



PHD

**Metal-based Catalysis for a Sustainable and Circular Plastics Economy
(Alternative Format Thesis)**

Payne, Jack

Award date:
2023

Awarding institution:
University of Bath

[Link to publication](#)

Alternative formats

If you require this document in an alternative format, please contact:
openaccess@bath.ac.uk

Copyright of this thesis rests with the author. Access is subject to the above licence, if given. If no licence is specified above, original content in this thesis is licensed under the terms of the Creative Commons Attribution-NonCommercial 4.0 International (CC BY-NC-ND 4.0) Licence (<https://creativecommons.org/licenses/by-nc-nd/4.0/>). Any third-party copyright material present remains the property of its respective owner(s) and is licensed under its existing terms.

Take down policy

If you consider content within Bath's Research Portal to be in breach of UK law, please contact: openaccess@bath.ac.uk with the details. Your claim will be investigated and, where appropriate, the item will be removed from public view as soon as possible.

Metal-based Catalysis for a Sustainable and Circular Plastics Economy

Jack M. Payne

A thesis submitted for the degree of Doctor of Philosophy

Department of Chemistry

University of Bath

October 2022

COPYRIGHT

Attention is drawn to the fact that copyright of this thesis rests with the author. A copy of this thesis has been supplied on condition that anyone who consults it is understood to recognise that its copyright rests with the author and that they must not copy it or use material from it except as permitted by law or with the consent of the author.



Centre for **Sustainable
& Circular** Technologies



UNIVERSITY OF
BATH

Acknowledgements

There are a number of people I would like to thank for making my PhD such an enjoyable and rewarding experience. Firstly, I would like to thank my supervisors, Prof. Matthew Jones and Dr. Emma Emanuelsson, for their unwavering support and guidance over the last 3 years. I feel extremely privileged to have worked under the supervision of such excellent mentors who allowed me the academic freedom to explore my own ideas and from whom I have learnt so much. I am also grateful to Dr. Andrew Sutton of Oak Ridge National Laboratory for productive quarterly discussions during the early stages of the PhD.

I am also hugely grateful to the CDT in Sustainable Chemical Technologies, and more broadly the CSCT, for the diverse array of training and development opportunities they provided me throughout my PhD. In particular, I would like to thank Francesca Guiso Gallisai, Aida De Heras and Amanda Crowe for all their hard work and support during my studies with everything CSCT-related. I would also like to thank the EPSRC for funding (EP/L016354/1) and Cohort 18 for their support and camaraderie.

I am also thankful for the assistance and expertise provided by a number of characterisation specialists based within MC² at the University of Bath. In particular, I would like to extend my gratitude to Dr. Tim Woodman and Dr. John Lowe for their invaluable NMR support, in addition to Dr. Mary Mahon and Dr. Gabriele Kociok-Köhn for X-ray crystallography assistance. I am also grateful to Dr. Shaun Reeksting for help with mass spectrometry and to Dr. Rémi Castaing and Dr. Martin Levere for SEC support.

I have also been incredibly fortunate to have been a part of such a welcoming and supportive research group. I would therefore like to thank all members of the Jones group, both past and present, namely Dr. Paul McKeown, Dr. Oliver Driscoll, Jack Stewart and Sandeep Kaler. A particular thank you to Paul for his expertise and tireless support during my MRes project and the first year of my PhD. I would like to extend my thanks to all members of the 5W SusChemLab and office for making work such an enjoyable place to come into each day and for fruitful discussions. A particular mention to Emma Daniels, Matthew Oshinowo, Fannie Burgevin, Alejandro Bara Estaún, Muhammad Kamran, Ella Clark and Kieran Moore. It has been a pleasure to work with such talented scientists and engineers, from which I have also greatly benefitted myself.

I am also extremely grateful for the opportunity to have co-supervised 5 master's project students, namely Binty Sankoh, Georgie Wright, Alvin Hong, William Brewer and Jack Hughes, across both chemistry and chemical engineering during my PhD. I would like to thank them for all their hard work during their research projects and for helping me grow as a

researcher. I am also thankful to Dr. Parimala Shivaprasad and Dr. Mutiah Mutiah for all their help related to training and work undertaken on the SDR. I also want to express my deepest gratitude to both Matthew and Paul for running the crystals presented in this thesis. Beyond the lab, Dr. Henry Shere deserves a special thank you for accompanying me through no less than 3 national lockdowns. I have also greatly enjoyed being a part of such a friendly and sociable chemistry department, particularly the weekly football and touch rugby matches.

Finally, I want to thank my family and friends for their continued love and support, and my partner, Ellie, for everything. Mum, Dad, I could not have asked for better parents or role models in life and this thesis, along with all the opportunities I have been fortunate enough to experience in life thus far, would not have been possible without you. Thank you for everything.

Abstract

Whilst plastics have played an instrumental role in the development of modern-day society, current practices within industry are unsustainable and require urgent revision. Central to the pursuit of a sustainable and circular plastics economy is the development of renewable alternatives and diversification of existing waste management strategies. **Chapter 1** aims to introduce and expand on these concepts, principally focusing on the catalytic chemical recycling of two commercial polyesters, namely poly(lactic acid) (PLA) and poly(ethylene terephthalate) (PET).

In **Chapter 2**, a range of Al(III)-complexes based on a novel ligand framework, namely the catalen, were prepared and characterised using a range of techniques. These Al(III)-catalen complexes were subsequently trialed in the ring-opening polymerisation (ROP) of *rac*-lactide (*rac*-LA) for the production of PLA, a bio-based polymer. Such initiators were found to exhibit unprecedented activity in the melt (TOFs up to 45,300 h⁻¹), whilst an unusual stereoselectivity switch dependent on the nature of the ligand substituents employed was observed under solution conditions {Al(**1**)Me, $P_r = 0.30$; Al(**3**)Me, $P_r = 0.72$ }.

In **Chapter 3**, metal diversification of these complexes was explored in pursuit of catalysts active for PLA degradation. Metal exchange was found to adversely impact polymerisation activity under both melt and solution conditions. The first example of PLA methanolysis mediated by a discrete Mg(II)-complex was demonstrated under relatively mild conditions (80 °C). Preliminary work extended the scope of such catalysts to the chemical recycling of PET.

In **Chapter 4**, Zn(II)- and Mg(II)-complexes based on a simple monoanionic tridentate {ONN} ligand (**1H**) were prepared and characterised. Zn(**1**)₂ and Mg(**1**)₂ were found to facilitate rapid PLA methanolysis under mild conditions (50 °C) and are among the fastest reported to date. Catalyst versatility and selectivity was further explored through the chemical upcycling of various commercial polyesters and the use of mixed plastic waste feeds. Metal exchange was found to dramatically influence catalyst activity, which appeared system dependent, whilst elevated temperatures were found to adversely impact PLA methanolysis.

In **Chapter 5**, a series of well-defined Zn(II)-half-salan complexes were synthesised and characterised. These complexes were shown to mediate the mild and selective degradation of various commercial polyesters and polycarbonates. The first example of discrete metal-mediated poly(bisphenol A carbonate) (BPA-PC) methanolysis being appreciably active at room temperature was demonstrated, with further kinetic analysis confirming Zn(**2**)₂ to be the fastest catalyst reported to date. A completely circular upcycling approach for bottle-grade PET waste was demonstrated through the production of several renewable poly(ester-amide)s (PEAs).

Publications

All publications produced as part of work undertaken during the Integrated PhD in Sustainable Chemical Technologies are detailed below. *N.B.* Publications 3, 4, 5, 6 and 8 constitute to the work presented in this thesis.

- [1] **J. Payne**, P. McKeown, M. D. Jones, *Polym. Degrad. Stab.* **2019**, *165*, 170–181.
- [2] **J. Payne**, P. McKeown, M. F. Mahon, E. A. C. Emanuelsson, M. D. Jones, *Polym. Chem.* **2020**, *11*, 2381–2389.
- [3] **J. Payne**, P. McKeown, G. Kociok-Köhn, M. D. Jones, *Chem. Commun.* **2020**, *56*, 7163–7166. *N.B.* Publication 2 in Chapter 2.
- [4] **J. Payne**, P. McKeown, O. Driscoll, G. Kociok-Köhn, E. A. C. Emanuelsson, M. D. Jones, *Polym. Chem.* **2021**, *12*, 1086–1096. *N.B.* Publication 3 in Chapter 3.
- [5] **J. Payne**, M. D. Jones, *ChemSusChem* **2021**, *14*, 4041–4070. *N.B.* Publication 1 in Chapter 1.
- [6] **J. M. Payne**, G. Kociok-Köhn, E. A. C. Emanuelsson, M. D. Jones, *Macromolecules* **2021**, *54*, 8453–8469. *N.B. N.B.* Publication 4 in Chapter 4.
- [7] J. Stewart, M. Fuchs, **J. Payne**, O. Driscoll, G. Kociok-Köhn, B. D. Ward, S. Herres-Pawlis, M. D. Jones, *RSC Adv.* **2022**, *12*, 1416–1424.
- [8] **J. M. Payne**, M. Kamran, M. G. Davidson, M. D. Jones, *ChemSusChem* **2022**, *15*, e202200255. *N.B.* Publication 5 in Chapter 5.

Additional online articles published concerning the work presented in Chapters 3 and 5 include:

- [9] **Chapter 3:** The Conversation, Plastic pollution: how chemical recycling technology could help fix it, <https://theconversation.com/plastic-pollution-how-chemical-recycling-technology-could-help-fix-it-156346>, (Accessed: 26th September 2022).
- [10] **Chapter 3:** World Economic Forum, Here’s everything you need to know about chemical recycling – and how it could solve our plastic problem, <https://www.weforum.org/agenda/2021/04/plastic-pollution-chemical-recycling-technology/>, (Accessed: 26th September 2022).
- [11] **Chapter 5:** University of Bath Press Release, Upcycling plastic waste into more valuable materials could make recycling pay for itself, <https://www.bath.ac.uk/announcements/upcycling-plastic-waste-into-more-valuable-materials-could-make-recycling-pay-for-itself/>, (Accessed: 26th September 2022).

Conferences

Work detailed in this thesis was presented at the following selected conferences:

- **07/2019 – CSCT Summer Showcase**
Oral and poster presentation – University of Bath, UK
- **12/2020 – CSCT Winter Showcase**
Poster presentation – online
- **07/2021 – CSCT Summer Showcase**
3MT and poster presentation – online
- **09/2021 – Bolland Symposium**
Poster presentation – University of Bath, UK
- **06/2022 – Bordeaux Polymer Conference (BPC)**
Poster presentation – University of Bordeaux, France
- **06/2022 – Bolland Symposium**
Oral presentation – University of Bath, UK
- **06/2022 - CSCT Summer Showcase**
Poster presentation – University of Bath, UK
- **08/2022 – American Chemical Society (ACS) Fall Meeting**
Oral and poster presentation – Chicago, Illinois, USA

Additional selected conferences attended in-person include:

- **10/2019 – One Young World (OYW) Summit**
London, UK
- **04/2022 – Research and Development (R&D) European PhD Seminar**
Hosted by Procter and Gamble (P&G), Frankfurt, Germany

Additional selected conferences attended online include:

- **05/2021 – Climate Exp0**
- **06/2021 – Dalton - Joint Interest Group Meeting**
- **07/2021 – UK Catalysis Hub Summer Conference**

Awards and Prizes

Selected awards and prizes achieved during the Integrated PhD in Sustainable Chemical Technologies are listed below:

- **07/2019 – BP Advancing Energy Scholarship**
- **10/2019 – One Young World (OYW) Ambassador**
- **07/2021 – Best Poster Prize**
CSCT Summer Showcase – online
- **07/2021 – Abel + Imray Prize Nomination for ‘Best Peer-Reviewed Research Paper’ by a CSCT Student between 2019 – 2020**
CSCT Summer Showcase – online
- **09/2021 – Inorganic Poster Runner-Up**
Bolland Symposium – University of Bath, UK
- **04/2022 – P&G European PhD Seminar Fellow**
- **05/2022 – Member of the Royal Society of Chemistry (MRSC)**
- **06/2022 – Finalist for ‘The Janet Scott Prize for Collaborative Research in Sustainability’**
CSCT Summer Showcase – University of Bath, UK

N.B. Co-supervised a final year MChem project student (J. W. J. Hughes) who was awarded the **Infineum Prize for ‘Best Final Year Project in Inorganic Chemistry’** at the University of Bath in July 2022.

Contents

Acknowledgements	i
Abstract	iii
Publications	iv
Conferences	v
Awards and Prizes	vi
List of Abbreviations	xiii
PhD Aims and Objectives	1
Chapter 1. Introduction (Publication 1)	2
1. Preamble.....	3
1.1. Statement of Authorship.....	4
1.2. Post-publication Commentary.....	35
1.2.1. Chemical recycling of PLA.....	35
1.2.1.1. Transesterification to alkyl lactates.....	35
1.2.1.2. Reductive depolymerisation.....	36
1.2.1.3. New methods.....	37
1.2.2. Chemical recycling of PET.....	38
1.2.2.1. Methanolysis to dimethyl terephthalate (DMT).....	38
1.2.2.2. Aminolysis to diamines of terephthalic acid.....	39
1.2.2.3. Glycolysis to bis(2-hydroxyethyl) terephthalate (BHET).....	40
1.2.2.4. Reductive depolymerisation.....	41
1.3. References.....	43
Chapter 2. Development of Industrially Relevant Aluminium Catalysts for PLA Production (Publication 2)	45
2. Preamble.....	46
2.1. Introduction.....	47
2.1.1. Synthesis.....	47
2.1.1.1. Lactic acid production.....	47
2.1.1.2. Polycondensation of lactic acid.....	47
2.1.1.3. ROP of lactide.....	48
2.1.2. Stereocontrol.....	50
2.1.2.1. Stereoisomerism of lactic acid and lactide.....	50
2.1.2.2. Tacticity of PLA.....	50
2.1.3. Polymer characterisation.....	52

2.1.3.1. Nuclear magnetic resonance (NMR) spectroscopy	52
2.1.3.2. Size exclusion chromatography (SEC)	53
2.1.3.3. MALDI time-of-flight mass spectrometry (MALDI-ToF)	54
2.1.3.4. Differential scanning calorimetry (DSC).....	55
2.1.3.5. Thermogravimetric analysis (TGA).....	55
2.1.4. Metal-based initiators for ROP of lactide	55
2.1.4.1. Industry standard	55
2.1.4.2. Aluminium(III).....	56
2.2. Statement of Authorship	62
2.3. Experimental	67
2.3.1. General experimental methods.....	67
2.3.2. General polymerisation procedures	67
2.3.2.1. Lactide polymerisation	67
2.3.2.2 Lactide polymerisation kinetics.....	68
2.3.3. Synthesis and characterisation.....	69
2.3.3.1. Tridentate {ONN} ligand precursor	69
2.3.3.2. Catalen ligands	69
2.3.3.3. Al(III)-catalen complexes	70
2.3.3.4. Representative NMR spectra.....	74
2.3.4. Polymer characterisation.....	81
2.3.4.1. Representative ¹ H NMR spectrum.....	81
2.3.4.2. Representative SEC spectrum	81
2.3.4.3. Representative homonuclear decoupled ¹ H NMR spectra	82
2.3.4.4. MALDI-ToF spectra.....	83
2.3.5. Crystallographic data	84
2.3.5.1. Special refinement details	84
2.3.6. Polymerisation kinetic data.....	86
2.4. Post-publication Commentary	87
2.5. References.....	89
Chapter 3. Metal Diversification in Pursuit of Catalysts Active for the Chemical Recycling of Polyesters (Publication 3).....	93
3. Preamble	94
3.1. Statement of Authorship	95
3.2. Experimental	107

3.2.1. General experimental methods.....	107
3.2.2. General polymerisation procedures.....	107
3.2.2.1. Lactide polymerisation.....	107
3.2.2.2. Lactide polymerisation kinetics.....	107
3.2.3. General PLA degradation procedures.....	107
3.2.3.1. PLA methanolysis.....	107
3.2.3.2. PLA methanolysis kinetics.....	108
3.2.4. General PET degradation procedures.....	108
3.2.4.1. PET glycolysis.....	108
3.2.5. Synthesis and characterisation.....	108
3.2.5.1. Zn(II)-catalen complexes.....	108
3.2.5.2. Mg(II)-catalen complexes.....	110
3.2.5.3. Representative NMR spectra.....	112
3.2.6. Polymer characterisation.....	115
3.2.6.1. Representative ¹ H NMR spectrum.....	115
3.2.6.2. Representative SEC spectra.....	115
3.2.6.3. Representative homonuclear decoupled ¹ H NMR spectra.....	116
3.2.6.4. MALDI-ToF spectra.....	116
3.2.7. Degradation characterisation.....	117
3.2.7.1. Representative ¹ H NMR spectra of PLA methanolysis.....	117
3.2.7.2. Representative ¹ H NMR spectrum of PET glycolysis.....	119
3.2.8. Crystallographic data.....	120
3.2.8.1. Special refinement details.....	120
3.3. Post-publication Commentary.....	122
3.4. References.....	123
Chapter 4. Exploring the Potential of a Ligand Building Block (Publication 4).....	124
4. Preamble.....	125
4.1. Statement of Authorship.....	126
4.2. Experimental.....	144
4.2.1. General experimental methods.....	144
4.2.2. General polymerisation procedures.....	144
4.2.2.1. Lactide polymerisation.....	144
4.2.2.2. Lactide polymerisation kinetics.....	144
4.2.3. General PLA degradation procedures.....	144

4.2.3.1. PLA methanolysis	144
4.2.3.2. PLA methanolysis kinetics.....	145
4.2.4. General PET degradation procedures	145
4.2.4.1. PET glycolysis.....	145
4.2.4.2. PET methanolysis.....	145
4.2.4.3. PET aminolysis.....	145
4.2.4.3.1. <i>N,N'</i> -dibenzylterephthalamide (DBT)	146
4.2.4.3.2. <i>N,N'</i> -bis(2-hydroxyethyl)terephthalamide (BHETA).....	146
4.2.4.3.3. <i>N,N'</i> -bis(3-(aminomethyl)benzyl)terephthalamide (3-AMBT).....	146
4.2.5. General PCL degradation procedures	146
4.2.5.1. PCL methanolysis.....	146
4.2.6. Synthesis and characterisation.....	147
4.2.6.1. Metal complexes based on 1H	147
4.2.6.2. Representative NMR spectra.....	148
4.2.7. Polymer characterisation.....	153
4.2.7.1. Representative ¹ H NMR spectrum.....	153
4.2.7.2. Representative SEC spectra	153
4.2.7.3. Representative homonuclear decoupled ¹ H NMR spectra	154
4.2.7.4. MALDI-ToF spectra.....	154
4.2.8. Degradation characterisation.....	155
4.2.8.1. PLA methanolysis	155
4.2.8.2. PET glycolysis.....	157
4.2.8.3. Representative ¹ H NMR spectra of PET methanolysis.....	157
4.2.8.4. Representative NMR spectra of PET aminolysis	158
4.2.8.5. Representative ¹ H NMR spectrum of PCL methanolysis	159
4.2.9. Degradation plots.....	160
4.2.9.1. Representative degradation plots for PLA methanolysis	160
4.2.9.2. Comparative catalyst performance plot for PET glycolysis.....	162
4.2.10. Crystallographic data	163
4.3. Post-publication Commentary	164
4.4. References.....	167
Chapter 5. Metal-mediated Chemical Upcycling Strategies for Commercial Polyester and Polycarbonate Waste (Publication 5).....	168
5. Preamble	169

5.1. Introduction.....	170
5.1.1. Polycarbonates	170
5.1.1.1. Industrial production of BPA-PC.....	170
5.1.1.2. Toxicity of BPA.....	171
5.1.1.3. End-of-life (EoL) options	172
5.1.2. Chemical recycling of BPA-PC	172
5.1.2.1. Alcoholysis	173
5.1.2.1.1. Metal-mediated transesterification.....	173
5.1.2.1.2. Organocatalysed transesterification	176
5.1.2.2. Glycolysis	178
5.1.2.3. Other methods.....	182
5.1.2.4. Summary.....	182
5.2. Statement of Authorship.....	184
5.3. Experimental.....	194
5.3.1. General experimental methods.....	194
5.3.2. General polymerisation procedures	194
5.3.2.1. Lactide polymerisation	194
5.3.2.2. PEA production.....	194
5.3.3. General PLA degradation procedures.....	195
5.3.3.1. PLA methanolysis	195
5.3.3.2. PLA methanolysis kinetics	195
5.3.4. General PET degradation procedures	195
5.3.4.1. PET glycolysis	195
5.3.4.2. PET aminolysis	195
5.3.4.2.1. <i>N,N'</i> -bis(2-aminoethyl)terephthalamide (BAETA).....	195
5.3.5. General BPA-PC degradation procedures	196
5.3.5.1. BPA-PC methanolysis.....	196
5.3.5.2. BPA-PC methanolysis kinetics	196
5.3.5.3. BPA-PC glycolysis.....	196
5.3.6. General PPC degradation procedures	197
5.3.6.1. PPC methanolysis.....	197
5.3.7. Synthesis and characterisation	197
5.3.7.1. Half-salan ligands.....	197
5.3.7.2. Zn(II)-half-salan complexes.....	199

5.3.7.3. Representative NMR spectra.....	202
5.3.8. Polymer characterisation.....	210
5.3.8.1. PLA.....	210
5.3.8.1.1. Representative ¹ H NMR spectrum	210
5.3.8.1.2. Representative SEC spectra	210
5.3.8.1.3. Representative homonuclear decoupled ¹ H NMR spectrum.....	211
5.3.8.1.4. MALDI-ToF spectra.....	211
5.3.8.2. PEA.....	212
5.3.8.2.1. Representative ¹ H NMR spectra.....	212
5.3.8.2.2. Representative SEC spectrum	213
5.3.8.2.3. Thermal analysis	214
5.3.9. Degradation characterisation.....	215
5.3.9.1. PLA methanolysis	215
5.3.9.2. PET glycolysis.....	215
5.3.9.3. PET aminolysis.....	215
5.3.9.4. Representative ¹ H NMR spectra of BPA-PC methanolysis	216
5.3.9.5. Representative ¹ H NMR spectrum of BPA-PC ethanolysis	217
5.3.9.6. Representative ¹ H NMR spectrum of BPA-PC glycolysis.....	218
5.3.9.7. Representative ¹ H NMR spectra of PPC methanolysis.....	219
5.3.10. Crystallographic data	220
5.3.11. Additional polymerisation and degradation data.....	221
5.4. Post-publication Commentary	226
5.5. References	228
Chapter 6.	233
6. Concluding Remarks	233
6.1. Future Work	235
6.1.1. Chapter 2.....	235
6.1.2. Chapter 3.....	236
6.1.3. Chapter 4.....	238
6.1.4. Chapter 5.....	239
6.2. References.....	243

List of Abbreviations

- 3-AMBT – *N,N'*-bis(3-(aminomethyl)benzyl)terephthalamide
APC – bio-based aliphatic polycarbonate
BAETA – *N,N'*-bis(2-aminoethyl)terephthalamide
BD – 1,4-butanediol
BHE-BPA – bishydroxyethyl ether of BPA
BHEDMTA – bis(2-hydroxyethyl) dimethylterephthalamide
BHET – bis(2-hydroxyethyl) terephthalate
BHETA – *N,N'*-bis(2-hydroxyethyl)terephthalamide
BnOH – benzyl alcohol
BPA – bisphenol A
BPA-PC – poly(bisphenol A carbonate)
CAN – covalent adaptable network
CAPEX – capital expenditure
CD – compact disc
CE – chain-end methine
CHN – elemental microanalysis
CHO – cyclohexene oxide
CRM – chemical recycling to monomer
D – diffusion coefficient
D – dispersity (molecular weight distribution)
DBN – 1,5-diazabicyclo[4.3.0]non-5-ene
DBT – *N,N'*-dibenzylterephthalamide
DBU – 1,8-diazabicyclo[5.4.0]undec-7-ene
DC-BPA – di-carbonate BPA
DCM – dichloromethane
DCTB – *trans*-2-[3-(4-*tert*-butylphenyl)-2-methyl-2-propenylidene]malononitrile
DCYPE – 1,2-bis(dicyclohexylphosphino)ethane
DEC – diethyl carbonate
DES – deep eutectic solvent
DFDC – dimethyl 2,5-furandicarboxylate
DFT – density functional theory
2,3-DHB – 2,3-dihydro-5*H*-1,4-benzodioxepin-5-one
DMA – dynamic mechanical analysis
DMAd – dimethyl adipate
DMAP – 4-dimethylaminopyridine

DMC – dimethyl carbonate
DMCD – dimethyl cyclohexanedicarboxylate
DMF – dimethylformamide
DMSe – dimethyl sebacate
DMSu – dimethyl succinate
DMT – dimethyl terephthalate
DoE – design-of-experiments
DOSY – diffusional ordered spectroscopy
DOTP – dioctyl terephthalate
DP – degree of polymerisation
DPC – diphenyl carbonate
DPPE – 1,2-bis(diphenylphosphino)ethane
DSC – differential scanning calorimetry
EA – ethanolamine
EC – ethylene carbonate
EDG – electron donating group
ee – enantiomeric excess
EG – ethylene glycol
EoL – end-of-life
ESI – electronic supporting information
ESI-MS – electron-spray ionisation-mass spectrometry
Et-LA – ethyl lactate
EtOH – ethanol
EWG – electron withdrawing group
FDA – US Food and Drug Administration
FDCA – furandicarboxylic acid
GHG – greenhouse gas
GPGB – Great Pacific Garbage Patch
GVL – γ -valerolactone
3-HBA – 3-hydroxybutyric acid
HBpin – pinacolborane
HDPE – high-density polyethylene
HMDS – bis(trimethylsilyl)amine
HPPO – hydrogen peroxide propylene oxide
HSQC – heteronuclear single quantum coherence
IL – ionic liquid
Int – internal methine

IP – intellectual property
 k_{app} – apparent pseudo-first-order rate constant
 k_i – rate constant of initiation
 k_p – rate constant of propagation
 KMH – KOH-in-MeOH hydrolysis
 LA – lactide
 LCA – life cycle analysis
 M – metal centre
 M_i – total weight of polymer chains in the sample
 M_n – number average molecular weight
 $M_{n,theo}$ – theoretical number average molecular weight
 M_r – molecular mass
 M_w – weight average molecular weight
 MALDI-ToF – matrix-assisted laser desorption/ionisation time-of-flight
 MC-BPA – mono-carbonate BPA
 MeCN – acetonitrile
 Me-LA – methyl lactate
 MeOH – methanol
 2-Me-THF – 2-methyltetrahydrofuran
 MHE-BPA – monohydroxyethyl ether of BPA
 MOF – metal-organic framework
 MSA – methanesulfonic acid
 N_i – total number of polymer chains in the sample
 NHC – N-heterocyclic carbene
 NMR – nuclear magnetic resonance
 N,N -DMAc – N,N -dimethylacetamide
 NP – nanoparticle
 P_m – probability of isotactic enchainment
 P_r – probability of heterotactic enchainment
 PA – phthalic anhydride
 PBAT – poly(butylene adipate terephthalate)
 PBO – 2,2'-(1,4-phenylene)-bis(2-oxazoline)
 PBS – poly(butylene succinate)
 PC – propylene carbonate
 PCL – poly(ϵ -caprolactone)
 PCW – poster-consumer plastic waste
 PDK – poly(diketoenamine)

PDMS – polydimethylsiloxane
PEA – poly(ester-amide)
PEEP – poly(ethyl ethylene phosphate)
PEF – poly(ethylene furanoate)
PET – poly(ethylene terephthalate)
PG – propylene glycol
PHB – polyhydroxybutyrate
PLA – poly(lactic acid)
PMEP – poly(methyl ethylene phosphate)
PMHS – polymethylhydrosiloxane
PMMA – poly(methylmethacrylate)
PO – propylene oxide
PP – polypropylene
PPA – polyphthalaldehyde
PPC – poly(propylene carbonate)
PPE – polyphosphoester
ppm – parts per million
PPY – 4-pyrrolidinopyridine
PS – polystyrene
PVC – poly(vinyl chloride)
rac – racemic
RCD – ring-closing depolymerisation
RI – refractive index
ROCOP – ring-opening copolymerisation
ROP – ring-opening polymerisation
RPA – relative peak area
RT – room temperature
 S_{A-LA} – alkyl lactate selectivity
 S_{BPA} – BPA selectivity
 S_{cc} – cyclic carbonate selectivity
 S_{OC} – organic carbonate selectivity
 S_{PC} – propylene carbonate selectivity
SDR – spinning disc reactor
SEC – size exclusion chromatography
SIP – self-immolative polymer
SPS – solvent purification system
 T_c – crystallisation temperature

T_d – decomposition temperature
 T_g – glass transition temperature
 T_m – melting temperature
 T_{mc} – monomer ceiling temperature
 $\tau_{4/5}$ – structural index parameter/geometric preference value
TA – terephthalic acid
TBD – 1,5,7-triazabicyclo[4.4.0]dec-5-ene
TBT – titanium butoxide
TGA – thermogravimetric analysis
THETA – N^l, N^l, N^d, N^d -tetrakis-(2-hydroxyethyl)terephthalamide
THF – tetrahydrofuran
TMA – thermomechanical analysis
TMAF – tetramethylammonium fluoride
TMC – tetramethylammonium methyl carbonate
TMDS – 1,1,3,3-tetramethyldisiloxane
TMS – tetramethylsilane
TOF – turnover frequency
TPA – terephthalamide
VT-NMR – variable temperature nuclear magnetic resonance
 X_{int} – internal methine conversion
XRD – X-ray diffraction
 Y_{A-LA} – alkyl lactate yield (as determined by ^1H NMR analysis)
 Y_{BHET} – isolated yield of BHET
 Y_{DMT} – isolated yield of DMT
 Y_{TPA} – isolated yield of TPA

PhD Aims and Objectives

Overarching aims and objectives of the PhD are detailed below to contextualise the published work presented herein which follows as chapters. Indeed, this thesis is presented in an alternative format comprising of a portfolio of research papers, which adhere to the narrative established by the PhD objectives. Chapter preamble serves to link the papers together, whilst post-publication commentary allows for further comments and critique beyond that initially discussed in the publication.

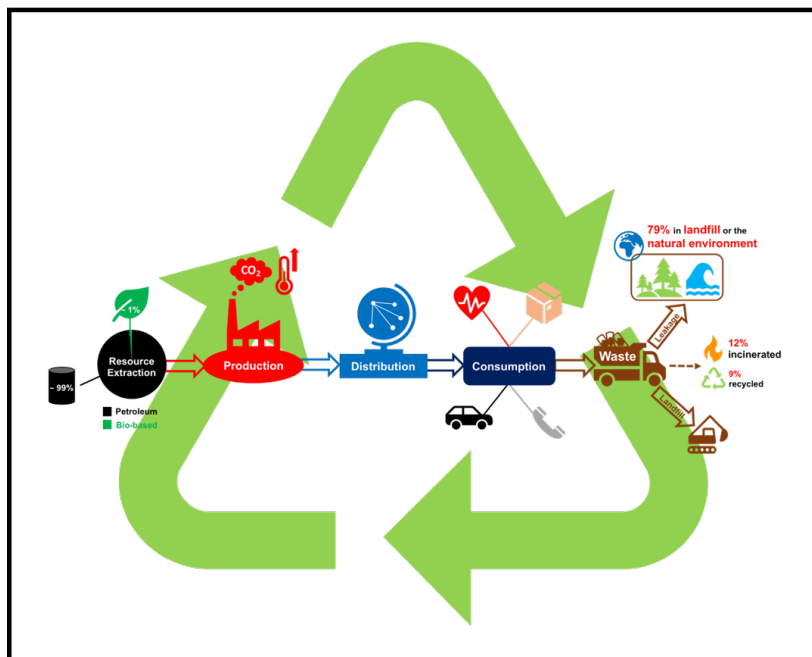
The aims and objectives of this PhD were to:

1. Develop simple, cheap and environmentally benign discrete metal-based catalysts for PLA production *via* the ROP of *rac*-LA, prioritising high activity and stereocontrol, particularly under industrially melt conditions (**Chapter 2**).
2. Assess the ability of such catalysts to facilitate the mild and selective degradation of various commercial polyesters, such as PLA and PET, with a particular focus on chemical upcycling into value-added products (*e.g.* green solvents and chemical building blocks) (**Chapters 3, 4 and 5**).
3. Explore judicious metal and ligand diversification for the optimisation of such systems for the chemical recycling of polyesters, whilst ensuring catalyst design remains industrially relevant in accordance to Aim 1 above (**Chapters 3, 4 and 5**).
4. Investigate the potential to extend catalyst scope to other types of plastics that possess cleavable linkages (*e.g.* polycarbonates) (**Chapters 5**).
5. Evaluate process scalability and intensification on a novel spinning disc reactor (SDR), adopting a combined experimental (*e.g.* design-of-experiments) and computational (*e.g.* MATLAB) approach for system optimisation (**work not detailed within this thesis**).

Chapter 1.

Introduction

Publication 1. The Chemical Recycling of Polyesters for a Circular Plastics Economy: Challenges and Emerging Opportunities



Acknowledgement: The work presented in this chapter has been published in the journal ‘*ChemSusChem*’, volume 14, issue 19, pages 4041–4070 and is reproduced with the permission of Wiley-VCH.

1. Preamble

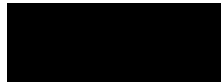
The “Plastic Age” has facilitated significant advancements in human development through disruptive and transformative innovation, notably in key sectors such as healthcare, transport and electronics.^[1-3] However, the current plastics economy remains fundamentally limited, characterised by a predominantly petroleum-based product portfolio that operates within a wasteful linear economy.^[4,5] Consequently, mounting environmental concerns has stimulated increasing public scrutiny, leading to some to call for outright bans on plastic use. However, plastics remain a tremendous source of social, economic and environmental value, pillars central to a truly sustainable future.^[6,7] Thus, such materials will play a key role in enabling the transition towards net zero.

The purpose of this chapter is to first provide an overview of the plastics industry and identify key challenges and opportunities, particularly relating to feedstock selection and current end-of-life (EoL) options. The concept of chemical recycling will then be introduced as a possible enabler for a sustainable and circular plastics economy and compared with the industry standard; mechanical recycling. Specifically, Chapter 1 aims to highlight a number of key advantages associated with chemical recycling, for example long-term material value retention and possible economic incentives through the derivatisation of platform/value-added chemicals (*e.g.* lactate esters). Governing depolymerisation thermodynamic and kinetic principles will be discussed before highlighting the crucial role catalysis will play in the commercialisation of future processes. Social, economic and environmental challenges associated with the uptake of such technology will then be presented before introducing polyesters as a possible class of plastics amenable to chemical recycling.

Two commercial polyesters, namely poly(lactic acid) (PLA) and poly(ethylene terephthalate) (PET), feature extensively in this thesis and thus form the primary focus of this chapter. A comprehensive overview of key contributions and recent developments for the catalytic chemical recycling of PLA and PET will be discussed, with a particular focus on upcycling strategies (*e.g.* solvolysis, alcoholysis and reductive depolymerisation) and the use of metal-based catalysts. Indeed, Chapter 1 will highlight discrete metal-mediated systems remain rare despite being a promising solution for a number of key challenges in the field, including process efficiency and selectivity.

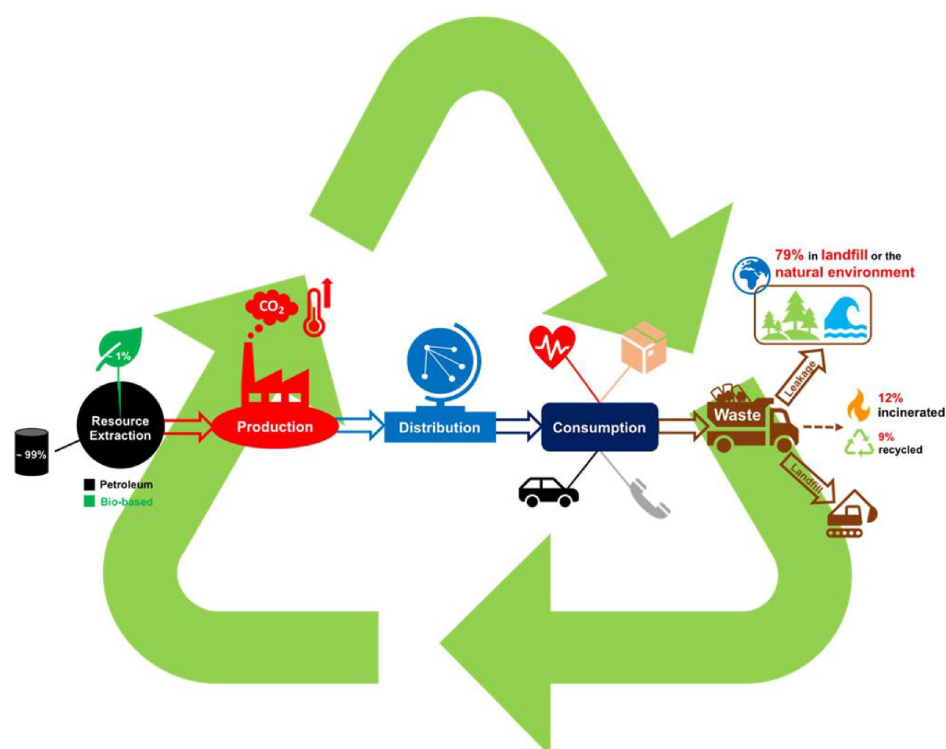
Finally, developments pertaining to the emergence of new materials (*e.g.* covalent adaptable networks (CANs) and self-immolative polymers (SIPs)) with the potential to revolutionise the plastics industry will be briefly introduced. Throughout this chapter emerging opportunities and challenges are critically discussed within the context of industrial feasibility.

1.1. Statement of Authorship

This declaration concerns the article entitled:			
The Chemical Recycling of Polyesters for a Circular Plastics Economy: Challenges and Emerging Opportunities			
Publication status (tick one)			
Draft manuscript <input type="checkbox"/> Submitted <input type="checkbox"/> In review <input type="checkbox"/> Accepted <input type="checkbox"/> Published <input checked="" type="checkbox"/>			
Publication details (reference)	J. Payne, M. D. Jones, <i>ChemSusChem</i> 2021 , <i>14</i> , 4041–4070 (DOI: 10.1002/cssc.202100400)		
Copyright status (tick the appropriate statement)			
I hold the copyright for this material <input checked="" type="checkbox"/> Copyright is retained by the publisher, but I have been given permission to replicate the material here <input type="checkbox"/>			
Candidate's contribution to the paper (provide details, and also indicate as a percentage)	<p>The candidate predominantly executed the work presented in the paper.</p> <p>JMP was responsible for conducting a comprehensive literature review on the chemical recycling of polyesters, focusing primarily on PLA and PET. The purpose of this review was to provide a complete literature overview in order to introduce the main body of the thesis research. The manuscript was initially prepared by JMP with editorial feedback from MDJ prior to submission. JMP was the corresponding author.</p> <p>Formulation of ideas:</p> <p>Review scope was prepared by JMP and discussed with MDJ for editorial advice. [JMP = 90%, MDJ = 10%]</p> <p>Design of methodology:</p> <p>The structure of the review was designed by JMP. [JMP = 100%]</p> <p>Experimental work:</p> <p>The literature search and manuscript preparation were completed by JMP with minor editing from MDJ. [JMP = 90%, MDJ = 10%]</p> <p>Presentation of data in journal format:</p> <p>All of the figures, tables and schemes were prepared by JMP. [JMP = 100%]</p>		
Statement from Candidate	This paper reports on original research I conducted during the period of my Higher Degree by Research candidature.		
Signed		Date	6/6/2022

The Chemical Recycling of Polyesters for a Circular Plastics Economy: Challenges and Emerging Opportunities

Jack Payne^{*(a)} and Matthew D. Jones^{*(b)}



Whilst plastics have played an instrumental role in human development, growing environmental concerns have led to increasing public scrutiny and demands for outright bans. This has stimulated considerable research into renewable alternatives, and more recently, the development of alternative waste management strategies. Herein, the aim was to highlight recent developments in the catalytic chemical recycling of two commercial polyesters, namely poly(lactic acid) (PLA) and poly(ethylene terephthalate) (PET). The concept of chemical recycling

is first introduced, and associated opportunities/challenges are discussed within the context of the governing depolymerisation thermodynamics. Chemical recycling methods for PLA and PET are then discussed, with a particular focus on upcycling and the use of metal-based catalysts. Finally, the attention shifts to the emergence of new materials with the potential to modernise the plastics economy. Emerging opportunities and challenges are discussed within the context of industrial feasibility.


1. Introduction


Plastics have played a crucial role in human development since their commercialisation in the 20th century, revolutionising key sectors such as transport, communications and healthcare.^[1] Whilst their inherent strength and durability is revered during their functional lifetime, such properties render plastics a pervasive environmental pollutant at end-of-life. The industries reliance on a depleting fossil feedstock, coupled with a linear model, serves to confound mounting environmental concerns (Figure 1).^[1–3] It has been estimated of the 8.3 billion tonnes of plastic manufactured between 1950 to 2015, 6.3 billion tonnes is now waste, with 79% accumulating in either landfill or the natural environment.^[6] Whilst prevalent on land, ocean plastics exemplify current levels of plastic pollution within the environment.^[7,8] In 2018, it was reported the Great Pacific Garbage Patch (GPGP) consisted of approximately 1.8 trillion plastic fragments, collectively weighing 79000 tonnes, and continues to grow annually.^[9] It is therefore unsurprising recent initiatives have emerged proposing plastics be banned outright, perhaps most notably in packaging applications, and replaced by alternative materials such as paper, glass and aluminium. However, in the face of increasing public scrutiny, it is imperative research continues to underpin informed decisions to avoid unintended environmental consequences. Indeed, despite being traditionally perceived as less environmentally friendly, life cycle analysis (LCA) has shown a poly(ethylene terephthalate) (PET) bottle to be significantly less carbon intensive relative to its glass and aluminium counterpart.^[9] Moreover, the social and economic value of plastics is often overlooked. In Europe, the plastics economy comprised close to

60000 companies, supporting 1.6 million jobs and turning over €360 billion in 2018.^[10] Consequently, a solution to the plastics dilemma is rather more complex than an outright plastic ban. A complete system redesign of the economy is required to mitigate anthropogenic activity and ensure its long-term future. It is clear feedstock selection requires urgent revision with petroleum-based products accounting for approximately 99% of all processed plastics, consuming approximately 6% of oil produced globally, which is projected to increase to 20% by 2050.^[2,11] Bio-based plastics represent a promising solution, but market penetration remains low (<1%) due to a high production cost and inferior performance, for some applications, relative to conventional synthetic plastics.^[3,12] Nonetheless, it is anticipated increasing public awareness, coupled with legislation and a high oil price, will drive the uptake of bio-based products. However, the plastic industry is characterised by a high product turnover, owing to an anticipated life expectancy of typically less than 1 year.^[2,11] Indeed, 1 million plastic bottles are produced per minute, with single-use plastics equating for 47% of the waste stream.^[2,13] Consequently, in pursuit of a sustainable plastics economy, utilisation of a renewable feedstock is not the answer unless it is complemented by comprehensive waste management strategies. This necessitates sufficient collection and sorting infrastructure to manage the large quantities of waste produced and minimise leakage. However, 32% of plastic packaging waste escapes current collection systems, whilst emerging economies have little to no infrastructure.^[2,5,7] Therefore, the waste crisis can be expected to worsen in the absence of positive, proactive intervention as plastics remain in the growth phase, with use expected to double within the next 20 years and production projected to exceed 1 billion tonnes per year by 2050.^[2,14] Presently, 40% of post-consumer plastic waste (PCW) is destined for landfill, where non-biodegradable plastics can persist for decades.^[1,2,5] Whilst immediate environmental impact is limited to land use and collection/transport, obvious benefits include potential greenhouse gas (GHG) sequestration and targeted waste depositing. Alternatively, industrial composting can facilitate the degradation of biodegradable plastics, such as poly(lactic acid) (PLA), limiting their environmental impact.^[5] However, both methods align with a linear model and fail to capture embedded material value. Whilst incineration represents a possible waste valorisation strategy, consuming 14% of PCW, comprehensive LCAs favour recycling both in terms of energy use and GHG production.^[15,16] Thus, it is clear recycling will play a pivotal role in facilitating the industries transition to

[a] J. Payne
Centre for Sustainable and Circular Technologies
University of Bath
Claverton Down, Bath, BA2 7AY (UK)
E-mail: jmp63@bath.ac.uk

[b] Prof. M. D. Jones
Department of Chemistry
University of Bath
Claverton Down, Bath, BA2 7AY (UK)
E-mail: mj205@bath.ac.uk

 This publication is part of a collection of invited contributions focusing on "Chemical Upcycling of Waste Plastics". Please visit chemsuschem.org/collections to view all contributions.

 © 2021 The Authors. ChemSusChem published by Wiley-VCH GmbH. This is an open access article under the terms of the Creative Commons Attribution License, which permits use, distribution and reproduction in any medium, provided the original work is properly cited.

a bio-based circular model, one concerned with material recapture and reuse.^[1,25] Mechanical recycling is extensively exploited in the reprocessing of plastic packaging, accounting almost entirely for Europe's (EU 28+2) average packaging recycling rate, which equated to 42% in 2018.^[10] However, the process is limited by eventual material downcycling, owing to thermomechanical degradation facilitated by the harsh remelting conditions used.^[5] Plastic oxidation over their functional lifetime increases their susceptibility to such detrimental side reactions during reprocessing.^[17] Consequently, there is an industry appetite to diversify the existing portfolio of plastic waste management strategies, with a particular focus on preserving, or indeed upcycling, waste material market value. A potential solution to this is chemical recycling, which will form the primary focus of this Review.

Recently, there have been a number of comprehensive polymer recycling Reviews published.^[5,17–22] However, with the field rapidly expanding, numerous advancements have been made in recent years. Herein, we aim to highlight recent developments in the sustainable chemical recycling of two commercial polyesters, namely PLA and PET. The concept of chemical recycling will first be introduced, highlighting challenges and opportunities within the context of depolymerisation thermodynamics. Chemical recycling methods for PLA and PET will then be discussed, with a particular focus on upcycling and the use of metal-based catalysts. We do not intend this to be an exhaustive account but instead endeavour to highlight key contributions and contextualize their impact. Emerging opportunities and challenges within the field are discussed within the context of industrial feasibility.

2. Chemical Recycling of Plastics

2.1. Principle of chemical recycling

The chemical recycling of plastic waste exploits a chemical transformation (e.g., hydrolysis, transesterification, hydrosilylation, etc.) to either recapture virgin monomer (closed-loop) or directly convert it into other useful synthetic chemicals/feedstocks (open-loop). Central to this concept is the polymer backbone bearing functionality susceptible to cleavage, for

example, ester linkages found in polyesters. Potential benefits relative to mechanical recycling include:

1. removes material downcycling, thus promoting the long-term retention of material value within the plastics economy
2. potential for upcycling plastic waste, enabling value-added chemicals to be accessed for enhanced economic performance
3. access raw virgin feedstocks, such as lactic acid from PLA, whilst preserving product quality.^[5,17,22–24]

2.2. Depolymerisation energetics

In order to adopt a systemic approach to depolymerisation, it is important to first consider the fundamental thermodynamic and kinetic principles governing polymerisation.^[17,22,25] Traditionally, exergonic polymerisations ($\Delta G_p < 0$) are driven by a large exothermic enthalpic (ΔH_p) driving force.^[5,26] Intuitively, this must dominate an entropic (ΔS_p) forfeit conceded due to a reduction in degrees of freedom as monomer is consumed. At polymerisation equilibrium, the change in Gibbs free energy (ΔG_p) is zero, and thus a critical temperature (T_c) can be described exclusively as a function of $\Delta H_p/\Delta S_p$. Traditionally, ΔH_p and ΔS_p are negative and T_c is termed the ceiling temperature.^[17,27] Systems that favour polymerisation below T_c and depolymerisation above T_c will form the basis of this Review (Figure 2). Industrially relevant polymer ($M_n > 10000 \text{ g mol}^{-1}$) can be produced by careful consideration of the reaction conditions used in alignment with the Carother's equation and Le Châtelier's principle.^[17,28] It is thus clear the magnitude of $\Delta H_p/\Delta S_p$ dictates the temperature difference between complete polymerisation and the reverse process; depolymerisation.

However, polymer composition has significant ramifications on T_c and therefore their amenability to chemical recycling. Polyolefins consist of inherently inert sp^3 -hybridised C–C and C–H bonds and thus require harsh conditions (250–400 °C) to overcome high activation barriers ($E_a = 150\text{--}300 \text{ kJ mol}^{-1}$) associated with pyrolysis.^[17,29] However, preceding catalytic pyrolysis methods utilising temperatures $\geq 500 \text{ °C}$ have been reported.^[22,30–32] Product selectivity is also problematic, generally characterised by downgrading to fuels and waxes of varying chain length and saturation, owing to a homogenous polymer



Jack Payne is a Ph.D. student at the Centre for Sustainable and Circular Technologies (CSCT). Jack holds master's degrees (hons) in Chemistry (First Class) and Sustainable Chemical Technologies (Distinction) from the University of Bath. He has previous industrial experience working for Shell on the development of novel diesel performance additives. His current research spans both chemistry and engineering, focusing on the application of metal-based catalysis for renewable polymer production and chemical recycling of plastics.



Matthew Jones is a Professor of Inorganic Chemistry at the University of Bath. He obtained his Ph.D. in 2003 under the supervision of Professors Brian Johnson and Melinda Duer at Cambridge University. After a brief sojourn in industry he moved back to academia in 2004 as a PDRA in the group of Professor Matthew Davidson at Bath, where he remained being promoted from research fellow (2007), lecturer (2012), senior lecturer (2012), reader (2017) and finally to Professor (2019). He has graduated 13 Ph.D. students and his current work focusses on novel catalysts for polymer production and degradation.

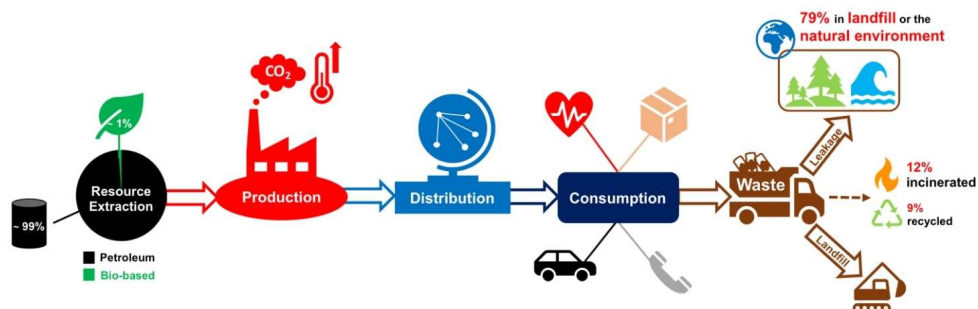


Figure 1. Linear model of a petroleum-based plastics economy.

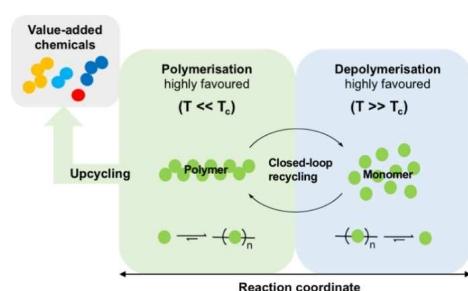


Figure 2. Overview of chemical recycling from an energetic perspective, considering closed-loop recycling and upcycling.

backbone.^[22,30–34] High-density poly(ethylene) (HDPE) offers minimal monomer recovery (22–25%), whilst high monomer yields (up to 94%) have been reported for poly(propylene) (PP).^[17,35,36] Such methods are practical from a plastic accumulation perspective and offer some net energy/material recovery. However, their high energy intensity releases damaging CO₂ emissions into the environment. Thus, it is clear the development of selective and mild recycling strategies for polyolefins remains a prevalent challenge in the field. However, extreme exergonicity renders chemical recycling unsuitable, though this is not to say alternative strategies should not be aggressively pursued to mitigate plastic pollution. Indeed, polyolefins accounted for almost two-thirds of global plastic production in 2015.^[11] Since such materials are not the primary focus of this report, we direct the interested reader to two excellent Reviews that highlight recent developments within the field.^[17,22]

Polyolefins represent an exergonic threshold, with chemical recycling lending itself to exergonicities approaching neutrality. Coates and Getzler recently described the ideal system as one that exhibits sufficient polymerisation exergonicity as to achieve high conversion and molecular weights rapidly, whilst retaining high selectivity under mild conditions. These features should be reflected just above T_c in the corresponding depolymerisation process.^[17] However, polymers can become kinetically trapped

in the absence of a reactive chain-end due to end-capping, which can be as simple as a proton. This increases the thermal stability of the polymer well beyond its T_c , necessitating thermodynamic and kinetic driving forces be considered in tandem during polymer design.^[17] A sustainable plastics economy relies on leveraging the intricate balance between polymerisation and depolymerisation energetics to deliver a truly sustainable and circular product portfolio. However, the current waste crisis poses an interesting dilemma: should research focus on developing recycling strategies compatible with existing products or favour a complete system redesign? We argue both avenues should be pursued in parallel to ensure future growth endeavours to address existing challenges, whilst anticipating future needs and concerns.

2.3. Catalysis

Catalysis will undoubtedly play a crucial role in ensuring the commercial viability of chemical recycling by improving reaction efficiency and reducing waste. Indeed, catalysis is exploited in approximately 90% of industrial chemical processes and contributes over £50 billion to the UK economy annually.^[37] Whilst pyrolysis is highly material dependent, catalysis offers the opportunity to precisely engineer the process conditions used and products manufactured. An excellent example of metal-based catalysis underpinning commercial viability is that of Ziegler-Natta applied to olefin polymerisation. Such catalysts enabled commercialisation of the process in 1954, ushering in an era of unprecedented economic and academic investment in order to realise the tangible societal benefits of plastics.^[17,38] For example, plastic components lower the environmental impact of vehicles by a factor of 4, whilst plastic insulation saves 250 times the energy used for its production.^[39] Whilst this has led to significant developments in the field of polymerisation catalysis, our attention must now be diverted towards depolymerisation in equal measure to mitigate plastic pollution and ensure the plastic economy's long-term future. Before considering plastics amenable to chemical recycling, focusing on polyesters and the application of metal-based catalysts, we will

first consider societal and economic challenges associated with the uptake of such technology.

2.4. Society, infrastructure and economics

Chemical recycling has long been an established technology with commercial examples including the PETCORE system, the Eastman Chemical Company (EEC) method and the DuPont process.^[40] However, such processes are sensitive to feed impurities, requiring a pre-treatment step. This coupled with high capital expenditure (CAPEX) and process costs relative to cheap petrochemical feedstock has limited their widespread application. Common waste stream contaminants include foreign debris and other plastics arising due to sorting mistakes or in instances when separation is difficult to achieve (for example PE and PP).^[22] Poly(vinyl chloride) (PVC) is particularly problematic due to its propensity to eliminate HCl upon heat treatment, which can lead to reactor corrosion, precluding mechanical recycling.^[41] Indeed, PVC contamination as low as 100 ppm has previously been reported to adversely impact the quality of the recycled product.^[42] Plastics are also inherently heterogeneous, containing numerous additives (e.g., plasticizers, stabilizers and pigments) for performance and aesthetic purposes.^[43] Beyond the manufacturer, their identity is often unknown due to intellectual property (IP) rights. Consequently, if treated in isolation with respect to product commercialisation, their potentially detrimental impact on polymer recyclability remains unknown until end-of-life, at which point it is too late. Moving forward, industry/consumers may need to concede on product expectations when additives are used solely for aesthetic purposes (e.g., pigments in carbonated drinks bottles) unless green alternatives that uphold recyclability can be developed. Education will play a key role in reducing resistance to such change and promoting consumer engagement. Multi-component and composite plastics serve to confound the aforementioned challenges.^[22] We therefore identify a clear opportunity to collaborate fruitfully with industry to deliver transferable research and avoid such pitfalls. For emerging materials, this necessitates embedding recyclability at the design phase whilst maintaining a competitive cost-to-performance ratio.

However, despite a clear industry appetite for robust and selective recycling strategies, a serious imbalance remains between waste generation and recovery.^[5,22] This can be attributed to both a lack of infrastructure (e.g., collection and sorting) and insufficient waste management portfolio. Indeed, only 14% of plastic packaging collected is intended for recycling, with closed-loop (i.e., collected and reprocessed for the same application) accounting for just 2%.^[22] It has been estimated for PET chemolysis facilities to be economically viable they require a minimum throughput of 1.5×10^5 tonnes p/a.^[44] Significant capital investment will undoubtedly underpin realising this future, but industry has been cautious. Five recent signatories of the "The New Plastics Economy Global Commitment" pledged \$200+ million towards enabling a circular plastics economy.^[45] Whilst promising, this remains low relative

to the projected \$15–20 billion of CAPEX required annually to achieve a recovery rate of 50% by 2030.^[46] Aggressive investment strategies can be incentivised through developing renewable products/processes that compete with, or indeed outperform, their petrochemical-based counterpart. Industry must also adopt a mindset that values plastic waste as an untapped resource, which is anticipated to grow from 260 to 460 million tonnes between 2016–2030 based on current disposal rates.^[46] Moreover, recycled content demand is expected to exceed 5 million tonnes by 2025, equivalent to 25 million barrels of oil being left in the ground.^[45] Over the last decade, global petrochemical and plastic industry investment has totalled between \$80–100 billion each year.^[46] If such funds can be directed towards enabling a sustainable and circular plastics economy, we remain optimistic of taking significant strides towards achieving 2025 targets.^[45] Legislation will also undoubtedly play a crucial role in ascertaining a circular plastics economy, whether it be through promoting the uptake of renewable technology (e.g., economic subsidies) or influencing consumer habits. Moreover, such policy need not be inherently complex to achieve significant disruption. For example, following the introduction of a simple 5p plastic bag charge in 2015, plastic bag sales reduced by 86% between 2015–2018 among England's major supermarkets, removing over 9 billion plastic bags out of circulation.^[47] However, policy requires standardisation with regards to plastic disposal. In the UK, such policy can vary considerably between local and regional authorities owing to a certain degree of devolution, which generates discontinuity at a national level. This leads to consumer frustration and confusion, which encourages sorting mistakes and a tendency not to recycle. Efficient recycling strategies will only achieve their desired environmental impact if all components in the supply chain are connected and operate harmoniously.

Whilst we focus on the development of waste management strategies in this Review, this is not to say it is inherently any more, or less, important than any other individual component in the supply chain. It is imperative all components are developed in tandem to deliver an integrated plastics economy that practices circularity and sustainability. It is only by adopting this stance that meaningful change can be realised within the next decade and beyond.

2.5. Polyesters

Polyesters represent ideal candidates for chemical recycling owing to the presence of a highly polar sp^2 -hybridised carbonyl bond (C=O), which is susceptible to nucleophilic attack. It is therefore unsurprising most progress in catalytic chemical recycling pertains to polar plastics.^[22] Society's varied polyester use demands equally diverse recycling strategies, rendering a "one-solution-fits-all" scenario unrealistic. We encourage the scientific community to exploit the inherently vibrant and diverse field of carbonyl chemistry in system and product design.^[48] It is envisaged an indefinite chemical recycling closed-loop will increase recycled content in today's products, reducing society's dependence on depleting fossil reserves,

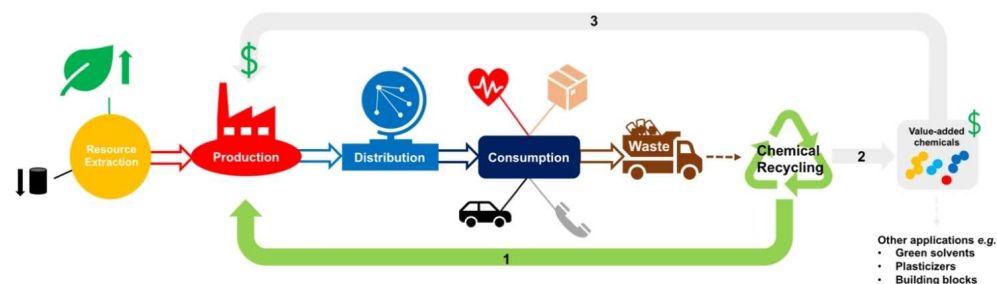


Figure 3. Diagram representing the potential for chemical recycling to introduce circularity into the plastics economy: (1) closed-loop recycling or (2) transformation of plastic waste into value-added chemicals that can be used in higher-value applications or recirculated to access higher-value plastics (3).

whilst promoting the uptake of bio-based alternatives. However, it is the potential to access higher-value chemicals for use in both the plastic industry and beyond that creates a unique differentiating value proposition relative to other waste management strategies (Figure 3). This will be particularly adventurous for plastics where recovering the monomer may be economically unviable. Recently, a number of promising advancements have been made, although numerous key challenges remain. For research to be considered industrially relevant, it must fulfil the following criteria:

1. high process efficiency under mild conditions
2. high product selectivity in the presence of mixed plastics
3. robust catalysts tolerant to common plastic waste stream contaminants, including additives and debris
4. simple catalyst recovery and reuse, maintaining performance between cycles
5. metal-based systems should exploit the use of cheap and earth-abundant metals in combination with scalable ligands.

The aforementioned criteria will provide the framework by which recent developments in the field will be assessed. The plastic waste crisis demands the development of recycling strategies for both emerging and established plastics in parallel. We adopt this approach in this Review, first considering developments for PLA, an emerging bio-based plastic, before discussing those pertaining to PET, an established polyester with a significantly higher market share.^[11]

3. Chemical Recycling of Poly(lactic acid)

3.1. Poly(lactic acid)

PLA is a renewable and biodegradable aliphatic polyester based on a repeating lactic acid monomer (Figure 4), sourced from the microbial fermentation of starch-rich feedstocks, such as corn and sugar.^[5,49,50] Industrially, PLA is produced from the ring-opening polymerisation (ROP) of L-lactide under solvent-free conditions. This method exploits a $\text{Sn}(\text{Oct})_2$ (Oct = 2-ethylhexanoate) catalyst operating via a coordination–insertion mechanism to produce poly(L-lactic acid) (PLLA) of high and well-

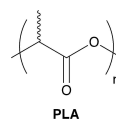


Figure 4. Polymeric structure of PLA.

defined M_n .^[51] Toxicity concerns associated with the industry standard $[\text{Sn}(\text{Oct})_2]$ has stimulated considerable research into sustainable and biocompatible alternatives.^[51–54] This remains an active area of research although it falls beyond the scope of this Review and thus will not be discussed further. PLA has been the subject of intense academic interest over the last 20 years owing to its green credentials.^[5,11,55–59] PLA possesses intrinsic biocompatibility and thus has been widely exploited in the biomedical industry. Common applications include use in tissue scaffolds, sutures and drug delivery systems.^[5,60,61] PLA has also found use in food and packaging material applications.^[5,11,55–58,60]

Despite being a commercially available polymer, its widespread use has been limited by a high production cost relative to traditional synthetic plastics. This can be attributed to complexity associated with the fermentation and purification of lactic acid, accounting for approximately 50% of total production costs.^[62] It is therefore unsurprising PLA accounted for just 13.9% of bioplastic production in 2019.^[63] Thus, research has been devoted to reducing production costs by targeting the production of lactide directly in one-step processes, exploiting the use of shape-selective catalysis and gas-phase reactions.^[64–70] However, it is clear PLA will play a prominent role in a future plastics economy as the uptake of bio-based products increases.^[5] Indeed, the production and use of PLA has the potential to reduce GHG emissions and non-renewable energy use by 40 and 25%, respectively, compared to traditional petroleum-based plastics, including PE and PET.^[3,5,71,72] In 2018, Total Corbion constructed a new 75000 tonne p/a plant in Thailand, signifying market growth.^[73]

However, despite its green credentials, PLA waste is a potential contributor to plastic pollution if irresponsibly handled at end-of-life. PLA is often praised as a biodegradable

alternative, although this leads to the misconception that it readily degrades in the natural environment.^[74] PLA biodegrades efficiently into CO₂ and H₂O under industrial composting conditions, requiring elevated temperatures (60 °C) and high relative humidity in the presence of thermophilic microbes.^[5,75–79] Complete biodegradation has been reported within 30 days under such conditions.^[75,79] Conversely, degradation can take up to a year in domestic composters at 20 °C, which can be reduced to 12 weeks above 25 °C.^[80,81] PLA's tendency to persist in the marine environment raises further concerns. Recent studies observed no degradation within 1 year under laboratory conditions simulating static seawater, although weight loss was noted under dynamic conditions via mechanical processes.^[82–85]

In light of such challenges, there is a clear need to develop sustainable chemical recycling strategies to assist incorporation of PLA into the circular economy. Given PLA's relatively low, but increasing, market share at present, this represents a unique opportunity to potentially introduce large-scale commercialisation and complementary recycling methods in parallel. This would assist plastic pollution mitigation from the outset, whilst providing a model framework for future product design/deployment.

3.2. Hydrolysis to lactic acid

PLA hydrolysis produces lactic acid, which has been identified as a future platform chemical for the production of a wide range of value-added commodity chemicals (Figure 5).^[5,86,87] Current lactic acid production capacity is approximately 400 000 tonnes p/a, which is projected to increase annually by 5–8%.^[5,18,88] Lactic acid is envisaged to play a crucial role in ascertaining a low-carbon future, underpinned by a bio-based circular economy. Consequently, considerable research has been devoted to PLA hydrolysis.

PLA hydrolysis is known to proceed via two possible mechanisms, dictated by the rate of water diffusion relative to bond breaking. This is dependent on a number of parameters including molecular weight, pH and temperature. Homogeneous sample mass loss dominates when water diffusivity is high, whilst heterogeneous surface erosion is observed when water diffusivity is low.^[89,90] McKeown and Jones^[89] recently published a detailed account of PLA hydrolysis, particularly from a mechanistic perspective. Here we do not intend to reproduce such work but instead highlight key contributions.

Pioneering work by Tsuji et al.^[91–97] details early developments within the field. Initial work considered a 5 wt% solution of PLLA ($M_n = 170\,000 \text{ g mol}^{-1}$) between 180–350 °C.^[91] An optimum hydrolysis temperature of 250 °C was found, achieving 90% L-lactic acid yield within 20 min ($E_a = 51.0 \text{ kJ mol}^{-1}$). Above 250 °C, racemisation became more prevalent, culminating in lactic acid decomposition into CO₂, CO and CH₄ at 350 °C. Degradation via a homogenous mass loss mechanism was found to proceed independent of reaction temperature (120–250 °C) and PLA phase (melt or solid).^[92] Such high reaction temperatures are characteristic of PLA hydrolysis owing to its

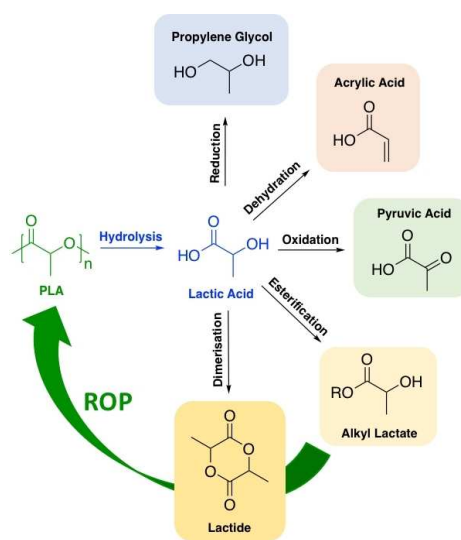


Figure 5. Hydrolysis of PLA to lactic acid with examples of further transformations to value-added commodity chemicals. Similar transformations are possible starting from alkyl lactates, whilst the green arrow highlights possible circularity (via lactide) in the PLA supply chain.^[89]

inherent insolubility in the reaction media, rendering the process energy intensive. The effect of average block length on the degradation of stereoblock PLA has also been investigated.^[94] Rapid degradation of atactic segments was observed, whilst a decrease in hydrolysis rate was noted for increasing stereoblock length. Hirao and Ohara^[98] have demonstrated the application of microwave heating to achieve enhanced hydrolysis rates. Using a relatively concentrated solution of PLA (75 wt%, $M_n = 96\,000 \text{ g mol}^{-1}$), maximum lactic acid yield was achieved within 800 min at 170 °C, which could be reduced to 120 min under microwave irradiation. However, this process is limited to 45% lactic acid yield before racemisation reduces optical purity of the final product.

Piemonte and Gironi^[99,100] have contributed substantially to the field from a kinetic perspective. Recent studies have investigated hydrolysis between 140–180 °C for varying concentrations of PLA (5–50 wt%), observing 95% conversion to lactic acid within 120 min between 160–180 °C. The kinetic reaction rate was found to be independent of PLA concentration and characterised by two distinct reaction mechanisms: (1) a two-phase reaction ($E_a = 53.2 \text{ kJ mol}^{-1}$) and (2) an autocatalytic effect ($E_a = 36.9 \text{ kJ mol}^{-1}$). This autocatalytic effect had previously been reported by Siparsky et al.^[101] and arises due to an increase in the number of carboxylic acid end groups as hydrolysis proceeds, which decreases the pH of the solution. Villani and co-workers^[102] have subsequently extended this kinetic model to higher reaction temperatures (170–200 °C), achieving complete PLA conversion within 90 min.

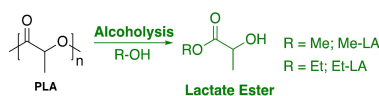
Given the challenge of solubilising PLA in H₂O, water/ethanol mixtures (50% ethanol) between 40–90 °C have recently been reported.^[103,104] The presence of ethanol causes the polymer to swell, facilitating enhanced water diffusivity, which reduces the activation barrier [$E_a(\text{H}_2\text{O}) = 101.4 \text{ kJ mol}^{-1}$, $E_a(\text{H}_2\text{O}/\text{EtOH}) = 93.4 \text{ kJ mol}^{-1}$]. It was predicted oligomers suitable for repolymerisation could be obtained after 29 h at 90 °C, whilst prolonged reaction would achieve 95% yield of lactic acid after approximately 41 h. Whilst such conditions are considerably less energy intensive relative to traditional hydrolysis systems, such reaction times are unreasonable at an industrial scale.

To overcome this challenge, commercial processes typically use a strong inorganic acid (H₂SO₄, HNO₃) or base [NaOH, Ca(OH)₂] catalyst.^[5,105] A patented example is described by Coszach et al.^[106] who demonstrated PLA hydrolysis in both the presence and absence of NaOH, the latter being particularly commercially advantageous since it removes the need for harsh and highly corrosive reagents. The hydrolysis process proceeded between 80 and 180 °C with pressures of up to 10 bar. In the absence of catalyst, reaction temperatures can be as high as 350 °C.^[89] Unsurprisingly, to the best of our knowledge, no examples of PLA hydrolysis mediated by a discrete metal-based catalyst have been reported. This is presumably due to their sensitivity to hydrolytic degradation, highlighting the need for robust metal-based catalysts in pursuit of sustainable PLA hydrolysis. Song et al.^[107] have demonstrated the use of ionic liquids (ILs) for the relatively mild hydrolysis of PLA. [Bmim][OAc] was identified as the outstanding candidate, achieving up to 94% lactic acid yield within 2 h at 130 °C ($E_a = 133.9 \text{ kJ mol}^{-1}$). The product was recovered by addition of calcium carbonate to precipitate calcium lactate in good yield (up to 76%). Promisingly, [Bmim][OAc] could be recycled seven times with no decrease in performance. However, this system is limited by a high catalyst loading (50 wt% based on PLA), which is unscalable based on catalyst cost (Sigma Aldrich, 100 g, £200).

Enzymatic processes have also previously been reported.^[5,108–111] Whilst their industrial feasibility is hindered by possible scalability issues, it is clear biocatalysis will play an increasingly important role in enabling the bioeconomy.^[112–114]

3.3. Transesterification to alkyl lactates

Whilst the depolymerisation of PLA to lactic acid is one circular economy approach, perhaps a more attractive option is the direct transformation of waste feedstock into value-added chemicals. Consequently, the transesterification of PLA into alkyl lactates (lactate esters) has received increasing attention (Scheme 1). Low-molecular lactate esters have been identified as potential green solvent replacements for traditional petrochemical-based solvents owing to their inherent biodegradability and low toxicity. Moreover, their low vapour pressure ensures they are safer and easier to handle than conventional solvents. As such, lactate esters lend themselves to a diverse range of sectors, including the pharmaceuticals, agriculture and



Scheme 1. Metal-mediated alcoholysis of PLA to afford lactate esters, otherwise referred to as alkyl lactates.^[89]

polymer industry.^[5,115,116] There is also the potential to realise enhanced economic performance through waste upcycling, a particularly attractive quality to industry. The Et-LA market is estimated to reach \$92 million by 2024 and currently trades at £2.54–3.49 per kg relative to £1.69 per kg for virgin PLA.^[42,117] Traditionally, such materials are resource and energy intensive to produce, providing significant scope for process optimisation in accordance to the 12 principles of green chemistry.^[5,118] Recently, the metal-mediated alcoholysis of lactide has been shown to be an effective alternative.^[119–121] However, this method is arguably an inefficient use of a direct PLA precursor and fails to utilise the PLA waste stream. We will therefore focus on PLA transesterification methods.

Numerous patented processes have been reported for PLA alcoholysis, detailing the use of a range of solid acid/base catalysts (CaO, Montmorillonite K10, Nafion-H) and solvents (ILs, toluene, lactate esters, chloroform, alcohols).^[89,105] DuPont possesses a patent for PLA degradation into various lactate esters (R=Me, Et and *n*Bu) in the presence of H₂SO₄, achieving high conversion (69–87%) within 2 h between 150 and 190 °C.^[122] However, the acid catalyst used is both highly corrosive and toxic, and thus effort in the literature has focused on developing more environmentally friendly alternatives.

To this end, Song et al.^[123] reported the first example of PLA ($M_w = 400000 \text{ g mol}^{-1}$) methanolysis mediated by a range of ILs (Figure 6). [Bmim][OAc] was identified as the outstanding candidate, consistent with PLA hydrolysis, achieving up to 93% Me-LA yield within 3 h at 115 °C ($E_a = 38.3 \text{ kJ mol}^{-1}$). [Bmim][OAc] could be recycled 6 times without a reduction in activity, although a high loading was noted (50 wt% based on PLA). The use of ILs in combination with simple metal salts [e.g., Zn(OAc)₂ and FeCl₃] has also been shown to facilitate PLA degradation under milder conditions.^[124,125] For example, 2[Bmim][OAc]-Zn(OAc)₂ achieved 92% Me-LA yield within 2 h at 110 °C, consistent with a lower activation energy ($E_a = 21.0 \text{ kJ mol}^{-1}$). This synergistic reactivity enhancement can likely be attributed to greater C=O activation in the presence of Lewis acid metals, facilitated by enhanced PLA dissolution. Despite ILs exhibiting superior activity and easier product separation relative to H₂SO₄, their scalability remains limited by their high cost and intrinsic viscosity.

Organocatalysts have also been reported for PLA transesterification (Figure 6).^[126] Hedrick and co-workers^[127] have demonstrated the use of 4-pyrrolidinopyridine (PPY) and 4-dimethylaminopyridine (DMAP) for the alcoholysis of PLA, focusing on controlled degradation to target molecular weights. Recently, Enthaler and co-workers^[128] extended the use of DMAP for PLA methanolysis under microwave irradiation,

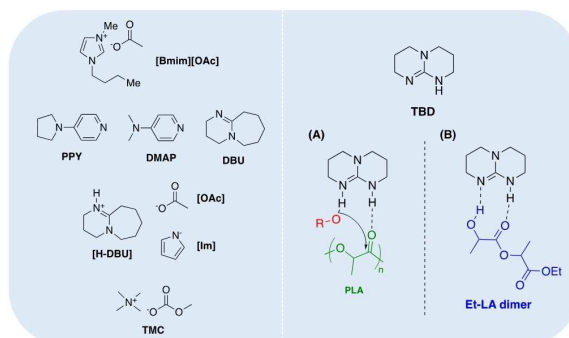


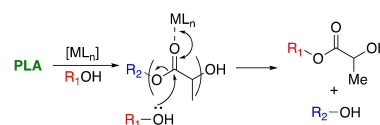
Figure 6. Selected examples of organocatalysts reported for PLA transesterification. (A) Proposed dual-activation transesterification mechanism for TBD and (B) reaction inhibition by intramolecular binding of lactate dimer to TBD.

achieving high Me-LA yield within 10 min at 180 °C. The use of MeOH in a large excess (23.1 equiv.) allows the reaction to proceed under neat conditions, negating the need for potentially harmful solvents that are typically a significant source of waste in industry.^[5] Moreover, this simple catalytic system exhibited reasonable tolerance to plastic contaminants and additives for PLA sourced from 16 commodity applications. High activity was retained on substituting DMAP for 1,8-diazabicyclo[5.4.0]undec-7-ene (DBU). Liu et al.^[129] recently reported DBU-based protic ILs for PLA ($M_w = 400000 \text{ g mol}^{-1}$) alcoholysis. Preliminary screening found [H-DBU][OAc] offered the highest Me-LA yield, achieving 91% within 5 h at 100 °C. High lactate ester yields (76–89%) were retained for higher-chain alcohols under comparable conditions. Substitution of the anion for an imidazole-based derivative afforded [H-DBU][Im], capable of achieving 87% Me-LA yield within 1 h at 70 °C.^[130] This remarkable activity enhancement enabled polymer scope to be expanded to PET and poly(bisphenol A) carbonate (BPA-PC), demonstrating catalyst versatility. McKeown et al.^[131] recently reported tetramethylammonium methyl carbonate (TMC) as a simple and cheap organocatalyst for versatile polymer degradation including PET, BPA-PC and poly(ϵ -caprolactone) (PCL). Promisingly, 100% Me-LA yield could be achieved within 1 h at 50 °C in THF. High activity was retained down to reasonably low catalyst loadings (0.5 mol%), which is commonly a limiting feature among organocatalysts, perhaps most notably in ILs. Leibfarth et al.^[132] have demonstrated 1,5,7-triazabicyclo[4.4.0]dec-5-ene (TBD) to be an extremely efficient catalyst for PLA degradation. Indeed, TBD exhibited extremely high activity, achieving >90% Et-LA yield within 3 min at room temperature, which could be extended to a range of primary alcohols including MeOH, BuOH and BnOH. TBD's remarkable activity can likely be attributed to a dual-activation mechanism, characterised by simultaneous activation of both the carbonyl group and incoming alcohol via H-bonding (Figure 6a). Interestingly, transesterification of the ethyl lactate dimer proceeded significantly slower relative to bulk PLA ($M_n = 76700 \text{ g mol}^{-1}$). This retardation event was attributed to the formation of an

intramolecular complex between the dimer and TBD, which subsequently inhibits activation of a further ethanol molecule (Figure 6b). An enantiomeric excess (*ee*) of >95% confirmed preservation of stereochemistry in the lactate product from PLLA.

Despite product racemisation risking potentially costly and complex product separation, retention of stereochemistry in the final lactate product often remains overlooked in the literature. Whilst TBD clearly represents the benchmark for PLA alcoholysis from an activity standpoint, with degradation under ambient conditions adventitious both economically and environmentally, TBD remains limited by properties akin to H_2SO_4 . Moreover, this system utilises CH_2Cl_2 , a possible carcinogenic solvent, and thus is limited in practice relative to the 12 principles of green chemistry.^[118] A possible solution to this is metal-mediated degradation (Scheme 2), although literature examples remain scarce despite the plethora of initiators reported for lactide polymerisation.^[51,52,54]

The first example of metal-mediated PLA alcoholysis dates back to 1945, concerning the use of ZnCl_2 with temperatures up to 150 °C.^[133] A range of studies using commercially available metal salts have since been reported. Sánchez and Collinson^[134] reported a strategy using $\text{Zn}(\text{OAc})_2$ for the selective degradation of PLA into Me-LA from a 1:1 mixture of PLA and PET. At the boiling point of methanol, 65% Me-LA yield was obtained after 15 h. Under these conditions, PET was found to be non-reactive and insoluble, which enabled solid PET to be separated by filtration post-reaction. The formation of $\text{Zn}(\text{lactate})_2$ was



Scheme 2. General metal-mediated degradation mechanism of PLA into a lactate ester via transesterification with an alcohol, where R_1 and R_2 denote the alcohol chain length and growth polymer chain, respectively.

detected by IR spectroscopy, possibly implicating this as the active species. Liu et al.^[135] investigated the activity of a wide range of simple, commercially available salts including NaOAc, NaOH, NaOMe, Zn(Octanoate)₂, AlCl₃ and SnCl₄·5H₂O. FeCl₃ was identified as the outstanding candidate, achieving 87% conversion to Me-LA within 4 h at 130 °C in the absence of solvent ($E_a = 32.4 \text{ kJ mol}^{-1}$). The catalyst could be reused 6 times without any appreciable loss in activity following recovery via distillation of the lactate product. This is particularly impressive given catalyst recovery is often a limiting industrial feature of homogeneous catalysis. Recently, Enthaler and co-workers^[136–139] have extensively reported the use of simple metal salts for PLA alcoholysis under microwave irradiation. Commercially available alkali halide salts of the general formula MX, such as KF, LiCl and KBr, were found to be potent catalysts for PLA ($M_n = 43600\text{--}150400 \text{ g mol}^{-1}$) methanolysis between 140–160 °C. Indeed, KF was shown to facilitate high yields of Me-LA within 10 min and could be reused up to three times.^[136] It is anticipated the potassium cation activates the carbonyl to nucleophilic attack, whilst the fluoride anion simultaneously assists proton transfer. Sn(Oct)₂ has also been shown to facilitate methanolysis for various end-of-life sources of PLA ($M_n = 43600\text{--}150400 \text{ g mol}^{-1}$).^[137] High Me-LA yields were achieved between 140–180 °C at low catalyst loadings (0.05–0.25 mol%), observing turnover frequencies (TOFs) up to 36900 h^{-1} at 180 °C. The scalability of this process was demonstrated at a 50 g scale using a PLA cup. Interestingly, the amount of MeOH was found to significantly impact Me-LA yield, observing a reduction from quantitative to negligible yield upon shifting from 15.4 to 11.6 equiv. Plichta et al.^[140] had previously reported the use of Sn(Oct)₂ for the partial alcoholysis of high molecular weight PLA ($M_w = 217000 \text{ g mol}^{-1}$) in the presence of protic reagents, such as diols, diacids and macromolecules, for the design of block copolymers. To address toxicity concerns associated with Sn(Oct)₂, Enthaler and co-workers explored the use of environmentally benign alternatives, including bismuth- and zinc-based salts.^[138,139] Promisingly, TOFs up to 13800 and 45000 h^{-1} were observed for bismuth subsalicylate and Zn(OAc)₂, respectively, at 180 °C using 0.1 mol% catalyst. However, in both instances a large excess of MeOH (67.5 equiv.) was required, which limits process scalability. A reoccurring theme of this group's work is to assess the impact of various sources of end-of-life PLA (e.g., cup, bottle, coloured lids, contaminants) and mixed plastic waste streams (e.g., PLA + PET, nylon-6, PVC, BPA-PC) on catalyst activity and selectivity, both of which are integral for ensuring industrial viability. For both bismuth subsalicylate and Zn(OAc)₂, high Me-LA yield (>99%) was retained irrespective of PLA source.^[138,139] Conversely, Me-LA yield was found to vary more significantly for the alkali halide and Sn(Oct)₂ systems, observing moderate to high yields (43–128%). Note yields greater than 100% were observed in instances when the starting material was assumed to be 100% PLA but contained a substantial number of additives by mass (e.g., black sushi box). Generally, high activity and selectivity was retained in the presence of mixed waste streams, observing the concomitant degradation of BPA-PC with PLA, whilst nylon-6 and PET remain intact.^[136,137,139] Sobota

and co-workers^[141] have explored the use of cheap and abundant magnesium and calcium catalysts for the solvothermal alcoholysis of PLA ($M_n = 64200\text{--}115700 \text{ g mol}^{-1}$). Using metallic magnesium or Mg(*n*Bu)₂, efficient alcoholysis was achieved at 200 °C within 1 h using a wide range of linear and branched alcohols. Ethanolysis was scaled up to 1.5 kg, noting retention of polymer stereochemistry in the lactate product, confirmed by polarimetry. High reaction temperatures were favoured to avoid the use of excess alcohol, despite reasonable Et-LA yields (71–88%) being attainable as low as 100 °C in the presence of 4–10 equiv. of ethanol. In the absence of catalyst, high-temperature regimes (220–260 °C) were required in the presence of 4 equiv. of ethanol based on ester linkages. Such high temperatures are consistent with work by Hirao et al.^[142] for the ethanolysis and butanolysis of PLA ($M_n = 96000 \text{ g mol}^{-1}$), which required conventional heating up to 210 °C and a large excess of alcohol (10 equiv.), although enhanced reaction rates were observed under microwave irradiation. Commercially available alkali/alkaline metals (Li–K/Mg–Ba) and selected alkoxides [e.g., Na(OEt), K(OEt), Ca(OMe)₂], in addition to organometallic/chloride zinc, tin and aluminium reagents, were also investigated.^[141] All reagents exhibited good activity, achieving between 64–91% Et-LA yield at 200 °C within 1 h under autogenous pressure. Interestingly, the formation of Ca(lactate)₂ was observed for calcium-mediated alcoholysis, consistent with work by Sánchez and Collinson.^[134]

Whilst such methods have the potential to overcome industry concerns associated with catalyst recovery and equipment corrosion, there is a clear opportunity to preserve activity under significantly milder conditions. This can likely be achieved through judicious choice of the metal-ligand employed, although literature examples of discrete metal-based complexes remain limited (Figure 7). Whitelaw et al.^[143] have previously reported a series of zirconium and hafnium(IV)-salalen complexes for the production and degradation of PLA. It was proposed the addition of excess MeOH during post polymerisation work up facilitated the formation of a bismethoxide analogue, which appeared active for PLA methanolysis. The Hf^{IV}-salalen (R=Me) complex was found to degrade PLA samples of varying tacticities (atactic and isotactic; $M_n = 10000\text{--}200000 \text{ g mol}^{-1}$), achieving 75% conversion to Me-LA within 24 h at room temperature for a commercial PLLA source ($M_n = 200000 \text{ g mol}^{-1}$). However, ligand complexity limits the scalability of these systems, highlighting the need for facile ligand preparation. Zn^{II}-complexes are arguably the most studied for PLA recycling due to a strong literature precedent as highly active initiators for lactide polymerisation, coupled with zinc being an inexpensive and biocompatible metal.^[51,52,54] Fliedel et al.^[144] reported the first example of a Zn^{II}-complex for the controlled degradation of PLA, namely a dinuclear zinc-carbene complex. The addition of methanol to a heteroleptic (NHC)-ZnEt (Cl) pre-catalyst generated the active species in situ. Low-molecular-weight PLLA ($M_n = 18410 \text{ g mol}^{-1}$) was degraded exclusively to oligomers ($M_n \approx 2000 \text{ g mol}^{-1}$) and Me-LA (28%) after 24 h at room temperature. Ejfler and co-workers^[145] explored the use of a homoleptic Zn^{II}{ON}₂ for the controlled transesterification of PLA into Me-LA via an oligomeric precip-

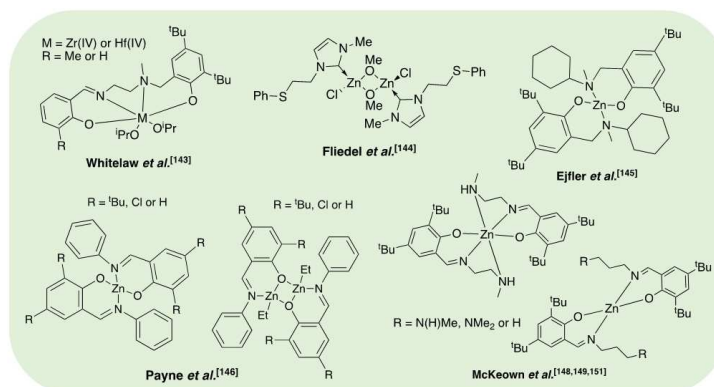
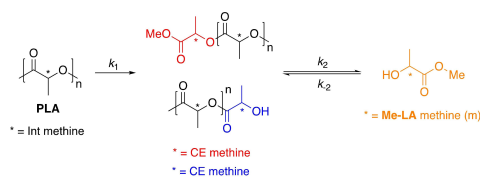


Figure 7. Discrete metal-based catalysts reported for the transesterification of PLA.

itation strategy, using alcohol as an anti-solvent. However, this process was limited to PLA of low molecular weight. Recently, Payne et al.^[146] reported a series of well-defined mono- and dimeric Zn^{II}-Schiff base complexes for lactide polymerisation and PLA methanolysis. Schiff bases are traditionally easy to prepare and purify in high yield, and thus are ideal candidates for ligand scale-up. Moreover, their functional versatility provides significant scope for catalyst fine-tuning, and thus they lend themselves to the field of PLA recycling, which remains in its infancy.^[5] Interestingly, whilst dimers outperformed their monomeric counterparts in the polymerisation of *rac*-LA, reduced activity was generally observed in the methanolysis of a PLA cup ($M_n = 45150 \text{ g mol}^{-1}$). This was attributed to inferior catalyst stability, highlighting the importance of robust pre-catalysts. Zn^{II}{ON}₂ (R=Cl, H) were identified as the outstanding candidates, achieving 100% Me-LA yield within 8 h at 80 °C in THF. It is anticipated the carbonyl is activated by the Lewis acidic Zn^{II}-centre, consistent with enhanced activity upon shifting from an electron-donating (R = *t*Bu) to -withdrawing ligand backbone (R=Cl). McKeown et al.^[147] had previously reported a series of aminopiperidine-based Zn^{II} and Mg^{II}{ONN} complexes for lactide polymerisation. Extensive transesterification was observed during polymer purification, although ligand complexity precluded a complete degradation study. Recent work by Jones and co-workers sought to simplify the ligand backbone with a particular focus on preserving activity. To this end, McKeown et al.^[148] developed a Zn^{II}-Schiff base complex bearing a simple ethylenediamine ligand, which exhibited high activity (TOF = 114000 h⁻¹) for lactide polymerisation. This was conducted under industrially relevant immortal conditions in the melt at 180 °C, demonstrating high catalyst tolerance, a desirable quality of a degradation catalyst. Román-Ramírez et al.^[149] have subsequently performed an in-depth kinetic study of PLA methanolysis using this Zn^{II}-complex. Experimental design identified temperature (40–130 °C) and catalyst loading (4–16 wt%) as the main variables influencing PLA degradation.

Mass transfer limitations related to PLA particle size and stirring speed were considered negligible. Various PLA samples ($M_n = 44350\text{--}71900 \text{ g mol}^{-1}$) were degraded, achieving conversions up to 100% Me-LA within 1 h at 90 °C in THF. PLA consumption proceeded with a pseudo-first-order kinetic profile, whilst the production of Me-LA was shown to proceed via a two-step process through the intermediate formation of chain-end groups ($E_a = 39\text{--}65 \text{ kJ mol}^{-1}$; Scheme 3). A subsequent study investigated the use of this Zn^{II}-complex in PLA methanolysis using various end-of-life sources (cup, toy and 3D printed material) between 70–110 °C.^[150] As expected, the largest deviations in Me-LA selectivity and conversion were observed for the toy, which contained the highest number of additives. Recently, McKeown et al.^[151] demonstrated shifting to a propylenediamine analogue [R=N(H)Me] to have significant ramifications on activity. Indeed, rapid degradation of a PLA cup ($M_n = 45150 \text{ g mol}^{-1}$) was realised, obtaining 81% Me-LA yield within 30 min at 50 °C in THF. The corresponding ethylenediamine analogue exhibited significantly reduced activity (12% Me-LA in 6 h) under comparable conditions (4 wt% catalyst, 40 °C), highlighting the importance of structure–activity relationships.^[149] Substitution of the propylenediamine substituent (R=NMe₂) resulted in reduced activity, although remained high, observing



Scheme 3. Two-step reaction sequence for the production of Me-LA from PLA via the intermediate formation of chain-end groups. Consequently, the methine groups can be categorised as internal (int), chain-end (CE) and those corresponding directly to the alkyl lactate (Me-LA).^[149]

84% Me-LA within 1 h. This system was scaled up to 12.5 g of PLA and found tolerant to the presence of PET. Scale up experiments have since used these Zn^{II}-complexes for the production of higher-chain alkyl lactates including ethyl, propyl and butyl lactate.^[117,152] Removal of the amine group (R=H) resulted in a dramatic reduction in activity under identical conditions, implicating the amine group in the reaction. It is anticipated the Lewis acidic Zn^{II}-centre and amine group activate the incoming carbonyl group and alcohol respectively, analogous to the dual-activation mechanism proposed for TBD (Figure 6). A recent kinetic study revealed these complexes to adopt unusual behaviour, noting curved Arrhenius plots and variable activation energies, whilst observing the formation of Me-LA as low as -20°C .^[153] Yang et al.^[154] recently reported Zn(HMDS)₂ as a highly efficient catalyst for the transesterification of a variety of polyesters including PLA, poly(β -butyrolactone) (PBL), poly(δ -valerolactone) (PVL) and PCL. Promisingly, 99% Me-LA yield was achieved within 2 h at room temperature, although a high catalyst loading (1.0 mol%) and large excess of MeOH (24.7 equiv.) were used. The process was scaled up to 11.0 g of PLA ($M_n=49900\text{ g mol}^{-1}$) using 5 wt% catalyst, characterised firstly by the ROP of *rac*-LA, followed by polymer purification and finally degradation with MeOH. Whilst promising, it is important to acknowledge PLA samples degraded were not commercially sourced and instead directly produced from *rac*-LA. Consequently, the impact of additives and polymer processing on the amenability of the final PLA product to chemical recycling were not considered, and thus are not industrially representative. Zn(HMDS)₂ also possesses a reason-

ably high market price (1 g, £123, Sigma Aldrich), limiting scalability.

Whilst significant developments have been made within the last 5 years, a number of challenges remain. Although consideration of mixed plastic waste streams on catalyst activity and selectivity is becoming increasingly assessed, it is imperative it becomes routine to overcome inevitable barriers to industrial application. Additionally, whilst the recovery and reuse of simple commercially available metal salts has been well established, it remains overlooked for discrete metal-based systems. A possible solution to this is immobilisation on a support, although heterogeneous-based systems for PLA alcoholysis remain scarce. The pursuit of more active and robust catalysts should assist in addressing this concern, ultimately targeting a system that operates in air under ambient conditions. Work has also primarily focused on zinc; however, concerns associated with its long-term availability have created an appetite for metal diversification.^[155] Here, we argue prioritisation of cheap, earth-abundant and environmentally benign metals (e.g., Mg, Fe, Ca) to ensure a sustainable future. For inspiration, the scientific community need not look further than the plentiful and diverse array of initiators reported for lactide polymerisation. A summary of the systems discussed in the preceding section is provided in Table 1.

3.4. Reductive depolymerisation

PLA degradation methods discussed thus far retain carbonyl functionality in the final product, either as a carboxylic acid

Table 1. Summary of selected metal-based and organocatalysts reported for PLA transesterification.^[a]

Catalyst	MeOH/ester unit (n/n)	Cat. [mol%]	T [°C]	t [h]	PLA conv. [%]	S _{Me-LA} [%]	Y _{Me-LA} [%]	Ref.
ILs								
[Bmim][OAc]	5:1	2 ^[b]	115	3	97	96	93	[123]
2[Bmim][OAc]-Zn(OAc) ₂	5:1	1 ^[b]	110	2	97	95	92	[124]
[H-DBU][OAc]	5:1	5	100	5	100	91	91	[129]
[H-DBU][Im]	5:1	10	70	1	100	87	87	[130]
Organocatalysts								
DMAP	23.2:1	5	180 ^[c]	0.17	–	–	97	[128]
TMC	7:1	4 ^[b]	50	1	100 ^[d]	100 ^[d]	100 ^[d]	[131]
TBD	3:1	1	25	0.033	100	100	>95	[132]
Metal-based								
Zn(OAc) ₂	5.3:1	1.4	65	15	90 ^[e]	72	65	[134]
FeCl ₃	5:1	1	130	4	96	91	87	[135]
KF	23.1:1	1	180 ^[c]	0.17	–	–	98	[136]
Sn(Oct) ₂	15.4:1	0.05	180 ^[c]	0.017	–	–	33	[137]
bismuth subsalicylate	67.5:1	0.1	180 ^[c]	0.017	–	–	23	[138]
Zn(OAc) ₂	67.5:1	0.1	180 ^[c]	0.017	–	–	75	[139]
Hf(IV)-salalen (R=Me)	25.5:1	1	25	24	>99 ^[f]	75	75	[143]
(NHC)-ZnEt(Cl) pre-catalyst	0.5:1	0.5	25	24	89 ^[f]	31	28	[144]
Zn ^{II} (ON) ₂ (R=Cl, H)	7:1	8 ^[b]	80	8	100 ^[d]	100 ^[d]	100 ^[d]	[146]
Zn ^{II} (ONN) ₂ st	7:1	8 ^[b]	50	3	85 ^[d]	45 ^[d]	38 ^[d]	[149]
Zn ^{II} (ONN) ₂ st (R=N(H)Me)	7:1	4 ^[b]	50	0.5	100 ^[d]	81 ^[d]	81 ^[d]	[151]
Zn ^{II} (ONN) ₂ st (R=NMe ₂)	7:1	4 ^[b]	50	1	100 ^[d]	84 ^[d]	84 ^[d]	[151]
Zn ^{II} (ONN) ₂ st (R=H)	7:1	4 ^[b]	50	3	29 ^[d]	17 ^[d]	5 ^[d]	[151]
Zn(HMDS) ₂	24.7:1	1	25	2	100	99	99	[154]

[a] S_{Me-LA} and Y_{Me-LA} refer to selectivity and yield of Me-LA, respectively. Yields determined by ¹H NMR analysis unless otherwise stated. [b] Catalyst loading reported as wt%. [c] Microwave irradiation, power: 850 W. [d] Values determined by ¹H NMR (CDCl₃) analysis following solvent removal in vacuo. [e] Depolymerisation by mass of PLA recovered. Initial waste stream contained 1:1 mixture of [PLA]/[PET]. [f] Depolymerisation based on ΔM_n [determined by gel permeation chromatography (GPC) in THF] before and after degradation.

(hydrolysis) or ester group (transesterification). Adjusting the reducing agent employed enables a diverse range of value-added chemicals to be accessed directly from plastic waste.

Hydrogenation processes have been reported for the production of alcohols and alkanes (Figure 8). Krall et al.^[156] reported the use of a ruthenium(II)-PNN pincer complex for the hydrogenation of various polyesters and polycarbonates. The active species is generated in situ by abstraction of the Cl ligand using KO^tBu. Employing a solvent mixture of THF and anisole, a PLA cup was successfully reduced to propylene glycol (PG). The active species is generated in situ by abstraction of the Cl (PG), achieving quantitative yield within 24 h at 160 °C and 54 bar (H₂). Recently, Klankermayer and co-workers^[157] investigated the use of a Ru^{II}-triphos complex for the recycling of polyesters and polycarbonates. Quantitative PG yield was achieved within 16 h at 140 °C and 100 bar (H₂), employing either 1,4-dioxane or PG as the reaction solvent, with bis(trifluoromethane)sulfonimide (HNTf₂) as a co-catalyst. Selective degradation of PLA in the presence of PET was demonstrated and scaled up to 11.4 g. Subsequently, Enthaler and co-workers^[158] have applied a commercially available Ru-MACHO-BH complex to this process. This system was found to be tolerant to the presence of dyes and additives, observing PLA reduction to PG under significantly milder conditions with shorter reaction times (120–140 °C, 30–45 bar, <6 h). Mixed waste streams were also considered with a PLA and poly(propylene) mixture affording PG and MeOH. Shuklov et al.^[159] have exploited the use of a barium-promoted copper chromite (Cu/Cr/Ba) heterogeneous catalyst at 150 bar (H₂) for the reduction of PLA and lactide to PG. This process is characterised by a tandem reaction whereby Me-LA is initially formed by methanolysis, which is subsequently reduced to PG via hydrogenation. A modest PG yield (50%) was observed at 100 °C within 15 h, achieving 90% *ee*. Reaction temperatures up to 150 °C were pursued, resulting in increased yield at the expense of severe product racemisation. The use of a high catalyst loading (133 wt%) is circumvented by facile recovery by centrifugation, a limiting feature of the homoge-

neous ruthenium-based systems. Catalyst recyclability was demonstrated for lactide transformations. In principle, these processes make use of a waste feedstock to access green PG, which is traditionally produced from the petroleum-based hydrogen peroxide propylene oxide (HPPO) process at a scale of approximately 1 million tonnes per year.^[159] Simple 1,2-diols, such as PG, are high-value speciality chemical intermediates used in a diverse range of applications, including the manufacture of biodegradable polyester fibres, unsaturated polyester resins and pharmaceuticals, to name but a few.^[160]

Hydrosilylation strategies are also a possible route to higher-value chemicals such as silyl ethers (Figure 8). Feghali and Cantat^[161] reported the first example of a metal-free hydrosilylation process for a wide range of polyethers, polyesters and polycarbonates under ambient conditions, catalysed by B(C₆F₅)₃. For PLA, the use of an air-stable and inexpensive hydrosilane, namely 1,1,3,3-tetramethyldisiloxane (TMDS), yielded propane in excellent yield (>99%, 1 h) in CH₂Cl₂. Alternatively, substitution of TMDS for triethylsilane (Et₃SiH) afforded silylated propylene glycol (Si-PG), achieving 65% yield within 16 h. Besides low energy intensity, a particular advantage of this recycling system is its tolerance to additives and mixed plastic waste. The same group has subsequently investigated the use of Brookhart's iridium(III) catalyst for PLA degradation, among other polymers.^[162] Using Et₃SiH, a mixture of Si-PG and propanol were formed at 65 °C in chlorobenzene after 60 h. Silylated propanol (*n*PrO-Si) was selectively formed at 90 °C in the presence of excess silane. PLA (3D printing material) was degraded despite the presence of additives, demonstrating high catalyst tolerance. As observed for B(C₆F₅)₃, the use of TMDS afforded propane, although prolonged reaction times and higher temperatures were required (12 h, 110 °C), yielding a valuable silicon polymer as a by-product, namely polydimethylsilyloxane (PDMS).

Whilst such methods demonstrate the versatile products accessible from plastic waste, the use of scarce and expensive rare-earth metals, in combination with often complex ligands, is

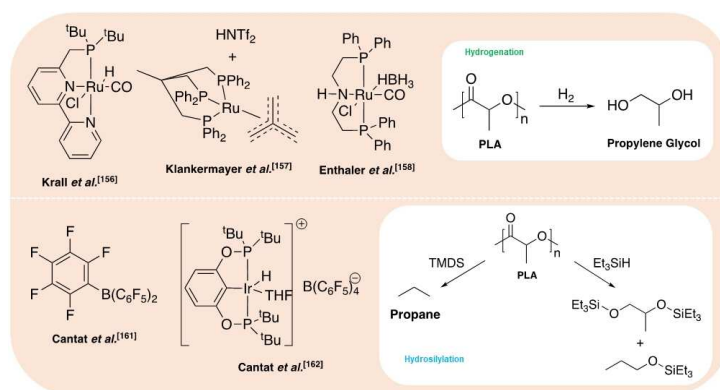


Figure 8. Selected metal-based and organocatalysts reported for the hydrogenation (top) and hydrosilylation (bottom) of PLA.

clearly undesirable. Moreover, such processes typically rely on harsh reaction conditions/toxic reagents, providing significant scope for optimisation. To this end, Nunes et al.^[163] recently reported a cheap, reusable and environmentally benign dioxomolybdenum complex $\{\text{MoO}_2\text{Cl}_2(\text{H}_2\text{O})_2\}$ for the reductive depolymerisation of PLA into propane using various silanes on a gram scale. This method further demonstrates the potential to access products traditionally derived from depleting fossil fuel resources, whilst simultaneously making use of polymethylhydroxysilane (PMHS), a by-product of the silicone industry. PLA from various end-of-life sources (cup and 3D printing material) were degraded, requiring prolonged reaction (20–40 h) at 110 °C in toluene, whilst PG was implicated as a potential reaction intermediate. A summary of the systems discussed in the preceding section is provided in Table 2.

3.5. Other products

In the absence of exogeneous reagents, thermal degradation methods have been widely reported for the chemical recycling of PLA. High reaction temperatures are required, often affording lactide amongst other products, owing to competing side reactions and potential racemisation/epimerisation. We direct the interested reader to an excellent Review by McKeown and Jones^[89] that provides a succinct overview of the thermal degradation mechanisms discussed herein. Pioneering work by McNeill and Leiper investigated the thermal degradation of PLA between 250–450 °C under programmed heating conditions (10 °C min⁻¹).^[164] PLA degradation was found to proceed in one step and product distribution was temperature dependent, confirmed by isothermal studies.^[165] CO₂ was observed as the major product, with lactide and cyclic oligomers also present. Acetaldehyde formation via *cis*-elimination was observed at 230 °C with higher temperatures favouring the formation of CO₂. Short chain alkenes such as ethylene, propylene and methyl ketene were also observed at higher temperatures. Thermal degradation proceeded via a back-biting mechanism, confirmed by acetylation of the chain ends enhancing polymer

thermal stability by approximately 30 °C. Subsequent work in the field has investigated the addition of simple metal salts on thermal degradation characteristics, with a particular focus on polymer processability at end-of-life.^[166–177] Industrially, PLA production relies on a Sn(Oct)₂ catalyst and thus residual Sn^{II} species in the final polymer are common. Trace metal residues often adversely impact polymer thermal stability, reducing the onset degradation temperature. Nishida et al.^[167,176] have previously shown the selective formation of L-LA from PLLA via an intramolecular unzipping mechanism mediated by tin, contrasting random intermolecular transesterification. Sn^{II} carboxylate end groups were found to drastically reduce the activation energy (from 175 to 85 kJ mol⁻¹, depending on tin concentration), enabling onset weight loss as low as 150 °C. Poorer depolymerisation control was noted in the absence of Sn^{II}, favouring the formation of oligomers and *meso*-LA. Calcium and magnesium oxides have also been shown to operate via an unzipping mechanism, observing a comparable activation energy trend relative to tin.^[171,173,175] Product racemisation was found to be both temperature and metal dependent. CaO was found to selectively form L-LA at high temperatures (< 300 °C); however, extensive *meso*-LA formation was noted below 250 °C. Conversely, racemisation with MgO was less prevalent and high selectivity towards L-LA was retained below 270 °C. Trace residual organocatalyst (DBU) and Zn^{II}, Fe^{III} and Al^{III} cations have also been explored for PLA pyrolysis.^[169,177,178]

Pyrolysis potentially represents a route of least resistance to tackling plastic waste due to existing industrial precedent. However, such processes are energy intensive and offer limited value return for PLA, often returning the cyclic monomer, lactide. Beyond pyrolysis, Enthaler and co-workers^[139,179] have demonstrated lactide recapture is possible via microwave irradiation in the presence of zinc-based salts, achieving TOFs up to approximately 260 h⁻¹ between 200–210 °C. However, where possible, it is imperative to pursue upcycling for emerging products to promote market penetration through economic incentives to industry. Recent work by Slater et al.^[180] reported the synthesis of high-value lactate-containing metal-organic frameworks (MOFs) from waste PLA, further highlight-

Table 2. Summary of selected metal-based and organocatalysts reported for the hydrogenation and hydrosilylation of PLA.

Catalyst	Cat. [mol %]	Solvent	T [°C]	H ₂ [bar]	t [h]	PLA conv. [%]	Product(s)	Yield ^[a] [%]	Ref.
Hydrogenation									
Ruthenium(II)-PNN pincer	2 ^[b]	anisole/THF	160	54.4	24	100	PG	> 99	[156]
Ru ^{II} -triphos complex	1 ^[c]	1,4-dioxane or PG	140	100	16	100	PG	> 99	[157]
Ru-MACHO-BH complex	0.5	THF	140	45	3	100	PG	> 99	[158]
(Cu/Cr/Ba) heterogeneous catalyst	133 ^[d]	MeOH	100	150	15	–	PG	50 ^[e]	[159]
Hydrosilylation									
B(C ₆ F ₅) ₃	2	CH ₂ Cl ₂	25	Silane (equiv.)	1	100	propane	> 99 ^[f]	[161]
	5	CH ₂ Cl ₂	25	TMDS (2.0)	16	–	Si-PG	65	[161]
Brookhart's iridium(III) catalyst	0.5	chlorobenzene	65	Et ₃ SiH (3.3)	60	100	Si-PG/nPrO-Si	64:31	[162]
	1	chlorobenzene	90	Et ₃ SiH (3.0)	60	100	nPrO-Si	92	[162]
MoO ₂ Cl ₂ (H ₂ O) ₂	2	toluene	110	Et ₃ SiH (excess)	40	–	propane	95	[163]
	1	toluene	100	PMHS (2.0)	40	–	propane	95	[163]
				PhSiH ₃ (1.5)	20	100	propane	100	[163]

[a] Yields determined by ¹H NMR analysis unless otherwise stated. [b] KOtBu employed as a co-catalyst in a loading ratio of 50:1:2 {[ester repeat unit]/[catalyst precursor]/[KOtBu]}. [c] HNTf₂ employed as a co-catalyst in a loading ratio of 100:1:1 {[ester repeat unit]/[catalyst precursor]/[HNTf₂]}. [d] Catalyst loading reported as wt%. [e] PG yield based on GC. [f] Propane yield based on GC-MS analysis.

ing the potentially vibrant product portfolio attainable from waste PLA. Alkyl lactylactates, the dimeric precursor to lactate esters, have also attracted interest owing to properties akin to their monomer.^[5] Group I,^[119,141] group II^[119–121,141] and Al^[141,181,182] have been reported, although primarily limited to the alcoholysis of lactide, with the exception of work by Sobota and co-workers.^[141] We identify this as an emerging area of opportunity, particularly with regards to translating such catalysts to PLA. Indeed, catalysts that exhibit modest activity are perhaps desirable where controlled and selective partial depolymerisation is required. A tailored approach to catalyst development will undoubtedly provide use to systems that might otherwise be overlooked.

4. Chemical Recycling of Poly(ethylene terephthalate)

4.1. Poly(ethylene terephthalate)

Whilst the development of recycling technologies in tandem with emerging bioplastics is central to the industry's transition, there is also a pressing need to address waste concerns associated with the current product portfolio. Indeed, bio-based plastics accounted for just 1% of all processed plastics in 2019.^[63] PET (Figure 9) is a commercially important polyester, which exhibits high mechanical strength, good barrier properties and high optical clarity.^[42,183] Consequently, PET has been widely exploited in the packaging industry, which consumed 38% of plastics produced globally in 2015, with PET accounting for 22.6% of plastic use in the sector.^[11] PET has also found use in the construction, transport and textiles industry.^[183] Industrially, PET is manufactured via a four-step process. Firstly, bis(2-hydroxyethyl) terephthalate (BHET) is produced from the esterification of ethylene glycol (EG) with terephthalic acid (TA). Transesterification of EG with dimethyl terephthalate (DMT) was widely used up until the 1960s, although slower reaction rates and high corrosivity rendered it obsolete. The second and third stage are characterised by the pre-polymerisation of BHET and subsequent melt condensation to form low- M_n PET (suitable for fibres), respectively. Finally, solid-state polymerisation is used to access PET of high M_n , suitable for drinks bottles.^[42,184] For PET synthesis, antimony-based catalysts, such as Sb_2O_3 and $Sb(OAc)_3$, are generally considered the most effective and thus are routinely used.^[185]

Traditionally, EG and TA are sourced from petroleum-based feedstocks, although the synthesis of bio-based PET is possible. Presently, Bio-PET in circulation is only 30% bio-based (Bio-PET30), corresponding to renewably sourced EG from biomass,

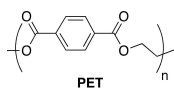


Figure 9. Polymeric structure of PET.

and is currently marketed by several well-known brands such as Coca-Cola and Pepsi.^[42,186,187] Whilst 100% bio-based PET remains a long-term ambition of the industry, technical constraints associated with renewable TA production have limited commercialisation. Promisingly, Bio-PET is compatible with existing processing and recycling equipment, although it remains non-biodegradable. This serves to highlight that bio-based polymers are not inherently biodegradable and that irresponsibly handled PET waste is a major source of plastic pollution.

The mechanical recycling of PET is well established but is limited by eventual material downcycling, with ductility decreasing from 310 to 2.9% after just three cycles. This necessitates recycled PET be repurposed into lower-value products, such as fibres (72%) in carpeting, which can no longer be recycled.^[42,188] Moreover, PET waste streams are easily contaminated by PVC and PLA, rendering the recycled product of low-grade quality, which can no longer be mechanically recycled.^[42] However, the commercial viability of mechanical recycling relies on a high (\geq \$75 per barrel) and stable oil price. Below \$65 per barrel, the economics become challenging, which inhibits recycling efforts as noted in 2015.^[46]

A possible solution to this is chemical recycling. Beyond long-term material value retention, the possibility of accessing higher-value products offers a potential route to decoupling PET recycling from a volatile oil market. Addressing this clear industry appetite is paralleled by the opportunity to enact timely and meaningful action. Relative to PLA, there is an exhaustive body of literature concerning the chemical recycling of PET, and we highlight a number of excellent Reviews.^[44,184,189–193] We do not intend to reproduce such work but instead provide a brief overview of traditional methods with a particular focus on upcycling and recent developments in catalysis.

4.2. Hydrolysis to terephthalic acid

Traditionally, PET hydrolysis requires high-temperature (200–250 °C) and -pressure regimes (1.4–2 MPa) under either acid, basic or neutral conditions to afford TA and EG.^[189] Acid hydrolysis is typically facilitated by concentrated H_2SO_4 (minimum 87 wt%), although other inorganic acids such as HNO_3 and H_3PO_4 have been reported.^[44,189,194,195] A major limitation of this method is the large quantities of inorganic and aqueous waste produced, coupled with high system corrosivity. Alkaline hydrolysis typically relies on a solution of NaOH or KOH of a concentration between 4–20 wt% to afford EG and the corresponding disodium or dipotassium terephthalate salt.^[189,192,196,197] EG can be recovered via distillation, whilst pure TA can be isolated by neutralisation of the reaction mixture with a strong inorganic acid (e.g., H_2SO_4). This method can tolerate highly contaminated post-consumer PET such as metalised PET film.^[189] Neutral hydrolysis involves the use of water or steam in the presence of a transesterification catalyst, typically an alkali metal acetate.^[44,192,198,199] This method remedies concerns associated with equipment corrosion and waste disposal

prevalent in acid and alkali-based methods. However, the process is limited by low TA purity, necessitating further purification at the expense of increased process cost and complexity.^[189] Consequently, hydrolysis is not widely used in industry for the production of food-grade recycled PET. Comparatively, hydrolysis is a slow process due to water being a poor nucleophile. Enzymatic-based processes (PETase) have also been reported. Recently, Tournier et al.^[200] reported the fastest PETase to date, capable of achieving a minimum of 90% conversion to monomers within 10 h, equating to a productivity of 16.7 g L⁻¹ h⁻¹. This represents a remarkable improvement relative to previously reported systems, which exhibited limited productivity, highlighting the rapidly progressing field of biocatalysis as a possibly feasible bioremediation strategy in the future.^[201–204]

4.3. Methanolysis to dimethyl terephthalate

As noted for hydrolysis, PET methanolysis relies on high temperatures (18–280 °C) and pressures (2–4 MPa) to afford DMT and EG, which can be used as raw starting materials for polymer production.^[44,205,206] Zinc acetate is most commonly employed as a transesterification catalyst; however, magnesium acetate, cobalt acetate, lead dioxide and aryl sulfonic acid salts have also been reported.^[189] Recently, McKeown et al.^[131] reported the first example of organocatalysed PET methanolysis using TMC (Figure 6). Promisingly, DMT could be isolated in good yield (72%) at temperatures as low as 100 °C under ambient pressure, although prolonged reaction times (16 h) were required. PET depolymerisation in supercritical methanol has also been reported, generally observing enhanced reaction rates due to higher density and kinetic energy in the supercritical state.^[189,207–210] Due to the propensity of DMT to undergo transesterification, catalyst deactivation is required following reaction termination. Whilst the process is reasonably tolerant to contaminants, water perturbs the process, resulting in catalyst deactivation and the formation of various azeotropes. A limiting feature of this process is the resulting complex product feed, comprising glycols, alcohols and phthalate derivatives, which renders DMT separation both costly and time consuming.^[44,189] Presently, the cost of methanolysis-derived DMT is approximately double that of virgin DMT, and thus is unable to compete with cheap petroleum feedstocks. Moreover, market penetration is limited by manufacturers favouring TA as a feedstock for PET production due to greater process performance. Whilst DMT can be hydrolysed to TA, this incurs considerable additional cost to the process. Consequently, the use of methanolysis-derived DMT as a feedstock in the future relies on technological innovation and a high oil price, or indeed a shift from petroleum entirely.

4.4. Ammonolysis to terephthalamide

PET ammonolysis typically employs liquor ammonia between 70–180 °C under pressure (2 MPa) in either the presence or

absence of catalyst, typically zinc acetate.^[189,211] The main degradation products are 1,4-benzene dicarboxamide, otherwise known as terephthalamide (TPA), and EG. TPA serves as an intermediate to terephthalonitrile, which can be subsequently reduced via hydrogenation into either *p*-xylenediamine or 1,4-bis(aminomethyl)cyclohexane. Low-pressure ammonolysis is also possible using ammonia in an EG environment, catalysed by zinc acetate (0.05 wt%). TPA was recovered in 87% yield at 70 °C using a PET/NH₃ ratio of 1:6.^[189] Whilst not directly amenable to polymer reprocessing, TPA and its derivatives represent potentially useful building blocks for the production of both saturated and unsaturated terephthalamides, which are discussed in further detail herein. Unsurprisingly, PET ammonolysis has received little interest in the literature, likely due to limited substrate scope and commercial interest.

4.5. Aminolysis to diamines of terephthalic acid

Presently, there are no known examples of PET aminolysis use at a commercial scale. However, partial aminolysis is exploited for enhancing PET properties (e.g., fibre colouration) in the manufacture of fibres with defined processing properties.^[189,191] Aminolytic chain cleavage of PET affords diamines of TA and EG and is thermodynamically more favourable than alcoholysis owing to enhanced nucleophilicity. Consequently, aminolysis is typically conducted under milder reaction conditions (20–100 °C) in both the presence or absence of catalyst. Commonly used aqueous solutions of primary amine include methylamine, ethylamine, ethanolamine and anhydrous *n*-butylamine.^[44,189]

Fukushima et al.^[212] have reported the organocatalysed aminolysis of PET waste mediated by TBD, employing a diverse range of aliphatic, allylic and aromatic amines. Typical reaction conditions afforded 63–89% yield within 1–2 h at 110–120 °C. The resulting crystalline terephthalamides exhibited attractive thermal (m.p. up to 301 °C) and mechanical properties with potential uses as additives, modifiers and building blocks for high-performance materials. The origin of these desirable properties was attributed to amide hydrogen bonding and structural rigidity of the monomer. Further computational study concluded the bifunctionality of TBD plays a crucial role in aminolysis, in particular activation of the carbonyl, differentiating TBD from other organic bases such as DBU. Such behaviour had previously been discussed for PLA degradation mediated by TBD (Figure 6). Deep eutectic solvents (DES) have also been reported as highly efficient organocatalysts for PET aminolysis. Musale and Shukla^[213] employed choline chloride·2 ZnCl₂ (5 wt%) in the production of *N*¹,*N*¹,*N*⁴,*N*⁴-tetrakis-(2-hydroxyethyl)-terephthalamide (THETA) and TA, and bis(2-hydroxyethylene) terephthalamide (BHETA), achieving 82, 83 and 95% yield within 30 min under reflux (PET/amine = 1:6).

Metal-mediated examples of PET aminolysis include sodium acetate, potassium sulfate and dibutyl tin oxide for the production of BHETA using excess ethanolamine (EA).^[214–216] BHETA has possible uses as an environmentally benign corrosion inhibitor for the protection of steel structures. This is highly desirable as powerful corrosion inhibitors tend to be

toxic and carcinogenic.^[216] Microwave-assisted methods for PET aminolysis have also been reported. Cheap and non-toxic simple metal salts, such as sodium acetate, sodium bicarbonate and sodium/potassium sulfate are frequently used, achieving excellent product yield (> 85%) within minutes.^[217–219] Heterogeneous and recyclable β -zeolite acid catalyst and montmorillonite KSF clay catalyst have also been reported, affording BHETA in good yield (85–88%).^[220] Here, the resulting product was found to undergo a cyclisation reaction under reflux mediated by polyphosphoric acid to produce 2,2'-(1,4-phenylene)-bis(2-oxazoline) (PBO), a possible chain extender/coupling agent or cross-linker.

An excellent Review by George and Kurian^[44] highlights the possible applications of PET aminolysed products, which include antibacterial drugs,^[221] adhesion promoters^[222] and polyol components for rigid polyurethane foams.^[223] Despite the diverse chemistry and breadth of applications of aminolysis-derived products, the area remains vastly underexplored. Additionally, to the best of our knowledge, there are no known examples of homogeneous PET aminolysis mediated by discrete metal-based complexes. Thus, there is clear scope for further catalyst optimisation. Surprisingly, no examples of PET thiolysis or phosphorolysis have been reported to date. We identify these as potential avenues for accessing vibrant and diverse products of untapped potential. The impact of mixed plastic waste on the activity and recyclability of these catalysts remains unaddressed.

4.6. Glycolysis to bis(2-hydroxyethyl) terephthalate

PET glycolysis is a well-established commercial process operated by a number of leading global companies such as DuPont, Shell and Eastman Kodak.^[44] Indeed, the first patents detailing PET glycolysis were filed over 50 years ago, rendering it the oldest recycling method for PET.^[224–227] Consequently, glycolysis is the most widely used chemical recycling method for PET, characterised by cleavage of the ester bond via insertion of a glycol, most commonly EG, to produce BHET.^[44] Higher-chain alcohols such as PG and 1,4-butanediol (BD) have also been reported.^[228,229] Typically, high temperatures (180–240 °C) and prolonged reaction times (0.5–8 h) in the presence of a transesterification catalyst, often a metal acetate, are required to achieve appreciable conversion. Whilst numerous metal acetate catalysts have been reported in the literature, zinc acetate is considered the benchmark.^[42,44,189] Additionally, a large excess of EG (EG/PET \geq 5:1) is used to mediate the formation of higher chain oligomers, thus favouring the formation of BHET.^[42] The method lends itself to the recovery of post-industrial PET waste where the incoming feed is of known origin and high quality.^[44]

Organocatalysts have been widely reported as efficient catalysts for PET glycolysis. Wang et al.^[230] employed urea (10 wt%) as a cheap and reusable catalyst, achieving 100% PET depolymerisation and approximately 80% BHET yield under optimal reaction conditions [3 h, 180 °C, $m(\text{PET})/m(\text{EG}) = 1:4$]. DFT and complementary experimental study revealed hydrogen bond formation between EG and urea playing a crucial role in

the enhanced reaction rate. In 2011, Fukushima et al.^[231] explored the use of a commercially available guanidine for PET glycolysis, namely TBD (1.0 mol%). After 3.5 h at 190 °C, BHET was isolated in 78% yield following recrystallisation to remove residual impurities (e.g., oligomers and additives). The observed activity was comparable to that reported for commonly used metal acetates/alkoxide catalysts. The excess of unreacted EG and TBD catalyst could be recycled more than 5 times. Further computational study confirmed TBD and EG activate PET through hydrogen bond formation, consistent with previous studies.^[132,212,230] Prior work in this group reported a highly efficient N-heterocyclic (NHC) carbene catalyst derived from a commercially available imidazolium IL.^[232] NHC catalysis enabled PET glycolysis to be conducted under reflux in anhydrous tetrahydrofuran to afford BHET, noting significantly milder reaction conditions and a shortened reaction time of 1 h. The commercial potential of NHC catalysis for PET depolymerisation is reflected in a patent filed in 2006.^[233] Indeed, nucleophilic NHCs have previously been exploited for the production of PET via the transesterification of DMT with EG.^[234] Beyond TBD and NHCs, a comprehensive study by Fukushima et al.^[235] investigated other nitrogen-containing bases for PET glycolysis, including DMAP, DBU and 1,5-diazabicyclo[4.3.0]non-5-ene (DBN) to name but a few. Recently, TBD and DBU have been explored as catalysts for transesterification and amidation reactions using EG, EA and ethylenediamine, employing methylbenzoate as a model system for PET.^[236] Whilst traditional organocatalysts generally exhibit high activity for PET glycolysis, they remain limited by activity loss incurred over repeated use due to oxodegradative reactions or competing side reactions.^[22] The most recent advancements in this area concerns the development of amidine and guanidine-type eutectic salts, which exhibit superior stability and efficiency.^[235,237] Jehanno et al.^[237] reported the first example of an industrially relevant organocatalyst, namely a TBD/methanesulfonic acid complex (TBD/MSA, 1:1). This protic ionic salt combined the high catalytic activity of the free base with superb thermal stability (> 400 °C), achieving 91% BHET yield within 2 h at 180 °C. Moreover, the catalyst could be recycled at least 5 times.

Unsurprisingly, ILs have also seen extensive use as catalysts for PET glycolysis.^[230,238–243] Beyond benefits noted for PLA, the reaction products are easily separated from the IL by addition of water followed by filtration, enabling facile catalyst recovery and reuse. This is a limiting feature of glycolysis catalysed by traditional compounds such as metal acetates. Wang et al.^[238] investigated the use of acidic, basic and neutral ILs in the glycolysis of waste PET using EG. Acidic ILs exhibited poor stability above 180 °C, whilst basic ILs were limited by a complex and high production cost. Neutral ILs were preferred based on cost and performance. [Bmim][Cl] was selected as the ideal catalyst due to its high stability, despite exhibiting inferior performance to [Bmim][Br], which achieved 99% PET depolymerisation within 8 h at 180 °C.^[239] No reaction occurred between PET and the IL, and depolymerisation proceeded to be first-order using [Bmim][Cl] ($E_a = 232.79 \text{ kJ mol}^{-1}$). Yue et al.^[240] further explored basic ILs as degradation catalysts, identifying [Bmim][OH] as the outstanding candidate. Under the optimal

conditions, 71% BHET yield was obtained within 2 h at 190 °C, although a relatively high catalyst loading (5 wt%) is noted. Recently, ILs embedded with first-row transition metals (e.g., Fe, Co and Zn) have been reported.^[241,242] Generally, enhanced activity is observed relative to traditional ILs, attributed to the presence of a Lewis acidic metal centre facilitating enhanced nucleophilic attack. For example, Wang et al.^[241] noted [Bmim]₂[CoCl₄] achieved 81% BHET yield within 1.5 h at 175 °C and could be recycled up to 6 times. Enhanced thermal stability was also noted, promoting industrial relevance. A common drawback of ILs is their high cost. However, Sun et al.^[243] recently reported a low cost (\$1.2 kg⁻¹) and biocompatible IL, cholinium phosphate ([Ch]₃[PO₄]) for the glycolytic degradation of PET. Under metal-free conditions, 61% BHET yield was achieved within 4 h at 180 °C. A low catalyst cost is paramount if ILs are to be considered industrially viable in the future given the high catalyst loadings commonly reported (20–25 wt%).^[238,239,241–243] Recent work has focused on DESs as a cheaper, less toxic and often biodegradable alternative to ILs.^[244,245] Recently, Wang et al.^[244] reported the use of 4(urea)·(ZnCl₂) (5 wt%) for PET glycolysis, obtaining 83% BHET yield within 30 min at 170 °C. This reaction time is equivalent to that taken by a supercritical method under 15.3 MPa at 450 °C, highlighting the importance of catalysis to optimising process efficiency.^[246] Zhou et al.^[245] further extended the scope of DESs for the production of dioctyl terephthalate (DOTP), a green and non-toxic plasticizer, from PET waste using 2-ethyl-1-hexanol. A summary of the organocatalysts discussed for PET glycolysis is provided in Figure 10.

PET glycolysis mediated by metal-based catalysts has also been reported. Pingale et al.^[247] investigated the use of various metal chlorides (e.g., Zn, Li, Mg and Fe) for the catalytic degradation of waste PET bottle. Zinc chloride (0.5 wt%) was found to be most active, achieving 73% BHET yield within 8 h under reflux (197 °C, *n*(PET)/*n*(EG) = 1:10). A reactivity series of Zn > Pr/Nd > Mg > Li > Fe was proposed, although the optimal PET/EG molar ratio varied with metal type. Whilst such salts are cheap and readily available, they remain limited by slow reaction rates, harsh reaction conditions and difficulties asso-

ciated with catalyst recovery. Consequently, subsequent research has sought to address such concerns. Pingale and Shukla^[248] explored the use of environmentally friendly catalysts such as sodium carbonate and sodium bicarbonate. The latter afforded 65% BHET yield, competitive with zinc acetate. More importantly, microwave-assisted depolymerisation (800 W) enabled the reaction time to be reduced from 8 h to 35 min relative to conventional electric heating under identical conditions (5 wt% catalyst, PET/EG = 1:6). In a subsequent study, Lopez-Fonseca et al.^[249] [JP1] extensively investigated the use of simple and eco-friendly metal salts, such as sodium and potassium sulfate, for PET glycolysis at a reasonably large scale (30 g). Comparably high BHET yield (≈70%) was obtained within 1 h at 196 °C using zinc acetate and sodium carbonate (1 mol%) in the presence of a large excess of EG. Zhu et al.^[250] have previously reported a series of recyclable solid acid catalysts including sulfated oxides of zinc (SO₄²⁻/ZnO), titanium (SO₄²⁻/TiO₂) and their binary oxide (SO₄²⁻/ZnO-TiO₂). SO₄²⁻/ZnO-TiO₂-200–300 °C (note 200–300 °C refers to calcination temperature range) exhibited the highest catalytic activity with a PET conversion and BHET selectivity of 100 and 72%, respectively, after 3 h at 180 °C under atmospheric pressure. Catalytic activity was attributed to a high surface area and predominance of Lewis acid sites. Whilst the catalyst could be reused up to four times, potential pollution concerns coupled with their corrosive nature limits scalability. Porous structures such as zeolites (e.g., β-zeolite and γ-zeolite) have been investigated as environmentally friendly alternatives that retain a high surface area for PET glycolysis.^[251]

Recently, nanoparticles have received increasing attention as heterogeneous transesterification catalysts for PET glycolysis owing to their facile preparation, high surface area and recyclability. Bartolome et al.^[252] reported the use of superparamagnetic γ-Fe₂O₃ nanoparticles (average size: 10.5 ± 1.4 nm, surface area: 147 m²g⁻¹) for PET glycolysis. The reaction proceeded at 300 °C and 1.1 MPa, achieving >90% BHET yield within 1 h using an exceptionally low catalyst loading (0.05 wt%).

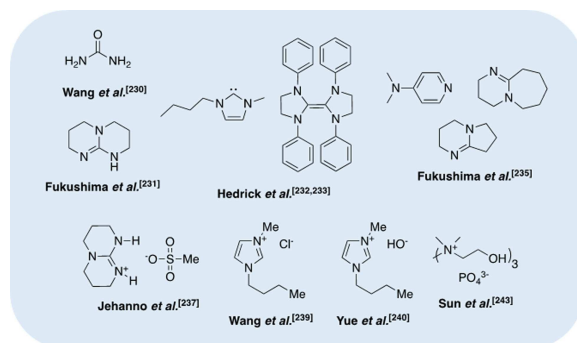


Figure 10. Selected organocatalysts reported for PET glycolysis.

High catalytic activity was attributed to the γ -Fe₂O₃ nanoparticles ability to facilitate glycolysis via redox reactions, high area surface promoting more active sites, thermal stability and good crystallinity. Promisingly, the γ -Fe₂O₃ nanoparticles could be easily separated by magnetic decantation post reaction and were reused 10 times. Metal-oxide doped silica nanoparticles (Mn₂O₄/SNPs) have also been investigated as recoverable transesterification catalysts for PET degradation.^[253,254] Metal oxides of zinc, manganese and cerium were deposited on silica nanospheres of various diameters (60–750 nm) using ultrasonic irradiation. Manganese oxide-doped silica nanoparticles (1 wt%) afforded the highest BHET yield (> 90%), observing equilibration within 80 min at 300 °C and 1.1 MPa. Smaller nanosphere supports promoted superior catalyst distribution, likely due to a higher surface area/volume ratio, resulting in enhanced activity. Imran et al.^[255] have reported mesoporous mixed-metal oxide spinels of manganese, cobalt and zinc as novel catalysts for PET glycolysis. ZnMn₂O₄ was found to be most active, yielding 92% BHET within 60 min at 260 °C and 5 atm. It was found that the cation pair, positioning within the crystal structure and spinel geometry influenced catalytic efficiency. Despite ease of catalyst recovery and reuse, such systems remain limited by their high energy intensity (260–300 °C, 1–5 atm). Recent developments include the utilisation of Fe₃O₄-boosted multiwalled carbon nanotubes (MWCNT) and ultrasmall cobalt nanoparticles for PET glycolysis under milder reaction conditions.^[256,257] Indeed, for the former, 100% BHET yield was obtained within 2 h at 190 °C, whilst the catalyst could be reused in at least 8 sequential runs.^[256] Promisingly, the latter reported a water-free BHET precipitation method that enabled direct reuse of the remaining EG solution, thus simplifying product separation.^[257]

Despite the extensive metal-based systems previously discussed, examples of PET glycolysis mediated by discrete metal-based complexes remain rare (Figure 11). Most notably, Troev et al.^[258] reported a Ti^{IV}-phosphate catalyst (0.3 wt%) for the glycolysis of PET fibres, achieving 98% conversion to BHET within 150 min between 190–200 °C, outperforming Zn(OAc)₂ (PET/EG = 1:3). No noticeable change in depolymerisation activity relative to Zn(OAc)₂ was observed upon shifting to bottle-grade PET, although greater optical clarity in isolated BHET was noted. The design premise of this catalyst was to combine the high activity of traditional titanium alkoxides with a thermal stabiliser (e.g., trialkyl phosphate) to circumvent undesirable yellowing in the product arising from competing side degradation reaction. Indeed, simple titanium alkoxides [e.g., titanium-butoxide (TBT)] have been reported as highly

active catalysts for PET degradation.^[259–261] Consequently, this work represents an excellent example of addressing industry challenges through judicious catalyst design. Wang et al.^[262] reported sodium titanium tris(glycolate) [Ti(OCH₂CH₂O)₃Na₂] as a catalyst for PET recycling via glycolysis. This catalyst offered significantly higher activity than sodium carbonate or tetrabutyl titanate, ascertaining 85% BHET yield within 3 h at 190 °C (1 mol% catalyst loading, PET/EG = 1:12). Ti(OCH₂CH₂O)₃Na₂ was found to be more tolerant to lower catalyst loadings relative to zinc acetate, although it was generally outperformed. Promisingly, Ti(OCH₂CH₂O)₃Na₂ could also be used to repolymerise BHET to form recycled PET (rPET), culminating in a completely circular recycling strategy. Recently, Esquer and García^[263] reported the use of commercially available phosphine ligands [e.g., 1,2-bis(dicyclohexylphosphino)ethane (dcype) and 1,2-bis(diphenylphosphino)ethane (dppf)] in combination with cheap and air-stable metal pre-catalysts, for example CoCl₂. Typical reaction conditions used 1.5 mol% catalyst and a large excess of EG, obtaining poor to good BHET yield (10–75%) within 3 h at 190 °C. Monodentate ligands typically afforded lower BHET yields relative to bidentate ligands, which varied with the metal precursor, with Co-based systems generally appearing more active. Whilst this system is limited by poorer activity relative to previous systems, the use of air stable reagents is desirable. Polymer scope was expanded to polyurethane for the production of polyols. In all instances, no attempt to recover the homogeneous catalyst were made. Thus, challenges associated with catalyst recovery and colour in the final product remain. Whilst heterogenization is a possible solution, such catalysts do not often maintain high BHET selectivity and typically require higher temperatures than other catalysts discussed.

Example applications of PET glycolized products include the production of unsaturated polyester resins,^[228,264,265] polyurethanes,^[266,267] epoxy resins,^[268] vinyl esters,^[269] polymer concretes,^[270–272] textile dyes^[273] and plasticizers.^[245,274] Recently, Beckham and co-workers reported an excellent example of waste PET upcycling.^[261] More specifically, reclaimed PET was upcycled into higher-value reinforced plastics (FRPs), namely an unsaturated polyester and vinyl ester. The upcycled FRPs have a market price of \$2.60/lb relative to \$0.51 and \$0.31/lb for clear and green-coloured PET flakes, respectively. Additionally, the upcycled FRPs have the potential to realise a 57% total supply chain energy saving and a reduction in GHG emissions by 40% over standard petroleum-derived FRPs. It is therefore clear PET glycolysis represents a tangible route to accessing a diverse

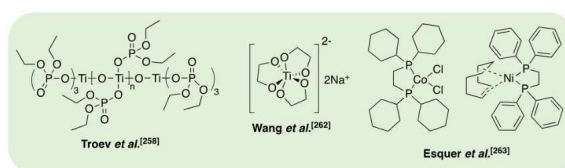


Figure 11. Selected examples of discrete metal-based catalysts reported for PET glycolysis.

range of value-added products. Moreover, catalysis will undoubtedly underpin the commercial viability of such processes in the future. Whilst we have treated the assessment of organo- and metal-based catalysts in isolation, this is not to say their future application cannot be complementary. Indeed, Dove and co-workers recently exploited cooperativity between Lewis acid (metal salts) and organic bases for the enhanced glycolysis of PET.^[275] Whilst we have aimed to detail major developments in catalytic systems thus far, we acknowledge certain omissions may be of potential use to the scientific community. As such, we direct the interested reader to a thorough Review by Kosloski-Oh et al.^[276] that includes catalytic examples of those omitted, for example polyoxometalates and MOFs. A detailed account of supercritical and microwave-assisted methods for PET glycolysis is provided by George and Kurian.^[44] A summary of catalysts reported for PET glycolysis is provided in Table 3 in addition to an overview of the chemical recycling methods discussed (Figure 12).

4.7. Reductive depolymerisation

Metal-based catalysts exploited in the reductive depolymerisation of PLA (Figure 8) have also been applied to PET. Krall

et al.^[156] reported the first example of PET hydrogenation mediated by a ruthenium(II)-PNN pincer complex. Using conditions identical to those discussed for PLA [THF/anisole, 54 bar (H₂) at 160 °C], bottle-grade PET was successfully reduced to 1,4-benzenedimethanol (> 99%) and EG within 24 h. The use of a used water bottle suggests the catalyst is robust to impurities and additives, although the system remains limited by its high energy intensity. Substitution of the pyridine arm for an amine resulted in a loss in catalytic activity, implicating this substituent as an active component in the degradation mechanism. Clarke and co-workers have previously screened a series of ruthenium(II)-catalysts bearing tridentate aminophosphine ligands for the hydrogenation of diester model compounds.^[277] Product selectivity was found to be dependent on ligand structure, identifying an ethylenediamine variant of a Ru^{II}-sulfoxide complex as the outstanding candidate (Figure 13). Using a solvent mixture of THF and anisole, 73% conversion to 1,4-benzenedimethanol was achieved within 48 h under optimal conditions [2 mol% cat, BuOK/cat = 20:1, 50 bar (H₂)]. Recently, Klankermayer and co-workers^[157] reported the use of two ruthenium(II)-complexes bearing tridentate phosphine ligands (triphos and triphos-xyl) for the hydrogenation of PET in the presence of a co-catalyst; HNTf₂ (1 mol%) (Figure 13). Substitution of the phenyl groups with xyl (3,5-dimethylphenyl)

Table 3. Summary of selected metal-based and organocatalysts reported for PLA glycolysis.

Catalyst	EG/ester unit (w/w)	Cat. [wt %]	T [°C]	t [h]	PET conv. [%]	Y _{BHET} ^[a] [%]	Ref.
Organocatalysts							
Urea	4:1	10	180	3	100	80	[230]
TBD	5.2:1	0.7	190	3.5	100	78	[231]
DMAP	5.2:1	16	190	1.67	100	94 ^[b]	[235]
DBU	5.2:1	13	190	0.11	100	99 ^[b]	[235]
DBN	5.2:1	15	190	0.12	100	99 ^[b]	[235]
TBD/MSA (1:1)	20:1 ^[c]	0.5:1 ^[d]	180	2	100	91	[237]
ILs							
[Bmim][Cl]	4:1	20	180	8	45	–	[238,239]
[Bmim][Br]	4:1	20	180	8	99	–	[238,239]
[Bmim][OH]	10:1	5	190	2	100	71	[240]
[Bmim] ₂ [CoCl ₄]	11.7:1	16.7	175	1.5	100	81	[241]
[Ch ₃] ₃ [PO ₄]	4:1	20	180	4	100	61	[243]
DESSs							
4(urea)·(ZnCl ₂)	4:1	5	170	0.5	100	83	[244]
Metal-based							
ZnCl ₂	10:1 ^[c]	0.5	197	8	–	73	[247]
NaHCO ₃	6:1 ^[c]	5	– ^[e]	0.58	–	65	[248]
Zn(OAc) ₂	7.6:1 ^[c]	1:100 ^[d]	196	1	–	≈ 70	[249]
Na ₂ CO ₃	7.6:1 ^[c]	1:100 ^[d]	196	1	–	≈ 70	[249]
SO ₄ ²⁻ /ZnO-TiO ₂ -200–300 °C	5.6:1	0.3	180	3	100	72	[250]
β-zeolite	6:1	1	196	8	100	66	[251]
γ-zeolite	6:1	1	196	8	100	65	[251]
Ti(IV)-phosphate catalyst	2.8:1 ^[c]	0.3	190–200	2.5	100	98 ^[b]	[258]
Ti(OCH ₂ CH ₂ O) ₂ Na ₂	12:1 ^[c]	1:100 ^[d]	190	3	–	85	[262]
[Co(dcape)]Cl ₂	11.1:1	1.5:100 ^[d]	190	3	–	75	[263]
[Ni(COD)] ₂ /dppe (1:2)	11.1:1	1:100 ^[d]	190	3	100	67	[263]
Nanocatalysts							
γ-Fe ₂ O ₃	3.3:1	0.05	300 ^[f]	1	–	> 90	[252]
Mn ₂ O ₃ /SNPs	11:1 ^[c]	1	300 ^[f]	1.33	–	> 90	[253,254]
ZnMn ₂ O ₄	11.5:1 ^[c]	1	260 ^[g]	1	–	92	[255]
Fe ₃ O ₄ -boosted MWCNT	10:1	5	190	2	100	100	[256]

[a] Y_{BHET} refers to isolated yield of BHET unless otherwise stated. [b] Yield reported as a mass fraction of the products as determined by GPC. [c] Molar ratios are listed. [d] Molar ratio of [catalyst]/[PET]. [e] No temperature reported. Microwave irradiation used, power = 800 W. [f] Reaction performed at approximately 1.1 MPa. [g] Reaction performed at 5 atm.

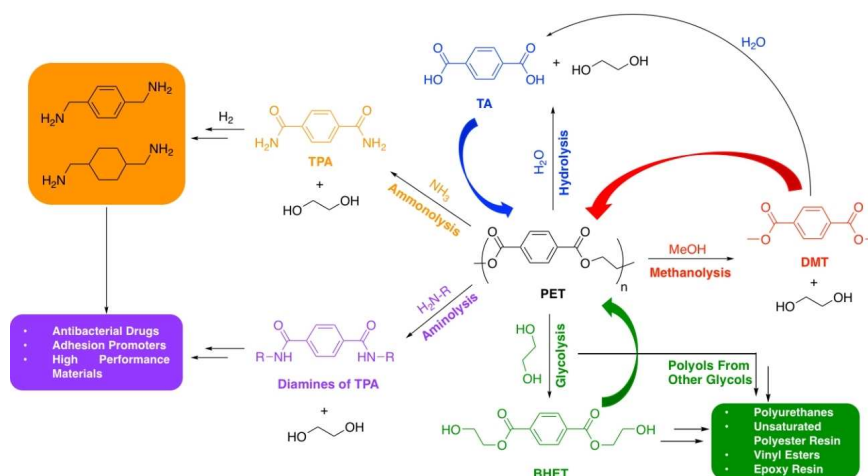


Figure 12. Summary of chemical recycling options for PET with example applications of value-added products. Note: green, red and blue arrows denote recycled products directly amenable to polymer reprocessing.

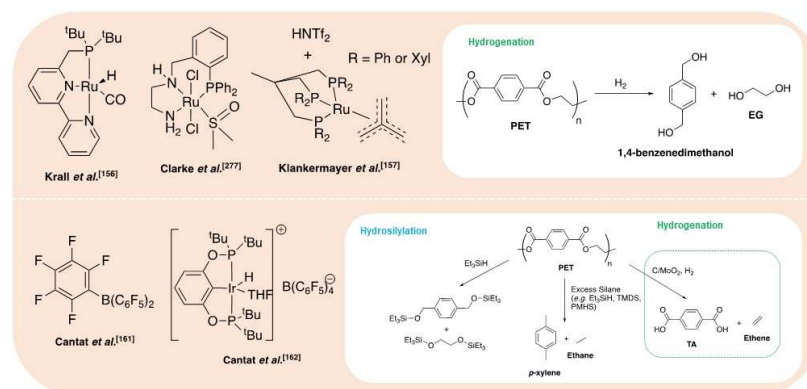


Figure 13. Selected metal-based and organocatalysts reported for the hydrogenation (top) and hydrosilylation (bottom) of PET.

resulted in enhanced PET conversion and selectivity to 1,4-benzenedimethanol. Promisingly, high conversion (>99%) and product selectivity (86–99%) were retained for a variety of commercial PET sources (e.g., bottle, yoghurt pot and sport jersey), demonstrating catalyst robustness. A selective separation method for PET and PLA via catalytic hydrogenation was proposed. Moreover, process scale-up (>10 g) demonstrated the hydrogenation of PET bottle flake could proceed in the presence of a PP bottle cap and PE label. A drawback of this method are the harsh reaction conditions employed [140 °C, 100 bar (H₂)] and prolonged reaction times (16 h), although low catalyst loadings are acknowledged (0.2 mol %).

Hydrosilylation methods have also been reported for PET (Figure 13). In 2015, Feghali and Cantat^[161] reported a two-step catalytic process using B(C₆F₅)₃ (2 mol %) for the production of 1,4-benzenedimethanol, characterised by hydrosilylation followed by hydrolysis. Using Et₃SiH, green PET flakes were converted into two silyl ethers, namely silylated 1,4-benzenedimethanol (85%) and EG (72%), within 3 h at RT. The formation of such silyl ethers is attractive since they can be used as sources of alkoxide groups in Ullman's coupling reactions to prepare ethers.^[278] These disilyl ethers were subsequently hydrolysed to 1,4-benzenedimethanol and EG using 2.1 equiv. of TBAF·3H₂O. 1,4-Benzenedimethanol is a valuable building block for the production of pesticides, perfumes and dyes and is

directly accessible via the aforementioned hydrogenation routes. In the presence of excess silane and at high catalyst loadings, PET could be converted into *p*-xylene and ethane in up to 49% yield under prolonged stirring (16 h). Enhanced *p*-xylene yields of 82 and 75% were realised upon substituting Et₃SiH for TMDS and PMHS, respectively. High catalyst tolerance was demonstrated in the presence of mixed waste feeds, which included PLA and PVC. Moreover, the reaction conditions employed are significantly milder relative to previously reported systems, thus lending itself to industry. However, B(C₆F₅)₃ is limited by a high cost comparable to precious rare earth metals. Subsequent work in this group has utilised Brookhart's iridium (III) catalyst for PET hydrosilylation.^[162] Lower catalyst loadings (1 mol %) are noted relative to B(C₆F₅)₃, albeit at the expense of elevated temperatures (70 °C) and prolonged reaction times (72 h). Moreover, hydrosilylation products of PET were isolated in lower yields (48–63%). Catalyst versatility was demonstrated by application to the hydrosilylation of polycarbonates (PPC and BPA-PC), which typically proceeded more rapidly relative to polyesters at lower catalyst loadings. The use of undesirable toxic halogenated solvents (CH₂Cl₂ and chlorobenzene) is noted in both systems, respectively.^[161,162] The environmental impact of toxic solvent waste is of particular concern upon upscaling. Recently, Nunes et al.^[163] reported a cheap and air-stable dioxomolybdenum complex, MoO₂Cl₂(H₂O)₂. Employing PhSiH₃ as the reducing agent, *p*-xylene could be obtained in 65% yield after 4 days under notably harsher reaction conditions than those previously reported (chlorobenzene, 160 °C). No evidence of 1,4-benzenedimethanol as an intermediate was observed and prolonged reaction (7 days) resulted in complete disappearance of the NMR signal pertaining to EG, suggesting reduction to ethane. High catalyst and silane loadings of 5 and 6 mol %, respectively, were used, although potential economic benefits offset low catalyst activity. Indeed, such work provides scope for future optimisation. Catalyst tolerance was demonstrated using multiple sources of PET (e.g., bottle, sport jersey and pillow filling), maintaining reasonable *p*-xylene yields (62–65%). In 2020, Marks and co-workers reported a carbon-supported single-site molybdenum-dioxo catalyst (C/MoO₂) for

the reduction of PET to TA and EG.^[279] Using a PET + PP system to model a bottle, 87% yields of TA, ethylene and trace acetaldehyde (<5%) were observed within 24 h at 260 °C (1 atm H₂, Ester/Mo = 40:1). Catalyst stability and recyclability was successfully demonstrated, averaging 90% TA yield over 4 consecutive runs (24 h, 260 °C, 1 atm H₂, Ester/Mo = 40:1). A summary of the systems discussed is provided in Table 4.

4.8. Other products

The catalytic pyrolysis of PET remains underexplored as solvolysis methods generally offer superior product selectivity. Typically, high temperature regimes (400–700 °C) are used, notably higher relative to PLA. Moreover, the resulting degradation feeds are often complex mixtures of solids, liquids and gases that require costly and extensive separations. The impregnation of simple metal salts (e.g., CuCl₂) have been shown to dramatically increase the extent of PET cracking.^[280] The use of calcium oxide and calcium hydroxide, among other metal salts, produces benzene-rich oils with a significantly higher benzene content relative to thermal pyrolysis.^[281–284] Indeed, product distribution has been shown to be highly dependent on the metal oxide catalyst employed.^[282] For example, a mixture of Ca(OH)₂ and NiO favoured the formation of synthesis gas (CO + H₂), which is an important building block used in numerous industrial processes, perhaps most notably the Fischer–Tropsch process for hydrocarbon production.^[285] Conversely, a considerable reduction in gaseous products was observed using TiO₂. A notable drawback of this method is the production of sublimate materials such as TA and benzoic acid, which can result in pipe blockages leading to plant downtime. To this end, Masuda et al.^[284] demonstrated FeOOH as a cheap catalyst that yields no sublimate material, highlighting the importance of catalyst design in circumventing by-product production. Recently, El-Sayed and Yuan^[286] provided an excellent account of using waste plastic, including PET, as a source of organic linker in the production of MOFs. Such

Table 4. Summary of selected metal-based and organocatalysts reported for the hydrogenation and hydrosilylation of PET.

Catalyst	Cat. [mol %]	Solvent	T [°C]	H ₂ [bar]	t [h]	PET conv. [%]	Product(s)	Yield ^[a] [%]	Ref.
Hydrogenation									
ruthenium(II)-PNN pincer	2 ^[b]	anisole/THF	160	54.4	24	100	1,4-benzenedimethanol; EG	> 99	[156]
Ru ^{II} -triphos complex (R = xyl)	0.2 ^[c]	1,4-dioxane	140	100	16	100	1,4-benzenedimethanol; EG	> 99	[157]
Ru ^{II} -sulfoxide complex	2 ^[d]	anisole/THF	110	50	48	–	1,4-benzenedimethanol; EG	73	[277]
C/MoO ₂	2.5	–	260	1.0	24	–	TA; EG; trace acetaldehydes	87; 87; < 5	[279]
Hydrosilylation									
B(C ₆ F ₅) ₃	2	CH ₂ Cl ₂	25	Et ₃ SiH (4.3)	3	–	Si-1,4benzenedimethanol; Si-EG	85; 72 ^[e]	[161]
	5	CH ₂ Cl ₂	25	TMDS (6.0)	16	–	<i>p</i> -xylene; ethane	82; – ^[f]	[161]
	7.5	CH ₂ Cl ₂	25	PMHS (11.0)	16	–	<i>p</i> -xylene; ethane	75; – ^[f]	[161]
Brookhart's iridium(III) catalyst	1	chlorobenzene	70	Et ₃ SiH (6.0)	72	–	Si-1,4benzenedimethanol; Si-EG	63; 48 ^[e]	[162]
MoO ₂ Cl ₂ (H ₂ O) ₂	5	chlorobenzene	160	PhSiH ₃ (6.0)	96	–	<i>p</i> -xylene; EG	65	[163]

[a] Product yields refer to ¹H NMR analysis unless otherwise stated. [b] KOtBu employed as a co-catalyst in a loading ratio of 50:1:2 {[ester repeat unit]/[catalyst precursor]/[KOtBu]}. [c] HNTf₂ employed as a co-catalyst in a loading ratio of 500:1:5 {[ester repeat unit]/[catalyst precursor]/[HNTf₂]}. [d] KOtBu employed as a co-catalyst in a loading ratio of 50:1:20 {[ester repeat unit]/[catalyst precursor]/[KOtBu]}. [e] Isolated yield. [f] *p*-Xylene yield obtained by GC-MS analysis. Ethane yield not determinable by ¹H NMR spectroscopy owing to insolubility of PET in CH₂Cl₂.

materials have broad applicability ranging from gas storage and separation through to catalysis and sensing.

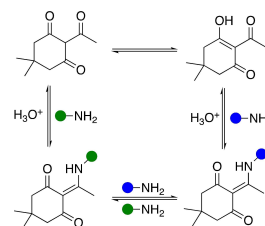
5. Emerging Materials

In the preceding sections we have highlighted chemical recycling strategies for two commercial polyesters, namely PLA and PET. For such materials, the development of future waste management strategies relies on retrospective action to combat plastic pollution. However, as the plastic industry transitions to a low-carbon and circular future, it is imperative recyclability is embedded at the design phase. In this final section, we aim to highlight key contributions and promising developments in this area.

5.1. Covalent adaptable networks

Thermoset materials are widely used in demanding engineering applications owing to their high mechanical strength and elasticity. Such favourable properties are derived from cross-linking via permanent covalent networks, which render the material unsuitable for physical or solution processing. Consequently, material down-cycling via mechanical processing is often the optimal outcome.^[22] A promising solution to PCW thermosets is the use of covalent adaptable networks (CANs). Such dynamic covalent networks are reversible in nature and can be controllably biased in accordance to a stimuli response such as light, heat or pH.^[287–289] Indeed, the dynamic bonds provide exchangeable anchor points within the network to facilitate material remoulding and repair with the potential for self-healing and retention of structural integrity.^[22,290] Numerous CAN systems have been reported to date, which include carbonate,^[291] imine,^[292,293] urea,^[294] ester^[295] and thioester motifs.^[296] Despite the vast array of CAN materials reported, complete depolymerisation to monomer(s) remains challenging. Additionally, the presence of such dynamic networks complicates further transformations in the overall recycling process. Nonetheless, monomer recovery has been reported for hemiaminal^[297] and boroxine^[298] systems among other motifs.^[22]

Helms and co-workers recently reported the closed-loop recycling of plastics enabled by dynamic covalent diketoenamine bonds (Scheme 4).^[299] Promisingly, the starting monomers could be efficiently recaptured and isolated from additives (e.g., dyes, inorganic fillers, flame retardants) and fibres present in the poly(diketoenamine)s (PDKs) under strongly acidic conditions in water. The potential to decouple monomers from material additives will undoubtedly assist market penetration in the future. Current work in the field remains focused on improving the overall sustainability of chemically recyclable thermosets and we direct the interested reader to a recent Review by Worch and Dove.^[22]

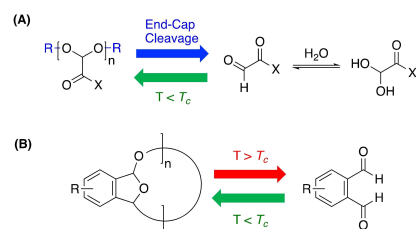


Scheme 4. Dynamic diketoenamine bonds for the production of a CAN material.^[299]

5.2. Self-immolative polymers

Self-immolative polymers (SIPs) have attracted considerable interest in recent years owing to their ability to “trigger” complete depolymerisation for on-demand material disposal applications.^[300] SIP degradation is typically irreversible in nature, akin to biodegradable polymers, although chemical recyclability is possible when monomeric units are recovered. Traditionally, reversible SIPs exhibit a low T_c observing polymer stability below this temperature. Cleavable end-capping units have been shown to provide sufficient chain stability above T_c for SIPs with extremely low ceiling temperatures ($T_c < 20^\circ\text{C}$), enabling practical applications.^[22,300] Examples of SIPs include polyglyoxylates^[301] and polyphthalaldehydes (PPA) as shown in Scheme 5.^[302] We envision such materials will play an important role in the future economy owing to their ability to exhibit well-defined complete depolymerisation. This is a major limitation of current biodegradable polymers, which exhibit differing degradation profiles depending on a variety of external environmental factors, including temperature and humidity.

Since non-composite SIPs typically exhibit poor mechanical properties, recent work in the field has focused on material property enhancement. A recent example includes the development of a thermally robust PPA with potential applications as a thermoplastic material.^[303] Zimmerman and co-workers recently reported a trigger-responsive self-amplifying degradable polymer based on a 3-iodopropyl acetal moiety.^[304] Acid catalysed hydrolysis promotes chain cleavage and liberation of the triggering species in stoichiometric quantities, resulting in



Scheme 5. Example SIPs: (A) Polyglyoxyls and (B) PPA.^[22]

accelerated degradation. Indeed, mechanically initiated chain scission via sonication has also been reported.^[305,306]

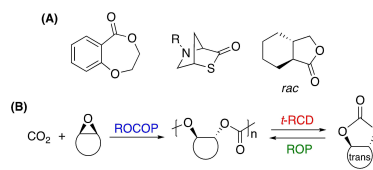
Beyond this, polyphosphoesters (PPEs), such as poly(methyl ethylene phosphate) (PMEP) and poly(ethyl ethylene phosphate) (PEEP), have also been reported as SIPs.^[307] Such poly(alkyl ethylene phosphate)s were shown to undergo back-biting hydrolysis under basic conditions, liberating alkyl (2-hydroxyethyl) hydrogen phosphate as the primary degradation product. PPEs are used in a diverse range of applications from flame retardants and tissue engineering through to drug and gene delivery systems.^[308]

5.3. Polyolefin mimics

The underlying thermodynamics of highly exergonic polymerisations (e.g., olefins) ensures reversing such transformations will remain challenging. A possible solution to this is the development of polyolefin mimics. Such materials retain many of the revered properties of polyolefins but are less environmentally persistent owing to the presence of cleavable linkages. Examples include polyphosphonates^[309] and polyesters^[310] among others.^[311] Recently, Wurm and co-workers reported long-chain polyorthoesters^[312] and polypyrophosphates^[313] as degradable alternatives to PE. Post polymerisation hydrogenation of the polyorthoesters yielded hard, solid materials with thermal properties similar to PE. Hydrogenated and non-hydrogenated co-polymers were found to hydrolyse slowly when exposed to atmospheric moisture, the rate of which was dependent on the orthoester substituent in solution. Conversely, the polypyrophosphates were found to hydrolyse rapidly under neutral, basic and acidic conditions. These materials have potential applications in the biomedical field or for advanced packaging. Whilst promising, it is important to note such materials do not address the loss of embedded material value to the natural environment or eutrophication resulting from nutrient saturation.

5.4. Monomer diversification

In pursuit of a plastics economy decoupled from fossil fuels, monomer sourcing considerations are becoming increasingly important. Additionally, it is imperative the industries pursuit of sustainability and circularity informs the selection of appropriate alternative feedstocks. Coates and Getzler^[17] recently defined the most attractive ROP monomers for chemical recycling to monomer (CRM) as large rings (7–11-membered) or five- and six-membered rings that possess multiple non- sp^3 -hybridised atoms or ring fusions (Scheme 6a). Such structural features increase ΔH_p , affording polymers that lend themselves to chemical recycling. We identify the economic derivatisation of such monomers from biomass as a key challenge in the future. Indeed, it is conceivable to access such monomers via the CRM of polymer derived from a different initial feedstock. For example, *trans*-[4.3.0] carbonates could be sourced from the ring-closing depolymerisation (RCD) of polycarbonates pro-

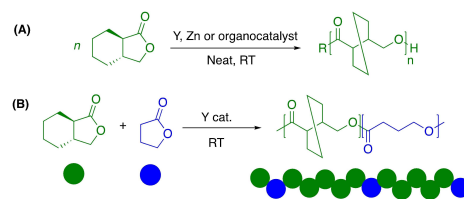


Scheme 6. (A) Selected lactone monomers that can undergo ROP and CRM.^[17] (B) Polycarbonate synthesis via ROCOP followed by RCD to afford *trans*-[4.3.0] carbonates.

duced via the ring-opening copolymerisation (ROCOP) of CO₂ and epoxide (Scheme 6b).^[17] Whilst high monomer cost relative to cheap petrochemical feedstocks has limited bio-based plastics thus far, cost is expected to decrease with scale-up. Indeed, the valorisation of polymer waste through CRM or upcycling may assist in overcoming a high initial monomer cost.

5.5. Cost and performance competitiveness

Whilst the plastic economies transition relies on the development of new materials, it is imperative they remain cost- and performance-competitive with existing synthetic plastics. Desirable material properties of emerging plastics include: a low glass transition temperature (T_g), high melting temperature (T_m), good ductility and high tensile strength.^[22] Whilst significant effort is devoted to advancing this research front, their inherent recyclability must not be overlooked to avoid potential pitfalls. Significant advancements with regards to bio-based polyesters have been made in recent years. Chen and co-workers reported a polyester based on γ -butyrolactone with *trans*-ring fusion at the α - and β -positions. Such *trans*-ring fusion renders the monomer polymerizable at room temperature under solvent-free conditions in the presence of a transition-metal (e.g., yttrium or zinc)^[314] or organocatalyst^[315] (Scheme 7a). Promisingly, the resulting polymer could be repeatedly recycled by means of thermolysis or chemolysis, recovering monomer in quantitative yield.^[314] Subsequently, this monomer has been copolymerised with a cyclic lactone (Scheme 7b) to afford a chemically recyclable copolymer with barrier and mechanical



Scheme 7. Chemically recyclable bio-based homopolymer (A) and copolymer (B) based on a fused ring γ -butyrolactone monomer.^[316]

properties competitive with existing commodity plastics such as PE and PET.^[316] Sustainable and recyclable biopolyesters reported thus far typically employ an aliphatic backbone and examples of novel aromatic polyesters remain rare despite a clear market need, exemplified by PET. Shaver and co-workers^[317,318] have reported a novel aromatic polyester with complete chemical recyclability back to monomer mediated by an Al^{III}-salen catalyst (Scheme 8). Such examples offer the prospect of a future plastics economy portfolio of robust and chemically recyclable plastics, surmounting the expectations of current first generation biopolyesters derived from cyclic lactones such as lactide.^[17,22]

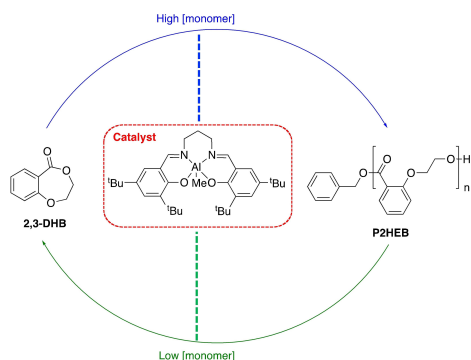
6. Conclusions and Outlook

Despite mounting environmental concerns, plastics will continue to play a dominant role in human development for the foreseeable future. It is therefore of critical importance we adopt proactive action to deliver disruptive and transformative change within a meaningful timeframe. Central to this notion is the decoupling of plastics from depleting fossil reserves and a shift towards a circular economic model, one concerned with material recapture and reuse. This will require the development of alternative waste management strategies, for which there is a clear industry appetite. Recycling represents a promising enabler to this transition. Mechanical recycling remains the industry standard but is limited by eventual material down-cycling, which creates uncertainty surrounding retention of material-value in the long-term. A possible solution to this is chemical recycling, which encompasses depolymerisation to monomer and degradation to value-added products. Examples from this Review include the derivatisation of alkyl lactates (e.g., green solvent) and terephthalamides (e.g., building blocks for high performance materials) from poly(lactic acid) (PLA) and poly(ethylene terephthalate) (PET) waste respectively. The potential to realise enhanced economic performance will

undoubtedly play a crucial role in overcoming inevitable barriers to adoption within industry. Additionally, catalysis will likely underpin the commercial viability of such processes and we have highlighted recent developments concerning PLA and PET. Despite recent progress, it is clear current methods remain limited by a number of factors including the use of expensive and/or highly corrosive reagents, harsh operating conditions or prolonged reaction times. Catalyst recovery often remains overlooked and the impact of mixed plastic waste on catalyst activity and product separation remains poorly understood. Such challenges provide scope for future process optimisation with metal-based catalysis a possible solution, although literature examples remain limited. In accordance with criteria previously described by Worch and Dove,^[22] we propose the following targets to encourage the development of industrially viable and sustainable chemical recycling strategies using metal-based systems:

1. exploit the use of cheap and earth-abundant metals in combination with scalable ligands
2. simple catalyst recovery and reuse, maintaining performance between cycles both in batch or flow
3. robust catalysts tolerant to common plastic waste stream contaminants including additives and debris
4. high process efficiency under mild conditions ($\geq 90\%$, $< 100^\circ\text{C}$, $\leq 1\text{ h}$)
5. maintain high product selectivity ($\geq 90\%$, $< 10\%$ per plastic) and process efficiency in the presence of mixed plastics.

It is clear a "one-solution-fits-all" approach is unrealistic, and we expect such criteria to direct the development of a diverse array of chemical recycling strategies. Additionally, future catalyst design should pursue the incorporation of Lewis acidic and H-bonding motifs, factors known to promote enhanced degradation activity. Whilst we anticipate mixed plastic waste to remain a major challenge, we expect the emergence of switchable catalysis (e.g., photo- and electrochemically induced) to offer new solutions to such problems. It is important to recognise a future circular model will be imperfect and thus susceptible to leakage. Embedding polymer recyclability and biodegradability at the design phase will assist in circumventing such challenges. Moving forward, it is imperative such materials remain cost and performance competitive with existing synthetic plastics. Moreover, we do not expect future innovation to be limited to the plastic materials themselves and anticipate developments in reaction engineering, and so forth, to assist in the transition.^[319] As the field garners increasing momentum, industry can expect significant advancements within the next 10 years. It is therefore prudent lessons learned from PLA and PET be applied to existing and emerging materials, for example poly(ethylene furanoate) (PEF).^[11] Whilst many catalytic chemical recycling processes remain immature relative to established thermal pyrolytic methods, we remain optimistic of its potential to modernise the plastics economy. Indeed, British Petroleum (BP) recently announced the development of its BP Infinia recycling technology for unrecyclable PET, highlighting the field's industrial relevance.^[320] Finally, it is imperative policy and legislation endeavour to deliver a platform that provides continuity between all invested stakeholders. This will remove



Scheme 8. A fully recyclable aromatic bio-based polyester based on the ROP of 2,3-dihydro-5H-1,4-benzodioxepin-5-one (2,3-DHB) mediated by an Al^{III}-salen complex.^[317]

barriers that currently confound the plastic waste crisis and accelerate the uptake and implementation of such technology.

Acknowledgements

We would like to thank the EPSRC for funding (EP/L016354/1) for a PhD studentship to JP.

Conflict of Interest

The authors declare no conflict of interest.

Keywords: catalysis · chemical recycling · circular economy · polyesters · upcycling

- [1] R. C. Thompson, C. J. Moore, F. S. vom Saal, S. H. Swan, *Philos. Trans. R. Soc. B* **2009**, *364*, 2153–2166.
- [2] Ellen MacArthur Foundation, The New Plastics Economy: Rethinking the Future of Plastics, <https://www.ellenmacarthurfoundation.org/publications/the-new-plastics-economy-rethinking-the-future-of-plastics>, (Accessed: 16th November 2020).
- [3] Y. Zhu, C. Romain, C. K. Williams, *Nature* **2016**, *540*, 354–362.
- [4] R. A. Sheldon, M. Norton, *Green Chem.* **2020**, *22*, 6310–6322.
- [5] J. Payne, P. McKeown, M. D. Jones, *Polym. Degrad. Stab.* **2019**, *165*, 170–181.
- [6] R. Geyer, J. R. Jambeck, K. L. Law, *Sci. Adv.* **2017**, *3*, e1700782.
- [7] J. R. Jambeck, R. Geyer, C. Wilcox, T. R. Siegler, M. Perryman, A. Andrady, R. Na, *Science* **2015**, *347*, 768–771.
- [8] L. Lebreton, B. Slat, F. Ferrari, B. Sainte-Rose, J. Aitken, R. Marthouse, S. Hajbane, S. Cunsolo, A. Schwarz, A. Levivier, K. Noble, P. Debeljak, H. Maral, R. Schoeneich-Argent, R. Brambini, J. Reisser, *Sci. Rep.* **2018**, *8*, 4666.
- [9] J. Pasqualino, M. Menesesab, F. Castells, *J. Food Eng.* **2011**, *103*, 357–365.
- [10] PlasticsEurope, Plastics – the Facts 2019. An Analysis of European Plastics Production, Demand and Waste Data, https://www.plasticseurope.org/application/files/9715/7129/9584/FINAL_web_version_Plastics_the_facts2019_14102019.pdf, (Accessed: 16th November 2020).
- [11] M. Rabnawaz, I. Wyman, R. Auras, S. Cheng, *Green Chem.* **2017**, *19*, 4737–4753.
- [12] J. H. Song, R. J. Murphy, R. Narayan, G. B. H. Davies, *Philos. Trans. R. Soc. B* **2009**, *364*, 2127–2139.
- [13] Guardian, A Million Bottles a Minute: World's Plastic Binge 'as Dangerous as Climate Change', <https://www.theguardian.com/environment/2017/jun/28/a-million-a-minute-worlds-plastic-bottle-binge-as-dangerous-as-climate-change>, (Accessed: 16th November 2020).
- [14] E. Gabirondo, A. Sangroniz, A. Etxeberria, S. Torres-Giner, H. Sardon, *Polym. Chem.* **2020**, *11*, 4861–4874.
- [15] C. A. Bernardo, C. L. Simões, M. L. Costa Pinto, *AIP Conf. Proc.* **2016**, *1779*, 140001–140005.
- [16] J. Zheng, S. Suh, *Nat. Clim. Change* **2019**, *9*, 374–378.
- [17] G. W. Coates, Y. D. Y. L. Getzler, *Nat. Rev. Mater.* **2020**, *5*, 501–516.
- [18] D. K. Schneiderman, M. A. Hillmyer, *Macromolecules* **2017**, *50*, 3733–3749.
- [19] X. Zhang, M. Fevre, G. O. Jones, R. M. Waymouth, *Chem. Rev.* **2018**, *118*, 839–885.
- [20] A. Rahimi, J. M. Garcia, *Nat. Chem. Rev.* **2017**, *1*, 0046.
- [21] M. Hong, E. X.-Y. Chen, *Green Chem.* **2017**, *9*, 3692–3706.
- [22] J. C. Worch, A. P. Dove, *ACS Macro Lett.* **2020**, *9*, 1494–1506.
- [23] J. Hopewell, R. Dvorak, E. Kosior, *Philos. Trans. R. Soc. B* **2009**, *364*, 2115–2126.
- [24] A. Soroudi, I. Jakubowicz, *Eur. Polym. J.* **2013**, *49*, 2839–2858.
- [25] S. C. Greer, *J. Phys. Chem. B* **1998**, *102*, 5413–5422.
- [26] A. Duda, S. Penczek, *Macromolecules* **1990**, *23*, 1636–1639.
- [27] G. Odian, *Principles of Polymerisation*, Wiley-Interscience, John-Wiley & Sons, 4th edn **2004**.
- [28] H. L. Le Châtelier, *C. R. Acad. Sci.* **1884**, *99*, 786–789.
- [29] R. Miranda, J. Yang, C. Roy, C. Vasile, *Polym. Degrad. Stab.* **2001**, *72*, 469–491.
- [30] A. S. Burange, M. B. Gawande, F. L. Y. Lam, R. V. Jayaram, R. Luque, *Green Chem.* **2015**, *17*, 146–156.
- [31] J. F. Mastral, C. Berruico, M. Gea, J. Ceamanos, *Polym. Degrad. Stab.* **2006**, *91*, 3330–3338.
- [32] R. Aguado, M. Olazar, M. J. San José, B. Gaisán, *J. Bilbao. Energy Fuels* **2002**, *16*, 1429–1437.
- [33] X. Jia, C. Qin, T. Friedberger, Z. Guan, Z. Huang, *Sci. Adv.* **2016**, *2*, e1501591.
- [34] J. Aguado, D. P. Serrano, J. M. Escola, *Ind. Eng. Chem. Res.* **2008**, *47*, 7982–7992.
- [35] L. S. Diaz-Silvarrey, K. Zhang, A. N. Phan, *Green Chem.* **2018**, *20*, 1813–1823.
- [36] R. R. Guddeti, R. Knight, E. D. Grossmann, *Ind. Eng. Chem. Res.* **2000**, *39*, 1171–1176.
- [37] UK Catalysis Hub, <https://ukcatalysishub.co.uk/wp-content/uploads/2020/04/Cat-Hub2018-key-areas.pdf>, (Accessed: 22nd November 2020).
- [38] H. Sinn, W. Kaminsky, *Adv. Organomet. Chem.* **1980**, *18*, 99–149.
- [39] PlasticsEurope, Plastics – the Facts 2017. An Analysis of European Plastics Production, Demand and Waste Data, https://www.plasticseurope.org/application/files/5715/1717/4180/Plastics_the_facts_2017_FINAL_for_website_one_page.pdf, (Accessed: 22nd November 2020).
- [40] J. Aguado, D. P. Serrano, G. San Miguel, *Global NEST J.* **2007**, *9*, 12–19.
- [41] J. Yu, L. Sun, C. Ma, Y. Qiao, H. Yao, *Waste Manage.* **2016**, *48*, 300–314.
- [42] F. M. Lamberti, L. A. Román-Ramírez, J. Wood, *J. Polym. Environ.* **2020**, *28*, 2551–2571.
- [43] J. N. Hahladakis, C. A. Velis, R. Weber, E. Iacovidou, P. Purnell, *J. Hazard. Mater.* **2018**, *344*, 179–199.
- [44] N. George, T. Kurian, *Ind. Eng. Chem. Res.* **2014**, *53*, 14185–14198.
- [45] Ellen MacArthur Foundation, The New Plastics Economy Global Commitment: 2019 Progress Report, <https://www.ellenmacarthurfoundation.org/assets/downloads/Global-Commitment-2019-Progress-Report.pdf> (Accessed: 24th November 2020).
- [46] McKinsey & Company, How plastics waste recycling could transform the chemical industry, <https://www.mckinsey.com/industries/chemicals/our-insights/how-plastics-waste-recycling-could-transform-the-chemical-industry> (Accessed: 24th November 2020).
- [47] UK Government, Plastic bag sales in 'big seven' supermarkets down 86% since 5p charge, <https://www.gov.uk/government/news/plastic-bag-sales-in-big-seven-supermarkets-down-86-since-5p-charge> (Accessed: 24th November 2020).
- [48] J. Otera, *Modern Carbonyl Chemistry*, Wiley-VCH, John-Wiley & Sons, edn 1, **2000**.
- [49] M. A. Abdel-Rahman, Y. Tashiro, K. Sonomoto, *Biotechnol. Adv.* **2013**, *31*, 877–902.
- [50] M. A. Abdel-Rahman, Y. Tashiro, K. Sonomoto, *J. Biotechnol.* **2011**, *156*, 286–301.
- [51] O. Dechy-Cabaret, B. Martin-Vaca, D. Bourissou, *Chem. Rev.* **2004**, *104*, 6147–6176.
- [52] C. M. Thomas, *Chem. Soc. Rev.* **2010**, *39*, 165–173.
- [53] M. J. Stanford, A. P. Dove, *Chem. Soc. Rev.* **2010**, *39*, 486–494.
- [54] R. H. Platel, L. M. Hodgson, C. K. Williams, *Polym. Rev.* **2008**, *48*, 11–63.
- [55] E. T. H. Vink, K. R. Rábago, D. A. Glassner, B. Springs, R. P. O'Connor, J. Kolstad, P. R. Gruber, *Macromol. Biosci.* **2004**, *4*, 551–564.
- [56] R. Auras, B. Harte, S. Selke, *Macromol. Biosci.* **2004**, *4*, 835–864.
- [57] C. J. Weber, V. Haugaard, R. Festersen, G. Bertelsen, *Food Addit. Contam.* **2002**, *19*, 172–177.
- [58] E. Castro-Aguirre, F. Iñiguez-Franco, H. Samsudin, X. Fang, R. Auras, *Adv. Drug Delivery Rev.* **2016**, *107*, 333–366.
- [59] J. Lunt, *Polym. Degrad. Stab.* **1998**, *59*, 145–152.
- [60] K. M. Nampoothiri, N. J. Nair, R. P. John, *Bioresour. Technol.* **2010**, *101*, 8493–8501.
- [61] A. J. R. Lasprilla, G. A. R. Martinez, B. H. Lunelli, A. L. Jardini, R. M. Filho, *Biotechnol. Adv.* **2012**, *30*, 321–328.
- [62] P. VanWouwe, M. Dusselier, E. Vanleeuw, B. Sels, *ChemSusChem* **2016**, *9*, 907–921.
- [63] European Bioplastics, Facts and Figures, https://docs.european-bioplastics.org/publications/EUBP_Facts_and_figures.pdf, (Accessed: 4th December 2020).
- [64] R. De Clercq, M. Dusselier, C. Poleunis, D. P. Debecker, L. Giebeler, S. Oswald, E. Makshina, B. F. Sels, *ACS Catal.* **2018**, *8*, 8130–8139.

- [65] M. Ghadamyari, S. Chaemchuen, K. Zhou, M. Dusselier, B. F. Sels, B. Mousavi, F. Verpoort, *Catal. Commun.* **2018**, *114*, 33–36.
- [66] M. Dusselier, P. Van Wouwe, A. Dewaele, P. A. Jacobs, B. F. Sels, *Science* **2015**, *349*, 78–80.
- [67] R. De Clercq, M. Dusselier, E. Makshina, B. F. Sels, *Angew. Chem. Int. Ed.* **2018**, *57*, 3074–3078; *Angew. Chem.* **2018**, *130*, 3128–3132.
- [68] P. P. Upare, Y. K. Hwang, J.-S. Chang, D. W. Hwang, *Ind. Eng. Chem. Res.* **2012**, *51*, 4837–4842.
- [69] P. P. Upare, J. W. Yoon, D. W. Hwang, U. H. Lee, Y. K. Hwang, D. Y. Hong, J. C. Kim, J. H. Lee, S. K. Kwak, H. Shin, H. Kim, J.-S. Chang, *Green Chem.* **2016**, *18*, 5978–5983.
- [70] S. Heo, H. W. Park, J. H. Lee, Y. K. Chang, *ACS Sustainable Chem. Eng.* **2019**, *7*, 6178–6184.
- [71] E. Shen, L. Worrell, M. K. Patel, *Biofuels Bioprod. Biorefin.* **2012**, *6*, 625–639.
- [72] W. J. Groot, T. Borén, *Int. J. Life Cycle Assess.* **2010**, *15*, 970–984.
- [73] Total, Thailand: Total Corbion PLA Starts-up its 75,000 Tonnes Per Year Bioplastics Plant, <https://www.total.com/media/news/press-releases/thailand-total-corbion-pla-starts-its-75000-tonnes-year-bioplastics-plant>, (Accessed: 4th December 2020).
- [74] T. P. Haider, C. Völker, J. Kramm, K. Landfester, F. R. Wurm, *Angew. Chem. Int. Ed.* **2019**, *58*, 50–62; *Angew. Chem.* **2019**, *131*, 50–63.
- [75] C. Danylyuk, R. Erickson, S. Burrows, R. Auras, *J. Test. Eval.* **2010**, *38*, 717–723.
- [76] G. Kale, R. Auras, S. P. Singh, R. Narayan, *Polym. Test.* **2007**, *26*, 1049–1061.
- [77] H. K. Ahn, M. S. Huda, M. C. Smith, W. Mulbray, W. F. Schmidt, J. B. Reeves, *Bioresour. Technol.* **2011**, *102*, 4930–4933.
- [78] S. M. Emadian, T. T. Onay, B. Demirel, *Waste Manage.* **2017**, *59*, 526–536.
- [79] G. Kale, T. Kijchavengkul, R. Auras, M. Rubino, S. E. Selke, S. P. Singh, *Macromol. Biosci.* **2007**, *7*, 255–277.
- [80] K. L. G. Ho, A. L. Pometto, P. N. Hinz, A. Gadea-Rivas, J. A. Briceño, A. Rojas, *J. Environ. Polym. Degrad.* **1999**, *7*, 167–172.
- [81] E. Rudnik, Briassoulis, *Ind. Crops Prod.* **2011**, *33*, 648–658.
- [82] A. R. Bagheri, C. Laforscha, A. Greiner, S. Agarwal, *Global Challenges* **2017**, *1*, 1700048.
- [83] H. Tsuji, K. Suzuyoshi, *Polym. Degrad. Stab.* **2002**, *75*, 347–355.
- [84] M. Nazareth, M. R. C. Marques, M. C. A. Leite, Í. B. Castro, *J. Hazard. Mater.* **2019**, *366*, 714–722.
- [85] H. Tsuji, K. Suzuyoshi, *Polym. Degrad. Stab.* **2002**, *75*, 357–365.
- [86] U. S. Department of Energy, Top Value Added Chemicals from Biomass, <https://www.nrel.gov/docs/fy04osti/35523.pdf>, (Accessed: 7th December 2020).
- [87] Y. Fan, C. Zhou, X. Zhu, *Catal. Rev. Sci. Eng.* **2009**, *51*, 293–324.
- [88] M. Dusselier, P. V. Wouwe, A. Dewaele, E. Makshina, B. F. Sels, *Energy Environ. Sci.* **2013**, *6*, 1415–1442.
- [89] P. McKeown, M. D. Jones, *Sustainable Chem.* **2020**, *1*, 1–22, DOI: 10.3390/suschem1010001.
- [90] F. Von Burkersroda, L. Schedl, A. Göpferich, *Biomaterials* **2002**, *23*, 4221–4231.
- [91] H. Tsuji, H. Daimon, K. Fujie, *Biomacromolecules* **2003**, *4*, 835–840.
- [92] H. Tsuji, T. Saeki, T. Tsukegi, H. Daimon, K. Fujie, *Polym. Degrad. Stab.* **2008**, *93*, 1956–1963.
- [93] H. Tsuji, M. Ogiwara, S. K. Saha, T. Sakaki, *Biomacromolecules* **2006**, *7*, 380–387.
- [94] M. H. Rahaman, H. Tsuji, *Polym. Degrad. Stab.* **2013**, *98*, 709–719.
- [95] H. Tsuji, *Macromol. Biosci.* **2005**, *5*, 569–597.
- [96] H. Tsuji, Y. Ikada, *J. Appl. Polym. Sci.* **1997**, *63*, 855–863.
- [97] “Hydrolytic Degradation”: H. Tsuji in *Poly(Lactic Acid)*, Wiley, Hoboken, NJ, **2010**, pp. 343–381.
- [98] K. Hirao, H. Ohara, *Polym. Rev.* **2011**, *51*, 1–22.
- [99] V. Piemonte, F. Gironi, *J. Polym. Environ.* **2013**, *21*, 313–318.
- [100] V. Piemonte, F. Gironi, *J. Polym. Environ.* **2013**, *21*, 275–279.
- [101] G. L. Siparsky, K. J. Voorhees, F. Miao, *J. Environ. Polym. Degrad.* **1998**, *6*, 31–41.
- [102] C. Annesini Maria, S. Frattari, F. Gironi, V. Piemonte, R. Sabia, C. Villani, *J. Polym. Environ.* **2018**, *26*, 4396–4404.
- [103] F. Iniguez-Franco, R. Auras, K. Dolan, S. Selke, D. Holmes, M. Rubino, H. Soto-Valdez, *Polym. Degrad. Stab.* **2018**, *149*, 28–38.
- [104] R. Auras, G. Burgess, D. Holmes, X. Fang, M. Rubino, H. Soto-Valdez, *Polymer* **2016**, *99*, 315–323.
- [105] M. Niaounakis, *Eur. Polym. J.* **2019**, *114*, 464–475.
- [106] P. Coszach, J.-C. Bogaert, J. Wilocq, US Pat. 8431683 B2, **2013**.
- [107] X. Song, H. Wang, X. Yang, F. Liu, S. Yu, S. Liu, *Polym. Degrad. Stab.* **2014**, *110*, 65–70.
- [108] R. T. MacDonald, S. P. McCarthy, R. A. Gross, *Macromolecules* **1996**, *29*, 7356–7361.
- [109] Á. Girard, H. Garreau, M. Vert, S. Li, *Polym. Degrad. Stab.* **2001**, *71*, 61–67.
- [110] H. Cai, V. Dave, R. A. Gross, S. P. McCarthy, *J. Polym. Sci. Part B* **1996**, *34*, 2701–2708.
- [111] S. Li, S. McCarthy, *Macromolecules* **1999**, *32*, 4454–4456.
- [112] Y. Tokiwa, B. P. Calabria, C. U. Ugwu, S. Aiba, *Int. J. Mol. Sci.* **2009**, *10*, 3722–3742.
- [113] J. Chapman, A. E. Ismail, C. Z. Dinu, *Catalysts* **2018**, *8*, 238–264.
- [114] R. A. Sheldon, J. M. Woodley, *Chem. Rev.* **2018**, *118*, 801–838.
- [115] C. T. Bowmer, R. N. Hooftman, A. O. Hanstveit, P. W. M. Venderbosch, N. van der Hoeven, *Chemosphere* **1998**, *37*, 1317–1333.
- [116] C. S. M. Pereira, V. M. T. M. Silva, A. E. Rodrigues, *Green Chem.* **2011**, *13*, 2658–2671.
- [117] F. M. Lamberti, L. A. Román-Ramírez, P. McKeown, M. D. Jones, J. Wood, *Processes* **2020**, *8*, 738.
- [118] ACS, 12 Principles of Green Chemistry, <https://www.acs.org/content/acs/en/greenchemistry/principles/12-principles-of-green-chemistry.html>, (Accessed: 14th December 2020).
- [119] K. Phomphrai, S. Pracha, P. Phonjanthuek, M. Pohmakotr, *Dalton Trans.* **2008**, 3048–3050.
- [120] D. Bykowski, A. Grala, P. Sobota, *Tetrahedron Lett.* **2014**, *55*, 5286–5289.
- [121] A. Grala, J. Efler, L. B. Jerzykiewicz, P. Sobota, *Dalton Trans.* **2011**, *40*, 4042–4044.
- [122] L. D. Brake, US Pat. 5264617, **1993**.
- [123] X. Song, X. Zhang, H. Wang, F. Liu, S. Yu, S. Liu, *Polym. Degrad. Stab.* **2013**, *98*, 2760–2764.
- [124] X. Song, Z. Bian, Y. Hui, H. Wang, F. Liu, S. Yu, *Polym. Degrad. Stab.* **2019**, *168*, 108937.
- [125] H. Liu, R. Zhao, X. Song, F. Liu, S. Yu, S. Liu, X. Ge, *Catal. Lett.* **2017**, *147*, 2298–2305.
- [126] C. Jehanno, M. M. Pérez-Madriral, J. Demarteau, H. Sardo, A. P. Dove, *Polym. Chem.* **2019**, *10*, 172–186.
- [127] F. Nederberg, E. F. Connor, T. Glausser, J. L. Hedrick, *Chem. Commun.* **2001**, 2066–2067.
- [128] C. Alberti, N. Damps, R. R. R. Meißner, S. Enthaler, *ChemistrySelect* **2019**, *4*, 6845–6848.
- [129] F. Liu, J. Guo, P. Zhao, Y. Gu, J. Gao, M. Liu, *Polym. Degrad. Stab.* **2019**, *167*, 124–129.
- [130] M. Liu, J. Guo, Y. Gu, J. Gao, F. Liu, *ACS Sustainable Chem. Eng.* **2018**, *6*, 15127–15134.
- [131] P. McKeown, M. Kamran, M. G. Davidson, M. D. Jones, L. A. Román-Ramírez, J. Wood, *Green Chem.* **2020**, *22*, 3721–3726.
- [132] F. A. Leibfarth, N. Moreno, A. P. Hawker, J. D. Shand, *J. Polym. Sci. Part A* **2012**, *50*, 4814–4822.
- [133] E. M. Filachione, J. H. Lengel, C. H. Fisher, *Ind. Eng. Chem.* **1945**, *37*, 388–390.
- [134] A. C. Sánchez, R. S. Collinson, *Eur. Polym. J.* **2011**, *47*, 1970–1976.
- [135] H. Liu, X. Song, F. Liu, S. Liu, S. Yu, *J. Polym. Res.* **2015**, *22*, 135–141.
- [136] C. Alberti, N. Damps, R. R. R. Meißner, M. Hofmann, D. Rijono, S. Enthaler, *Adv. Sustainable Syst.* **2020**, *4*, 1900081.
- [137] M. Hofmann, C. Alberti, F. Scheliga, R. R. R. Meißner, S. Enthaler, *Polym. Chem.* **2020**, *11*, 2625–2629.
- [138] C. Alberti, H. R. Kricheldorf, S. Enthaler, *ChemistrySelect* **2020**, *5*, 12313–12316.
- [139] E. Cheung, C. Alberti, S. Enthaler, *ChemistryOpen* **2020**, *9*, 1224–1228.
- [140] A. Plichta, P. Lisowska, A. Kundys, A. Zychewicz, M. Dębowski, Z. Florjańczyk, *Polym. Degrad. Stab.* **2014**, *108*, 288–296.
- [141] R. Petrus, D. Bykowski, P. Sobota, *ACS Catal.* **2016**, *6*, 5222–5235.
- [142] K. Hirao, Y. Nakatsuchi, H. Ohara, *Polym. Degrad. Stab.* **2010**, *95*, 925–928.
- [143] E. L. Whitelaw, M. G. Davidson, M. D. Jones, *Chem. Commun.* **2011**, *47*, 10004–10006.
- [144] C. Fliedel, D. Vila-Viçosa, M. J. Calhorda, S. Dagonne, T. Avilés, *ChemCatChem* **2014**, *6*, 1357–1367.
- [145] D. Jędrzkiewicz, I. Czełusniak, M. Wierzejewska, S. Szafert, J. Efler, *J. Mol. Catal. A* **2015**, *396*, 155–163.
- [146] J. Payne, P. McKeown, M. F. Mahon, E. A. C. Emanuelsson, M. D. Jones, *Polym. Chem.* **2020**, *11*, 2381–2389.
- [147] P. McKeown, J. Brown-Humes, M. G. Davidson, M. F. Mahon, T. J. Woodman, M. D. Jones, *Dalton Trans.* **2017**, *46*, 5048–5057.

- [148] P. McKeown, S. N. McCormick, M. F. Mahon, M. D. Jones, *Polym. Chem.* **2018**, *9*, 5339–5347.
- [149] L. A. Román-Ramírez, P. McKeown, M. D. Jones, J. Wood, *ACS Catal.* **2019**, *9*, 409–416.
- [150] L. A. Román-Ramírez, P. McKeown, C. Shah, J. Abraham, M. D. Jones, J. Wood, *Ind. Eng. Chem. Res.* **2020**, *59*, 11149–11156.
- [151] P. McKeown, L. A. Román-Ramírez, S. Bates, J. Wood, M. D. Jones, *ChemSusChem* **2019**, *12*, 5233–5238.
- [152] L. A. Román-Ramírez, M. Powders, P. McKeown, M. D. Jones, J. Wood, *J. Polym. Environ.* **2020**, *28*, 2956–2964.
- [153] L. A. Román-Ramírez, P. McKeown, M. D. Jones, J. Wood, *ACS Omega* **2020**, *5*, 5556–5564.
- [154] R. Yang, G. Xu, C. Lv, B. Dong, L. Zhou, Q. Wang, *ACS Sustainable Chem. Eng.* **2020**, *8*, 18347–18353.
- [155] "Elemental Sustainability and the Importance of Scarce Element Recovery": A. J. Hunt, T. J. Farmer, J. H. Clark in *Element Recovery and Sustainability* (Ed.: A. Hunt), RSC, **2013**, chap. 1, pp. 1–28.
- [156] E. M. Krall, T. W. Klein, R. J. Andersen, A. J. Nett, R. W. Glasgow, D. S. Reader, B. C. Dauphinais, S. P. Mc Ilrath, A. A. Fischer, M. J. Carney, D. J. Hudson, N. J. Robertson, *Chem. Commun.* **2014**, *50*, 4884–4887.
- [157] S. Westhues, J. Idel, J. Klankermayer, *Sci. Adv.* **2018**, eaat9669.
- [158] T.-O. Kandler, C. Alberti, E. Fedorenko, N. Santangelo, S. Enthaler, *ChemistryOpen* **2020**, *9*, 401–404.
- [159] I. A. Shuklov, N. V. Dubrovina, J. Schulze, W. Tietz, K. Kühlein, A. Börner, *Chem. Eur. J.* **2014**, *20*, 957–960.
- [160] E. Balaraman, E. Fogler, D. Milstein, *Chem. Commun.* **2012**, *48*, 1111–1113.
- [161] E. Feghali, T. Cantat, *ChemSusChem* **2015**, *8*, 980–984.
- [162] L. Monsigny, J.-C. Berthet, T. Cantat, *ACS Sustainable Chem. Eng.* **2018**, *6*, 10481–10488.
- [163] B. F. S. Nunes, M. Conceição Oliveira, A. C. Fernandes, *Green Chem.* **2020**, *22*, 2419–2425.
- [164] I. C. McNeill, H. A. Leiper, *Polym. Degrad. Stab.* **1985**, *11*, 267–285.
- [165] I. C. McNeill, H. A. Leiper, *Polym. Degrad. Stab.* **1985**, *11*, 309–326.
- [166] F. Kopinke, M. Remmler, K. Mackenzie, M. Moder, O. Wachsen, *Polym. Degrad. Stab.* **1996**, *53*, 329–342.
- [167] H. Nishida, T. Mori, S. Hoshihara, Y. Fan, Y. Shirai, T. Endo, *Polym. Degrad. Stab.* **2003**, *81*, 515–523.
- [168] O. Wachsen, K. Platkowski, K. H. Reichert, *Polym. Degrad. Stab.* **1997**, *57*, 87–94.
- [169] D. Cam, M. Marucci, *Polymer* **1997**, *38*, 1879–1884.
- [170] Y. Fan, H. Nishida, Y. Shirai, Y. Tokiwa, T. Endo, *Polym. Degrad. Stab.* **2004**, *86*, 197–208.
- [171] Y. Fan, H. Nishida, T. Mori, Y. Shirai, T. Endo, *Polymer* **2004**, *45*, 1197–1205.
- [172] H. Nishida, Y. Fan, T. Mori, N. Oyagi, T. Endo, *Ind. Eng. Chem. Res.* **2005**, *44*, 1433–1437.
- [173] Y. Fan, H. Nishida, S. Hoshihara, Y. Shirai, Y. Tokiwa, T. Endo, *Polym. Degrad. Stab.* **2003**, *79*, 547–562.
- [174] L. Feng, S. Feng, X. Bian, G. Li, X. Chen, *Polym. Degrad. Stab.* **2018**, *157*, 212–223.
- [175] Y. Fan, H. Nishida, Y. Shirai, T. Endo, *Green Chem.* **2003**, *5*, 575–579.
- [176] T. Mori, H. Nishida, Y. Shirai, T. Endo, *Polym. Degrad. Stab.* **2004**, *84*, 243–251.
- [177] H. Abe, N. Takahashi, K. J. Kim, M. Mochizuki, Y. Doi, *Biomacromolecules* **2004**, *5*, 1606–1614.
- [178] O. Coulembier, S. Moins, J. M. Raquez, F. Meyer, L. Mespouille, E. Duquesne, P. Dubois, *Polym. Degrad. Stab.* **2011**, *96*, 739–744.
- [179] C. Alberti, S. Enthaler, *ChemistrySelect* **2020**, *5*, 14759–14763.
- [180] B. Slater, S.-O. Wong, A. Duckworth, A. J. P. White, M. R. Hill, B. P. Ladewig, *Chem. Commun.* **2019**, *55*, 7319–7322.
- [181] H. Kampová, E. Riemlová, J. Kličarová, V. Pejchal, J. Merna, P. Vlasák, P. Švec, Z. Růžicková, A. Růžicka, *J. Organomet. Chem.* **2015**, *778*, 35–41.
- [182] K. V. Zaitsev, V. S. Cherepakhin, A. Zhrebek, A. Kononikhin, E. Nikolaev, A. V. Churakov, *J. Organomet. Chem.* **2018**, *875*, 11–23.
- [183] F. Welle, *Resour. Conserv. Recycl.* **2011**, *55*, 865–875.
- [184] F. Awaja, D. Pavel, *Eur. Polym. J.* **2005**, *41*, 1453–1477.
- [185] S. M. Biros, B. M. Bridgewater, A. Villeges-Estrada, J. M. Tanski, G. Parkin, *Inorg. Chem.* **2002**, *41*, 4051–4057.
- [186] C. Vilela, A. F. Sousa, A. C. Fonseca, A. C. Serra, J. F. J. Coelho, C. S. R. Freire, A. J. D. Silvestre, *Polym. Chem.* **2014**, *5*, 3119–3141.
- [187] S. A. Miller, *ACS Macro Lett.* **2013**, *2*, 550–554.
- [188] J. M. García, *Chem* **2016**, *1*, 813–815.
- [189] V. Sinha, M. R. Patel, J. V. Patel, *J. Polym. Environ.* **2010**, *18*, 8–25.
- [190] S. M. Al-Salem, P. Lettieri, J. Baeyens, *Waste Manage.* **2009**, *29*, 2625–2643.
- [191] G. P. Karayannidis, D. S. Achilias, *Macromol. Mater. Eng.* **2007**, *292*, 128–146.
- [192] D. Paszun, T. Spychaj, *Ind. Eng. Chem. Res.* **1997**, *36*, 1373–1383.
- [193] A. M. Al-Sabagh, F. Z. Yehia, Gh. Eshaq, A. M. Rabie, A. E. ElMetwally, *Egypt. J. Pet.* **2016**, *25*, 53–64.
- [194] C. G. G. Namboori, M. S. Haith, *J. Appl. Polym. Sci.* **1968**, *12*, 1999–2005.
- [195] G. E. Brown Jr., R. C. O'Brien, R. C. US Pat. 3952053, **1976**.
- [196] J. Pitat, V. Holcik, M. A. Bacak, GB Pat. 822834, **1959**.
- [197] J. Benzaria, B. Durif-Varambon, F. Dawans, J. B. Gaillard, Eur. Pat. 59775, **1994**.
- [198] J. W. Mandoki, U. S. Pat. 4605762, **1986**.
- [199] B. I. Rosen, U. S. Pat. 5095145, **1992**.
- [200] V. Tournier, C. M. Topham, A. Gilles, B. David, C. Folgoas, E. Moya-Leclair, E. Kamionka, M.-L. Desrousseaux, H. Texier, S. Gavalda, M. Cot, E. Guémar, M. Dalibey, J. Nomme, G. Cioci, S. Barbe, M. Chateau, I. André, S. Duquesne, A. Marty, *Nature* **2020**, *580*, 216–219.
- [201] S. Yoshida, K. Hiraga, T. Takehana, I. Taniguchi, H. Yamaji, Y. Maeda, K. Toyohara, K. Miyamoto, Y. Kimura, K. Oda, *Science* **2016**, *351*, 1196–1199.
- [202] U. T. Bornscheuer, *Science* **2016**, *351*, 1154–1155.
- [203] R. Wei, W. Zimmermann, *Microb. Biotechnol.* **2017**, *10*, 1308–1322.
- [204] F. Kawai, T. Kawabata, M. Oda, *Appl. Microbiol. Biotechnol.* **2019**, *103*, 4253–4268.
- [205] R. Lotz, G. Wick, C. Neuhaus, U. S. Pat. 3321510, **1967**.
- [206] H. Gruschke, W. Hammerschick, W. Medem, U. S. Pat. 3403115, **1968**.
- [207] M. Goto, H. Koyamoto, A. Kodama, T. Hirose, S. Nagaoka, *J. Phys. Condens. Matter* **2002**, *14*, 11427–11430.
- [208] M. Genta, T. Iwaya, M. Sasaki, M. Goto, T. Hirose, *Ind. Eng. Chem. Res.* **2005**, *44*, 3894–3900.
- [209] Y. Yang, Y. Lu, H. Xiang, Y. Xu, Y. Li, *Polym. Degrad. Stab.* **2002**, *75*, 185–191.
- [210] M. Goto, *J. Supercrit. Fluids* **2009**, *47*, 500–507.
- [211] K. P. Blackmon, D. W. Fox, S. J. Shafer, Eur. Pat. 365842, **1988**.
- [212] K. Fukushima, J. M. Lecuyer, D. S. Wei, H. W. Horn, G. O. Jones, H. A. Al-Megren, A. M. Alabdulrahman, F. D. Alsewailam, M. A. McNeil, J. E. Rice, J. L. Hedrick, *Polym. Chem.* **2013**, *4*, 1610–1616.
- [213] R. M. Musale, S. R. Shukla, *Int. J. Plast. Technol.* **2016**, *20*, 106–120.
- [214] S. R. Shukla, A. M. Harad, *Polym. Degrad. Stab.* **2006**, *91*, 1850–1854.
- [215] M. E. Tawfik, S. B. Eskander, *Polym. Degrad. Stab.* **2010**, *95*, 187–194.
- [216] M. E. Tawfik, N. M. Ahmed, S. B. Eskander, *J. Appl. Polym. Sci.* **2011**, *120*, 2842–2855.
- [217] N. D. Pingale, S. R. Shukla, *Eur. Polym. J.* **2009**, *45*, 2695–2700.
- [218] Y. S. Parab, N. D. Pingale, S. R. Shukla, *J. Appl. Polym. Sci.* **2012**, *125*, 1103–1107.
- [219] R. V. Shah, V. S. Borude, S. R. Shukla, *J. Appl. Polym. Sci.* **2013**, *127*, 323–328.
- [220] Y. S. Parab, R. V. Shah, S. R. Shukla, *Curr. Chem. Lett.* **2012**, *1*, 81–90.
- [221] V. S. Palekar, A. J. Damle, S. R. Shukla, *Eur. J. Med. Chem.* **2009**, *44*, 5112–5116.
- [222] R. K. Soni, M. Teotia, K. Dutt, *J. Appl. Polym. Sci.* **2010**, *118*, 638–645.
- [223] T. Spychaj, E. Fabrycy, S. Spychaj, M. Kacperski, *J. Mater. Cycles Waste Manage.* **2001**, *3*, 24–31.
- [224] F. Siclari, D. Ruta, F. Cauzzi, Ital. Pat. 729187, **1966**.
- [225] J. Heinz, H. Ramm, H. Richardt, Ger. Pat. 1247291, **1967**.
- [226] K. Miura, Y. Kagiya, T. Ichikawa, Jpn. Pat. 6823449, **1968**.
- [227] H. Grushke, M. Mayer, Ger. Pat. 1290929, **1969**.
- [228] U. R. Vaidya, V. M. Nadkarni, *Ind. Eng. Chem. Res.* **1987**, *26*, 194–198.
- [229] S. H. Mansour, N. E. Ikladious, *Polym. Test.* **2002**, *21*, 497–505.
- [230] Q. Wang, X. Yao, S. Tang, X. Lu, X. Zhang, S. Zhang, *Green Chem.* **2012**, *14*, 2559–2566.
- [231] K. Fukushima, O. Coulembier, J. M. Lecuyer, H. A. Almegren, A. M. Alabdulrahman, F. D. Alsewailam, M. A. McNeil, P. Dubois, R. M. Waymouth, H. W. Horn, J. E. Rice, J. L. Hedrick, *J. Polym. Sci. Part A* **2011**, *49*, 1273–1281.
- [232] N. E. Kamber, Y. Tsujii, K. Keets, R. M. Waymouth, R. C. Pratt, G. W. Nycy, J. L. Hedrick, *J. Chem. Educ.* **2010**, *87*, 519–521.
- [233] J. L. Hedrick, G. W. Nycy, R. M. Waymouth, US Pat. 7053221 B2, **2006**.
- [234] G. W. Nycy, J. A. Lamboy, E. F. Connor, R. M. Waymouth, J. L. Hedrick, *Org. Lett.* **2002**, *4*, 3587–3590.
- [235] K. Fukushima, D. J. Coady, G. O. Jones, H. A. Almegren, A. M. Alabdulrahman, F. D. Alsewailam, H. W. Horn, J. E. Rice, J. L. Hedrick, *J. Polym. Sci. Part A* **2013**, *51*, 1606–1611.

- [236] H. W. Horn, G. O. Jones, D. S. Wei, K. Fukushima, J. M. Lecuyer, D. J. Coady, J. L. Hedrick, J. E. Rice, *J. Phys. Chem. A* **2012**, *116*, 12389–12398.
- [237] C. Jehanno, I. Flores, A. P. Dove, A. J. Müller, F. Ruipérez, H. Sardon, *Green Chem.* **2018**, *20*, 1205–1212.
- [238] H. Wang, Y. Liu, Z. Li, X. Zhang, S. Zhang, Y. Zhang, *Eur. Polym. J.* **2009**, *45*, 1535–1544.
- [239] H. Wang, Z. Li, Y. Liu, X. Zhang, S. Zhang, *Green Chem.* **2009**, *11*, 1568–1575.
- [240] Q. F. Yue, C. X. Wang, L. N. Zhang, Y. Ni, Y. X. Jin, *Polym. Degrad. Stab.* **2011**, *96*, 399–403.
- [241] Q. Wang, Y. Geng, X. Lu, S. Zhang, *ACS Sustainable Chem. Eng.* **2015**, *3*, 340–348.
- [242] H. Wang, R. Yan, Z. Li, X. Zhang, S. Zhang, *Catal. Commun.* **2010**, *11*, 763–767.
- [243] J. Sun, D. Liu, R. P. Young, A. G. Cruz, N. G. Isern, T. Schuerg, J. R. Cort, B. A. Simmons, S. Singh, *ChemSusChem* **2018**, *11*, 781–792.
- [244] Q. Wang, X. Yao, Y. Geng, Q. Zhou, X. Lu, S. Zhang, *Green Chem.* **2015**, *17*, 2473–2479.
- [245] L. Zhou, X. Lu, Z. Ju, B. Liu, H. Yao, J. Xu, Q. Zhou, Y. Hu, S. Zhang, *Green Chem.* **2019**, *21*, 897–906.
- [246] M. Imran, B. K. Kim, M. Han, B. G. Cho, D. H. Kim, *Polym. Degrad. Stab.* **2010**, *95*, 1686–1693.
- [247] N. D. Pingale, V. S. Palekar, S. R. Shukla, *J. Appl. Polym. Sci.* **2010**, *115*, 249–254.
- [248] N. D. Pingale, S. R. Shukla, *Eur. Polym. J.* **2008**, *44*, 4151–4156.
- [249] R. López-Fonseca, I. Duque-Ingunza, B. de Rivas, S. Arnaiz, J. I. Gutiérrez-Ortiz, *Polym. Degrad. Stab.* **2010**, *95*, 1022–1028.
- [250] M. Zhu, S. Li, Z. Li, X. Lu, S. Zhang, *Chem. Eng. J.* **2012**, *185–186*, 168–177.
- [251] S. R. Shukla, V. S. Palekar, N. D. Pingale, *J. Appl. Polym. Sci.* **2008**, *110*, 501–506.
- [252] L. Bartolome, M. Imran, K. G. Lee, A. Sangalang, J. K. Ahn, D. H. Kim, *Green Chem.* **2014**, *16*, 279–286.
- [253] M. Imran, K. Lee, Q. Imtiaz, B. Kim, M. Han, B. Cho, D. Kim, *J. Nanosci. Nanotechnol.* **2011**, *11*, 824–828.
- [254] R. Wi, M. Imran, G. Lee, S. Yoon, B. Cho, D. Kim, *J. Nanosci. Nanotechnol.* **2011**, *11*, 6544–6549.
- [255] M. Imran, D. H. Kim, W. A. Al-Masry, A. Mahmood, A. Hassan, S. Haider, S. M. Ramay, *Polym. Degrad. Stab.* **2013**, *98*, 904–915.
- [256] A. M. Al-Sabagh, F. Z. Yehia, D. R. K. Harding, G. Eshaaq, A. E. ElMetwally, *Green Chem.* **2016**, *18*, 3997–4003.
- [257] F. R. Veregue, C. T. Pereira da Silva, M. P. Moisés, J. G. Meneguín, M. R. Guilherme, P. A. Arroyo, S. L. Favaro, E. Radovanovic, E. M. Girotto, A. W. Rinaldi, *ACS Sustainable Chem. Eng.* **2018**, *6*, 12017–12024.
- [258] K. Troev, G. Grancharov, R. Tsevi, I. Gitsov, *J. Appl. Polym. Sci.* **2003**, *90*, 1148–1152.
- [259] F. Pardal, G. Tersac, *Polym. Degrad. Stab.* **2006**, *91*, 2567–2578.
- [260] F. Pardal, G. Tersac, *Polym. Degrad. Stab.* **2007**, *92*, 611–616.
- [261] N. A. Rorrer, S. Nicholson, A. Carpenter, M. J. Biddy, N. J. Grundl, G. T. Beckham, *Joule* **2019**, *3*, 1006–1027.
- [262] S. Wang, C. Wang, H. Wang, X. Chen, S. Wang, *Polym. Degrad. Stab.* **2015**, *114*, 105–114.
- [263] R. Esquer, J. J. García, *J. Organomet. Chem.* **2019**, *902*, 120972.
- [264] D. J. Suh, O. O. Park, K. H. Yoon, *Polymer* **2000**, *41*, 461–466.
- [265] U. R. Vaidya, V. M. Nadkarni, *J. Appl. Polym. Sci.* **1987**, *34*, 235–245.
- [266] U. R. Vaidya, V. M. Nadkarni, *J. Appl. Polym. Sci.* **1989**, *38*, 1179–1190.
- [267] U. R. Vaidya, V. M. Nadkarni, *J. Appl. Polym. Sci.* **1988**, *35*, 775–785.
- [268] A. M. Atta, A. F. El-Kafrawy, M. H. Aly, A. A. Abdel-Aziz, *Prog. Org. Coat.* **2007**, *58*, 13–22.
- [269] A. M. Atta, S. I. Elnagdy, M. E. Abdel-Raouf, S. M. Elsaed, A. A. Abdel-Aziz, *J. Polym. Res.* **2005**, *12*, 373–383.
- [270] M. E. Tawfik, S. B. Eskander, *J. Elastomers Plast.* **2006**, *38*, 65–79.
- [271] K. S. Rebeiz, D. W. Fowler, D. R. Paul, *J. Appl. Polym. Sci.* **1992**, *44*, 1649–1655.
- [272] J. Kim, D. Jeong, C. Son, Y. Lee, E. Kim, I. I. Moon, *Korean J. Chem. Eng.* **2007**, *24*, 1076–1083.
- [273] S. R. Shukla, A. M. Harad, L. S. Jawale, *Polym. Degrad. Stab.* **2009**, *94*, 604–609.
- [274] K. Dutt, R. K. Soni, *Iran. Polym. J.* **2013**, *22*, 481–491.
- [275] K. R. Delle Chiaie, F. R. McMahon, E. J. Williams, M. J. Price, A. P. Dove, *Polym. Chem.* **2020**, *11*, 1450–1453.
- [276] S. C. Kosloski-Oh, Z. A. Wood, Y. Manjarrez, J. Pablo de los Rios, M. E. Fieser, *Mater. Horiz.* **2021**, *8*, 1084–1129.
- [277] J. A. Fuentes, S. M. Smith, M. T. Scharbert, I. Carpenter, D. B. Cordes, A. M. Z. Slawin, M. L. Clarke, *Chem. Eur. J.* **2015**, *21*, 10851–10860.
- [278] S. Bhadra, W. I. Dzik, L. J. Goossen, *J. Am. Chem. Soc.* **2012**, *134*, 9938–9941.
- [279] Y. Kratish, J. Li, S. Liu, Y. Gao, T. J. Marks, *Angew. Chem. Int. Ed.* **2020**, *59*, 19857–19861; *Angew. Chem.* **2020**, *132*, 20029–20033.
- [280] S. J. Chiu, W. H. Cheng, *Polym. Degrad. Stab.* **1999**, *63*, 407–412.
- [281] T. Yoshioka, E. Kitagawa, T. Mizoguchi, A. Okuwaki, *Chem. Lett.* **2004**, *33*, 282–283.
- [282] T. Yoshioka, T. Handa, G. Grause, Z. Lei, H. Inomata, T. Mizoguchi, *J. Anal. Appl. Pyrolysis* **2005**, *73*, 139–144.
- [283] S. Kumagai, G. Grause, T. Kameda, T. Yoshioka, *J. Mater. Cycles Waste Manage.* **2014**, *16*, 282–290.
- [284] T. Masuda, Y. Miwa, K. Hashimoto, Y. Ikeda, *Polym. Degrad. Stab.* **1998**, *61*, 217–224.
- [285] I. Wender, *Fuel Process. Technol.* **1996**, *48*, 189–297.
- [286] E.-S. El-Sayed, D. Yuan, *Green Chem.* **2020**, *22*, 4082–4104.
- [287] M. Podgoński, B. D. Fairbanks, B. E. Kirkpatrick, M. McBride, A. Martinez, A. Dobson, N. J. Bongiardina, C. N. Bowman, *Adv. Mater.* **2020**, *32*, 1906876.
- [288] S. J. Rowan, S. J. Cantrill, G. R. L. Cousins, J. K. M. Sanders, J. F. Stoddart, *Angew. Chem. Int. Ed.* **2002**, *41*, 898–952; *Angew. Chem.* **2002**, *114*, 938–993.
- [289] P. Chakma, D. Konkolewicz, *Angew. Chem. Int. Ed.* **2019**, *58*, 9682–9695; *Angew. Chem.* **2019**, *131*, 9784–9797.
- [290] N. Roy, B. Bruchmann, J.-M. Lehn, *Chem. Soc. Rev.* **2015**, *44*, 3786–3807.
- [291] R. L. Snyder, D. J. Fortman, G. X. De Hoe, M. A. Hillmyer, W. R. Dichtel, *Macromolecules* **2018**, *51*, 389–397.
- [292] P. Taynton, H. Ni, C. Zhu, K. Yu, S. Loob, Y. Jin, H. J. Qi, W. Zhang, *Adv. Mater.* **2016**, *28*, 2904–2909.
- [293] Z. Zou, C. Zhu, Y. Li, X. Lei, W. Zhang, J. Xiao, *Sci. Adv.* **2018**, *4*, No. eaaq0508.
- [294] Y. Zhang, H. Ying, K. R. Hart, Y. Wu, A. J. Hsu, A. M. Coppola, T. A. Kim, K. Yang, N. R. Sottos, S. R. White, J. Cheng, *Adv. Mater.* **2016**, *28*, 7646–7651.
- [295] K. Yu, Q. Shi, M. L. Dunn, T. Wang, H. J. Qi, *Adv. Funct. Mater.* **2016**, *26*, 6098–6106.
- [296] B. T. Worrell, M. K. McBride, G. B. Lyon, L. M. Cox, C. Wang, S. Mavila, C.-H. Lim, H. M. Coley, C. B. Musgrave, Y. Ding, C. N. Bowman, *Nat. Commun.* **2018**, *9*, 2804.
- [297] J. M. García, G. O. Jones, K. Virwani, B. D. McCloskey, D. J. Boday, G. M. ter Huurne, H. W. Horn, D. J. Coady, A. M. Bintaieb, A. M. S. Alabdulrahman, F. Alsewailam, H. A. A. Almegre, J. L. Hedrick, *Science* **2014**, *344*, 732–735.
- [298] W. A. Ogdan, Z. Guan, *J. Am. Chem. Soc.* **2018**, *140*, 6217–6220.
- [299] P. R. Christensen, A. M. Scheuermann, K. E. Loeffler, B. A. Helms, *Nat. Chem.* **2019**, *11*, 442–448.
- [300] R. E. Yardley, A. R. Kenaree, E. R. Gillies, *Macromolecules* **2019**, *52*, 6342–6360.
- [301] B. Fan, J. F. Trant, A. D. Wong, E. R. Gillies, *J. Am. Chem. Soc.* **2014**, *136*, 10116–10123.
- [302] J. A. Kaitz, C. E. Diesendruck, J. S. Moore, *J. Am. Chem. Soc.* **2013**, *135*, 12755–12761.
- [303] J. P. Lutz, O. Davydovich, M. D. Hannigan, J. S. Moore, P. M. Zimmerman, A. J. McNeil, *J. Am. Chem. Soc.* **2019**, *141*, 14544–14548.
- [304] K. A. Miller, E. G. Morado, S. R. Samanta, B. A. Walker, A. Z. Nelson, S. Sen, D. T. Tran, D. J. Whitaker, R. H. Ewaldt, P. V. Braun, S. C. Zimmerman, *J. Am. Chem. Soc.* **2019**, *141*, 2838–2842.
- [305] C. E. Diesendruck, G. I. Peterson, H. J. Kulik, J. A. Kaitz, B. D. Mar, P. A. May, S. R. White, T. J. Martinez, A. J. Boydston, J. S. Moore, *Nat. Chem.* **2014**, *6*, 623–628.
- [306] X. Hu, T. Zeng, C. C. Husic, M. J. Robb, *J. Am. Chem. Soc.* **2019**, *141*, 15018–15023.
- [307] K. N. Bauer, L. Liu, M. Wagner, D. Andrienko, F. R. Wurm, *Eur. Polym. J.* **2018**, *108*, 286–294.
- [308] T. Steinbach, F. R. Wurm, *Angew. Chem. Int. Ed.* **2015**, *54*, 6098–6108; *Angew. Chem.* **2015**, *127*, 6196–6207.
- [309] H. Busch, E. Schiebel, A. Sicking, S. Mecking, *Macromolecules* **2017**, *50*, 7901–7910.
- [310] D. Myers, T. Witt, A. Cyriac, M. Bown, S. Mecking, C. K. Williams, *Polym. Chem.* **2017**, *8*, 5780–5785.
- [311] F. Stempfle, P. Ortman, S. Mecking, *Chem. Rev.* **2016**, *116*, 4597–4641.
- [312] T. Haider, O. Shyshov, O. Suraeva, I. Lieberwirth, M. von Delius, F. R. Wurm, *Macromolecules* **2019**, *52*, 2411–2420.
- [313] H. T. Tee, I. Lieberwirth, F. R. Wurm, *Macromolecules* **2019**, *52*, 1166–1172.

- [314] J.-B. Zhu, E. M. Watson, J. Tang, E. Y. X. Chen, *Science* **2018**, *360*, 398–403.
- [315] R. M. Cywar, J.-B. Zhu, E. Y. X. Chen, *Polym. Chem.* **2019**, *10*, 3097–3106.
- [316] A. Sangroniz, J.-B. Zhu, X. Tang, A. Etxeberria, E. Y. X. Chen, *Nat. Commun.* **2019**, *10*, 3559.
- [317] E. Lizundia, V. A. Makwana, A. Larrañaga, J. L. Vilas, M. P. Shaver, *Polym. Chem.* **2017**, *8*, 3530–3538.
- [318] J. P. MacDonald, M. P. Shaver, *Polym. Chem.* **2016**, *7*, 553–559.
- [319] I. Vollmer, M. J. F. Jenks, M. C. P. Roelands, R. J. White, T. van Harmelen, P. de Wild, G. P. van der Laan, F. Meirer, J. T. F. Keurentjes, B. M. Weckhuysen, *Angew. Chem. Int. Ed.* **2020**, *59*, 15402–15423; *Angew. Chem.* **2020**, *132*, 15524–15548.
- [320] BP, BP's New Technology to Enable Circularity for Unrecyclable PET Plastic Waste, <https://www.bp.com/en/global/corporate/news-and-insights/press-releases/bp-new-technology-to-enable-circularity-for-unrecyclable-pet-plastic-waste.html>, (Accessed: 25th January 2021).

Manuscript received: February 25, 2021
Revised manuscript received: April 1, 2021
Accepted manuscript online: April 7, 2021
Version of record online: May 5, 2021

1.2. Post-publication Commentary

Whilst publication 1 provides a comprehensive overview for the chemical recycling of PLA and PET, the field is rapidly expanding, and thus the post-publication commentary aims to highlight key recent developments. This should not be considered exhaustive and particular focus will be made for (discrete) metal-mediated systems, which are most pertinent herein.

1.2.1. Chemical recycling of PLA

1.2.1.1. Transesterification to alkyl lactates

Recently, Mazzeo and co-workers have reported a series of discrete Zn(II)- and Mg(II)-complexes supported by tridentate {ONN} Schiff-base-type ligands that facilitate rapid PLA methanolysis under ambient conditions.^[8,9] Indeed, such progress promises to create new opportunities for low energy PLA recycling and inform future catalyst design. A detailed account of this work is provided in the post-publication commentary of Chapter 4.

Interestingly, Lamberti *et al.*^[10] have exploited synergistic dual catalytic systems for PLA alcoholysis. Zn(OAc)₂ and DMAP were found to exhibit the most pronounced Lewis acid-base pair cooperative effect, achieving 97% Me-LA yield within 80 min at 130 °C in THF {5 wt% total catalyst loading ($m(\text{Zn}(\text{OAc})_2) = m(\text{DMAP}) = 0.05 \text{ g}$), $n_{\text{ester}}:n_{\text{MeOH}} = 1:9$ }. Mechanistically it is proposed the dual-activation mechanism is akin to that noted for TBD in publication 1 (Figure 6), whereby Zn(OAc)₂ and DMAP activate the carbonyl and incoming nucleophile respectively. Comparatively, the use of either Zn(OAc)₂ or DMAP exclusively resulted in reduced activity, requiring up to 300 min for the latter to achieve comparably high Me-LA yield under identical conditions. A reduction in reaction temperature and the use of EtOH coincided with a significant decrease in process efficiency. In a follow up study, Zn(OAc)₂:TBD was found to exhibit superior activity, highlighting the importance of Lewis acid/base compatibility and scope for further system optimisation.^[11] Whilst such conditions are generally more forcing compared to literature examples, the process lends itself to industry owing to the use of cheap, air-stable and commercially available transesterification catalysts, confounded by process ease and scalability.

In publication 1, ionic liquids reported for PLA transesterification are generally limited by their high cost. However, Xie *et al.*^[12] recently reported a cost-effective quaternary ammonium fluoride catalyst (Figure 1.1), specifically tetramethylammonium fluoride (TMAF) (**1**), which can be readily prepared from inexpensive commercial precursors, namely potassium fluoride (KF) and tetramethylammonium hydroxide (NMe₄OH). Whilst TMAF exhibited modest activity for PLA methanolysis, requiring elevated temperatures between 90 – 110 °C to achieve near quantitative Me-LA yield within 1 h ($m_{\text{PLA}} = 0.1 \text{ g}$, 25 mL of 0.01 mol dm⁻³

TMAF methanol solution}, excellent thermal and chemical stability is noted. Additionally, TMAF could be easily recovered and retained good catalyst performance across 5 reuse cycles, whilst GPC and NMR analysis implicated the F⁻ anion as the active centre. Although limited by process efficiency, this work promises to create new opportunities for the development of low cost organocatalysts for PLA recycling, further increasing their industrial relevance.

Promisingly, Liptrot and co-workers have also shown the potential of a rigidly oriented diamine (**2**) to selectively degrade PLA in the presence of either poly(caprolactone) (PCL) or PET (Figure 1.1).^[13] Given the abundance of commercial diamines, such findings promise to stimulate new developments within the field, whilst analogous phosphamides offer a possible solution to handling issues associated with air-sensitivity.

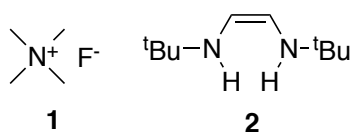


Figure 1.1. Organocatalysts reported by Xie *et al.*^[12] (**1**) and English *et al.*^[13] (**2**) for PLA transesterification.

1.2.1.2. Reductive depolymerisation

Reductive depolymerisation is garnering increasing momentum as a promising strategy for the recycling of plastic waste, exemplified by a number of recent reviews.^[14,15] Notably, Lehnertz *et al.*^[16] recently reported the first example of PLA depolymerisation into lactic acid over a solid supported catalyst under aqueous conditions. Indeed, 94% lactic acid recovery was possible after 20 min in the presence of Ru/CeO₂, although high catalyst loadings (25 mg, 22 wt%) and harsh reaction conditions {200 °C, 100 bar H₂, 5 mL of H₂O} are noted. However, such high catalyst loadings are circumvented by the ease of catalyst recovery, although a re-reduction step is required to restore initial catalytic performance. Promisingly, the direct recycling of a mixed plastic feed comprising of polyhydroxybutyrate (PHB), PLA and PET was demonstrated, observing the formation of 3-hydroxybutyric acid (3-HBA) and lactic acid in high yield. The PET remained largely intact and could subsequently be isolated by filtration (96% recovery) before being redirected for recycling. Presently, the role of the H₂ reductant remains poorly understood, whilst techno-economic and life cycle analysis is required to further assess commercial viability.

Additionally, Cantat and co-workers have recently reported the use of a lanthanum(III) tris(amide) catalyst and Schwartz's reagent (Figure 1.2), namely La[N(SiMe₃)₂]₃ (**3**) and [Cp₂Zr(H)Cl] (**4**) respectively, to mediate the reductive depolymerisation of various commercial polyesters and polycarbonates.^[17,18] Furthermore, **3** represents the first example

of a 4f-metal complex being used in chemical depolymerisation, which proceeded readily under mild conditions for PLA and PET in the presence of pinacolborane (HBpin) as a hydride source. Promisingly, high selectivity was retained towards diols and alcohols following hydrolysis, although a high catalyst cost is noted in both instances, which hinders scalability. Indeed, cheap and simple metal-based salts, such as $Zn(OAc)_2 \cdot 2H_2O$, have also been reported as highly efficient and recyclable catalysts for such processes.^[19]

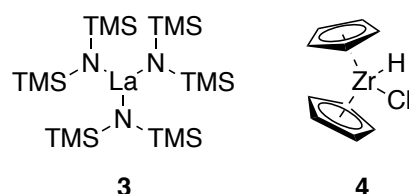


Figure 1.2. Metal-based catalysts reported by Cantat and co-workers that facilitate the reductive depolymerisation of various commercial polyesters and polycarbonates.^[17,18]

1.2.1.3. New methods

Traditionally, the recovery of *L*-lactide (*L*-LA) from PLLA has been limited by low selectivity and competing side reactions owing to a high monomer ceiling temperature (T_{mc}), which necessitates the use of either high reaction temperatures or multistep processes. In recent seminal work, Cederholm *et al.*^[20] addressed such issues through suppression of the T_{mc} by exploiting the impact of solvent interactions on the monomer-polymer equilibrium. Indeed, selecting solvents that strongly interact with the monomer, for example dimethylformamide (DMF), enabled high molecular weight PLLA ($M_n = 14,000 \text{ g mol}^{-1}$, $D = 1.13$) to be directly converted into *L*-LA within 1 – 4 h at 140 °C, observing high conversion (> 95%) and excellent selectivity (98 – 99%). Promisingly, high process efficiency was retained on exchanging the solvent for a green alternative, namely γ -valerolactone (GVL), and *L*-LA could be isolated and controllably repolymerised, thus closing the polymer loop (Figure 1.3). It is suggested this approach may be amenable to other monomer-polymer systems and will undoubtedly be a source of inspiration for future circular material design.

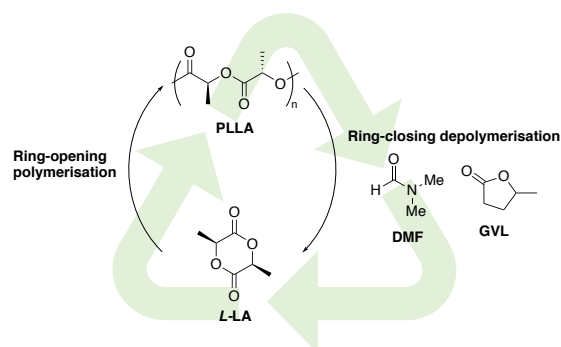
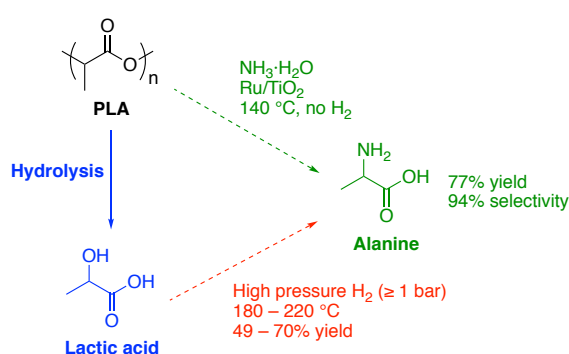


Figure 1.3. Closed-loop recycling of PLLA by exploiting monomer-polymer-solvent interactions.

Notably, Ma and co-workers have developed a novel one-pot catalytic approach to upcycle PLA waste into alanine, which is widely used in the food and pharmaceutical sector, by a simple ammonia solution treatment over a Ru/TiO₂ catalyst (Scheme 1.1).^[21] Importantly, no external H₂ is required, the reaction yields 77% alanine after 94 h at 140 °C under N₂ { $m_{PLA} = 0.25$ g, $n_{metal}:n_{ester} = 0.048$, 30 mL of NH₃·H₂O (25 wt%)} and an overall process selectivity of 94% can be achieved across 8 catalytic cycles. Crucially, the reaction proceeds under milder conditions relative to the amination of lactic acid {180 – 220 °C, ≥ 1 bar H₂, 49 – 70% yield of alanine}. Besides representing the first example of PLA aminolysis, this work also highlights the potential of plastic waste, in some instances, to be a more amenable feedstock for high value chemical production relative to platform chemicals such as lactic acid.



Scheme 1.1. Chemical upcycling of PLA and lactic acid into alanine *via* aminolysis.

Beyond such methods, it is anticipated emerging recycling technologies reviewed by Vollmer *et al.*^[22] will also find applications for PLA, which can be extended to PET. This is exemplified by recent work utilising PLA waste as a feedstock for solar-driven H₂ generation *via* photo-reforming.^[23,24]

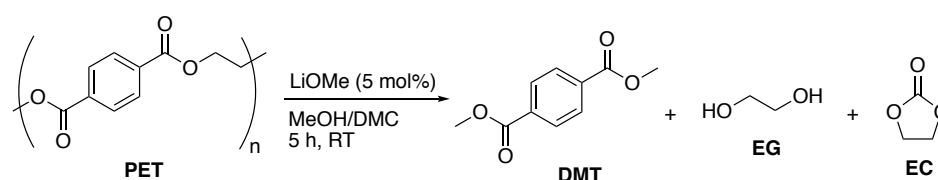
1.2.2. Chemical recycling of PET

Whilst the chemical recycling of PLA remains in its infancy, the field is vastly more developed for PET, which is reflected in both the diversity and number of examples reported to date. Consequently, developments pertaining to PET hydrolysis and ammonolysis will not be considered, although a number of recent reviews compliment the discussion provided in publication 1.^[25-28]

1.2.2.1. Methanolysis to dimethyl terephthalate (DMT)

Pioneering work by Hedrick *et al.*^[29] has previously shown PET methanolysis to be possible under ambient conditions in the presence of a patented N-heterocyclic carbene (NHC) catalyst, although the yield of DMT is limited to *ca.* 80%. A subsequently patented process by Essaddam *et al.*^[30] afforded superior product yield through judicious choice of the inorganic

base and organic solvent employed. However, this system remains limited by the use of a high catalyst loading (20 mol%), toxic halogenated solvent and prolonged reaction time (24 h). Recently, Nakajima and co-workers addressed such challenges by capturing ethylene glycol (EG) with dimethyl carbonate (DMC) to generate an ethylene carbonate (EC) by-product, which biased the product equilibrium towards DMT (Scheme 1.2).^[31] This enabled PET methanolysis catalysed by LiOMe (5 mol%) to proceed rapidly at room temperature, achieving *ca.* 90% DMT yield within 5 h $\{m_{PET} = 100 \text{ mg}, n_{ester}:n_{MeOH} = 1:4, 1.5 \text{ mL of DMC}\}$. Additionally, highly pure DMT could be isolated *via* filtration and washing with H₂O, whilst EC could potentially be used in battery applications following purification. It is envisaged this method will be applicable to other depolymerisation processes hindered by product equilibria, creating new opportunities for low-energy and selective chemical recycling.



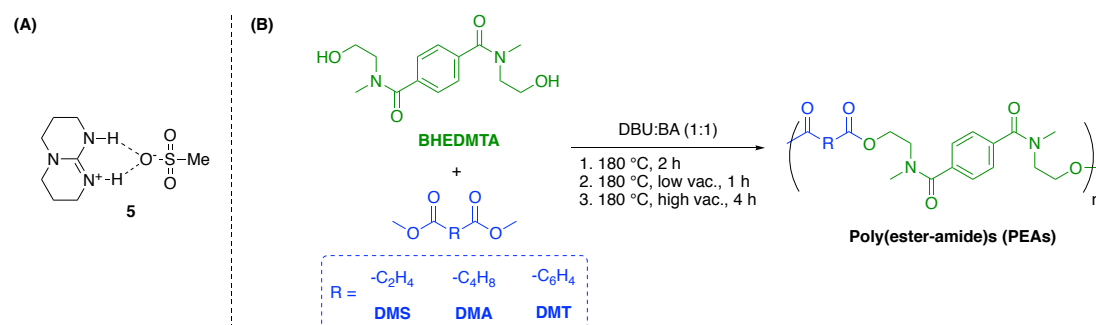
Scheme 1.2. Transesterification of PET in a MeOH/DMC mixture under ambient conditions in the presence of a metal-alkoxide catalyst.

Comparatively, Pham *et al.*^[32] exploited the use of a co-solvent, namely dichloromethane (DCM), to facilitate PET methanolysis under ambient conditions in the presence of a simple, cheap and non-toxic metal salt, namely K₂CO₃. However, a prolonged reaction time (24 h) was required to achieve comparable DMT yield (up to 93%) despite the use of a large excess of MeOH and DCM $\{m_{PET} = 1 \text{ g}, n_{ester}:n_{MeOH}:n_{DCM} = 1:50:50\}$, although a lower catalyst loading is noted (2 mol%). Whilst the use of a toxic halogenated co-solvent is undesirable from a scale-up perspective, this could possibly be remedied through the use of a green alternative, which provides scope for further system optimisation.

1.2.2.2. Aminolysis to diamines of terephthalic acid

Recently, Demarteau *et al.*^[33] employed a thermally stable protic ionic salt (TBD:MSA; Scheme 1.3, **5** in **A**) to catalyse the depolymerisation of PET in the presence of various diamines, yielding high value terephthalamides in moderate to excellent yield (55 – 93%). Upon isolation (87% yield), bis(2-hydroxyethyl) dimethylterephthalamide (BHEDMTA) was used as a synthon, in combination with various dimethyl esters, for the production of several poly(ester-amide)s (PEAs), relying on organocatalysed (DBU:BA) polycondensation in the melt (Scheme 1.3, **B**). Promisingly, molecular weights up to 10,000 g mol⁻¹ were observed and multifunctional diols were explored as a method of inducing crosslinking to overcome limitations associated with low *M_n*. Importantly, this work promises to stimulate exciting new

developments relating to the use of such building blocks for the production of higher value-added materials, exemplified by a number of recent examples.^[34,35]



Scheme 1.3. (A) TBD:MSA organocatalyst (**5**) reported by Sardon and co-workers, and; (B) melt polycondensation of BHEDMTA with various dimethyl esters for PEA production.^[33]

1.2.2.3. Glycolysis to bis(2-hydroxyethyl) terephthalate (BHET)

PET glycolysis continues to receive significant attention within the field, however, newly reported systems generally exhibit comparable activity to those reviewed in publication 1. Consequently, such systems will not be discussed herein, which have been comprehensively reviewed by a number of recent reports.^[25,28] Indeed, organocatalytic strategies continue to dominate the literature, whilst discrete homogeneous metal-based examples remain rare.^[36,37] Despite this clear opportunity, only one example, to the best of our knowledge, has been reported beyond those detailed in publication 1. Specifically, Deng *et al.*^[38] utilised an inexpensive and easily prepared tropine-Zn(OAc)₂ complex (**6**), which afforded 100% PET conversion and a BHET yield of 82% within 2 h at 190 °C ($m_{PET} = 5$ g, $m_{PET}:m_{catalyst}:m_{EG} = 20:1:5$) (Figure 1.4). Promisingly, **6** could also be recycled, although a steady decrease in activity was observed across 5 reuse cycles (down to *ca.* 77% PET conversion under identical conditions), which could be attributed to a gradual loss of catalyst during the recovery process.

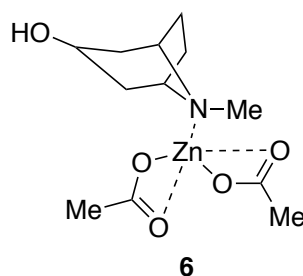
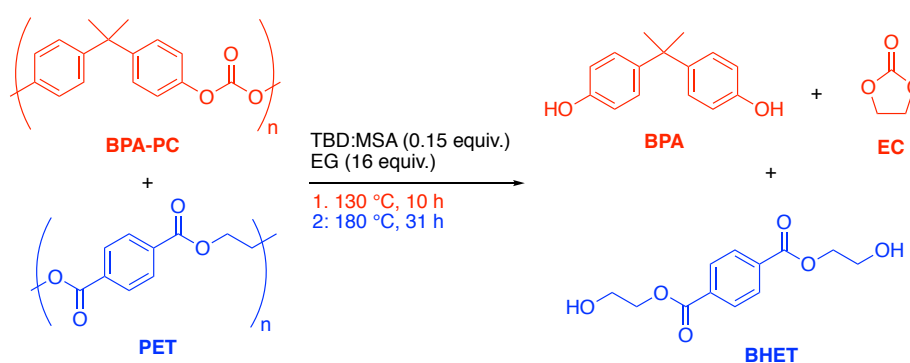


Figure 1.4. A highly active tropine-Zn(OAc)₂ catalyst (**6**) reported by Deng *et al.*^[38] for PET glycolysis.

Encouragingly, selective recycling is receiving increasing interest owing to industrial relevance, although literature examples remain limited. Notably, Sardon and co-workers have

recently employed a thermally stable and recyclable organocatalyst (Scheme 1.3, **5** in **A**) for the solvent-free and selective upcycling of mixed PET and poly(bisphenol A carbonate) (BPA-PC) waste (Scheme 1.4).^[39] The process enables monomer recovery, yielding BHET and bisphenol A (BPA) *via* sequential degradation, which relies on leveraging the difference in activation energy between PET and BPC-PC glycolysis. Furthermore, judicious choice of the nucleophile allows the production of various high value cyclic carbonates. Crucially, it is proposed this method could be applicable to other mixed plastic waste streams and highly contaminated commercial blends.



Scheme 1.4. Selective glycolysis of a mixed PET/BPC-PC feed in the presence of TBD:MSA.

Subsequently, Thielemans *et al.*^[40] have reported the ultrafast and selective degradation of a mixed PET/BPA-PC feed *via* an inexpensive KOH-in-MeOH hydrolysis (KMH) process. Principally, this study serves to further highlight the diversity of possible solutions to such prevalent challenges within the field.

1.2.2.4. Reductive depolymerisation

Recently, a number of significant advancements have been made concerning the reductive depolymerisation of PET.^[14] Consequently, a number of high impact examples have been chosen to highlight such progress.

Remarkably, Jing *et al.*^[41] have reported the first example of upgrading various aromatic plastic waste mixtures containing C-O and/or C-C linkages to arenes (75 – 85% yield) *via* catalytic hydrogenolysis over a Ru/Nb₂O₅ catalyst. For PET a total product yield of *ca.* 84% was obtained within 8 h at 280 °C, observing a mixed feed comprised of *p*-xylene (45%), toluene (41%) and benzene (14%) {m(feedstock) = m(Ru/Nb₂O₅) = 30 mg, 4 g of octane, 5 bar H₂}. Recently, Marks and co-workers employed a solvent-free tandem hydrogenolytic approach using two air- and moisture-stable catalysts, namely Hf(OTf)₄ and Pd/C, to depolymerise various commodity polyesters including PET.^[42] The process proceeds in high yield and selectively under 1 atmosphere of H₂, affording near quantitative conversion of terephthalic acid and ethane within 24 h at 265 °C. Finally, in a complimentary study, Li *et*

al.^[43] have developed a simple one-pot PET upcycling strategy that exploits a dual-promotion effect through the synergistic coupling of CO₂ hydrogenation and PET methanolysis. This in turn allows the thermodynamic constraints associated with CO₂ to be overcome, which is utilised as a solvent precursor. Specifically, PET initially undergoes methanolysis to yield DMT, which is subsequently hydrogenated to either dimethyl cyclohexanedicarboxylate (DMCD) or *p*-xylene.

Whilst such examples remain hindered by the use of high temperature and pressure regimes, they will undoubtedly inspire key future developments, particularly relating to the use of tandem catalysis. This could potentially help address a number of key challenges within the field, for example CO₂ utilisation and selective recycling.

1.3. References

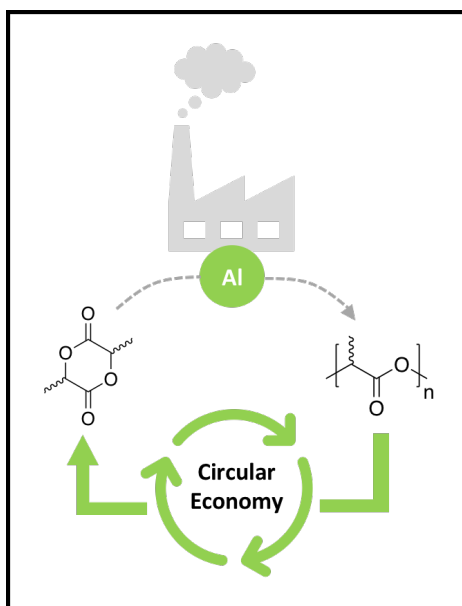
- [1] R. C. Thompson, C. J. Moore, F. S. vom Saal, S. H. Swan, *Philos. Trans. R. Soc. B* **2009**, *364*, 2153–2166.
- [2] R. A. Sheldon, M. Norton, *Green Chem.* **2020**, *22*, 6310–6322.
- [3] C. Jehanno, J. W. Alty, M. Roosen, S. De Meester, A. P. Dove, E. Y.-X. Chen, F. A. Leibfarth, H. Sardon, *Nature* **2022**, *603*, 803–814.
- [4] J. Payne, P. McKeown, M. D. Jones, *Polym. Degrad. Stab.* **2019**, *165*, 170–181.
- [5] Z. O. G. Schyns, M. P. Shaver, *Macromol. Rapid Commun.* **2021**, *42*, 2000415.
- [6] Plastics Europe, Plastics - the Facts 2021. An Analysis of European Plastics Production, Demand and Waste Data, <https://plasticseurope.org/knowledge-hub/plastics-the-facts-2021/>, (Accessed: 30th June 2022).
- [7] Ellen MacArthur Foundation, The New Plastics Economy: Rethinking the Future of Plastics, <https://ellenmacarthurfoundation.org/the-new-plastics-economy-rethinking-the-future-of-plastics>, (Accessed: 30th June 2022).
- [8] F. Santulli, M. Lamberti, M. Mazzeo, *ChemSusChem* **2021**, *14*, 5470–5475.
- [9] F. Santulli, G. Gravina, M. Lamberti, C. Tedesco, M. Mazzeo, *Mol. Catal.* **2022**, *528*, 112480.
- [10] F. M. Lamberti, A. Ingram, J. Wood, *Processes* **2021**, *9*, 921.
- [11] F. M. Lamberti, L. A. Román-Ramírez, A. P. Dove, J. Wood, *Polymers* **2022**, *14*, 1763.
- [12] S. Xie, Z. Sun, T. Liu, J. Zhang, T. Li, X. Ouyang, X. Qiu, S. Luo, W. Fan, H. Lin, *J. Catal.* **2021**, *402*, 61–71.
- [13] L. E. English, M. D. Jones, D. J. Liptrot, *ChemCatChem* **2022**, *14*, e2021019.
- [14] A. C. Fernandes, *Green Chem.* **2021**, *23*, 7330–7360.
- [15] C. Wang, O. El-Sepelgy, *Curr. Opin. Green Sustain. Chem.* **2021**, *32*, 100547.
- [16] M. S. Lehnertz, J. B. Mensah, R. Palkovits, *Green Chem.* **2022**, *24*, 3957–3963.
- [17] M. Kobylarski, J.-C. Berthet, T. Cantat, *Chem. Commun.* **2022**, *58*, 2830–2833.
- [18] L. Donnelly, M. Kobylarski, J.-C. Berthet, T. Cantat, **2022**, ChemRxiv preprint DOI: 10.26434/chemrxiv-2022-xtzxx.
- [19] A. C. Fernandes, *ChemSusChem* **2021**, *5*, 4228–4233.
- [20] L. Cederholm, J. Wohler, P. Olsén, M. Hakkarainen, K. Odellius, *Angew. Chem. Int. Ed.* **2022**, e202204531.
- [21] S. Tian, Y. Jiao, Z. Gao, Y. Xu, L. Fu, H. Fu, W. Zhou, C. Hu, G. Liu, M. Wang, D. Ma, *J. Am. Chem. Soc.* **2021**, *143*, 16358–16363.

- [22] I. Vollmer, M. J. F. Jenks, M. C. P. Roelands, R. J. White, T. van Harmelen, P. de Wild, G. P. van der Laan, F. Meirer, J. T. F. Keurentjes, B. M. Weckhuysen, *Angew. Chem. Int. Ed.* **2020**, *59*, 15402–15423.
- [23] T. Uekert, M. F. Kuehnel, D. W. Wakerley, E. Reisner, *Energy Environ. Sci.* **2018**, *11*, 2853–2857.
- [24] T. Uekert, H. Kasap, E. Reisner, *J. Am. Chem. Soc.* **2019**, *141*, 15201–15210.
- [25] E. Barnard, J. J. R. Arias, W. Thielemans, *Green Chem.* **2021**, *23*, 3765–3789.
- [26] M. Dolores de Dios Caputto, R. Navarro, J. López Valentín, Á. Marcos-Fernández, *J. Polym. Sci.* **2022**, 1–15.
- [27] K. Ghosal, C. Nayak, *Mater. Adv.* **2022**, *3*, 1974–1992.
- [28] M. Chu, Y. Liu, X. Lou, Q. Zhang, J. Chen, *ACS Catal.* **2022**, *12*, 4659–4679.
- [29] J. L. Hedrick, P. Kilickiran, G. W. Nyce, R. M. Waymouth, US Pat. 6911546 B2, **2005**.
- [30] H. Essaddam, US Pat. 9550713 B1, **2017**.
- [31] S. Tanaka, J. Sato, Y. Nakajima, *Green Chem.* **2021**, *23*, 9412–9416.
- [32] D. D. Pham, J. Cho, *Green Chem.* **2021**, *23*, 511–525.
- [33] J. Demarteau, I. Olazabal, C. Jehanno, H. Sardon, *Polym. Chem.* **2020**, *11*, 4875–4882.
- [34] Y.-H. Chen, P. Ranganathan, Y.-H. Lee, S.-P. Rwei, *ACS Sustainable Chem. Eng.* **2021**, *9*, 3518–3528.
- [35] J. M. Payne, M. Kamran, M. G. Davidson, M. D. Jones, *ChemSusChem* **2022**, *15*, e202200255.
- [36] C. Jehanno, M. M. Pérez-Madrigal, J. Demarteau, H. Sardon, A. P. Dove, *Polym. Chem.* **2019**, *10*, 172–186.
- [37] H. Sardon, M. Valle, X. Lopez de Pariza, M. Ximenis, J. M.W. Chan, *Angew. Chem. Int. Ed.* **2022**, e202203043.
- [38] L. Deng, R. Li, Y. Chen, J. Wang, H. Song, *J. Mol. Liq.* **2021**, *334*, 116419.
- [39] C. Jehanno, J. Demarteau, D. Mantione, M. C. Arno, F. Ruipérez, J. L. Hedrick, A. P. Dove, H. Sardon, *Angew. Chem. Int. Ed.* **2021**, *60*, 6710–6717.
- [40] J. J. R. Arias, E. Barnard, W. Thielemans, *ChemSusChem* **2022**, e202200625.
- [41] Y. Jing, Y. Wang, S. Furukawa, J. Xia, C. Sun, M. J. Hülsey, H. Wang, Y. Guo, X. Liu, N. Yan, *Angew. Chem. Int. Ed.* **2021**, *60*, 5527–5535.
- [42] Y. Kratish, T. J. Marks, *Angew. Chem. Int. Ed.* **2022**, *61*, e202112576.
- [43] Y. Li, M. Wang, X. Liu, C. Hu, D. Xiao, D. Ma, *Angew. Chem. Int. Ed.* **2022**, *61*, e2021172.

Chapter 2.

Development of Industrially Relevant Aluminium Catalysts for PLA Production

Publication 2: Novel hybrid aluminium(iii)–catalen complexes as highly active catalysts for lactide polymerisation: towards industrial relevance



Acknowledgement: The work presented in this chapter has been published in the journal *‘Chemical Communications’*, volume 56, issue 52, pages 7163–7166 and is reproduced with the permission of the Royal Society of Chemistry. The electronic supporting information (ESI) has been amended into a supporting experimental section for clarity. Additional figures (*e.g.* representative NMR spectra) have been added, where appropriate, to support the work presented herein.

2. Preamble

In Chapter 1, PLA was introduced as a promising commercial bio-based polymer with applications in the biomedical and packaging industry.^[1-6] However, despite being revered for its green credentials, PLA waste is still a potential contributor to plastic pollution since biodegradation occurs exclusively under industrial compositing conditions.^[7-9] Therefore, Chapter 1 focused primarily on the need to develop sustainable chemical recycling strategies to remedy such concerns, however, issues remain surrounding its production. Indeed, toxicity concerns associated with the industry standard catalyst, namely Sn(Oct)₂, has created an industry appetite for the development of more sustainable and biocompatible alternatives.^[10-13]

Consequently, Chapter 2 aims to expand on the introduction to PLA provided in Chapter 1 through a mini-review. Possible monomer and PLA production processes will be discussed in greater detail before introducing relevant mechanistic pathways, specifically metal-mediated coordination-insertion and activated-monomer. The concept of stereocontrol will then be introduced and the subsequent relationship between polymer tacticity and observed material properties highlighted. Finally, polymer characterisation techniques (*e.g.* NMR spectroscopy, SEC and MALDI-ToF) will be presented before discussing initiators reported for lactide polymerisation, focusing on metal-based systems, principally Al(III), which are most pertinent herein.

Initiators based on Al(III) have been extensively studied for the ring-opening polymerisation (ROP) of cyclic esters due to it being a cheap, abundant and biocompatible metal.^[12,14] Traditionally, Al(III)-based initiators exhibit good stereocontrol but low activity, typically requiring elevated temperatures (≥ 70 °C) and high catalyst loadings (~ 1 mol%) to be appreciably active. Furthermore, literature examples are limited almost exclusively to solution phase production, whilst the development of initiators that retain both high activity and stereocontrol under industrially relevant melt conditions remains a prevalent challenge in the field.^[15,16]

In this chapter, adventitious features of two well established ligands, namely the salen (*e.g.* easily prepared and functionally versatile) and catam (*e.g.* non-covalent interactions), are integrated into the design of a novel hybrid ligand framework: the catalen. Crucially, in combination with Al(III), such initiators were found to facilitate rapid PLA production in the melt, furnishing polymer of high M_n ($> 10,000$ g mol⁻¹) under industrially relevant loadings (0.033 mol%) for the first time. Additionally, high activity is retained in solution under ambient conditions, observing an unusual stereoselectivity switch dependent on the ligand substituents employed.

2.1. Introduction

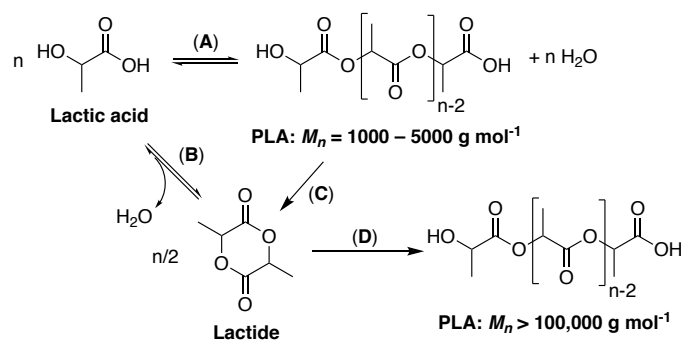
2.1.1. Synthesis

2.1.1.1. Lactic acid production

As previously discussed in Chapter 1, PLA is a renewable and biodegradable aliphatic polyester based on a repeating lactic acid monomer, sourced from the microbial fermentation of starch-rich feedstocks, such as corn and sugar.^[17,18] Indeed, industrial scale lactic acid production relies on a batch fermentation process, which typically takes between 3 – 6 days and accounts for *ca.* 50% of total PLA production costs. Whilst optimal process efficiency is observed under high concentrations of lactic acid, a neutral pH is maintained to preserve optimal activity of the bacteria employed. This is achieved through either the addition of Ca(OH)₂ or CaCO₃ to produce calcium lactate, which readily crystallises. Crude lactic acid is then liberated *via* acidification with H₂SO₄.^[7,19-21] In the last 10 years, significant attention has been devoted to process cost reduction *via* the development of one-step processes (*e.g.* shape-selective catalysis and gas-phase reactions) for lactide production, as highlighted in Chapter 1.^[8]

2.1.1.2. Polycondensation of lactic acid

PLA can be produced *via* the polycondensation of lactic acid, which liberates H₂O (Scheme 2.1, **A**).^[7,22] However, this step-growth process is limited by inherently poor polymerisation control, resulting in PLA of low number average molecular weight ($M_n = 1000 - 5000 \text{ g mol}^{-1}$).



Scheme 2.1. Synthesis routes for PLA of low and high M_n .

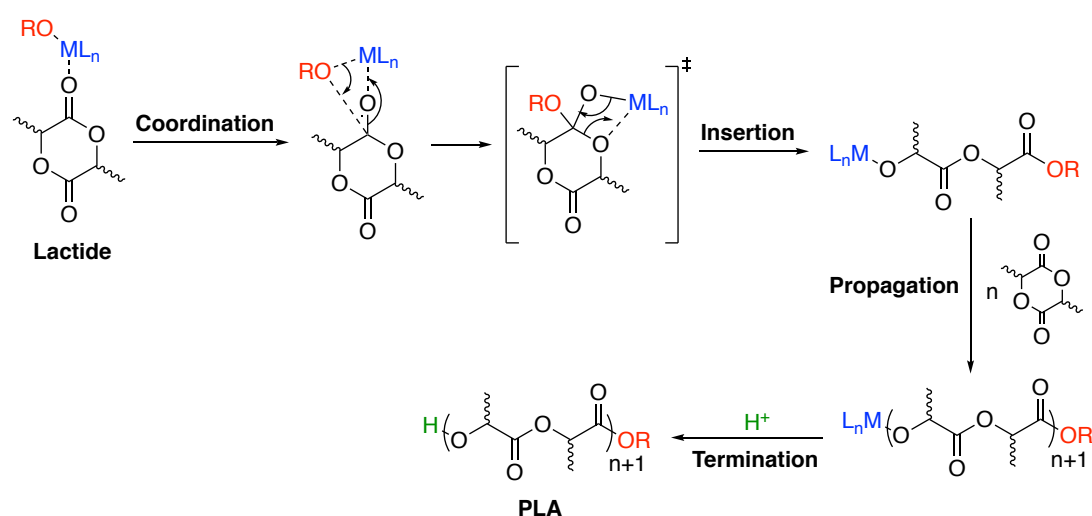
Additionally, the lactic acid starting material can undergo intermolecular condensation to generate lactide, a six-membered by-product (Scheme 2.1, **B**), which further inhibits polymerisation control. Indeed, in accordance to the Carother's equation (Equation 2.1), this back-biting equilibrium reaction reduces the conversion (p) of lactic acid to PLA, resulting in a low degree of polymerisation (DP):

$$DP = \frac{1}{1-p} \quad (2.1)$$

Furthermore, the presence of H₂O impurities can induce chain transfer, further exacerbating PLA chain growth inhibition. Consequently, chain-coupling agents, such as acid chlorides or anhydrides, are commonly used to access PLA of sufficiently high M_n ($\geq 10,000$ g mol⁻¹) for industrial application, albeit at the expense of increased process cost and complexity.^[7,19,22,23] Alternatively, superior monomer conversion to PLA is also possible through the use of elevated temperatures and reduced pressures, which promotes the removal of the H₂O by-product, shifting the polymerisation equilibrium in favour of the PLA product, as per Le Châtelier's principle (Scheme 2.1, **A**).^[24] However, this is not conducive to low energy polymer production, and thus is undesirable in the face of mounting environmental concerns and public scrutiny. There is therefore a clear opportunity to develop more sustainable and environmentally friendly synthesis routes. One such example is lactide production *via* the ring-closing depolymerisation (RCD) of low M_n PLA (Scheme 2.1, **C**), followed by ROP (Scheme 2.1, **D**).^[6,7,19,25]

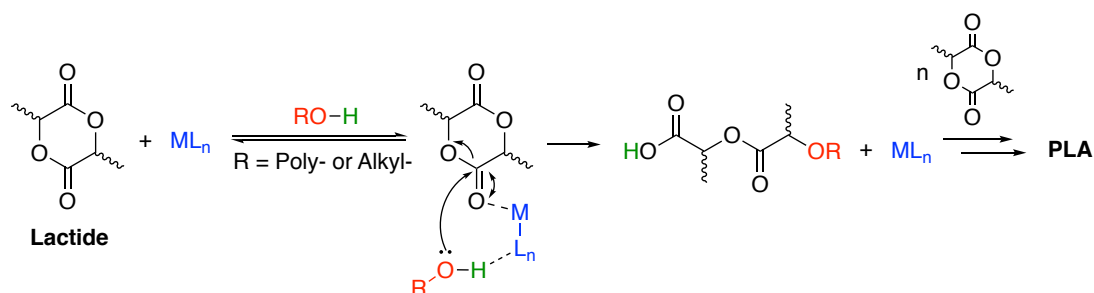
2.1.1.3. ROP of lactide

Pioneering work by Carothers *et al.*^[26] in the 1930s demonstrated the first example of PLA production *via* the ROP of lactide (LA), which is employed on an industrial scale to access PLA of high and well-defined M_n (Scheme 2.1, **D**).^[5-7,19,25,27] The ROP of lactide, as with all polymerisation processes, is intrinsically entropically unfavourable ($\Delta S_{(\text{ROP of lactide})} = -41.1$ J K⁻¹ mol⁻¹). However, this is offset by a dominant thermodynamic driving force arising from the ring-strain relief provided during ring-opening of the monomer ($\Delta H_{(\text{ROP of lactide})} = -23.0$ kJ mol⁻¹).^[7,27] A variety of ROP methods have been reported in the literature, including anionic and cationic-mediated systems.^[6,7,19] However, this introduction will focus on two mechanisms, namely coordination-insertion and activated-monomer, which are most relevant herein.



Scheme 2.2. Metal-mediated coordination-insertion mechanism for the ROP of lactide. *N.B.* H⁺ corresponds to a proton source, such as an acid, alcohol or H₂O.

The coordination-insertion mechanism (Scheme 2.2) is characterised by activation of the lactide monomer *via* coordination of the carbonyl carbon to a Lewis acidic metal centre (M) bearing a labile ligand, typically an alkoxide (-OR). A four-membered ring intermediate is subsequently formed through insertion of the M-OR bond. Ring-opening ensues *via* cleavage of the acyl bond, generating a new metal-alkoxide bond. Propagation proceeds through the insertion of incoming lactide monomer units until the addition of a proton source, which terminates the polymerisation reaction. The growing polymer chain is characterised by two distinct terminal functional end-groups: 1. An ester group furnished from the alkoxide insertion step, and; 2. A metal-based end-cap, which is converted to a hydroxyl group through hydrolysis of the M-O bond during the termination step.^[7] Good polymerisation control is often achieved by virtue of the growing polymer chain being retained on the metal centre, allowing PLA of high and well-defined M_n ($> 100,000 \text{ g mol}^{-1}$) to be accessed. Additionally, coordination-insertion can be performed in the monomer melt (*i.e.* under solvent-free conditions), circumventing the use of potentially expensive and toxic solvents, which are routinely used in traditional anionic and cationic-mediated systems.^[7,11] Consequently, the metal-mediated coordination-insertion mechanism is of significant commercial interest and is widely considered the most synthetically useful method of choice in the ROP of lactide.^[6,7,19]



Scheme 2.3. Metal-mediated activated-monomer mechanism for the ROP of lactide in the presence of a co-initiator, typically an alcohol.

Comparatively, an activated-monomer mechanism (Scheme 2.3) proceeds for the ROP of lactide in the absence of a labile group on a coordinatively unsaturated metal centre, which necessitates the use of a co-initiator, typically an alcohol.^[28]

The ROP of lactide can also be conducted under metal-free conditions through the use of an organocatalyst, which has been widely reported in the literature.^[29-33] Furthermore, diverse and functional polymer architectures (*e.g.* polymer stars) are accessible through judicious choice of the initiating system employed.^[34,35] However, such chemistry falls beyond the scope of this thesis and thus is not discussed in greater detail herein. In summary, both the metal-mediated coordination-insertion and activated-monomer mechanism represent two of the most commercially attractive methods for producing PLA, and thus are the methods of choice used in this work.

2.1.2. Stereocontrol

2.1.2.1. Stereoisomerism of lactic acid and lactide

Lactic acid possesses intrinsic chirality owing to the presence of a chiral centre at the α -carbon relative to the terminal ester functional group, resulting in two optically active enantiomers: *L* (-) and *D* (+), affording three distinct configurations: *L*-, *D*- and *meso*-lactide (*L*-LA, *D*-LA and *meso*-LA, respectively) (Figure 2.1). Lactide can be sourced commercially either as the pure *L*-isomer or a 50:50 racemic mixture comprising of the *L*- and *D*-isomers, namely *rac*-lactide (*rac*-LA).^[1,5,7,36]

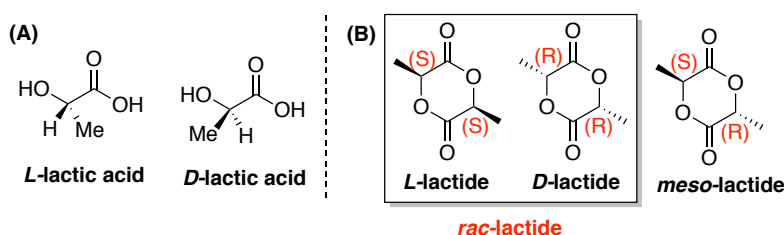


Figure 2.1. Stereoisomers of lactic acid (A) and lactide (B).

2.1.2.2. Tacticity of PLA

Tacticity refers to the relative stereochemistry of adjacent chiral centres within a macromolecule, which is dependent on both the configuration of the monomer and the order of insertion. Indeed, tacticity can have significant ramifications on the overall materials exhibited by the final polymer, which dictates end application.^[1,5,7] PLA can exhibit a variety of different tacticities, as seen in Figure 2.2, owing to the presence of two chiral centres per monomer unit. Possible stereochemical configurations are as follows:

1. **Isotactic:** A semi-crystalline material characterised by the presence of *-SS-* or *-RR-* repeat units, indicating all adjacent chiral centres possess the same stereochemical configuration. Consequently, all substituents reside on the same side along the polymer backbone. Isotactic PLLA and PDLA can be accessed *via* the ROP of *L*- and *D*-LA, respectively, in the absence of epimerisation, which induces the interconversion of stereocentres during polymerisation.
2. **Atactic:** An amorphous material that lacks long-range order owing to a completely random arrangement of stereocentres along the polymer backbone.
3. **Heterotactic:** Characterised by the presence of *-SSRR-* linkages within each repeat unit arising from the alternating insertion of *L*- and *D*-LA.
4. **Syndiotactic:** A semi-crystalline polymer, accessible *via* the ROP of *meso*-LA, that possesses alternating stereochemistry between adjacent chiral centres (*i.e.* *-SR-*), such that substituents alternate between sides along the polymer backbone.^[7]

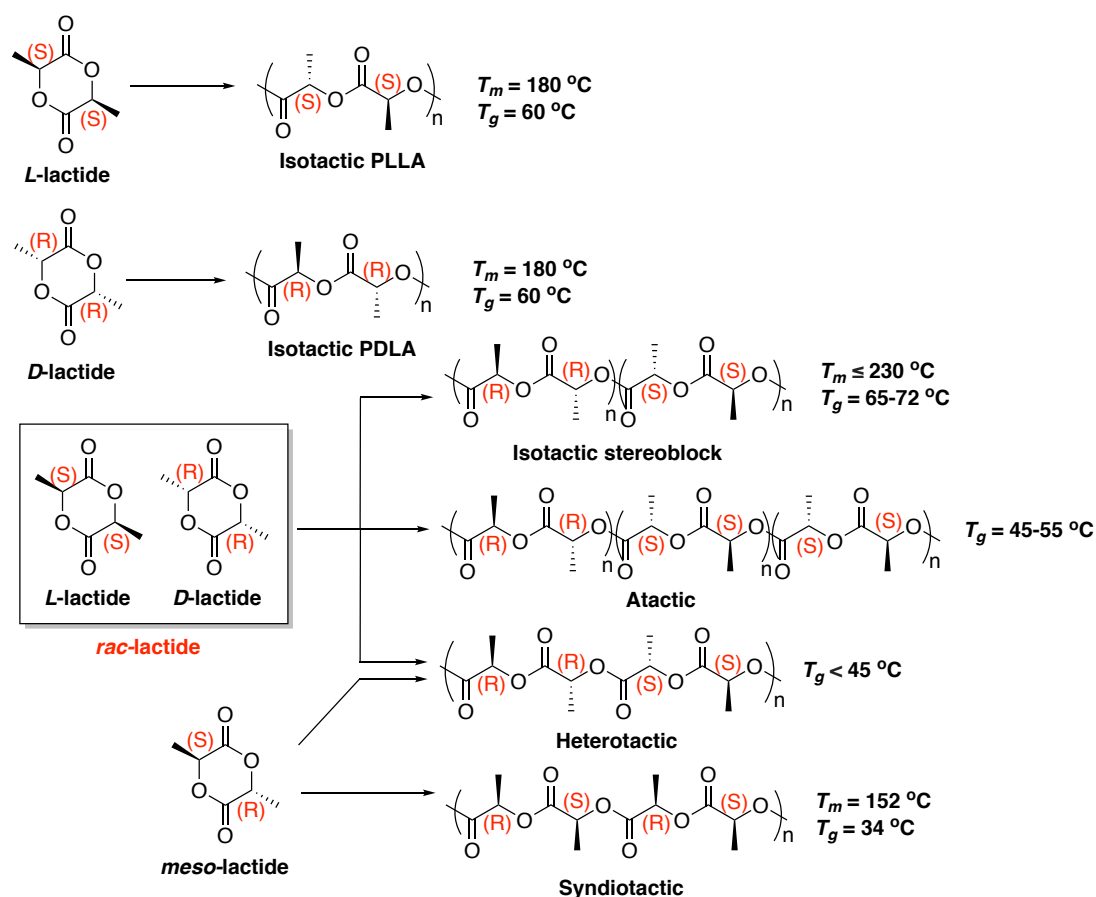


Figure 2.2. Possible tacticities accessible through the ROP of L-, D- and meso-LA for PLA production.

Tacticity plays a key role in influencing the degree of polymer crystallinity, and thus the extent to which polymer chains interact, which dictates the material properties exhibited by the final PLA product. Indeed, homopolymers of isotactic PLLA and PDLA (Figure 2.2) exhibit a high degree of crystallinity and regularity, reflected in a high and well-defined melting point ($T_m = 180\text{ }^\circ\text{C}$), whilst the T_m of atactic PLA remains undefined.^[7,37] Additionally, enhanced thermal properties for PLLA and PDLA can be realised through stereocomplexation (T_m up to $230\text{ }^\circ\text{C}$), either through mixing neat polymer chains or connected block-copolymers.^[38,39] Such work promises to expand the current product portfolio for PLA, which remains limited to predominantly single-use, disposable applications, owing to its generally poor heat resistance, brittleness and intrinsic hydrolytic instability.^[5,7,19] Another parameter frequently used to characterise polymeric materials is the glass transition temperature (T_g). Specifically, the T_g represents the temperature at which a polymer transitions from a hard, brittle material to a flexible, ‘glass-like’ state.^[7] Furthermore, manipulation of the T_g through precise control of polymer tacticity, crystallinity and M_n enables the material properties of the final polymer to be engineered to the desired end application. Consequently, catalyst development in pursuit of the stereoselective synthesis of PLA has attracted significant interest over the last 20 years.

Indeed, isotactic PLA represents the most commercially attractive option due to it possessing superior thermal and mechanical properties.^[7,25] However, before discussing metal-based initiators for PLA production, commonly used polymer characterisation methods will first be introduced.

2.1.3. Polymer characterisation

2.1.3.1. Nuclear magnetic resonance (NMR) spectroscopy

Monomer conversion is a parameter widely used to assess initiator activity for lactide polymerisation *via* inspection of the methine region ($\delta = 5.00 - 5.26$ ppm) using ^1H NMR spectroscopic analysis.^[40] The DP is observed to be directly proportional to monomer conversion, which can be calculated using Equation 2.2, where the relative peak area of the monomer ($RPA_{monomer}$) is normalised to 1:

$$\text{PLA conversion (\%)} = \frac{RPA_{polymer}}{RPA_{polymer} + RPA_{monomer}} \times 100 \quad (2.2)$$

Intuitively, consideration of conversion with time allows one to ascertain catalyst activity. Additionally, possible catalyst stereoselectivity can be probed through determination of polymer tacticity, which relies on the use of ^1H - ^1H homonuclear decoupling. For PLA produced *via* the ROP of *rac*-LA, five overlapping quartets are observed in the methine region due to methine-methyl coupling and the different stereochemical configurations possible. However, decoupling simplifies the methine region to five distinct singlets, with each peak corresponding to a series of four lactyl units, otherwise known as tetrads, as seen in Figure 2.3. below.^[40,41]

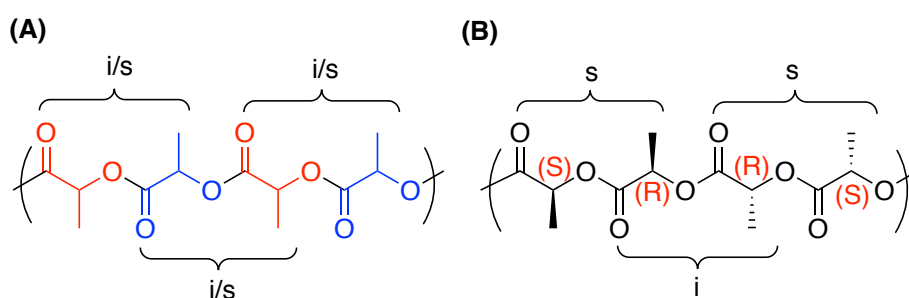


Figure 2.3. Polymeric backbone of PLA: (A) possible stereochemical relationships in a tetrad, with red and blue representing four separate lactyl units, and; (B) a tetrad example, where ‘i’ and ‘s’ denote an isotactic and syndiotactic unit respectively.

In the absence of detrimental epimerisation and transesterification side reactions, PLA produced from *rac*-LA can display up to five possible tetrads, specifically: *iii*, *isi*, *sis*, *sii* and *iis*, as shown in Figure 2.4.

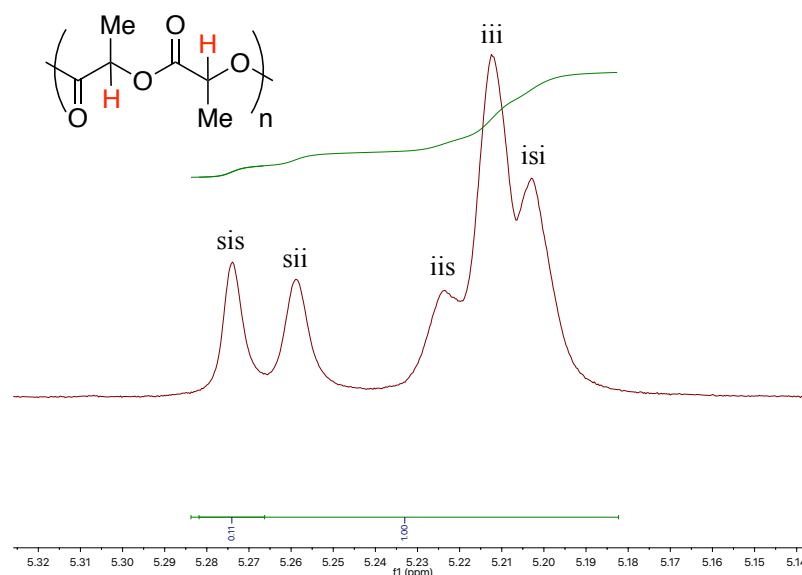


Figure 2.4. Homonuclear decoupled ^1H NMR (CDCl_3 , 400 MHz) spectrum of atactic PLA produced from *rac*-LA, displaying the five tetrad possibilities in the methine region.^[41,42]

In seminal work, Coates and co-workers found the probability of racemic/heterotactic enchainment, denoted as P_r , could be determined using Equation 2.3:^[42]

$$P_r = \sqrt{2[RPA_{sis}]} \quad (2.3)$$

Where RPA_{sis} corresponds to the relative peak area of the *sis* tetrad. The probability of meso/isotactic enchainment, denoted as P_m , can then be readily calculated as the sum of P_r and P_m is equal to 1. Possible polymer microstructure assignments based on P_r and P_m are tabulated in Table 2.1 below.^[43]

Table 2.1. PLA tacticity assignment based on P_r and P_m values.^[43]

P_r	P_m	Tacticity
$0.5 < P_r \leq 1$	$0 \leq P_m < 0.5$	Heterotactic
$0 \leq P_r < 0.5$	$0.5 < P_m \leq 1$	Isotactic
$P_r = 0.5$	$P_m = 0.5$	Atactic

2.1.3.2. Size exclusion chromatography (SEC)

SEC is an analytical technique used to determine both the molecular weight (M_w and M_n) and relative dispersity (\mathcal{D}) in a polymeric sample, which can be calculated using Equations 2.4–2.6 (from left to right):

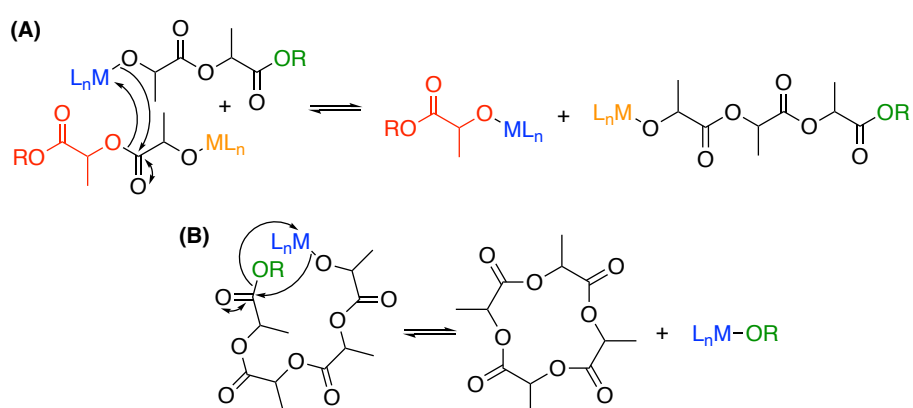
$$M_w = \frac{\sum M_i^2 N_i}{\sum M_i N_i}; M_n = \frac{\sum M_i N_i}{\sum N_i}; \mathcal{D} = \frac{M_w}{M_n} \quad (2.4-2.6)$$

Where N_i and M_i correspond to the total number and weight of polymer chains in the sample, respectively. Note M_w denotes the weight average molecular weight, whilst M_n refers to the

number average molecular weight, which describes the statistical average molecular weight of each polymer chain in the sample. Intuitively, D represents the breadth of M_w distribution within the polymer batch, with narrow dispersities often desirable. Indeed, D has a value ≥ 1 , which tends towards unity as polymer chains approach a uniform chain length.^[44] SEC relies on the use of a column containing porous microbeads, which exploits size exclusion principles to selectively separate molecules within a sample based on size. Specifically, small molecules readily diffuse into the column, and thus elute slowly, whilst large polymeric chains are excluded, resulting in faster elution. Refractive index (RI) response is the most commonly used detection method for analysing the SEC eluent, although a number of alternative methods are available. RIS relies on monitoring the change in refractive index of the sample relative to a cell of pure solvent, which is then calibrated against a known standard, for example polystyrene (PS), which exhibits a narrow distribution. However, since the hydrodynamic volume of a polymer in solution is sensitive to solvent effects, and dependent on the polymer type, observed M_w and M_n values cannot be considered absolute. Thus, a correction factor of 0.58 is routinely used for PLLA when detected against PS standards.^[45]

2.1.3.3. MALDI time-of-flight mass spectrometry (MALDI-ToF)

Matrix-assisted laser desorption/ionisation time-of-flight (MALDI-ToF) mass spectrometry is frequently used to complement SEC analysis for polymeric materials, assisting with monomer repeat unit and polymer end-group determination. Indeed, MALDI-ToF analysis provides spectra of enhanced resolution, enabling the quantification of individual polymer chain masses. Moreover, unexpected repeat unit masses provides insight into possible detrimental transesterification side reactions, as shown for PLA in Scheme 2.4 below.



Scheme 2.4. Inter- (A) and intramolecular (B) transesterification mechanisms for PLA.

MALDI-ToF is a multi-step procedure, the first of which focuses on selecting a suitable matrix and ion source to facilitate ionisation and charging of the polymer. The sample then undergoes desorption into the gas phase under irradiation, provided by a pulsed laser, prior to ionisation.

Finally, the ionised molecules undergo acceleration within a ToF spectrometer, which allows the time taken to reach the detector to be correlated to the ion mass, which obeys an inversely proportional relationship. Consideration of the distribution of said masses allows key information to be extracted about the polymeric material, as detailed above. However, the technique remains limited to a maximum M_n value of *ca.* 10,000 g mol⁻¹ owing to the need for the sample to be readily ionisable and susceptible to an electric field for analysis purposes. Consequently, the spectrum obtained may not necessarily be representative of the polymer sample analysed.^[41,46]

2.1.3.4. Differential scanning calorimetry (DSC)

The thermal properties of a polymeric material can be investigated using DSC analysis. The technique measures the heat flux required by a sample to maintain a prescribed heating rate relative to a reference. The difference in measured heat flux (exo- or endothermic) can then be subsequently plotted against temperature. This allows key material phase changes of the sample to be evaluated, namely the T_g and T_m , in addition to the crystallisation temperature (T_c).^[41,46]

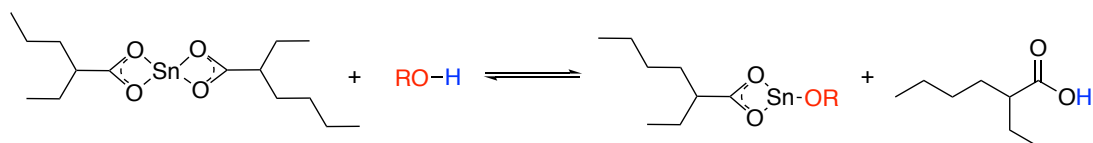
2.1.3.5. Thermogravimetric analysis (TGA)

Polymer degradation profiles can be ascertained using TGA analysis, which measures the sample mass change as a function of temperature. This allows key parameters such as T_{ons} and T_{inf} to be identified, which correspond to the temperature at which the polymer begins to thermally decompose and the fastest observed rate of degradation, respectively. Such parameters are of crucial importance to industry, where temperatures above the polymer melting point are often employed during processing.^[41,46]

2.1.4. Metal-based initiators for ROP of lactide

2.1.4.1. Industry standard

Industrially, PLA is manufactured *via* the ROP of *L*-LA under solvent-free conditions, which proceeds through a coordination-insertion mechanism (Scheme 2.2) in the presence of Sn(Oct)₂ {180 – 210 °C, [Sn(Oct)₂] = 100 – 1000 ppm } (Scheme 2.5).^[7,47,48] Sn(Oct)₂ is used due to it being cheap, commercially available and robust. Moreover, it exhibits high activity and exceptional solubility in cyclic esters, enabling PLLA of high and well-defined M_n to be produced, often in the presence of a co-initiator.^[48,49]



Scheme 2.5. Structure of tin(II) 2-ethylhexanoate, otherwise known as tin(II) octanoate; $\text{Sn}(\text{Oct})_2$. *N.B.* The presence of a co-initiator, commonly an alcohol, serves to generate the active species *via* an alkoxide exchange mechanism.^[7,10,48,49]

However, despite being approved by the US food and drug administration (FDA), toxicity concerns associated with $\text{Sn}(\text{Oct})_2$ has created an appetite for the development of sustainable and biocompatible alternatives, as noted in Chapter 1. Indeed, the suitability of $\text{Sn}(\text{Oct})_2$ for producing PLA destined for certain biomedical applications has been challenged in the literature.^[7,10,49] Moreover, difficulties associated with the complete removal of trace Sn residues from the polymer melt serve to confound such concerns.^[7,10,12,49] $\text{Sn}(\text{Oct})_2$ also offers no stereocontrol in the ROP of *rac*-LA, and thus an optically pure feed of *L*-LA is required, resulting in additional monomer processing costs.^[10,12,48,49] There is therefore a clear opportunity to address such challenges through the development of environmentally benign alternatives that exhibit both high catalyst activity and enhanced stereocontrol, particularly under industrially relevant melt conditions. Discrete metal-based alternatives represent a promising solution to this challenge, which remains an active area of research within the field. Indeed, examples based on a variety of different metals, including Mg(II), Zn(II) and group(IV), have been extensively reported.^[10-13,15,16] However, initiators based on Al(III) are most relevant to this chapter, and thus will form the basis of discussion herein.

2.1.4.2. Aluminium(III)

Al(III) is a cheap, abundant and biocompatible metal, which lends itself to the ROP of cyclic esters.^[12,14] Simple Al(III)-based initiators, such as $\text{Al}(\text{O}^i\text{Pr})_3$, have been reported to be highly active for the ROP of lactide, however, exhibit poor polymerisation control owing to a high degree of transesterification.^[50,51] Consequently, ligands with greater steric bulk have been explored as a means of achieving superior polymerisation and stereocontrol *via* expansion of the metals coordination sphere. Al(III)-complexes supported by tetradentate bis(phenolate) {ONNO} ligands are of particular importance to this chapter, particularly the so called ‘salen’ pro-ligand. Indeed, such ligands are easily accessible in high yield and purity *via* a simple imine condensation reaction, whilst also being functionally versatile, which provides significant scope for catalyst fine-tuning.

Early examples of isoselective Al(III)-initiators relied on the use of chiral salen-based pro-ligands as depicted in Figure 2.5. below. The first example of a highly stereoselective Al(III)-

initiator was reported in seminal work by Spassky *et al.*^[52] (**7**) who employed the use of an enantiomerically pure binaphthyl salen ligand backbone. *R*-**7** facilitates the ROP of *rac*-LA at 70 °C in toluene, whilst exhibiting an initial preference for *D*-LA insertion. Stereocomplexation was achieved through the preferential insertion of *L*-LA at high conversion, evidenced by an increase in polymer melting temperature ($T_m = 185 - 187$ °C). Highly isotactic PLA was obtained *via* an enantiomorphic site control mechanism, whereby the order of monomer insertion is dictated by the initial chiral preference of the initiator, which is retained throughout the polymerisation process. The versatility of this system has been subsequently demonstrated through the production of syndiotactic PLA from *meso*-LA and the use of racemic initiator (*rac*-**7**) to afford polymer with superior melting temperatures ($T_m = 210 - 230$ °C).^[53-56]

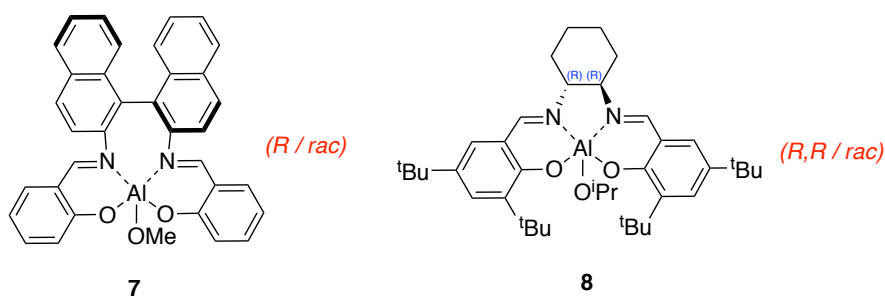


Figure 2.5. Early isoselective Al(III)-initiators reported by Spassky (**7**) and Feijen (**8**).^[52,57,58]

Feijen and co-workers exploited the use of Jacobsen's ligand in combination with Al(III) (**8**) to produce highly isotactic PLA from *rac*-LA under both solution {70 °C, toluene, [*rac*-LA]:[Al] = 62:1, 12 days, $P_m = 0.93$ } and melt {130 °C, [*rac*-LA]:[Al] = 200:1, 2 days, $P_m = 0.88$ } conditions.^[57,58] *R,R*-**8** retained an enantiomorphic site control mechanism, akin to that noted for *R*-**7**, observing a preference for *L*-LA insertion, although poor activity was observed. Comparatively, *rac*-**8** facilitated isoselective enchainment, resulting in an enhanced polymer melting temperature ($T_m \sim 185$ °C). Saha *et al.*^[59] prepared analogous dinuclear complexes of Zr(IV) and Hf(IV), which exhibited superior activity at the expense of diminished stereocontrol (atactic PLA) relative to **8**, highlighting the importance of structure-activity relationships.

Initial developments within the field primarily focused on shifting towards achiral initiators that retain salen pro-ligand functionality. Indeed, catalyst fine tuning has received significant attention in the literature and is typically achieved through modification of the phenyl substituents, R, and nitrogen backbone, Y, as shown in Figure 2.6.

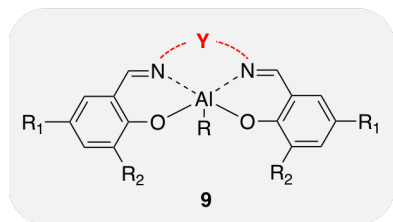
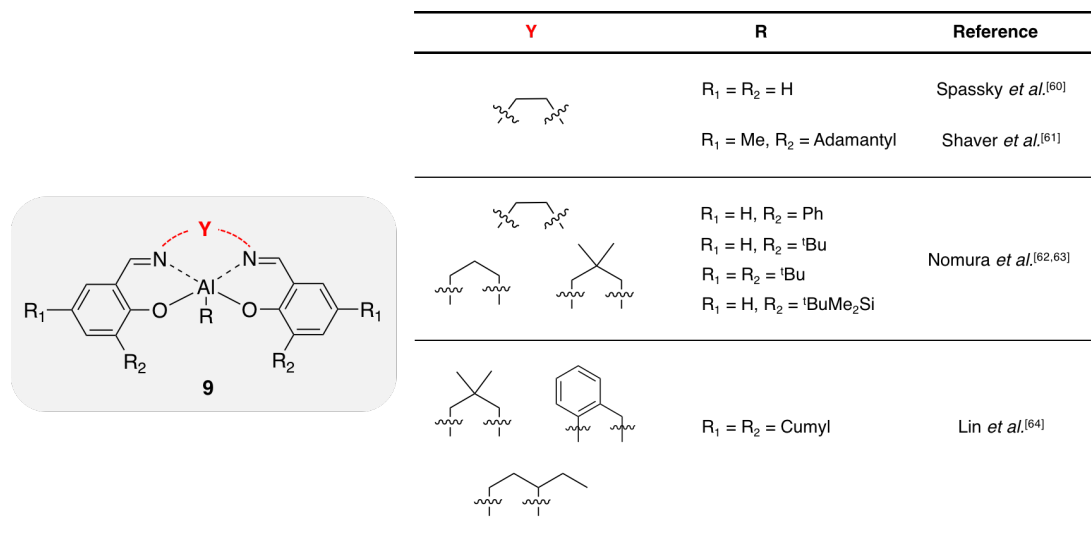


Figure 2.6. Achiral Al(III)-salen initiators reported by Spassky *et al.*^[60], Shaver *et al.*^[61], Nomura *et al.*^[62,63] and Lin *et al.*^[63]

Spassky *et al.*^[60] reported a simple deviation by employing two unsubstituted aryl groups connected by an ethylenediamine backbone (Figure 2.6). Isotactic PLA was obtained through a chain-end control mechanism, whereby insertion of the incoming monomer unit is dictated by the previous. Shaver *et al.*^[61] reported a subtle variation of this system through diversification of the aryl substituents, employing methyl and adamantyl moieties at the *para* (R₁) and *ortho* (R₂) positions, respectively. Importantly, excellent stereoselectivity was observed, enabling highly isotactic PLA ($P_m = 0.88$) to be furnished, which could be retained under immortal conditions in toluene {70 °C, [*rac*-LA]:[Al]:[BnOH] = 1000:1:10}. Steric and electronic effects were extensively investigated in a follow up study by Nomura and co-workers.^[62,63] Increased ligand flexibility along the nitrogen backbone was shown to impart enhanced activity, whilst stereocontrol was most readily dictated by steric bulk at the *ortho* position. Remarkably, near perfectly isotactic PLA was accessible in toluene at 70 °C {[*rac*-LA]:[Al] = 100:1, 14 h, $P_m = 0.98$, $T_m = 209$ °C} through the use of a neopentyl linker and ^tBuMe₂Si *ortho* substituent. Good isoselectivity was retained at elevated temperatures under solvent-free conditions {130 °C: [*rac*-LA]:[Al] = 300:1, 30 min, $P_m = 0.92$, $T_m = 189$ °C; 180 °C: [*rac*-LA]:[Al] = 300:1, 20 min, $P_r = 0.16$, $T_m = 176$ °C}, although an obvious suppression in the polymer melting temperature was conceded. Such findings are generally consistent with work by Lin *et al.*^[64] who found bulky cumyl groups (Me₂PhC-) occupying both the R₁ and R₂ positions to impart superior stereocontrol relative to their ^tBu analogues. Whilst such initiators exhibited moderate activity for the ROP of *rac*-LA, excellent isoselectivity was observed in toluene {70 °C, $P_m = 0.94 - 0.97$, 12 – 24 h, $T_m = 203 - 205$ °C}. Inspired by such work, Hormnirun *et al.*^[65] explored the impact of reduced ligand flexibility through the

introduction of aromatic linkers (Figure 2.7), observing trends akin to those reported by Nomura and co-workers.^[62,63]

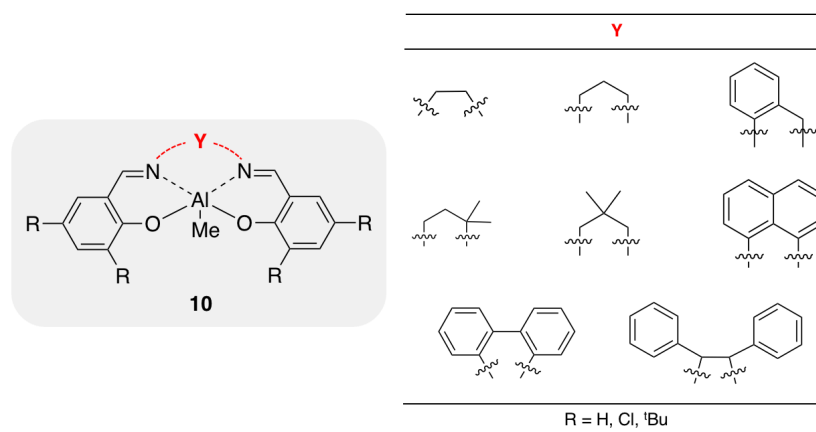


Figure 2.7. Achiral Al(III)-salen initiators reported by Hormnirun *et al.*^[65]

The salen pro-ligand can be further derivatised through partial and complete reduction to afford the corresponding salalen and salan counterpart (Figure 2.8), respectively, which retain the adventitious properties ascribed to the salens. Consequently, such ligands have also been extensively explored in combination with Al(III) for lactide polymerisation.^[66-75]

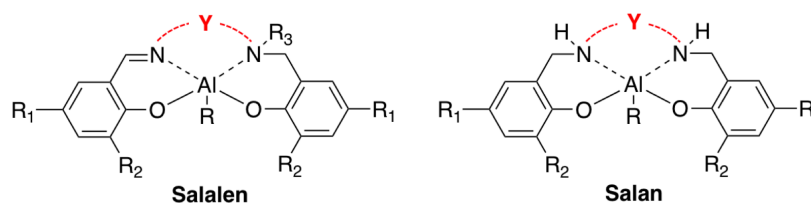


Figure 2.8. General structure of salalen- and salan-type ligands in combination with Al(III). *N.B.* Y corresponds to the backbone linker.

Whilst it is clear significant advancements have been made within the last 20 years, particularly relating to stereocontrol under solution conditions, a number of key challenges remain. Indeed, Al(III)-initiators typically require the use of elevated temperatures ($> 70\text{ }^{\circ}\text{C}$) and high catalyst loadings ($\sim 1\text{ mol } \%$) to be appreciably active. Thus, scope remains for the development of alternative systems that exhibit both high activity and stereocontrol, particularly under industrially relevant melt conditions.

Recently, Romain *et al.*^[76,77] reported a series of highly active Al(III)-initiators supported by catam-type ligand scaffolds that facilitate rapid lactide polymerisation under ambient conditions (Figure 2.9). Complexes **11–13** were found to furnish PLA with a slight isotactic bias ($P_m = 0.60$) within 90 min in THF at room temperature (RT) $\{[rac\text{-LA}]:[\text{Al}]:[\text{BnOH}] = 100:1:1\}$. Promisingly, high activity was retained for **13** under immortal conditions $\{\text{toluene}, 90\text{ }^{\circ}\text{C}, [rac\text{-LA}]:[\text{Al}]:[\text{BnOH}] = 1000:1:9, P_m = 0.55\}$. Exchange of the ethyl backbone for a

more flexible substituted propyl linker, as seen in **14–16**, was found to have significant ramifications on stereocontrol. Indeed, **14** and **16** produced highly heterotactic PLA ($P_r = 0.90$), whilst retaining high activity under analogous conditions to those noted for **11–13**. Such subtle changes in ligand design serve to highlight the importance of fine-tuning metal-ligand cooperative effects within such systems. Crucially, the -NH donor group was found to play a key role in facilitating non-covalent interactions with the active species, which partly accounts for the enhanced activity of the catam relative to its salen and salan counterparts. Indeed, exchange of the -NH donors for -NMe, as seen in **15**, coincided with a complete loss in activity at RT. Furthermore, in accordance to previous work by Tolman and co-workers, activity enhancement can also likely be attributed to the catam providing a lower ligand framework distortion energy.^[78-80] Whilst **13** and **16** were found to be active for PLA production under melt conditions (41 – 77% monomer conversion within 3 to 4 min), low molecular weight polymer ($M_n \sim 5,000 \text{ g mol}^{-1}$) was obtained.

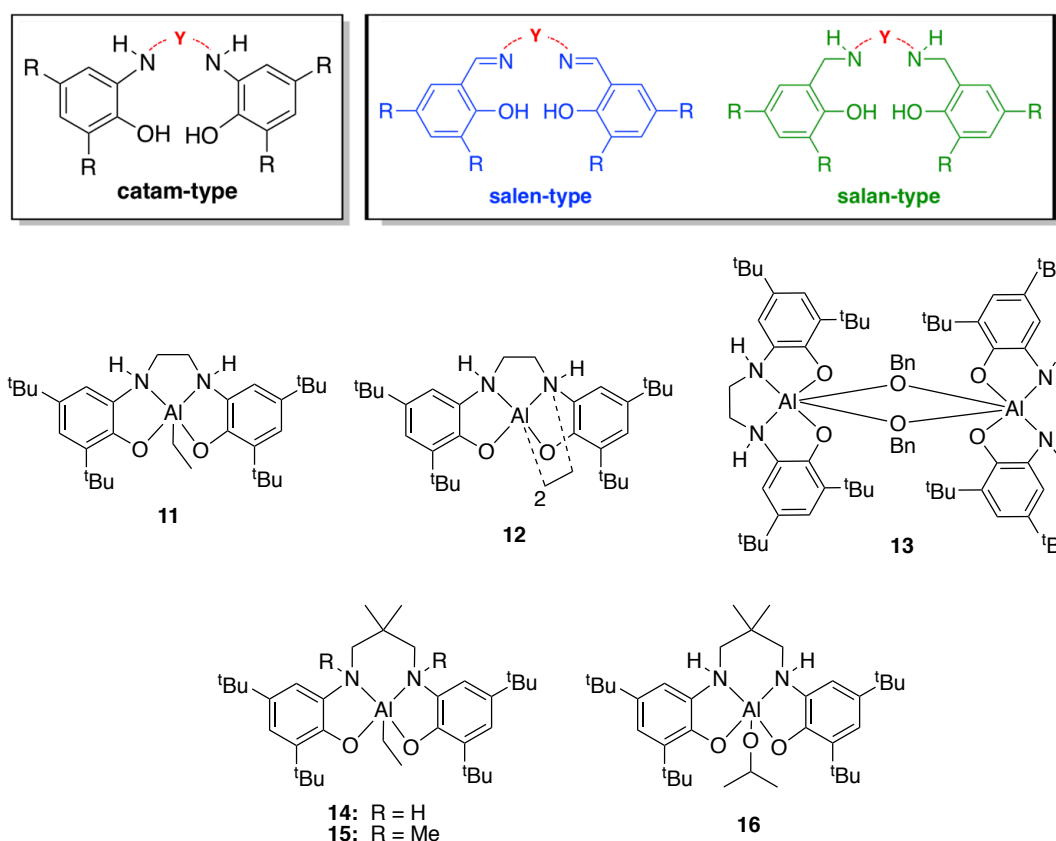


Figure 2.9. Highly active Al(III)-catam complexes reported by Romain *et al.*^[76,77] for lactide polymerisation under ambient conditions.

Prior to this work, few examples of Al(III)-initiators exhibiting appreciable activity for the solution phase production of PLA under ambient conditions had been reported, which are

depicted in Figure 2.10.^[81-84] Indeed, translating such activity to the melt phase production of PLA remains a prevalent challenge in the field for Al(III)-complexes.

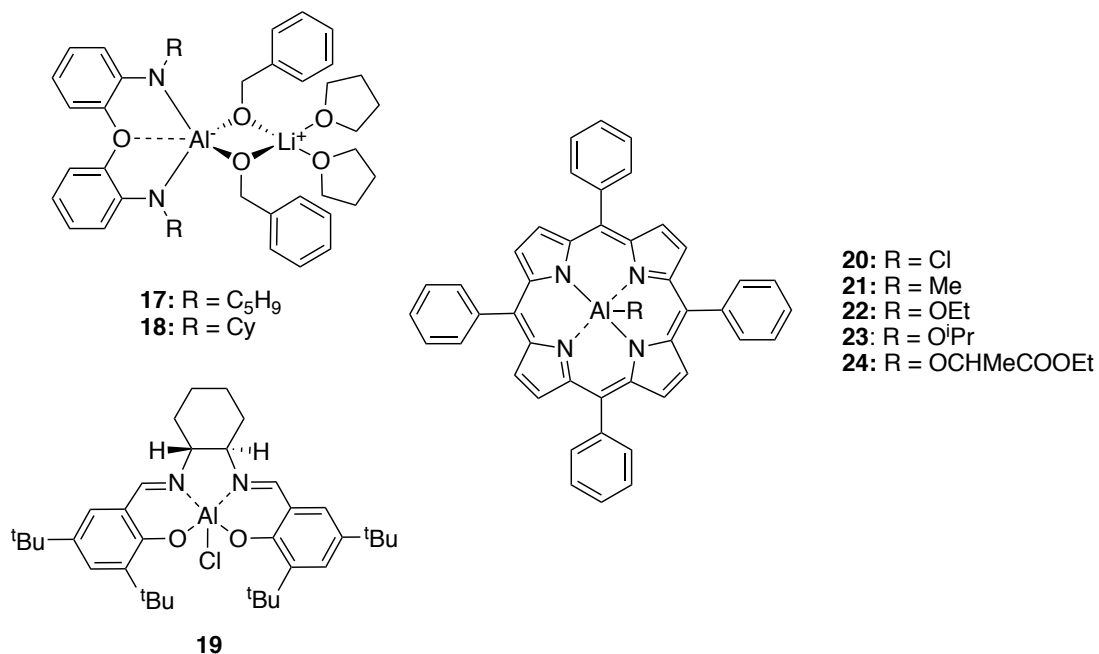
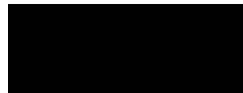


Figure 2.10. Selected examples of Al(III)-initiators active for lactide polymerisation under ambient conditions reported by Hild *et al.*^[81] (**17–18**), Robert *et al.*^[82] (**19**) and by both Praban *et al.*^[83] and Anker *et al.*^[84] for the tetraphenylporphyrin complexes (**20–24**). *N.B.* Cy refers to a cyclohexane substituent.

2.2. Statement of Authorship

This declaration concerns the article entitled:			
Novel hybrid aluminium(iii)-catalen complexes as highly active catalysts for lactide polymerisation: towards industrial relevance			
Publication status (tick one)			
Draft manuscript <input type="checkbox"/> Submitted <input type="checkbox"/> In review <input type="checkbox"/> Accepted <input type="checkbox"/> Published <input checked="" type="checkbox"/>			
Publication details (reference)	J. Payne, P. McKeown, G. Kociok-Köhn, M. D. Jones, <i>Chem. Commun.</i> 2020 , 56, 7163–7166 (DOI: 10.1039/D0CC02733B)		
Copyright status (tick the appropriate statement)			
I hold the copyright for this material <input checked="" type="checkbox"/> Copyright is retained by the publisher, but I have been given permission to replicate the material here <input type="checkbox"/>			
Candidate's contribution to the paper (provide details, and also indicate as a percentage)	<p>The candidate predominantly executed the work presented in the paper.</p> <p>Formulation of ideas:</p> <p>Ideas were discussed and planned with PM and MDJ. The manuscript draft was prepared by JMP with editing from PM and MDJ during the editing stage. [JMP = 70%, PM = 10%, GKK = 0%, MDJ = 20%]</p> <p>Design of methodology:</p> <p>Experiments were discussed and planned with PM and MDJ. [JMP = 80%, PM = 10%, GKK = 0%, MDJ = 10%]</p> <p>Experimental work:</p> <p>Experimental work and data analysis were conducted by JMP. X-ray crystallographic data was collected and processed by PM, GKK and MDJ. [JMP = 80%, PM = 10%, GKK = 5%, MDJ = 5%]</p> <p>Presentation of data in journal format:</p> <p>All figures, tables and schemes were prepared by JMP. [JMP = 100%]</p>		
Statement from Candidate	This paper reports on original research I conducted during the period of my Higher Degree by Research candidature.		
Signed		Date	6/6/2022

Cite this: *Chem. Commun.*, 2020, 56, 7163Received 15th April 2020,
Accepted 22nd May 2020

DOI: 10.1039/d0cc02733b

rsc.li/chemcomm

Novel hybrid aluminium(III)–catalen complexes as highly active catalysts for lactide polymerisation: towards industrial relevance†

Jack Payne,^{ab} Paul McKeown,^{ab} Gabriele Kociok-Köhn^b and Matthew D. Jones^{ab*}

Herein, we report a series of highly active Al(III)-complexes based on a novel hybrid ligand: the catalen. Their application in the production of polylactide under both solution, and industrially preferred melt conditions, is demonstrated. Potential structural diversification to broaden initiator scope is discussed.

Whilst plastics remain deeply embedded in modern day society, growing environmental concerns within industry has stimulated considerable research into renewable alternatives.¹ Polylactide (PLA) has received significant commercial interest owing to its green credentials and ability to compete with existing petroleum-based plastics, particularly within the packaging sector.^{2,3} Industrially, PLA is produced from L-lactide under solvent-free conditions, relying on a Sn(Oct)₂ catalyst.⁴ However, toxicity concerns surrounding Sn(IV) has created an appetite for biocompatible and sustainable alternatives. Initiators based on Mg(n)^{5–8} and Zn(n)^{5,7,9–16} have thus been extensively reported, but those pertinent to this report exploit Al(III) bearing tetradentate bis(phenolate) ligands. Early examples by Spassky *et al.*¹⁷ and Feijen *et al.*^{18,19} relied on chiral salen-based initiators, achieving exceptional isoselectivity ($P_r = 0.05–0.12$). Development of the field saw the emergence of achiral initiators retaining the salen pro-ligand functionality.^{20–25} Ligand scope significantly expanded with the emergence of subsequently reduced derivatisations, namely salalens^{26–30} and salans.^{31–35} Such ligand classes are traditionally easy to synthesise and functionally versatile, providing significant scope for catalyst fine-tuning. However, whilst it is clear the field has developed significantly within the last 20 years, particularly from a stereoselectivity standpoint, Al(III)-complexes remain limited by their poor activity, often requiring elevated conditions ($T > 70$ °C) and high catalyst loadings

(~1 mol%) to be appreciably active. Recently, Romain *et al.*^{36,37} reported the first example of a series of highly active Al(III)-complexes bearing a catam-type ligand scaffold. Exceptional activity was observed, achieving full conversion to PLA with a slight isotactic bias ($P_r = 0.4$) within 90 minutes at room temperature (RT) {THF, [*rac*-LA]:[I]:[BnOH] = 100:1:1}. Interestingly, shifting from an ethyl to substituted propyl backbone had significant ramifications on stereoselectivity, producing highly heterotactic PLA ($P_r = 0.9$), highlighting the importance of structure–activity relationships. However, producing highly isotactic PLA, whilst retaining activity, remains a prevalent challenge in the field, particularly under industrially preferred melt conditions. Whilst highly efficient metal-free organo-catalysts have also been reported in the ROP of *rac*-LA in solution, retaining high activity in the melt remains a major limitation, with Al(III)-complexes a possible solution.^{1,38}

Herein, we report the preparation and characterisation of a series of highly active Al(III)-complexes based on a novel hybrid ligand framework: the catalen. Their application in the ROP of *rac*-LA in solution, and under industrially preferred melt conditions, is discussed.

The catalen ligands, and subsequently derived Al(III)-complexes, were prepared under mild conditions as depicted in Scheme 1. Despite significant effort, attempts to isolate Al(2)Me proved unsuccessful. The solid-state structure of all complexes prepared was determined *via* single crystal X-ray diffraction (XRD), with the exception of Al(3)Me (Fig. 1). Al(1)Me exhibited a distorted trigonal bipyramidal geometry ($\tau_5 = 0.62$), whilst [Al(1–3){OBn}]₂ conformed reasonably well with an octahedral geometry {[Al(2){OBn}]₂: O(1)–Al(1)–N(2), O(2)–Al(1)–N(1) = 88.2(3), 172.2(3)}.

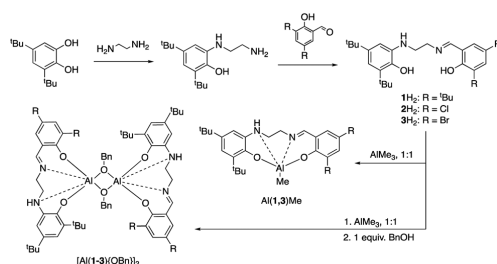
An Al(1)–N(1) bond length of *ca.* 2 Å confirmed retention of the imine functionality on coordination to the Al(III) centre for all complexes. The methoxy bridge analogue of [Al(1){OBn}]₂ was isolated on exposure of Al(1)Me to air, presumably through migration of the terminal –Me, and characterised by XRD but not pursued in polymerisation studies (see ESI†). ¹H NMR spectroscopic analysis of [Al(1–3){OBn}]₂ revealed characteristic singlet peaks at *ca.* $\delta = 7.50$ and 5.50 ppm corresponding to ArCHN and –NH resonances respectively. The –NH resonance

^a Centre for Sustainable and Circular Technologies, University of Bath, Claverton Down, Bath, BA2 7AY, UK

^b Department of Chemistry, University of Bath, Claverton Down, Bath, BA2 7AY, UK. E-mail: mj205@bath.ac.uk

† Electronic supplementary information (ESI) available: Full details of the experimental protocols with selected spectra and raw data. CCDC 1996836–1996840. For ESI and crystallographic data in CIF or other electronic format see DOI: 10.1039/d0cc02733b

Communication



Scheme 1 Ligands and Al(III)-complexes prepared in this study.

was absent in Al(1,3)Me, presumably due to enhanced structural fluxionality. More interestingly, the $-\text{OBn}\{\text{CH}_2\}$ resonances appeared as two distinct diastereotopic doublets, indicating [Al(1-3){OBn}]₂ to be asymmetric with the potential to exert catalytic-site stereocontrol (see ESI[†]). ¹³C{¹H} NMR spectroscopic analysis was consistent with XRD and ¹H NMR spectroscopic analysis, observing poor signal resolution for [Al(1-3){OBn}]₂, indicative of fluxionality, confounded by poor solubility. Diffusional ordered spectroscopy (DOSY) analysis of a monomeric vs. dimeric system comparison, namely Al(1)Me and [Al(1){OBn}]₂ respectively, confirmed the species to exist exclusively in solution with diffusion constants (*D*) of 0.66 and $0.46 \times 10^{-9} \text{ m}^2 \text{ s}^{-1}$ respectively (see ESI[†]), with no aggregation observed. These diffusion coefficients are in good agreement with the predicted molecular weights {Al(1)Me, [Al(1){OBn}]₂: *M_r* = 520.74, 1225.66 g mol⁻¹; *M_{r,DOSY}* = 527.7, 1173.2 g mol⁻¹}.³⁹ All Al(III)-complexes were in generally good agreement with elemental analysis (EA) data obtained, although *C*% values slightly lower than expected were observed for Al(1,3)Me and [Al(1-2){OBn}]₂, due to suspected hydrolysis and the presence of H₂O respectively.

All complexes were trialed in the ROP of *rac*-LA in solution (25 and 80 °C) and under industrially preferred melt conditions (130 and 180 °C) in the absence of solvent (Tables 1 and 2). [Al(1-3){OBn}]₂ were treated as monomeric such that one -OBn moiety was associated per Al centre. Unless otherwise stated, it is proposed the polymerisation proceeded *via* the classical coordination mechanism since [Al(1-3){OBn}]₂ were derived

from Al(1-3)Me on reaction with BnOH. It was envisaged introducing the 'catam' component into the ligand backbone would impart enhanced activity, whilst retention of the 'salen' component would provide rigidity, and therefore the potential to exert stereocontrol.

All complexes were highly active in the melt, atypical of traditional aluminium-based systems.^{18,19,30,31} Al(1)Me exhibited fair polymerisation control, affording atactic PLA of moderate dispersities (*D* = 1.35). Comparable activity and superior *M_n* control was observed in the analogous [Al(1){OBn}]₂ system. Al(3)Me exhibited superior activity compared to Al(1)Me, presumably due to a less hindered and more Lewis acidic Al(III) centre. Remarkably, a TOF of 45 300 h⁻¹ (Table 1, entry 3) was observed, the highest reported thus far for aluminium, though literature studies in the melt remain limited despite industrial relevance.^{18,19,30,31,37} Whilst moderately heterotactic PLA (*P_r* = 0.64) was produced, poor *M_n* control (relative to theoretical values) and broad dispersities (*D* = 1.81) were observed, implying *k_p* ≫ *k_t*, which subsequently inhibited homogenous polymerisation. Moderate heterotacticity (*P_r* = 0.64–0.65) and poor control (*M_n* = 93 100–146 200 g mol⁻¹) was retained for [Al(2-3){OBn}]₂ despite a reduction in activity. It is suggested the introduction of an electron-withdrawing ligand scaffold inhibits catalyst dissociation under these conditions, essentially maintaining the dimeric structure, such that less active species is available. A reduction in activity down the [Al(1-3){OBn}]₂ series, contrary to that noted for Al(1,3)Me, can likely be attributed to said dissociation effect, confounded by poorer solubility in the melt. The activity of Al(1,3)Me and the [Al(3){OBn}]₂ was also investigated under industrially relevant catalyst and monomer loadings, targeting PLA of *M_n* comparable to commercial products (*M_n* ~ 45 000 g mol⁻¹). Promisingly, high activity in the melt was retained upon reducing the catalyst loading to 0.033 mol%. To the best of our knowledge, this is the first example of aluminium-based complexes exhibiting significant activity under industrially relevant conditions. Prolonged reaction times resulted in polymer of narrower dispersities (*D* = 1.24–1.35) with a lower than expected *M_n* (13 700–14 700 g mol⁻¹). For [Al(3){OBn}]₂, it is proposed an increase in temperature assists the dissociation of [Al(3){OBn}]₂, resulting in superior *M_n* control (Table 1, entry 8).

The remarkable activity exhibited by the Al(III)-complexes in the melt was retained in solution, particularly at elevated

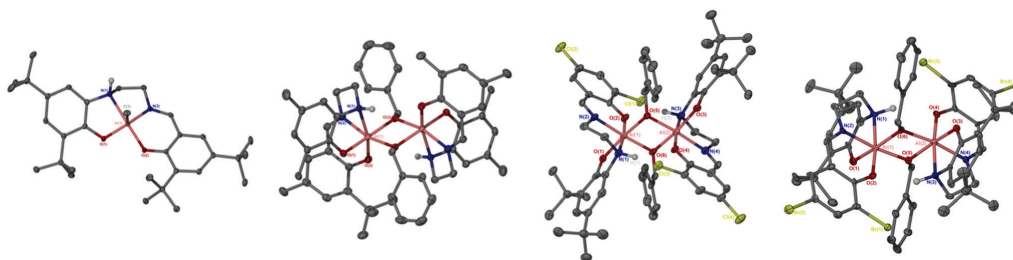


Fig. 1 Solid state structures for Al(1)Me and [Al(1-3){OBn}]₂ from left to right with ellipsoids shown at 30% probability level and all hydrogens omitted for clarity except those bound to nitrogen atoms. For [Al(1){OBn}]₂, ^tBu methyl groups have also been omitted for clarity.

Table 1 Melt polymerisation of *rac*-LA using Al(III)-complexes

Init.	Time/min	[<i>rac</i> -LA]:[Al]:[BnOX]	Conv. ^a /%	$M_{n,theo}^b/g\ mol^{-1}$	$M_n^c/g\ mol^{-1}$	D^d	P_r^d
Al(1)Me/BnOH	2	300:1:1	94	40 700	26 800	1.35	0.46
	19	3000:1:10	83	35 950	14 700	1.35	0.46
Al(3)Me/BnOH	0.33	300:1:1	83	35 950	119 900	1.81	0.64
	11	3000:1:10	90	39 000	13 950	1.28	0.60
[Al(1){OBn}] ₂	2	300:1:1	88	38 100	40 900	1.42	0.46
[Al(2){OBn}] ₂	5	300:1:1	76	32 950	146 200	1.52	0.64
[Al(3){OBn}] ₂	8	300:1:1	74	32 100	93 100	1.39	0.65
	32 ^e	3000:1:10	82	35 550	13 700	1.24	0.62

Conditions: *rac*-LA (1.0 g), solvent free (130 °C). ^a Determined via ¹H NMR spectroscopy. ^b Theoretical average number molecular weight (M_n) dependent on conversion and co-initiator added $\{(M_{n,LA} \times 3 \times \%_{conv}) + M_{n,BnOH}\}$. ^c Determined via GPC analysis (in THF). ^d Determined via homonuclear decoupled NMR spectroscopy. ^e 9 equivalents of BnOH added to achieve $\{[Al]:[BnOH] = 1:10\}$. A correction factor of 0.58 has been applied to reported M_n values.⁴⁰

Table 2 Solution polymerisation of *rac*-LA using Al(III)-complexes

Init.	Time/h	[<i>rac</i> -LA]:[Al]:[BnOX]	Conv. ^a /%	$M_{n,theo}^b/g\ mol^{-1}$	$M_n^c/g\ mol^{-1}$	D^d	P_r^d
Al(1)Me/BnOH	0.5	100:1:1	97	14 100	9200	1.33	0.36
	8 ^e	100:1:1	62	9050	6050	1.06	0.30
Al(3)Me/BnOH	0.5	100:1:1	97	14 100	9350	1.33	0.64
	8 ^e	100:1:1	81	11 750	7850	1.08	0.72
[Al(1){OBn}] ₂	0.5	100:1:1	96	13 950	11 200	1.64	0.38
	8 ^e	100:1:1	62	9050	6950	1.06	0.31
[Al(2){OBn}] ₂	0.5	100:1:1	94	13 650	85 200	1.56	0.64
	0.5 ^f	100:1:2	91	6900	7100	1.10	0.67
	8 ^e	100:1:1	<10	—	—	—	—
	8 ^g	100:1:1	0	—	—	—	—
[Al(3){OBn}] ₂	0.5	100:1:1	97	14 100	57 700	1.97	0.65
	8 ^e	100:1:1	<10	—	—	—	—
	8 ^g	100:1:1	0	—	—	—	—

Conditions: *rac*-LA (0.5 g), solvent (toluene, 80 °C). ^a Determined via ¹H NMR spectroscopy. ^b Theoretical average number molecular weight (M_n) dependent on conversion and co-initiator added $\{(M_{n,LA} \times \%_{conv}) + M_{n,BnOH}\}$. ^c Determined via GPC analysis (in THF). ^d Determined via homonuclear decoupled NMR spectroscopy. ^e RT (25 °C) in DCM. ^f 1 equiv. of BnOH added to achieve $\{[Al]:[BnOH] = 1:2\}$. ^g RT (25 °C) in THF. M_n , D and P_r values for [Al(2-3){OBn}]₂ at RT in DCM could not be determined due to insufficient polymeric material being isolated. A correction factor of 0.58 has been applied to reported M_n values.⁴⁰

conditions. All complexes achieved >94% conversion within 30 minutes at 80 °C (Table 2). Previously reported salen²³ and salan³² systems analogous to Al(1)Me achieved 19% and 77% conversion after 3 and 5 days respectively {toluene, 70 °C, [*rac*-LA]:[I]:[BnOH] = 100:1:1}.³⁶ Romain *et al.*³⁷ have previously attributed the enhanced reactivity of the catam to the presence of an -NH hydrogen donor, which readily interacts with the reactive species. Generally, fair M_n control and moderate dispersities ($D = 1.33$ – 1.64) were observed, with the exception of [Al(2-3){OBn}]₂, consistent with the melt. The addition of 1 equiv. of BnOH resulted in significantly enhanced M_n and D control for [Al(2){OBn}]₂ at 80 °C, suggesting a more efficient initiation process (Table 2, entry 8; see ESI[†]). General reactivity trends discussed for Al(1,3)Me were retained in solution, and could be extended to the dimeric series owing to enhanced solubility under these conditions. The production of moderately isotactic PLA ($P_r = 0.36$) was observed with an electron-donating caten backbone bearing the ^tBu substituents. Adopting electron-withdrawing substituents resulted in a shift to moderate heteroselectivity ($P_r = 0.64$ – 0.65), highlighting the importance of structure–activity relationships. Enhanced stereoselectivity ($P_r = 0.30$ – 0.72) and narrower dispersities ($D = 1.06$ – 1.09) were observed at RT in DCM, whilst reasonable M_n control was retained, achieving between 62–81% conversion within 8 h

(TOF = 8–10 h⁻¹). Prior to this, very few examples of aluminium-based complexes exhibiting appreciable activity at room temperature have been reported.^{36,37,41–44} Moreover, near identical stereoselectivities between Al(1,3)Me and their dimeric counterparts suggests an identical active species. Since Al(1,3)Me exhibit good polymerisation control under solution conditions, this implies [Al(1-3){OBn}]₂ dissociation to be kinetically limited. Slow and incomplete dissociation is supported by stability testing of [Al(2){OBn}]₂ with *rac*-LA in CDCl₃, with the ¹H NMR remaining virtually unchanged after 24 h at RT (see ESI[†]). Consequently, low activity was observed for [Al(2-3){OBn}]₂ (Table 2, entries 9 and 12), which was exacerbated by poor catalyst solubility under the reaction conditions. However, such limitations associated with catalyst dissociation could be mitigated by forming the benzoxy-bridged species *in situ*, evidenced by Al(3)Me. Interestingly, no reaction occurred on substituting the solvent for THF, despite achieving complete dissolution, likely owing to competitive binding of the solvent with lactide. MALDI-ToF analysis of polymeric material produced using [Al(1){OBn}]₂ (Table 2, entry 6) confirmed the polymer to be -OBn and -H end-capped. No secondary series were observed suggesting the polymerisation to be well-controlled in the absence of detrimental transesterification side reactions, consistent with the GPC data. No evidence of

transesterification was observed for $[\text{Al}(2)\{\text{OBn}\}]_2$ in the presence of benzyl alcohol (Table 2, entry 8), suggesting the broader dispersities are a result of a slow initiation rate compared to propagation, likely due to limited complex dissociation (see ESI†).

Since comparable solution polymerisation performance was observed between $[\text{Al}(1,3)\text{Me}]$ and their benzoxy-bridged counterparts, a kinetic study was pursued for $[\text{Al}(1-3)\{\text{OBn}\}]_2$ at 80 °C (see ESI†). All complexes were observed to be extremely active, achieving k_{app} values between $(6.2\text{--}10.8) \times 10^{-2} \text{ min}^{-1}$. Interestingly, $[\text{Al}(2)\{\text{OBn}\}]_2$ exhibited the lowest activity ($k_{\text{app}} = 6.2 \times 10^{-2} \pm 0.0072 \text{ min}^{-1}$) despite bearing the most electron withdrawing catalen backbone.

In conclusion, a series of highly active $\text{Al}(\text{m})$ -complexes based on a novel catalen ligand framework have been reported. Extremely high activity in the melt was demonstrated, which was retained under solution conditions, with $[\text{Al}(3)\text{Me}]$ culminating in the most active aluminium-based system to date in the melt. Work is ongoing to optimise activity and stereocontrol *via* diversification of both the ligand and metal.

We wish to thank the University of Bath and MC₂ for use of analysis facilities. We thank the EPSRC for funding (EP/L016354/1 – JP) and (EP/P016405/1 – PM).

Conflicts of interest

There are no conflicts to declare.

References

- J. Payne, P. McKeown and M. D. Jones, *Polym. Degrad. Stab.*, 2019, **165**, 170–181.
- J. Lunt, *Polym. Degrad. Stab.*, 1998, **59**, 145–152.
- D. Garlotta, *J. Polym. Environ.*, 2001, **9**, 63–84.
- O. Dechy-Cabaret, B. Martin-Vaca and D. Bourissou, *Chem. Rev.*, 2004, **104**, 6147–6176.
- M. H. Chisholm, J. Gallucci and K. Phomphrai, *Inorg. Chem.*, 2002, **41**, 2785–2794.
- B. M. Chamberlain, M. Cheng, D. R. Moore, T. M. Ovitt, E. B. Lobkovsky and G. W. Coates, *J. Am. Chem. Soc.*, 2001, **123**, 3229–3238.
- P. McKeown, S. N. McCormick, M. F. Mahon and M. D. Jones, *Polym. Chem.*, 2018, **9**, 5339–5347.
- T. Rosen, I. Goldberg, V. Venditto and M. Kol, *J. Am. Chem. Soc.*, 2016, **138**, 12041–12044.
- D. E. Stasiw, A. M. Luke, T. Rosen, A. B. League, M. Mandal, B. D. Neisen, C. J. Cramer, M. Kol and W. B. Tolman, *Inorg. Chem.*, 2017, **56**, 14366–14372.
- P. M. Schäfer, M. Fuchs, A. Ohligschläger, R. Rittinghaus, P. McKeown, E. Akin, M. Schmidt, A. Hoffmann, M. A. Liauw, M. D. Jones and S. Herres-Pawlis, *ChemSusChem*, 2017, **10**, 3547–3556.
- J. Börner, I. Dos Santos Vieira, A. Pawlis, A. Döring, D. Kuckling and S. Herres-Pawlis, *Chem. – Eur. J.*, 2011, **17**, 4507–4512.
- J. Börner, U. Florke, K. Huber, A. Döring, D. Kuckling and S. Herres-Pawlis, *Chem. – Eur. J.*, 2009, **15**, 2362–2376.
- Y. Gong and H. Ma, *Chem. Commun.*, 2019, **55**, 10112–10115.
- A. Thevenon, C. Romain, M. S. Bennington, A. J. P. White, H. J. Davidson, S. Brooker and C. K. Williams, *Angew. Chem., Int. Ed.*, 2016, **55**, 8680–8685.
- M. Cheng, A. B. Attygalle, E. B. Lobkovsky and G. W. Coates, *J. Am. Chem. Soc.*, 1999, **121**, 11583–11584.
- J. Payne, P. McKeown, M. F. Mahon, E. A. C. Emanuelsson and M. D. Jones, *Polym. Chem.*, 2020, **11**, 2381–2389.
- N. Spassky, M. Wisniewski, C. Pluta and A. LeBorgne, *Macromol. Chem. Phys.*, 1996, **197**, 2627–2637.
- Z. Y. Zhong, P. J. Dijkstra and J. Feijen, *Angew. Chem., Int. Ed.*, 2002, **41**, 4510–4513.
- Z. Zhong, P. J. Dijkstra and J. Feijen, *J. Am. Chem. Soc.*, 2003, **125**, 11291–11298.
- M. Wisniewski, A. LeBorgne and N. Spassky, *Macromol. Chem. Phys.*, 1997, **198**, 1227–1238.
- E. D. Cross, L. E. N. Allan, A. Decken and M. P. Shaver, *J. Polym. Sci., Part A: Polym. Chem.*, 2013, **51**, 1137–1146.
- N. Nomura, R. Ishii, M. Akakura and K. Aoi, *J. Am. Chem. Soc.*, 2002, **124**, 5938–5939.
- N. Nomura, R. Ishii, Y. Yamamoto and T. Kondo, *Chem. – Eur. J.*, 2007, **13**, 4433–4451.
- H.-L. Chen, S. Dutta, P.-Y. Huang and C.-C. Lin, *Organometallics*, 2012, **31**, 2016–2025.
- P. Hornmair, E. L. Marshall, V. C. Gibson, R. I. Pugh and A. J. P. White, *Proc. Natl. Acad. Sci. U. S. A.*, 2006, **103**, 15343–15348.
- E. L. Whitelaw, G. Loraine, M. F. Mahon and M. D. Jones, *Dalton Trans.*, 2011, **40**, 11469–11473.
- E. L. Whitelaw, M. F. Mahon and M. D. Jones, *Inorg. Chem.*, 2010, **49**, 7176–7181.
- A. Pilon, K. Press, I. Goldberg, M. Kol, M. Mazzeo and M. Lamberti, *J. Am. Chem. Soc.*, 2014, **136**, 2940–2943.
- P. McKeown, M. G. Davidson, J. P. Lowe, M. F. Mahon, L. H. Thomas, T. J. Woodman and M. D. Jones, *Dalton Trans.*, 2016, **45**, 5374–5387.
- P. McKeown, M. G. Davidson, G. Kociok-Köhn and M. D. Jones, *Chem. Commun.*, 2016, **52**, 10431–10434.
- M. D. Jones, L. Brady, P. McKeown, A. Buchard, P. M. Schafer, L. H. Thomas, M. F. Mahon, T. J. Woodman and J. P. Lowe, *Chem. Sci.*, 2015, **6**, 5034–5039.
- P. Hornmair, E. L. Marshall, V. C. Gibson, A. J. P. White and D. J. Williams, *J. Am. Chem. Soc.*, 2004, **126**, 2688–2689.
- H. Du, A. H. Velders, P. J. Dijkstra, J. Sun, Z. Zhong, X. Chen and J. Feijen, *Chem. – Eur. J.*, 2009, **15**, 9836–9845.
- K. Press, I. Goldberg and M. Kol, *Angew. Chem., Int. Ed.*, 2015, **54**, 14858–14861.
- R. Hador, A. Botta, V. Venditto, S. Lipstman, I. Goldberg and M. Kol, *Angew. Chem., Int. Ed.*, 2019, **58**, 14679–14685.
- S. Gesslbauer, H. Cheek, A. J. P. White and C. Romain, *Dalton Trans.*, 2018, **47**, 10410–10414.
- S. Gesslbauer, R. Savela, Y. Chen, A. J. P. White and C. Romain, *ACS Catal.*, 2019, **9**, 7912–7920.
- N. E. Kamber, W. Jeong, R. M. Waymouth, R. C. Pratt, B. G. G. Lohmeijer and J. L. Hedrick, *Chem. Rev.*, 2007, **107**, 5813–5840.
- R. Evans, Z. Deng, A. K. Rogerson, A. S. McLachlan, J. J. Richards, M. Nilsson and G. A. Morris, *Angew. Chem., Int. Ed.*, 2013, **52**, 3199–3202.
- J. Baran, A. Duda, A. Kowalski, R. Szymanski and S. Penczek, *Macromol. Rapid Commun.*, 1997, **18**, 325–333.
- F. Hild, P. Haquette, L. Brelot and S. Dagorne, *Dalton Trans.*, 2010, **39**, 533–540.
- C. Robert, T. E. Schmid, V. Richard, P. Haquette, S. K. Raman, M.-N. Rager, R. M. Gauvin, Y. Morin, X. Trivelli, V. Guérineau, I. del Rosal, L. Maron and C. M. Thomas, *J. Am. Chem. Soc.*, 2017, **139**, 6217–6225.
- S. Praban, P. Pirojmitpong, V. Balasanthiran, S. Jayaraj, M. H. Chisholm, J. Tantirungrotechai and K. Phomphrai, *Dalton Trans.*, 2019, **48**, 3223–3230.
- M. Anker, C. Balasanthiran, V. Balasanthiran, M. H. Chisholm, S. Jayaraj, K. Mathieu, P. Pirojmitpong, S. Praban, B. Raya and W. J. Simonsick, *Dalton Trans.*, 2017, **46**, 5938–5945.

2.3. Experimental

Exemplar procedures, full characterisation data and representative spectra are provided herein, see ESI for full details: <https://www.rsc.org/suppdata/d0/cc/d0cc02733b/d0cc02733b1.pdf>

2.3.1. General experimental methods

The synthesis and characterisation of all Al(III)-catalen complexes was performed under an inert atmosphere of argon using standard Schlenk or Glovebox techniques. All chemicals used were purchased from Sigma-Aldrich and used as received, with the exception of *rac*-LA, which was recrystallised once from anhydrous toluene prior to use. All dry solvents used in handling Al(III)-complexes were obtained *via* SPS (solvent purification system). ^1H and $^{13}\text{C}\{^1\text{H}\}$ NMR spectra were obtained on either a Bruker 400 or 500 MHz spectrometer and referenced to residual solvent resonances.^[85] HSQC experiments were run on a Bruker 500 MHz spectrometer. Coupling constants (J) are provided in Hertz (Hz) to the nearest integer. CDCl_3 was dried over CaH_2 prior to use with Al(III)-complexes. C_6D_6 was degassed and stored over molecular sieves for use with Al(III)-complexes. All ligands were prepared *via* novel synthetic procedures and characterised by high-resolution electron-spray ionisation-mass spectrometry (ESI-MS) in positive mode. CHN microanalysis was performed by Elemental Microanalysis under an inert atmosphere. Diffusional ordered spectroscopy (DOSY) NMR analysis was carried out on a Bruker 500 MHz instrument.^[86] The standard Bruker pulse sequence ledsp2s used was with 8 scans recorded per gradient level. A gradient strength between 1600 to 1750 μs was used with a diffusion time of 0.05 s. Eight gradient strengths were used between 10 to 90 %. Data was processed using DOSY methods.

Single crystal X-ray data was collected on an EOS SuperNova diffractometer with Cu K α radiation ($\lambda = 1.54184 \text{ \AA}$) at 150(2) K. All structures were solved by direct methods and refined on all F^2 data using the SHELXL-2014 or 2017 suite of programs. All hydrogen atoms were included in idealised positions and refined using the riding model. All refinement details are given in the .cif file.

2.3.2. General polymerisation procedures

2.3.2.1. Lactide polymerisation

Polymerisations were conducted in a J Young's ampoule under argon. All melt polymerisations were performed in the absence of solvent. Initial melt polymerisations were performed with *rac*-LA (1.0 g, 6.94 mmol) to which the required amount of metal complex and benzyl alcohol co-initiator (BnOH, 2.4 μL , 0.023 mmol) were loaded in a Glovebox filled with argon $\{[rac\text{-LA}]:[\text{Al}]:[\text{BnOH}] = 300:1:1\}$. The ampoule was then submerged in a

preheated oil bath (130 °C) and the polymerisation start time commenced on melting of the monomer. The reaction was deemed finished once a polymer melt of sufficient viscosity stopped the stirrer bar. The reaction was then quenched in air and the product dissolved in DCM (20 mL) with stirring. The solvent was then removed *in vacuo* and a crude ¹H NMR spectrum of the polymer was obtained. The polymer was then washed with copious amounts of MeOH (80 mL) to remove initiator and any unreacted monomer, dried *in vacuo* and retained for materials characterisation. This procedure was repeated for melt polymerisations conducted at 180 °C, which maintained a constant [*rac*-LA]:[BnOH] ratio {[*rac*-LA]:[Al]:[BnOH] = 3000:1:10}. For solution polymerisations, *rac*-LA (0.5 g, 3.47 mmol) was dissolved in anhydrous toluene (5 mL) with the required amount of metal complex and BnOH (3.6 μL, 0.035 mmol). The flask was then placed in a preheated oil bath (80 °C) and stirred for 30 min. The reaction was then quenched in air, the solvent removed *in vacuo* and a crude ¹H NMR spectrum of the polymer was obtained. The polymer was then purified as described for melt polymerisations. This method was repeated for solution polymerisations performed at RT. *N.B.* For polymerisations using [Al(**1-3**){OBn}]₂, the initiator was treated as monomeric such that there is one -OBn moiety associated per Al centre, thus no additional BnOH was required for {[*rac*-LA]:[Al]:[BnOH] = 300:1:1 or 100:1:1}. For {[*rac*-LA]:[Al]:[BnOH] = 3000:1:10}, treating [Al(**3**){OBn}]₂ as monomeric required the addition of 9 equivalents of BnOH (2.2 μL, 0.022 mmol).

All polymer molecular weights were characterised by SEC, which was performed with a 1 mL min⁻¹ flow rate at 35 °C with a THF eluent using a PLgel 5 μm MIXED-D 300 × 7.5 mm column. The system was referenced against 11 narrow molecular weight polystyrene standards with detection *via* refractive index response. Polymer tacticity was determined *via* homonuclear decoupled ¹H NMR (CDCl₃) spectroscopic analysis of the methine region in accordance to relationships described by Coates *et al.*^[42] MALDI-ToF mass spectra were determined on a Bruker Autoflex speed instrument using DCTB (*trans*-2-[3-(4-*tert*-butylphenyl)-2-methyl-2-propenylidene]malononitrile, 10 μL, 10 mg mL⁻¹ in THF) as the matrix and ionised using NaTFA (2 μL, 0.1 M in THF) for PLA (10 μL, 5 mg mL⁻¹ in THF). After centrifugation, homogeneous samples of PLA (2 μL) were spotted onto a polished steel plate and data was collected in linear positive mode.

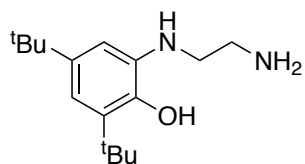
2.3.2.2 Lactide polymerisation kinetics

Reaction kinetic analysis was performed using the solution polymerisation procedure detailed in section 2.3.2.1. {toluene, 80 °C, [*rac*-LA]:[Al]:[BnOH] = 100:1:1}. Aliquots were taken under a dynamic flow of argon, obtaining 5 data points across the total reaction time for [Al(**1-**

3){OBn}₂. Plotting ln([LA]₀ / [LA]_t) against time afforded a straight line fit with the gradient equivalent to the pseudo first-order rate constant (*k_{app}*).

2.3.3. Synthesis and characterisation

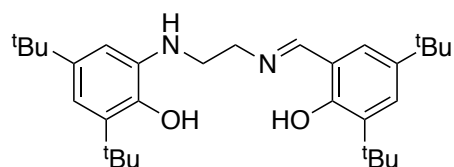
2.3.3.1. Tridentate {ONN} ligand precursor



1H: Isolated as a light-blue powder (2.50 g, 9.46 mmol, 70%). To a solution of 3,5-di-*tert*-butylcatechol (3.0 g, 13.5 mmol) in MeCN (20 mL), ethylenediamine (0.9 mL, 13.5 mmol) in MeCN (2 mL) was added dropwise with stirring and then refluxed at 100 °C for 1 h. The solution was allowed to cool to RT slowly and then stirred for 3 h to afford a light-blue precipitate, which was isolated by filtration, washed with MeCN (10 mL) and dried *in vacuo*. ¹H NMR (CDCl₃, 400 MHz): δ = 6.97 (s, 1H; ArH), 6.86 (s, 1H; ArH), 3.13 (t, *J* = 5 Hz, 2H; CH₂), 2.86 (t, *J* = 6 Hz, 2H; CH₂), 1.42 (s, 9H; C(CH₃)₃), 1.28 (s, 9H; C(CH₃)₃). *N.B.* Unaccounted for -OH, -NH and -NH₂ resonances likely due to rapid proton exchange in solution. ¹³C {¹H} NMR (CDCl₃, 125 MHz): δ = 146.3, 142.0, 135.8, 135.6, 117.8, 116.0 (Ar), 50.6, 41.2 (CH₂), 35.0, 34.5, (C(CH₃)₃), 31.8, 30.0 (CH₃). ESI-MS (+ve, MeOH): Calculated *m/z* [C₁₆H₂₉N₂O]⁺ = 265.2280; found *m/z* = 265.2371.

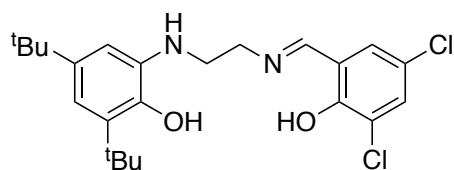
2.3.3.2. Catalen ligands

General synthesis procedure: To a solution of **1H** (0.67 g, 2.53 mmol) in MeCN (20 mL), 3,5-dichloro-2-hydroxybenzaldehyde (0.48 g, 2.53 mmol) or 3,5-dibromo-2-hydroxybenzaldehyde (0.71 g, 2.53 mmol) was added portion wise and the solution stirred for 30 min at RT. The solvent was removed *in vacuo*, replaced with *n*-hexane (10 mL) and stirred for 1 h. A yellow powder was isolated by filtration and dried *in vacuo*. *N.B.* For **1H₂** upon the addition of 3,5-di-*tert*-butyl-2-hydroxybenzaldehyde (0.44 g, 1.89 mmol), the solution was stirred at 0 °C for 30 min. The solvent was removed *in vacuo* to afford a green oil from which a green solid was obtained upon further drying under a dynamic vacuum. The solid was isolated and used without further purification.

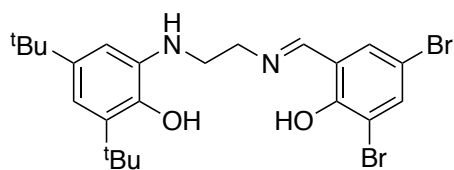


1H₂: Isolated as a green solid (0.78 g, 1.62 mmol, 86%). ¹H NMR (CDCl₃, 400 MHz): δ = 13.59 (s, 2H; OH), 8.40 (s, 1H; ArCHN), 7.40 (d, *J* = 3 Hz, 1H; ArH), 7.10 (d, *J* = 3 Hz, 1H; ArH), 6.99 (d, *J* = 2 Hz, 1H; ArH), 6.91 (d, *J* = 2 Hz, 1H; ArH), 3.80 (t, *J* = 6 Hz, 2H; CH₂), 3.40 (t, *J* = 6 Hz, 2H; CH₂), 1.45 (s, 9H; C(CH₃)₃), 1.41 (s, 9H; C(CH₃)₃), 1.31 (s, 9H; C(CH₃)₃), 1.29 (s, 9H; C(CH₃)₃). *N.B.* Unaccounted for -NH resonance likely due to rapid proton exchange in solution. ¹³C {¹H} NMR (CDCl₃, 100 MHz): δ = 167.7 (ArCHN), 158.2, 140.4, 140.2, 137.0,

136.8, 127.3, 127.2, 126.2, 126.2, 118.0, 116.1, 110.6 (Ar), 59.8, 59.4 (CH₂), 35.2, 35.2, 34.3, 34.3 (C(CH₃)₃), 31.7, 31.6, 29.6, 29.6 (CH₃). ESI-MS (+ve, MeCN): Calculated m/z [C₃₁H₄₉N₂O₂]⁺ = 481.3794; found m/z = 481.3927.

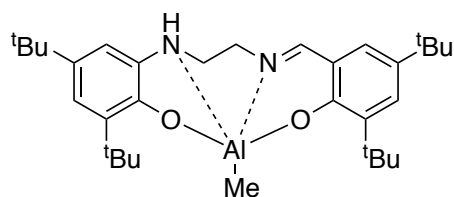


2H₂: Isolated as a yellow powder (0.70 g, 1.60 mmol, 63%). ¹H NMR (CDCl₃, 400 MHz): δ = 14.28 (s, 1H; OH), 8.24 (s, 1H; ArCHN), 7.40 (s, 1H; ArH), 7.11 (s, 1H; ArH), 6.98 (s, 1H; ArH), 6.89 (s, 1H; ArH), 3.86 (t, *J* = 5 Hz, 2H; CH₂), 3.46 (t, *J* = 5 Hz, 2H; CH₂), 1.40 (s, 9H; C(CH₃)₃), 1.28 (s, 9H; C(CH₃)₃). *N.B.* Unaccounted for -OH and -NH resonances likely due to rapid proton exchange in solution. ¹³C {¹H} NMR (CDCl₃, 100 MHz): δ = 165.1 (ArCHN), 146.5, 143.0, 136.6, 133.1, 132.6, 130.2, 129.2, 124.5, 124.2, 116.4, 112.7 (Ar), 47.3 (CH₂), 35.3, 34.9, 34.8, 34.6 (C(CH₃)₃), 31.8, 31.7, 29.9, 29.6 (CH₃). *N.B.* Unaccounted for Ar and -CH₂ resonances indicative of structural fluxionality on the ¹³C {¹H} timescale, resulting in poor signal intensity. Additional -C(CH₃)₃ and -CH₃ resonances observed indicating inequivalence, possibly due to structural tautomerisation as previously noted by Wieghardt and co-workers.^[87] ESI-MS (+ve, MeCN): Calculated m/z [C₂₃H₃₁Cl₂N₂O₂]⁺ = 438.1796; found m/z = 438.1786.



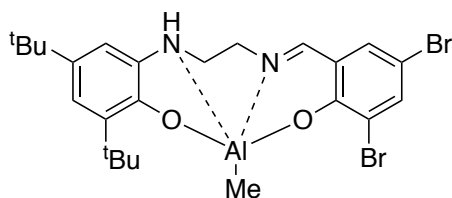
3H₂: Isolated as a yellow powder (0.92 g, 1.75 mmol, 69%). ¹H NMR (CDCl₃, 400 MHz): δ = 14.45 (s, 1H; OH), 8.20 (s, 1H; ArCHN), 7.69 (d, *J* = 2 Hz, 1H; ArH), 7.29 (d, *J* = 2 Hz, 1H; ArH), 6.98 (d, *J* = 2 Hz, 1H; ArH), 6.89 (d, *J* = 2 Hz, 1H; ArH), 3.85 (t, *J* = 6 Hz, 2H; CH₂), 3.46 (t, *J* = 6 Hz, 2H; CH₂), 1.40 (s, 9H; C(CH₃)₃), 1.28 (s, 9H; C(CH₃)₃). *N.B.* Unaccounted for -OH and -NH resonances likely due to rapid proton exchange in solution. ¹³C {¹H} NMR (CDCl₃, 100 MHz): δ = 164.9 (ArCHN), 145.3, 142.4, 138.0, 133.0, 119.8, 114.6, 112.9, 109.4, 108.6 (Ar), 47.3 (CH₂), 36.5, 34.8 (C(CH₃)₃), 31.8, 29.9 (CH₃). *N.B.* Unaccounted for Ar and -CH₂ resonances indicative of structural fluxionality on the ¹³C {¹H} timescale, resulting in poor signal intensity. ESI-MS (+ve, MeCN): Calculated m/z [C₂₃H₃₁Br₂N₂O₂]⁺ = 527.0732; found m/z = 527.0869.

2.3.3.3. Al(III)-catalen complexes



Al(1)Me: Isolated as a yellow solid (0.20 g, 0.38 mmol, 38%). To a pre-stirred solution of **1H₂** (0.48 g, 1 mmol) in dry toluene (10 mL) at 0 °C for 5 min, AlMe₃ (0.5 mL, 1 mmol) was added dropwise with stirring. The solution was allowed to gradually warm to RT where it was stirred for 2 h. The solvent was then removed *in vacuo*, replaced with *n*-hexane (5 mL) and stirred for 5 min to afford a yellow solid, which was isolated by cannula filtration and dried *in vacuo* at 80 °C for

4 h. ^1H NMR (C_6D_6 , 400 MHz): $\delta = 7.75$ (s, 1H; ArCHN), 7.48 (s, 1H; ArH), 7.23 (s, 1H; ArH), 6.79 (s, 1H; ArH), 6.77 (s, 1H; ArH), 2.71 (t, $J = 12$ Hz, 1H; CH), 2.41 (d, $J = 7$ Hz, 1H; CH), 2.31 (t, $J = 9$ Hz, 1H; CH), 2.21 (d, $J = 14$ Hz, 1H; CH), 1.81 (s, 9H; $\text{C}(\text{CH}_3)_3$), 1.75 (s, 9H; $\text{C}(\text{CH}_3)_3$), 1.45 (s, 9H; $\text{C}(\text{CH}_3)_3$), 1.37 (s, 9H; $\text{C}(\text{CH}_3)_3$), -0.38 (s, 3H; CH_3). *N.B.* Unaccounted for -NH resonance likely due to rapid proton exchange in solution. $^{13}\text{C}\{^1\text{H}\}$ NMR (C_6D_6 , 100 MHz): $\delta = 171.7$ (ArCHN), 165.2, 156.0, 141.5, 138.4, 137.6, 137.2, 131.9, 131.6, 122.9, 118.0, 117.6 (Ar), 55.6, 49.9 (CH_2), 35.8, 35.8, 34.5, 34.2 ($\text{C}(\text{CH}_3)_3$), 32.2, 31.7, 29.9, 29.7 (CH_3). *N.B.* Unaccounted for Ar resonance likely due to overlap with solvent peak (C_6D_6 , $\delta = 128.1$). Al-Me resonance absent, indicative of structural fluxionality. Elemental analysis: Calculated for $\text{C}_{32}\text{H}_{49}\text{AlN}_2\text{O}_2$: C, 73.81 %; H, 9.49 %; N, 5.38 %. Found: C, 69.50 %; H, 9.66 %; N, 4.78%. Elemental analysis more consistent with a degree of hydroxide during analysis, indicating poor hydrolytic stability. Al(1)OH, theoretical: $\text{C}_{31}\text{H}_{47}\text{AlN}_2\text{O}_3$: C, 71.23 %; H, 9.06 %; N, 5.36 %.

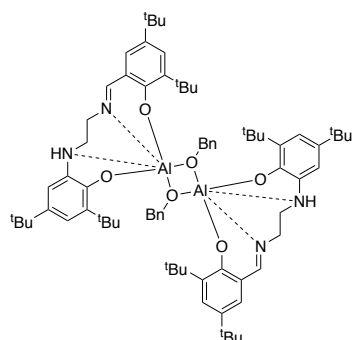


Al(3)Me: Isolated as a light-brown solid (0.25 g, 0.44 mmol, 44%). To a solution of AlMe_3 (0.5 mL, 1 mmol) in dry toluene (10 mL), $\mathbf{3H}_2$ (0.53 g, 1 mmol) was added portion wise over 5 min under a dynamic

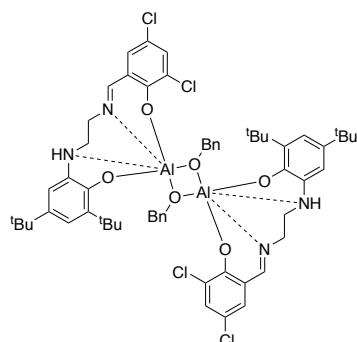
flow of argon with stirring. The solution was stirred at RT for 1 h. The solvent was then removed *in vacuo*, replaced with *n*-hexane (10 mL) and stirred for 3 days from which a light-brown solid was isolated by cannula filtration and dried *in vacuo* at 80 °C for 4 h. ^1H NMR (C_6D_6 , 400 MHz): $\delta = 7.68$ (s, 1H; ArCHN), 7.46 (s, 1H; ArH), 6.74 (s, 2H; ArH), 6.67 (s, 1H; ArH), 2.52 (t, $J = 11$ Hz, 1H; CH), 2.31 (t, $J = 11$ Hz, 2H; CH), 2.11 (s, 1H; CH), 1.73 (s, 9H; $\text{C}(\text{CH}_3)_3$), 1.43 (s, 9H; $\text{C}(\text{CH}_3)_3$), -0.47 (s, 3H; CH_3). *N.B.* Unaccounted for -NH resonance likely due to rapid proton exchange in solution. $^{13}\text{C}\{^1\text{H}\}$ NMR (C_6D_6 , 100 MHz): $\delta = 169.5$ (ArCHN), 162.3, 155.8, 141.2, 138.7, 138.1, 134.7, 131.2, 123.1, 119.0, 118.5, 117.6, 106.0 (Ar), 55.4, 49.0 (CH_2), 34.5, 34.2 ($\text{C}(\text{CH}_3)_3$), 32.2, 31.7 (CH_3), -8.10 (Al-Me). Elemental analysis: Calculated for $\text{C}_{24}\text{H}_{31}\text{AlBr}_2\text{N}_2\text{O}_2$: C, 50.90 %; H, 5.52 %; N, 4.95 %. Found: C, 47.08 %; H, 5.26 %; N, 4.52 %. Elemental analysis more consistent with a degree of hydroxide during analysis, indicating poor hydrolytic stability. Al(3)OH, theoretical: C, 48.61 %; H, 5.14 %; N, 4.93 %.

General complexation procedure for $[\text{Al}(\mathbf{1-3})\{\text{OBn}\}]_2$: To a pre-stirred solution of either $\mathbf{1H}_2$ (0.48 g, 1 mmol) or $\mathbf{3H}_2$ (0.53 g, 1 mmol) in dry toluene (10 mL) at 0 °C for 5 min, AlMe_3 (0.5 mL, 1 mmol) was added dropwise and the solution stirred for 1 h at RT. BnOH (0.10 mL, 1 mmol) was then added dropwise and the solution stirred for 1 h. A light-yellow solid was isolated by cannula filtration and dried *in vacuo* at 80 °C for 4 h. *N.B.* For $[\text{Al}(\mathbf{2})\{\text{OBn}\}]_2$ no pre-stirring was required such that to a solution of $\mathbf{2H}_2$ (0.44 g, 1 mmol) in dry toluene (10

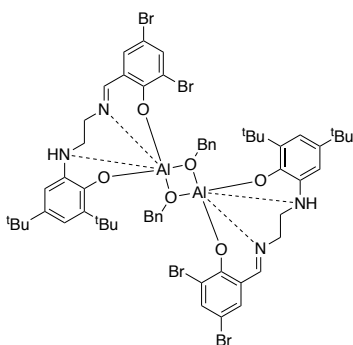
mL), AlMe₃ (0.5 mL, 1 mmol) was added dropwise at RT and the solution stirred for 1 h. [Al(2){OBn}]₂ was then prepared and isolated as detailed above.



[Al(1){OBn}]₂: Isolated as a yellow solid (0.20 g, 0.33 mmol, 33%). ¹H NMR (C₆D₆, 400 MHz): δ = 7.86 (s, 1H; ArCHN), 7.41 (s, 1H; ArH), 7.35 (s, 2H; ArH), 7.29 (s, 1H; ArH), 7.06 (s, 1H; ArH), 7.00 (s, 3H; ArH), 6.95 (s, 1H; ArH), 4.90 (s, 1H; NH), 4.76 (d, *J* = 12 Hz, 1H; Ar-CH), 4.38 (d, *J* = 13 Hz, 1H; Ar-CH), 3.71 (d, *J* = 4 Hz, 1H; CH), 2.62 (t, *J* = 14 Hz, 1H; CH), 2.51 (d, *J* = 8 Hz, 1H; CH), 1.87 (s, 1H; CH), 2.02 (s, 9H; C(CH₃)₃), 1.42 (s, 9H; C(CH₃)₃), 1.38 (s, 9H; C(CH₃)₃), 1.30 (s, 9H; C(CH₃)₃). ¹³C{¹H} NMR (CDCl₃, 100 MHz): δ = 169.7 (ArCHN), 157.7, 141.5, 137.2, 135.9, 130.2, 130.0, 129.0, 128.7, 128.4, 127.8, 127.40, 127.2, 126.8, 122.1, 120.5, 117.5 (Ar), 65.6, 49.4, 47.1 (CH₂), 35.6, 34.9, 34.1, 34.0 (C(CH₃)₃), 31.9, 31.6, 30.8, 29.4 (CH₃). *N.B.* Unaccounted for Ar resonances indicative of structural fluxionality on the ¹³C{¹H} timescale, resulting in low signal intensity. Elemental analysis: Calculated for C₇₆H₁₀₆Al₂N₄O₆: C, 74.48 %; H, 8.72 %; N, 4.57 %. Found: C, 71.64 %; H, 8.21 %; N, 4.64%. Elemental analysis more consistent with hydrated complex, indicative of hygroscopicity. [Al(1){OBn}]₂·3H₂O, theoretical: C, 71.33 %; H, 8.82 %; N, 4.38 %.



[Al(2){OBn}]₂: Isolated as a yellow solid (0.21 g, 0.37 mmol, 37%). ¹H NMR (C₆D₆, 400 MHz): δ = 7.41 (s, 3H; ArCHN, ArH), 7.29 (s, 5H; ArH), 6.94 (s, 1H; ArH), 6.58 (s, 1H; ArH), 5.62 (s, 1H; NH), 4.63 (d, *J* = 14 Hz, 1H; Ar-CH), 3.70 (d, *J* = 13 Hz, 1H; Ar-CH), 3.12 (s, 1H; CH), 2.85 (d, *J* = 17 Hz, 1H; CH), 2.27 (s, 1H; CH), 2.12 (s, 1H; CH), 1.34 (s, 9H; C(CH₃)₃), 1.26 (s, 9H; C(CH₃)₃). ¹³C{¹H} NMR (CDCl₃, 100 MHz): δ = 165.2 (ArCHN), 136.9, 134.2, 131.4, 131.3, 128.7, 128.4, 127.7, 126.8, 122.3, 119.1, 117.8 (Ar), 34.9, 34.2 (C(CH₃)₃), 31.9, 29.5 (CH₃). *N.B.* Unaccounted for Ar and ¹³C resonances indicative of structural fluxionality on the ¹³C{¹H} timescale, resulting in low signal intensity. Elemental analysis: Calculated for C₆₀H₇₀Al₂Cl₄N₄O₆: C, 63.27 %; H, 6.19 %; N, 4.92 %. Found: C, 60.25 %; H, 5.78 %; N, 4.65 %. Elemental analysis more consistent with hydrated complex, indicative of hygroscopicity. [Al(2){OBn}]₂·3H₂O, theoretical: C, 60.40 %; H, 6.42 %; N, 4.70 %.



[Al(**3**){OBn}]₂: Isolated as a yellow solid (0.50 g, 0.76 mmol, 76%). ¹H NMR (C₆D₆, 400 MHz): δ = 7.71 (s, 1H; ArCHN), 7.39 (s, 2H; ArH), 7.31 (s, 4H; ArH), 7.01 (d, *J* = 5 Hz, 1H; ArH), 6.88 (s, 1H; ArH), 6.73 (s, 1H; ArH), 5.65 (s, 1H; NH), 4.61 (d, *J* = 17 Hz, 1H; Ar-CH), 3.64 (d, *J* = 17 Hz, 1H; Ar-CH), 3.16 (s, 1H; CH), 2.81 (t, *J* = 14 Hz, 1H; CH), 2.25 – 2.15 (m, 2H; CH), 1.33 (s, 9H; C(CH₃)₃), 1.26 (s, 9H; C(CH₃)₃). ¹³C{¹H} NMR (CDCl₃, 100 MHz): δ = 165.2 (ArCHN), 142.1, 139.7, 138.0, 136.9, 135.3, 129.2, 128.9, 128.4, 127.8, 126.8, 125.5, 122.3, 121.0, 117.7 (Ar), 48.0 (CH₂), 34.9, 34.2 (C(CH₃)₃), 31.9, 29.5 (CH₃). *N.B.* Unaccounted for Ar and -CH₂ resonances indicative of structural fluxionality on the ¹³C{¹H} timescale, resulting in low signal intensity. Elemental analysis: Calculated for C₆₀H₇₀Al₂Br₄N₄O₆: C, 54.73 %; H, 5.36 %; N, 4.25 %. Found: C, 54.94 %; H, 5.40 %; N, 3.92 %.

2.3.3.4. Representative NMR spectra

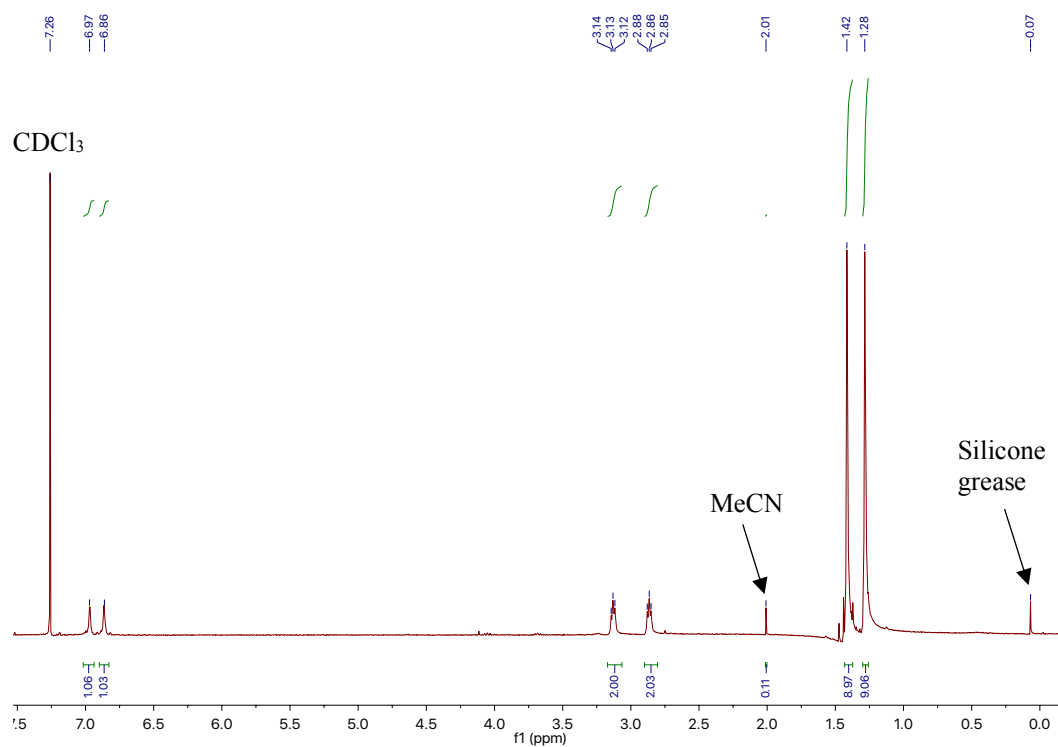


Figure 2.11. ¹H NMR (CDCl₃, 400 MHz) spectrum of 1H.

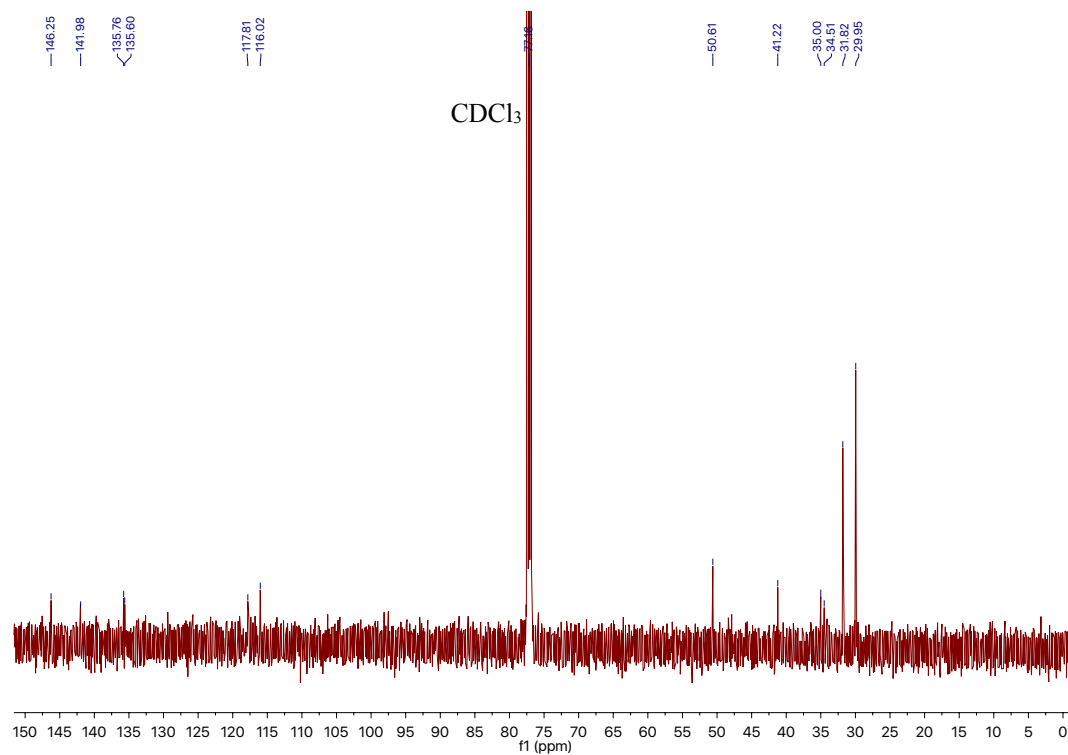


Figure 2.12. ¹³C{¹H} NMR (CDCl₃, 125 MHz) spectrum of 1H.

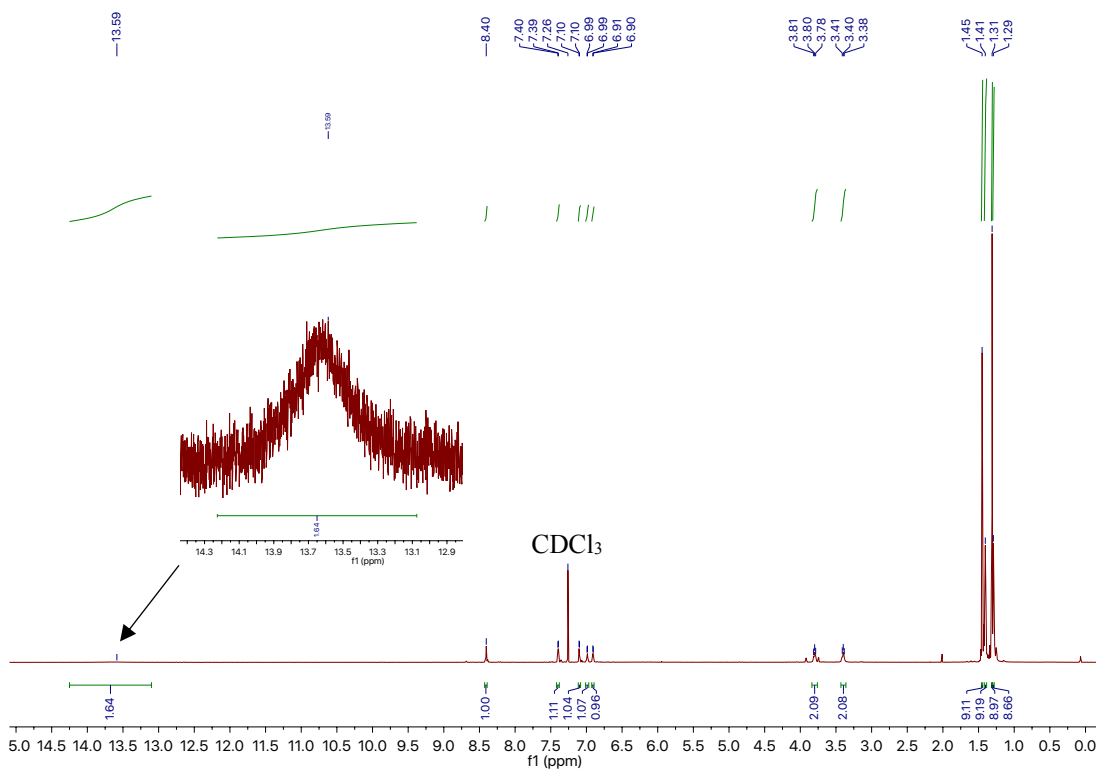


Figure 2.13. ¹H NMR (CDCl₃, 400 MHz) spectrum of 1H₂.

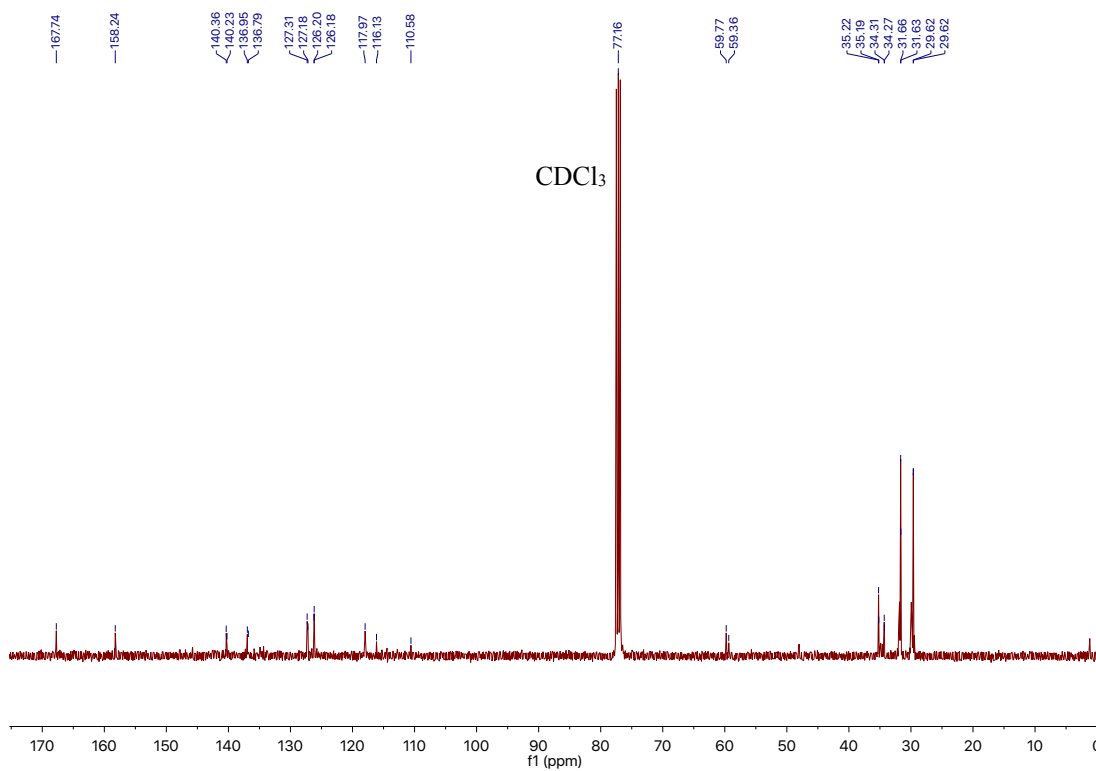


Figure 2.14. ¹³C{¹H} NMR (CDCl₃, 100 MHz) spectrum of 1H₂.

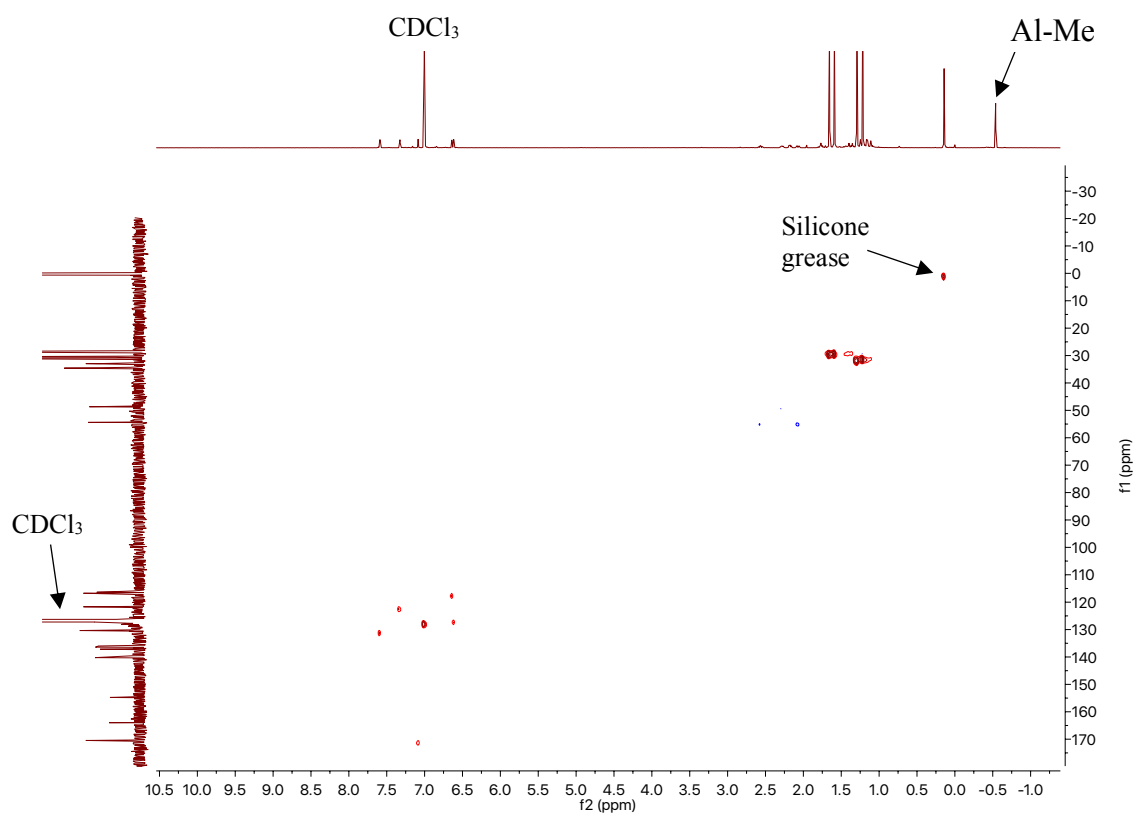


Figure 2.15. HSQC NMR (C_6D_6 , 500 MHz) spectrum of Al(1)Me with Al-Me resonance absent, indicative of structural fluxionality. *N.B.* Figure 2 in ESI.

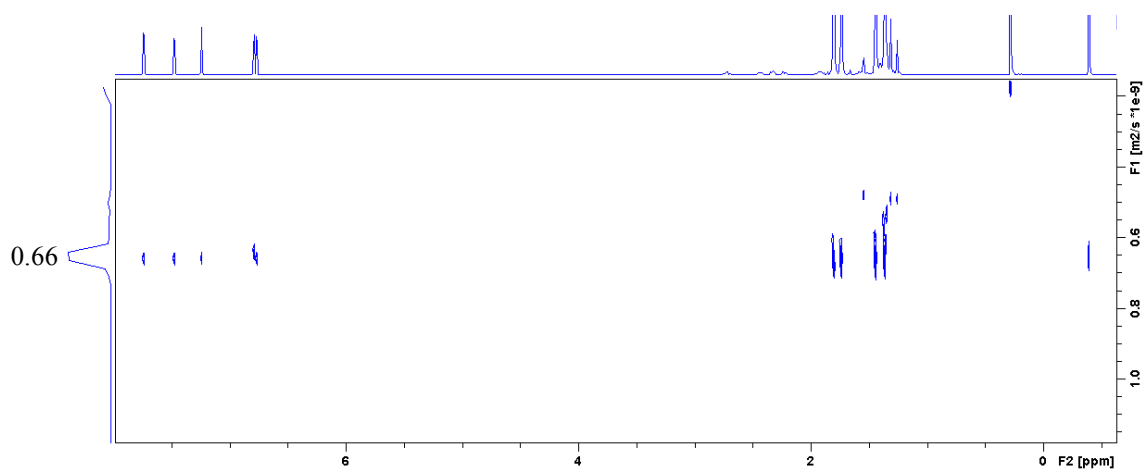


Figure 2.16. DOSY NMR (C_6D_6 , 500 MHz) spectrum of Al(1)Me, indicating only one species present in solution, with a diffusion constant of $0.66 \times 10^{-9} \text{ m}^2 \text{ s}^{-1}$. *N.B.* Figure 1 in ESI.

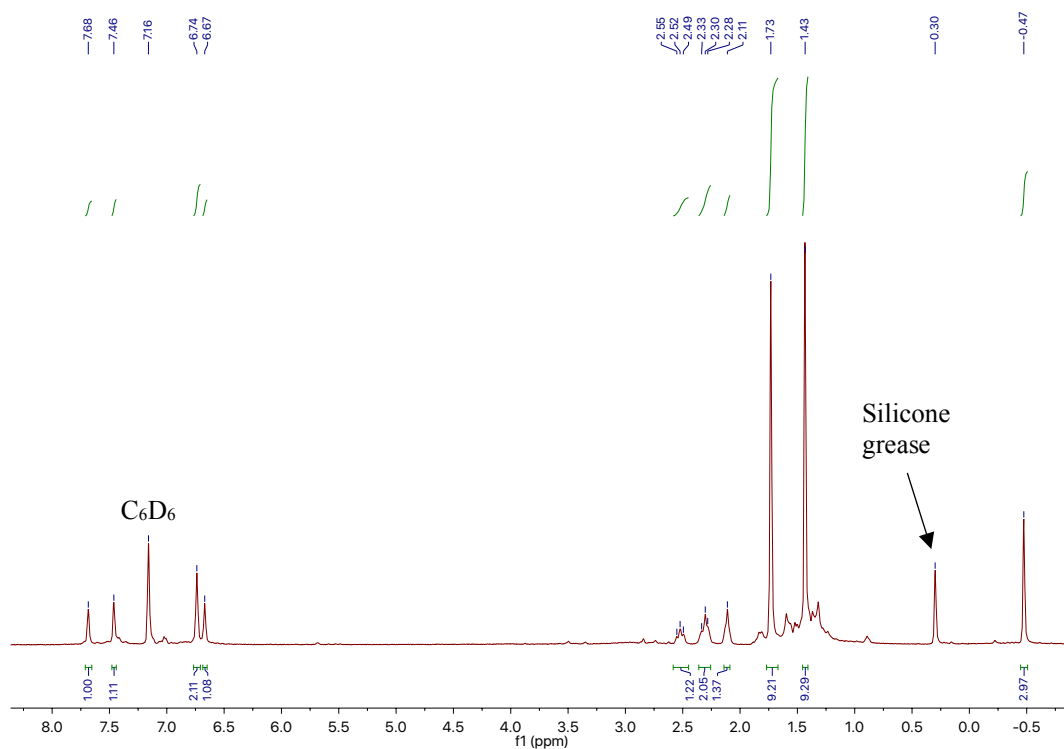


Figure 2.17. ¹H NMR (C₆D₆, 400 MHz) spectrum of Al(3)Me.

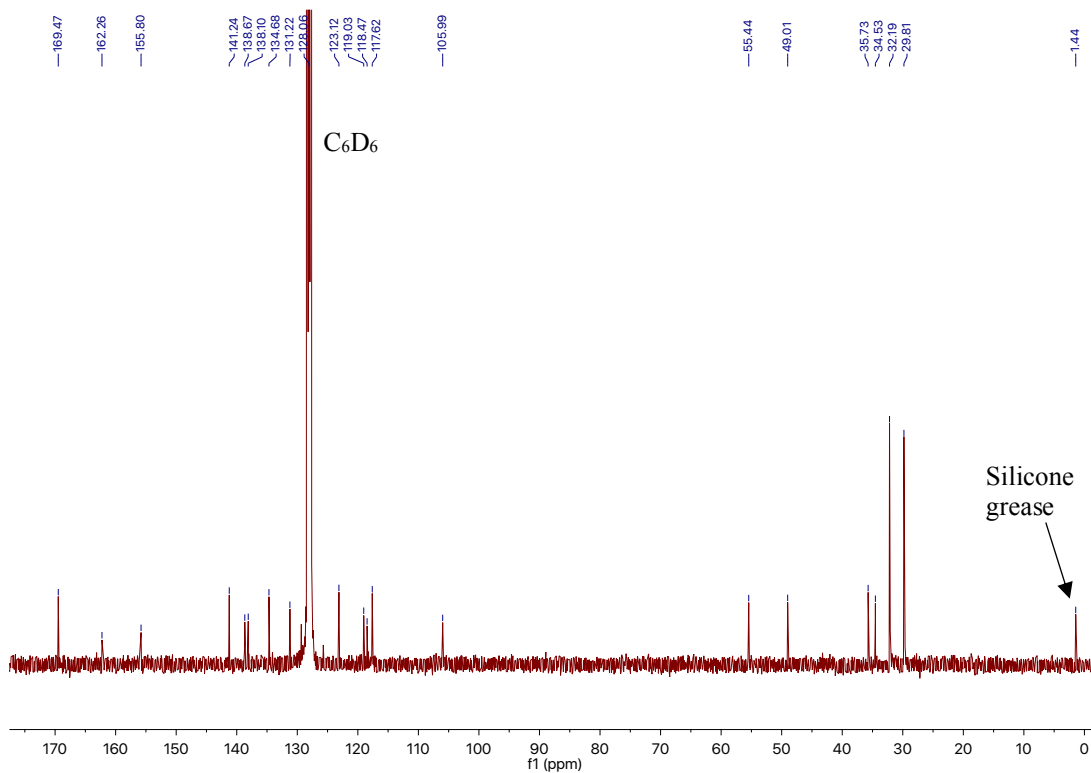


Figure 2.18. ¹³C{¹H} NMR (C₆D₆, 400 MHz) spectrum of Al(3)Me.

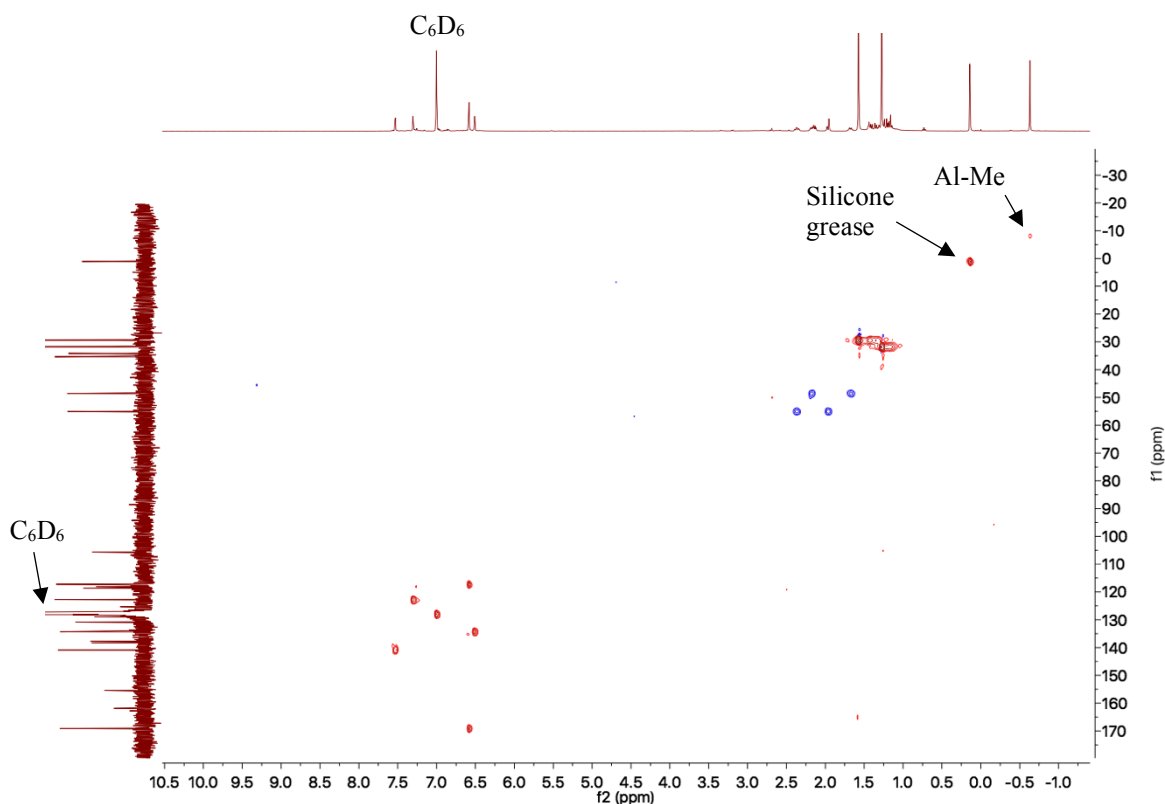


Figure 2.19. HSQC NMR (C_6D_6 , 500 MHz) spectrum of $\text{Al}(\mathbf{3})\text{Me}$ with Al-Me peak present at *ca.* $\delta = -8.10$ ppm. *N.B.* Figure 3 in ESI.

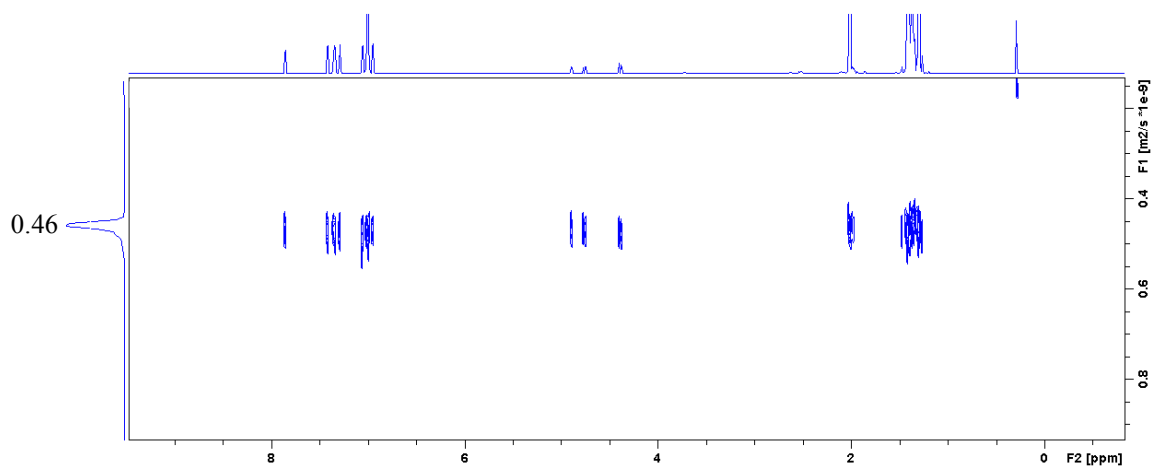


Figure 2.20. DOSY NMR (C_6D_6 , 500 MHz) spectrum of $[\text{Al}(\mathbf{1})\{\text{OBn}\}]_2$, indicating only one species present in solution, with a diffusion constant of $0.46 \times 10^{-9} \text{ m}^2 \text{ s}^{-1}$. *N.B.* Figure 4 in ESI.

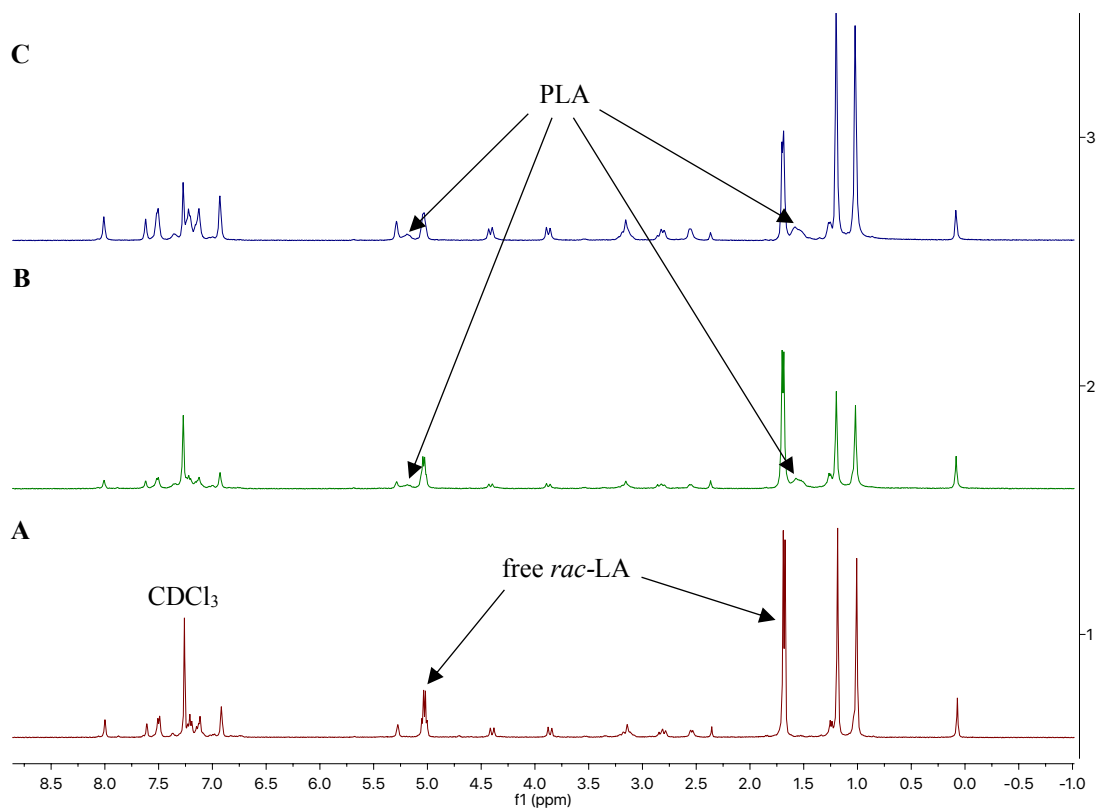


Figure 2.21. Stacked ¹H NMR (CDCl₃, 400 MHz) spectra assessing the stability of [Al(**2**){OBn}]₂ with *rac*-LA {[Al(**2**){OBn}]₂:*rac*-LA] = 1:1}: (A) 10 min at RT; (B) 24 h at RT, and; (C) 1 h at 80 °C. *N.B.* Figure 5 in ESI.

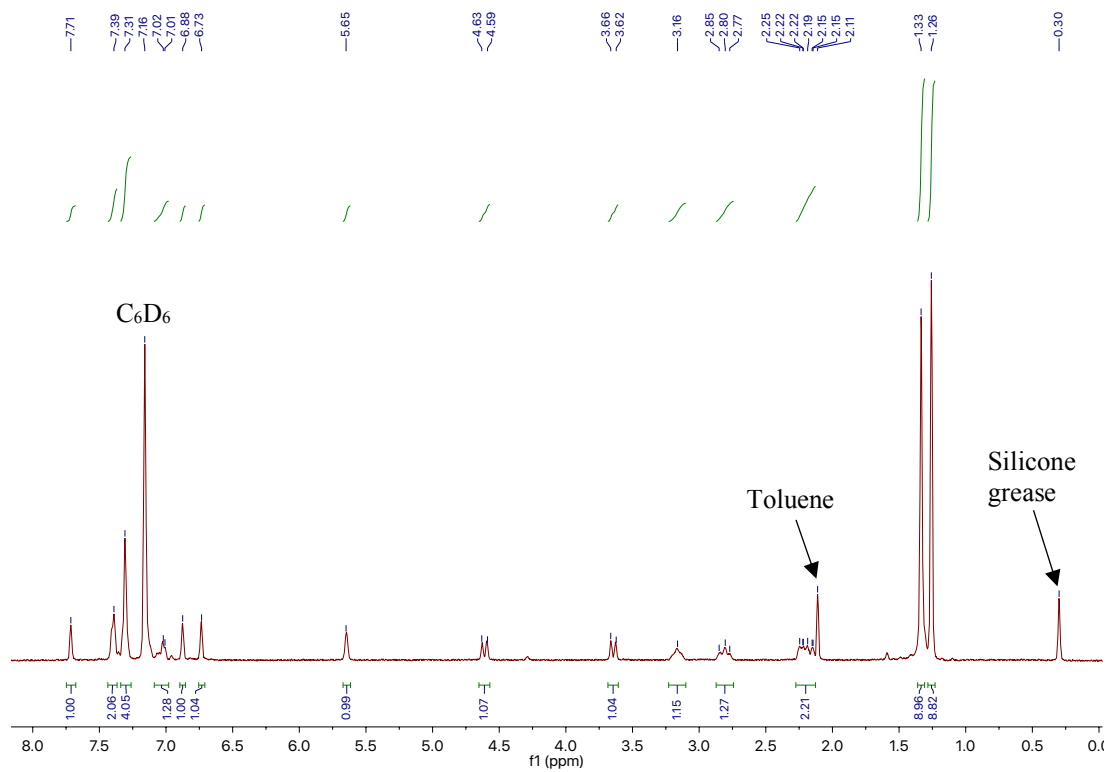


Figure 2.22. ^1H NMR (C_6D_6 , 400 MHz) spectrum of $[\text{Al}(\mathbf{3})\{\text{OBn}\}]_2$.

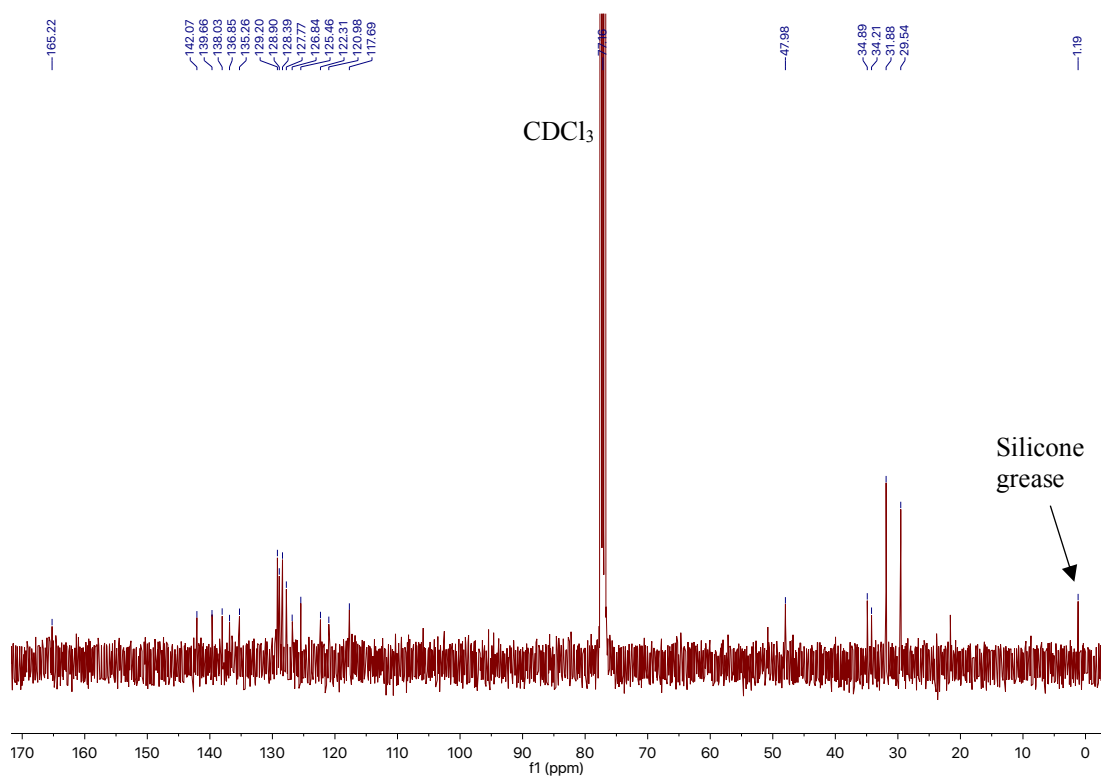


Figure 2.23. $^{13}\text{C}\{^1\text{H}\}$ NMR (CDCl_3 , 100 MHz) spectrum of $[\text{Al}(\mathbf{3})\{\text{OBn}\}]_2$.

2.3.4. Polymer characterisation

2.3.4.1. Representative ^1H NMR spectrum

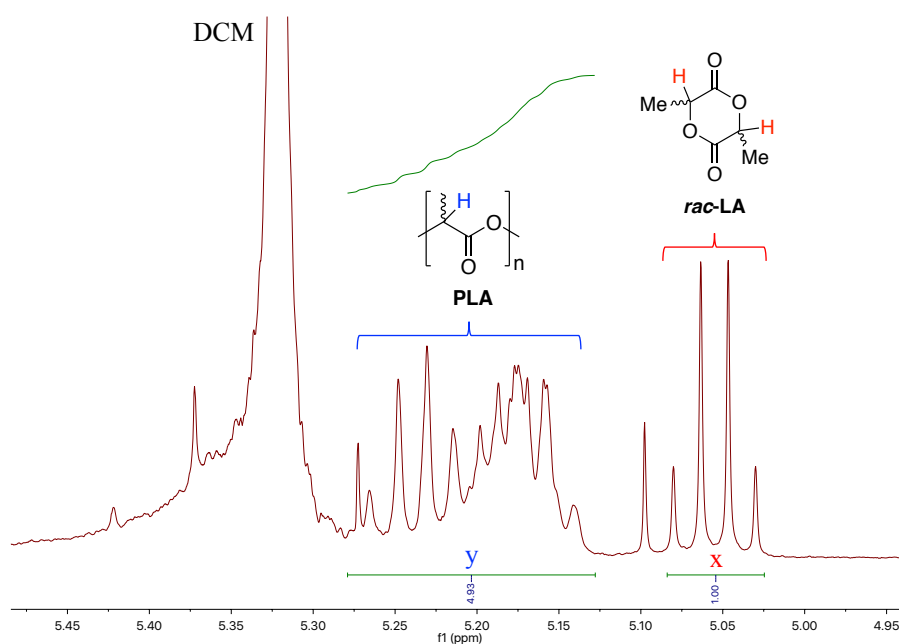


Figure 2.24. ^1H NMR (CDCl_3 , 400 MHz) spectrum of crude PLA obtained from the melt polymerisation of *rac*-LA at 130 °C using $\text{Al}(\mathbf{3})\text{Me}$ $\{[rac\text{-LA}]:[\text{Al}]:[\text{BnOH}] = 300:1:1\}$ (Table 1, Entry 3 in publication 2). PLA conversion = $[y/(x+y)] \times 100\%$. *N.B.* Figure 6 in ESI.

2.3.4.2. Representative SEC spectrum

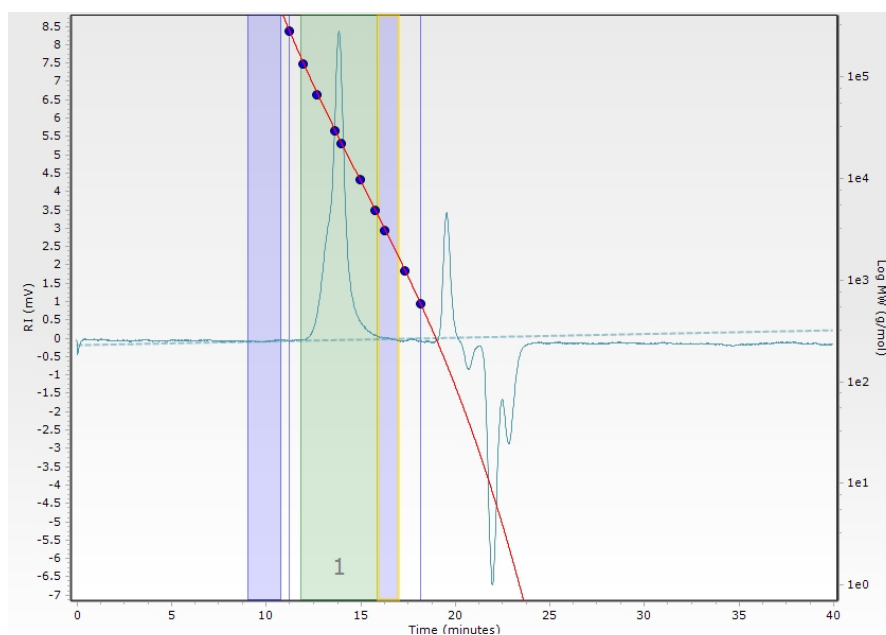


Figure 2.25. Monomodal SEC spectrum of purified PLA obtained from the melt polymerisation of *rac*-LA at 180 °C using $[\text{Al}(\mathbf{3})\{\text{OBn}\}]_2$ $\{[rac\text{-LA}]:[\text{Al}]:[\text{BnOH}] = 3000:1:10\}$ (Table 1, Entry 8 in publication 2). *N.B.* Figure 7 in ESI.

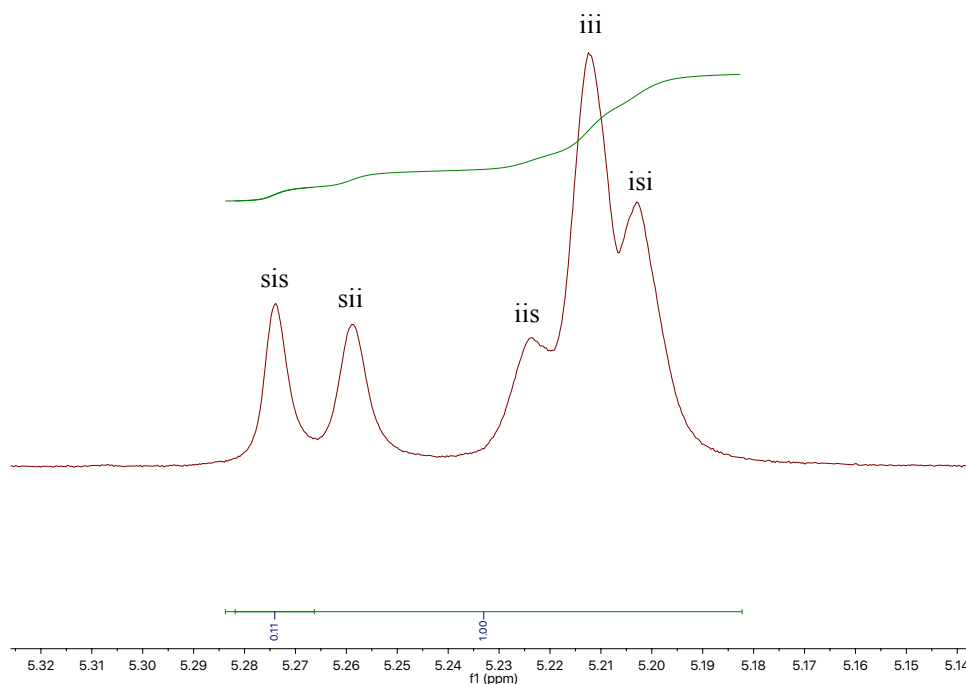


Figure 2.28. Homonuclear decoupled ^1H NMR (CDCl_3 , 400 MHz) spectrum of purified atactic PLA ($P_r = 0.46$) from the melt polymerisation of *rac*-LA using $\text{Al}(\mathbf{1})\text{Me}$ at $130\text{ }^\circ\text{C}$ (Table 1, Entry 1 in publication 2), displaying the five tetrad possibilities in the methine region.^[42] *N.B.* Figure 10 in ESI.

2.3.4.4. MALDI-ToF spectra

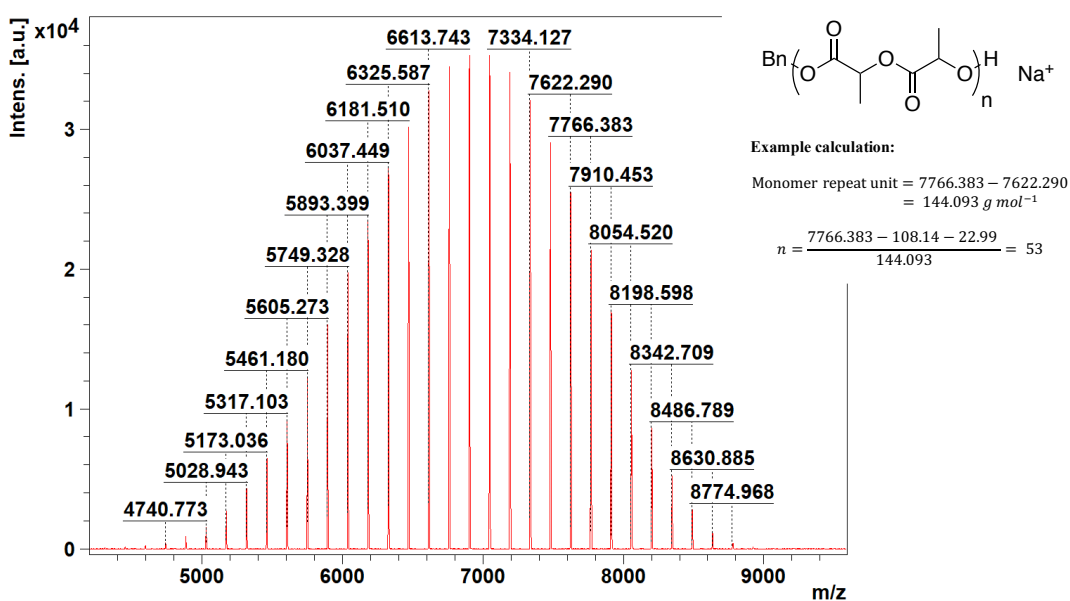


Figure 2.29. MALDI-ToF spectrum of PLA produced using $[\text{Al}(\mathbf{1})\{\text{OBn}\}]_2$ at RT in DCM $\{[rac\text{-LA}]:[\text{Al}]:[\text{BnOH}] = 100:1:1\}$ (Table 2, Entry 6 in publication 2). *N.B.* Figure 11 in ESI.

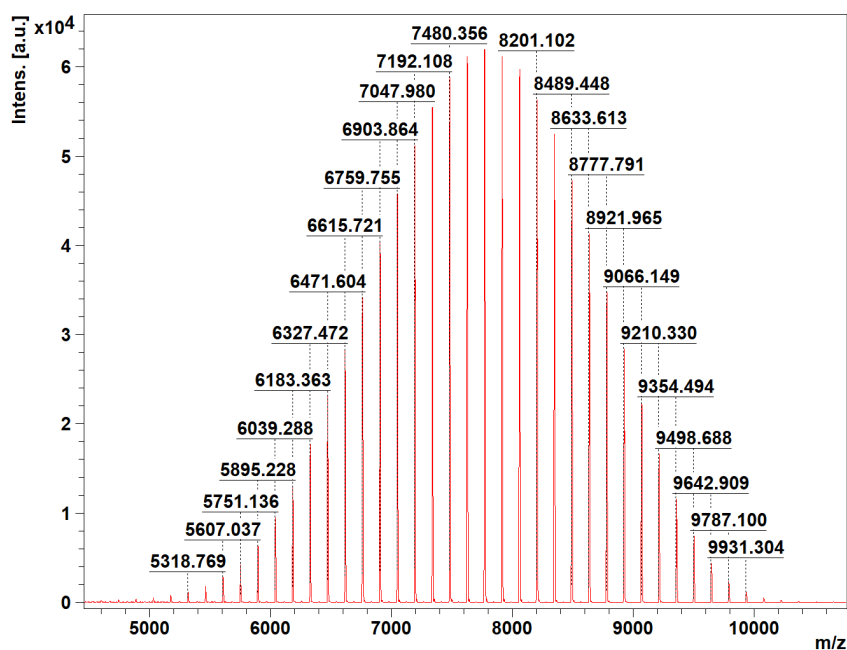


Figure 2.30. MALDI-ToF spectrum of PLA produced using $[\text{Al}(\mathbf{2})\{\text{OBn}\}]_2$ with the addition of 1 equivalent of BnOH at 80 °C in toluene (Table 2, Entry 8 in publication 2). *N.B.* Figure 12 in ESI.

2.3.5. Crystallographic data

2.3.5.1. Special refinement details

$\text{Al}(\mathbf{1})\text{Me}$: Crystal was weakly diffracting, achieving a completeness of 95.6 % (66.601°). The structure is nevertheless unambiguous and a testament to modern diffractometers.

$[\text{Al}(\mathbf{1})\text{OBn}]_2$: The -NH hydrogen atom has been located in the difference Fourier map and was refined with bond length restraint. One of the ^tBu groups in the dimeric complex shows rotational disorder in the ratio 40:60. Atoms within this disorder have been refined using ADP restraints. The cavity in the unit cell contains 1.75 solvent molecules of toluene or 0.875 per asymmetric unit, distributed over three sites. Every solvent molecule is sitting on a centre of inversion. One solvent molecule was refined with 50% occupation, the second one with 25% and the third one with 12.5% occupation. The methyl group of the lowest occupied toluenes has been refined with bond length restraints and all atoms in the lowest occupied toluenes have been refined with ADP restraints.

$[\text{Al}(\mathbf{1})\text{OMe}]_2$: Methyl groups of one ^tBu (C24) groups disordered over two positions (55:45), minor component treated isotropically.

$[\text{Al}(\mathbf{3})\text{OBn}]_2$: ISOR restraints applied to carbon atoms (C22,45) directly attached to bromine groups.

Table 2.2. Crystallographic data of Al(1)Me, [Al(1-3){OBn}]₂ and [Al(1){OMe}]₂. *N.B.*

Table 1 in ESI.

Compound reference	Al(1)Me	[Al(1)OBn] ₂	[Al(1)OMe] ₂	[Al(2)OBn] ₂	[Al(3)OBn] ₂
Chemical formula	C ₃₂ H ₄₉ AlN ₂ O ₂	C _{88.25} H ₁₂₀ Al ₂ N ₄ O ₆	C ₃₂ H ₄₉ AlN ₂ O ₃	C ₈₁ H ₉₄ Al ₂ Cl ₂ N ₄ O ₆	C ₈₁ H ₉₄ Al ₂ Br ₄ N ₄ O ₆
Formula Mass	520.71	1386.84	536.71	1415.36	1593.20
Crystal system	Triclinic	Triclinic	Monoclinic	Monoclinic	Monoclinic
<i>a</i> /Å	9.6309(7)	10.1019(6)	12.4849(9)	9.8297(11)	9.8437(7)
<i>b</i> /Å	11.5396(8)	14.8501(12)	14.4299(9)	29.388(8)	29.300(4)
<i>c</i> /Å	15.2779(10)	15.5646(11)	18.0897(11)	25.847(2)	26.1541(19)
<i>α</i> /°	103.549(6)	111.216(7)	90	90	90
<i>β</i> /°	102.775(6)	103.321(6)	91.719(6)	94.656(9)	94.073(7)
<i>γ</i> /°	98.081(6)	97.899(6)	90	90	90
Unit cell volume/Å ³	1576.3(2)	2054.4(3)	3257.5(4)	7442(2)	7524.2(13)
Temperature/K	150(2)	150(2)	150(2)	150(2)	150(2)
Space group	<i>P</i> $\bar{1}$	<i>P</i> $\bar{1}$	<i>P</i> 2 ₁ / <i>c</i>	<i>P</i> 2 ₁ / <i>n</i>	<i>P</i> 2 ₁ / <i>n</i>
No. of formula units per unit cell, <i>Z</i>	2	1	4	4	4
Radiation type	Cu K α	Cu K α	Cu K α	Cu K α	Cu K α
No. of reflections measured	9363	13154	10718	48475	24315
No. of independent reflections	5330	7395	5621	13140	12986
<i>R</i> _{int}	0.0397	0.0672	0.0626	0.2112	0.1514
Final <i>R</i> _{<i>I</i>} values (<i>I</i> > 2 σ (<i>I</i>))	0.0503	0.0669	0.0925	0.1028	0.0991
Final <i>wR</i> (<i>F</i> ²) values (<i>I</i> > 2 σ (<i>I</i>))	0.1299	0.1486	0.2158	0.2049	0.1696
Final <i>R</i> _{<i>I</i>} values (all data)	0.0629	0.1144	0.1502	0.2233	0.2207
Final <i>wR</i> (<i>F</i> ²) values (all data)	0.1403	0.1784	0.2491	0.2770	0.2342

Table 2.3. Selected bond lengths for Al(1)Me and [Al(1-3){OBn}]₂. *N.B.* Table 2 in ESI.

Init.	Bond	Bond length / Å
Al(1)Me		2.1603(17), 1.9827(19)
[Al(1){OBn}] ₂	Al(1)-N(1) {amine}, Al(1)-	2.122(3), 2.027(3)
[Al(2){OBn}] ₂	N(2) {imine}	2.088(7), 2.020(6)
[Al(3){OBn}] ₂		2.072(9), 2.014(10)

Table 2.4. Selected bond angles for Al(1)Me and [Al(1-3){OBn}]₂ with calculated τ_5 value for the former. Ideal square pyramidal geometry corresponds to $\tau_5 = 0$. *N.B.* Table 3 in ESI.

Init.	Bond	Bond angle / °	τ_5
Al(1)Me	O(1)-Al(1)-N(2), O(2)-Al(1)-N(1)	124.13(7), 161.30(7)	0.62
[Al(1){OBn}] ₂		92.09(11), 166.54	-
[Al(2){OBn}] ₂	O(1)-Al(1)-N(2), O(2)-Al(1)-N(1)	88.2(3), 172.2(3)	-
[Al(3){OBn}] ₂		89.0(4), 171.6(4)	-

2.3.6. Polymerisation kinetic data

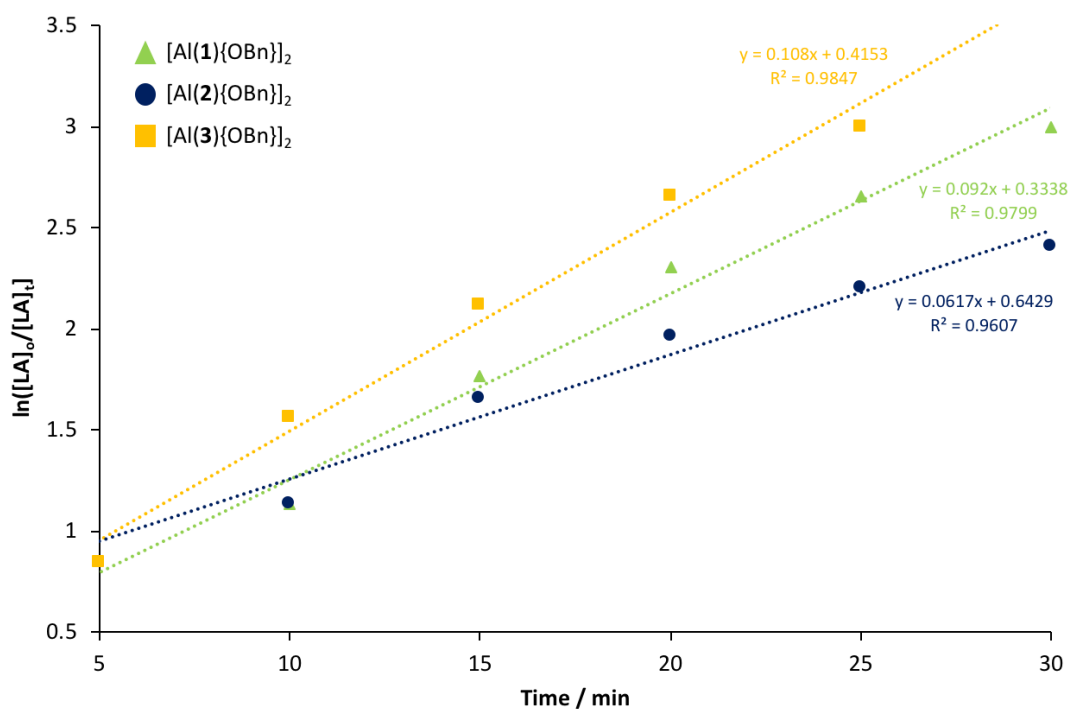


Figure 2.31. First-order logarithmic plot for the polymerisation of *rac*-LA at 80 °C in toluene using $[Al(1-3)\{OBn\}_2]$ $\{[rac\text{-LA}]:[Al][BnOH] = 100:1:1\}$. Note $[LA]_0 = 0.69 \text{ mol dm}^{-3}$. *N.B.* Figure 13 in ESI.

2.4. Post-publication Commentary

Building on previous work, Romain *et al.*^[88] recently investigated the impact of chirality on catalyst aggregation and activity for the ROP of cyclic esters, including lactide. Consequently, a range of novel enantiopure chiral Al(III)-complexes based on the catam ligand scaffold were prepared (Figure 2.32). Enantiopure *S,S*-**25** was found to be the most active, furnishing PLLA of high molecular weight ($M_n = 13,200 \text{ g mol}^{-1}$) and narrow dispersities ($D = 1.3$) within 4.5 min (TOF > $100,000 \text{ h}^{-1}$) under industrially relevant melt conditions $\{150 \text{ }^\circ\text{C}, [L\text{-LA}]:[\text{Al}]:[\text{iPrOH}] = 10,000:1:99\}$. Remarkably, this corresponds to a TOF in excess of $100,000 \text{ h}^{-1}$, surpassing the activity noted for Al(**3**)Me in Chapter 2 (TOF = $45,300 \text{ h}^{-1}$), culminating in the fastest system reported to date for Al(III). Comparatively, *R,R*-**25** and its achiral derivative exhibited inferior performance relative to *S,S*-**25** for lactide polymerisation. Indeed, further kinetic analysis found catalyst chirality induces the formation of homo- and heterodimeric species, which drastically impacts polymerisation activity. This work could potentially provide useful insights into the kinetically limited dissociation discussed for the Al(III)-catam dimers, helping to inform future catalyst design. Indeed, such work promises to compliment findings detailed in Chapter 2, creating new opportunities to realise the untapped potential of Al(III)-initiators for the melt phase production of PLA, with literature examples remaining scarce.^[63,88-90]

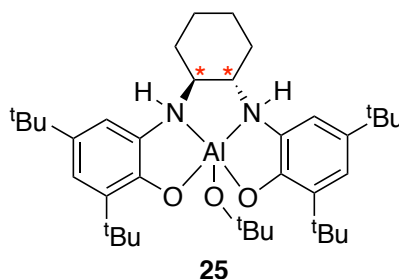


Figure 2.32. Chiral Al(III)-complexes supported by a catam ligand scaffold reported by Romain and co-workers.^[88] *N.B.* Chiral centre denoted by (*).

In Chapter 2, a pronounced stereoselectivity switch dependent on the nature of the ligand backbone employed was observed for the solution phase production of PLA in DCM at RT $\{\text{Al}(\mathbf{1})\text{Me}, P_r = 0.30; \text{Al}(\mathbf{3})\text{Me}, P_r = 0.72\}$, which remains poorly understood. In a comparable study, Gibson and co-workers have previously shown the ancillary ligands of Al(III)-complexes bearing tetradentate bis(aminophenoxide) ligands to dramatically impact polymer microstructure, ranging from highly isotactic ($P_m = 0.79$) to very highly heterotactic ($P_r = 0.96$).^[72] Further computational study should be pursued to understand the origin of this stereocontrol, which is fundamental to future catalyst design and optimisation. Indeed, Marshall *et al.*^[91] and D'Alterio *et al.*^[92] have previously used density functional theory (DFT)

to provide mechanistic insight into the stereoselective ROP of lactide using metal-based catalysts. Such studies will undoubtedly provide a source of inspiration for addressing this challenge.

Finally, Al(III)-complexes have also been reported as highly efficient catalysts for the production of alkyl lactylactates *via* the alcoholysis of lactide.^[93,94] Given such products are the dimeric precursors of lactate esters, it was postulated whether the activity discovered in Chapter 2 could be translated to PLA methanolysis. Consequently, Al(3)Me was selected, owing to its exceptional performance, and trialed in the metal-mediated degradation of PLA into methyl lactate (Me-LA) using the general procedure detailed in section 3.2.3.1. However, Al(3)Me was found to be inactive, observing negligible PLA consumption ($X_{int} = 5\%$) and no evidence of Me-LA formation after 8 h at 80 °C (Figure 2.33). This was presumably due to a combination of poor hydrolytic stability and adverse electronic/steric effects.

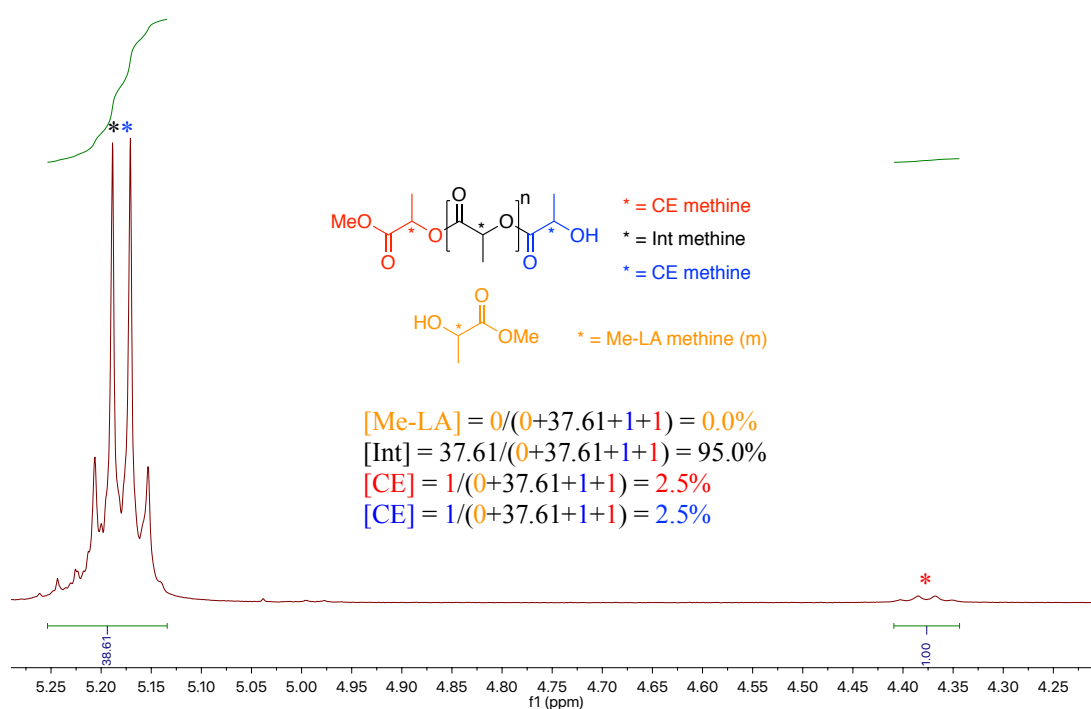


Figure 2.33. ^1H NMR (CDCl_3 , 400 MHz) spectrum of attempted PLA cup (0.25 g, $M_n = 45,510$ g mol $^{-1}$) methanolysis into Me-LA using Al(3)Me (8 wt%, 0.02 g, 1 mol% relative to ester linkages) at 80 °C for 8 h in THF (solvent removed).

2.5. References

- [1] R. Auras, B. Harte, S. Selke, *Macromol. Biosci.* **2004**, *4*, 835–864.
- [2] C. J. Weber, V. Haugaard, R. Festersen, G. Bertelsen, *Food Addit. Contam.* **2002**, *19*, 172–177.
- [3] A. J. R. Lasprilla, G. A. R. Martinez, B. H. Lunelli, A. L. Jardini, R. M. Filho, *Biotechnol. Adv.* **2012**, *30*, 321–328.
- [4] E. Castro-Aguirre, F. Iñiguez-Franco, H. Samsudin, X. Fang, R. Auras, *Adv. Drug Delivery Rev.* **2016**, *107*, 333–366.
- [5] J. Lunt, *Polym. Degrad. Stab.* **1998**, *59*, 145–152.
- [6] K. M. Nampoothiri, N. J. Nair, R. P. John, *Bioresour. Technol.* **2010**, *101*, 8493–8501.
- [7] J. Payne, P. McKeown, M. D. Jones, *Polym. Degrad. Stab.* **2019**, *165*, 170–181.
- [8] J. Payne, M. D. Jones, *ChemSusChem* **2021**, *14*, 4041–4070.
- [9] P. McKeown, M. D. Jones, *Sustainable Chem.* **2020**, *1*, 1–22.
- [10] O. Dechy-Cabaret, B. Martin-Vaca, D. Bourissou, *Chem. Rev.* **2004**, *104*, 6147–6176.
- [11] C. M. Thomas, *Chem. Soc. Rev.* **2010**, *39*, 165–173.
- [12] R. H. Platel, L. M. Hodgson, C. K. Williams, *Polym. Rev.* **2008**, *48*, 11–63.
- [13] M. J. Stanford, A. P. Dove, *Chem. Soc. Rev.* **2010**, *39*, 486–494.
- [14] A. J. Hunt, T. J. Farmer, J. H. Clark in *Element Recovery and Sustainability*, (Eds.: A. J. Hunt), RSC, **2013**, pp. 1–28.
- [15] M. J.-L. Tschan, R. M. Gauvin, C. M. Thomas, *Chem. Soc. Rev.* **2021**, *50*, 13587–13608.
- [16] O. Santoro, X. Zhang, C. Redshaw, *Catalysts* **2020**, *10*, 800.
- [17] M. A. Abdel-Rahman, Y. Tashiro, K. Sonomoto, *Biotechnol. Adv.* **2013**, *31*, 877–902.
- [18] M. A. Abdel-Rahman, Y. Tashiro, K. Sonomoto, *J. Biotechnol.* **2011**, *156*, 286–301.
- [19] D. Garlotta, *J. Polym. Environ.* **2001**, *9*, 63–84.
- [20] R. Datta, M. Henry, *J. Chem. Technol. Biotechnol.* **2016**, *81*, 1119–1129.
- [21] P. VanWouwe, M. Dusselier, E. Vanleeuw, B. Sels, *ChemSusChem* **2016**, *9*, 907–921.
- [22] K. Ishihara, S. Ohara, H. Yamamoto, *Science* **2000**, *290*, 1140–1142.
- [23] B. Y. Y. Zhao, Z. Wang, J. Wang, H. Mai, F. Yang, *J. Appl. Polym. Sci.* **2004**, *91*, 2143–2150.
- [24] H. L. Le Châtelier, *C. R. Acad. Sci.* **1884**, *99*, 786–789.
- [25] E. T. H. Vink, K. R. Rábago, D. A. Glassner, B. Springs, R. P. O'Connor, J. Kolstad, P. R. Gruber, *Macromol. Biosci.* **2004**, *4*, 551–564.
- [26] W. H. Carothers, G. L. Dorough, F. J. van Natta, *J. Am. Chem. Soc.* **1932**, *54*, 761–772.

- [27] A. Duda, S. Penczek, *Macromolecules* **1990**, *23*, 1636–1639.
- [28] S. C. Roşca, D. A. Rosca, V. Dorcet, C. M. Kozak, F. M. Kerton, J. F. Carpentier, Y. Sarazin, *Dalton Trans.* **2013**, *42*, 9361–9375.
- [29] N. E. Kamber, W. Jeong, R. M. Waymouth, R. C. Pratt, B. G. G. Lohmeijer, J. L. Hedrick, *Chem. Rev.* **2007**, *107*, 5813–5840.
- [30] B. G. G. Lohmeijer, R. C. Pratt, F. Leibfarth, J. W. Logan, D. A. Long, A. P. Dove, F. Nederberg, J. Choi, C. Wade, R. M. Waymouth, J. L. Hedrick, *Macromolecules* **2006**, *39*, 8574–8583.
- [31] F. Nederberg, E. F. Connor, M. Möller, T. Glauser, J. L. Hedrick, *Angew. Chem. Int. Ed.* **2001**, *40*, 2712–2715.
- [32] R. C. Pratt, B. G. G. Lohmeijer, D. A. Long, R. M. Waymouth, J. L. Hedrick, *J. Am. Chem. Soc.* **2006**, *128*, 4556–4557.
- [33] A. P. Dove, R. C. Pratt, B. G. G. Lohmeijer, R. M. Waymouth, J. L. Hedrick, *J. Am. Chem. Soc.* **2005**, *127*, 13798–13799.
- [34] D. J. A. Cameron, M. P. Shaver, *Chem. Soc. Rev.* **2011**, *40*, 1761–1776.
- [35] R. Tong, *Ind. Eng. Chem. Res.* **2017**, *56*, 4207–4219.
- [36] Y. Fan, C. Zhou, X. Zhu, *Catal. Rev. Sci. Eng.* **2009**, *51*, 293–324.
- [37] S. Brochu, R. E. Prud'Homme, I. Barakat, R. Jerome, *Macromolecules* **1995**, *28*, 5230–5239.
- [38] H. Tsuji, *Macromol. Biosci.* **2005**, *5*, 569–597.
- [39] H. Tsuji, T. Tajima, *Polym. Int.* **2015**, *64*, 54–65.
- [40] A. Buchard, C. M. Bakewell, J. Weiner, C. K. Williams in *Organometallics and Renewables*, (Eds.: M. A. R. Meier, B. M. Weckhuysen, P. C. A. Bruijninx), Springer Heidelberg, **2012**, pp. 175–224.
- [41] P. McKeown, PhD Thesis, University of Bath (UK), **2017**.
- [42] B. M. Chamberlain, M. Cheng, D. R. Moore, T. M. Ovitt, E. B. Lobkovsky, G. W. Coates, *J. Am. Chem. Soc.* **2001**, *123*, 3229–3238.
- [43] J. Coudane, C. Ustariz-Peyret, G. Schwach, M. Vert, *J. Polym. Sci. Pol. Chem.* **1997**, *35*, 1651–1658.
- [44] B.-T. Ko, C.-C. Lin, *J. Am. Chem. Soc.* **2001**, *123*, 7973–7977.
- [45] J. Baran, A. Duda, A. Kowalski, R. Szymanski, S. Penczek, *Macromol. Rapid Commun.* **1997**, *18*, 325–333.
- [46] J. Beament, PhD Thesis, University of Bath (UK), **2019**.
- [47] P. R. Gruber, US. Pat. 6326458 B1, **2001**.
- [48] R. E. Drumright, P. R. Gruber, D. E. Henton, *Adv. Mater.* **2000**, *12*, 1841–1846.
- [49] H. R. Kricheldorf, I. Kreiser-Saunders, A. Stricker, *Macromolecules* **2000**, *33*, 702–709.

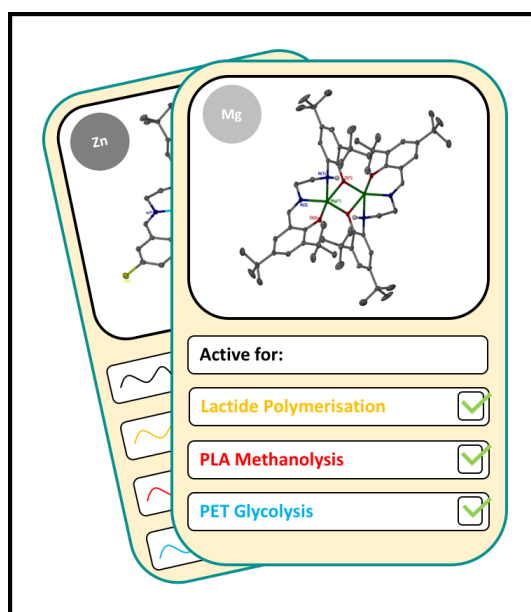
- [50] P. Dubois, C. Jacobs, R. Jerome, P. Teyssie, *Macromolecules* **1991**, *24*, 2266–2270.
- [51] A. Kowalski, A. Duda, S. Penczek, *Macromolecules* **1998**, *31*, 2114–2122.
- [52] N. Spassky, M. Wisniewski, C. Pluta, A. LeBorgne, *Macromol. Chem. Phys.* **1996**, *197*, 2627–2637.
- [53] T. M. Ovitt, G. W. Coates, *J. Am. Chem. Soc.* **1999**, *121*, 4072–4073.
- [54] T. M. Ovitt, G. W. Coates, *J. Polym. Sci., Part A: Polym. Chem.* **2000**, *38*, 4686–4692.
- [55] C. P. Radano, G. L. Baker, M. R. Smith, *J. Am. Chem. Soc.* **2000**, *122*, 1552–1553.
- [56] K. Majerska, A. Duda, *J. Am. Chem. Soc.* **2004**, *126*, 1026–1027.
- [57] Z. Y. Zhong, P. J. Dijkstra, J. Feijen, *Angew. Chem. Int. Ed.* **2002**, *41*, 4510–4513.
- [58] Z. Zhong, P. J. Dijkstra, J. Feijen, *J. Am. Chem. Soc.* **2003**, *125*, 11291–11298.
- [59] T. K. Saha, V. Ramkumar, D. Chakraborty, *Inorg. Chem.* **2011**, *50*, 2720–2722.
- [60] M. Wisniewski, A. LeBorgne, N. Spassky, *Macromol. Chem. Phys.* **1997**, *198*, 1227–1238.
- [61] E. D. Cross, L. E. N. Allan, A. Decken, M. P. Shaver, *J. Polym. Sci., Part A: Polym. Chem.* **2013**, *51*, 1137–1146.
- [62] N. Nomura, R. Ishii, M. Akakura, K. Aoi, *J. Am. Chem. Soc.* **2002**, *124*, 5938–5939.
- [63] N. Nomura, R. Ishii, Y. Yamamoto, T. Kondo, *Chem. Eur. J.* **2007**, *13*, 4433–4451.
- [64] H.-L. Chen, S. Dutta, P.-Y. Huang, C.-C. Lin, *Organometallics* **2012**, *31*, 2016–2025.
- [65] P. Hormnirun, E. L. Marshall, V. C. Gibson, R. I. Pugh, A. J. P. White, *Proc. Natl. Acad. Sci. U. S. A.* **2006**, *103*, 15343–15348.
- [66] E. L. Whitelaw, G. Loraine, M. F. Mahon, M. D. Jones, *Dalton Trans.* **2011**, *40*, 11469–11473.
- [67] S. L. Hancock, M. F. Mahon, M. D. Jones, *Dalton Trans.* **2013**, *42*, 9279–9285.
- [68] M. D. Jones, L. Brady, P. McKeown, A. Buchard, P. M. Schafer, L. H. Thomas, M. F. Mahon, T. J. Woodman, J. P. Lowe, *Chem. Sci.* **2015**, *6*, 5034–5039.
- [69] A. Pilone, K. Press, I. Goldberg, M. Kol, M. Mazzeo, M. Lamberti, *J. Am. Chem. Soc.* **2014**, *136*, 2940–2943.
- [70] P. McKeown, M. G. Davidson, J. P. Lowe, M. F. Mahon, L. H. Thomas, T. J. Woodman, M. D. Jones, *Dalton Trans.* **2016**, *45*, 5374–5387.
- [71] P. McKeown, M. G. Davidson, G. Kociok-Köhn, M. D. Jones, *Chem. Commun.* **2016**, *52*, 10431–10434.
- [72] P. Hormnirun, E. L. Marshall, V. C. Gibson, A. J. P. White, D. J. Williams, *J. Am. Chem. Soc.* **2004**, *126*, 2688–2689.
- [73] H. Du, A. H. Velders, P. J. Dijkstra, J. Sun, Z. Zhong, X. Chen, J. Feijen, *Chem. Eur. J.* **2009**, *15*, 9836–9845.
- [74] K. Press, I. Goldberg, M. Kol, *Angew. Chem. Int. Ed.* **2015**, *54*, 14858–14861.
- [75] R. Hador, A. Botta, V. Venditto, S. Lipstman, I. Goldberg, M. Kol, *Angew. Chem. Int. Ed.* **2019**, *58*, 14679–14685.

- [76] S. Gesslbauer, H. Cheek, A. J. P. White, C. Romain, *Dalton Trans.* **2018**, *47*, 10410–10414.
- [77] S. Gesslbauer, R. Savela, Y. Chen, A. J. P. White, C. Romain, *ACS Catal.* **2019**, *9*, 7912–7920.
- [78] D. E. Stasiw, M. Mandal, B. D. Neisen, L. A. Mitchell, C. J. Cramer, W. B. Tolman, *Inorg. Chem.* **2017**, *56*, 725–728.
- [79] J. A. Macaranas, A. M. Luke, M. Mandal, B. D. Neisen, D. J. Marell, C. J. Cramer, W. B. Tolman, *Inorg. Chem.* **2018**, *57*, 3451–3457.
- [80] E. E. Marlier, J. A. Macaranas, D. J. Marell, C. R. Dunbar, M. A. Johnson, Y. DePorre, M. O. Miranda, B. D. Neisen, C. J. Cramer, M. A. Hillmyer, W. B. Tolman, *ACS Catal.* **2016**, *6*, 1215–1224.
- [81] F. Hild, P. Haquette, L. BreLOT, S. Dagorne, *Dalton Trans.* **2010**, *39*, 533–540.
- [82] C. Robert, T. E. Schmid, V. Richard, P. Haquette, S. K. Raman, M.-N. Rager, R. M. Gauvin, Y. Morin, X. Trivelli, V. Guérineau, I. del Rosal, L. Maron, C. M. Thomas, *J. Am. Chem. Soc.* **2017**, *139*, 6217–6225.
- [83] S. Praban, P. Piromjitpong, V. Balasanthiran, S. Jayaraj, M. H. Chisholm, J. Tantirungrotechai, K. Phomphrai, *Dalton Trans.* **2019**, *48*, 3223–3230.
- [84] M. Anker, C. Balasanthiran, V. Balasanthiran, M. H. Chisholm, S. Jayaraj, K. Mathieu, P. Piromjitpong, S. Praban, B. Raya, W. J. Simonsick, *Dalton Trans.* **2017**, *46*, 5938–5945.
- [85] G. R. Fulmer, A. J. M. Miller, N. H. Sherden, H. E. Gottlieb, A. Nudelman, B. M. Stoltz, J. E. Bercaw, K. I. Goldberg, *Organometallics* **2010**, *29*, 2176–2179.
- [86] R. Evans, Z. Deng, A. K. Rogerson, A. S. McLachlan, J. J. Richards, M. Nilsson, G. A. Morris, *Angew. Chem. Int. Ed.* **2013**, *52*, 3199–3202.
- [87] K. S. Min, T. Weyhermüller, E. Bothe, K. Wieghardt, *Inorg. Chem.* **2004**, *43*, 2922–2931.
- [88] S. Gesslbauer, G. Hutchinson, A. J. P. White, J. Burés, C. Romain, *ACS Catal.* **2021**, *11*, 4084–4093.
- [89] J. Payne, P. McKeown, G. Kociok-Köhn, M. D. Jones, *Chem. Commun.* **2020**, *56*, 7163–7166.
- [90] J. Gao, D. Zhu, W. Zhang, G. A. Solan, Y. Ma, W.-H. Sun, *Inorg. Chem. Front.* **2019**, *6*, 2619–2652.
- [91] E. L. Marshall, V. C. Gibson, H. S. Rzepa, *J. Am. Chem. Soc.* **2005**, *127*, 6048–6051.
- [92] M. C. D'Alterio, C. De Rosa, G. Talarico, *Chem. Commun.* **2021**, *57*, 1611–1614.
- [93] H. Kampová, E. Riemlová, J. Klikarová, V. Pejchal, J. Merna, P. Vlasák, P. Švec, Z. Růžicková, A. Růžička, *J. Organomet. Chem.* **2015**, *778*, 35–41.
- [94] K. V. Zaitsev, V. S. Cherepakhin, A. Zhrebker, A. Kononikhin, E. Nikolaev, A. V. Churakov, *J. Organomet. Chem.* **2018**, *875*, 11–23.

Chapter 3.

Metal Diversification in Pursuit of Catalysts Active for the Chemical Recycling of Polyesters

Publication 3: Make or break: Mg(II)- and Zn(II)-catalen complexes for PLA production and recycling of commodity polyesters



Acknowledgement: The work presented in this chapter has been published in the journal *‘Polymer Chemistry’*, volume 12, issue 8, pages 1086–1096 and is reproduced with the permission of the Royal Society of Chemistry. The electronic supporting information (ESI) has been amended into a supporting experimental section for clarity. Additional figures (*e.g.* representative NMR spectra) have been added, where appropriate, to support the worked presented herein.

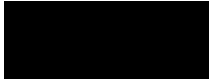
3. Preamble

A range of Al(III)-catalen initiators were shown to exhibit unprecedented activity in the melt phase production of PLA in Chapter 2. Given the mechanistic similarities between metal-mediated PLA production and degradation, principally the metal centre acting as a Lewis acid to assist nucleophilic attack of the carbonyl, it was envisioned such activity might be transferable.^[1-3] However, such complexes were found to be inactive for PLA methanolysis, presumably due to a combination of poor hydrolytic stability and adverse electronic/steric effects. Indeed, given the use of wet solvents in this process, the development of robust metal-based pre-catalysts was considered of paramount importance. This opportunity was further confounded by the lack of metal-mediated examples reported to date as noted in Chapter 1.

In this chapter, metal diversification is explored as a possible solution to these challenges. Zn(II) was selected owing to an established literature precedence for such initiators being highly active for PLA production and, more recently, degradation, whilst also being cheap and biocompatible.^[4-14] Beyond comparable advantages with its use, Mg(II) was selected as a comparison due to it possessing a similar charge and valency, enabling metal-ligand cooperative effects to be further probed. Furthermore, the use of a divalent metal centre in combination with stoichiometric quantities of catalen ligand (1:1) should promote the formation of homoleptic dimers, which were predicted to exhibit superior stability relative to their aluminium-based counterparts. To ensure industrial relevance, all polyester samples used in degradation studies were commercially sourced.

In Chapter 3, metal diversification is shown to adversely impact polymerisation activity under both melt and solution conditions. However, the first example of PLA methanolysis mediated by a discrete Mg(II)-complex is demonstrated under relatively mild conditions (80 °C). Interestingly, their Zn(II)-analogues exhibited significantly reduced activity, possibly evidencing detrimental catalyst aggregation, which appeared less prevalent in the Mg(II)-complexes. Indeed, kinetically limited dissociation was highlighted in Chapter 2 for the Al(III)-catalen dimers as a possible cause for poor polymerisation control in solution. Preliminary work extended the polymer chemical recycling scope to PET from various sources, demonstrating catalyst versatility.

3.1. Statement of Authorship

This declaration concerns the article entitled:	
Make or break: Mg(II)- and Zn(II)-catalen complexes for PLA production and recycling of commodity polyesters	
Publication status (tick one)	
Draft manuscript <input type="checkbox"/> Submitted <input type="checkbox"/> In review <input type="checkbox"/> Accepted <input type="checkbox"/> Published <input checked="" type="checkbox"/>	
Publication details (reference)	J. Payne, P. McKeown, O. Driscoll, G. Kociok-Köhn, E. A. C. Emanuelsson, M. D. Jones, <i>Polym. Chem.</i> 2021 , 12, 1086-1096 (DOI: 10.1039/D0PY01519A)
Copyright status (tick the appropriate statement)	
I hold the copyright for this material <input checked="" type="checkbox"/> Copyright is retained by the publisher, but I have been given permission to replicate the material here <input type="checkbox"/>	
Candidate's contribution to the paper (provide details, and also indicate as a percentage)	<p>The candidate predominantly executed the work presented in the paper.</p> <p>Formulation of ideas:</p> <p>Ideas were discussed and planned with PM, EE and MDJ. The manuscript draft was prepared by JMP with editing from PM and MDJ during the editing stage. [JMP = 80%, PM = 5%, OD = 0%, GKK = 0%, EE = 5%, MDJ = 10%]</p> <p>Design of methodology:</p> <p>Experiments were discussed and planned with PM and MDJ. [JMP = 80%, PM = 10%, OD = 0%, GKK = 0%, EE = 0%, MDJ = 10%]</p> <p>Experimental work:</p> <p>Experimental work and data analysis were conducted by JMP. X-ray crystallographic data was collected and processed by PM, GKK and MDJ. OD assisted with collecting kinetic data for PLA methanolysis. [JMP = 80%, PM = 10%, OD = 2%, GKK = 3%, EE = 0%, MDJ = 5%]</p> <p>Presentation of data in journal format:</p> <p>All figures, tables and schemes were prepared by JMP. [JMP = 100%]</p>
Statement from Candidate	This paper reports on original research I conducted during the period of my Higher Degree by Research candidature.
Signed	
Date	7/6/2022



Cite this: *Polym. Chem.*, 2021, **12**, 1086

Make or break: Mg(II)- and Zn(II)-catalen complexes for PLA production and recycling of commodity polyesters†

Jack Payne,^a Paul McKeown,^b Oliver Driscoll,^b Gabriele Kociok-Köhn,^b Emma A. C. Emanuelsson^c and Matthew D. Jones^b

Recently we reported a series of highly active Al(III)-complexes bearing a catalen ligand support for lactide polymerisation, observing unprecedented activity in the melt. Herein we report diversification of the metal to furnish a series of well-defined dimeric Zn(II)- and Mg(II)-complexes, which were fully characterised by X-ray crystallography and NMR spectroscopy. The production of biocompatible atactic PLA from *rac*-LA in solution and under industrially preferred solvent-free conditions was demonstrated, typically observing good activity and M_n control with a broad range of dispersities ($D = 1.08$ – 2.04). Mg(II)-Complexes were shown to facilitate the relatively mild methanolysis of PLA, achieving up to 64% conversion to Me-LA within 8 h at 80 °C in THF. Further kinetic analysis found [Mg(**1,3**)₂] to have k_{app} values of 0.628 ± 0.0536 {4 wt% cat. loading} and 0.265 ± 0.0193 h⁻¹ {8 wt% cat. loading} respectively for the rate of consumption of PLA. Preliminary work extended polymer scope to PET from various sources, demonstrating catalyst versatility.

Received 30th October 2020,
Accepted 23rd December 2020
DOI: 10.1039/d0py01519a

rsc.li/polymers

Introduction

Inexpensive, lightweight and robust, plastics remain a tremendous source of social and economic value, providing 1.6 million jobs and turning over € 360 billion in 2018 in Europe alone.^{1,2} However, the current plastics economy remains fundamentally limited, dominated by petroleum-based products operating within a linear model, which underpins mounting environmental concerns.^{3–8} Ocean plastics typify the severity of current plastic pollution with the Great Pacific Garbage Patch (GPGP), an accumulation zone of ocean plastics, encompassing *ca.* 1.6 million km², equivalent to three times the area of France.⁹ This has stimulated considerable research into renewable and environmentally friendly alternatives, for example poly(lactic acid) (PLA). Traditionally produced from the metal-mediated ring-opening polymerisation (ROP) of lactide (LA), a bio-based monomer feedstock, PLA has

subsequently found commercial use in both the packaging and biomedical sector.^{3,10–14} Recent research has primarily sought to address toxicity concerns associated with the industry standard, Sn(Oct)₂, through the development of biocompatible and environmentally benign alternatives.^{15–17} Consequently, a diverse range of metals have been explored, including Al(III)^{18–35} and group(IV),^{36–49} with a particular focus on retaining activity whilst maintaining stereocontrol. Metals most pertinent to this report include Zn(II) and Mg(II), which are cheap and non-toxic. Zinc complexes have previously been shown to be highly effective initiators for the ROP of LA, generally observing high activity in solution.^{50–64} Pioneering work by Coates and co-workers reported a highly heteroselective Zn(II)-complex bearing a β-diiminate ligand, achieving up to $P_r = 0.94$ in the ROP of *rac*-LA at 0 °C.⁶⁵ Dizinc catalysts supported by macrocyclic ligands developed by Williams and co-workers remain the fastest reported to date under solution conditions, exhibiting high TOFs (up to 60 000 h⁻¹) at room temperature in THF.⁶⁶ The most isoselective Zn(II)-complex known is an aminophenolate initiator reported by Ma and co-workers, which achieved $P_r = 0.07$ at –40 °C.⁶⁷ McKeown *et al.*⁶⁸ have reported a series of simple Zn(II)-Schiff Base complexes capable of achieving TOFs in excess of 100 000 h⁻¹ under immortal conditions in the melt. Recently, Hermann *et al.*⁶⁹ reported a highly active and robust zinc-guanidine complex capable of producing colourless, high molecular weight ($M_n \sim 150\,000$ g mol⁻¹) PLA within minutes under solvent-free

^aCentre for Sustainable and Circular Technologies, University of Bath, Claverton Down, Bath, BA2 7AY, UK

^bDepartment of Chemistry, University of Bath, Claverton Down, Bath, BA2 7AY, UK. E-mail: mj205@bath.ac.uk

^cDepartment of Chemical Engineering, University of Bath, Claverton Down, Bath, BA2 7AY, UK

† Electronic supplementary information (ESI) available: Full details of the experimental protocols with selected spectra and raw data. CCDC 2041361–2041367. For ESI and crystallographic data in CIF or other electronic format see DOI: 10.1039/d0py01519a

conditions ($k_p = 1.43 \pm 0.09 \text{ L mol}^{-1} \text{ s}^{-1}$), culminating in the fastest reported system to date, significantly outperforming Sn(Oct)₂. Magnesium complexes have also received significant interest in the ROP of LA.^{70–82} Chisholm and co-workers have reported numerous Mg(II)-complexes for the production of heterotactic PLA ($P_r = 0.90–0.96$).^{51,83–85} Both Coates *et al.*⁵⁰ (Zn(II), $P_r = 0.94$; Mg(II), atactic PLA) and Ma *et al.*⁵⁸ (Zn(II), $P_r = 0.20$; Mg(II), $P_r = 0.81$) have previously shown metal exchange to dramatically impact stereocontrol. Despite such promising advancements, the widespread use of PLA remains limited by a high production cost.^{3,11} Additionally, if not disposed of appropriately, PLA is a potential contributor to the plastic waste crisis.^{3,86} Plastic pollution mitigation requires the industry adopts a circular model, one concerned with material recapture and reuse, with recycling a potential solution.^{1,3,7} Whilst mechanical recycling is traditionally employed, its long-term suitability is limited by eventual material downcycling.^{2,87} A possible alternative is chemical recycling, which enables value-added products such as lactate esters, lactic acid and acrylic acid to be accessed.^{3,88,89} Lactic acid has been identified as a platform chemical, whilst lactate esters have been cited as potential green solvent replacements owing to their low toxicity and biodegradability.^{90–93} It is anticipated the potential for enhanced socio-economic performance will drive market penetration and reduce PLA production costs.⁹⁴ Indeed, the ethyl lactate market is projected to reach \$ 92 million by 2024 and currently trades at £ 2.54–3.49 per kg relative to £ 1.69 per kg for virgin PLA.^{91,95} PLA recycling processes include hydrolysis^{96–103} and alcoholysis.^{104–115} Hydrogenation^{116–118} and hydrosilylation¹¹⁹ processes exploiting ruthenium and iridium have also been reported. Simple, commercially available metal salts and precursors (*e.g.* FeCl₃) have been shown to facilitate the transesterification of PLA, typically in the presence of methanol to afford methyl lactate (Me-LA).^{120–122} Sobota and co-workers demonstrated the transesterification of PLA using a wide range of alcohols in the presence of Mg(II) and Ca(II) pre-catalysts, typically operating under high temperature and pressure regimes.¹¹¹ Organocatalysts have also been exploited in PLA degradation, for example triazabicyclodecene (TBD), 4-(dimethylamino)pyridine (DMAP) and tetramethylammonium methyl carbonate.^{112–114} McKeown *et al.*¹²³ recently demonstrated a homoleptic Zn(II)-complex bearing a propylenediamine backbone to be highly active for PLA methanolysis, achieving 84% conversion to Me-LA ($Y_{\text{Me-LA}}$) within 1 h at 50 °C. The corresponding ethylenediamine analogue exhibited significantly reduced activity ($Y_{\text{Me-LA}} = 12\%$ in 6 h) under comparable conditions (40 °C), highlighting the importance of structure-activity relationships.^{109,123} However, the use of metal-based catalysts for this purpose remains rare despite the plethora reported for LA polymerisation. There is also a clear appetite to diversify metal scope to address potential long-term availability concerns associated with zinc.¹²⁴

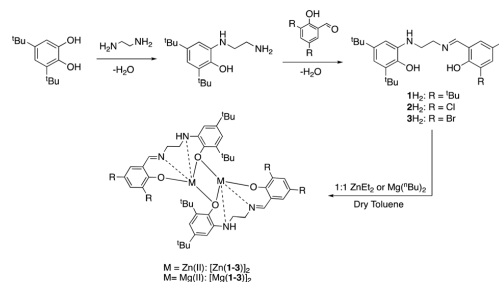
We recently reported a series of highly active Al(III)-complexes supported by a catalan framework for lactide polymerisation, observing unprecedented activity in the melt.³⁵ However, these complexes are inactive for PLA methanolysis.

Herein, we report diversification of the metal to Zn(II) and Mg(II) in pursuit of catalysts active for PLA degradation, for which there is existing literature precedent.^{109,111,123} Consequently, a range of well-defined dimeric Zn(II)- and Mg(II)-catalan complexes were prepared, employing a new and emerging class of ligands in the area. Their application to the ROP of *rac*-LA in solution, and under industrially preferred melt conditions, is discussed. The relatively mild metal-mediated methanolysis of PLA into Me-LA is reported. Preliminary work diversifying polyester scope is also demonstrated.

Results and discussion

Synthesis

The catalan ligands were prepared *via* a simple two-step synthesis (Scheme 1), exploiting successive condensation reactions, and characterised by ¹H NMR spectroscopy and mass spectrometry (MS). ¹H NMR spectroscopic analysis revealed a characteristic singlet at *ca.* $\delta = 8.40$ ppm, corresponding to a HC=N resonance, confirming formation of the imine. The –CH₂ resonances were observed as two distinct triplets between *ca.* $\delta = 3.40$ and 3.80 ppm. Dimeric complexes of Zn(II) and Mg(II) were then prepared in anhydrous toluene and recrystallised from the reaction solvent (Scheme 1). All complexes were characterised by single crystal X-ray diffraction (XRD) as shown in Fig. 1. Selected bond lengths and angles for [Zn(1–3)]₂ and [Mg(1–3)]₂ are provided in the ESI† A Zn(1)–N(2) and Mg(1)–N(2) bond length of *ca.* 2 Å confirmed retention of the imine functionality present in 1–3H₂ upon coordination to the metal centre. In all instances, τ_5 values tended towards 1, indicative of a distorted trigonal bipyramidal geometry (see ESI†). Interestingly, a highly unusual tetrameric Mg(II)-complex based on an amine-deprotonated derivative of 2H₂ was isolated and characterised by XRD (Fig. 2). Direct concentration of the same solution led to the isolation of [Mg(2)]₂ in good purity. The tetramer exhibited an Mg(1)–N(1) bond length of *ca.* 0.20 Å shorter relative to [Mg(2)]₂ as expected {Mg(1)–N(1): tetramer, 2.078(4); [Mg(2)]₂, 2.2181(19)}. Tetrameric analogues based on 1,3H₂ and Zn(II) were not



Scheme 1 Catalan ligand preparation and subsequently derived Zn(II)- and Mg(II)-complexes.

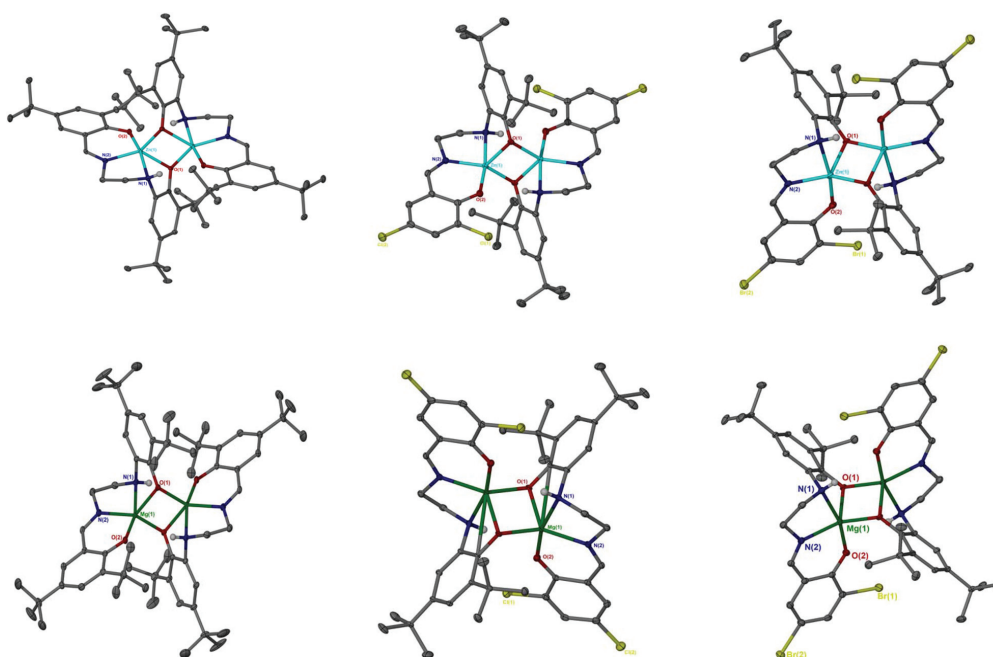


Fig. 1 Solid-state structures of $[\text{Zn}(\mathbf{1-3})]_2$ (top left to right) and $[\text{Mg}(\mathbf{1-3})]_2$ (bottom left to right). Ellipsoids shown at 30% probability with the exception of $[\text{Mg}(\mathbf{2-3})]_2$, which is shown at 50% probability. All hydrogen atoms except those bound to nitrogen or involved in hydrogen bonding, as noted for $[\text{Mg}(\mathbf{2-3})]_2$, have been omitted for clarity.

observed, whilst synthesis reattempts were unsuccessful. ^1H NMR spectroscopic analysis of $[\text{Zn}(\mathbf{1-3})]_2$ and $[\text{Mg}(\mathbf{1-3})]_2$ revealed characteristic singlets at *ca.* $\delta = 8.00$ and 4.50 ppm

corresponding to ArCHN and $-\text{NH}$ resonances respectively. More interestingly, diastereotopic $-\text{CH}_2$ resonances between *ca.* $\delta = 3.50$ and 4.00 ppm were observed, indicating the ligand is locked in position once coordinated (see ESI †). $^{13}\text{C}\{^1\text{H}\}$ NMR spectroscopic analysis was consistent with ^1H NMR and XRD analysis. It is proposed the dimeric structure observed in the solid-state is retained in solution. $\text{Zn}(\text{II})$ - and $\text{Mg}(\text{II})$ -complexes were in generally good agreement with elemental analysis (EA) data obtained, demonstrating their purity. However, C% values were consistently low on $[\text{Mg}(\mathbf{2-3})]_2$, potentially due to air and moisture sensitivity confounded by high hygroscopicity, consistent with the $\text{Al}(\text{III})$ -catalens.^{3,5}

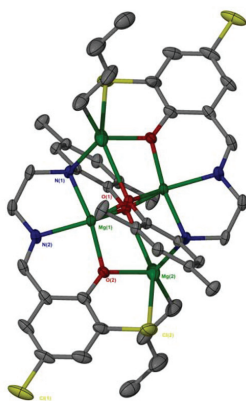


Fig. 2 Solid-state structure of a tetrameric $\text{Mg}(\text{II})$ -complex based on an amine-deprotonated derivative of 2H_2 . Ellipsoids shown at 30% probability. All hydrogen atoms and methyl groups of the ^tBu groups have been omitted for clarity.

Polymerisation of *rac*-LA

All $\text{Zn}(\text{II})$ - and $\text{Mg}(\text{II})$ -complexes were trialed in the ROP of *rac*-LA under solvent-free conditions (130 and 180 $^\circ\text{C}$) in alignment with industrial practices (Table 1). Industrially, solvents are a significant source of waste and thus catalysts that operate under melt conditions are highly desirable.^{3,15,68,69} All initiators were also tested out under solution conditions (80 $^\circ\text{C}$) (Table 2). The lactide monomer, *rac*-LA, was recrystallised from anhydrous toluene once prior to use and benzyl alcohol (BnOH) was employed as a co-initiator. Conversion was determined *via* analysis of the methine region (*ca.* $\delta = 4.9$ – 5.2 ppm) using ^1H NMR spectroscopy. To ensure one

Table 1 Melt polymerisation of *rac*-LA using [Zn(1–3)]₂ and [Mg(1,3)]₂

Init.	Time/min	[<i>rac</i> -LA]:[M]:[BnOH]	Conv. ^a /%	$M_{n,theo}^b$ /g mol ⁻¹	M_n^c /g mol ⁻¹	\bar{D}^d	P_r^d
[Zn(1)] ₂	20	300 : 1 : 1	69	29 900	28 600	1.37	0.57
	90	3000 : 1 : 10	68	29 500	23 500	2.04	0.53
[Zn(2)] ₂	17	300 : 1 : 1	63	27 300	21 600	1.24	0.54
	60	3000 : 1 : 10	69	29 900	25 150	1.58	0.52
[Zn(3)] ₂	16	300 : 1 : 1	69	29 900	23 050	1.37	0.57
	50	3000 : 1 : 10	60	26 000	22 750	1.91	0.52
[Mg(1)] ₂	20 ^e	300 : 1 : 1	69	29 900	—	—	—
	120	3000 : 1 : 10	64	27 750	8750	1.58	0.49
[Mg(3)] ₂	8	300 : 1 : 1	71	30 800	17 900	1.50	0.54
	70	3000 : 1 : 10	69	29 900	16 800	2.00	0.50

Reaction conditions: *rac*-LA (1.0 g), solvent-free (130 °C). ^a Determined *via* ¹H NMR spectroscopy. ^b Theoretical average number molecular weight (M_n) dependent on conversion and co-initiator added $\{(M_{r,LA} \times 3 \times \%_{conv}) + M_{n,BnOH}\}$. ^c Determined *via* GPC analysis (in THF). ^d Determined *via* homonuclear decoupled NMR spectroscopy. ^e Insufficient polymeric material isolated for material characterisation. N.B. {[*rac*-LA]:[M]:[BnOH]} = 3000 : 1 : 10} were performed at 180 °C. [M]:[BnOH] = 1 : 1 corresponds to 1 equivalent of BnOH per metal centre. Monomer conversion plateau between 60–70% can be attributed to reduced catalyst activity coupled with mass transfer limitations.

Table 2 Solution polymerisation of *rac*-LA using [Zn(1–3)]₂ and [Mg(1,3)]₂

Init.	Time/h	[<i>rac</i> -LA]:[M]:[BnOH]	Conv. ^a /%	$M_{n,theo}^b$ /g mol ⁻¹	M_n^c /g mol ⁻¹	\bar{D}^d	P_r^d
[Zn(1)] ₂	8	100 : 1 : 1	60	8750	124 00 ^e	1.08 ^e	0.61
[Zn(2)] ₂	8 ^f	100 : 1 : 1	31	4550	—	—	—
[Zn(3)] ₂	8 ^f	100 : 1 : 1	21	3150	—	—	—
[Mg(1)] ₂	1.5	100 : 1 : 1	94	13 650	13 900	1.17	0.46
[Mg(3)] ₂	8	100 : 1 : 1	77	12 000	9400	1.63	0.48

Reaction conditions: *rac*-LA (0.5 g), solvent (toluene, 80 °C). ^a Determined *via* ¹H NMR spectroscopy. ^b Theoretical average number molecular weight (M_n) dependent on conversion and co-initiator added $\{(M_{r,LA} \times \%_{conv}) + M_{n,BnOH}\}$. ^c Determined *via* GPC analysis (in THF). ^d Determined *via* homonuclear decoupled NMR spectroscopy. ^e Bimodal GPC observed, distributions treated together for reported M_n and \bar{D} values. ^f Insufficient polymeric material isolated for material characterisation. N.B. [M]:[BnOH] = 1 : 1 corresponds to 1 equivalent of BnOH per metal centre.

–OBn moiety was associated per metal centre, both Zn(II)- and Mg(II)-complexes were treated as monomeric. It is proposed [Zn(1–3)]₂ and [Mg(1–3)]₂ operate *via* an activated-monomer mechanism. To investigate this the stability of [Zn(1)]₂ with excess BnOH was studied using ¹H NMR (CDCl₃), which confirmed [Zn(1)]₂ to be stable at both room temperature and 80 °C (see ESI†). Due to a poor isolation yield (0.065 g, 14%), [Mg(2)]₂ was not pursued in polymerisation studies but was expected to exhibit comparable activity to [Mg(3)]₂ based on previous work.³⁵

All Zn(II)-complexes exhibited good activity at 130 °C, achieving reasonably high conversion within 20 minutes {[*rac*-LA]:[M]:[BnOH]} = 300 : 1 : 1} (Table 1). [Zn(2–3)]₂ exhibited superior activity relative to [Zn(1)]₂, presumably owing to a more Lewis acid Zn(II)-centre. [Zn(1)]₂ exhibited excellent M_n control ($M_{n,theo}$ = 29 900 g mol⁻¹, M_n = 28 600 g mol⁻¹; Table 1, entry 1), whilst reasonable M_n control was maintained for [Zn(2–3)]₂, observing moderate dispersities (\bar{D} = 1.24–1.37) in all cases. Reducing the catalyst loading to 0.033 mol% at 180 °C to simulate industrial conditions resulted in prolonged polymerisation times, achieving between 60–69% within 50 to 90 minutes {[*rac*-LA]:[M]:[BnOH]} = 3000 : 1 : 10} (Table 1). The reactivity trend noted for [Zn(1–3)]₂ was exacerbated under these conditions, likely due to an increase in temperature

assisting catalyst dissociation and solubility. Interestingly, [Zn(1)]₂ exhibited poorer M_n control ($M_{n,theo}$ = 29 500 g mol⁻¹, M_n = 23 500 g mol⁻¹; Table 1, entry 2), whilst comparable control was retained for [Zn(2–3)]₂ under these conditions. Generally, a lower M_n value than expected (relative to theoretical values) was observed, possibly indicative of side transesterification reactions, consistent with the broader dispersities observed (\bar{D} = 1.58–2.04). Reactivity trends discussed for [Zn(1–3)]₂ could be extended to the Mg(II)-catalen series, observing comparable activity between [Zn(1)]₂ and [Mg(1)]₂ at 130 °C (Table 1). Both [Mg(1,3)]₂ exhibited reduced activity relative to their Zn(II) counterparts at 180 °C, suggesting the active species to be inherently less active, despite [Mg(3)]₂ (71%, 8 min; Table 1, entry 9;) outperforming [Zn(3)]₂ (69%, 16 min; Table 1, entry 5;) at 130 °C. However, significantly lower M_n values relative to those reported for the Al(III)-catalens (M_n = 160 500–252 100 g mol⁻¹) were observed, implying k_p to be significantly slower relative to k_t , possibly due to a mechanism shift. Under both sets of conditions, [Mg(1,3)]₂ exhibited poor M_n control ($M_{n,theo}$ = 27 750–30 800 g mol⁻¹, M_n = 8750–17 900 g mol⁻¹). MALDI-ToF analysis confirmed the polymer (Table 1, entry 8) to be –OBn and –H end-capped with multiple series present indicating a high degree of transesterification (see ESI†), consistent with the broad dispersities

observed ($D = 1.50\text{--}2.00$). Metal exchange was found to have no impact on stereocontrol, observing the production of atactic PLA in all instances ($P_r = 0.49\text{--}0.57$).

Under solution conditions $\{[rac\text{-LA}]:[M]:[BnOH] = 100:1:1\}$ (Table 2), $[Zn(1)]_2$ exhibited good polymerisation control, producing PLA of reasonably well-defined M_n ($M_{n,theo} = 8750\text{ g mol}^{-1}$, $M_n = 12\,400\text{ g mol}^{-1}$; Table 2, entry 1) and narrow dispersities ($D = 1.08$). GPC analysis revealed the M_n distribution to be bimodal in nature (see ESI†). Surprisingly, $[Zn(2\text{--}3)]_2$ exhibited poorer activity relative to $[Zn(1)]_2$, achieving between 21–31% conversion within 8 h, contrary to reactivity trends discussed for the melt (Table 1). This activity loss could potentially be due to greater catalyst aggregation under these conditions, which limits availability of the active species. Indeed, kinetically limited dissociation was previously reported for the Al(III)-catalens, resulting in a loss in polymerisation control.³⁵ This trend was reflected in the Mg(II)-series but appeared less prevalent, consistent with observations in the melt. Promisingly, both $[Mg(1,3)]_2$ outperformed their Zn(II) counterpart, achieving 94% and 77% conversion within 1.5 and 8 h respectively. MALDI-ToF analysis confirmed polymer produced by $[Mg(3)]_2$ (Table 2, entry 5) to be $-OBn$ and $-H$ end-capped and transesterified, consistent with GPC analysis ($M_{n,theo} = 12\,000\text{ g mol}^{-1}$, $M_n = 9400\text{ g mol}^{-1}$, $D = 1.63$; Table 2, entry 5) (see ESI†). Interestingly, $[Mg(1)]_2$ also facilitated intermolecular transesterification, consistent with a 72 g mol^{-1} peak separation in the MALDI-ToF spectra (see ESI†), but maintained excellent polymerisation control ($M_{n,theo} = 13\,650\text{ g mol}^{-1}$, $M_n = 13\,900\text{ g mol}^{-1}$, $D = 1.17$; Table 2, entry 4). It is possible transesterification was exacerbated during polymer work up in the presence of MeOH, consistent with the melt (Table 1, entries 7–10). $[Mg(1,3)]_2$ produced atactic polymer ($P_r = 0.46\text{--}0.48$), whilst $[Zn(1)]_2$ afforded PLA with a slight heterotactic bias ($P_r = 0.61$). In summary, all Zn(II)- and Mg(II)-complexes exhibited good activity in the production of biocompatible atactic PLA, although non-competitively with the industry standard; Sn(Oct)₂.

Polymerisation kinetics

To ascertain a better understanding of metal-ligand cooperative effects on activity, a kinetic study was pursued using $[Zn(1)]_2$ and $[Mg(1)]_2$ as a model system. A plot of $\ln([LA]_0/[LA]_t)$ against time exhibited a linear relationship, indicating the reaction to be pseudo-first-order with respect to the consumption of *rac*-LA (Fig. 3). $[Mg(1)]_2$ exhibited an apparent rate constant (k_{app}) of 0.0206 min^{-1} , over 12 orders of magnitude higher relative to $[Zn(1)]_2$ ($k_{app} = 0.0017\text{ min}^{-1}$), consistent with solution results (Table 2). Indeed, $[Zn(1)]_2$ also exhibited an induction period of *ca.* 40 minutes, potentially evidencing catalyst aggregation under these conditions. No induction period was observed for $[Mg(1)]_2$, highlighting judicious choice of the metal can circumvent such limitations. It is tentatively suggested such aggregation is H-bonding in nature, although metal influence remains poorly understood. GPC analysis of the aliquots retained for $[Mg(1)]_2$ confirmed the polymerisation to be well controlled and living (Fig. 4). This was demon-

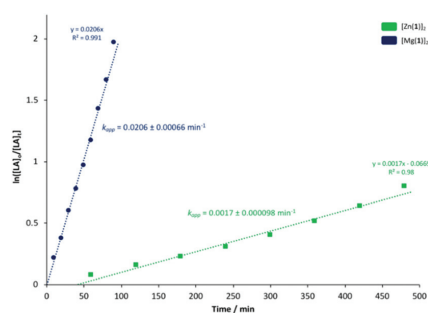


Fig. 3 Pseudo-first-order logarithmic plot for the polymerisation of *rac*-LA at 80 °C in toluene ($[rac\text{-LA}]:[M]:[BnOH] = 100:1:1$) using $[Zn(1)]_2$ and $[Mg(1)]_2$. N.B. $[LA]_0 = 0.69\text{ mol dm}^{-3}$.

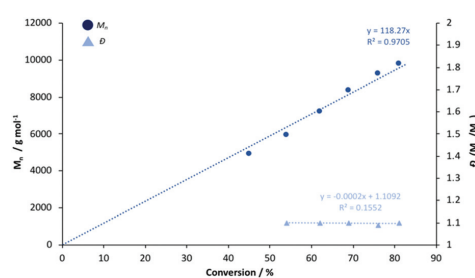


Fig. 4 Linear plot of M_n and D against conversion for the polymerisation of *rac*-LA at 80 °C in toluene ($[rac\text{-LA}]:[M]:[BnOH] = 100:1:1$) using $[Mg(1)]_2$.

strated by a linear increase in M_n with conversion whilst maintaining narrow dispersities. A slightly lower $M_{r,monomer}$ relative to ideal PLA was observed ($M_{r,theo} = 144.12\text{ g mol}^{-1}$, $M_r = 118.27\text{ g mol}^{-1}$), which could likely be attributed to minor transesterification, consistent with MALDI-ToF analysis (see ESI†).

Polyester recycling

PLA degradation. $[Zn(1\text{--}3)]_2$ and $[Mg(1,3)]_2$ were investigated in the metal-mediated degradation of PLA into Me-LA in solution at 80 °C (Fig. 5 and Table 3). Whilst Me-LA is a possible green solvent replacement, it is also a potentially valuable chemical to the PLA supply chain since it can be directly converted to lactide.^{3,91} Commercially available polymer (0.25 g, PLLA cup, $M_n = 45\,510\text{ g mol}^{-1}$) and catalyst were dissolved in either THF or anhydrous toluene under Ar, with heat and stirring assisting dissolution. MeOH was then added and the conversion to Me-LA was determined *via* ¹H NMR analysis of the methine region (*ca.* $\delta = 4.2\text{--}5.2\text{ ppm}$). The production of Me-LA has previously been shown to proceed *via* a two-step process through the intermediate formation of chain-end groups (see ESI†).^{109,123}

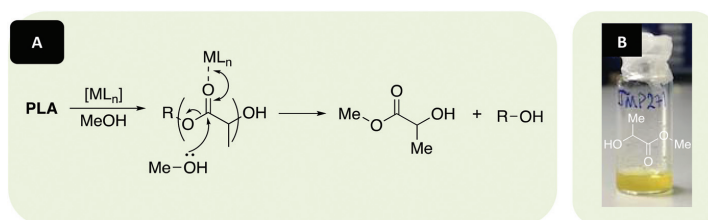


Fig. 5 (A) Metal-mediated degradation mechanism of PLA into methyl lactate (Me-LA) via transesterification with MeOH, where R denotes the growth polymer chain. (B) Example of recycled product (Me-LA). N.B. Discolouration in Me-LA product (B, liquid) originates from catalyst used ($[\text{Mg}(\mathbf{1})]_2$ – yellow solid).

Table 3 Degradation of PLA into Me-LA using $[\text{Zn}(\mathbf{1-3})]_2$ and $[\text{Mg}(\mathbf{1,3})]_2$

Catalyst	Time/h	$T/^\circ\text{C}$	Cat. loading/wt%	$Y_{\text{Me-LA}}/\%$	$S_{\text{Me-LA}}/\%$	$X_{\text{int}}/\%$	$k_{\text{app}}/\text{h}^{-1}$
$[\text{Zn}(\mathbf{1})]_2$	8	80	8	19	28	68	—
	8	80	4	4	9	46	—
	8 ^a	80	8	51	53	96	—
	8 ^a	80	4	7	12	57	—
$[\text{Zn}(\mathbf{2})]_2$	8	80	8	0	0	42	—
	8	80	4	0	0	20	—
	8 ^a	80	8	4	9	44	—
	8 ^a	80	4	0	0	28	—
$[\text{Zn}(\mathbf{3})]_2$	8	80	8	0	0	36	—
	8 ^a	80	8	0	0	37	—
$[\text{Mg}(\mathbf{1})]_2$	8	80	2	10	36	28	—
	8	80	4	64	66	97	0.628
	8	80	8	31	56	55	0.0819
$[\text{Mg}(\mathbf{3})]_2$	8	80	2	13	38	34	—
	8	80	4	42	63	67	—
	8	80	8	64	77	83	0.265

Reaction conditions: 0.25 g of PLLA cup ($M_n = 45\,510\text{ g mol}^{-1}$), $V_{\text{THF}}:V_{\text{MeOH}} = 4:1$, $n_{\text{MeOH}}:n_{\text{ester}} = 7:1$, $[\text{Zn}(\mathbf{1-3})]_2 = 4\text{--}8\text{ wt\%}$ cat. loading (0.24–0.58 mol% relative to ester linkages), $[\text{Mg}(\mathbf{1,3})]_2 = 2\text{--}8\text{ wt\%}$ cat. loading (0.13–0.57 mol% relative to ester linkages). $Y_{\text{Me-LA}}$, $S_{\text{Me-LA}}$ and X_{int} determined by $^1\text{H NMR}$ upon solvent removal. ^a Solvent: Anhydrous toluene, $V_{\text{toluene}}:V_{\text{MeOH}} = 4:1$.

Consequently, the methine groups can be categorised as internal (int), chain-end (CE) and those corresponding directly to the alkyl lactate (Me-LA). Conversion of internal methine units (X_{int}), methyl lactate selectivity ($S_{\text{Me-LA}}$) and Me-LA yield ($Y_{\text{Me-LA}}$) are tabulated in Table 3 below. $[\text{Zn}(\mathbf{1})]_2$ exhibited reasonably poor activity at 8 wt%, achieving 19% conversion to Me-LA within 8 h in THF with poor selectivity (Table 3, entry 1). Promisingly, superior activity and selectivity ($Y_{\text{Me-LA}} = 51\%$, $S_{\text{Me-LA}} = 53\%$) was observed upon shifting to a non-coordinating solvent, namely anhydrous toluene (Table 3, entry 3). This implies THF competes with the degrading polymeric chain with respect to coordination to the Zn(II)-centre, consistent with the near complete consumption of PLA ($X_{\text{int}} = 96\%$). Interestingly, shifting to a more electron withdrawing catalan backbone in $[\text{Zn}(\mathbf{2-3})]_2$ had a detrimental impact on $Y_{\text{Me-LA}}$, achieving 0% conversion to Me-LA under analogous conditions in THF. Whilst contrary to previous work by Payne *et al.*,¹¹⁰ this was consistent with solution polymerisation results (Table 2). Indeed, previously described solution reactivity trends were retained for PLA degradation. Since this behaviour was retained in anhydrous toluene, it is suggested the afore-

mentioned activity loss due to possible catalyst aggregation (Table 2) likely persists under these conditions. It is possible bulky ^tBu substituents promote the dissociation of $[\text{Zn}(\mathbf{1})]_2$ in solution, resulting in superior activity relative to $[\text{Zn}(\mathbf{2-3})]_2$. $[\text{Mg}(\mathbf{1})]_2$ significantly outperformed its Zn(II)-counterpart, achieving 31% conversion to Me-LA with good selectivity in THF at 8 wt% (Table 3, entry 13). Interestingly, significantly enhanced activity was realised upon decreasing the catalyst loading to 4 wt% ($Y_{\text{Me-LA}} = 64\%$, $S_{\text{Me-LA}} = 66\%$, $X_{\text{int}} = 97\%$), possibly evidencing a reduction in catalyst aggregation due to dilution. To improve industrial feasibility and investigate the limit of this effect, the catalyst loading was further reduced to 2 wt%. Significantly reduced $Y_{\text{Me-LA}}$ relative to 4 wt% was observed (Table 3, entries 11 and 12), implying unavailability of the active species predominates, consistent with $[\text{Mg}(\mathbf{3})]_2$ (Table 3, entry 14). In light of this, $[\text{Zn}(\mathbf{1-3})]_2$ were investigated at 4 wt% in both THF and anhydrous toluene at 80 °C, although no activity enhancement was observed. $[\text{Mg}(\mathbf{3})]_2$ exhibited superior activity relative to $[\text{Zn}(\mathbf{3})]_2$, achieving 42% conversion to Me-LA within 8 h at 4 wt% (Table 3, entry 15). Whilst lower relative to $[\text{Mg}(\mathbf{1})]_2$, enhanced $Y_{\text{Me-LA}}$ and $S_{\text{Me-LA}}$

was observed at 8 wt% (Table 3, entry 16). This implies the liberated species to be inherently more active relative to $[\text{Mg}(\text{1})]_2$ and that possible catalyst aggregation dominates at 4 wt%. Judicial choice of the metal had previously been shown to circumvent such challenges in the solution polymerisation of *rac*-LA (Fig. 3). Degradation reactions using $[\text{Mg}(\text{1,3})]_2$ in anhydrous toluene were not pursued in alignment with the 12 principles of green chemistry.¹²⁵ Overall, mass transfer limitations due to polymer particle size and stirring speeds were considered negligible based on previous work by Román-Ramírez *et al.*,¹⁰⁹ which employed a homoleptic $\text{Zn}(\text{n})$ -complex bearing an ethylenediamine Schiff-base ligand.

PLA degradation kinetics. $[\text{Mg}(\text{1})]_2$ and $[\text{Mg}(\text{3})]_2$ were identified as the outstanding candidates and thus pursued for further kinetic analysis. Reaction progress was monitored hourly for the first 4 hours for ^1H NMR (CDCl_3) analysis of the methine region. A final aliquot was taken after 8 hours for analysis, totalling 5 data points (Fig. 6). PLA consumption was assumed to adopt pseudo-first-order kinetics in accordance to previous work by Román-Ramírez *et al.*¹⁰⁹ Consequently, the gradient of the logarithmic plot is equivalent to the apparent rate constant, k_{app} (Table 3 and Fig. 6). $[\text{Mg}(\text{1})]_2$ exhibited a k_{app} value of 0.628 ± 0.0536 and $0.0819 \pm 0.0213 \text{ h}^{-1}$ at 4 and 8 wt% respectively in THF, indicating an increase in catalyst loading results in a statistically significant decrease in activity. $[\text{Mg}(\text{3})]_2$ was found to have a k_{app} value of $0.265 \pm 0.0193 \text{ h}^{-1}$, lower relative to $[\text{Mg}(\text{1})]_2$, consistent with preliminary methanolysis results (Table 3). Comparable $Y_{\text{Me-LA}}$ values (Table 4) were observed relative to Table 3, indicating good reproducibility. Whilst promising, these k_{app} value remain lower compared to previously reported $\text{Zn}(\text{n})$ -complexes ($k_{\text{app}} = 0.44\text{--}12.0 \text{ h}^{-1}$) operating between 50 to 80 °C under analogous reaction conditions.^{109,110,123} However, to the best of our knowledge, $[\text{Mg}(\text{1,3})]_2$ represent the first example of PLA methanolysis mediated by a well-defined discrete $\text{Mg}(\text{n})$ -complex, operating under significantly milder conditions relative to Petrus *et al.*,¹¹¹ who relied upon metallic Mg or $\text{Mg}(\text{tBu})_2$ as pre-catalysts. For $[\text{Mg}(\text{1,3})]_2$, inspection of the ^1H NMR (Table 3,

Table 4 PLLA cup degradation using $[\text{Mg}(\text{1,3})]_2$ in THF at 80 °C

Catalyst	$Y_{\text{Me-LA}}/\%$	$k_{\text{app}}/\text{h}^{-1}$
$[\text{Mg}(\text{1})]_2^a$	76	0.628 ± 0.0536
$[\text{Mg}(\text{1})]_2^b$	38	0.0819 ± 0.0213
$[\text{Mg}(\text{3})]_2^c$	63	0.265 ± 0.0193

Reaction conditions: 0.25 g of PLLA cup ($M_n = 45\,510 \text{ g mol}^{-1}$), $V_{\text{THF}} : V_{\text{MeOH}} = 4 : 1$, $n_{\text{MeOH}} : n_{\text{ester}} = 7 : 1$. Error associated with k_{app} calculated using linear regression. ^a $[\text{Mg}(\text{1})]_2 = 4 \text{ wt\%}$ cat. loading (0.29 mol% relative to ester linkages). ^b $[\text{Mg}(\text{1})]_2 = 8 \text{ wt\%}$ cat. loading (0.57 mol% relative to ester linkages). ^c $[\text{Mg}(\text{3})]_2 = 8 \text{ wt\%}$ cat. loading (0.53 mol% relative to ester linkages). N.B. $Y_{\text{Me-LA}}$ refers to maximum Me-LA conversion determined *via* ^1H NMR (CDCl_3) after 8 h prior to solvent (THF) removal.

entries 12 and 16) following solvent removal revealed the formation of a new $\text{Mg}(\text{n})$ -species, although its identity remains unclear. It is suggested the dimeric framework dissociates in solution, affording a heteroleptic complex of the general formula $\text{Mg}(\text{1,3})\text{L}$, where L could be methoxy, lactyl or higher chain oligomers, as previously described by Jones and co-workers.¹²³ Consequently, $[\text{Mg}(\text{1,3})]_2$ should strictly be regarded as pre-catalysts and this can likely be extended to the remaining $\text{Zn}(\text{n})$ -complexes.

PET degradation. Presently, bio-based plastics account for ca. 1% of all processed plastics, with PLA accounting for just 13.9% of bioplastic production in 2019.¹²⁶ Consequently, our attention shifted to PET, a commercial polyester widely exploited in the packaging industry, which consumed 38% of plastics produced globally in 2015, with PET accounting for 22.6% of plastic use in the sector.¹³ Glycolysis is the most widely used chemical recycling method for PET, characterised by cleavage of the ester bond *via* insertion of a glycol, commonly ethylene glycol (EG), to produce bis(2-hydroxyethyl) terephthalate (BHET) or higher alcohol derivatives. BHET can then be repolymerised to virgin PET or used as a precursor in the production of unsaturated polyester resins.^{127–131} In light of this, preliminary work sought to apply $[\text{Zn}(\text{1,3})]_2$ and $[\text{Mg}(\text{1})]_2$ to the glycolysis of PET. $[\text{Mg}(\text{3})]_2$ was not investigated due to insufficient yield. Typically, high temperatures (180–240 °C) and prolonged reaction times (0.5–8 h) in the presence of a transesterification catalyst, often a metal acetate, are required to achieve appreciable conversion. Whilst numerous metal acetate catalysts have been reported in the literature, zinc acetate is considered the benchmark.^{127,132}

Consequently, $\text{Zn}(\text{OAc})_2 \cdot 2\text{H}_2\text{O}$ (Sigma Aldrich) was chosen as an air-stable, commercially available reference. Additionally, high EG : PET ($\geq 5 : 1$) are used to mediate the formation of higher chain oligomers, thus favouring the formation of BHET.¹²⁷ As such, a reaction temperature of 180 °C in the presence of 8 wt% catalyst and 27.5 equivalents of EG was chosen (Table 5). Two sources of PET were selected: 1. A carbonated drinks bottle ($M_n \sim 40\,000 \text{ g mol}^{-1}$) and 2. Thin-films, representing waste from the manufacturing industry (Fig. 7).

Typically, a 6–12% reduction in Y_{BHET} (isolated yield) was observed on accounting for residual H_2O (1.3–3.5 equivalents)

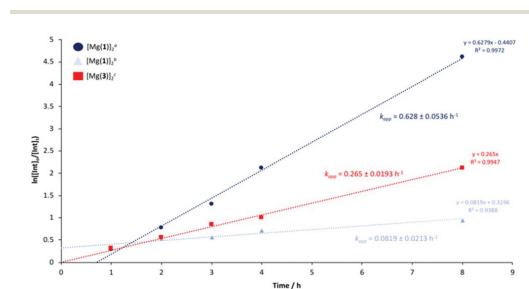


Fig. 6 Pseudo-first-order logarithmic plot for the degradation of PLLA cup using $[\text{Mg}(\text{1})]_2$ and $[\text{Mg}(\text{3})]_2$ in THF at 80 °C. ^a $[\text{Mg}(\text{1})]_2 = 4 \text{ wt\%}$ cat. loading (0.29 mol% relative to ester linkages). ^b $[\text{Mg}(\text{1})]_2 = 8 \text{ wt\%}$ cat. loading (0.57 mol% relative to ester linkages). ^c $[\text{Mg}(\text{3})]_2 = 8 \text{ wt\%}$ cat. loading (0.53 mol% relative to ester linkages).

Table 5 PET degradation into BHET using selected Zn(II)- and Mg(II)-catalen complexes at 180 °C

Catalyst	Time/h	$T/^\circ\text{C}$	Cat. loading/wt%	EG/equiv.	Y_{BHET} (wet) (g/%)	$\text{H}_2\text{O}/\text{equiv.}$	Corrected Y_{BHET} (%)
Ref	4	180	8	27.5	0.16 (48%)	2.0	42
	2 ^a	180	8	27.5	0.14 (42%)	2.1	37
$[\text{Zn}(\text{1})]_2$	4	180	8	27.5	0.20 (61%)	3.3	49
$[\text{Zn}(\text{3})]_2$	4	180	8	27.5	0.16 (48%)	1.3	44
$[\text{Mg}(\text{1})]_2$	3	180	8	27.5	0.20 (61%)	2.7	51
	0.75 ^a	180	8	27.5	0.14 (42%)	3.5	34
	3 ^b	180	8	27.5	0.18 (55%)	2.4	46

Reaction conditions: 0.25 g of carbonated drinks bottle ($M_n \sim 40\,000 \text{ g mol}^{-1}$), 27.5 equivalents of EG (relative to ester linkages), Ref: $\text{Zn}(\text{OAc})_2 \cdot 2\text{H}_2\text{O} = 8 \text{ wt\% cat. loading}$ (0.02 g, 7 mol% relative to ester linkages), $[\text{Zn}(\text{1,3})]_2 = 8 \text{ wt\% cat. loading}$ (0.02 g, 1.3–1.4 mol% relative to ester linkages), $[\text{Mg}(\text{1})]_2 = 8 \text{ wt\% cat. loading}$ (0.02 g, 1.5 mol% relative to ester linkages). ^a PET thin-film (0.25 g). ^b PET (0.25 g, carbonated drinks bottle) + PVC (0.025 g, 10 wt%, Sigma Aldrich, $M_n \sim 22\,000 \text{ g mol}^{-1}$). N.B. Y_{BHET} (wet) refers to the isolated yield of BHET recrystallised from deionised H_2O , followed by drying at 90 °C for 3 h *in vacuo*. Residual H_2O (equiv.) was determined *via* $^1\text{H NMR}$ (D_2O -DMSO) analysis. A corrected Y_{BHET} is provided accounting for the complete removal of H_2O .

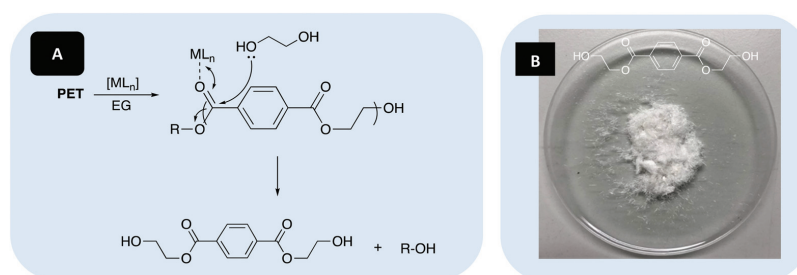


Fig. 7 (A) Metal mediated glycolysis of poly(ethylene terephthalate) (PET) into bis(2-hydroxyethyl) terephthalate (BHET) in the presence of ethylene glycol (EG), where R denotes the growth polymer chain. (B) Example of recycled product (BHET).

after drying, and thus cannot be considered absolute. Consequently, the discussion of Y_{BHET} herein will refer to the corrected value. $[\text{Zn}(\text{1,3})]_2$ exhibited comparable performance to the reference, achieving between 44–49% Y_{BHET} within 4 h at 180 °C. Promisingly, $[\text{Mg}(\text{1})]_2$ exhibited superior activity, ascertaining the highest Y_{BHET} observed, achieving 51% within 3 h under analogous conditions. For this system, tolerance stability was successfully demonstrated in the presence of 10 wt% PVC, retaining comparable Y_{BHET} (46%; Table 5, entry 7). PVC contamination as low as 100 ppm has previously been reported to adversely impact the quality of the final recycled product, owing to the production of acid catalysts that facilitate chain scission under melt reprocessing conditions ($T = 160 \text{ }^\circ\text{C}$) routinely employed in industry.¹²⁷ Thus, this result is particularly promising from an industrial perspective. Both $[\text{Mg}(\text{1})]_2$ and $\text{Zn}(\text{OAc})_2 \cdot 2\text{H}_2\text{O}$ exhibited superior activity on substituting the carbonated drinks bottle for thin-films, owing to superior sample dissolution. Remarkably, $[\text{Mg}(\text{1})]_2$ achieved 34% Y_{BHET} within 45 minutes, vastly outperforming the reference, which afforded comparable conversion within 2 h ($Y_{\text{BHET}} = 37\%$; Table 5, entry 2). Whilst reaction times reflect the time taken to achieve complete PET dissolution, indicative of reaction completion, Y_{BHET} less than 50% were typically observed. It is possible the production of higher

chain oligomers is partly responsible.^{127–132} In summary, $[\text{Zn}(\text{1,3})]_2$ and $[\text{Mg}(\text{1})]_2$ exhibited superior activity for PET glycolysis relative to $\text{Zn}(\text{OAc})_2 \cdot 2\text{H}_2\text{O}$, despite the wt% of the reference corresponding to a significantly higher zinc loading, highlighting the importance of structure-activity relationships.

Conclusions

A range of dimeric Zn(II)- and Mg(II)-catalen complexes were prepared and fully characterised. The production of biocompatible atactic PLA in solution and under industrially preferred solvent-free conditions was demonstrated, typically observing good activity and M_n control with a broad range of dispersities ($D = 1.08\text{--}2.04$). Mg(II)-Complexes were shown to facilitate the relatively mild methanolysis of PLA, achieving up to 64% conversion to Me-LA within 8 h at 80 °C in THF. Further kinetic analysis found $[\text{Mg}(\text{1,3})]_2$ to have k_{app} values of 0.628 ± 0.0536 {4 wt% cat. loading} and $0.265 \pm 0.0193 \text{ h}^{-1}$ {8 wt% cat. loading} respectively. For $[\text{Mg}(\text{1})]_2$, increasing the catalyst loading to 8 wt% resulted in a statistically significant reduction in activity ($0.0819 \pm 0.0213 \text{ h}^{-1}$), potentially evidencing catalyst aggregation, which appeared prevalent in the

Zn(II)-complexes. Preliminary work extended polymer scope to PET from various sources, demonstrating catalyst versatility.

Conflicts of interest

The authors declare no conflict of interest.

Acknowledgements

We wish to thank the EPSRC for funding and the University of Bath and MC² for use of their analysis facilities. We would like to thank the EPSRC for funding (EP/L016354/1) for a PhD studentship to J. P. and (EP/P016405/1) for P. M. We thank Avery Dennison for kindly providing waste PET thin-films used in this study.

References

- R. A. Sheldon and M. Norton, *Green Chem.*, 2020, **22**, 6310–6322.
- PlasticsEurope, *Plastics – the Facts 2019. An Analysis of European Plastics Production, Demand and Waste Data*, 2019, https://www.plasticseurope.org/application/files/9715/7129/9584/FINAL_web_version_Plastics_the_facts2019_14102019.pdf, (Accessed: 13th October 2020).
- J. Payne, P. McKeown and M. D. Jones, *Polym. Degrad. Stab.*, 2019, **165**, 170–181.
- R. Geyer, J. R. Jambeck and K. L. Law, *Sci. Adv.*, 2017, **3**, 1–5.
- R. C. Thompson, C. J. Moore, F. S. vom Saal and S. H. Swan, *Philos. Trans. R. Soc., B*, 2009, **364**, 2153–2166.
- Y. Zhu, C. Romain and C. K. Williams, *Nature*, 2016, **540**, 354–362.
- Ellen MacArthur Foundation, *The New Plastics Economy: Rethinking the future of plastics*, 2016, <https://www.ellenmacarthurfoundation.org/publications/the-new-plastics-economy-rethinking-the-future-of-plastics>, (Accessed: 7th January 2019).
- J. R. Jambeck, R. Geyer, C. Wilcox, T. R. Siegler, M. Perryman, A. Andrady and R. Na, *Science*, 2015, **347**, 768–771.
- L. Lebreton, B. Slat, F. Ferrari, B. Sainte-Rose, J. Aitken, R. Marthouse, S. Hajbane, S. Cunsolo, A. Schwarz, A. Levivier, K. Noble, P. Debeljak, H. Maral, R. Schoeneich-Argent, R. Brambini and J. Reisser, *Sci. Rep.*, 2018, **8**, 4666.
- E. T. H. Vink, K. R. Rábago, D. A. Glassner, B. Springs, R. P. O'Connor, J. Kolstad and P. R. Gruber, *Macromol. Biosci.*, 2004, **4**, 551–564.
- E. T. H. Vink, D. A. Glassner, J. Kolstad, R. J. Wooley and R. P. O'Connor, *Biotechnology*, 2007, **3**, 58–81.
- J. Lunt, *Polym. Degrad. Stab.*, 1998, **59**, 145–152.
- M. Rabnawaz, I. Wyman, R. Auras and S. Cheng, *Green Chem.*, 2017, **19**, 4737–4753.
- R. E. Drumright, P. R. Gruber and D. E. Henton, *Adv. Mater.*, 2000, **12**, 1841–1846.
- O. Dechy-Cabaret, B. Martin-Vaca and D. Bourissou, *Chem. Rev.*, 2004, **104**, 6147–6176.
- R. H. Platel, L. M. Hodgson and C. K. Williams, *Polym. Rev.*, 2008, **48**, 11–63.
- H. R. Kricheldorf, I. Kreiser-Saunders and A. Stricker, *Macromolecules*, 2000, **33**, 702–709.
- N. Spassky, M. Wisniewski, C. Pluta and A. LeBorgne, *Macromol. Chem. Phys.*, 1996, **197**, 2627–2637.
- Z. Y. Zhong, P. J. Dijkstra and J. Feijen, *Angew. Chem., Int. Ed.*, 2002, **41**, 4510–4513.
- Z. Zhong, P. J. Dijkstra and J. Feijen, *J. Am. Chem. Soc.*, 2003, **125**, 11291–11298.
- N. Nomura, R. Ishii, M. Akakura and K. Aoi, *J. Am. Chem. Soc.*, 2002, **124**, 5938–5939.
- N. Nomura, R. Ishii, Y. Yamamoto and T. Kondo, *Chem. – Eur. J.*, 2007, **13**, 4433–4451.
- H.-L. Chen, S. Dutta, P.-Y. Huang and C.-C. Lin, *Organometallics*, 2012, **31**, 2016–2025.
- E. L. Whitelaw, G. Loraine, M. F. Mahon and M. D. Jones, *Dalton Trans.*, 2011, **40**, 11469–11473.
- A. Pilone, K. Press, I. Goldberg, M. Kol, M. Mazzeo and M. Lamberti, *J. Am. Chem. Soc.*, 2014, **136**, 2940–2943.
- P. McKeown, M. G. Davidson, G. Kociok-Köhn and M. D. Jones, *Chem. Commun.*, 2016, **52**, 10431–10434.
- P. Hormnirun, E. L. Marshall, V. C. Gibson, A. J. P. White and D. J. Williams, *J. Am. Chem. Soc.*, 2004, **126**, 2688–2689.
- P. Hormnirun, E. L. Marshall, V. C. Gibson, R. I. Pugh and A. J. P. White, *Proc. Natl. Acad. Sci. U. S. A.*, 2006, **103**, 15343–15348.
- H. Du, A. H. Velders, P. J. Dijkstra, J. Sun, Z. Zhong, X. Chen and J. Feijen, *Chem. – Eur. J.*, 2009, **15**, 9836–9845.
- J. Feijen, *Chem. – Eur. J.*, 2009, **15**, 9836–9845.
- K. Press, I. Goldberg and M. Kol, *Angew. Chem., Int. Ed.*, 2015, **54**, 14858–14861.
- R. Hador, A. Botta, V. Venditto, S. Lipstman, I. Goldberg and M. Kol, *Angew. Chem., Int. Ed.*, 2019, **58**, 14679–14685.
- S. Gesslbauer, H. Cheek, A. J. P. White and C. Romain, *Dalton Trans.*, 2018, **47**, 10410–10414.
- S. Gesslbauer, R. Savela, Y. Chen, A. J. P. White and C. Romain, *ACS Catal.*, 2019, **9**, 7912–7920.
- J. Payne, P. McKeown, G. Kociok-Köhn and M. D. Jones, *Chem. Commun.*, 2020, **56**, 7163–7166.
- A. J. Chmura, M. G. Davidson, M. D. Jones, M. D. Lunn, M. F. Mahon, A. F. Johnson, P. Khunkamchoo, S. L. Roberts and S. S. F. Wong, *Macromolecules*, 2006, **39**, 7250–7257.
- A. J. Chmura, M. G. Davidson, C. J. Frankis, M. D. Jones and M. D. Lunn, *Chem. Commun.*, 2008, 1293–1295.
- A. J. Chmura, M. G. Davidson, C. J. Frankis, M. D. Jones and M. D. Lunn, *Chem. Commun.*, 2008, 1293–1295.
- A. Sauer, A. Kapelski, C. Fliedel, S. Dagorne, M. Kol and J. Okuda, *Dalton Trans.*, 2013, **42**, 9007–9023.
- E. Sergeeva, J. Kopilov, I. Goldberg and M. Kol, *Inorg. Chem.*, 2010, **49**, 3977–3979.

- 41 S. Gendler, S. Segal, I. Goldberg, Z. Goldschmidt and M. Kol, *Inorg. Chem.*, 2006, **45**, 4783–4790.
- 42 A. Stopper, J. Okuda and M. Kol, *Macromolecules*, 2012, **45**, 698–704.
- 43 J.-C. Buffet and J. Okuda, *Polym. Chem.*, 2011, **2**, 2758–2763.
- 44 C. Romain, B. Heinrich, S. B. Laponnaz and S. Dagorne, *Chem. Commun.*, 2012, **48**, 2213–2215.
- 45 X. Wang, A. Thevenon, J. L. Brosmer, I. Yu, S. I. Khan, P. Mehrkhodavandi and P. L. Diaconescu, *J. Am. Chem. Soc.*, 2014, **136**, 11264–11267.
- 46 M. D. Jones, S. L. Hancock, P. McKeown, P. M. Schafer, A. Buchard, L. H. Thomas, M. F. Mahon and J. P. Lowe, *Chem. Commun.*, 2014, **50**, 15967–15970.
- 47 M. D. Jones, L. Brady, P. McKeown, A. Buchard, P. M. Schafer, L. H. Thomas, M. F. Mahon, T. J. Woodman and J. P. Lowe, *Chem. Sci.*, 2015, **6**, 5034–5039.
- 48 E. L. Whitelaw, M. F. Mahon and M. D. Jones, *Inorg. Chem.*, 2010, **49**, 7176–7181.
- 49 E. L. Whitelaw, M. G. Davidson and M. D. Jones, *Chem. Commun.*, 2011, **47**, 10004–10006.
- 50 B. M. Chamberlain, M. Cheng, D. R. Moore, T. M. Ovitt, E. B. Lobkovsky and G. W. Coates, *J. Am. Chem. Soc.*, 2001, **123**, 3229–3238.
- 51 M. H. Chisholm, J. C. Gallucci and K. Phomphrai, *Inorg. Chem.*, 2005, **44**, 8004–8010.
- 52 H.-Y. Chen, H.-Y. Tang and C.-C. Lin, *Macromolecules*, 2006, **39**, 3745–3752.
- 53 J. Börner, U. Florke, K. Huber, A. Doring, D. Kuckling and S. Herres-Pawlis, *Chem. – Eur. J.*, 2009, **15**, 2362–2376.
- 54 D. J. Darensbourg and O. Karroonnirun, *Inorg. Chem.*, 2010, **49**, 2360–2371.
- 55 J. Börner, I. dos Santos Vieira, A. Pawlis, A. Döring, D. Kuckling and S. Herres-Pawlis, *Chem. – Eur. J.*, 2011, **17**, 4507–4512.
- 56 H. Wang and H. Ma, *Chem. Commun.*, 2013, **49**, 8686–8688.
- 57 C. Fliedel, D. Vila-Viçosa, M. J. Calhorda, S. Dagorne and T. Avilés, *ChemCatChem*, 2014, **6**, 1357–1367.
- 58 H. Wang, Y. Yang and H. Ma, *Macromolecules*, 2014, **47**, 7750–7764.
- 59 Y. Yang, H. Wang and H. Ma, *Inorg. Chem.*, 2015, **54**, 5839–5854.
- 60 T. Rosen, Y. Popowski, I. Goldberg and M. Kol, *Chem. – Eur. J.*, 2016, **22**, 11533–11536.
- 61 P. M. Schäfer, M. Fuchs, A. Ohligschläger, R. Rittinghaus, P. McKeown, E. Akin, M. Schmidt, A. Hoffmann, M. A. Liauw, M. D. Jones and S. Herres-Pawlis, *ChemSusChem*, 2017, **10**, 3547–3556.
- 62 D. E. Stasiw, A. M. Luke, T. Rosen, A. B. League, M. Mandal, B. D. Neisen, C. J. Cramer, M. Kol and W. B. Tolman, *Inorg. Chem.*, 2017, **56**, 14366–14372.
- 63 S. Abbina and G. Du, *ACS Macro Lett.*, 2014, **3**, 689–692.
- 64 C. K. Williams, L. E. Breyfogle, S. K. Choi, W. Nam, V. G. Young, M. A. Hillmyer and W. B. Tolman, *J. Am. Chem. Soc.*, 2003, **125**, 11350–11359.
- 65 M. Cheng, A. B. Attygalle, E. B. Lobkovsky and G. W. Coates, *J. Am. Chem. Soc.*, 1999, **121**, 11583–11584.
- 66 A. Thevenon, C. Romain, M. S. Bennington, A. J. P. White, H. J. Davidson, S. Brooker and C. K. Williams, *Angew. Chem., Int. Ed.*, 2016, **55**, 8680–8685.
- 67 C. Kan, J. Hu, Y. Huang, H. Wang and H. Ma, *Macromolecules*, 2017, **50**, 7911–7919.
- 68 P. McKeown, S. N. McCormick, M. F. Mahon and M. D. Jones, *Polym. Chem.*, 2018, **9**, 5339–5347.
- 69 Al. Hermann, S. Hill, A. Metz, J. Heck, A. Hoffmann, L. Hartmann and S. Herres-Pawlis, *Angew. Chem., Int. Ed.*, 2020, **59**(48), 21778–21784.
- 70 J. Kasperczyk and M. Bero, *Polymer*, 2000, **41**, 391–395.
- 71 L. F. Sánchez-Barba, A. Garcés, M. Fajardo, C. Alonso-Moreno, J. Fernández-Baeza, A. Otero, A. Antiñolo, J. Tejada, A. Lara-Sánchez and M. I. López-Solera, *Organometallics*, 2007, **26**, 6403–6411.
- 72 V. Poirier, T. Roisnel, J.-F. Carpentier and Y. Sarazin, *Dalton Trans.*, 2009, 9820–9827.
- 73 C. A. Wheaton, P. G. Hayes and B. J. Ireland, *Dalton Trans.*, 2009, 4832–4846.
- 74 L. Wang and H. Ma, *Macromolecules*, 2010, **43**, 6535–6537.
- 75 L. F. Sánchez-Barba, A. Garcés, J. Fernández-Baeza, A. Otero, C. Alonso-Moreno, A. Lara-Sánchez and A. M. Rodríguez, *Organometallics*, 2011, **30**, 2775–2789.
- 76 H.-J. Chuang, H.-L. Chen, J.-L. Ye, Z.-Y. Chen, P.-L. Huang, T.-T. Liao, T.-E. Tsai and C.-C. Lin, *J. Polym. Sci., Part A: Polym. Chem.*, 2013, **51**, 696–707.
- 77 A. Garcés, L. F. Sánchez-Barba, J. Fernández-Baeza, A. Otero, M. Honrado, A. Lara-Sánchez and A. M. Rodríguez, *Inorg. Chem.*, 2013, **52**, 12691–12701.
- 78 W. Yi and H. Ma, *Inorg. Chem.*, 2013, **52**, 11821–11835.
- 79 M. J. Walton, S. J. Lancaster and C. Redshaw, *ChemCatChem*, 2014, **6**, 1892–1898.
- 80 K. Devaine-Pressing, J. H. Lehr, M. E. Pratt, L. N. Dawe, A. A. Sarjeant and C. M. Kozak, *Dalton Trans.*, 2015, **44**, 12365–12375.
- 81 H. Wang, J. Guo, Y. Yang and H. Ma, *Dalton Trans.*, 2016, **45**, 10942–10953.
- 82 P. McKeown, J. Brown-Humes, M. G. Davidson, M. F. Mahon, T. J. Woodman and M. D. Jones, *Dalton Trans.*, 2017, **46**, 5048–5057.
- 83 M. H. Chisholm, K. Choojun, A. S. Chow, G. Fraenkel and J. C. Gallucci, *Inorg. Chem.*, 2013, **52**, 11302–11310.
- 84 M. H. Chisholm, K. Choojun, J. C. Gallucci and P. M. Wambua, *Chem. Sci.*, 2012, **3**, 3445–3457.
- 85 M. H. Chisholm, J. Gallucci and K. Phomphrai, *Inorg. Chem.*, 2002, **41**, 2785–2794.
- 86 T. P. Haider, C. Völker, J. Kramm, K. Landfester and F. R. Wurm, *Angew. Chem., Int. Ed.*, 2019, **58**, 50–62.
- 87 J. Hopewell, R. Dvorak and E. Kosior, *Philos. Trans. R. Soc., B*, 2009, **364**, 2115–2126.
- 88 M. Hong and E. X.-Y. Chen, *Green Chem.*, 2017, **9**, 3692–3706.
- 89 P. McKeown and M. D. Jones, *Sustainable Chem.*, 2020, **1**, 1–22.

- 90 C. T. Bowmer, R. N. Hooftman, A. O. Hanstveit, P. W. M. Venderbosch and N. van der Hoeven, *Chemosphere*, 1998, **37**, 1317–1333.
- 91 C. S. M. Pereira, V. M. T. M. Silva and A. E. Rodrigues, *Green Chem.*, 2011, **13**, 2658–2671.
- 92 M. Dusselier, P. V. Wouwe, A. Dewaele, E. Makshina and B. F. Sels, *Energy Environ. Sci.*, 2013, **6**, 1415–1442.
- 93 Y. Fan, C. Zhou and X. Zhu, *Catal. Rev. Sci. Eng.*, 2009, **51**, 293–324.
- 94 V. Piemonte, S. Sabatini and F. Gironi, *J. Polym. Environ.*, 2013, **21**, 640–647.
- 95 F. M. Lamberti, L. A. Román-Ramírez, P. Mckeown, M. D. Jones and J. Wood, *Processes*, 2020, **8**, 738.
- 96 H. Tsuji, T. Saeki, T. Tsukegi, H. Daimon and K. Fujie, *Polym. Degrad. Stab.*, 2008, **93**, 1956–1963.
- 97 V. Piemonte and F. Gironi, *J. Polym. Environ.*, 2013, **21**, 313–318.
- 98 P. Coszach, J.-C. Bogaert and J. Willocq, *US Pat*, 8431683B2, 2013.
- 99 C. F. VanNostrum, T. F. J. Veldhuis, G. W. Bos and W. E. Hennink, *Polymer*, 2004, **45**, 6779–6787.
- 100 H. Tsuji, H. Daimon and K. Fujie, *Biomacromolecules*, 2003, **4**, 835–840.
- 101 F. Codari, S. Lazzari, M. Soos, G. Storti, M. Morbidelli and D. Moscatelli, *Polym. Degrad. Stab.*, 2012, **97**, 2460–2466.
- 102 K. Odellius, A. Höglund, S. Kumar, M. Hakkarainen, A. K. Ghosh, N. Bhatnagar and A. C. Albertsson, *Biomacromolecules*, 2011, **12**, 1250–1258.
- 103 K. Hirao, Y. Nakatsuchi and H. Ohara, *Polym. Degrad. Stab.*, 2010, **95**, 925–928.
- 104 L. D. Brake, *US Pat*, 5264617, 1993.
- 105 X. Song, X. Zhang, H. Wang, F. Liu, S. Yu and S. Liu, *Polym. Degrad. Stab.*, 2013, **98**, 2760–2764.
- 106 X. Song, H. Wang, X. Zheng, F. Liu and S. Yu, *J. Appl. Polym. Sci.*, 2014, **131**, 40817–40822.
- 107 C. Flidel, D. Vila-Viçosa, M. J. Calhorda, S. Dagorne and T. Avilés, *ChemCatChem*, 2014, **6**, 1357–1367.
- 108 E. L. Whitelaw, M. G. Davidson and M. D. Jones, *Chem. Commun.*, 2011, **47**, 10004–10006.
- 109 L. A. Román-Ramírez, P. Mckeown, M. D. Jones and J. Wood, *ACS Catal.*, 2019, **9**, 409–416.
- 110 J. Payne, P. McKeown, M. F. Mahon, E. A. C. Emanuelsson and M. D. Jones, *Polym. Chem.*, 2020, **11**, 2381–2389.
- 111 R. Petrus, D. Bykowski and P. Sobota, *ACS Catal.*, 2016, **6**, 5222–5235.
- 112 F. A. Leibfarth, N. Moreno, A. P. Hawker and J. D. Shand, *J. Polym. Sci., Part A: Polym. Chem.*, 2012, **50**, 4814–4822.
- 113 F. Nederberg, E. F. Connor, T. Glausser and J. L. Hedrick, *Chem. Commun.*, 2001, 2066–2067.
- 114 P. McKeown, M. Kamran, M. G. Davidson, M. D. Jones, L. A. Román-Ramírez and J. Wood, *Green Chem.*, 2020, **22**, 3721–3726.
- 115 A. C. Sánchez and R. S. Collinson, *Eur. Polym. J.*, 2011, **47**, 1970–1976.
- 116 S. Westhues, J. Idel and J. Klankermayer, *Sci. Adv.*, 2018, 1–9.
- 117 E. M. Krall, T. W. Klein, R. J. Andersen, A. J. Nett, R. W. Glasgow, D. S. Reader, B. C. Dauphinais, S. P. Mc Ilrath, A. A. Fischer, M. J. Carney, D. J. Hudson and N. J. Robertson, *Chem. Commun.*, 2014, **50**, 4884–4887.
- 118 T.-O. Kindler, C. Alberti, E. Fedorenko, N. Santangelo and S. Enthaler, *ChemistryOpen*, 2020, **9**, 401–404.
- 119 L. Monsigny, J.-C. Berthet and T. Cantat, *ACS Sustainable Chem. Eng.*, 2018, **6**, 10481–10488.
- 120 H. Liu, X. Song, F. Liu, S. Liu and S. Yu, *J. Polym. Res.*, 2015, **22**, 135–141.
- 121 C. Alberti, N. Damps, R. R. R. Meißner, M. Hofmann, D. Rijono and S. Enthaler, *Adv. Sustainable Syst.*, 2020, **4**, 1900081.
- 122 M. Hofmann, C. Alberti, F. Scheliga, R. R. R. Meißner and S. Enthaler, *Polym. Chem.*, 2020, **11**, 2625–2629.
- 123 P. McKeown, L. A. Román-Ramírez, S. Bates, J. Wood and M. D. Jones, *ChemSusChem*, 2019, **12**, 5233–5238.
- 124 A. J. Hunt, T. J. Farmer and J. H. Clark, *Chapter 1 Elemental Sustainability and the Importance of Scarce Element Recovery*, in *Element Recovery and Sustainability*, ed. A. Hunt, RSC, 2013, ch. 1, pp. 1–28.
- 125 ACS, *12 Principles of Green Chemistry*, <https://www.acs.org/content/acs/en/greenchemistry/principles/12-principles-of-green-chemistry.html>, (Accessed: 19th October 2020).
- 126 European Bioplastics, *Facts and Figures*, https://docs.european-bioplastics.org/publications/EUBP_Facts_and_figures.pdf, (Accessed: 20th October 2020).
- 127 F. M. Lamberti, L. A. Román-Ramírez and J. Wood, *J. Polym. Environ.*, 2020, **28**, 2551–2571.
- 128 V. Sinha, M. R. Patel and J. V. Patel, *J. Polym. Environ.*, 2010, **18**, 8–25.
- 129 S. M. Al-Salem, P. Lettieri and J. Baeyens, *Waste Manage.*, 2009, **29**, 2625–2643.
- 130 G. P. Karayannidis and D. S. Achilias, *Macromol. Mater. Eng.*, 2007, **292**, 128–146.
- 131 D. Paszun and T. Szychaj, *Ind. Eng. Chem. Res.*, 1997, **36**, 1373–1383.
- 132 K. R. Della Chiaie, F. R. McMahon, E. J. Williams, M. J. Price and A. P. Dove, *Polym. Chem.*, 2020, **11**, 1450–1453.

3.2. Experimental

Exemplar procedures, full characterisation data and representative spectra are provided herein, see ESI for full details: <https://www.rsc.org/suppdata/d0/py/d0py01519a/d0py01519a1.pdf>

3.2.1. General experimental methods

General methods detailed in section 2.3.1. of Chapter 2 were used. Commercial PLA samples were purchased (*Vegware*TM; R600Y-VW, $M_n \sim 45,510 \text{ g mol}^{-1}$) and used as received. Bottle-grade poly(ethylene terephthalate) (PET) (*The Coca-Cola Company*TM, $M_n \sim 40,000 \text{ g mol}^{-1}$) was sourced from a local grocery store (Fresh, University of Bath), rinsed with acetone and air-dried prior to use. PET thin-films represent waste from the manufacturing sector and were kindly donated by Avery Dennison.

3.2.2. General polymerisation procedures

3.2.2.1. Lactide polymerisation

PLA production and subsequent materials characterisation was conducted as detailed in section 2.3.2.1. of Chapter 2.

3.2.2.2. Lactide polymerisation kinetics

Polymerisation kinetic data was acquired according to the method described in section 2.3.2.2. of Chapter 2.

3.2.3. General PLA degradation procedures

3.2.3.1. PLA methanolysis

A J Young's flask was charged with metal complex (2 – 8 wt%, 0.0050 – 0.02 g, 0.13 – 0.58 mol% relative to ester linkages) and PLA pieces (0.25 g, $0.1 \times 0.1 \text{ cm}^2$, *Vegware*TM, PLLA cup, $M_n = 45,510 \text{ g mol}^{-1}$) in a Glovebox filled with argon. The polymer was dissolved in THF (4 mL) with heat and stirring assisting dissolution. The flask was submerged in a preheated oil bath (80 °C) to which MeOH (1 mL, 7 equivalents relative to ester linkages) was added. Aliquots were taken for ¹H NMR (CDCl₃) analysis of the methine region (*ca.* $\delta = 4.2 - 5.2$ ppm). After the reaction the solvent was removed *in vacuo* and the residual methyl lactate (Me-LA) was analysed further. This procedure was repeated for degradation reactions conducted in dry toluene (4 mL).

3.2.3.2. PLA methanolysis kinetics

Reaction kinetic analysis was performed using the degradation procedure detailed in section 3.2.3.1. [Mg(1)]₂ was tested at 4 and 8 wt% respectively (0.01 – 0.02 g, 0.29 – 0.57 mol% relative to ester linkages) in THF, whilst [Zn(1)]₂ was investigated at 8 wt% (0.02 g, 0.53 mol% relative to ester linkages) in dry toluene. Aliquots were taken under a dynamic flow of argon to obtain a minimum of 5 data points across the total reaction time. Plotting $\ln([\text{Int}]_0/[\text{Int}]_t)$ against time afforded a straight line fit with the gradient equivalent to the pseudo-first-order rate constant (k_{app}).

3.2.4. General PET degradation procedures

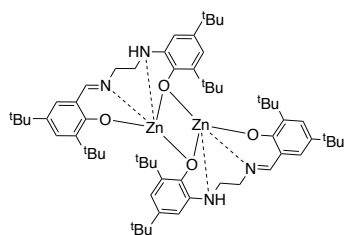
3.2.4.1. PET glycolysis

A J Young's flask was charged with metal complex (8 wt%, 0.02 g, 1.3 – 1.5 mol% relative to ester linkages) and bottle-grade PET pieces (0.25 g, 0.1 × 0.1 cm², *The Coca-Cola Company*TM, $M_n \sim 40,000 \text{ g mol}^{-1}$) in a Glovebox filled with argon. Ethylene glycol (EG) (2 mL, 27.5 equivalents relative to ester linkages) was added under a flow of argon before submerging the flask in a preheated oil bath (180 °C). The reaction solution was stirred for the desired amount of time or until a homogeneous solution was observed, indicating reaction completion. Following this the flask was removed and allowed to cool for a few minutes after which deionised H₂O (5 mL) was added, the flask vigorously shaken and rapidly filtered. The flask was rinsed with an additional portion of deionised H₂O (5 mL), which was used to stir the filter cake. The filtrate was retained and refrigerated (*ca.* 4 °C) for 18 h. Needle-like crystals of bis(2-hydroxyethyl) terephthalate (BHET) were isolated by filtration, washed with deionised H₂O (2 × 1 mL) and dried *in vacuo* at 90 °C for 3 h. This method was repeated for PET thin-films.

3.2.5. Synthesis and characterisation

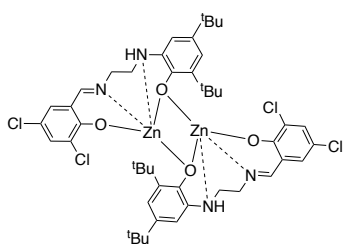
General procedures, full characterisation data and representative spectra for the ligand precursor (1H) and catalen ligands (1-3H₂) are detailed in sections 2.3.3.1, 2.3.3.2. and 2.3.3.4. of Chapter 2.

3.2.5.1. Zn(II)-catalen complexes



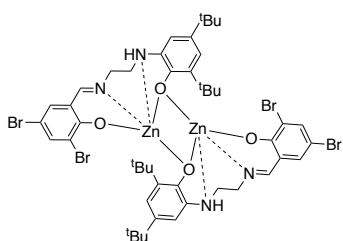
[Zn(1)]₂: Isolated as a light-green solid (0.45 g, 0.83 mmol, 83%). To a pre-stirred solution of 1H₂ (0.48 g, 1 mmol) in dry toluene (10 mL) at 0 °C for 5 min, ZnEt₂ (1 mL, 1 mmol) was added dropwise with stirring. The solution was allowed to gradually warm to RT, resulting in a light-green precipitate.

The precipitate was redissolved upon gentle heating and the solution stirred for 30 min at RT. Light-green crystals were isolated by cannula filtration and dried *in vacuo* at 80 °C for 4 h. ^1H NMR (CDCl_3 , 500 MHz): δ = 8.17 (s, 1H; ArCHN), 7.24 (d, J = 2 Hz, 1H; ArH), 7.00 (s, 1H; ArH), 6.95 (s, 1H; ArH), 6.73 (d, J = 2 Hz, 1H; ArH), 4.44 (s, 1H; NH), 3.99 – 3.93 (m, 1H; CH), 3.80 – 3.75 (m, 1H; CH), 3.62 – 3.57 (m, 2H; CH), 1.36 (s, 9H; $\text{C}(\text{CH}_3)_3$), 1.24 (s, 9H; $\text{C}(\text{CH}_3)_3$), 1.22 (s, 9H; $\text{C}(\text{CH}_3)_3$), 1.20 (s, 9H; $\text{C}(\text{CH}_3)_3$). $^{13}\text{C}\{^1\text{H}\}$ NMR (CDCl_3 , 100 MHz): δ = 170.9 (ArCHN), 169.0, 155.9, 140.6, 138.5, 137.8, 134.2, 132.7, 129.6, 129.0, 120.3, 117.4, 116.7 (Ar), 53.1, 44.6 (CH_2), 35.3, 35.1, 34.4, 33.8 ($\text{C}(\text{CH}_3)_3$), 31.8, 31.5, 30.3, 29.8 (CH_3). Elemental analysis: Calculated for $\text{C}_{62}\text{H}_{92}\text{N}_4\text{O}_4\text{Zn}_2$: C, 68.43 %; H, 8.52 %; N, 5.15 %. Found: C, 67.34 %; H, 8.32 %; N, 5.18 %.



$[\text{Zn}(\mathbf{2})]_2$: Isolated as a light-yellow solid (0.40 g, 0.80 mmol, 80%). To a solution of $\mathbf{2H}_2$ (0.44 g, 1 mmol) in dry toluene (10 mL), ZnEt_2 (1 mL, 1 mmol) was added dropwise at RT and the solution stirred for 30 min. A light-yellow solid precipitated, which was recrystallised from the reaction solvent prior to

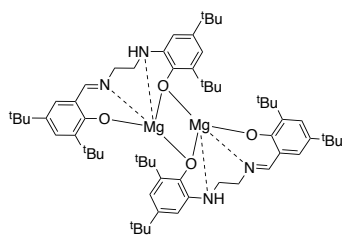
isolation by cannula filtration and dried *in vacuo* at 80 °C for 4 h. ^1H NMR (CDCl_3 , 500 MHz): δ = 8.09 (s, 1H; ArCHN), 7.18 (s, 1H; ArH), 7.16 (d, J = 3 Hz, 1H; ArH), 7.00 (d, J = 2 Hz, 1H; ArH), 6.80 (d, J = 3 Hz, 1H; ArH), 4.75 (s, 1H; NH), 3.83 – 3.81 (m, 1H; CH), 3.78 – 3.70 (m, 2H; CH), 3.58 – 3.54 (m, 1H; CH), 1.31 (s, 9H; $\text{C}(\text{CH}_3)_3$), 1.27 (s, 9H; $\text{C}(\text{CH}_3)_3$). $^{13}\text{C}\{^1\text{H}\}$ NMR (CDCl_3 , 125 MHz): δ = 168.4 (ArCHN), 164.6, 156.1, 139.1, 137.6, 132.8, 131.9, 131.9, 128.0, 120.8, 118.5, 117.0, 115.8 (Ar), 52.9, 44.6 (CH_2), 35.3, 34.5 ($\text{C}(\text{CH}_3)_3$), 31.9, 29.9 (CH_3). Elemental analysis: Calculated for $\text{C}_{46}\text{H}_{56}\text{Cl}_4\text{N}_4\text{O}_4\text{Zn}_2$: C, 55.17 %; H, 5.64 %; N, 5.59 %. Found: C, 53.50 %; H, 5.42 %; N, 5.51 %.



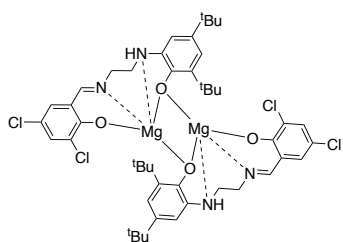
$[\text{Zn}(\mathbf{3})]_2$: Isolated as a light-yellow solid (0.52 g, 0.88 mmol, 88%). To a solution of $\mathbf{3H}_2$ (0.53 g, 1 mmol) in dry toluene (10 mL), ZnEt_2 (1 mL, 1 mmol) was added dropwise with stirring at RT and then stirred at 90 °C for 45 min. A light-yellow solid was isolated by cannula filtration and dried *in vacuo* at 80 °C

for 4 h. ^1H NMR (CDCl_3 , 500 MHz): δ = 8.06 (s, 1H; ArCHN), 7.46 (s, 1H; ArH), 7.17 (s, 1H; ArH), 7.01 (s, 1H; ArH), 6.98 (s, 1H; ArH), 4.80 (s, 1H; NH), 3.81 – 3.71 (m, 3H; CH), 3.61 – 3.55 (m, 1H; CH), 1.31 (s, 9H; $\text{C}(\text{CH}_3)_3$), 1.28 (s, 9H; $\text{C}(\text{CH}_3)_3$). $^{13}\text{C}\{^1\text{H}\}$ NMR (CDCl_3 , 100 MHz): δ = 168.37 (ArCHN), 165.4, 156.1, 139.1, 138.3, 137.7, 135.9, 131.8, 120.8, 119.4, 119.2, 117.2, 102.6 (Ar), 52.8, 44.5 (CH_2), 35.3, 34.5 ($\text{C}(\text{CH}_3)_3$), 31.9, 29.9 (CH_3). Elemental analysis: Calculated for $\text{C}_{46}\text{H}_{56}\text{Br}_4\text{N}_4\text{O}_4\text{Zn}_2$: C, 46.85 %; H, 4.79 %; N, 4.75 %. Found: C, 44.66 %; H, 4.40 %; N, 4.68 %.

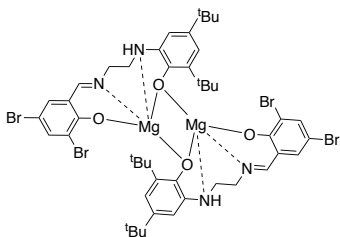
3.2.5.2. Mg(II)-catalen complexes



[Mg(1)]₂: Isolated as a light-yellow solid (0.12 g, 0.24 mmol, 24%). To a pre-stirred solution of 1H₂ (0.48 g, 1 mmol) in dry toluene (10 mL) at 0 °C, Mg(^tBu)₂ (1 mmol, 1 mL) was added dropwise with stirring. The solution was allowed to gradually warm to RT where it was stirred for 30 min. Light-yellow crystals were isolated after 3 days at –20 °C. Following XRD analysis, the solution was concentrated *in vacuo* and stored for a further 18 h at –20 °C to enhance product yield. A light-yellow solid was isolated by cannula filtration and dried *in vacuo* at 80 °C for 3 h. ¹H NMR (CDCl₃, 500 MHz): δ = 8.13 (s, 1H; ArCHN), 7.24 (d, *J* = 2 Hz, 1H; ArH), 7.00 (s, 1H; ArH), 6.96 (d, *J* = 2 Hz, 1H; ArH), 6.81 (d, *J* = 2 Hz, 1H; ArH), 4.22 (s, 1H; NH), 3.92 – 3.86 (m, 1H; CH), 3.81 – 3.76 (m, 1H; CH), 3.65 – 3.60 (m, 1H; CH), 3.52 – 3.47 (m, 1H; CH), 1.33 (s, 9H; C(CH₃)₃), 1.22 (s, 9H; C(CH₃)₃), 1.21 (s, 18H; C(CH₃)₃). ¹³C{¹H} NMR (CDCl₃, 125 MHz): δ = 171.2 (ArCHN), 167.5, 155.0, 139.9, 138.8, 138.0, 133.9, 132.3, 129.2, 128.8, 121.0, 119.5, 116.9 (Ar), 54.6, 45.6 (CH₂), 35.1, 35.1, 34.4, 33.8 (C(CH₃)₃), 31.8, 31.6, 30.4, 29.6 (CH₃). Elemental analysis: Calculated for C₆₂H₉₂N₄O₄Mg₂: C, 74.02 %; H, 9.22 %; N, 5.57 %. Found: C, 72.06 %; H, 9.22 %; N, 5.05 %.



[Mg(2)]₂: Isolated as a light-yellow solid (0.065 g, 0.14 mmol, 14%). To a solution of 2H₂ (0.44 g, 1 mmol) in dry toluene (10 mL), Mg(^tBu)₂ (1 mL, 1 mmol) was added dropwise with stirring at RT and the solution stirred for 30 min. The solution was concentrated *in vacuo*, observing precipitation of a light-yellow solid within 3 h, which was isolated by cannula filtration and dried *in vacuo* at 80 °C for 3 h. ¹H NMR (CDCl₃, 500 MHz): δ = 8.06 (s, 1H; ArCHN), 7.20 (s, 1H; ArH), 7.14 (s, 1H; ArH), 7.02 (s, 1H; ArH), 6.87 (s, 1H; ArH), 4.59 (s, 1H; NH), 3.79 – 3.57 (m, 4H; CH), 1.29 (s, 9H; C(CH₃)₃), 1.27 (s, 9H; C(CH₃)₃). ¹³C{¹H} NMR (CDCl₃, 125 MHz): δ = 168.7 (ArCHN), 163.3, 160.1, 155.3, 139.4, 137.9, 132.8, 131.7, 131.7, 121.3, 120.6, 117.0, 115.7 (ArH), 54.4, 45.4 (CH₂), 35.1, 34.5 (C(CH₃)₃), 31.9, 30.2 (CH₃). Elemental analysis: Calculated for C₄₆H₅₆Cl₄N₄O₄Mg₂: C, 60.09 %; H, 6.14 %; N, 6.09 %. Found: C, 44.70 %; H, 4.43 %; N, 3.40 %. Elemental analysis is consistently low on carbon, potentially indicative of the complex being air- and moisture sensitive.



[Mg(**3**)]₂: Isolated as a light-yellow solid (0.15 g, 0.15 mmol, 27%). To a solution of **3H**₂ (0.53 g, 1 mmol) in dry toluene (10 mL), Mg(^tBu)₂ (1 mL, 1 mmol) was added dropwise with stirring at RT and then stirred at 90 °C for 45 min. A light-yellow solid was isolated by cannula filtration and dried *in vacuo* at 80 °C for 3 h. ¹H NMR (CDCl₃, 500 MHz): δ = 8.04 (s, 1H; ArCHN), 7.48 (s, 1H; ArH), 7.15 (s, 1H; ArH), 7.04 (s, 1H; ArH), 7.03 (s, 1H; ArH), 4.59 (s, 1H; NH), 3.79 – 3.61 (m, 4H; CH), 1.29 (s, 9H; C(CH₃)₃), 1.27 (s, 9H; C(CH₃)₃). ¹³C {¹H} NMR (CDCl₃, 125 MHz): δ = 168.7 (ArCHN), 164.0, 155.3, 139.3, 138.2, 137.9, 135.6, 131.5, 121.3, 121.1, 118.9, 117.1, 102.4 (Ar), 54.1, 45.2 (CH₂), 35.1, 34.5 (C(CH₃)₃), 31.9, 30.1 (CH₃). Elemental analysis: Calculated for C₄₆H₅₆Br₄N₄O₄Mg₂: C, 50.36 %; H, 5.14 %; N, 5.11 %. Found: C, 45.66 %; H, 4.54 %; N, 4.41 %. Elemental analysis more consistent with hydrated complex, indicative of hygroscopicity. [Mg(**3**)]₂·6H₂O, theoretical: C, 45.84 %; H, 5.69 %; N, 4.65 %.

3.2.5.3. Representative NMR spectra

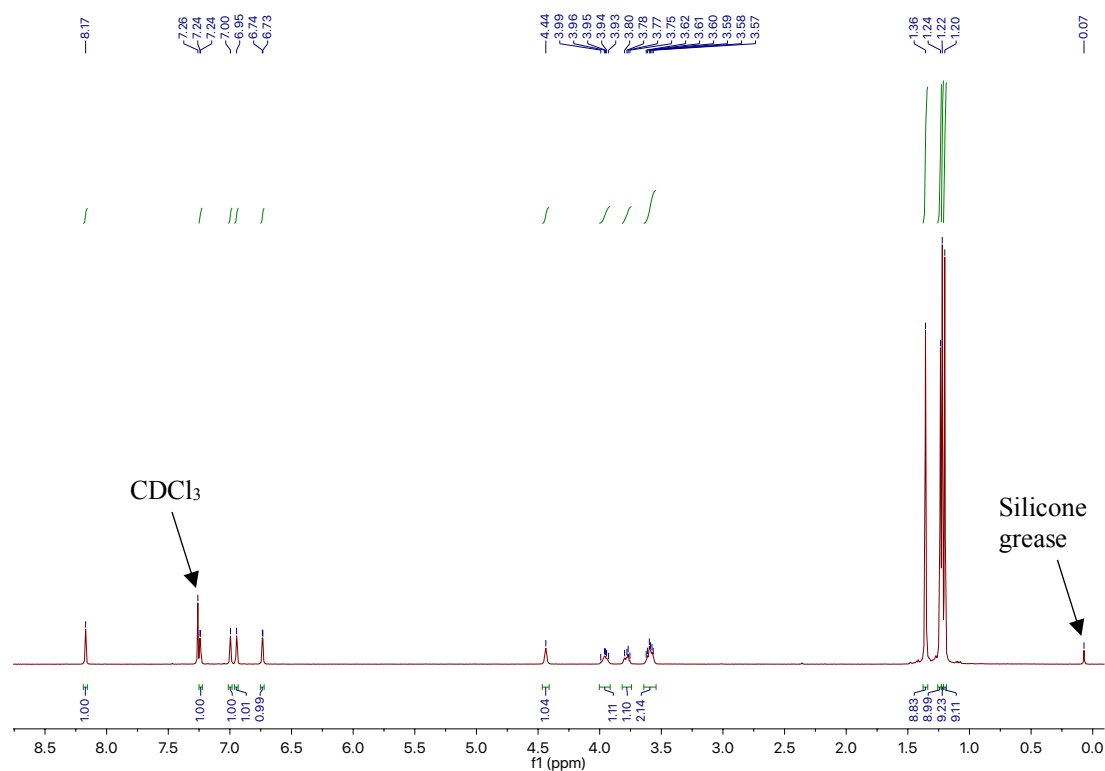


Figure 3.1. ¹H NMR (CDCl₃, 500 MHz) spectrum of [Zn(1)₂].

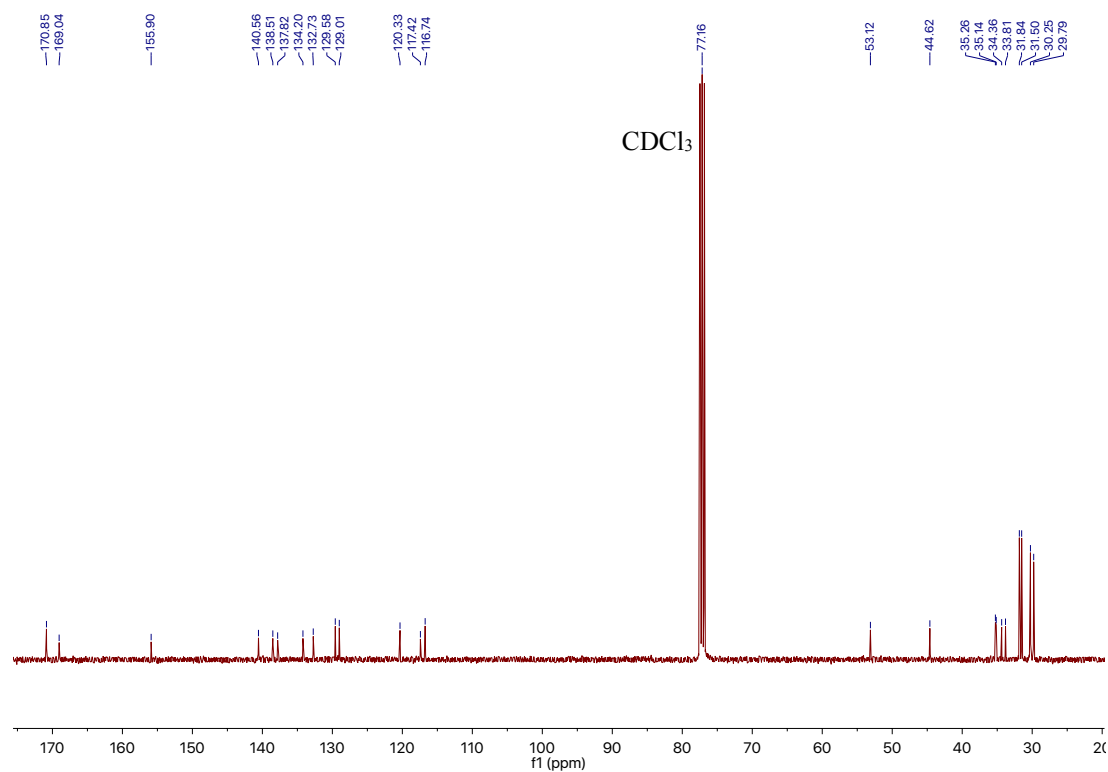


Figure 3.2. ¹³C {¹H} NMR (CDCl₃, 100 MHz) spectrum of [Zn(1)₂].

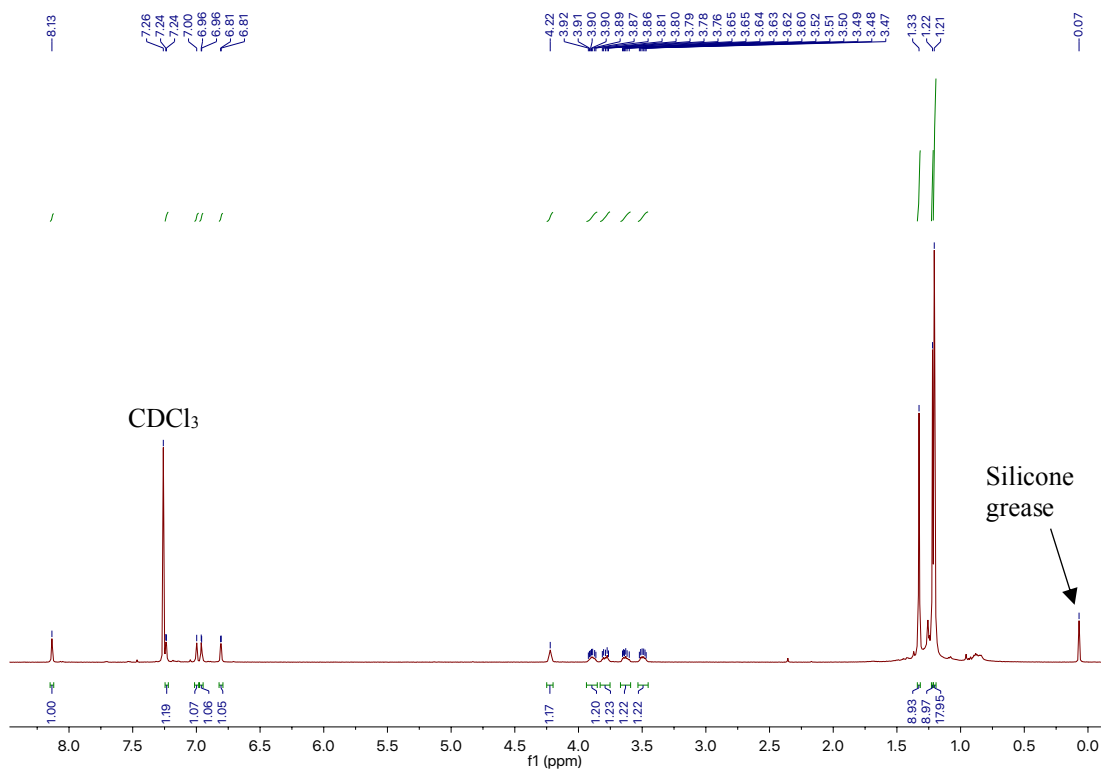


Figure 3.3. ¹H NMR (CDCl₃, 500 MHz) spectrum of [Mg(1)]₂.

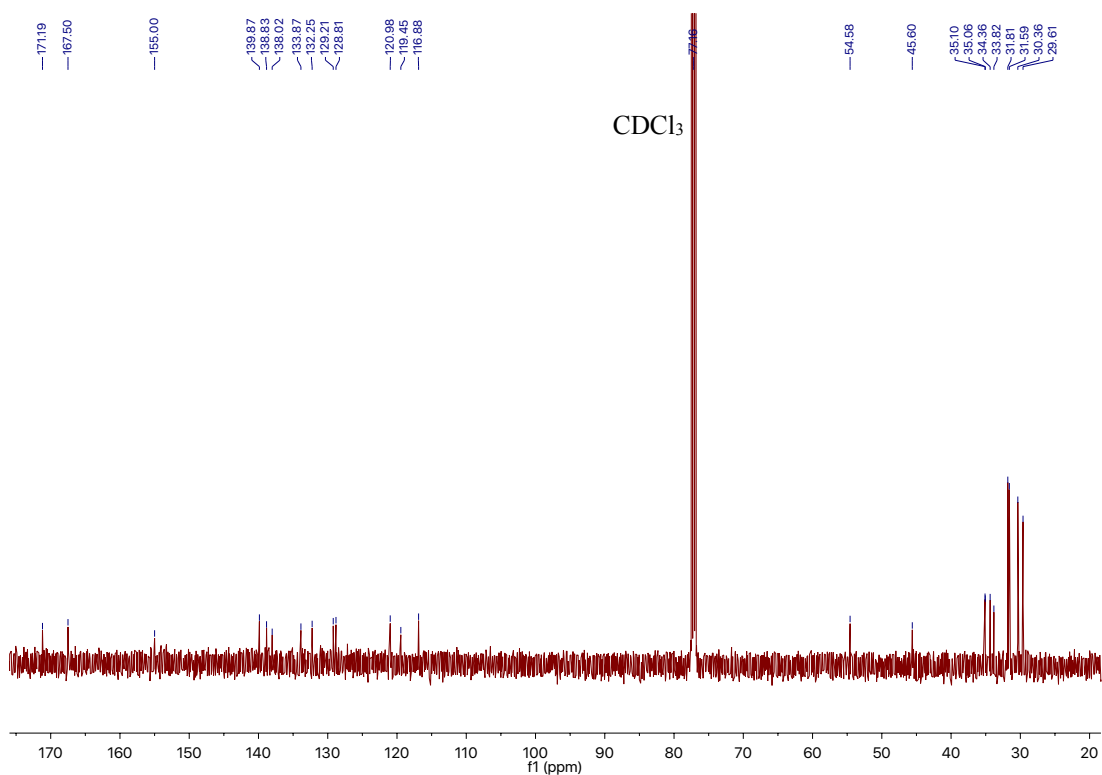


Figure 3.4. ¹³C {¹H} NMR (CDCl₃, 125 MHz) spectrum of [Mg(1)]₂.

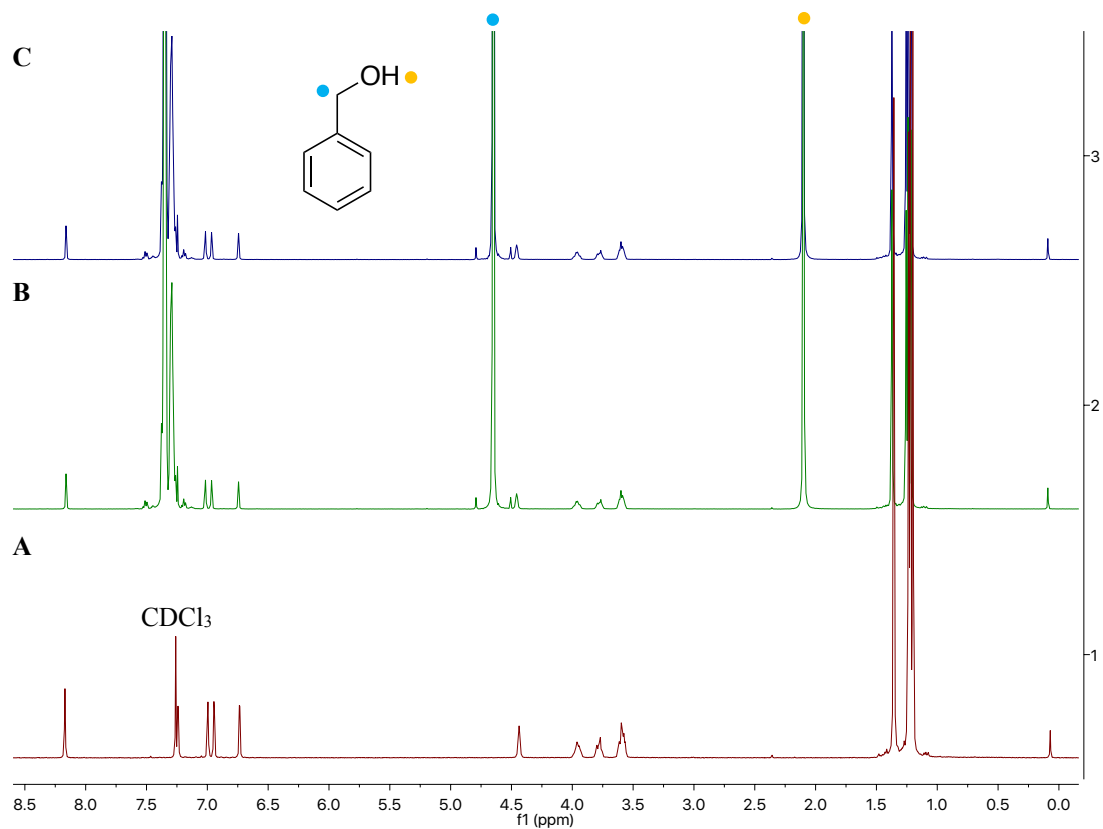


Figure 3.5. Stacked ¹H NMR (CDCl₃, 500 MHz) spectra assessing the stability of [Zn(**1**)]₂ with excess BnOH: (A) [Zn(**1**)]₂, (B) [Zn(**1**)]₂+ BnOH at RT, and; (C) [Zn(**1**)]₂+ BnOH at 80 °C for 1 h. *N.B.* Figure 1 in ESI.

3.2.6. Polymer characterisation

3.2.6.1. Representative ^1H NMR spectrum

A representative ^1H NMR spectrum of PLA is provided in section 2.3.4.1. of Chapter 2.

3.2.6.2. Representative SEC spectra

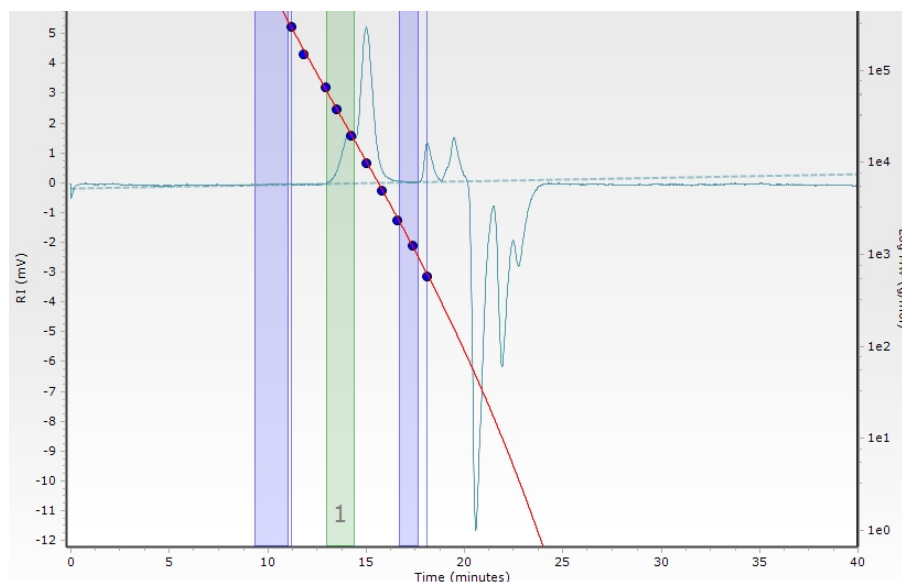


Figure 3.6. Bimodal SEC spectrum of purified PLA obtained from the solution polymerisation of *rac*-LA at 80 °C for 8 h using $[\text{Zn}(\mathbf{1})_2]$ $\{[rac\text{-LA}]:[\text{Zn}]:[\text{BnOH}] = 100:1:1\}$ (Table 2, Entry 1 in publication 3). *N.B.* Figure 4 in ESI.

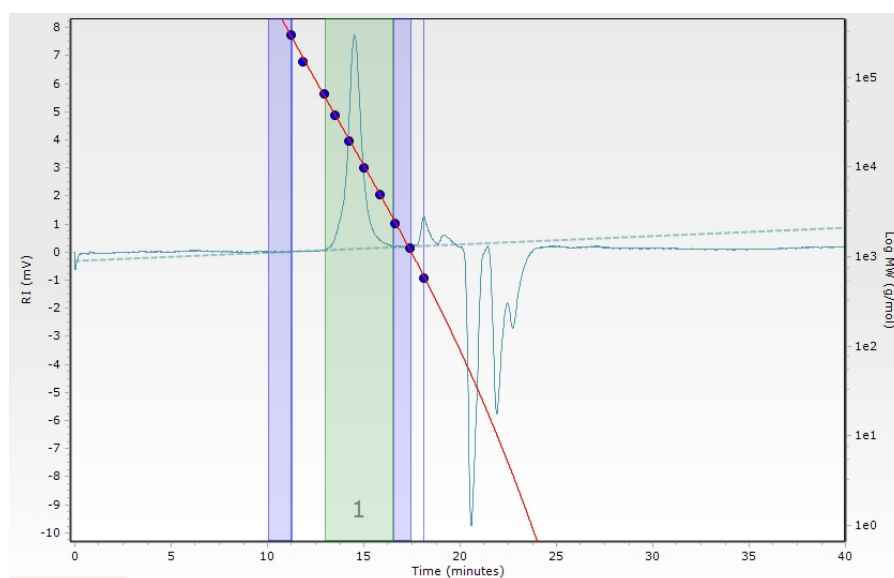


Figure 3.7. Monomodal SEC spectrum of purified PLA obtained from the solution polymerisation of *rac*-LA at 80 °C for 1.5 h using $[\text{Mg}(\mathbf{1})_2]$ $\{[rac\text{-LA}]:[\text{Mg}]:[\text{BnOH}] = 100:1:1\}$ (Table 2, Entry 4 in publication 3). *N.B.* Figure 5 in ESI.

3.2.6.3. Representative homonuclear decoupled ^1H NMR spectra

Representative spectra are provided in section 2.3.4.3. of Chapter 2.

3.2.6.4. MALDI-ToF spectra

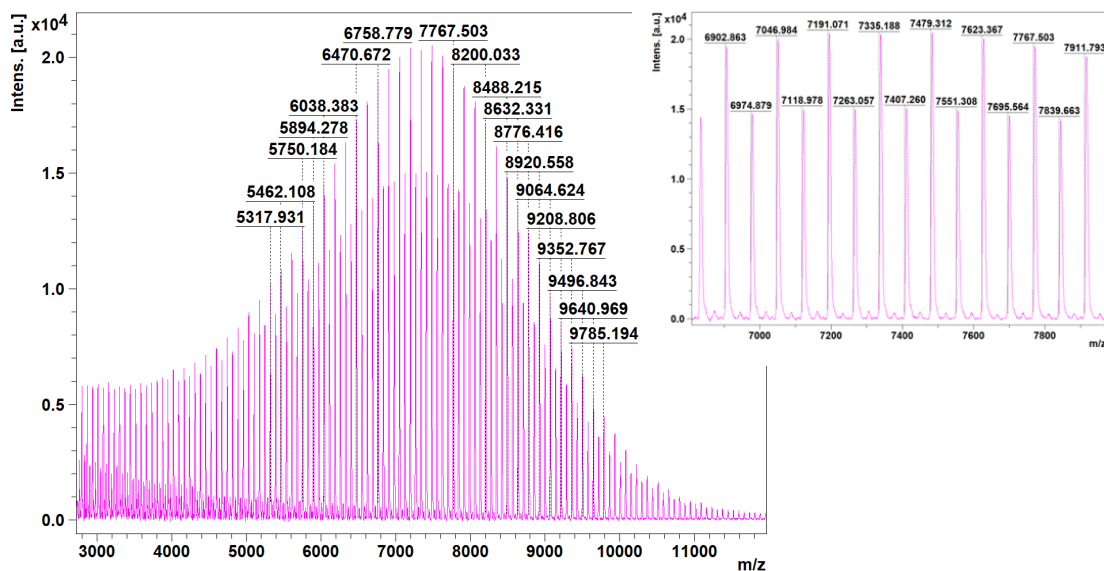


Figure 3.8. MALDI-ToF spectrum of purified PLA obtained from the solution polymerisation of *rac*-LA at 80 °C for 1.5 h using $[\text{Mg}(\mathbf{1})_2]$ $\{[rac\text{-LA}]:[\text{Mg}]:[\text{BnOH}] = 100:1:1\}$ (Table 2, Entry 4 in publication 3). Magnified version of main series provided to assist in identifying the repeat unit and end group. *N.B.* Figure 8 in ESI.

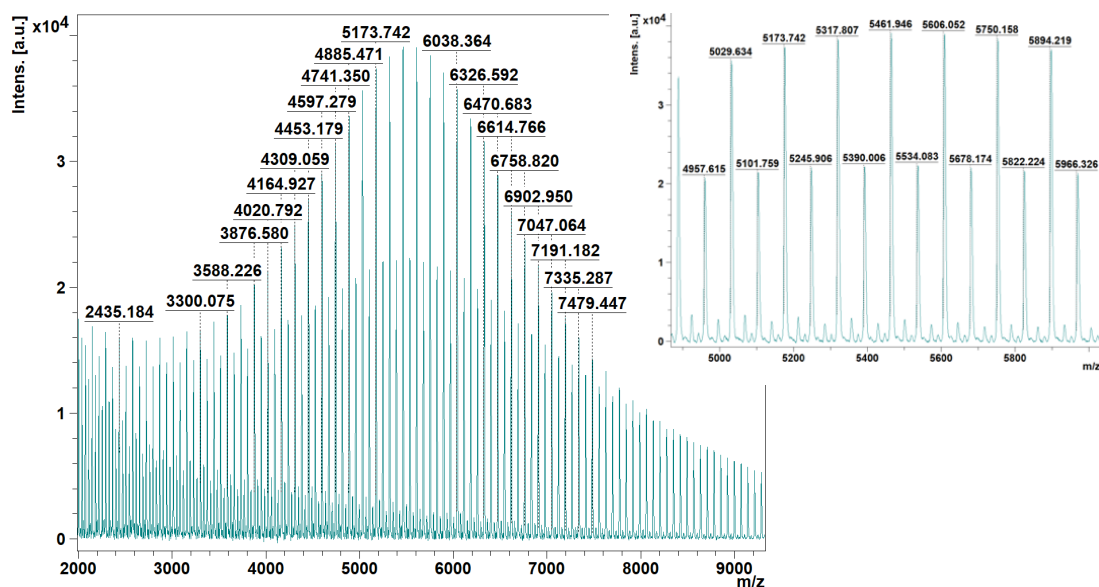


Figure 3.9. MALDI-ToF spectrum of purified PLA obtained from the melt polymerisation of *rac*-LA at 180 °C using $[\text{Mg}(\mathbf{1})_2]$ $\{[rac\text{-LA}]:[\text{Mg}]:[\text{BnOH}] = 3000:1:10\}$ (Table 1, Entry 8 in publication 3). Magnified version of main series provided to assist in identifying the repeat unit and end group. *N.B.* Figure 9 in ESI.

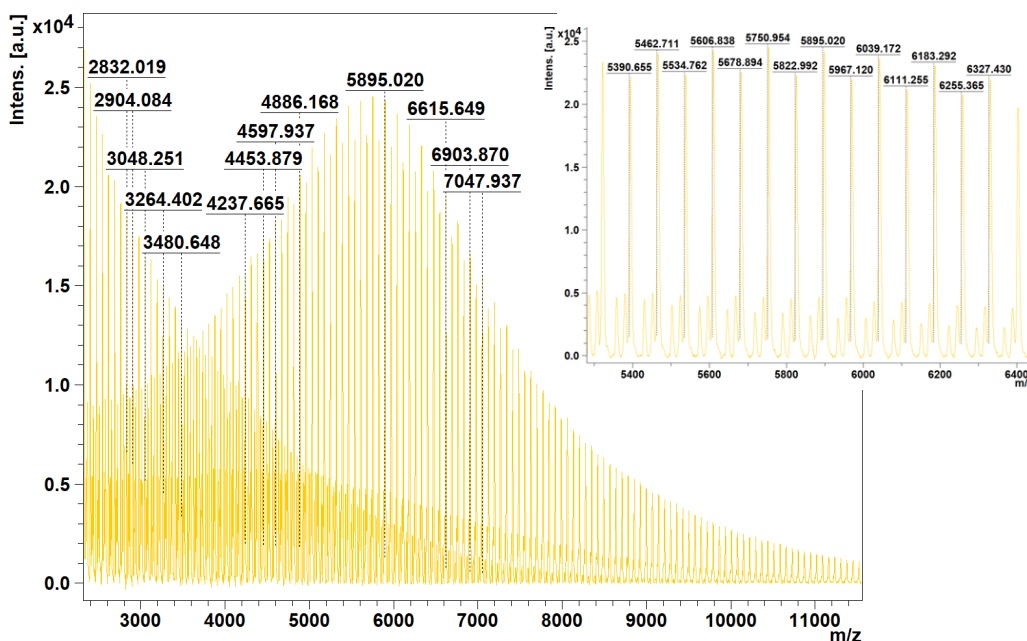
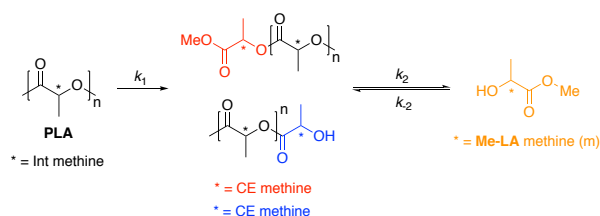


Figure 3.10. MALDI-ToF spectrum of purified PLA obtained from the solution polymerisation of *rac*-LA at 80 °C for 8 h using [Mg(3)]₂ {[*rac*-LA]:[Mg]:[BnOH] = 100:1:1} (Table 2, Entry 5 in publication 3). Magnified version of main series provided to assist in identifying the repeat unit and end group. *N.B.* Figure 10 in ESI.

3.2.7. Degradation characterisation

3.2.7.1. Representative ¹H NMR spectra of PLA methanolysis



Scheme 3.1. Two-step reaction sequence for the production of Me-LA from PLA *via* the intermediate formation of chain-end groups. Consequently, the methine groups can be categorised as internal (int), chain-end (CE) and those corresponding directly to the alkyl lactate (Me-LA).^[2]

Internal methine conversion (X_{int}), Me-LA selectivity (S_{Me-LA}) and Me-LA yield (Y_{Me-LA}) were calculated using Equations 3.1–3.3 below:^[11-12]

$$X_{int} = 1 - \frac{[Int]}{[Int]_0} \quad (3.1)$$

$$S_{Me-LA} = \frac{[Me-LA]}{[Int]_0 - [Int]} \quad (3.2)$$

$$Y_{Me-LA} = X_{int} S_{Me-LA} \quad (3.3)$$

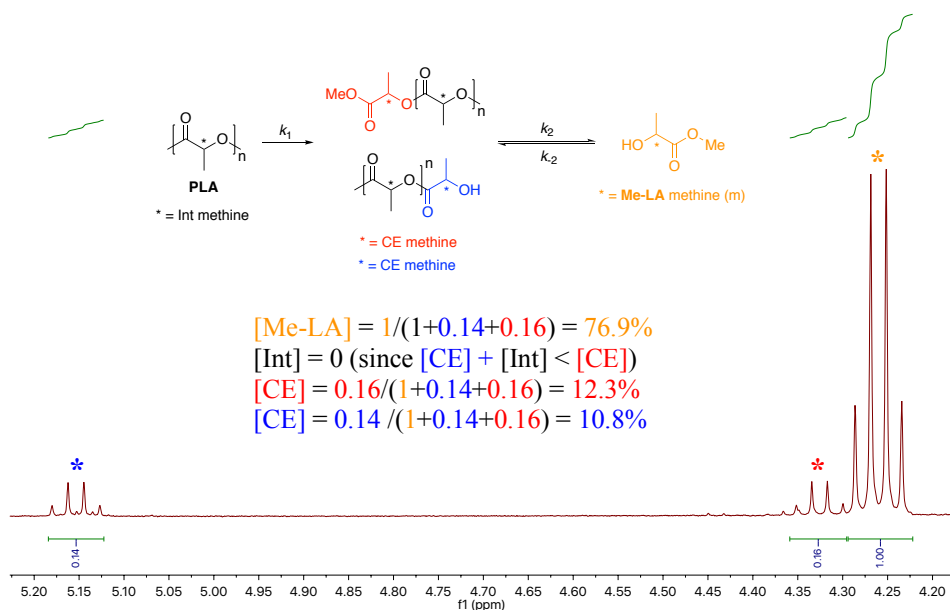


Figure 3.11. ^1H NMR (CDCl_3 , 400 MHz) spectrum of PLA cup (0.25 g, $M_n = 45,510 \text{ g mol}^{-1}$) degradation into Me-LA using $[\text{Mg}(\mathbf{1})_2]$ (4 wt%, 0.01 g, 0.29 mol% relative to ester linkages) at 80 °C for 8 h in THF (Table 4, Entry 1 in publication 3). $[Int] = 0$ indicative of complete PLA consumption. Consequently, no internal methine (*) resonance was observed, which would appear in the same region as (*). *N.B.* Figure 11 in ESI.

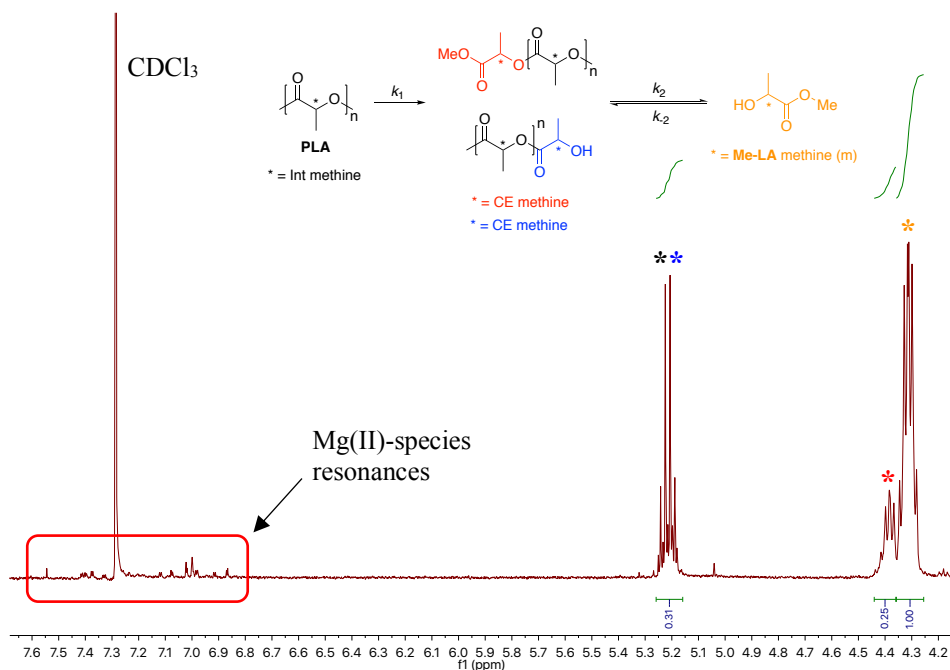


Figure 3.12. ^1H NMR (CDCl_3 , 400 MHz) spectrum of PLA cup (0.25 g, $M_n = 45,510 \text{ g mol}^{-1}$) degradation into Me-LA using $[\text{Mg}(\mathbf{1})_2]$ (4 wt%, 0.01 g, 0.29 mol% relative to ester linkages) at 80 °C for 8 h in THF (solvent removed). Aromatic resonances can be attributed to the presence of Mg(II)-species in the sample (Table 3, Entry 12 in publication 3). *N.B.* Figure 12 in ESI.

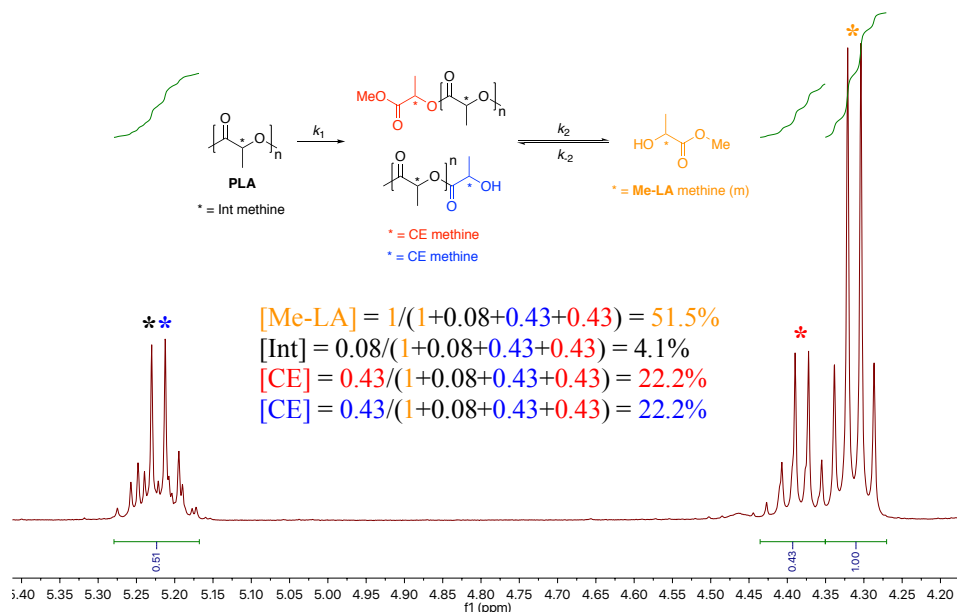


Figure 3.13. ^1H NMR (CDCl_3 , 400 MHz) spectrum of PLA cup (0.25 g, $M_n = 45,510 \text{ g mol}^{-1}$) degradation into Me-LA using $[\text{Zn}(\mathbf{1})_2]$ (8 wt%, 0.02 g, 0.53 mol% relative to ester linkages) at 80 °C for 8 h in dry toluene (solvent removed) (Table 3, Entry 3 in publication 3). *N.B.* Figure 13 in ESI.

3.2.7.2. Representative ^1H NMR spectrum of PET glycolysis

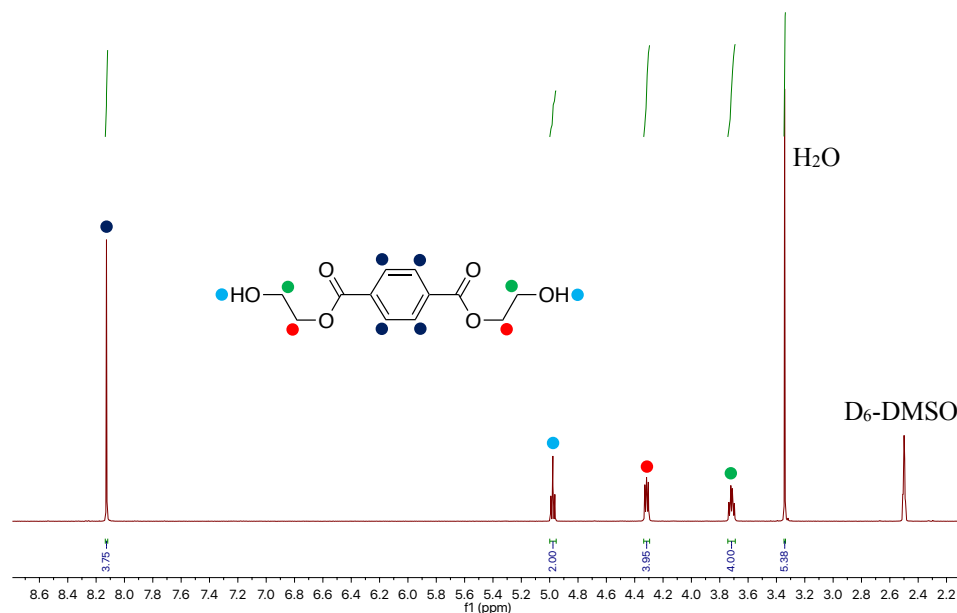


Figure 3.14. ^1H NMR ($\text{D}_6\text{-DMSO}$, 400 MHz) spectrum of recrystallised BHET from bottle-grade PET (0.25 g, $M_n \sim 40,000 \text{ g mol}^{-1}$) degradation using $[\text{Mg}(\mathbf{1})_2]$ (8 wt%, 0.02 g, 1.5 mol% relative to ester linkages) in 27.5 equivalents (2 mL) of EG at 180 °C for 3 h (Table 5, Entry 5 in publication 3). *N.B.* Figure 14 in ESI.

3.2.8. Crystallographic data

3.2.8.1. Special refinement details

[Zn(1)]₂: One solvent molecule of toluene is disordered over a centre of inversion and was refined with 50% occupation.

[Zn(3)]₂: Half the structure is generated by symmetry. One ^tBu group (C14) disordered over two positions in a ratio of 50:50.

[Mg(1)]₂: Three partial molecules of toluene contained in the unit cell with bond lengths subject to constraints. One ^tBu group (C23) disordered over two sites in a ratio of 78:22.

Table 3.1. Crystallographic data of [Zn(1-3)]₂. *N.B.* Table 1 in ESI.

Compound reference	[Zn(1)] ₂	[Zn(2)] ₂	[Zn(3)] ₂
Empirical formula	C ₈₃ H ₁₁₆ N ₄ O ₄ Zn ₂	C ₃₀ H ₃₆ Cl ₂ N ₂ O ₂ Zn	C ₃₀ H ₃₆ Br ₂ N ₂ O ₂ Zn
Formula Mass	1364.53	592.88	681.80
Crystal system	Triclinic	Monoclinic	Monoclinic
<i>a</i> /Å	9.5822(2)	9.8683(8)	10.0556(3)
<i>b</i> /Å	13.6635(3)	14.2238(12)	14.2825(3)
<i>c</i> /Å	15.4413(3)	20.5519(9)	20.6880(4)
<i>α</i> /°	98.426(2)	90	90
<i>β</i> /°	105.508	94.567(5)	95.646(2)
<i>γ</i> /°	99.504	90	90
Unit cell volume/Å ³	1882.26(7)	2875.6(4)	2956.78(12)
Temperature/K	150.0(3)	150(2)	150.01(10)
Space group	P-1	P 2 ₁ /c	P 2 ₁ /c
No. of formula units per unit cell, <i>Z</i>	1	4	4
Radiation type	Mo Kα	Cu Kα	Cu Kα
No. of reflections measured	45742	10029	15599
No. of independent reflections	8588	5054	5840
<i>R</i> _{int}	0.0391	0.0539	0.0181
Final <i>R</i> _i values (<i>I</i> > 2σ(<i>I</i>))	0.0363	0.0563	0.0408
Final <i>wR</i> (<i>F</i> ²) values (<i>I</i> > 2σ(<i>I</i>))	0.0848	0.1353	0.1003
Final <i>R</i> _i values (all data)	0.0539	0.0721	0.0426
Final <i>wR</i> (<i>F</i> ²) values (all data)	0.0939	0.1474	0.1019

Table 3.2. Crystallographic data of [Mg(1-3)]₂. *N.B.* DP refers to deprotonated amine as observed in the tetrameric analogue of [Mg(2)]₂, namely (Mg(2^{DP}))-tetramer. Table 2 in ESI.

Compound reference	[Mg(1)] ₂	[Mg(2)] ₂	Mg(2 ^{DP})-tetramer	[Mg(3)] ₂
Empirical formula	C ₈₄ H ₁₁₈ Mg ₂ N ₄ O ₄	C ₃₀ H ₃₆ Cl ₂ MgN ₂ O ₂	C ₂₇ H ₃₆ Cl ₂ Mg ₂ N ₂ O ₂	C ₃₀ H ₃₆ Br ₂ MgN ₂ O ₂
Formula Mass	1296.44	551.82	540.10	640.74
Crystal system	Monoclinic	Monoclinic	Triclinic	Monoclinic
<i>a</i> /Å	9.7766(3)	9.9229(4)	10.8720(12)	10.0761(5)
<i>b</i> /Å	31.3712(9)	14.2743(5)	11.0298(10)	14.3226(7)
<i>c</i> /Å	25.4191(5)	20.5348(5)	13.0224(12)	20.665(4)
<i>α</i> /°	90	90	112.876(9)	90
<i>β</i> /°	96.789(2)	95.319(3)	100.644(8)	96.011(10)
<i>γ</i> /°	90	90	93.112(8)	90
Unit cell volume/Å ³	7741.5(4)	2896.07(17)	1400.2(3)	2965.9(5)
Temperature/K	150.00(10)	150(2)	150.01(10)	150(2)
Space group	C 2/c	P 2 ₁ /c	P-1	P 2 ₁ /c
No. of formula units per unit cell, <i>Z</i>	4	4	2	4
Radiation type	Cu Kα	Mo Kα	Cu Kα	Cu Kα
No. of reflections measured	41029	20024	8571	11526
No. of independent reflections	7085	6390	5278	5538
<i>R</i> _{int}	0.0652	0.0489	0.0528	0.0451
Final <i>R</i> _i values (<i>I</i> > 2σ(<i>I</i>))	0.0725	0.0524	0.0768	0.0495
Final <i>wR</i> (<i>F</i> ²) values (<i>I</i> > 2σ(<i>I</i>))	0.1852	0.1352	0.1801	0.1346
Final <i>R</i> _i values (all data)	0.1026	0.0709	0.1275	0.0550
Final <i>wR</i> (<i>F</i> ²) values (all data)	0.2051	0.1483	0.2117	0.1409

Table 3.3. Selected bond lengths for [Zn(1-3)]₂ and [Mg(1-3)]₂. *N.B.* Table 3 in ESI.

Init.	Bond	Bond length / Å
[Zn(1)] ₂	Zn(1)-N(1) {amine}, Zn(1)- N(2) {imine}	2.2326(15), 2.0124(15)
[Zn(2)] ₂		2.204(3), 2.026(3)
[Zn(3)] ₂		2.212(2), 2.026(3)
[Mg(1)] ₂	Mg(1)-N(1) {amine}, Mg(1)-N(2) {imine}	2.236(2), 2.088(3)
[Mg(2)] ₂		2.2181(19), 2.0994(18)
[Mg(3)] ₂		2.221(3), 2.105(3)

Table 3.4. Selected bond angles for [Zn(1-3)]₂ and [Mg(1-3)]₂ with calculated τ_5 values. Ideal square pyramidal geometry corresponds to $\tau_5 = 0$. *N.B.* Table 4 in ESI.

Init.	Bond	Bond angle / °	τ_5
[Zn(1)] ₂	N(2)-Zn(1)-O(1), O(2)-Zn(1)-N(1)	133.43(5), 168.78(6)	0.59
[Zn(2)] ₂		126.55(10), 171.33(10)	0.75
[Zn(3)] ₂		126.22(9), 170.68(9)	0.74
[Mg(1)] ₂	O(1)-Mg(1)- N(2), O(2)- Mg(1)-N(1)	132.05(10), 164.11(9)	0.53
[Mg(2)] ₂		125.22(7), 166.45(7)	0.69
[Mg(3)] ₂		124.85(10), 165.92(11)	0.68

3.3. Post-publication Commentary

Key developments in the literature inspired by the work detailed in publication 3 include exchange of the catam fragment for a substituted thioether as reported by Stewart *et al.*^[15] (Figure 3.15, **26**). Indeed, Zn(II)-complexes supported by these thioether appended iminophenolate {ONS} ligands were found to exhibit superior activity for lactide polymerisation, achieving TOF values up to 250,000 h⁻¹ under immortal conditions in the melt $\{[rac\text{-LA}]:[\text{Zn}]:[\text{BnOH}] = 10,000:1:30 \text{ at } 180 \text{ }^\circ\text{C}\}$. Crystalline PLLA was also produced rapidly with minimal epimerisation, however, significantly reduced activity was observed on exchange with technical grade *rac*-LA, indicating poor catalyst stability. However, comparable PLA methanolysis performance to that discussed in publication 3 was observed, which could be extended to PET glycolysis. Interestingly, a number of Zn(II)-complexes were not amenable to kinetic sampling owing to sample quenching, which was attributed to poor hydrolytic stability, as noted in Chapter 2 for the Al(III)-catalens. Selective recycling using mixed waste feeds was not explored despite industrial relevance, presumably due to modest activity, which could be extended to this work.

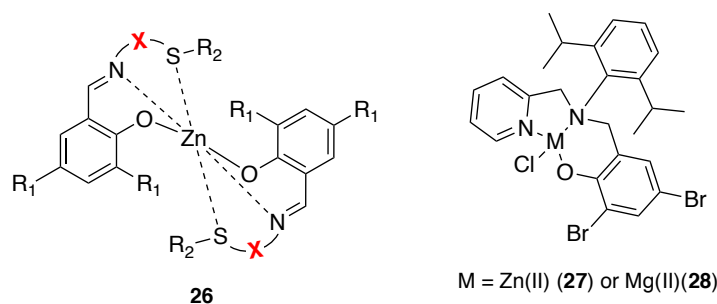


Figure 3.15. Zn(II)- and Mg(II)-complexes reported by Stewart *et al.*^[15] (**26**) and Hu *et al.*^[16] (**27** and **28**) for PLA production and recycling applications. *N.B.* X (in red) denotes variation of the substituted thioether backbone dependent on the amine precursor employed.

Comparatively, Han and co-workers have explored the substitution of a catam-type core derived from 2,6-diisopropylaniline with a labile pendant pyridine arm, generating an asymmetric {ONN} tertiary amine ligand.^[16] In combination with Zn(II) (**27**) and Mg(II) (**28**) (Figure 3.15), such complexes produced PLA of well-defined M_n and narrow dispersities ($D = 1.05 - 1.27$). However, markedly slower reaction times (typically 2 – 4 h) are noted in the melt at 130 °C relative to catalysts described in publication 3, despite the use of higher catalyst loadings (~ 1 mol%). Indeed, a fractional dependence on catalyst concentration suggests the catalytically active species aggregates during propagation, which inhibits activity. Crucially, this work highlights the negative impact of removing the H-bond donor provided by the catam moiety, which should be exploited in future catalyst design.

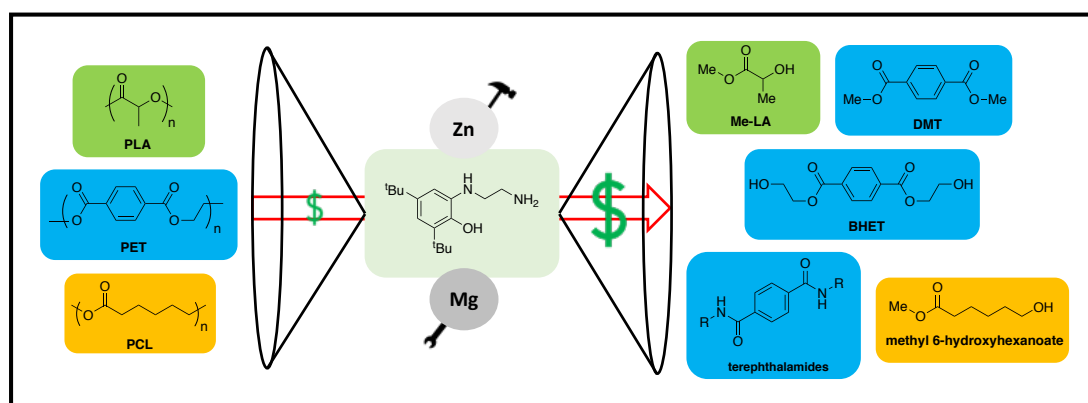
3.4. References

- [1] J. Payne, P. McKeown, M. D. Jones, *Polym. Degrad. Stab.* **2019**, *165*, 170–181.
- [2] J. Payne, M. D. Jones, *ChemSusChem* **2021**, *14*, 4041–40.
- [3] P. McKeown, M. D. Jones, *Sustainable Chem.* **2020**, *1*, 1–22.
- [4] O. Dechy-Cabaret, B. Martin-Vaca, D. Bourissou, *Chem. Rev.* **2004**, *104*, 6147–6176.
- [5] C. M. Thomas, *Chem. Soc. Rev.* **2010**, *39*, 165–173.
- [6] R. H. Platel, L. M. Hodgson, C. K. Williams, *Polym. Rev.* **2008**, *48*, 11–63.
- [7] M. J. Stanford, A. P. Dove, *Chem. Soc. Rev.* **2010**, *39*, 486–494.
- [8] C. A. Wheaton, P. G. Hayes, B. J. Ireland, *Dalton Trans.* **2009**, *0*, 4832–4846.
- [9] M. J.-L. Tschan, R. M. Gauvin, C. M. Thomas, *Chem. Soc. Rev.* **2021**, *50*, 13587–13608.
- [10] G. Xu, Q. Wang, *Green Chem.* **2022**, *24*, 2321–2346.
- [11] L. A. Román-Ramírez, P. Mckeown, M. D. Jones, J. Wood, *ACS Catal.* **2019**, *9*, 409–416.
- [12] P. McKeown, L. A. Román-Ramírez, S. Bates, J. Wood, M. D. Jones, *ChemSusChem* **2019**, *12*, 5233–5238.
- [13] R. Yang, G. Xu, C. Lv, B. Dong, L. Zhou, Q. Wang, *ACS Sustainable Chem. Eng.* **2020**, *8*, 18347–1835.
- [14] F. Santulli, M. Lamberti, M. Mazzeo, *ChemSusChem* **2021**, *14*, 5470–5475.
- [15] J. Stewart, M. Fuchs, J. Payne, O. Driscoll, G. Kociok-Köhn, B. D. Ward, S. Herres-Pawlis, M. D. Jones, *RSC Adv.* **2022**, *12*, 1416–1424.
- [16] M. Hu, X. Song, F. Wang, W. Zhang, W. Ma, F. Han, *New J. Chem.* **2022**, *46*, 1175–1181.

Chapter 4.

Exploring the Potential of a Ligand Building Block

Publication 4. Zn(II)- and Mg(II)-Complexes of a Tridentate {ONN} Ligand: Application to Poly(lactic acid) Production and Chemical Upcycling of Polyesters



Acknowledgement: The work presented in this chapter has been published in the journal ‘*Macromolecules*’ and is reproduced with permission from *Macromolecules*, **2021**, 54, 18, 8453–8469. Copyright 2021 American Chemical Society. The electronic supporting information (ESI) has been amended into a supporting experimental section for clarity.


4. Preamble

In Chapter 3, the importance of metal-ligand cooperativity on both polymerisation and degradation activity was highlighted. However, it was speculated such systems were hindered by possible catalyst aggregation in solution, providing significant scope for further optimisation. One possible solution was expansion of the catalen ligand suite *via* variation of the Schiff-base moiety, with the literature providing a bountiful source of inspiration.^[1-4] However, it was also postulated a tetradentate ligand backbone and dimeric configuration may potentially be hindering availability of the metal centre through steric crowding. Consequently, a reduction in ligand bulk was favourably pursued, identifying monoanionic tridentate ligands as a promising alternative. Indeed, McKeown *et al.*^[5-7] and Williams *et al.*^[8] have previously shown such ligands, in combination with Zn(II) and Mg(II), to lend themselves to PLA production and degradation.

Fortuitously, the catalen ligands rely on the synthesis of a simple tridentate {ONN} building block, which was identified as an ideal candidate for the production of homoleptic and monomeric Zn(II)- and Mg(II)-complexes. Moreover, this building block possesses H-bond donors at both the 1° and 2° amine positions, which were anticipated to impart enhanced reactivity as discussed in Chapter 2. Furthermore, a greater emphasis on selective recycling is explored in Chapter 4 to ensure catalyst development remains industrially relevant and transferable. Indeed, despite this clear need literature examples remain rare, as highlighted in both Chapter 1 and a number of recent high-impact reviews.^[9-11]

In this chapter, Zn(II)- and Mg(II)-complexes based on a tridentate {ONN} ligand are shown to facilitate rapid PLA methanolysis under mild conditions (50 °C) and are among the fastest reported to date. Interestingly, Zn(1)₂ was also found to be highly active for the solution phase production of PLA at room temperature. Catalyst versatility is demonstrated through the degradation of various commercial polyesters (*e.g.* PET and poly(caprolactone) (PCL)), employing a range of upcycling strategies (*e.g.* methanolysis, glycolysis and aminolysis) to achieve a broad value-added substrate scope. A selective recycling strategy for a mixed PLA/PET feed is also demonstrated on a multigram scale, whilst the application of discrete homogeneous metal-based catalysts to PET aminolysis and PCL methanolysis is reported for the first time. In all instances, metal exchange was found to significantly influence catalyst activity and was system dependent, whilst elevated temperatures adversely impacted PLA methanolysis.

4.1. Statement of Authorship

This declaration concerns the article entitled:			
Zn(II)- and Mg(II)-Complexes of a Tridentate {ONN} Ligand: Application to Poly(lactic acid) Production and Chemical Upcycling of Polyesters			
Publication status (tick one)			
Draft manuscript <input type="checkbox"/> Submitted <input type="checkbox"/> In review <input type="checkbox"/> Accepted <input type="checkbox"/> Published <input checked="" type="checkbox"/>			
Publication details (reference)	J. M. Payne, G. Kociok-Köhn, E. A. C. Emanuelsson, M. D. Jones, <i>Macromolecules</i> 2021 , <i>54</i> , 8453–8469 (DOI: 10.1021/acs.macromol.1c01207)		
Copyright status (tick the appropriate statement)			
I hold the copyright for this material <input type="checkbox"/> Copyright is retained by the publisher, but I have been given permission to replicate the material here <input checked="" type="checkbox"/>			
Candidate's contribution to the paper (provide details, and also indicate as a percentage)	<p>The candidate predominantly executed the work presented in the paper.</p> <p>Formulation of ideas:</p> <p>Ideas were discussed and planned with EE and MDJ. The manuscript draft was prepared by JMP with editing from MDJ during the editing stage. [JMP = 80%, GKK = 0%, EE = 5%, MDJ = 15%]</p> <p>Design of methodology:</p> <p>Experiments were discussed and planned with MDJ. [JMP = 90%, GKK = 0%, EE = 0%, MDJ = 10%]</p> <p>Experimental work:</p> <p>Experimental work and data analysis were conducted by JMP. X-ray crystallographic data was collected and processed by GKK and MDJ. [JMP = 90%, GKK = 5%, EE = 0%, MDJ = 5%]</p> <p>Presentation of data in journal format:</p> <p>All figures, tables and schemes were prepared by JMP. [JMP = 100%]</p>		
Statement from Candidate	This paper reports on original research I conducted during the period of my Higher Degree by Research candidature.		
Signed		Date	7/6/2022

Zn(II)- and Mg(II)-Complexes of a Tridentate {ONN} Ligand: Application to Poly(lactic acid) Production and Chemical Upcycling of Polyesters

Jack M. Payne, Gabriele Kociok-Köhn, Emma A. C. Emanuelsson, and Matthew D. Jones*

Cite This: *Macromolecules* 2021, 54, 8453–8469

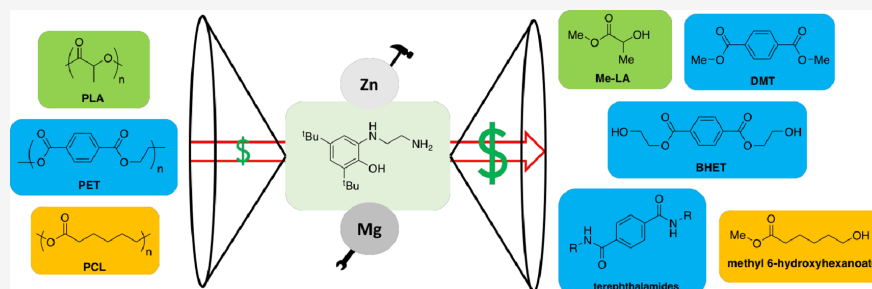
Read Online

ACCESS |

Metrics & More

Article Recommendations

Supporting Information



ABSTRACT: The synthesis and characterization of two homoleptic Zn(II)- and Mg(II)-complexes based on a simple tridentate {NNO} ligand are reported. The production of biocompatible atactic poly(lactic acid) (PLA) under industrially relevant melt conditions is demonstrated, noting high activity for Zn(1)₂ at room temperature in CH₂Cl₂ (TOF = 184 h⁻¹). Mg(1)₂ and Zn(1)₂ were shown to facilitate rapid PLA methanolysis into methyl lactate (Me-LA) under mild conditions, achieving up to 85% Me-LA yield within 30 min at 50 °C in THF. Further kinetic analysis found Mg(1)₂ and Zn(1)₂ to exhibit *k*_{app} values of 0.23 ± 0.0076 and 0.15 ± 0.0029 min⁻¹, respectively {8 wt % cat. loading}, among the highest reported thus far. Zn(1)₂ retained excellent activity for both poly(ethylene terephthalate) (PET) and poly(ε-caprolactone) (PCL) degradations, demonstrating catalyst versatility. Various upcycling strategies (e.g., methanolysis, glycolysis, and aminolysis) were employed to achieve a broad substrate scope, which included bis(2-hydroxyethyl) terephthalate (BHET), high value terephthalamides, and methyl 6-hydroxyhexanoate. Optimal glycolysis conditions using Zn(1)₂ enabled 64% BHET yield within 1 h at 180 °C, a rare example of PET glycolysis mediated by a discrete homogeneous metal-based catalyst. The application of such catalysts for PET aminolysis and PCL methanolysis has been reported for the first time.

INTRODUCTION

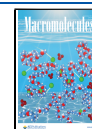
Plastics remain ubiquitous in society owing to their cheap manufacture and versatile material properties.¹ However, current practices are unsustainable and urgent revision is required to ensure the plastic economies' long-term future. Presently, plastic production relies heavily on a depleting and environmentally damaging fossil reserve, which accounts for ca. 99% of all processed plastics.² If irresponsibly handled at end-of-life (EoL), these products persist in the environment since they are typically robust and durable by design. This, coupled with a wasteful linear model, underpins plastic pollution, which represents one of the great environmental challenges of the 21st century.^{3–5} Indeed, plastic waste residing in either landfill or the natural environment, which equated to 79% of all plastics manufactured between 1950 and 2015, outweighs all living biomass (4 Gtonnes).^{4,6} Despite increasing public scrutiny, plastics remain in the growth phase with production projected to

exceed 1 billion tonnes per year by 2050.⁷ There is therefore a clear opportunity to develop renewable and biodegradable alternatives to address both existing environmental concerns and this anticipated increase in demand.

To this end, poly(lactic acid) (PLA) has emerged as one of the most promising bio-based replacements. Industrially, PLA production exploits the metal-mediated ring-opening polymerization (ROP) of L-lactide (L-LA) under solvent-free conditions.⁸ Revered for its green credentials, PLA has subsequently found commercial use in a diverse range of sectors, including

Received: June 7, 2021

Published: September 13, 2021



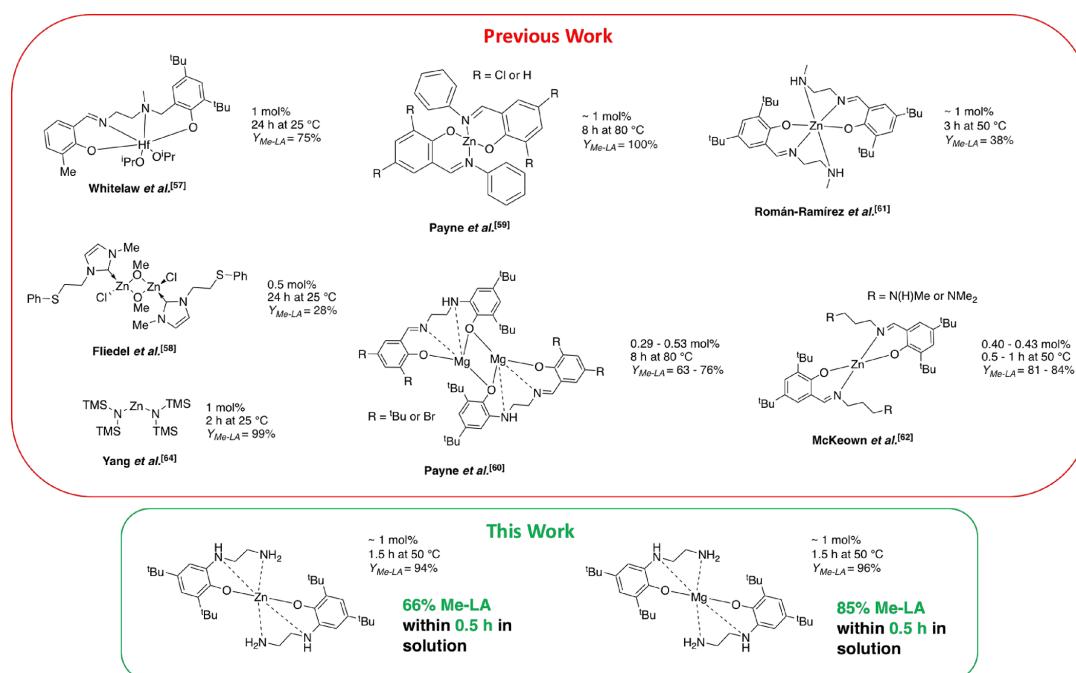


Figure 1. Selected examples of key and recent catalyst developments to date pertaining to metal-mediated PLA methanolysis, highlighting catalyst advancement reported herein. Catalyst loading, reaction conditions, and Me-LA yield upon solvent removal ($Y_{\text{Me-LA}}$) are provided for comparative purposes.

packaging and biomedical applications.^{2,9–17} However, toxicity concerns associated with the industry standard catalyst ($\text{Sn}(\text{Oct})_2$, Oct = 2-ethylhexanoate) have created an appetite for biocompatible and environmentally benign alternatives. Examples include the use of cheap and abundant metals, such as Mg(II) and Zn(II), whilst organocatalysts have also been reported.^{18–21} Whilst biodegradable materials offer the potential to remediate plastic accumulation in the environment, compostable materials align with a linear model, which fails to capture embedded material value.^{3,22}

Recycling processes have the potential to facilitate the economies' transition to a circular model, which prioritizes material recapture and reuse, principles central to a truly green and sustainable future.^{23–27} Mechanical recycling is routinely employed but is limited by eventual material downcycling, which necessitates product repurposing to less demanding uses.^{28,29} Conversely, chemical recycling preserves product quality over an infinite number of cycles, enabling depolymerization to monomer or degradation to other useful platform chemicals, such as lactic acid.^{30–32} Degradation is particularly advantageous due to the potential to access value-added products, which provides further economic incentives to industry. For example, PLA transesterification affords alkyl lactates, which have been touted as potential green solvent replacements. Moreover, ethyl lactate (Et-LA) currently trades at \$3.58–4.92 per kg, equating to a value multiplier between 1.5 and 2 relative to virgin PLA.^{33–36}

PLA recycling methods include pyrolysis^{37–40} and hydrolysis.^{41–44} Reductive depolymerization strategies based on hydrogenation^{45–47} and hydrosilylation^{48,49} have also been

reported. Traditionally, such processes rely on costly ruthenium- and iridium-based catalysts, although simple and cheap metal-based salts (e.g., $\text{Zn}(\text{OAc})_2 \cdot 2\text{H}_2\text{O}$ and $\text{MoO}_2\text{Cl}_2(\text{H}_2\text{O})_2$) have recently been reported.^{50,51} Metal-mediated PLA transesterification is most pertinent to this report, although literature examples remain limited. Simple, commercially available metal salts, such as FeCl_3 and ZnCl_2 , have been explored, typically in the presence of methanol to afford methyl lactate (Me-LA), under both solvothermal and microwave conditions.^{52–55} Sobota and co-workers demonstrated PLA transesterification using a variety of linear and branched alcohols mediated by Mg(II) and Ca(II) precatalysts, noting ethanolysis scale up to 1.5 kg and high temperature and pressure regimes to circumvent the use of excess alcohol.⁵⁶ Discrete metal-based catalysts based on group (IV),⁵⁷ Zn(II),^{58–63} and Mg(II)⁶⁰ have also been reported. McKeown *et al.*⁶² have previously reported a highly active Zn(II)-complex bearing a propylenediamine backbone ($\text{R} = \text{N}(\text{H})\text{Me}$), achieving 81% Me-LA yield within 30 min at 50 °C in THF. This was notably higher compared to the ethylenediamine analogue (12% Me-LA in 6 h) under comparable conditions (40 °C, 4 wt % cat. loading), highlighting the importance of structure–activity relationships.⁶¹ Recently, Yang *et al.*⁶⁴ demonstrated $\text{Zn}(\text{HMDS})_2$ as a highly efficient transesterification catalyst for various polyesters including PLA and poly(ϵ -caprolactone) (PCL). Promisingly, 99% Me-LA yield was obtained within 2 h under ambient conditions (1 mol % cat. loading), although a large excess of MeOH (24.7 equiv) was required. Key and recent catalyst developments to date pertaining to metal-mediated PLA methanolysis are depicted in Figure 1. Whilst organocatalysts have been identified as metal-

free alternatives, current systems remain limited by factors such as cost, toxicity/corrosivity, and high catalyst loadings. Example organocatalysts for PLA degradation include TBD,⁶⁵ DMAP,⁶⁶ TMC,⁶⁷ and ionic liquids.^{68–70}

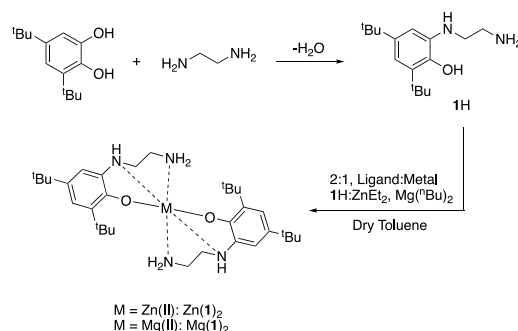
In addition to emerging plastics, it is imperative that sustainable recycling strategies are developed in tandem with established commercial polyesters, for example, poly(ethylene terephthalate) (PET). PET possesses a significantly larger market share relative to PLA, accounting for *ca.* 8% of global plastic production in 2015.² Widely used in packaging applications, it has also found use in the construction and textiles industry.⁷¹ PET is largely amenable to the chemical recycling strategies discussed for PLA and has been comprehensively reviewed in the literature.^{72–77} For example, PET can be depolymerized *via* glycolysis and methanolysis to produce bis(2-hydroxyethyl)terephthalate (BHET) and dimethyl terephthalate (DMT), respectively, which can be repolymerized or redirected for upcycling.^{73,77} PET aminolysis has also been reported, furnishing terephthalamides with potential use in the production of additives and high performance materials.⁷⁸ Glycolysis is the most widely used chemical recycling method for PET, often employing a metal acetate as the transesterification catalyst, with Zn(OAc)₂ generally considered the benchmark.^{77,79} Despite the plethora of catalysts reported, the use of discrete metal-based complexes for PET glycolysis remains rare.^{60,80–82} Notably, Troev *et al.*⁸⁰ reported a highly efficient Ti(IV)-phosphate catalyst, achieving 98% conversion to BHET within 150 min between 190 and 200 °C (0.3 wt % cat. loading, m(EG):m(PET) = 2.8:1). Whilst superior activity relative to Zn(OAc)₂ was observed for PET fibers, this was not retained for bottle-grade PET. Thus, it is clear that significant scope remains for process optimization through judicious catalyst design, which can be extended to PLA, with metal-mediated degradation a possible solution.

Inspired by the aforementioned challenges and opportunities in the field, herein we report the synthesis of a simple tridentate {NNO} ligand prior to complexation to Zn(II) and Mg(II). Their application to the ROP of *rac*-LA under industrially relevant melt conditions is demonstrated, noting high activity at room temperature (RT) in solution. High catalyst efficiency for PLA methanolysis under mild conditions is reported. Polyester scope diversification to PET and PCL highlights catalyst versatility, whilst various upcycling strategies (*e.g.*, glycolysis and aminolysis) were employed to achieve a broad substrate scope.

RESULTS AND DISCUSSION

Synthesis. A monoanionic tridentate {NNO} ligand (1H) was prepared *via* a facile condensation reaction (Scheme 1) and characterized by a combination of ¹H/¹³C{¹H} NMR spectroscopy and mass spectrometry (MS). Notably, ¹H NMR spectroscopic analysis revealed characteristic triplets between $\delta = 2.80$ and 3.20 ppm, corresponding to inequivalent –CH₂ resonances, consistent with the 1:1 product. Careful consideration of the stoichiometric quantities used, coupled with a MeCN wash, enabled 1H to be isolated in good yield (69%) with excellent purity. Indeed, this method represents a powerful synthetic strategy to accessing an asymmetric amine without the need for a protecting group, with potentially broad applicability. We have previously reported 1H as a building block in the synthesis of catalans, a new and emerging class of ligands in the field.^{60,83}

Scheme 1. Preparation of a Tridentate {NNO} Ligand (1H) and Subsequent Complexation to Afford Zn(1)₂ and Mg(1)₂



Homoleptic complexes of Zn(II) and Mg(II) were then prepared in anhydrous toluene and recrystallized from the reaction solvent in good yield (45–54%) (Scheme 1). Interestingly, a hexameric Zn(II)-complex was isolated and characterized by single-crystal X-ray diffraction (XRD), as shown in Figure 2. Selected bond lengths and angles are provided in the SI (Tables S2 and S3). Zn(1)–N(1) and Zn(1)–N(2) bond lengths of 2.229(2) and 2.096(3) Å, respectively, were observed, comparably longer relative to that of Zn(1)–O(1) {1.9912(19) Å}, as expected (Table S2). Zn(1) was found to adopt a distorted square pyramidal geometry ($\tau_5 = 0.14$, Table S3), whilst closer inspection of the asymmetric unit revealed the adventitious incorporation of dimethylsilanone (Me₂SiO) moieties, presumably derived from silicone grease. Such complexes are highly unusual and generally serendipitous in nature.⁸⁴ Given that silicone grease is typically inert and polymeric, the isolation of this complex provided an early indication of the depolymerization potential of these catalysts.

Despite significant efforts, further attempts to isolate crystals of Zn(1)₂ suitable for XRD analysis were unsuccessful, which could be extended to Mg(1)₂. ¹H NMR spectroscopic analysis of Zn(1)₂ revealed a characteristic singlet peak at $\delta = 2.08$ ppm corresponding to an –NH₂ moiety. –CH₂ resonances were observed as two distinct broad resonances at $\delta = 2.82$ and 2.99 ppm, respectively, suggesting the catalyst to be both symmetrical and fluxional (Figure S3). Interestingly, Mg(1)₂ exhibited a more complex ¹H NMR spectrum, possibly indicating a shift from a 4- to 6-coordinate metal center. Diastereotopic –CH₂ and –NH₂ resonances between *ca.* $\delta = 0.60$ and 2.60 ppm were observed, implying that the ligands are inequivalent and locked in position (Figure S6). HSQC analysis assisted with –NH and –NH₂ resonance assignment (Figures S5 and S8). ¹³C{¹H} NMR spectroscopic analysis was consistent with ¹H NMR analysis (Figures S4 and S7). Zn(1)₂ was in generally good agreement with the elemental analysis (EA) data obtained, demonstrating product purity. Conversely, Mg(1)₂ exhibited C % values slightly lower than expected, consistent with the monohydrate product (Mg(1)₂·H₂O), indicating the hygroscopic nature of the said complex.

Polymerization of *rac*-LA. Zn(1)₂ and Mg(1)₂ were trialed in the ROP of *rac*-LA under industrially preferred melt conditions (130 and 180 °C) (Table 1), negating the need for a solvent, which is typically a significant source of industrial waste.^{3,8,85,86} Initiator activity under solution conditions (25 and 80 °C) (Table 2) was also assessed. The lactide monomer, *rac*-

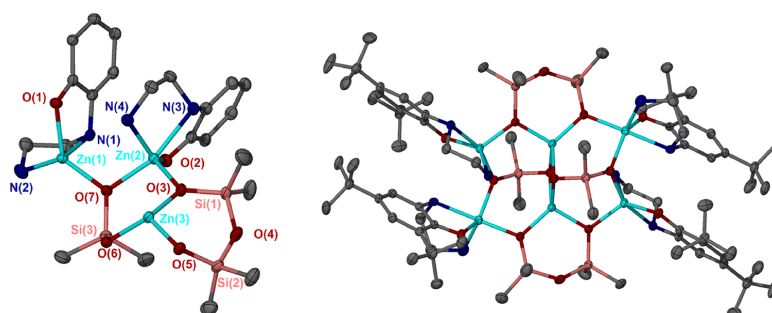


Figure 2. Solid-state structure of a Si-based Zn(1)₂ derivative including an asymmetric unit (left) and expanded structure (right). Ellipsoids shown at 50% probability level. All hydrogen atoms have been omitted from the asymmetric unit and expanded structure, in addition to ^tBu carbons for the former, for clarity.

Table 1. Melt Polymerization of *rac*-LA Using Zn(1)₂ and Mg(1)₂^c

Init.	time (min)	[<i>rac</i> -LA]:[M]:[BnOH]	Conv. ^a (%)	$M_{n,theo}$ ^b (g mol ⁻¹)	M_n ^c (g mol ⁻¹)	\bar{D} ^c	P_r ^d
Zn(1) ₂	<1	300:1:1	88	38,100	30,650	2.99	0.48
	8	3000:1:10	72	31,200	24,850	1.60	0.51
Mg(1) ₂	5	300:1:1	73	31,650	14,850	1.61	0.50
	60	3000:1:10	57	24,550	17,400	1.68	0.54

^aDetermined *via* ¹H NMR spectroscopy. ^bTheoretical average number molecular weight ($M_{n,theo}$) dependent on conversion and co-initiator added $\{(M_{r,LA} \times 3 \times \%_{conv}) + M_{n,BnOH}\}$. ^cDetermined *via* SEC analysis (in THF). ^dDetermined *via* homonuclear decoupled NMR spectroscopy. *N.B.* {[*rac*-LA]:[M]:[BnOH] = 3000:1:10} were performed at 180 °C. [M]:[BnOH] = 1:1 corresponds to 1 equiv of BnOH per metal center. ^eReaction conditions: *rac*-LA (1.0 g), solvent-free (130 °C).

Table 2. Solution Polymerization of *rac*-LA Using Zn(1)₂ and Mg(1)₂^k

Init.	time (min)	[<i>rac</i> -LA]:[M]:[BnOH]	Conv. ^a (%)	$M_{n,theo}$ ^b (g mol ⁻¹)	M_n ^c (g mol ⁻¹)	\bar{D} ^c	P_r ^d
Zn(1) ₂	10	100:1:1	97	14,100	6300	1.42	0.51
	90 ^e	100:1:1	99	14,350	<i>f</i>	<i>f</i>	<i>f</i>
	30 ^g	100:1:1	98	14,200	12,300 ^h	1.09 ^h	0.60 ^h
	30 ^j	100:1:1	36	5300	4300	2.07	0.59
Mg(1) ₂	120 ^g	1000:1:10	79	11,500	13,300	1.11	0.58
	10	100:1:1	78	11,350	5900	1.20	0.48
	480 ^g	100:1:1	68	9900	5950 ^h	1.11 ^h	0.45 ^h
	120 ^g	1000:1:10	7	1100	<i>j</i>	<i>j</i>	<i>j</i>

^aDetermined *via* ¹H NMR spectroscopy. ^bTheoretical average number molecular weight ($M_{n,theo}$) dependent on conversion and co-initiator added $\{(M_{r,LA} \times \%_{conv}) + M_{n,BnOH}\}$. ^cDetermined *via* SEC analysis (in THF). ^dDetermined *via* homonuclear decoupled NMR spectroscopy. ^eRT in toluene. ^fInsufficient polymeric material isolated for material characterization following degradation during polymer purification. ^gRT in CH₂Cl₂. ^hCrude polymer (*i.e.*, no MeOH wash). ⁱRT in THF. ^jInsufficient polymeric material isolated for material characterization due to low monomer conversion. *N.B.* [M]:[BnOH] = 1:1 corresponds to 1 equiv of BnOH per metal center. ^kReaction conditions: *rac*-LA (0.5 g), solvent (toluene, 80 °C). Unless otherwise stated, M_n , \bar{D} , and P_r values reported correspond to a purified polymer (*i.e.*, washed with MeOH).

LA, was recrystallized from anhydrous toluene once prior to use, and benzyl alcohol (BnOH) was employed as a co-initiator. Conversion was determined *via* analysis of the methine region (*ca.* δ = 4.9–5.2 ppm) using ¹H NMR analysis. It is assumed that both metal-complexes operate *via* an activated-monomer mechanism. To investigate this, the stability of Zn(1)₂ with excess BnOH was studied using ¹H NMR (CDCl₃), observing good stability at 25 and 80 °C (Figure S10). It was anticipated that the presence of H-donors within the ligand framework, notably the –NH moiety, would promote enhanced reactivity, consistent with previous works in the literature.^{83,87–89}

All metal complexes were highly active in the melt, achieving high conversion (73–88%) within minutes {[*rac*-LA]:[M]:[BnOH] = 300:1:1} (Table 1). Whilst Zn(1)₂ produced a highly

disperse polymer (\bar{D} = 2.99), reasonable M_n control was maintained ($M_{n,theo}$ = 38,100 g mol⁻¹, M_n = 30,650 g mol⁻¹; Table 1, entry 1). This can likely be attributed to a rapid polymerization time (<1 min), hindering homogeneity, resulting in suboptimal initiation. Superior polymerization control (\bar{D} = 1.60; Table 1, entry 2) was observed upon reducing the catalyst loading to 0.033 mol % at 180 °C {[*rac*-LA]:[M]:[BnOH] = 3000:1:10} (Table 1), consistent with a prolonged polymerization time (8 min). Mg(1)₂ exhibited poorer activity relative to Zn(1)₂ at 130 °C (Table 1, entry 3), which was exacerbated under industrially simulated conditions (57% in 60 min; Table 1, entry 4). Moreover, Mg(1)₂ exhibited poor M_n control ($M_{n,theo}$ = 31,650 g mol⁻¹, M_n = 14,850 g mol⁻¹; Table 1, entry 3) at 130 °C, possibly evidencing side

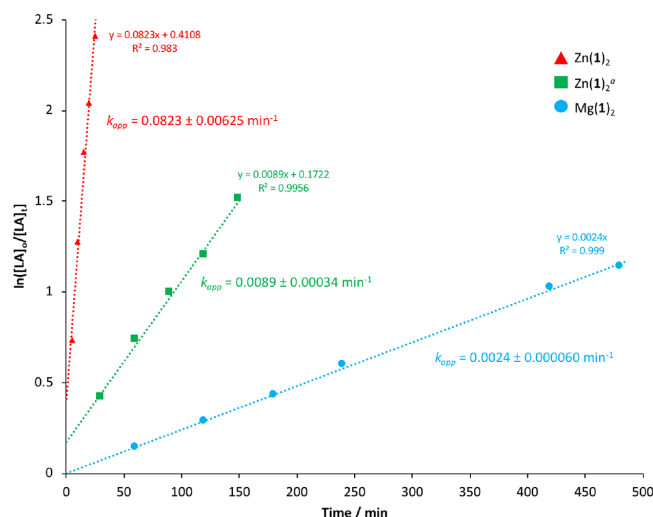


Figure 3. Pseudo-first-order logarithmic plot for the polymerization of *rac*-LA at RT in CH₂Cl₂ {[*rac*-LA]:[M]:[BnOH] = 100:1:1} using Zn(1)₂ and Mg(1)₂. Superscript *a* denotes [*rac*-LA]:[M]:[BnOH] = 1000:1:10. *N.B.* [LA]₀ = 0.69 mol dm⁻³. Data points at 300 and 360 min for Mg(1)₂ were not collected.

transesterification reactions, which can likely be extended to the remaining polymers. Indeed, in all instances, lower M_n values than expected (relative to theoretical) were observed, consistent with the moderate-to-broad dispersities ($\bar{D} = 1.60$ – 2.99) obtained. In all instances, the production of biocompatible atactic PLA ($P_r = 0.48$ – 0.54) was realized.

Initial work under solution conditions {[*rac*-LA]:[M]:[BnOH] = 100:1:1} (Table 2) focused on catalyst activity in toluene at 80 °C. Both complexes produced atactic PLA ($P_r = 0.48$ – 0.51), achieving high conversion (78–97%) within 10 min whilst observing reasonably low dispersities ($\bar{D} = 1.20$ – 1.42) and poor M_n control ($M_{n,theo} = 14,100$ and $11,350$ g mol⁻¹, $M_n = 6300$ and 5900 g mol⁻¹; Table 2, entries 1 and 7). Zn(1)₂ retained high activity at RT, achieving 99% within 1.5 h (Table 2, entry 2). Since *rac*-LA is insoluble under these conditions, the reaction solvent was exchanged for CH₂Cl₂ to assess the impact of complete initial monomer solubilization on catalyst activity. Enhanced activity was observed for Zn(1)₂, achieving 98% conversion within 30 min whilst producing crude PLA of well-defined M_n ($M_{n,theo} = 14,200$ g mol⁻¹, $M_n = 12,300$ g mol⁻¹; Table 2, entry 3) and narrow dispersity ($\bar{D} = 1.09$). Reasonably high activity and comparable polymerization control were maintained upon reducing the catalyst loading to 0.1 mol % {[*rac*-LA]:[M]:[BnOH] = 1000:1:10} (Table 2, entry 6). Exchanging the solvent for THF negatively influenced activity (36% in 30 min), despite achieving complete dissolution, suggesting that THF competes with lactide coordination (Table 2, entry 5). Comparatively, Mg(1)₂ exhibited significantly reduced activity in CH₂Cl₂ at RT, achieving 68% conversion within 8 h (Table 2, entry 8). Whilst crude PLA of narrow dispersity ($\bar{D} = 1.11$) was isolated, reduced M_n control ($M_{n,theo} = 9900$ g mol⁻¹, $M_n = 5950$ g mol⁻¹; Table 2, entry 8) was observed relative to Zn(1)₂. Additionally, a reduction in catalyst loading {[*rac*-LA]:[M]:[BnOH] = 1000:1:10} (Table 2, entry 10) resulted in negligible monomer conversion, consistent with poor catalyst tolerance noted in the melt (Table 1, entry 4). Whilst solvent exchange (toluene to CH₂Cl₂) had no impact on

stereocontrol for Mg(1)₂, yielding atactic PLA in all instances ($P_r = 0.45$ – 0.48), Zn(1)₂ exhibited a shift to PLA with a slight heterotactic bias ($P_r = 0.58$ – 0.60). Both Coates *et al.*⁹⁰ and Ma *et al.*⁹¹ have previously shown metal exchange to dramatically influence stereocontrol, which is absent in this work. Following polymer purification, M_n trends discussed for the melt were typically retained in solution, noting complete sample loss in some instances (Table 2, entries 2 and 9). Consequently, SEC analysis was employed to investigate the impact of polymer work-up using MeOH. Interestingly, for PLA produced using Zn(1)₂ (Table 2, entries 3 and 4), polymer purification coincided with a significant decrease in M_n ($M_{n,crude} = 12,300$ g mol⁻¹, $M_{n,pure} = 4300$ g mol⁻¹; Table 2, entries 3 and 4). Whilst this was reflected in an increase in dispersity ($\bar{D}_{crude} = 1.09$, $\bar{D}_{pure} = 2.07$; Table 2, entries 3 and 4), polymer tacticity was retained. MALDI-ToF analysis confirmed the purified polymer to be intermolecularly transesterified (Figure S31), consistent with the presence of multiple series and a peak separation of 72 g mol⁻¹, akin to PLA produced at 80 °C (Table 2, entry 1) (Figure S32). In contrast, the crude polymer displayed a single series with a peak separation of 144 g mol⁻¹ (Figure S30), corresponding to the monomer unit. MALDI-ToF analysis confirmed both the crude and purified polymers (Table 2, entries 3 and 4) to be –OBn and H-end capped. Very few methanolysis events are required to achieve a significant decrease in M_n . Consequently, the benzyloxy-end cap is detected exclusively (relative to –OMe and –H, as expected for methanolysis) since it is statistically dominant within the sample. Varying degrees of transesterification between samples (Tables 1 and 2) imply a dependence on both catalyst type and loading. Indeed, reducing the loading of Zn(1)₂ from 1 to 0.1 mol % was found to preserve sample integrity following polymer work-up, consistent with SEC analysis ($M_{n,theo} = 11,500$ g mol⁻¹, $M_n = 13,300$ g mol⁻¹, $\bar{D} = 1.11$; Table 2, entry 6). Shifting from methanol to higher chain alcohols (e.g., ethanol, propanol, and butanol) has previously been shown to coincide with a significant decrease in transesterification and thus is proposed

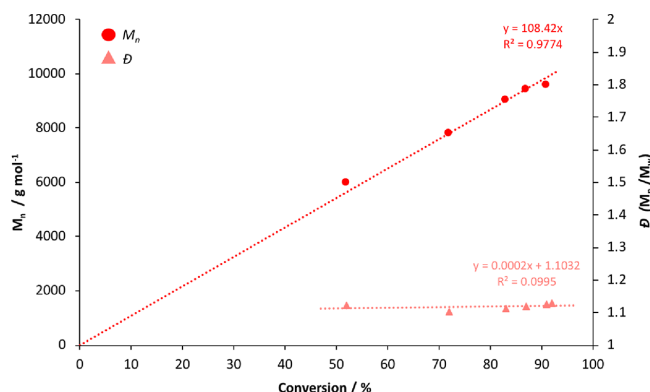
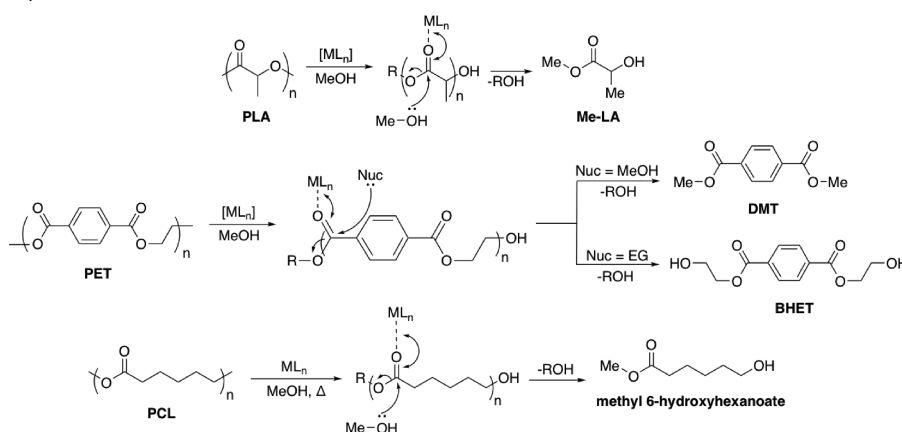


Figure 4. Plot of M_n and D against conversion for the solution polymerization of *rac*-LA in CH_2Cl_2 at RT $\{[rac\text{-LA}]:[M]:[BnOH] = 100:1:1\}$ using $\text{Zn}(\text{I})_2$.

Scheme 2. Metal-Mediated Degradation Mechanism of PLA, PET, and PCL via Transesterification, where R Denotes the Growing Polymer Chain



as an alternative polymer work-up procedure at higher catalyst loadings.³⁶ Sample loss and generally poorer M_n control implicate $\text{Mg}(\text{I})_2$ as a possibly better transesterification catalyst relative to $\text{Zn}(\text{I})_2$, consistent with the melt (Table 1, entry 3).

In summary, $\text{Zn}(\text{I})_2$ exhibited high activity in the melt, which was retained in solution. Careful consideration of the reaction conditions used, coupled with polymer work-up, enabled the rapid production of biocompatible PLA of well-defined M_n and low dispersities in solution. Metal exchange to $\text{Mg}(\text{II})$ typically resulted in a loss of activity and polymerization control.

Polymerization Kinetics. Metal exchange was found to have a dramatic impact on catalyst activity and polymerization control, notably under solution conditions (Table 2). Consequently, a kinetic study was pursued for $\text{Zn}(\text{I})_2$ and $\text{Mg}(\text{I})_2$ in CH_2Cl_2 at RT. A plot of $\ln([LA]_0/[LA]_t)$ against time exhibited a linear relationship, confirming the reaction to proceed pseudo-first-order with respect to the consumption of *rac*-LA (Figure 3).

$\text{Zn}(\text{I})_2$ exhibited an apparent rate constant (k_{app}) of 0.082 min^{-1} , outperforming $\text{Mg}(\text{I})_2$ ($k_{\text{app}} = 0.0024 \text{ min}^{-1}$) by a factor of over 30 under identical conditions $\{[rac\text{-LA}]:[M]:[BnOH] =$

$100:1:1\}$, consistent with solution results (Table 2). SEC analysis of aliquots retained for $\text{Zn}(\text{I})_2$ demonstrated a linear increase in M_n with conversion whilst maintaining narrow dispersities, indicating polymerization to be well-controlled (Figure 4). The apparent gradient ($M_t = 108.42 \text{ g mol}^{-1}$) is in reasonably good agreement with the theoretical monomer value ($M_t = 144.12 \text{ g mol}^{-1}$), indicating that one polymer chain is growing per $\text{Zn}(\text{II})$ center. Promisingly, $\text{Zn}(\text{I})_2$ retained superior activity ($k_{\text{app}} = 0.0089 \text{ min}^{-1}$) relative to $\text{Mg}(\text{I})_2$ upon reducing the catalyst loading to $0.1 \text{ mol } \%$ $\{[rac\text{-LA}]:[M]:[BnOH] = 1000:1:10\}$ (Figure 3).

The influence of metal exchange on activity can likely be attributed to aforementioned catalyst structural differences. For $\text{Zn}(\text{I})_2$, the structure is noted as symmetric and fluxional, indicating that the coordinating ligand is labile and thus the terminal $-\text{NH}_2$ may be more readily available for donation.

Whilst $\text{Zn}(\text{I})_2$ displayed impressive activity in solution at RT (TOFs up to 184 h^{-1}), this remains lower compared to the state-of-the-art catalysts, namely, dizinc catalysts, developed by Williams and co-workers (TOFs up to $60,000 \text{ h}^{-1}$ in THF).⁹²

Chemical Recycling of PLA. PLA Degradation. Both $\text{Zn}(\text{I})_2$ and $\text{Mg}(\text{I})_2$ were investigated in the metal-mediated degradation of PLA into Me-LA (Scheme 2). Me-LA is a possible green solvent replacement and potentially valuable chemical to the PLA supply chain since it can be directly converted to lactide, furthering a circular economy approach.^{3,34,77} The commercially available polymer (0.25 g, PLLA cup, $M_n = 45,510 \text{ g mol}^{-1}$) and catalyst were dissolved in THF with heat and stirring assisting dissolution. MeOH was then added, and product conversion (Me-LA) was determined by ^1H NMR analysis of the methine region (*ca.* $\delta = 4.2\text{--}5.2$ ppm). Catalyst tolerance to residual moisture was demonstrated through the use of wet-solvents, whilst $\text{Zn}(\text{I})_2$ appeared stable in air in solution (Figure S9). The production of Me-LA has previously been shown to proceed *via* a two-step process through the intermediate formation of chain-end groups (Figure S13).⁶¹ Consequently, the methine groups can be defined as internal (int), chain-end (CE), and those corresponding directly to the alkyl lactate (A-LA). Internal methine conversion (X_{int}), A-LA selectivity ($S_{\text{A-LA}}$), and A-LA yield ($Y_{\text{A-LA}}$) are tabulated in Tables 3 and 4 below. Overall, mass transfer limitations due to

Table 3. PLA Methanolysis Using $\text{Zn}(\text{I})_2$ and $\text{Mg}(\text{I})_2$ at 80 °C^e

catalyst	time (h)	<i>T</i> (°C)	cat. loading (wt %)	$Y_{\text{A-LA}}$ (%)	$S_{\text{A-LA}}$ (%)	X_{int} (%)
$\text{Zn}(\text{I})_2$	3	80	4	89	89	100
	3 ^a	80	4	48	52	93
	8 ^b	80	4	27	34	79
	3 ^c	80	4	71	71	100
	3 ^d	80	4	94	94	100
$\text{Mg}(\text{I})_2$	1.5	80	8	93	93	100
	3	80	4	91	91	100

^aPLA-based 3D printing material (0.25 g). ^bAlcohol: ethanol, $n_{\text{Et-OH}}:n_{\text{ester}} = 7:1$. ^cSolvent: 2-methyltetrahydrofuran (2Me-THF), $V_{2\text{Me-THF}}:V_{\text{MeOH}} = 4:1$. ^dPLLA cup (0.25 g) + PVC (0.025 g, 10 wt %, Sigma Aldrich, $M_n = 22,000 \text{ g mol}^{-1}$). ^eReaction conditions: 0.25 g of PLLA cup ($M_n = 45,510 \text{ g mol}^{-1}$), $V_{\text{THF}}:V_{\text{MeOH}} = 4:1$, $n_{\text{MeOH}}:n_{\text{ester}} = 7:1$, $\text{Zn}(\text{I})_2 = 4\text{--}8 \text{ wt \%}$ cat. loading (0.01–0.02 g, 0.48–0.96 mol % relative to ester linkages), $\text{Mg}(\text{I})_2 = 4\text{--}8 \text{ wt \%}$ cat. loading (0.01–0.02 g, 0.52–1.0 mol % relative to ester linkages).

polymer particle size and stirring speeds were considered negligible based on previous work by Román-Ramírez *et al.*,⁶¹ who employed a comparable homoleptic Zn(II)-complex based on an ethylenediamine Schiff-base ligand.

Preliminary work focused on PLA methanolysis at 80 °C in THF (Table 3). $\text{Zn}(\text{I})_2$ exhibited good activity, achieving complete PLA consumption ($X_{\text{int}} = 100\%$) and 89% conversion to Me-LA within 3 h at 4 wt % cat. loading (Table 3, entry 1). Comparable activity was maintained for $\text{Mg}(\text{I})_2$ ($Y_{\text{Me-LA}} = 91\%$, $S_{\text{Me-LA}} = 91\%$) under analogous conditions (Table 3, entry 7), contrasting polymerization results (Figure 3). Increasing the loading of $\text{Zn}(\text{I})_2$ to 8 wt % coincided with a reduction in degradation time to 1.5 h, as expected (Table 3, entry 6). Alternative commercial sources of PLA were also degraded using $\text{Zn}(\text{I})_2$ at 4 wt %. Substituting the cup for PLA-based 3D printing material coincided with a significant reduction in Me-LA yield and selectivity ($Y_{\text{Me-LA}} = 48\%$, $S_{\text{Me-LA}} = 52\%$), although near complete consumption of PLA ($X_{\text{int}} = 93\%$) was retained (Table 3, entry 2). This can likely be attributed to a higher concentration of additives inhibiting catalyst activity, consistent with an opaque reaction medium. However, excellent catalyst

Table 4. PLA Methanolysis Using $\text{Zn}(\text{I})_2$ and $\text{Mg}(\text{I})_2$ at 50 °C and Room Temperature^b

catalyst	time (h)	<i>T</i> (°C)	cat. loading (wt %)	$Y_{\text{A-LA}}$ (%)	$S_{\text{A-LA}}$ (%)	X_{int} (%)
$\text{Zn}(\text{I})_2$	6	50	2	28	35	80
	3	50	4	92	92	100
	1.5	50	8	82	82	100
	24	25	8	17	25	67
	16 ^a	25	8	55	81	68
$\text{Zn}(\text{OAc})_2 \cdot 2\text{H}_2\text{O}$	1.5	50	8	5	24	19
	1H	1.5	50	8	0	7
$\text{Mg}(\text{I})_2$	6	50	2	89	89	100
	3	50	4	81	81	100
	1.5	50	8	82	82	100
	5.5	25	8	85	85	100
$\text{Mg}(\text{OAc})_2 \cdot 4\text{H}_2\text{O}$	1.5	50	8	0	0	0

^a $n_{\text{MeOH}}:n_{\text{ester}} = 24.7:1$. ^bReaction conditions: 0.25 g of PLLA cup ($M_n = 45,510 \text{ g mol}^{-1}$), $V_{\text{THF}}:V_{\text{MeOH}} = 4:1$, $n_{\text{MeOH}}:n_{\text{ester}} = 7:1$, $\text{Zn}(\text{I})_2 = 4\text{--}8 \text{ wt \%}$ cat. loading (0.01–0.02 g, 0.48–0.96 mol % relative to ester linkages), $\text{Mg}(\text{I})_2 = 4\text{--}8 \text{ wt \%}$ cat. loading (0.01–0.02 g, 0.52–1.0 mol % relative to ester linkages), $\text{Zn}(\text{OAc})_2 \cdot 2\text{H}_2\text{O} = 8 \text{ wt \%}$ cat. loading (0.02 g, 2.6 mol % relative to ester linkages), 1H (*i.e.*, free ligand) = 8 wt % cat. loading (0.02 g, 2.1 mol % relative to ester linkages), $\text{Mg}(\text{OAc})_2 \cdot 4\text{H}_2\text{O} = 8 \text{ wt \%}$ cat. loading (0.02 g, 3.6 mol % relative to ester linkages).

tolerance was observed in the presence of poly(vinyl chloride) (PVC) (Table 3, entry 5), a pervasive waste stream contaminant, highlighting system sensitivity to feed impurities. 2Me-THF was investigated as a “greener” alternative to THF.⁹³ Poorer Me-LA yield and selectivity ($Y_{\text{Me-LA}} = 71\%$, $S_{\text{Me-LA}} = 71\%$) were observed, consistent with previous work by McKeown *et al.*⁶⁷ (Table 3, entry 4), highlighting the importance of catalyst–solvent compatibility. The use of EtOH for the production of ethyl lactate (Et-LA) was also demonstrated (Table 3, entry 3), noting a significant reduction in activity ($Y_{\text{Et-LA}} = 27\%$, $S_{\text{Et-LA}} = 34\%$ within 8 h), consistent with EtOH being a poorer nucleophile relative to MeOH.

In pursuit of a more sustainable recycling process, PLA methanolysis at 50 °C was also investigated (Table 4). Interestingly, a reduction in temperature had no appreciable impact on activity, contrasting our previous work,⁵⁹ observing comparable reactivity trends (Table 4, entries 2 and 3; entries 9 and 10). To improve industrial feasibility, the catalyst loading was further reduced to 2 wt % (Table 4, entries 1 and 8). Whilst a prolonged degradation time was required (6 h), $\text{Mg}(\text{I})_2$ exhibited excellent catalyst tolerance ($Y_{\text{Me-LA}} = 89\%$, $S_{\text{Me-LA}} = 89\%$) to trace impurities, whilst $\text{Zn}(\text{I})_2$ displayed a significant drop in productivity ($Y_{\text{Me-LA}} = 28\%$, $S_{\text{Me-LA}} = 35\%$). For comparison, $\text{Zn}(\text{OAc})_2 \cdot 2\text{H}_2\text{O}$ and $\text{Mg}(\text{OAc})_2 \cdot 4\text{H}_2\text{O}$ were tested as air-stable and commercially available alternatives (Table 4, entries 6 and 12). In both instances, inferior performance was observed, demonstrating the need for ligated catalysts. Additionally, free ligand (1H) was also shown to be inactive for PLA methanolysis ($Y_{\text{Me-LA}} = 0\%$, $S_{\text{Me-LA}} = 0\%$, $X_{\text{int}} = 7\%$), highlighting the importance of metal–ligand cooperativity (Table 4, entry 7). Degradation reactions were also performed at room temperature using $\text{Zn}(\text{I})_2$ and $\text{Mg}(\text{I})_2$ to investigate the temperature limit at 8 wt %. For $\text{Zn}(\text{I})_2$, a significant reduction in activity was observed relative to 50 °C, achieving incomplete PLA consumption ($X_{\text{int}} = 67\%$) and 17% Me-LA yield within 24

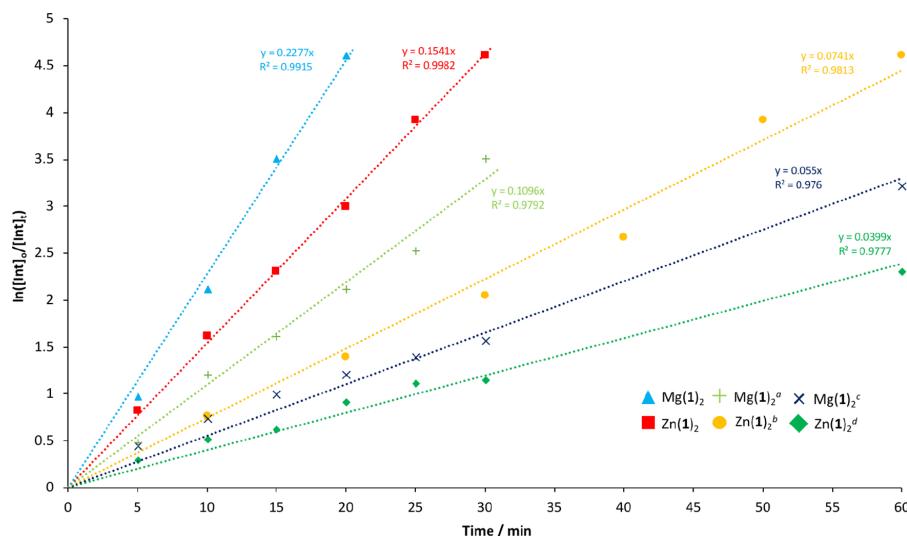


Figure 5. Pseudo-first-order logarithmic plot for the degradation of a PLA cup using Zn(1)_2 and Mg(1)_2 at 8 wt % cat. loading (0.02 g, 0.96–1 mol % relative to ester linkages) in THF at 50 °C. Superscript *a* denotes Mg(1)_2 = 4 wt % cat. loading (0.01 g, 0.52 mol % relative to ester linkages). Superscript *b* denotes Zn(1)_2 = 4 wt % cat. loading (0.01 g, 0.48 mol % relative to ester linkages). Superscript *c* denotes Mg(1)_2 = 4 wt % at 80 °C. Superscript *d* denotes Zn(1)_2 = 4 wt % at 80 °C.

h, as expected (Table 4, entry 4). The use of a large excess of MeOH (24.7 equiv) was found to compensate for this activity loss, achieving comparable PLA consumption ($X_{\text{int}} = 68\%$) within 16 h (Table 4, entry 5). Interestingly, a significantly higher Me-LA yield was obtained ($Y_{\text{Me-LA}} = 55\%$), presumably due to an equilibrium shift (Figure S13), consistent with enhanced product selectivity ($S_{\text{Me-LA}} = 81\%$). Whilst impressive, given the scarcity of metal-mediated degradations performed at room temperature, activity remains lower compared to a Zn(HMDS)_2 system reported by Wang and co-workers (99% Me-LA within 2 h under analogous conditions).⁶⁴ However, Zn(1)_2 represents a cheaper, more well-controlled and air-stable alternative to Zn(HMDS)_2 . Mg(1)_2 maintained reasonably good performance without the need for excess MeOH, achieving complete PLA consumption ($X_{\text{int}} = 100\%$) and 85% Me-LA yield within 5.5 h, highlighting the importance of structure–activity relationships (Table 4, entry 11). To the best of our knowledge, this is the first example of PLA methanolysis mediated by a discrete Mg(II) -complex at room temperature.

Degradation Kinetics. To investigate the effect of temperature and catalyst loading on activity, both Zn(1)_2 and Mg(1)_2 were pursued for further kinetic analysis. Reaction progress was monitored by taking aliquots for $^1\text{H NMR}$ (CDCl_3) analysis of the methine region at equal intervals, totaling between 4 and 7 data points (Figure 5). PLA consumption was assumed to adopt pseudo-first-order kinetics in accordance to previous work by Román-Ramírez *et al.*⁶¹ As such, the gradient of the logarithmic plot is equivalent to the apparent rate constant values, k_{app} , which are tabulated in Table 5 below.

Remarkably, Mg(1)_2 exhibited a k_{app} value of 0.23 min^{-1} using 8 wt % at 50 °C, culminating in one of the fastest and mildest metal-mediated PLA degradation systems reported to date.^{52–62,64} Indeed, near-complete PLA consumption ($X_{\text{int}} = 99\%$) and 85% Me-LA yield were achieved within 20 and 30 min, respectively (Figure 6). Metal exchange to Zn(II) was found to

Table 5. PLA Cup Degradation Using Zn(1)_2 and Mg(1)_2 in THF^a

catalyst	T (°C)	cat. loading (wt %)	time (h)	$Y_{\text{Me-LA}}$ (%)	k_{app} (min^{-1})
Mg(1)_2	50	8	1.5	96	0.23 ± 0.0076
		4	3	94	0.11 ± 0.0080
	80	4	3	79	0.055 ± 0.0026
Zn(1)_2	50	8	1.5	94	0.15 ± 0.0029
		4	3	91	0.074 ± 0.0048
	80	4	3	80	0.040 ± 0.0014

^aReaction conditions: 0.25 g of PLLA cup ($M_n = 45,510 \text{ g mol}^{-1}$), $V_{\text{THF}}:V_{\text{MeOH}} = 4:1$, $n_{\text{MeOH}}:n_{\text{ester}} = 7:1$, $\text{Zn(1)}_2 = 4\text{--}8 \text{ wt \%}$ cat. loading (0.01–0.02 g, 0.48–0.96 mol % relative to ester linkages), $\text{Mg(1)}_2 = 4\text{--}8 \text{ wt \%}$ cat. loading (0.01–0.02 g, 0.52–1.0 mol % relative to ester linkages). N.B. $Y_{\text{Me-LA}}$ refers to maximum Me-LA conversion in solution determined via $^1\text{H NMR}$ (CDCl_3).

result in a statistically significant reduction in activity ($k_{\text{app}} = 0.15 \text{ min}^{-1}$), contrasting polymerization kinetic results (Figure 3), although it remains competitive with the state-of-the-art catalysts.^{62,64} Such findings are consistent with Mg(1)_2 generally offering poorer polymerization control relative to Zn(1)_2 (Tables 1 and 2). In both instances, rapid initial CE production relative to Me-LA implies that chain scission proceeds randomly and is not limited to the polymer chain-end (Figure 7), consistent with previous reports.^{61,64} Interestingly, Zn(1)_2 exhibited a noticeably lower Me-LA yield ($Y_{\text{Me-LA}} = 66\%$) after 30 min relative to Mg(1)_2 ($Y_{\text{Me-LA}} = 85\%$) despite achieving complete PLA consumption. This can likely be attributed to equilibrium reversal facilitated by Zn(1)_2 being a superior polymerization catalyst (Figure 3), consistent with slower CE consumption (Figure 7).

However, Zn(1)_2 displayed activity over a factor of 10 higher relative to a comparable Zn(II) -Schiff base complex ($R = \text{N(H)Me}$) reported by Román-Ramírez *et al.*⁶¹ ($k_{\text{app}} = 0.01$

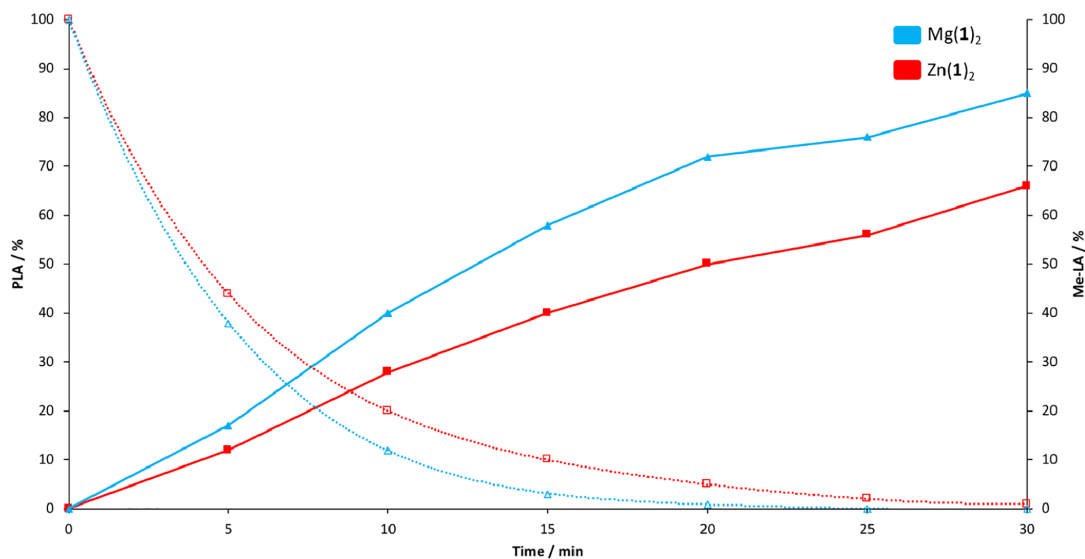


Figure 6. PLA cup degradation plot of conversion (PLA and Me-LA) vs time at 50 °C in THF using Mg(1)₂ and Zn(1)₂ at 8 wt % catalyst loading. N.B. Dashed lines refer to PLA consumption (primary axis), whilst bold lines refer to Me-LA yield (secondary axis).

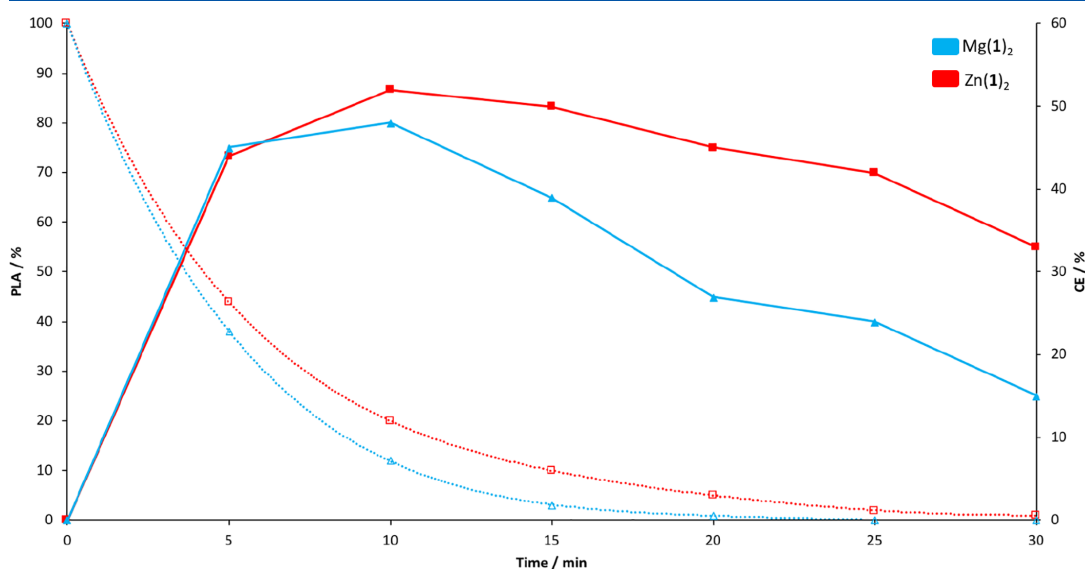


Figure 7. PLA cup degradation plot of conversion (PLA and CE) vs time at 50 °C in THF using Mg(1)₂ and Zn(1)₂ at 8 wt % catalyst loading. N.B. Dashed lines refer to PLA consumption (primary axis), whilst bold lines refer to CE yield (secondary axis).

min⁻¹ under identical conditions). This reactivity enhancement can likely be attributed to the incorporation of additional H-bond donors (–NH and –NH₂) within the ligand framework, which have previously been cited as playing a central role in enabling rapid transesterification.^{62,65,67} It is anticipated that shifting from an ethylene- to propylenediamine backbone would result in enhanced activity owing to a lower ligand distortion energy, consistent with the literature.⁶² For both metal complexes, a reduction in catalyst loading to 4 wt % coincided

with a statistically significant decrease in activity, as expected (Figure 5 and Table 5). Surprisingly, under such loadings, Mg(1)₂ and Zn(1)₂ exhibited *k*_{app} values of 0.055 and 0.040 min⁻¹, respectively, at 80 °C in THF, implying an increase in temperature results in a further reduction in activity (Figure 5 and Table 5). Indeed, both a reduction in catalyst loading and an increase in temperature resulted in slower CE consumption and lower Me-LA yield, exemplified by Zn(1)₂ (Figures S33–S36), which could be extended to Mg(1)₂ (Figures S41–S44).

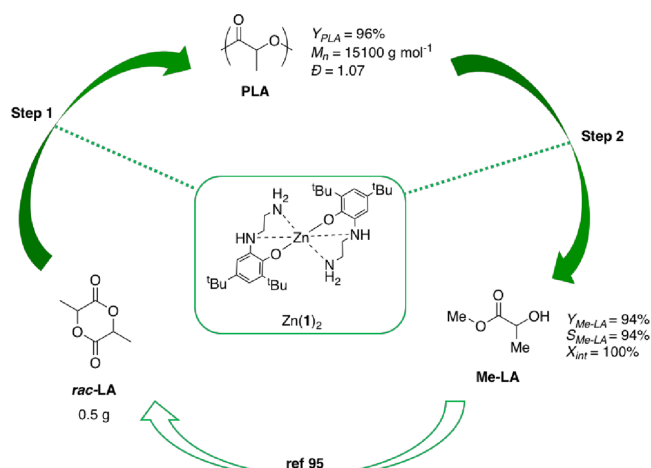


Figure 8. Two-step process for PLA production and transesterification. Reaction conditions are as follows: Step 1: 30 min at RT in CH₂Cl₂, {[rac-LA]:[M]:[BnOH]} = 100:1:1. Step 2: 1.5 h at 50 °C, V_{THF}:V_{MeOH} = 4:1, n_{MeOH}:n_{ester} = 7:1, Zn(1)₂ = 1 mol % relative to ester linkages, ~8 wt % cat. loading.

Generally, marginally higher Me-LA yields were observed under all conditions (Table 5) relative to preliminary methanolysis results (Tables 3 and 4), which can likely be attributed to equilibrium reversal due to removal of volatiles (THF + MeOH). Analysis of the ¹H NMR spectra after volatile removal revealed that Zn(1)₂ appears to remain intact at both 50 and 80 °C (Figures S14 and S15). The stability of Zn(1)₂ in excess MeOH provides further evidence for the ligand remaining coordinated to the Zn(II) center (Figure S11); however, coordination of the terminal amine to the metal during degradation cannot be excluded. Consequently, it is tentatively suggested that an increase in temperature promotes intermediate destabilization, consistent with Zn(1)₂ exhibiting a more sporadic PLA consumption profile at 4 wt % (Figure S35). Non-Arrhenius behavior has previously been reported for a Zn(II)-complex bearing a propylenediamine ligand.^{36,94} As such, it is proposed that lower temperatures and metal exchange assist intermediate stabilization, which possibly explains the aforementioned reactivity trends. Indeed, whilst Mg(1)₂ also appears to remain intact upon volatile removal at 50 °C (Figure S16), aromatic resonances appear to be significantly more shifted relative to Zn(1)₂, possibly evidencing a greater change in the metal coordination sphere during methanolysis.

In summary, both Mg(1)₂ and Zn(1)₂ facilitated rapid PLA methanolysis under mild conditions, albeit slower relative to TBD, which remains to be the benchmark.⁶⁵ Intermediate stabilization appeared to be metal- and temperature-dependent.

Concurrent PLA Production and Transesterification. Given the ability of Zn(1)₂ to facilitate both rapid PLA production and degradation in solution, a two-step proof-of-concept process was pursued (Figure 8). The first step involved the ROP of rac-LA in CH₂Cl₂ at RT {[rac-LA]:[M]:[BnOH]} = 100:1:1. The solvent was then removed *in vacuo*, and the resulting crude PLA was redissolved in THF prior to undergoing methanolysis at 50 °C. Comparable catalyst performance relative to the isolated steps was observed (Tables 2 and 4), indicating good reproducibility and catalyst stability. Upare *et al.*⁹⁵ have previously demonstrated lactide synthesis from Me-LA *via* a prepolymer route, providing further circularity to the PLA supply chain.

Chemical Recycling of PET. Whilst PLA represents a promising emerging bio-based plastic, market penetration remains low with bio-based plastics accounting for *ca.* 1% of global plastic production.⁷⁷ Consequently, our attention shifted to PET, a commercial polyester with a significantly higher market share. Whilst Mg(1)₂ exhibited superior activity for PLA methanolysis, Zn(1)₂ was pursued due to its ease of preparation, scalability, and stability. Unless otherwise stated, bottle-grade PET (M_n ≈ 40,000 g mol⁻¹) was used. Degradation products were isolated as solids and characterized by a combination of ¹H NMR and ¹³C{¹H} NMR spectroscopy (Figures S17 and S19–S25).

PET Methanolysis. Inspired by our recent success using an organocatalyst, namely, TMC,⁶⁷ preliminary work focused on PET methanolysis to afford DMT and EG (Scheme 2 and Table 6). Facile DMT recovery was possible *via* solvent removal followed by washing with MeOH to afford a white solid.

Using comparable reaction conditions to McKeown *et al.*,⁶⁷ Zn(1)₂ exhibited prolonged reaction times relative to TMC (16 h), although lower catalyst loadings are noted, achieving 48 and 88% DMT yield and PET depolymerization by mass, respectively, within 48 h at 100 °C (Table 6, entry 2). In the absence of a catalyst, a dramatic reduction in process efficiency

Table 6. PET Methanolysis into DMT Using Zn(1)₂^b

catalyst	time (h)	T (°C)	cat. loading (wt %)	Y _{DMT} (g/g)	m(PET) (g/g)
none	48	100		0 (0%)	0.23 (8%)
Zn(1) ₂	48	100	8	0.12 (48%)	0.0305 (88%)
	12 ^a	100	8	0.19 (76%)	
	1.5	150	8	0.18 (72%)	

^aPET thin film (0.25 g). *N.B.* Y_{DMT} refers to the isolated yield of pure DMT. m(PET) refers to the mass of PET recovered after methanolysis followed by drying at 140 °C for 3 h. The bracketed value corresponds to depolymerization by weight. Unless otherwise stated, complete PET dissolution was observed, indicative of reaction completion. ^bReaction conditions: 0.25 g of bottle-grade PET (M_n ≈ 40,000 g mol⁻¹), V_{Toluene}:V_{MeOH} = 4:1, n_{ester}:n_{MeOH} = 1:19, Zn(1)₂ = 8 wt % cat. loading (0.02 g, 2.5 mol % relative to ester linkages).

was observed, highlighting the ability of $\text{Zn}(\text{I})_2$ to facilitate PET methanolysis (Table 6, entry 1). Increasing the temperature to 150 °C resulted in a significant reduction in reaction time, achieving 72% DMT yield within 1.5 h, as expected (Table 6, entry 4). This can likely be attributed to general insolubility of the polymer at lower temperatures. However, this could be circumvented by exchanging bottle-grade PET for a thin film, representing waste from the manufacturing industry, consistent with previous work.⁶⁰ Indeed, complete PET dissolution was observed, affording 76% DMT within 12 h at 100 °C (Table 6, entry 3). Such conditions are significantly milder compared to traditional methods, which typically rely on elevated temperatures (180–280 °C) and pressures (20–40 atm) to be appreciably active.^{73,77} Whilst promising, we shifted our attention to glycolysis in pursuit of commercially in-demand chemicals.

PET Glycolysis. PET glycolysis is an established commercial process with the use of EG, furnishing both BHET and EG, which constitute the monomeric units of PET (Scheme 2). Value-added products from BHET include the production of unsaturated polyester resins, among others.^{73,77} Traditionally, high temperatures (180–240 °C) and prolonged reaction times (0.5–8 h) in the presence of a transesterification catalyst are required to achieve appreciable conversion.^{77,79} Moreover, high EG:PET ratios ($\geq 5:1$) are often used to mediate the formation of higher chain oligomers.⁷⁹ Consequently, a reaction temperature of 180 °C and an excess of EG (27.5 equiv) in the presence of 8 wt % $\text{Zn}(\text{I})_2$ were initially selected (Table 7). $\text{Zn}(\text{OAc})_2 \cdot 2\text{H}_2\text{O}$ (Sigma Aldrich) was chosen as an air-stable, commercially available reference. BHET was recovered *via* recrystallization from deionized H_2O .

Table 7. PET Glycolysis into BHET Using $\text{Zn}(\text{I})_2$ at 180 °C^a

catalyst	time (h)	T (°C)	cat. loading (wt %)	EG (equiv)	Y_{BHET} (g/%)
$\text{Zn}(\text{OAc})_2 \cdot 2\text{H}_2\text{O}$	4	180	8	27.5	0.16 (48%)
	2 ^a	180	8	27.5	0.14 (42%)
$\text{Zn}(\text{I})_2$	1	180	8	27.5	0.19 (58%)
	1 ^b	180	8	27.5	0.16 (48%)
	0.33 ^a	180	8	27.5	0.19 (59%)

^aPET thin film (0.25 g). ^bBottle-grade PET (0.25 g) + PVC (0.025 g, 10 wt %, Sigma Aldrich, $M_n \approx 22,000 \text{ g mol}^{-1}$). N.B. Y_{BHET} refers to the isolated yield of pure BHET recrystallized from deionized H_2O followed by drying at 90 °C for 3 h *in vacuo*. ^cReaction conditions: 0.25 g of bottle-grade PET ($M_n \approx 40,000 \text{ g mol}^{-1}$), 27.5 equiv (2 mL) of EG (relative to ester linkages). Ref: $\text{Zn}(\text{OAc})_2 \cdot 2\text{H}_2\text{O}$ = 8 wt % cat. loading (0.02 g, 7 mol % relative to ester linkages), $\text{Zn}(\text{I})_2$ = 8 wt % cat. loading (0.02 g, 2.5 mol % relative to ester linkages).

$\text{Zn}(\text{I})_2$ exhibited excellent activity, achieving complete PET consumption and 58% BHET yield within 1 h at 180 °C, among the most active discrete metal-based catalysts reported to date (Table 7, entry 3).^{60,80–82} Comparable process efficiency was retained in the presence of 10 wt % PVC ($Y_{\text{BHET}} = 48\%$, Table 7, entry 4), demonstrating good catalyst tolerance. This is particularly attractive from an industrial perspective since PVC contamination as low as 100 ppm has previously been reported to adversely impact the quality of the final recycled product.⁷⁹ Promisingly, complete PET consumption could be achieved

within 20 min using a thin film whilst retaining good BHET yield ($Y_{\text{BHET}} = 59\%$, Table 7, entry 5), consistent with methanolysis results (Table 6). For both sources of PET, $\text{Zn}(\text{I})_2$ outperformed $\text{Zn}(\text{OAc})_2 \cdot 2\text{H}_2\text{O}$, which displayed comparable reactivity trends (Table 7, entries 1 and 2). This is despite the reference being present in a large molar excess (7 mol %), highlighting the need for ligated catalysts. All reaction times reflect the time taken to achieve complete PET dissolution, indicative of reaction completion. However, BHET yields <60% were observed in all cases, likely due to the production of water-soluble higher chain oligomers.^{72–77,79} Indeed, ¹H NMR (D_6 -DMSO) analysis of a reaction aliquot after 1 h using $\text{Zn}(\text{I})_2$ (Table 7, entry 4) indicates the presence of BHET exclusively prior to the addition of deionized H_2O (Figure S18). The effect of catalyst loading, reaction time, and molar quantity of EG {n(EG)} on BHET yield was investigated, adopting a one-variable-at-a-time (OVAT) approach.

Initial work focused on variation of the catalyst loading between 2 and 8 wt % at 180 °C for 1 h (Figure 9). Overall, a reduction in catalyst loading coincided with a decrease in BHET yield ($Y_{\text{BHET}} = 36$ –58%), consistent with the literature.^{81,82,96,97} Complete PET consumption was maintained between 4 and 8 wt %, noting a reduction to 74% by mass at 2 wt %. Despite this, comparable BHET yield was retained between 2 and 4 wt % ($Y_{\text{BHET}} = 36$ –42%). Indeed, lowering the catalyst loading has previously been shown to increase BHET yield.⁹⁸

Given that the highest BHET yield was obtained at 8 wt % (Figure 9 and Table 7, entry 3), the influence of n(EG) (13.8–27.5 equiv, 1–2 mL) was investigated under identical reaction conditions (Figure 10). PET consumption and BHET yield appeared reasonably independent of n(EG), achieving 100% depolymerization by mass in all instances and a maximum yield of up to 64% using 20.6 equiv of EG. Previous work has highlighted a strong dependence of BHET yield on n(EG), possibly evidencing recrystallization limitations in this work.^{81,96–98}

To further optimize the BHET yield obtained using 20.6 equiv of EG (1.5 mL) (Figure 10), the effect of reaction time was also investigated. Indeed, previous reports have noted the enhanced BHET yield with prolonged reaction times.^{81,98,99} Consequently, the reaction time was varied between 1 and 3 h at 180 °C (Figure 11). A slight reduction in BHET yield from 64 to 58% is noted between 1 and 2 h prior to equilibration, consistent with the literature.^{81,96}

System optimization *via* an OVAT approach found the following conditions optimal for PET glycolysis using $\text{Zn}(\text{I})_2$: 1 h at 180 °C, 8 wt % cat. loading, 20.6 equiv of EG. Comparatively, $\text{Mg}(\text{I})_2$ offered significantly reduced activity under such conditions (Figure S45), highlighting the importance of system compatibility.

In summary, $\text{Zn}(\text{I})_2$ exhibited excellent activity, achieving 64% BHET yield within 1 h at 180 °C under optimal conditions. Such high activity can likely be attributed to the presence of H-bond donors, consistent with previous computational studies using organocatalysts, namely, TBD and urea.^{100,101}

Selective PLA–PET Degradation. Given the propensity of $\text{Zn}(\text{I})_2$ to facilitate both PLA and PET degradation, a selective chemical recycling strategy was envisaged. Despite industrial relevance, literature examples remain limited.^{45,48–50,102,103} Consequently, two strategies (A and B) are presented in Figure 12. Optimal conditions for both PLA methanolysis (Figure 5) and PET glycolysis (Figure S45) were used. Both strategies relied on PET being unreactive under methanolysis conditions,

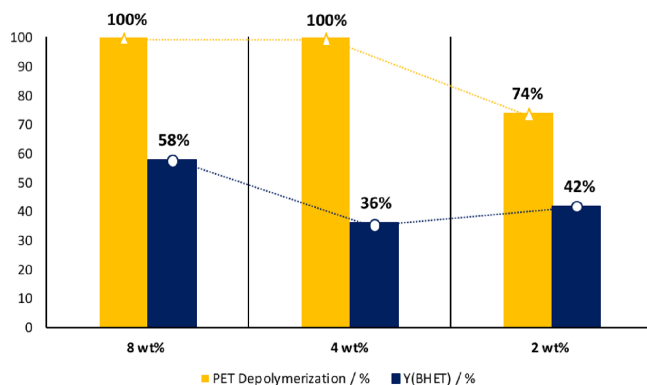


Figure 9. Plot of PET depolymerization by mass and BHET yield dependence on catalyst loading. Reaction conditions: 1 h at 180 °C, 0.25 g of bottle-grade PET ($M_n \approx 40,000 \text{ g mol}^{-1}$), 27.5 equiv (2 mL) of EG (relative to ester linkages), $\text{Zn}(\text{1})_2 = 2\text{--}8 \text{ wt \%}$ cat. loading (0.005–0.02 g, 0.64–2.5 mol % relative to ester linkages). *N.B.* Y_{BHET} refers to the isolated yield of pure BHET recrystallized from deionized H_2O followed by drying at 90 °C for 3 h *in vacuo*.

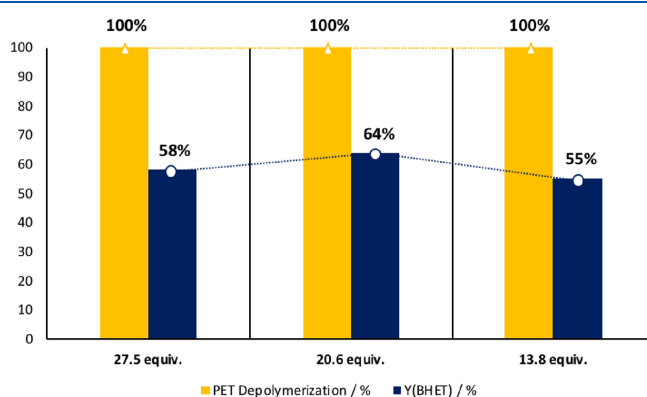


Figure 10. Plot of PET depolymerization by mass and BHET yield dependence on molar quantity of EG. Reaction conditions: 1 h at 180 °C, 0.25 g of bottle-grade PET ($M_n \approx 40,000 \text{ g mol}^{-1}$), 13.8–27.5 (1–2 mL) equiv of EG (relative to ester linkages), $\text{Zn}(\text{1})_2 = 8 \text{ wt \%}$ cat. loading (0.02 g, 2.5 mol % relative to ester linkages). *N.B.* Y_{BHET} refers to the isolated yield of pure BHET recrystallized from deionized H_2O followed by drying at 90 °C for 3 h *in vacuo*.

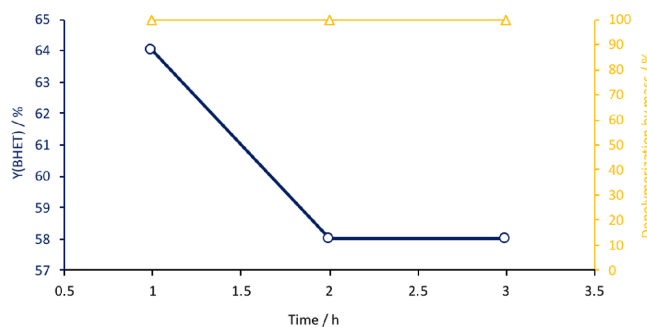


Figure 11. Plot of PET depolymerization by mass and BHET yield dependence on reaction time. Reaction conditions: 180 °C, 0.25 g of bottle-grade PET ($M_n \approx 40,000 \text{ g mol}^{-1}$), 20.6 equiv of EG (relative to ester linkages), $\text{Zn}(\text{1})_2 = 8 \text{ wt \%}$ cat. loading (0.02 g, 2.5 mol % relative to ester linkages). *N.B.* Y_{BHET} refers to the isolated yield of pure BHET recrystallized from deionized H_2O followed by drying at 90 °C for 3 h *in vacuo*.

which enabled separation post-reaction.¹⁰² Strategy A is characterized by catalyst recovery *via* distillation (2) to obtain

pure Me-LA post-methanolysis (1). Whilst this enabled $\text{Zn}(\text{1})_2$ to be reused for glycolysis (3), poorer activity was observed

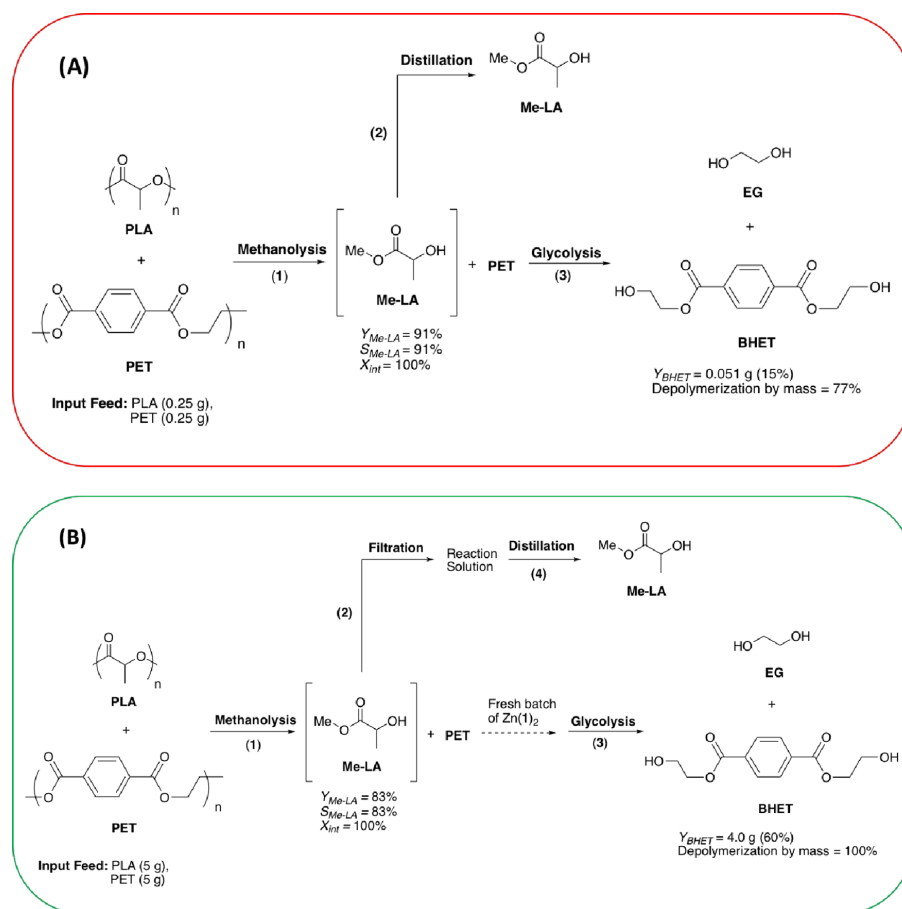


Figure 12. Selective chemical recycling strategies for a mixed PLA–PET feed. (A) Catalyst recovery-reuse *via* distillation. (B) Catalyst extraction *via* filtration. Input feed: PLA cup ($M_n \approx 45,510$ g mol⁻¹), bottle-grade PET ($M_n \approx 40,000$ g mol⁻¹). Reaction conditions used for (A): (1) 1.5 h at 50 °C, $V_{THF}:V_{MeOH} = 4:1$, $n_{MeOH}:n_{ester} = 7:1$, Zn(1)₂ = 8 wt % cat. loading (0.02 g, 0.96 mol % relative to ester linkages), (3) 1 h at 180 °C, 0.25 g of bottle-grade PET ($M_n \approx 40,000$ g mol⁻¹), 20.6 equiv (1.5 mL) of EG (relative to ester linkages), Zn(1)₂ = 8 wt % cat. loading (0.02 g, 2.5 mol % relative to ester linkages). *N.B.* Identical reaction conditions were used for (B), applying a quantity scale up factor of 20.

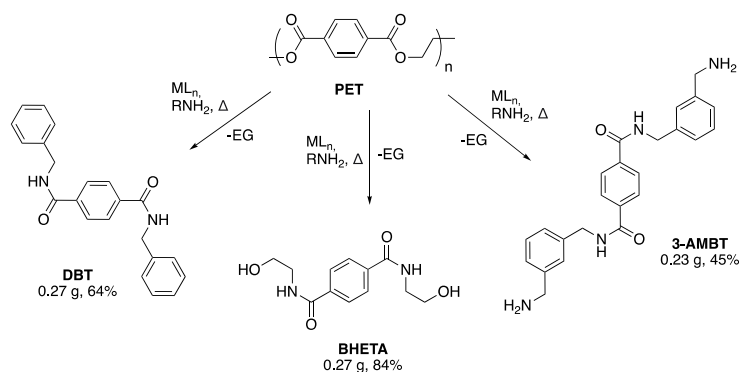
relative to the isolated step (Figure S45), noting incomplete PET consumption (77% by mass) and poorer BHET yield ($Y_{BHET} = 15\%$). This can likely be attributed to catalyst deactivation owing to the harsh distillation temperatures employed ($T = 170$ °C), consistent with activity loss relative to step (1). However, this could be circumvented in strategy B by introducing a filtration step prior to distillation, which necessitated a fresh batch of Zn(1)₂ to be added preglycolysis due to extraction in the filtrate. Process efficiency was preserved ($Y_{BHET} = 60\%$), enabling degradation to be performed on a milligram scale (5 g).

PET Aminolysis. To broaden substrate scope, bottle-grade PET was successfully broken down *via* aminolysis (Scheme 3). Hedrick and co-workers have previously shown TBD (~5 mol %) to be a potent catalyst for PET aminolysis, and thus identical reaction conditions were used for comparison (Table 8).⁷⁸ Since aminolysis is more thermodynamically favorable than glycolysis, notably milder conditions are noted (120–150 °C).^{72,73,77}

Reaction times (1–2 h) refer to the time taken to achieve complete PET dissolution, indicative of reaction completion. Facile product recovery was possible *via* washing or recrystallization, yielding white powders.

Both aliphatic and aromatic amines (6.0–16 equiv) were employed, furnishing high-value terephthalamides in good to excellent yield (45–84%), demonstrating catalyst versatility. Reactivity trends were consistent with previous work, generally requiring elevated temperatures, prolonged reaction times, or a large molar excess for aromatic amines owing to reduced nucleophilicity.⁷⁸ Promisingly, Zn(1)₂ remained competitive with TBD at a notably lower catalyst loading (2.5 mol %). PET aminolysis has also previously been reported to proceed within reasonable timeframes with no catalyst.^{78,104} Consequently, PET aminolysis in the absence of a catalyst was investigated (Table 8, entry 3). Using BHETA as a model system, a prolonged reaction time of 3 h is required to achieve comparable product yield (88%), highlighting reduced process efficiency. To

Scheme 3. Metal-Mediated PET Aminolysis into Terephthalamides (TPA) in the Presence of Both Aliphatic and Aromatic Amines

Table 8. PET Aminolysis into Terephthalamides Using Zn(1)₂^a

catalyst	time (h)	T (°C)	cat. loading (wt %)	amine (equiv)	TPA	Y _{TPA} (g/%)
Zn(1) ₂	2	150	8	6.0	DBT	0.27 (64%)
	2	120	8	6.4	BHETA	0.27 (84%)
	3	120	no cat.	6.4	BHETA	0.28 (88%)
	1	150	8	16	3-AMBT	0.23 (45%)

^aReaction conditions: Bottle-grade PET (0.24 g, $M_n \approx 40,000$ g mol⁻¹), Zn(1)₂ = 8 wt % cat. loading (0.019 g, 2.5 mol % relative to ester linkages), Benzyl amine (6.0 equiv), ethanolamine (6.4 equiv), and *m*-xylylenediamine (16 equiv) were used for the production of DBT, BHETA, and 3-AMBT, respectively. Y_{TPA} refers to the isolated yield of terephthalamide.

the best of our knowledge, such work encompasses the first example of PET aminolysis mediated by a homogeneous discrete metal-based catalyst.

PCL. PCL is a nonrenewable biodegradable polyester with potential biomedical applications.¹⁰⁵ Given a recent resurgence in the field, a clear opportunity exists to develop sustainable chemical recycling strategies (Scheme 2). Transesterification with MeOH affords methyl 6-hydroxyhexanoate. Whilst not directly amenable to repolymerization, this product possesses a relatively high market value (Fluorochem, 1 g, \$425.50), highlighting significant upcycling potential relative to PCL (Merck, 100 g, \$128.21). Initial work focused on the degradation of commercially available PCL beads ($M_n \approx 45,000$ g mol⁻¹) in THF using 8 wt % Zn(1)₂ (Table 9), whilst reaction progress was monitored using ¹H NMR (Figure S26).

Promisingly, methanolysis was possible at temperatures as low as 50 °C, contrary to previous work by McKeown *et al.*⁶⁷ using TMC (Table 9, entry 1). However, prolonged reaction times (20 h) were required to achieve appreciable product yield (69%) as noted by Wang and co-workers.⁶⁴ Increased resistance to degradation is possibly related to greater crystallinity and hydrophobicity relative to PLA.⁶⁷ To explore catalyst activity at higher temperatures, the solvent was exchanged with toluene. Increasing the reaction temperature to 100 °C resulted in a shorter reaction time and enhanced product yield, achieving 89% methyl 6-hydroxyhexanoate within 4 h (Table 9, entry 2).

Table 9. PCL Methanolysis into Methyl 6-Hydroxyhexanoate Using Zn(1)₂ and Mg(1)₂^c

catalyst	time (h)	T (°C)	cat. loading (wt %)	Y _{Methyl 6-hydroxyhexanoate} (%)
Zn(1) ₂	20 ^a	50	8	69
	4 ^b	100	8	89
	2 ^{b,c}	100	8	84
Mg(1) ₂	4 ^{b,d}	100	8	58

^aSolvent = THF, V_{THF}:V_{MeOH} = 4:1. ^bSolvent = toluene, V_{Toluene}:V_{MeOH} = 4:1. ^c0.25 g of PCL powder ($M_n \approx 10,000$ g mol⁻¹). ^d0.125 g of PCL beads ($M_n \approx 45,000$ g mol⁻¹), solvent = toluene, V_{Toluene}:V_{MeOH} = 2:1. N.B. Y_{Methyl 6-hydroxyhexanoate} refers to the product yield in solution as determined by ¹H NMR analysis (CDCl₃). ^eReaction conditions: 0.25 g of PCL beads ($M_n \approx 45,000$ g mol⁻¹), $n_{\text{PCL}}:n_{\text{MeOH}} = 1:11$ (based on ester linkages).

Mg(1)₂ exhibited poorer activity under identical reaction conditions (Table 9, entry 4), consistent with glycolysis results (Figure S45). Exchanging PCL beads for powder ($M_n \approx 10,000$ g mol⁻¹) enabled the reaction time to be reduced further (2 h), highlighting a dependence of degradation activity on M_n . A homogeneous solution was observed within 5 min under all conditions, indicating that sample dissolution is not rate-limiting. To the best of our knowledge, such work represents the first example of PCL methanolysis mediated by discrete metal-based complexes.

CONCLUSIONS

Homoleptic complexes of Zn(II) and Mg(II) based on a tridentate {NNO} ligand have been prepared and fully characterized. Zn(1)₂ exhibited high activity for the production of biocompatible atactic PLA under both industrially relevant melt conditions and at room temperature in CH₂Cl₂ (TOF = 184 h⁻¹). Both Mg(1)₂ and Zn(1)₂ were shown to facilitate rapid PLA methanolysis under mild conditions, achieving up to 85% Me-LA yield within 30 min at 50 °C in THF. Further kinetic analysis found Mg(1)₂ and Zn(1)₂ to exhibit k_{app} values of 0.23 ± 0.0076 and 0.15 ± 0.0029 min⁻¹, respectively {8 wt % cat. loading}, competitive with the state-of-the-art catalysts. Inferior performance was noted at elevated temperatures, potentially evidencing intermediate destabilization. Zn(1)₂ retained excellent activity for both PET and PCL degradation, demonstrating catalyst versatility, whilst a selective recycling

strategy for a mixed PLA–PET feed was demonstrated on a multigram scale. Various upcycling strategies (e.g., methanolysis, glycolysis, and aminolysis) were employed to achieve a broad substrate scope, which included BHET, high value terephthalamides, and methyl 6-hydroxyhexanoate. Optimal glycolysis conditions using Zn(1)₂ enabled 64% BHET yield within 1 h at 180 °C, a rare example of PET glycolysis mediated by a discrete homogeneous metal-based catalyst. The application of such catalysts for PET aminolysis and PCL methanolysis has been reported for the first time. In all instances, metal exchange was found to profoundly influence catalyst activity and appeared to be system-dependent. A possible new class of ligands for the field, we highlight significant scope for further optimization, which remains an ongoing endeavor.

■ ASSOCIATED CONTENT

Supporting Information

The Supporting Information is available free of charge at <https://pubs.acs.org/doi/10.1021/acs.macromol.1c01207>.

Crystallographic data of Si-based Zn(1)₂ derivative (CIF)

Experimental procedures, processed NMR spectra of the ligand and catalysts and associated stability testing, representative NMR spectra of polymers and degradation products, images of SEC traces and MALDI-ToF, homonuclear decoupled NMR spectrum of polymers, and degradation plots, and crystallographic data (PDF)

■ AUTHOR INFORMATION

Corresponding Author

Matthew D. Jones – Department of Chemistry, University of Bath, Bath BA2 7AY, United Kingdom; orcid.org/0000-0001-5991-5617; Phone: +44 (0)1225 384908; Email: mj205@bath.ac.uk

Authors

Jack M. Payne – Centre for Sustainable and Circular Technologies, University of Bath, Bath BA2 7AY, United Kingdom

Gabriele Kociok-Köhn – Department of Chemistry, University of Bath, Bath BA2 7AY, United Kingdom; orcid.org/0000-0002-7186-1399

Emma A. C. Emanuelsson – Department of Chemical Engineering, University of Bath, Bath BA2 7AY, United Kingdom; orcid.org/0000-0002-0937-4151

Complete contact information is available at: <https://pubs.acs.org/doi/10.1021/acs.macromol.1c01207>

Notes

The authors declare no competing financial interest.

■ ACKNOWLEDGMENTS

We wish to thank the EPSRC for funding and the University of Bath and MC² for use of their analysis facilities. We would like to thank the EPSRC for funding (EP/L016354/1) for a PhD studentship to J.P.

■ REFERENCES

- (1) Andrad, A. L.; Neal, M. A. Applications and societal benefits of plastics. *Philos. Trans. R. Soc., B* **2009**, *364*, 1977–1984.
- (2) Rabnawaz, M.; Wyman, I.; Auras, R.; Cheng, S. A roadmap towards green packaging: the current status and future outlook for

polyesters in the packaging industry. *Green Chem.* **2017**, *19*, 4737–4753.

(3) Payne, J.; McKeown, P.; Jones, M. D. A circular economy approach to plastic waste. *Polym. Degrad. Stab.* **2019**, *165*, 170–181.

(4) Geyer, R.; Jambeck, J. R.; Law, K. L. Production, use, and fate of all plastics ever made. *Sci. Adv.* **2017**, *3*, No. e1700782.

(5) Jambeck, J. R.; Geyer, R.; Wilcox, C.; Siegler, T. R.; Perryman, M.; Andrady, A.; Narayan, R.; Law, K. L. Plastic waste inputs from land into the ocean. *Science* **2015**, *347*, 768–771.

(6) Elhacham, E.; Ben-Uri, L.; Grozovski, J.; Bar-On, Y. M.; Milo, R. Global human-made mass exceeds all living biomass. *Nature* **2020**, *588*, 442–444.

(7) Gabirondo, E.; Sangroniz, A.; Etxeberria, A.; Torres-Giner, S.; Sardon, H. Poly(hydroxy acids) derived from the self-condensation of hydroxy acids: from polymerization to end-of-life options. *Polym. Chem.* **2020**, *11*, 4861–4874.

(8) Dechy-Cabaret, O.; Martin-Vaca, B.; Bourissou, D. Controlled Ring-Opening Polymerization of Lactide and Glycolide. *Chem. Rev.* **2004**, *104*, 6147–6176.

(9) Vink, E. T. H.; Rábago, K. R.; Glassner, D. A.; Springs, B.; O'Connor, R. P.; Kolstad, J.; Gruber, P. R. The Sustainability of NatureWorks™ Polylactide Polymers and Ingeo™ Polylactide Fibers: an Update of the Future. *Macromol. Biosci.* **2004**, *4*, 551–564.

(10) Vink, E. T. H.; Glassner, D. A.; Kolstad, J. J.; Wooley, R. J.; O'Connor, R. P. The eco-profiles for current and near-future NatureWorks® polylactide (PLA) production. *Biotechnol.* **2007**, *3*, 58–81.

(11) Lunt, J. Large-scale production, properties and commercial applications of polylactic acid polymers. *Polym. Degrad. Stab.* **1998**, *59*, 145–152.

(12) Auras, R.; Harte, B.; Selke, S. An Overview of Polylactides as Packaging Materials. *Macromol. Biosci.* **2004**, *4*, 835–864.

(13) Weber, C. J.; Haugaard, V.; Festersen, R.; Bertelsen, G. Production and applications of biobased packaging materials for the food industry. *Food Addit. Contam.* **2002**, *19*, 172–177.

(14) Castro-Aguirre, E.; Iñiguez-Franco, F.; Samsudin, H.; Fang, X.; Auras, R. Poly(lactic acid)—Mass production, processing, industrial applications, and end of life. *Adv. Drug Delivery Rev.* **2016**, *107*, 333–366.

(15) Nampoothiri, K. M.; Nair, N. J.; John, R. P. An overview of the recent developments in polylactide (PLA) research. *Bioresour. Technol.* **2010**, *101*, 8493–8501.

(16) Lasprilla, A. J. R.; Martinez, G. A. R.; Lunelli, B. H.; Jardini, A. L.; Filho, R. M. Poly-lactic acid synthesis for application in biomedical devices — A review. *Biotechnol. Adv.* **2012**, *30*, 321–328.

(17) Drumright, R. E.; Gruber, P. R.; Henton, D. E. Polylactic Acid Technology. *Adv. Mater.* **2000**, *12*, 1841–1846.

(18) Platel, R.; Hodgson, L.; Williams, C. Biocompatible Initiators for Lactide Polymerization. *Polym. Rev.* **2008**, *48*, 11–63.

(19) Thomas, C. M. Stereocontrolled ring-opening polymerization of cyclic esters: synthesis of new polyester microstructures. *Chem. Soc. Rev.* **2010**, *39*, 165–173.

(20) Stanford, M. J.; Dove, A. P. Stereocontrolled ring-opening polymerisation of lactide. *Chem. Soc. Rev.* **2010**, *39*, 486–494.

(21) Kamber, N. E.; Jeong, W.; Waymouth, R. M.; Pratt, R. C.; Lohmeijer, B. G. G.; Hedrick, J. L. Organocatalytic Ring-Opening Polymerization. *Chem. Rev.* **2007**, *107*, 5813–5840.

(22) Hong, M.; Chen, E. Y.-X. Chemically recyclable polymers: a circular economy approach to sustainability. *Green Chem.* **2017**, *19*, 3692–3706.

(23) Sheldon, R. A.; Norton, M. Green chemistry and the plastic pollution challenge: towards a circular economy. *Green Chem.* **2020**, *22*, 6310–6322.

(24) Sardon, H.; Dove, A. P. Plastics recycling with a difference. *Science* **2018**, *360*, 380–381.

(25) Garcia, J. M.; Robertson, M. L. The future of plastics recycling. *Science* **2017**, *358*, 870–872.

(26) Rahimi, A.; Garcia, J. M. Chemical recycling of waste plastics for new materials production. *Nat. Rev. Chem.* **2017**, *1*, 0046.

- (27) Coates, G. W.; Getzler, Y. D. Y. L. Chemical recycling to monomer for an ideal, circular polymer economy. *Nat. Rev. Mater.* **2020**, *5*, 501–516.
- (28) Hopewell, J.; Dvorak, R.; Kosior, E. Plastics recycling: challenges and opportunities. *Philos. Trans. R. Soc., B* **2009**, *364*, 2115–2126.
- (29) Ragaert, K.; Delva, L.; Van Geem, K. Mechanical and chemical recycling of solid plastic waste. *Waste Manage.* **2017**, *69*, 24–58.
- (30) McKeown, P.; Jones, M. D. The Chemical Recycling of PLA: A Review. *Sustainable Chem.* **2020**, *1*, 1–22.
- (31) Fan, Y.; Zhou, C.; Zhu, X. Selective Catalysis of Lactic Acid to Produce Commodity Chemicals. *Catal. Rev.: Sci. Eng.* **2009**, *51*, 293–324.
- (32) Dusselier, M.; Wouwe, P. V.; Dewaele, A.; Makshina, E.; Sels, B. F. Lactic acid as a platform chemical in the biobased economy: the role of chemocatalysis. *Energy Environ. Sci.* **2013**, *6*, 1415–1442.
- (33) Bowmer, C. T.; Hooftman, R. N.; Hanstveit, A. O.; Venderbosch, P. W. M.; van der Hoeven, N. The ecotoxicity and the biodegradability of lactic acid, alkyl lactate esters and lactate salts. *Chemosphere* **1998**, *37*, 1317–1333.
- (34) Pereira, C. S. M.; Silva, V. M. T. M.; Rodrigues, A. E. Ethyl lactate as a solvent: Properties, applications and production processes – a review. *Green Chem.* **2011**, *13*, 2658–2671.
- (35) Aparicio, S.; Alcalde, R. The green solvent ethyl lactate: an experimental and theoretical characterization. *Green Chem.* **2009**, *11*, 65–78.
- (36) Lamberti, F. M.; Román-Ramírez, L. A.; Mckeown, P.; Jones, M. D.; Wood, J. Kinetics of Alkyl Lactate Formation from the Alcoholysis of Poly(Lactic Acid). *Processes.* **2020**, *8*, 738.
- (37) Kopinke, F.; Remmler, M.; Mackenzie, K.; Moder, M.; Wachsen, O. Thermal decomposition of biodegradable polyesters—II. Poly(lactic acid). *Polym. Degrad. Stab.* **1996**, *53*, 329–342.
- (38) Fan, Y.; Nishida, H.; Shirai, Y.; Tokiwa, Y.; Endo, T. Thermal degradation behaviour of poly(lactic acid) stereocomplex. *Polym. Degrad. Stab.* **2004**, *86*, 197–208.
- (39) Aoyagi, Y.; Yamashita, K.; Doi, Y. Thermal degradation of poly[(R)-3-hydroxybutyrate], poly[ε-caprolactone], and poly[(S)-lactide]. *Polym. Degrad. Stab.* **2002**, *76*, 53–59.
- (40) Nishida, H.; Fan, Y.; Mori, T.; Oyagi, N.; Endo, T. Feedstock Recycling of Flame-Resisting Poly(lactic acid)/Aluminum Hydroxide Composite to l,l-lactide. *Ind. Eng. Chem. Res.* **2005**, *44*, 1433–1437.
- (41) Tsuji, H.; Saeki, T.; Tsukegi, T.; Daimon, H.; Fujie, K. Comparative study on hydrolytic degradation and monomer recovery of poly(l-lactic acid) in the solid and in the melt. *Polym. Degrad. Stab.* **2008**, *93*, 1956–1963.
- (42) Tsuji, H.; Daimon, H.; Fujie, K. A New Strategy for Recycling and Preparation of Poly(l-lactic acid): Hydrolysis in the Melt. *Biomacromolecules* **2003**, *4*, 835–840.
- (43) Codari, F.; Lazzari, S.; Soos, M.; Storti, G.; Morbidelli, M.; Moscatelli, D. Kinetics of the hydrolytic degradation of poly(lactic acid). *Polym. Degrad. Stab.* **2012**, *97*, 2460–2466.
- (44) Piemonte, V.; Gironi, F. Kinetics of Hydrolytic Degradation of PLA. *J. Polym. Environ.* **2013**, *21*, 313–318.
- (45) Westhues, S.; Idel, J.; Klankermayer, J. Molecular catalyst systems as key enablers for tailored polyesters and polycarbonate recycling concepts. *Sci. Adv.* **2018**, *4*, No. eaat9669.
- (46) Krall, E. M.; Klein, T. W.; Andersen, R. J.; Nett, A. J.; Glasgow, R. W.; Reader, D. S.; Dauphinais, B. C.; Mc Ilraith, S. P.; Fischer, A. A.; Carney, M. J.; Hudson, D. J.; Robertson, N. J. Controlled hydrogenative depolymerization of polyesters and polycarbonates catalyzed by ruthenium(II) PNN pincer complexes. *Chem. Commun.* **2014**, *50*, 4884–4887.
- (47) Kindler, T.-O.; Alberti, C.; Fedorenko, E.; Santangelo, N.; Enthaler, S. Ruthenium-Catalyzed Hydrogenative Degradation of End-of-Life Poly(lactide) to Produce 1,2-Propanediol as Platform Chemical. *ChemistryOpen.* **2020**, *9*, 401–404.
- (48) Monsigny, L.; Berthet, J.-C.; Cantat, T. Depolymerization of Waste Plastics to Monomers and Chemicals Using a Hydrosilylation Strategy Facilitated by Brookhart's Iridium(III) Catalyst. *ACS Sustainable Chem. Eng.* **2018**, *6*, 10481–10488.
- (49) Feghali, E.; Cantat, T. Room Temperature Organocatalyzed Reductive Depolymerization of Waste Polyethers, Polyesters, and Polycarbonates. *ChemSusChem* **2015**, *8*, 980–984.
- (50) Nunes, B. F. S.; Conceição Oliveira, M.; Fernandes, A. C. Dioxomolybdenum complex as an efficient and cheap catalyst for the reductive depolymerization of plastic waste into value-added compounds and fuels. *Green Chem.* **2020**, *22*, 2419–2425.
- (51) Fernandes, A. C. Reductive Depolymerization of Plastic Waste Catalyzed by Zn(OAc)₂ · 2H₂O. *ChemSusChem* **2021**, *14*, 1–7.
- (52) Liu, H.; Song, X.; Liu, F.; Liu, S.; Yu, S. Ferric chloride as an efficient and reusable catalyst for methanolysis of poly(lactic acid) waste. *J. Polym. Res.* **2015**, *22*, 135–141.
- (53) Hofmann, M.; Alberti, C.; Scheliga, F.; Meißner, R. R. R.; Enthaler, S. Tin(II) 2-ethylhexanoate catalyzed methanolysis of end-of-life poly(lactide). *Polym. Chem.* **2020**, *11*, 2625–2629.
- (54) Cheung, E.; Alberti, C.; Enthaler, S. Chemical Recycling of End-of-Life Poly(lactide) via Zinc-Catalyzed Depolymerization and Polymerization. *ChemistrySelect* **2020**, *9*, 1224–1228.
- (55) Alberti, C.; Kricheldorf, H. R.; Enthaler, S. Application of Bismuth Catalysts for the Methanolysis of End-of-Life Poly(lactide). *ChemistrySelect* **2020**, *5*, 12313–12316.
- (56) Petrus, R.; Bykowski, D.; Sobota, P. Solvothermal Alcoholysis Routes for Recycling Poly(lactide) Waste as Lactic Acid Esters. *ACS Catal.* **2016**, *6*, 5222–5235.
- (57) Whitelaw, E. L.; Davidson, M. G.; Jones, M. D. Group 4 salen complexes for the production and degradation of polylactide. *Chem. Commun.* **2011**, *47*, 10004–10006.
- (58) Fliedel, C.; Vila-Viçosa, D.; Calhorda, M. J.; Dagorne, S.; Avilés, T. Dinuclear Zinc–N-Heterocyclic Carbene Complexes for Either the Controlled Ring-Opening Polymerization of Lactide or the Controlled Degradation of Polylactide Under Mild Conditions. *ChemCatChem* **2014**, *6*, 1357–1367.
- (59) Payne, J.; McKeown, P.; Mahon, M. F.; Emanuelsson, E. A. C.; Jones, M. D. Mono- and dimeric zinc(II) complexes for PLA production and degradation into methyl lactate – a chemical recycling method. *Polym. Chem.* **2020**, *11*, 2381–2389.
- (60) Payne, J.; McKeown, P.; Driscoll, O.; Kociok-Köhn, G.; Emanuelsson, E. A. C.; Jones, M. D. Make or break: Mg(II)- and Zn(II)-catalen complexes for PLA production and recycling of commodity polyesters. *Polym. Chem.* **2021**, *12*, 1086–1096.
- (61) Román-Ramírez, L. A.; Mckeown, P.; Jones, M. D.; Wood, J. Poly(lactic acid) Degradation into Methyl Lactate Catalyzed by a Well-Defined Zn(II) Complex. *ACS Catal.* **2019**, *9*, 409–416.
- (62) McKeown, P.; Román-Ramírez, L. A.; Bates, S.; Wood, J.; Jones, M. D. Zinc Complexes for PLA Formation and Chemical Recycling: Towards a Circular Economy. *ChemSusChem* **2019**, *12*, 5233–5238.
- (63) Jędrzkiewicz, D.; Czełusniak, I.; Wierzejewska, M.; Szafert, S.; Ejfler, J. Well-controlled, zinc-catalyzed synthesis of low molecular weight oligolactides by ring opening reaction. *J. Mol. Catal. A: Chem.* **2015**, *396*, 155–163.
- (64) Yang, R.; Xu, G.; Lv, C.; Dong, B.; Zhou, L.; Wang, Q. Zn(HMDs)₂ as a Versatile Transesterification Catalyst for Polyesters Synthesis and Degradation toward a Circular Materials Economy Approach. *ACS Sustainable Chem. Eng.* **2020**, *8*, 18347–18353.
- (65) Leibfarth, F. A.; Moreno, N.; Hawker, A. P.; Shand, J. D. Transforming Polylactide into Value-Added Materials. *J. Polym. Sci.* **2012**, *50*, 4814–4822.
- (66) Nederberg, F.; Connor, E. F.; Glausser, T.; Hedrick, J. L. Organocatalytic chain scission of poly(lactides): a general route to controlled molecular weight, functionality and macromolecular architecture. *Chem. Commun.* **2001**, 2066–2067.
- (67) McKeown, P.; Kamran, M.; Davidson, M. G.; Jones, M. D.; Román-Ramírez, L. A.; Wood, J. Organocatalysis for versatile polymer degradation. *Green Chem.* **2020**, *22*, 3721–3726.
- (68) Song, X.; Zhang, X.; Wang, H.; Liu, F.; Yu, S.; Liu, S. Methanolysis of poly(lactic acid) (PLA) catalyzed by ionic liquids. *Polym. Degrad. Stab.* **2013**, *98*, 2760–2764.

- (69) Song, X.; Wang, H.; Zheng, X.; Liu, F.; Yu, S. Methanolysis of poly(lactic acid) using acidic functionalized ionic liquids as catalysts. *J. Appl. Polym. Sci.* **2014**, *131*, 40817–40822.
- (70) Liu, F.; Guo, J.; Zhao, P.; Gu, Y.; Gao, J.; Liu, M. Facile synthesis of DBU-based protic ionic liquid for efficient alcoholysis of waste poly(lactic acid) to lactate esters. *Polym. Degrad. Stab.* **2019**, *167*, 124–129.
- (71) Welle, F. Twenty years of PET bottle to bottle recycling—An overview. *Resour. Conserv. Recycl.* **2011**, *55*, 865–875.
- (72) Sinha, V.; Patel, M. R.; Patel, J. V. PET Waste Management by Chemical Recycling: A Review. *J. Polym. Environ.* **2010**, *18*, 8–25.
- (73) George, N.; Kurian, T. Recent Developments in the Chemical Recycling of Postconsumer Poly(ethylene terephthalate) Waste. *Ind. Eng. Chem. Res.* **2014**, *53*, 14185–14198.
- (74) Al-Salem, S. M.; Lettieri, P.; Baeyens, J. Recycling and recovery routes of plastic solid waste (PSW): a review. *Waste Manage.* **2009**, *29*, 2625–2643.
- (75) Al-Sabagh, A. M.; Yehia, F. Z.; Eshaq, G.; Rabie, A. M.; ElMetwally, A. E. Greener routes for recycling of polyethylene terephthalate. *Egypt. J. Pet.* **2016**, *25*, 53–64.
- (76) Kosloski-Oh, S. C.; Wood, Z. A.; Manjarrez, Y.; Pablo de los Rios, J.; Fieser, M. E. Catalytic methods for chemical recycling or upcycling of commercial polymers. *Mater. Horiz.* **2021**, *8*, 1084.
- (77) Payne, J.; Jones, M. D. The Chemical Recycling of Polyesters for a Circular Plastics Economy: Challenges and Emerging Opportunities. *ChemSusChem* **2021**, *14*, DOI: 10.1002/cssc.202100400.
- (78) Fukushima, K.; Lecuyer, J. M.; Wei, D. S.; Horn, H. W.; Jones, G. O.; Al-Megren, H. A.; Alabdulrahman, A. M.; Alsewaleim, F. D.; McNeil, M. A.; Rice, J. E.; Hedrick, J. L. Advanced chemical recycling of poly(ethylene terephthalate) through organocatalytic aminolysis. *Polym. Chem.* **2013**, *4*, 1610–1616.
- (79) Lamberti, F. M.; Román-Ramírez, L. A.; Wood, J. Recycling of Bioplastics: Routes and Benefits. *J. Polym. Environ.* **2020**, *28*, 2551–2571.
- (80) Troev, K.; Grancharov, G.; Tsevi, R.; Gitsov, I. A novel catalyst for the glycolysis of poly(ethylene terephthalate). *J. Appl. Polym. Sci.* **2003**, *90*, 1148–1152.
- (81) Wang, S.; Wang, C.; Wang, H.; Chen, X.; Wang, S. Sodium titanium tris(glycolate) as a catalyst for the chemical recycling of poly(ethylene terephthalate) via glycolysis and repolycondensation. *Polym. Degrad. Stab.* **2015**, *114*, 105–114.
- (82) Esquer, R.; García, J. J. Metal-catalysed Poly(Ethylene) terephthalate and polyurethane degradations by glycolysis. *J. Organomet. Chem.* **2019**, *902*, 120972.
- (83) Payne, J.; McKeown, P.; Kociok-Köhn, G.; Jones, M. D. Novel hybrid aluminium(iii)–catalen complexes as highly active catalysts for lactide polymerisation: towards industrial relevance. *Chem. Commun.* **2020**, *56*, 7163–7166.
- (84) Haiduc, I. Silicone Grease: A Serendipitous Reagent for the Synthesis of Exotic Molecular and Supramolecular Compounds. *Organometallics* **2004**, *23*, 3–8.
- (85) McKeown, P.; McCormick, S. N.; Mahon, M. F.; Jones, M. D. Highly active Mg(ii) and Zn(ii) complexes for the ring opening polymerisation of lactide. *Polym. Chem.* **2018**, *9*, 5339–5347.
- (86) Hermann, A.; Hill, S.; Metz, A.; Heck, J.; Hoffmann, A.; Hartmann, L.; Herres-Pawlis, S. Next Generation of Zinc Bisguanidine Polymerization Catalysts towards Highly Crystalline, Biodegradable Polyesters. *Angew. Chem., Int. Ed.* **2020**, *59*, 21778–21784.
- (87) Gesslbauer, S.; Cheek, H.; White, A. J. P.; Romain, C. Highly active aluminium catalysts for room temperature ring-opening polymerisation of *rac*-lactide. *Dalton Trans.* **2018**, *47*, 10410–10414.
- (88) Gesslbauer, S.; Savela, R.; Chen, Y.; White, A. J. P.; Romain, C. Exploiting Noncovalent Interactions for Room-Temperature Hetero-selective *rac*-Lactide Polymerization Using Aluminum Catalysts. *ACS Catal.* **2019**, *9*, 7912–7920.
- (89) Gesslbauer, S.; Hutchinson, G.; White, A. J. P.; Burés, J.; Romain, C. Chirality-Induced Catalyst Aggregation: Insights into Catalyst Speciation and Activity Using Chiral Aluminum Catalysts in Cyclic Ester Ring-Opening Polymerization. *ACS Catal.* **2021**, *11*, 4084–4093.
- (90) Chamberlain, B. M.; Cheng, M.; Moore, D. R.; Ovitt, T. M.; Lobkovsky, E. B.; Coates, G. W. Polymerization of Lactide with Zinc and Magnesium β -Diiminato Complexes: Stereoselective and Mechanism. *J. Am. Chem. Soc.* **2001**, *123*, 3229–3238.
- (91) Wang, H.; Yang, Y.; Ma, H. Stereoselectivity Switch between Zinc and Magnesium Initiators in the Polymerization of *rac*-Lactide: Different Coordination Chemistry, Different Stereoselective Mechanisms. *Macromolecules* **2014**, *47*, 7750–7764.
- (92) Thevenon, A.; Romain, C.; Bennington, M. S.; White, A. J. P.; Davidson, H. J.; Brooker, S.; Williams, C. K. Dizinc Lactide Polymerization Catalysts: Hyperactivity by Control of Ligand Conformation and Metallic Cooperativity. *Angew. Chem., Int. Ed.* **2016**, *55*, 8680–8685.
- (93) Aycock, D. F. Solvent Applications of 2-Methyltetrahydrofuran in Organometallic and Biphasic Reactions. *Org. Process Res. Dev.* **2007**, *11*, 156–159.
- (94) Román-Ramírez, L. A.; McKeown, P.; Jones, M. D.; Wood, J. Kinetics of Methyl Lactate Formation from the Transesterification of Poly(lactic acid) Catalyzed by Zn(II) Complexes. *ACS Omega* **2020**, *5*, 5556–5564.
- (95) Upare, P. P.; Hwang, Y. K.; Chang, J.-S.; Hwang, D. W. Synthesis of Lactide from Alkyl Lactate via a Prepolymer Route. *Ind. Eng. Chem. Res.* **2012**, *51*, 4837–4842.
- (96) López-Fonseca, R.; Duque-Ingunza, I.; de Rivas, B.; Arnaiz, S.; Gutiérrez-Ortiz, J. I. Chemical recycling of post-consumer PET wastes by glycolysis in the presence of metal salts. *Polym. Degrad. Stab.* **2010**, *95*, 1022–1028.
- (97) Jehanno, C.; Flores, I.; Dove, A. P.; Müller, A. J.; Ruipérez, F.; Sardon, H. Organocatalysed depolymerisation of PET in a fully sustainable cycle using thermally stable protic ionic salt. *Green Chem.* **2018**, *20*, 1205–1212.
- (98) Pingale, N. D.; Palekar, V. S.; Shukla, S. R. Glycolysis of postconsumer polyethylene terephthalate waste. *J. Appl. Polym. Sci.* **2010**, *115*, 249–254.
- (99) Delle Chiaie, K. R.; McMahon, F. R.; Williams, E. J.; Price, M. J.; Dove, A. P. Dual-catalytic depolymerization of polyethylene terephthalate (PET). *Polym. Chem.* **2020**, *11*, 1450–1453.
- (100) Fukushima, K.; Coulembier, O.; Lecuyer, J. M.; Almegren, H. A.; Alabdulrahman, A. M.; Alsewaleim, F. D.; McNeil, M. A.; Dubois, P.; Waymouth, R. M.; Horn, H. W.; Rice, J. E.; Hedrick, J. L. Organocatalytic Depolymerization of Poly(ethylene terephthalate). *J. Polym. Sci., Part A: Polym. Chem.* **2011**, *49*, 1273–1281.
- (101) Wang, Q.; Yao, X.; Tang, S.; Lu, X.; Zhang, X.; Zhang, S. Urea as an efficient and reusable catalyst for the glycolysis of poly(ethylene terephthalate) wastes and the role of hydrogen bond in this process. *Green Chem.* **2012**, *14*, 2559–2566.
- (102) Sánchez, A. C.; Collinson, R. S. The selective recycling of mixed plastic waste of polylactic acid and polyethylene terephthalate by control of process conditions. *Eur. Polym. J.* **2011**, *47*, 1970–1976.
- (103) Jehanno, C.; Demarteau, J.; Mantione, D.; Arno, M. C.; Ruipérez, F.; Hedrick, J. L.; Dove, A. P.; Sardon, H. Selective Chemical Upcycling of Mixed Plastics Guided by a Thermally Stable Organocatalyst. *Angew. Chem., Int. Ed.* **2021**, *133*, 6784–6791.
- (104) Tan, J. P. K.; Tan, J.; Park, N.; Xu, K.; Chan, E. D.; Yang, C.; Pionova, V. A.; Ji, Z.; Lim, A.; Shao, J.; Bai, A.; Bai, X.; Mantione, D.; Sardon, H.; Yang, Y. Y.; Hedrick, J. L. Upcycling Poly(ethylene terephthalate) Refuse to Advanced Therapeutics for the Treatment of Nosocomial and Mycobacterial Infections. *Macromolecules* **2019**, *52*, 7878–7885.
- (105) Woodruff, M. A.; Huttmacher, D. W. The return of a forgotten polymer—Polycaprolactone in the 21st century. *Prog. Polym. Sci.* **2010**, *35*, 1217–1256.

4.2. Experimental

Exemplar procedures, full characterisation data and representative spectra are provided herein, see ESI for full details: https://pubs.acs.org/doi/suppl/10.1021/acs.macromol.1c01207/suppl_file/ma1c01207_si_002.pdf

4.2.1. General experimental methods

General methods detailed in sections 2.3.1. and 3.2.1. of Chapter 2 and 3, respectively, were used. PLLA-based 3D printing material was kindly provided by Filamentive. PCL pellets ($M_n = 45,000 \text{ g mol}^{-1}$) and powder ($M_n = 10,000 \text{ g mol}^{-1}$) were sourced from Sigma-Aldrich.

4.2.2. General polymerisation procedures

4.2.2.1. Lactide polymerisation

PLA production and subsequent materials characterisation was conducted as detailed in section 2.3.2.1. of Chapter 2.

4.2.2.2. Lactide polymerisation kinetics

Polymerisation kinetic data was acquired according to the method described in section 2.3.2.2. of Chapter 2. *N.B.* For $\text{Zn}(\mathbf{1})_2$ {DCM, RT, [*rac*- LA]:[Zn]:[BnOH] = 100:1:1} following ^1H NMR (CDCl_3) analysis, samples were decanted into separate vials and retained for SEC analysis as per section 2.3.2.1. of Chapter 2.

4.2.3. General PLA degradation procedures

4.2.3.1. PLA methanolysis

PLA methanolysis was conducted as detailed in section 3.2.3.1. of Chapter 3.

The concurrent polymerisation-depolymerisation of PLA was characterised by a two-step process (Figure 8 in publication 4). First, the solution polymerisation of *rac*-LA using $\text{Zn}(\mathbf{1})_2$ {DCM, RT, [*rac*- LA]:[Zn]:[BnOH] = 100:1:1} was performed using the procedure detailed in section 2.3.2.1. of Chapter 2. Following reaction completion after 30 min (< 5% residual lactide), PLA and catalyst were isolated upon solvent removal and dried *in vacuo* for 1 h at RT, maintaining an argon atmosphere prior to step 2. Second, the degradation of PLA ($M_n = 15,100 \text{ g mol}^{-1}$, $D = 1.07$) was conducted using the method described in section 3.2.3.1. of Chapter 3 {8 wt%, 0.02 g, 0.96 mol% relative to ester linkages, 1.5 h at 50 °C in THF}.

For selective degradation experiments (*i.e.* a mixed PLA/PET feed) a modified method was used (Figure 12 in publication 4). For small scale reactions (PLA cup + bottle-grade PET, 1:1, 0.25 g:0.25 g) following reaction completion, catalyst and unreacted PET were recovered by vacuum distillation. Aliquots from the distillate were taken for ^1H NMR (CDCl_3) analysis of the methine region (*ca.* $\delta = 4.2 - 5.2$ ppm) before and after solvent removal *in vacuo*. Subsequent PET glycolysis was performed as per section 3.2.4.1. of Chapter 3. For large scale reactions (PLA cup + bottle-grade PET, 1:1, 5 g:5 g), unreacted PET was recovered by cannula filtration and dried *in vacuo* for 1 h at RT. A fresh batch of $\text{Zn}(\mathbf{1})_2$ was added (8 wt%, 0.4 g, 2.5 mol% relative to ester linkages) in a Glovebox filled with argon prior to glycolysis. A scale-up factor up of 20 was applied to the reagents used, whilst reaction and drying times were retained. Aliquots from the filtrate were taken for ^1H NMR (CDCl_3) analysis of the methine region (*ca.* $\delta = 4.2 - 5.2$ ppm) before and after solvent removal *in vacuo*.

4.2.3.2. PLA methanolysis kinetics

PLA methanolysis kinetic data was obtained according to the method detailed in section 3.2.3.2. of Chapter 3.

4.2.4. General PET degradation procedures

4.2.4.1. PET glycolysis

PET glycolysis was conducted as detailed in section 3.2.4.1. of Chapter 3.

4.2.4.2. PET methanolysis

A J Young's flask was charged with bottle-grade PET pieces (0.25 g, $0.1 \times 0.1 \text{ cm}^2$, *The Coca-Cola Company*TM, $M_n \sim 40,000 \text{ g mol}^{-1}$) and $\text{Zn}(\mathbf{1})_2$ (8 wt%, 0.02 g, 2.5 mol% relative to ester linkages) in a Glovebox filled with argon. Toluene (4 mL) and MeOH (1 mL, 19 equivalents relative to ester linkages) were added under a dynamic flow of argon and the flask was submerged in a pre-heated oil bath (100 °C). After the desired amount of time elapsed, residual PET fragments were isolated by filtration and weighed before and after drying at 140 °C for 3 h. The supernatant solvent was removed *in vacuo* and the solid residue washed with cold MeOH ($5 \times 2.5 \text{ mL}$) to afford dimethyl terephthalate (DMT) as a pale white solid. This procedure was repeated for degradations performed at 150 °C and for PET thin-films. *N.B.* filtration was not required when complete PET dissolution was observed, indicated by a homogenous solution.

4.2.4.3. PET aminolysis

Diamine terephthalamide products derived from PET aminolysis were prepared and characterised in accordance to previous work by Fukushima *et al.*^[12]

4.2.4.3.1. *N,N'*-dibenzylterephthalamide (DBT)

A J Young's flask was charged with bottle-grade PET pieces (0.24 g, $0.1 \times 0.1 \text{ cm}^2$, *The Coca-Cola Company*TM, $M_n \sim 40,000 \text{ g mol}^{-1}$) and $\text{Zn}(\mathbf{1})_2$ (8 wt%, 0.019 g, 2.5 mol % relative to ester linkages) in a Glovebox filled with argon. Benzyl amine (0.82 mL, 7.45 mmol) was added under a dynamic flow of argon. The flask was submerged in a preheated oil bath (150 °C) and stirred for 2 h, observing the formation of a pale-yellow slurry. The slurry was washed in THF (30 mL) and filtered to afford the title compound as a white powder, which was dried *in vacuo*. Yield = 0.27 g, 64%.

4.2.4.3.2. *N,N'*-bis(2-hydroxyethyl)terephthalamide (BHETA)

A J Young's flask was charged with bottle-grade PET pieces (0.24 g, $0.1 \times 0.1 \text{ cm}^2$, *The Coca-Cola Company*TM, $M_n \sim 40,000 \text{ g mol}^{-1}$) and $\text{Zn}(\mathbf{1})_2$ (8 wt%, 0.019 g, 2.5 mol% relative to ester linkages) in a Glovebox filled with argon. Ethanolamine (0.5 mL, 8 mmol) was added under a dynamic flow of argon. The flask was submerged in a preheated oil bath (120 °C) and stirred for 2 h, observing the formation of a white slurry. The slurry was washed in DCM (25 mL), filtered and washed with THF (25 mL) to afford the title compound as a white powder, which was dried *in vacuo*. Yield = 0.27 g, 84%.

4.2.4.3.3. *N,N'*-bis(3-(aminomethyl)benzyl)terephthalamide (3-AMBT)

A J Young's flask was charged with bottle-grade PET pieces (0.24 g, $0.1 \times 0.1 \text{ cm}^2$, *The Coca-Cola Company*TM, $M_n \sim 40,000 \text{ g mol}^{-1}$) and $\text{Zn}(\mathbf{1})_2$ (8 wt%, 0.019 g, 2.5 mol% relative to ester linkages) in a Glovebox filled with argon. *m*-Xylylenediamine (2.7 mL, 20 mmol) was added under a dynamic flow of argon. The flask was submerged in a preheated oil bath (150 °C) and stirred for 1 h, observing a clear homogeneous solution. The solution was transferred to a round-bottom flask containing deionised H₂O (50 mL), observing rapid precipitation of an off-white solid. The solution was heated vigorously with stirring and the insoluble was removed by filtration. The filtrate was retained and refrigerated (*ca.* 4 °C) for 20 h. The title compound was isolated as a white solid by filtration, which was dried *in vacuo*. Yield = 0.23 g, 45%.

4.2.5. General PCL degradation procedures

PCL methanolysis was conducted and characterised according to previous work by McKeown *et al.*^[13]

4.2.5.1. PCL methanolysis

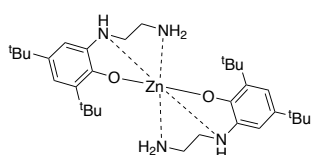
A J Young's flask was charged with PCL pellets (0.25 g, $M_n = 45,000 \text{ g mol}^{-1}$) and metal complex (8 wt%, 0.02 g, 1.5 – 1.6 mol% relative to ester linkages) in a Glovebox filled with

argon. Toluene (4 mL) and MeOH (1 mL, 11 equivalents relative to ester linkages) were added under a dynamic flow of argon and the flask was submerged in a pre-heated oil bath (100 °C), observing complete PCL dissolution within 5 min. Sample aliquots were taken under a flow of argon and analysed by ^1H NMR (CDCl_3) spectroscopy. This method was retained for PCL powder ($M_n = 10,000 \text{ g mol}^{-1}$) and degradations performed in THF at 50 °C.

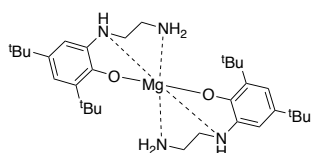
4.2.6. Synthesis and characterisation

A general synthesis procedure, full characterisation data and representative spectrum for the ligand precursor (**1H**) is provided in section 2.3.3.1. of Chapter 2.

4.2.6.1. Metal complexes based on **1H**



Zn(1)₂: Isolated as a white solid (0.63 g, 1.06 mmol, 53%). To a solution of **1H** (1.06 g, 4 mmol) in dry toluene (20 mL), ZnEt_2 (2 mL, 2 mmol) was added dropwise with stirring. The solution was stirred at RT for 1 h, observing a light grey precipitate, which was isolated by cannula filtration and dried *in vacuo* at 80 °C for 3 h to afford a white solid. ^1H NMR (CDCl_3 , 500 MHz): $\delta = 7.07$ (d, $J = 2$ Hz, 1H; ArH), 6.82 (d, $J = 2$ Hz, 1H; ArH), 2.99 (s, 2H; CH), 2.82 (s, 3H; CH, NH), 2.08 (s, 2H; NH_2), 1.47 (s, 9H; $\text{C}(\text{CH}_3)_3$), 1.24 (s, 9H; $\text{C}(\text{CH}_3)_3$). $^{13}\text{C}\{^1\text{H}\}$ NMR (CDCl_3 , 125 MHz): $\delta = 161.9$, 136.4, 131.4, 128.4, 121.5, 120.3 (Ar), 52.1, 38.8 (CH_2), 35.6, 34.0 ($\text{C}(\text{CH}_3)_3$), 32.1, 29.9 (CH_3). Elemental analysis: Calculated for $\text{C}_{32}\text{H}_{54}\text{N}_4\text{O}_2\text{Zn}$: C, 64.90 %; H, 9.19 %; N, 9.46 %. Found: C, 63.86 %; H, 9.01 %; N, 9.27 %.



Mg(1)₂: Isolated as an off-white solid (0.25 g, 0.45 mmol, 45%). To a solution of **1H** (0.53 g, 2 mmol) in dry toluene (10 mL), $\text{Mg}(\text{}^i\text{Bu})_2$ (1 mL, 1 mmol) was added dropwise with stirring, resulting in rapid precipitation of an off-white solid. The resulting suspension was stirred for 30 min at RT after which the solid was redissolved upon vigorous heating and left to recrystallise overnight at RT. The recrystallised product was isolated by cannula filtration and dried *in vacuo* at 80 °C for 4 h to afford an off-white solid. ^1H NMR (C_6D_6 , 500 MHz): $\delta = 7.46$ (s, 1H; ArH), 6.46 (s, 1H; ArH), 2.61 (t, $J = 12$ Hz, 1H; CH), 2.21 (s, 1H; CH), 2.19 (s, 1H; CH), 2.01 (s, 1H; NH), 1.88 (s, 9H; $\text{C}(\text{CH}_3)_3$), 1.82 (d, $J = 12$ Hz, 1H; CH), 1.43 (s, 9H; $\text{C}(\text{CH}_3)_3$), 0.92 (br s, 1H; NH), 0.63 (br s, 1H; NH). $^{13}\text{C}\{^1\text{H}\}$ NMR (C_6D_6 , 125 MHz): $\delta = 164.1$, 136.5, 132.8, 132.4, 121.8, 120.4 (Ar), 52.5, 38.2 (CH_2), 35.9, 34.3 ($\text{C}(\text{CH}_3)_3$), 32.5, 30.2 (CH_3). Elemental analysis: Calculated for $\text{C}_{32}\text{H}_{54}\text{N}_4\text{O}_2\text{Mg}$: C, 69.74 %; H, 9.88 %; N, 10.17 %. Found: C, 67.20 %; H, 9.52 %; N, 9.58 %. Elemental analysis more consistent with hydrated complex, indicative of hygroscopicity. $\text{Mg}(\mathbf{1})_2 \cdot \text{H}_2\text{O}$, theoretical: C, 67.53 %; H, 9.92 %; N, 9.84 %.

4.2.6.2. Representative NMR spectra

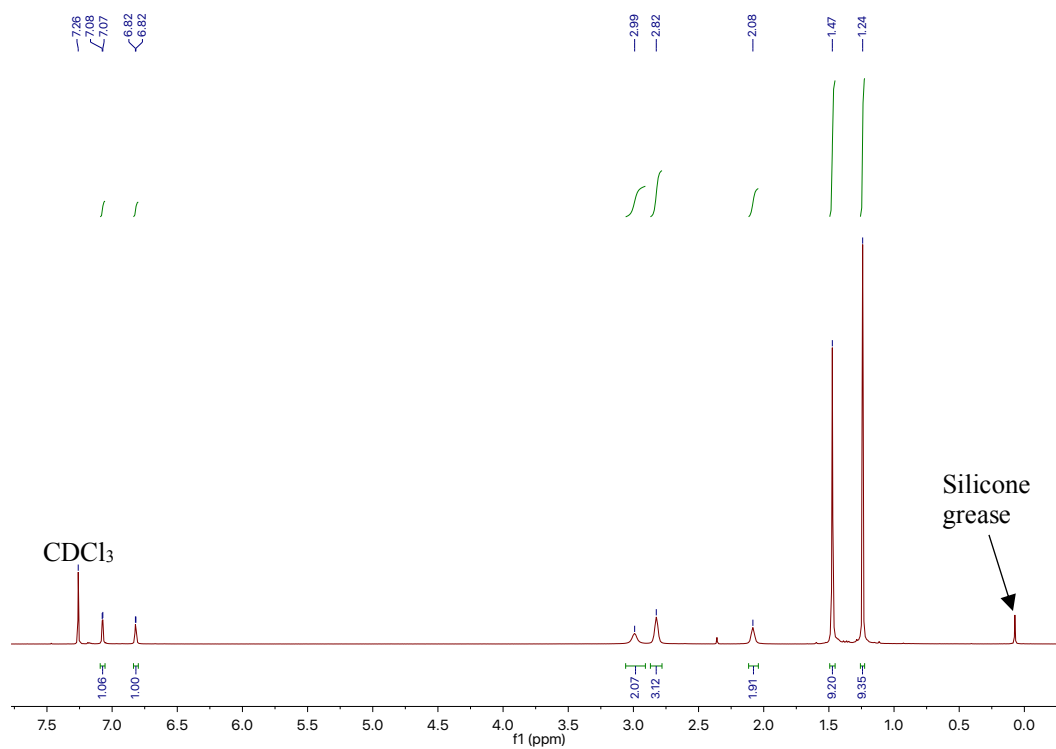


Figure 4.1. ^1H NMR (CDCl_3 , 500 MHz) spectrum of $\text{Zn}(\mathbf{1})_2$. *N.B.* Figure S3 in ESI.

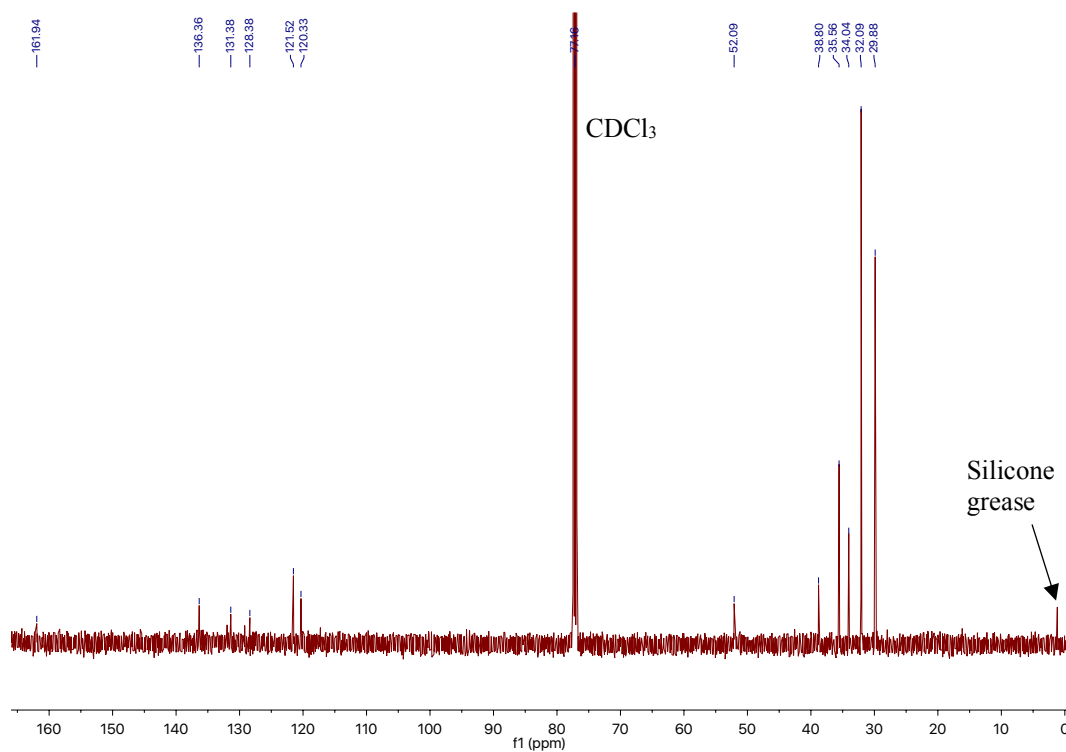


Figure 4.2. $^{13}\text{C}\{^1\text{H}\}$ NMR (CDCl_3 , 125 MHz) spectrum of $\text{Zn}(\mathbf{1})_2$. *N.B.* Figure S4 in ESI.

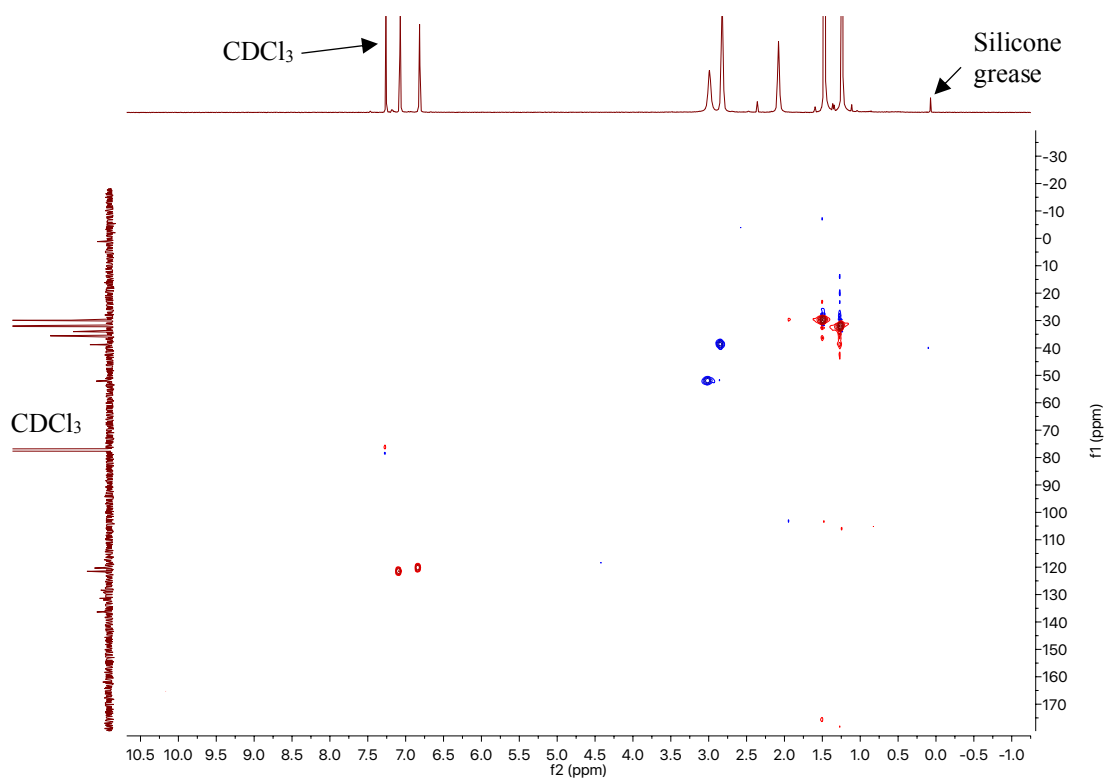


Figure 4.3. HSQC NMR (CDCl_3 , 125 MHz) spectrum of $\text{Zn}(\mathbf{1})_2$. *N.B.* Figure S5 in ESI.

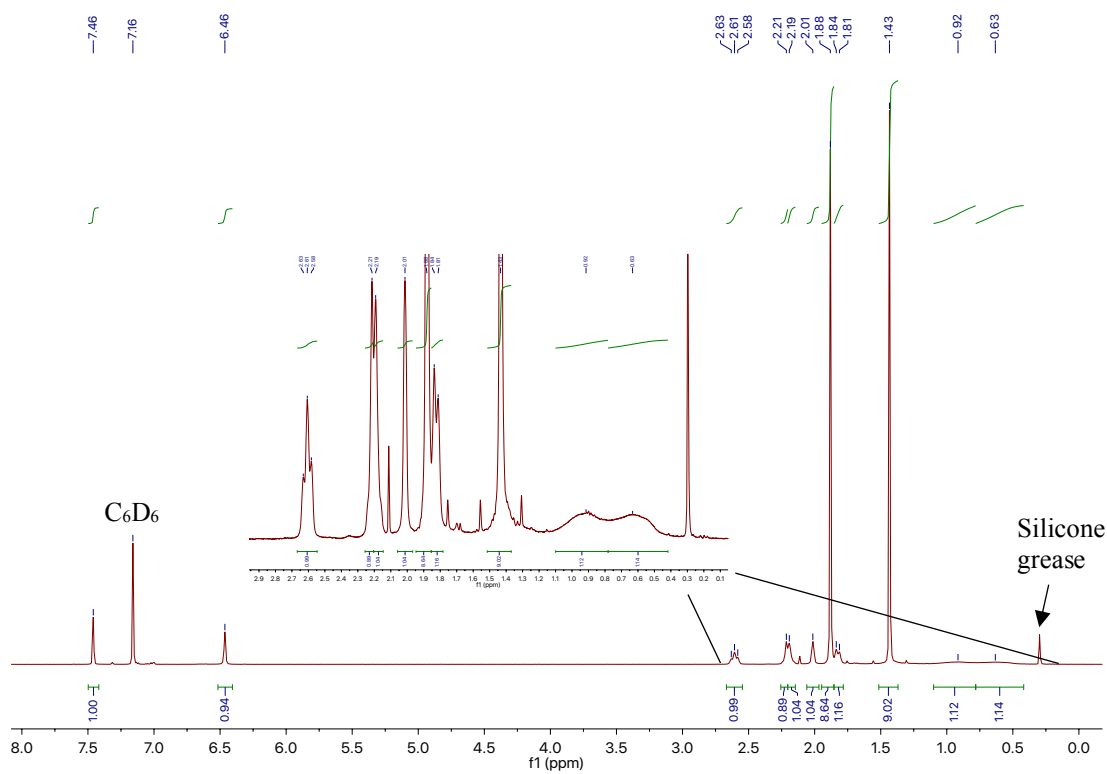


Figure 4.4. ^1H NMR (C_6D_6 , 500 MHz) spectrum of $\text{Mg}(\mathbf{1})_2$. *N.B.* Figure S6 in ESI.

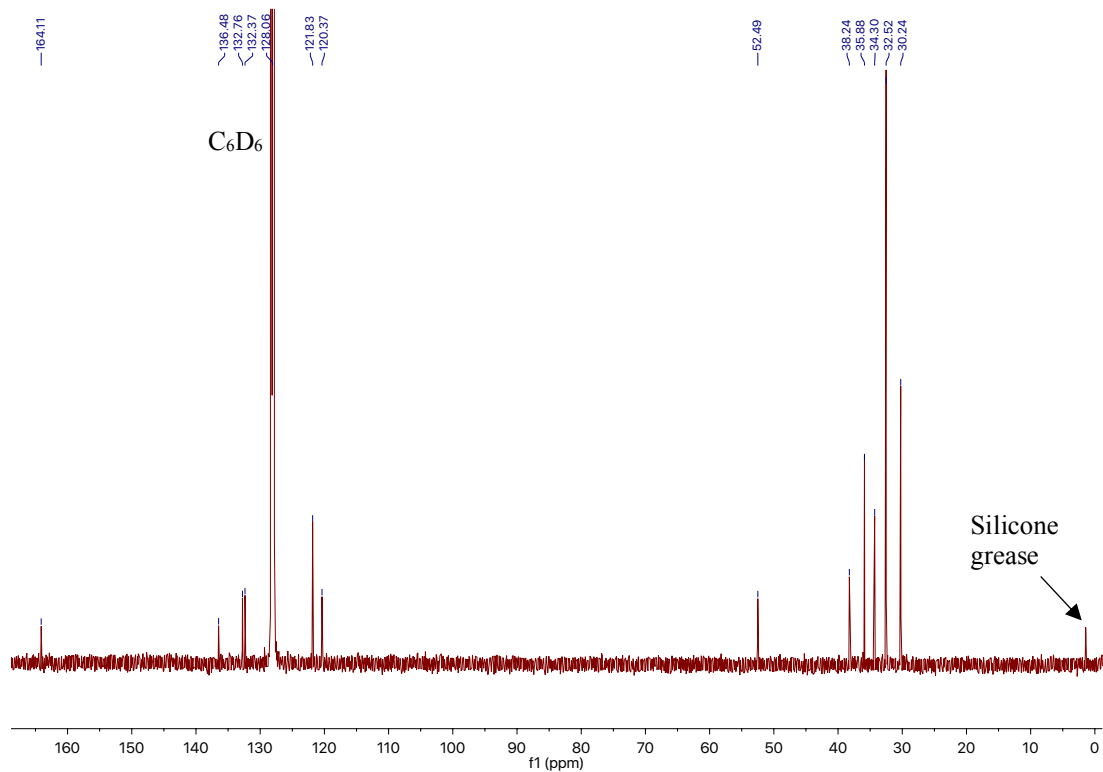


Figure 4.5. $^{13}\text{C}\{^1\text{H}\}$ NMR (C_6D_6 , 125 MHz) spectrum of $\text{Mg}(\mathbf{1})_2$. *N.B.* Figure S7 in ESI.

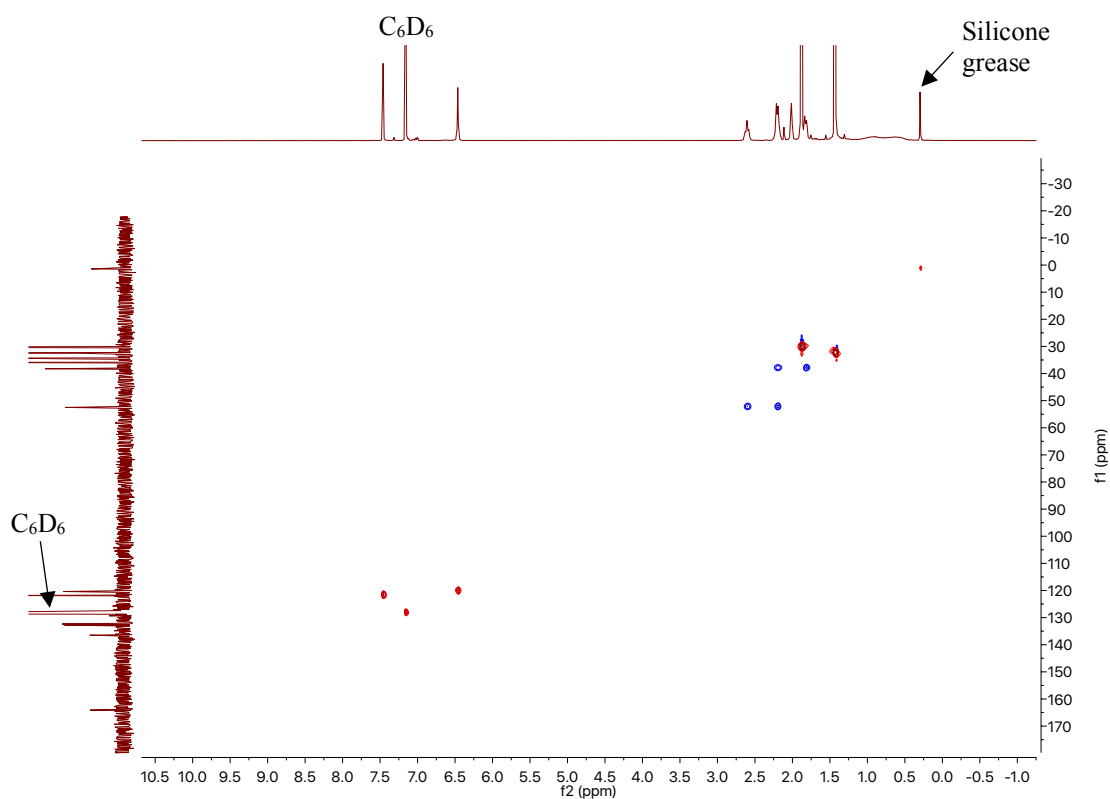


Figure 4.6. HSQC NMR (C_6D_6 , 125 MHz) spectrum of $Mg(1)_2$. *N.B.* Figure S8 in ESI.

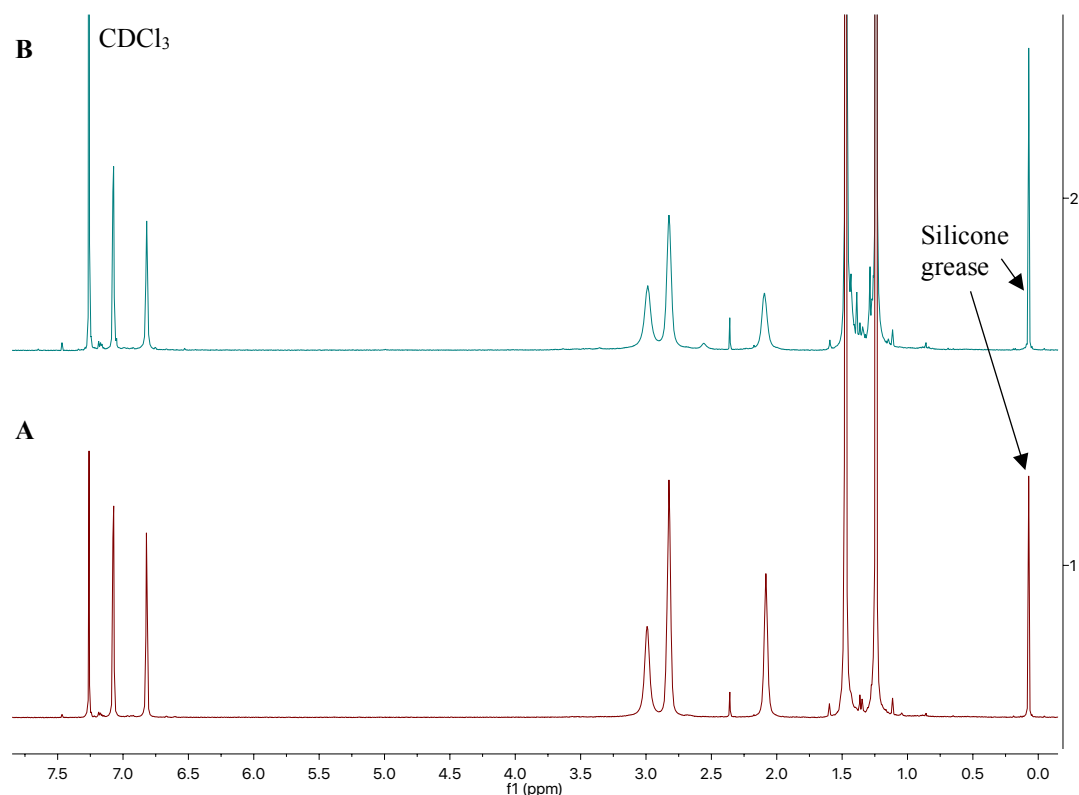


Figure 4.7. Stacked 1H NMR ($CDCl_3$, 500 MHz) spectra assessing the stability of $Zn(1)_2$ in air: (A) $Zn(1)_2$ under argon atmosphere, and; (B) $Zn(1)_2$ exposed to air for 24 h at RT. *N.B.* Figure S9 in ESI.

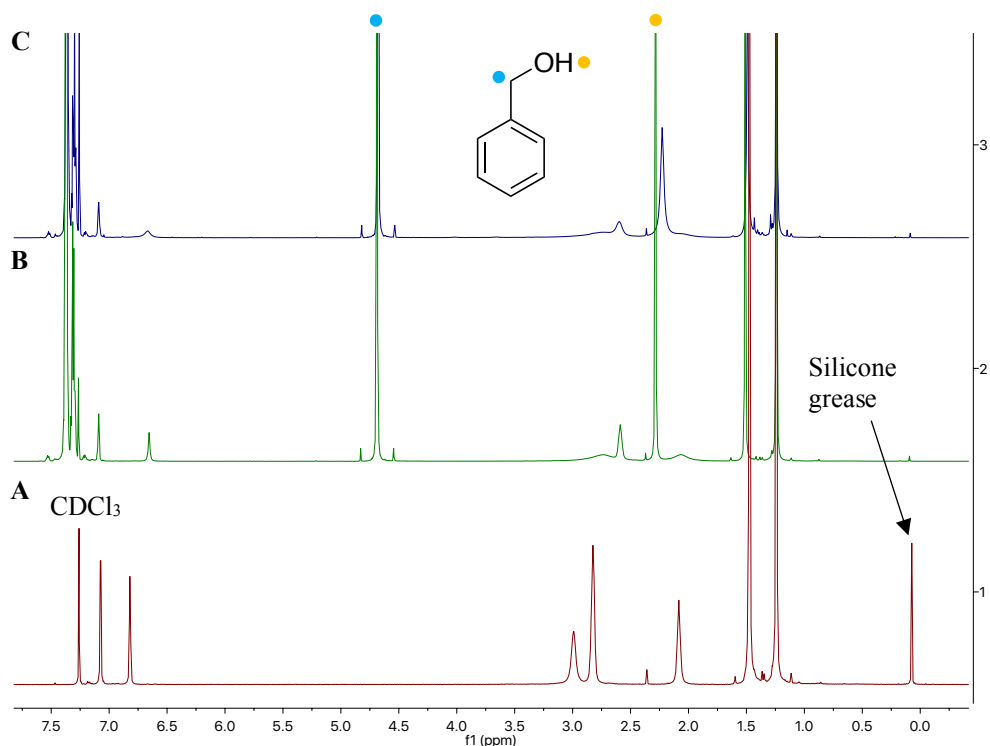


Figure 4.8. Stacked ¹H NMR (CDCl₃, 500 MHz) spectra assessing the stability of Zn(1)₂ with excess BnOH: (A) Zn(1)₂, (B) Zn(1)₂ + BnOH at RT, and; (C) Zn(1)₂ + BnOH at 80 °C for 30 min. *N.B.* Figure S10 in ESI.

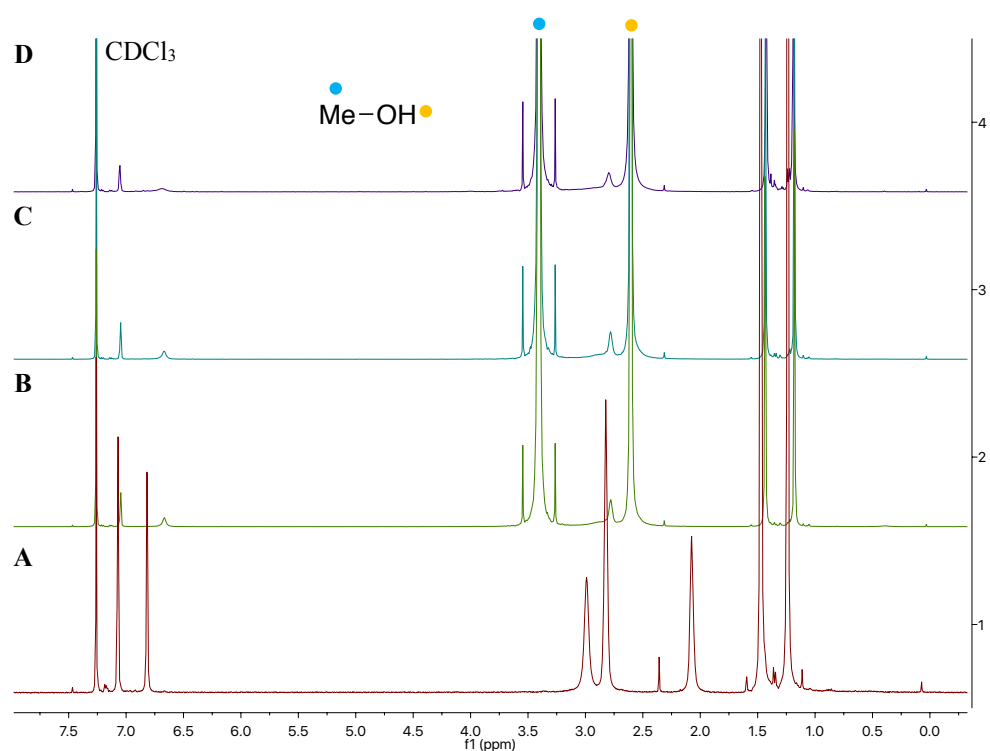


Figure 4.9. ¹H NMR (CDCl₃, 500 MHz) spectra assessing the stability of Zn(1)₂ with excess MeOH: (A) Zn(1)₂, (B) Zn(1)₂ + MeOH at RT, (C) Zn(1)₂ + MeOH at 50 °C for 30 min, and; (D) Zn(1)₂ + MeOH at 80 °C for 30 min. *N.B.* Figure S11 in ESI.

4.2.7. Polymer characterisation

4.2.7.1. Representative ^1H NMR spectrum

A representative ^1H NMR spectrum of PLA is provided in section 2.3.4.1. of Chapter 2.

4.2.7.2. Representative SEC spectra

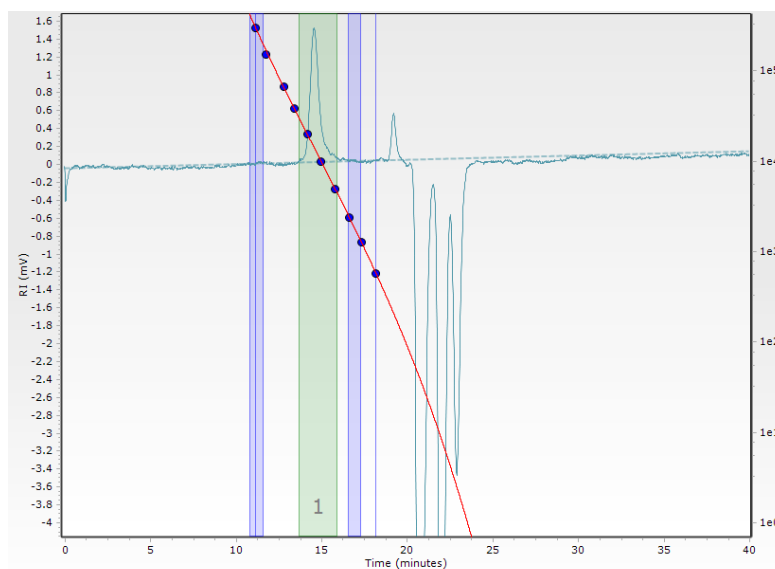


Figure 4.10. Monomodal SEC spectrum of crude PLA obtained from the solution polymerisation of *rac*-LA at RT for 30 min in DCM using $\text{Zn}(\mathbf{1})_2$ $\{[rac\text{-LA}]:[\text{Zn}]:[\text{BnOH}] = 100:1:1\}$ (Table 2, Entry 3 in publication 4). *N.B.* Figure S27 in ESI.

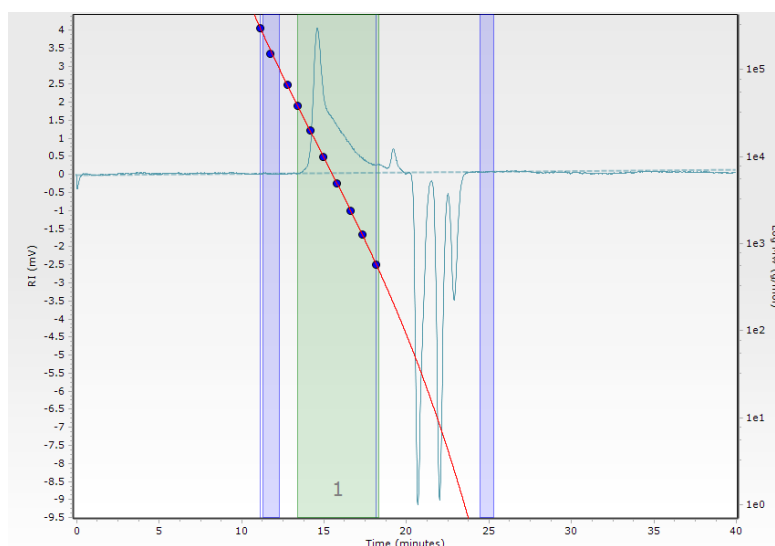


Figure 4.11. Monomodal SEC spectrum of purified PLA obtained from the solution polymerisation of *rac*-LA at RT for 30 min in DCM using $\text{Zn}(\mathbf{1})_2$ $\{[rac\text{-LA}]:[\text{Zn}]:[\text{BnOH}] = 100:1:1\}$ (Table 2, Entry 4 in publication 4). *N.B.* Broad profile indicative of high degree of transesterification following polymer purification. Figure S28 in ESI.

4.2.7.3. Representative homonuclear decoupled ^1H NMR spectrum

Representative spectra are provided in section 2.3.4.3. of Chapter 2.

4.2.7.4. MALDI-ToF spectra

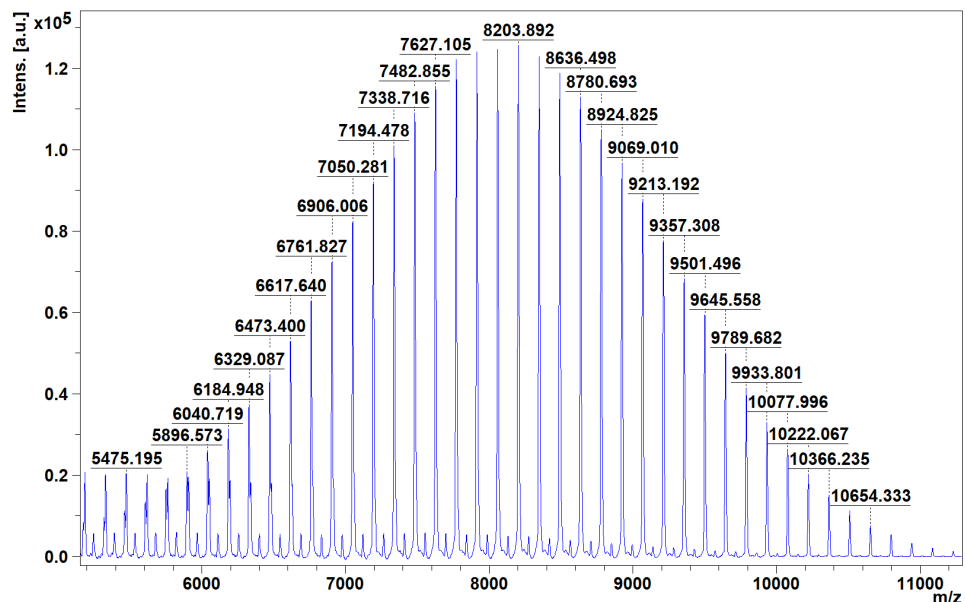


Figure 4.12. MALDI-ToF spectrum of crude PLA obtained from the solution polymerisation of *rac*-LA at RT for 30 min in DCM using $\text{Zn}(\mathbf{1})_2$ $\{[rac\text{-LA}]:[\text{Zn}]:[\text{BnOH}] = 100:1:1\}$ (Table 2, Entry 3 in publication 4). *N.B.* Figure S30 in ESI.

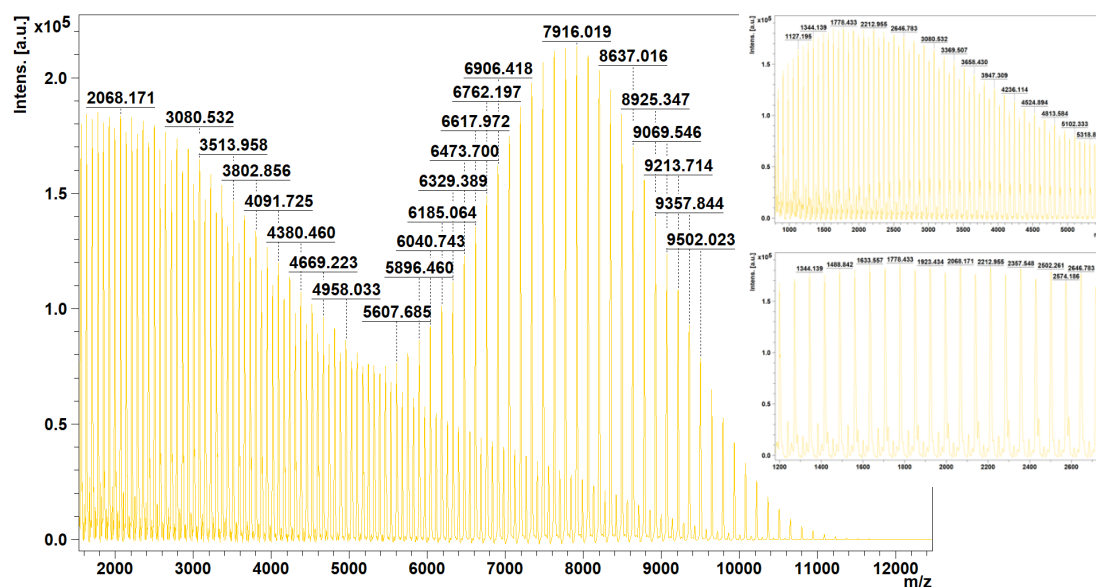


Figure 4.13. MALDI-ToF spectrum of purified PLA obtained from the solution polymerisation of *rac*-LA at RT for 30 min in DCM using $\text{Zn}(\mathbf{1})_2$ $\{[rac\text{-LA}]:[\text{Zn}]:[\text{BnOH}] = 100:1:1\}$ (Table 2, Entry 4 in publication 4). Magnified version of secondary series provided to assist in identifying the repeat unit and end group. *N.B.* Figure S31 in ESI.

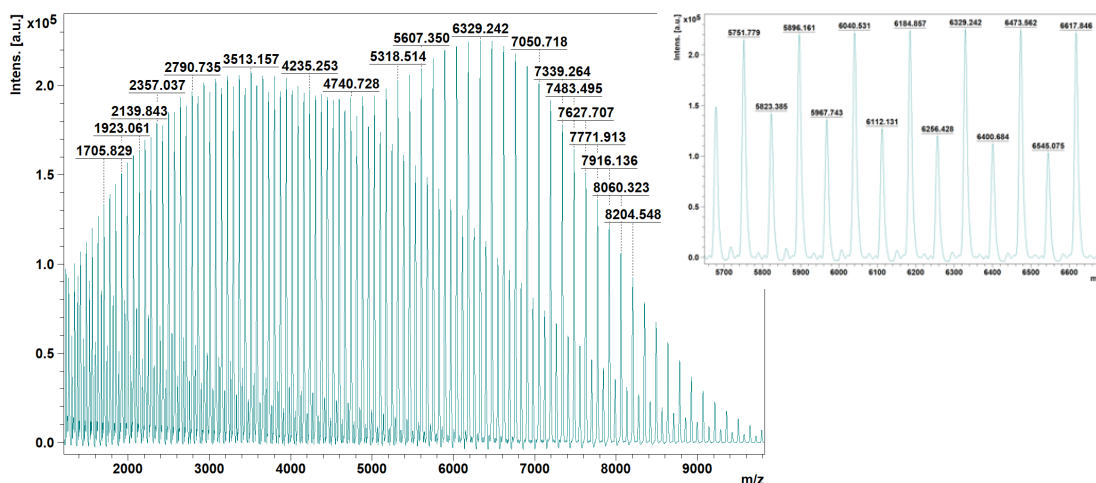


Figure 4.14. MALDI-ToF spectrum of purified PLA obtained from the solution polymerisation of *rac*-LA at 80 °C for 10 min in toluene using $\text{Zn}(\mathbf{1})_2$ $\{[rac\text{-LA}]:[\text{Zn}]:[\text{BnOH}] = 100:1:1\}$. Magnified version of secondary series provided to assist in identifying the repeat unit and end group. *N.B.* Figure S32 in ESI.

4.2.8. Degradation characterisation

4.2.8.1. PLA methanolysis

Representative ^1H NMR spectra of PLA methanolysis are provided in section 3.2.7.1. of Chapter 3.

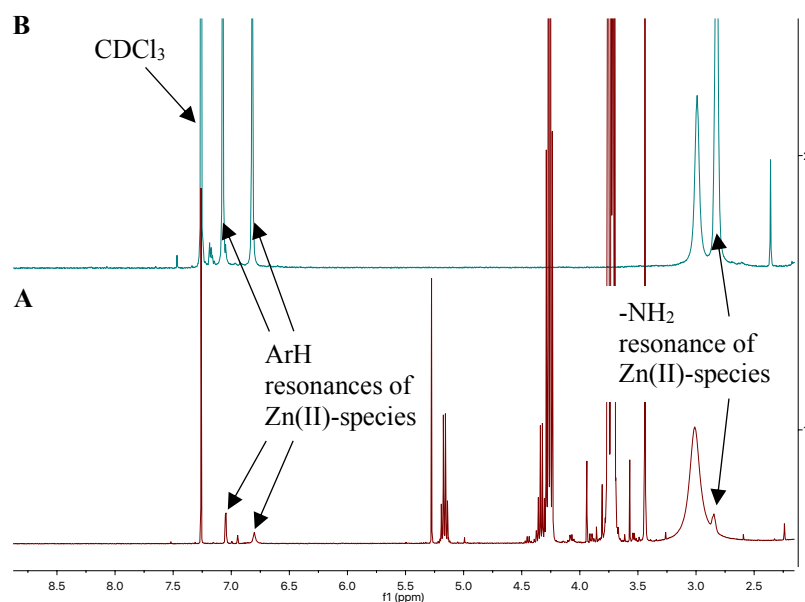


Figure 4.15. Stacked ^1H NMR (CDCl_3 , 400 (A) and 500 (B) MHz) spectra assessing the stability of $\text{Zn}(\mathbf{1})_2$ before and after PLA methanolysis: (A) PLA cup (0.25 g, $M_n = 45,510 \text{ g mol}^{-1}$) degradation into methyl lactate (Me-LA) using $\text{Zn}(\mathbf{1})_2$ (8 wt %, 0.02 g, 0.96 mol% relative to ester linkages) at 50 °C for 1.5 h in THF (solvent removed), and; (B) neat $\text{Zn}(\mathbf{1})_2$. *N.B.* Figure S14 in ESI.

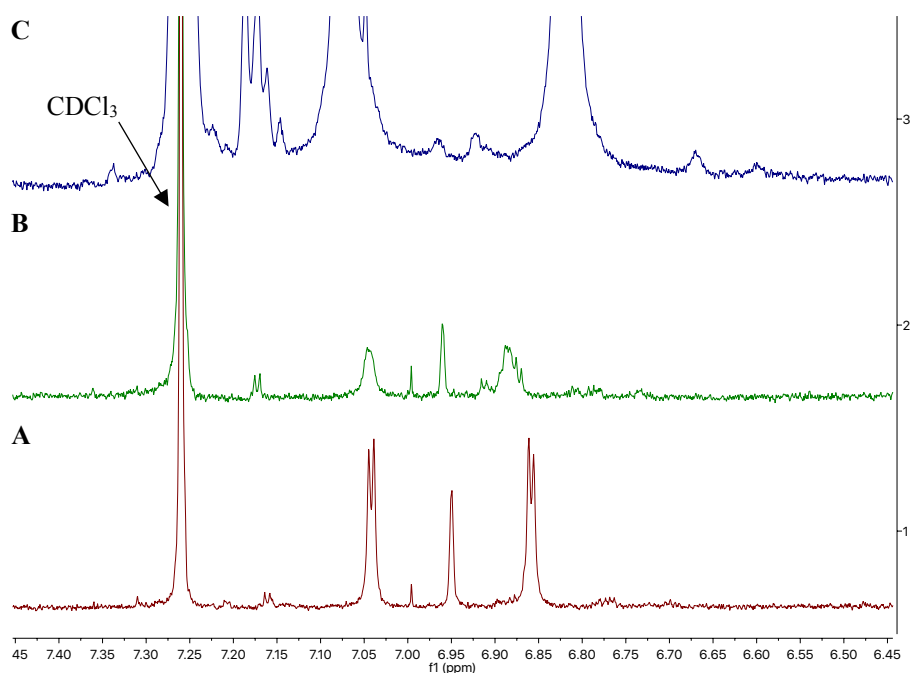


Figure 4.16. Stacked ¹H NMR (CDCl₃, 400 (A, B) and 500 (C) MHz) spectra assessing the stability of Zn(1)₂ before and after PLA methanolysis: PLA cup (0.25 g, $M_n = 45,510 \text{ g mol}^{-1}$) degradation into methyl lactate (Me-LA) using Zn(1)₂ (4 wt %, 0.01 g, 0.48 mol% relative to ester linkages) at 50 °C (A) and 80 °C (B) for 3 h in THF (solvent removed), and; (C) neat Zn(1)₂. *N.B.* Spectra focused on aromatic region to enable a clear comparison between Zn(II)-species. Figure S15 in ESI.

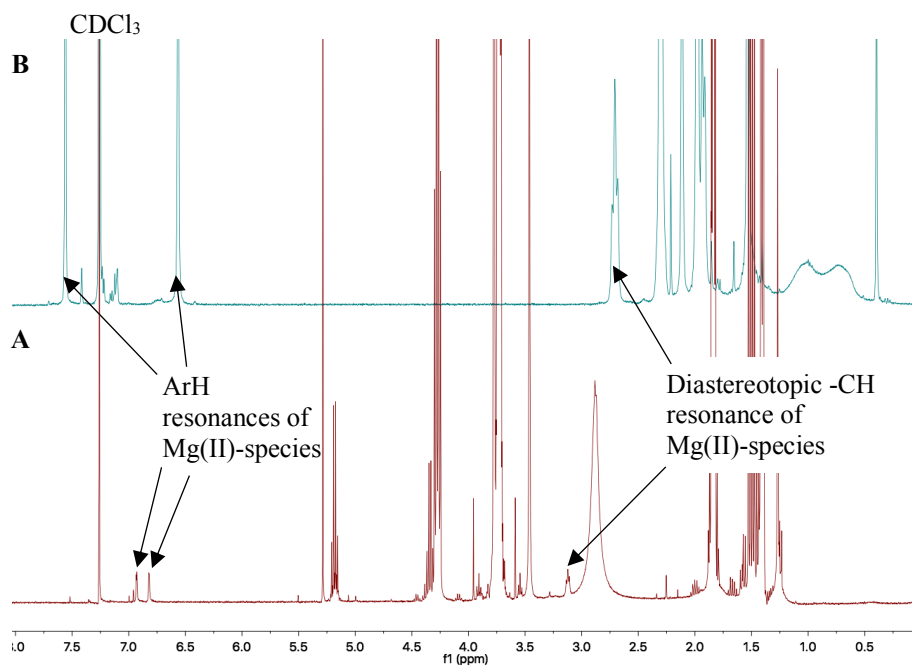


Figure 4.17. Stacked ¹H NMR (CDCl₃, 400 MHz) spectra assessing the stability of Mg(1)₂ before and after PLA methanolysis: (A) PLA cup (0.25 g, $M_n = 45,510 \text{ g mol}^{-1}$) degradation into methyl lactate (Me-LA) using Mg(1)₂ (8 wt %, 0.02 g, 1.0 mol% relative to ester linkages) at 50 °C for 1.5 h in THF (solvent removed), and; (B) neat Mg(1)₂. *N.B.* Figure S16 in ESI.

4.2.8.2. PET glycolysis

A representative ^1H NMR spectrum of BHET is provided in section 3.2.7.2. of Chapter 3.

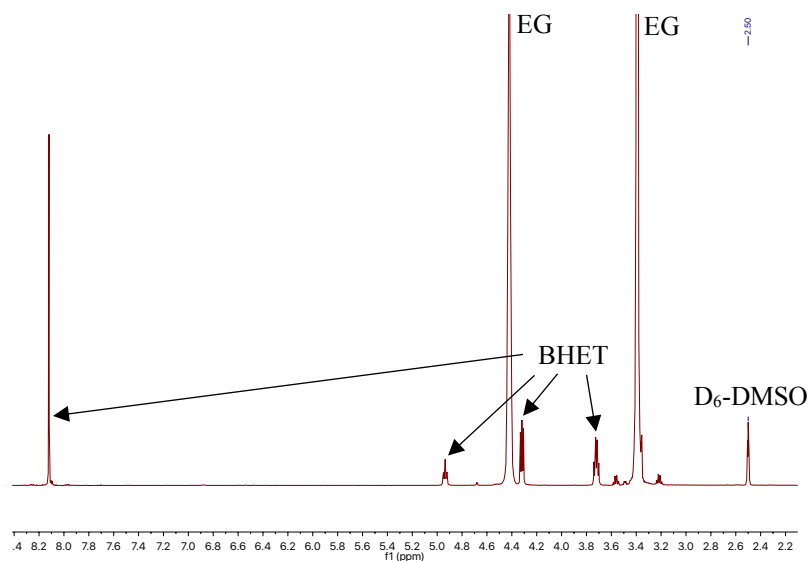


Figure 4.18. ^1H NMR ($\text{D}_6\text{-DMSO}$, 400 MHz) spectrum of bottle-grade PET (0.25 g, $M_n \sim 40,000 \text{ g mol}^{-1}$) glycolysis reaction aliquot (prior to addition of deionised water) using EG (2 mL, 27.5 equivalents relative to ester linkages) at 180 °C for 1 h in the presence of $\text{Zn}(\mathbf{1})_2$ (8 wt%, 0.02 g, 2.5 mol% relative to ester linkages) and PVC (0.025 g, 10 wt%) (Table 7, Entry 4 in publication 4). *N.B.* Figure S18 in ESI.

4.2.8.3. Representative ^1H NMR spectra of PET methanolysis

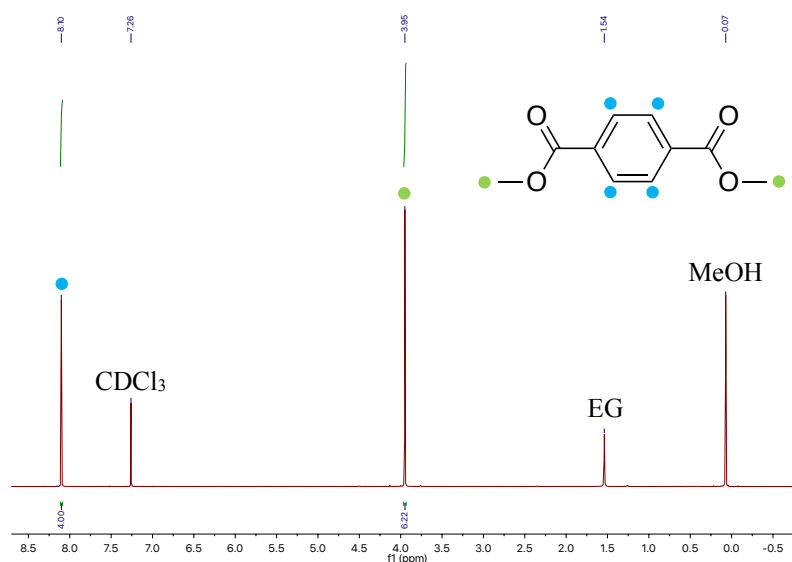


Figure 4.19. ^1H NMR (CDCl_3 , 400 MHz) spectrum of DMT obtained from the methanolysis of bottle-grade PET (0.25 g, $M_n \sim 40,000 \text{ g mol}^{-1}$) at 100 °C in toluene for 48 h in the presence of $\text{Zn}(\mathbf{1})_2$ (8 wt%, 0.02 g, 2.5 mol% relative to ester linkages) (Table 6, Entry 2 in publication 4). *N.B.* Figure S19 in ESI.

4.2.8.4. Representative NMR spectra of PET aminolysis

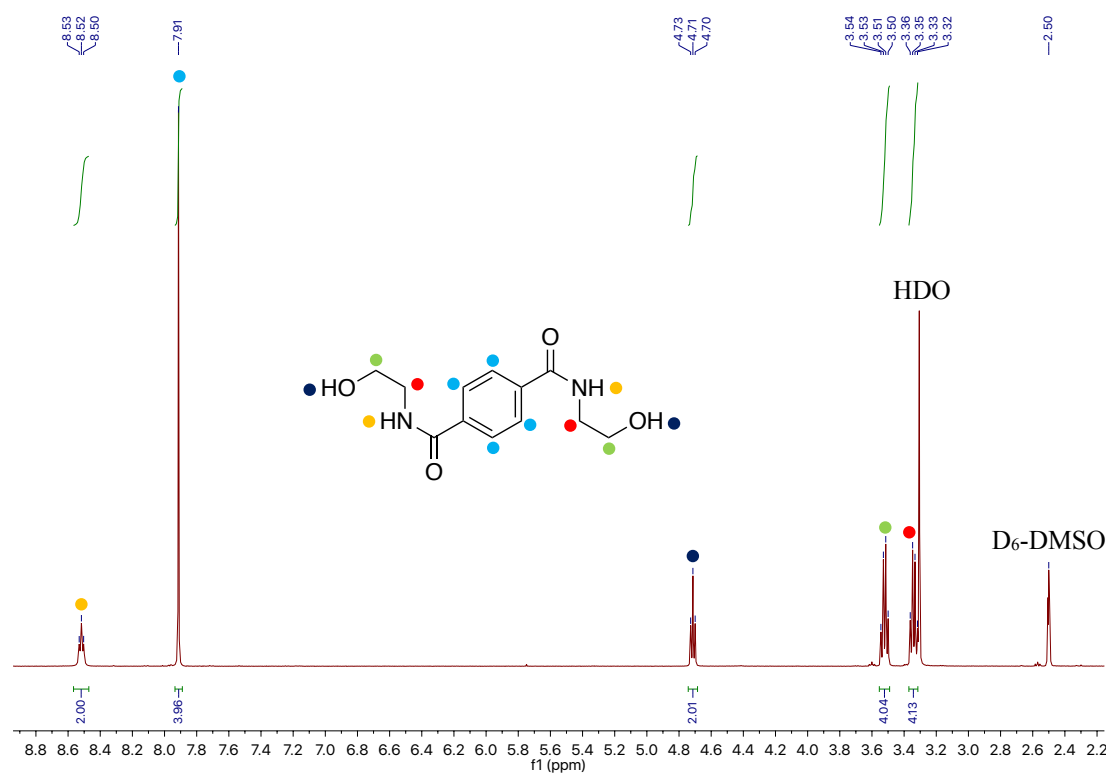


Figure 4.20. ^1H NMR ($\text{D}_6\text{-DMSO}$, 400 MHz) spectrum of BHETA. *N.B.* Figure S22 in ESI.

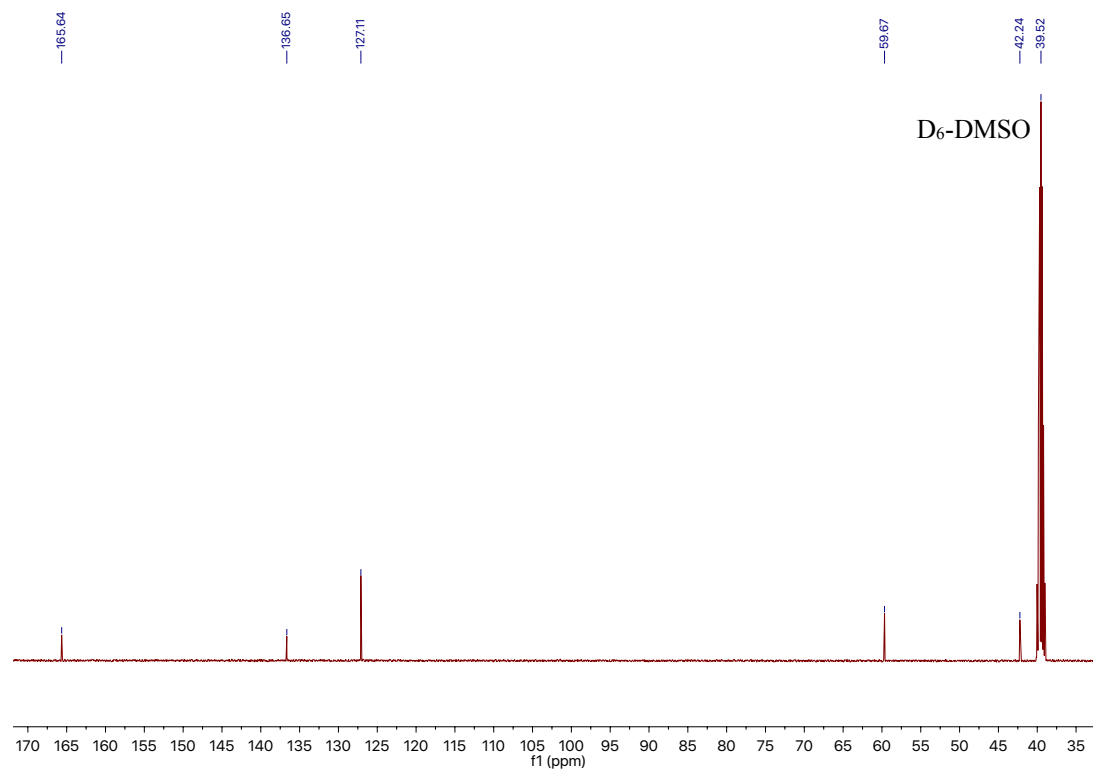


Figure 4.21. $^{13}\text{C}\{^1\text{H}\}$ NMR ($\text{D}_6\text{-DMSO}$, 125 MHz) spectrum of BHETA. *N.B.* Figure S23 in ESI.

4.2.8.5. Representative ^1H NMR spectrum of PCL methanolysis

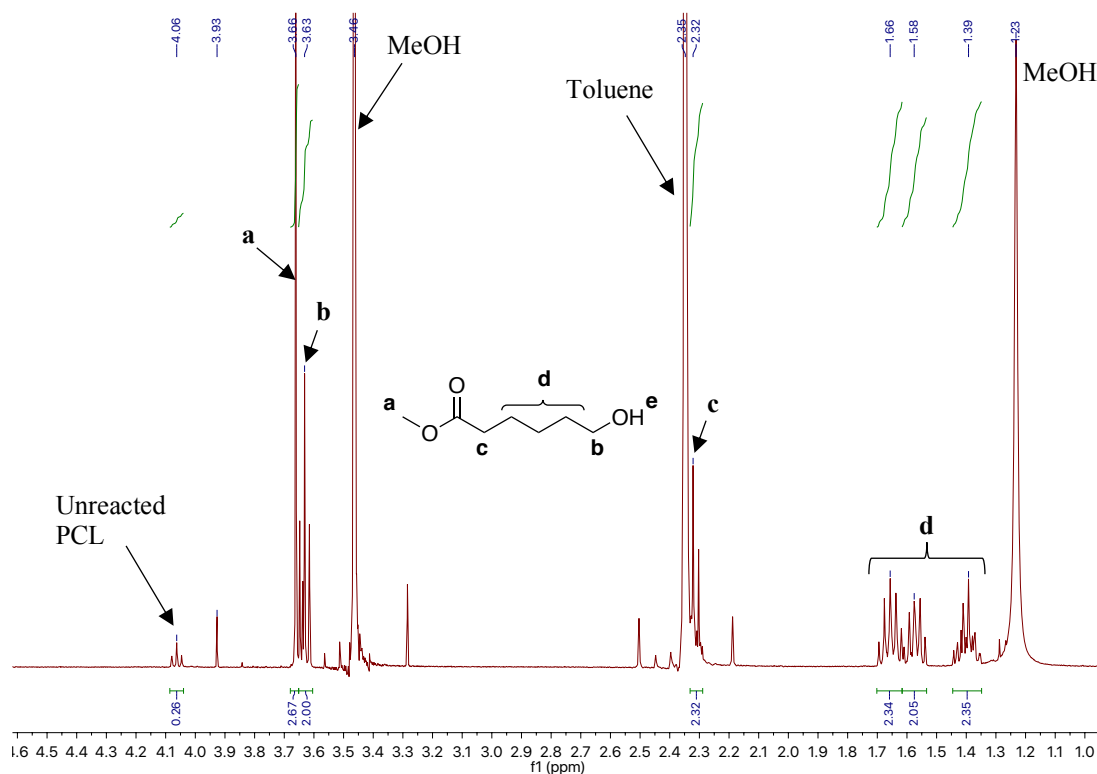


Figure 4.22. ^1H NMR (CDCl_3 , 400 MHz) spectrum of PCL pellet (0.25 g, $M_n = 45,000 \text{ g mol}^{-1}$) methanolysis reaction aliquot using $\text{Zn}(\mathbf{1})_2$ (8 wt%, 0.02 g, 1.5 mol% relative to ester linkages) after 4 h at 100 °C in toluene (Table 9, Entry 2 in publication 4). Relative peak area (RPA) of resonance (b) normalised to 2 to enable comparison with unreacted PCL to determine conversion to methyl 6-hydroxyhexanoate. *N.B.* Unaccounted for -OH resonance (e), likely due to rapid proton exchange in solution. Figure S26 in ESI.

4.2.9. Degradation plots

4.2.9.1. Representative degradation plots for PLA methanolysis

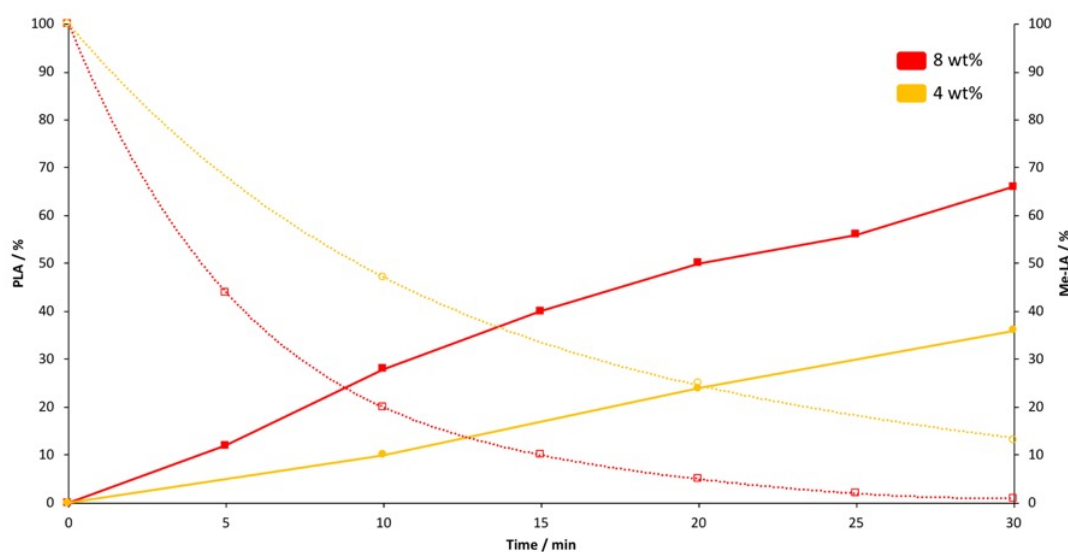


Figure 4.23. PLA cup (0.25 g, $M_n = 45,510 \text{ g mol}^{-1}$) degradation plot of conversion (PLA and Me-LA) vs time using Zn(1)_2 at 4 and 8 wt% (0.01 – 0.02 g, 0.48 – 0.96 mol% relative to ester linkages) in THF at 50 °C. *N.B.* Dashed lines refer to PLA consumption (primary axis), whilst bold lines refer to Me-LA yield (secondary axis). Figure S33 in ESI.

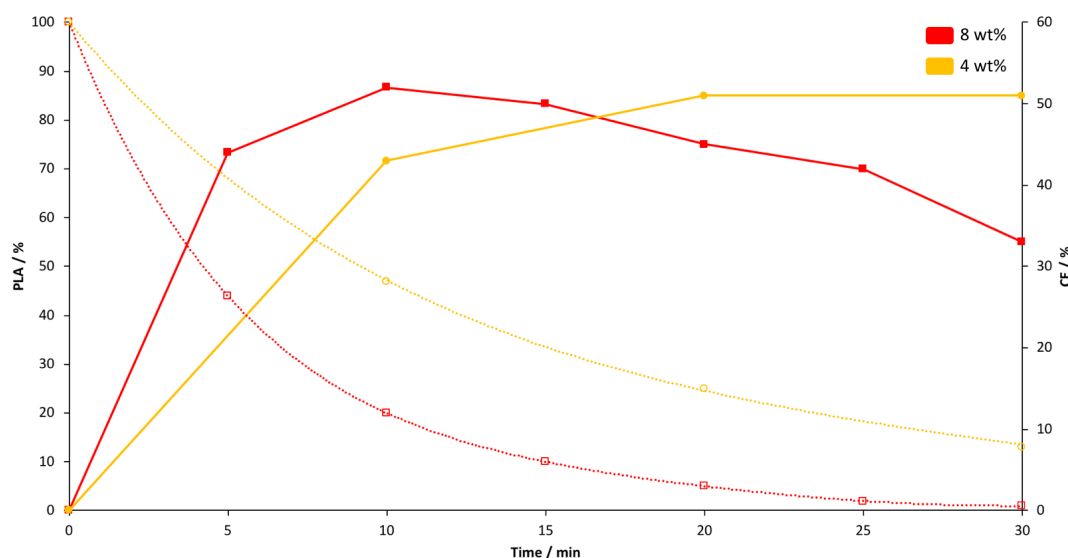


Figure 4.24. PLA cup (0.25 g, $M_n = 45,510 \text{ g mol}^{-1}$) degradation plot of conversion (PLA and CE) vs time using Zn(1)_2 at 4 and 8 wt% (0.01 – 0.02 g, 0.48 – 0.96 mol% relative to ester linkages) in THF at 50 °C. *N.B.* Dashed lines refer to PLA consumption (primary axis), whilst bold lines refer to CE yield (secondary axis). Figure S34 in ESI.

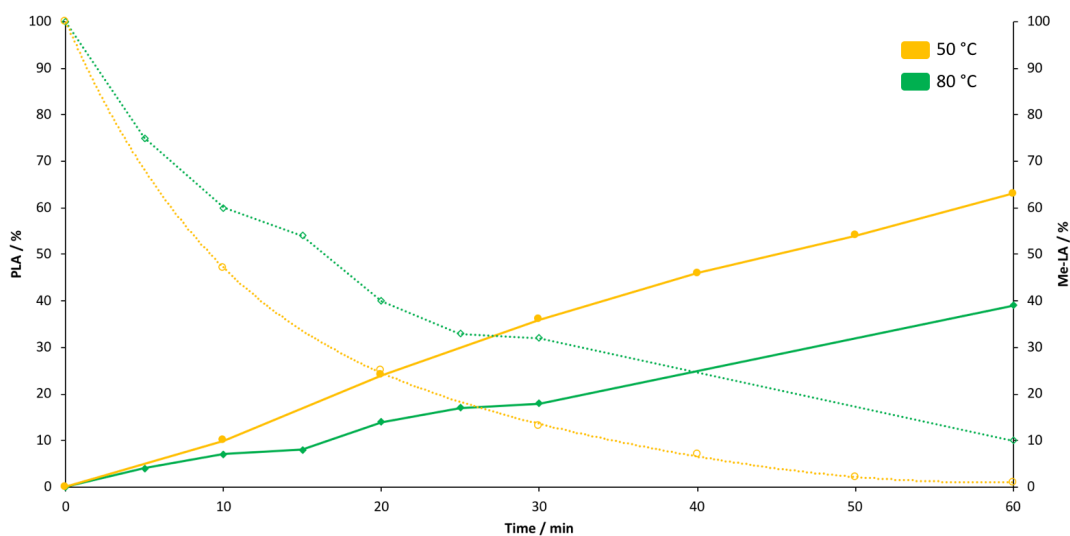


Figure 4.25. PLA cup (0.25 g, $M_n = 45,510 \text{ g mol}^{-1}$) degradation plot of conversion (PLA and Me-LA) vs time using $\text{Zn}(\mathbf{1})_2$ (4 wt%, 0.01 g, 0.48 mol% relative to ester linkages) in THF at 50 and 80 °C. *N.B.* Dashed lines refer to PLA consumption (primary axis), whilst bold lines refer to Me-LA yield (secondary axis). Figure S35 in ESI.

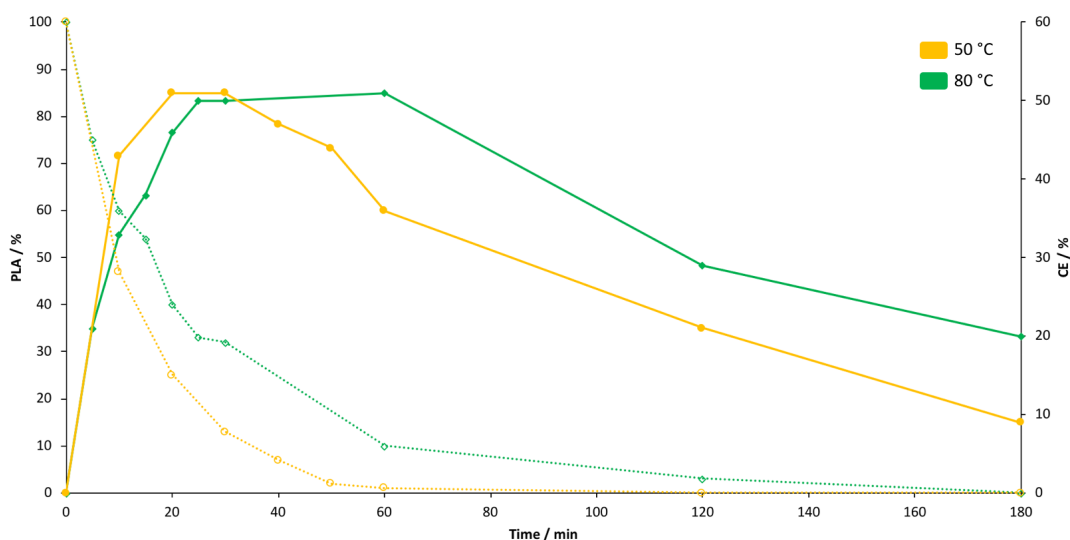


Figure 4.26. PLA cup (0.25 g, $M_n = 45,510 \text{ g mol}^{-1}$) degradation plot of conversion (PLA and CE) vs time using $\text{Zn}(\mathbf{1})_2$ (4 wt%, 0.01 g, 0.48 mol% relative to ester linkages) in THF at 50 and 80 °C. *N.B.* Dashed lines refer to PLA consumption (primary axis), whilst bold lines refer to CE yield (secondary axis). Figure S36 in ESI.

4.2.9.2. Comparative catalyst performance plot for PET glycolysis

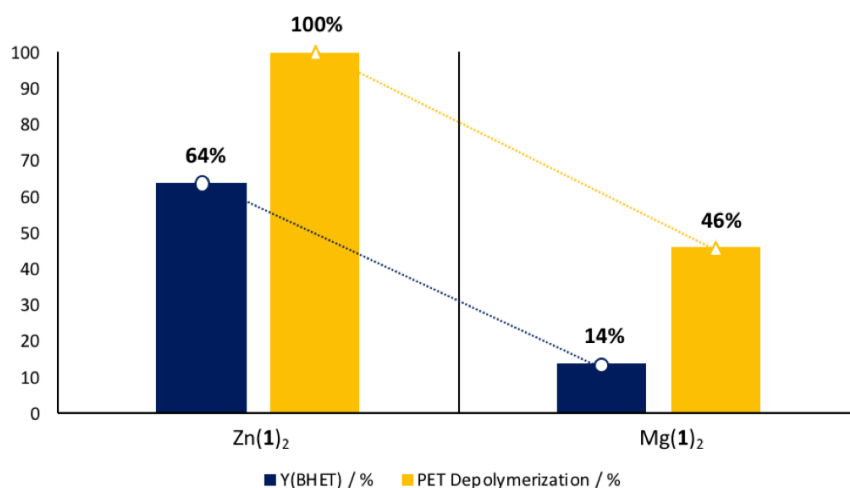


Figure 4.27. Comparative plot of Zn(1)₂ and Mg(1)₂ performance for PET glycolysis under optimal conditions. Reaction conditions: 1 h at 180 °C, bottle-grade PET (0.25 g, $M_n \sim 40,000$ g mol⁻¹), 20.6 equivalents (1.5 mL) of EG (relative to ester linkages), Zn(1)₂ = 8 wt% (0.02 g, 2.5 mol% relative to ester linkages), Mg(1)₂ = 8 wt% (0.02 g, 2.7 mol% relative to ester linkages). *N.B.* Y_{BHET} refers to the isolated yield of pure BHET recrystallised from deionised H₂O, followed by drying at 90 °C for 3 h *in vacuo*. Figure S45 in ESI.

4.2.10. Crystallographic data

Table 4.1. Crystallographic data of Si-based Zn(1)₂ derivative. *N.B.* Table S1 in ESI.

Compound reference	Si-based Zn(1) ₂ derivative
Empirical formula	C ₁₀₄ H ₁₇₆ N ₈ O ₁₄ Si ₆ Zn ₆
Formula Mass	2323.28
Crystal system	Triclinic
<i>a</i> /Å	13.6831(4)
<i>b</i> /Å	14.4983(3)
<i>c</i> /Å	16.1583(4)
<i>α</i> /°	86.515(2)
<i>β</i> /°	79.139(2)
<i>γ</i> /°	70.937(2)
Unit cell volume/Å ³	2975.45(14)
Temperature/K	150.00(10)
Space group	P-1
No. of formula units per unit cell, <i>Z</i>	1
Radiation type	Cu Kα
No. of reflections measured	45823
No. of independent reflections	11427
<i>R</i> _{int}	0.0492
Final <i>R</i> _I values (<i>I</i> > 2σ(<i>I</i>))	0.0434
Final <i>wR</i> (<i>F</i> ²) values (<i>I</i> > 2σ(<i>I</i>))	0.1142
Final <i>R</i> _I values (all data)	0.0537
Final <i>wR</i> (<i>F</i> ²) values (all data)	0.1202

Table 4.2. Selected bond lengths for Si-based Zn(1)₂ derivative. *N.B.* Table S2 in ESI.

Init.	Bond	Bond length / Å
Si-based Zn(1) ₂ derivative	Zn(1)-N(1), Zn(1)-N(2), Zn(1)-O(1)	2.229(2), 2.096(3), 1.9912(19)

Table 4.3. Selected bond angles for Si-based Zn(1)₂ derivative with calculated τ₅ value for Zn(1) centre. Ideal square pyramidal geometry corresponds to τ₅ = 0. *N.B.* Table S3 in ESI.

Init.	Bond	Bond angle / °	τ ₅
Si-based Zn(1) ₂ derivative	N(1)-Zn(1)-O(1), N(2)-Zn(1)-O(1)	80.31(8), 104.51(10)	0.14

4.3. Post-publication Commentary

Whilst developments pertaining to discrete homogeneous metal-mediated transesterification for PET and PCL remain limited, a number of key advancements have been reported for PLA.

Notably, Santulli *et al.*^[14] recently reported a simple and highly active heteroleptic Zn(II)-complex (**29**) bearing a tridentate {ONN} Schiff-base-type ligand for PLA methanolysis (Figure 4.28). Indeed, a range of isotactic PLA samples of varying molecular weights ($M_n = 14,000 - 90,000 \text{ g mol}^{-1}$) were degraded, observing quantitative consumption within 1 h in THF under ambient conditions $\{[\text{polyester linkages}]:[\text{Zn}] = 60, n_{\text{ester}}:n_{\text{MeOH}} = 1:6, k_{\text{app}} = 2.3 \text{ h}^{-1}\}$. Post-consumer PLA products (*e.g.* a cup and 3D printing filament) were also degraded, generally observing longer reaction times to achieve comparably high Me-LA yields (up to 100% for a PLA cup within 4 h). The rate of PLA methanolysis was shown to be independent of M_n in solution, indicating degradation proceeds *via* a random chain scission mechanism, consistent with observations discussed in publication 4. However, polymer tacticity was shown to influence degradation rate, which proceeded more slowly for atactic relative to isotactic samples owing to the formation of different diastereomer zinc species. Conversely, Zn(**1**)₂ exhibited comparable PLA methanolysis performance irrespective of polymer tacticity, highlighting both catalyst robustness and versatility. Promisingly, good process efficiency was retained on exposure to air and under solvent-free conditions, further highlighting the systems green credentials (*e.g.* process ease and waste reduction).

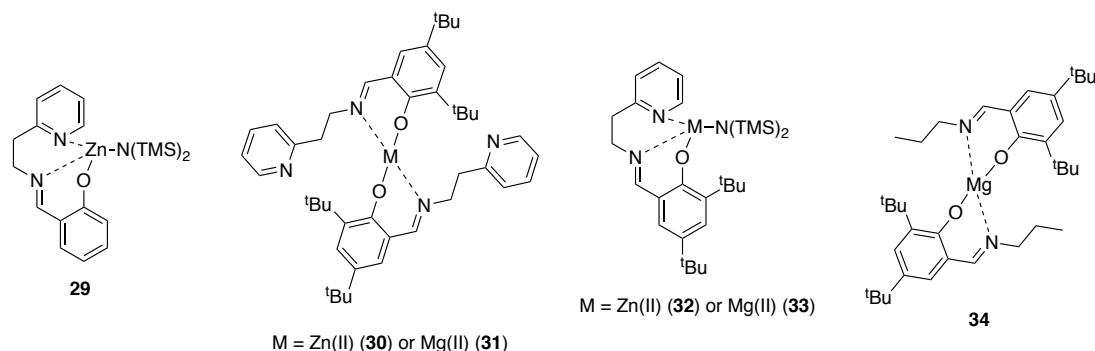
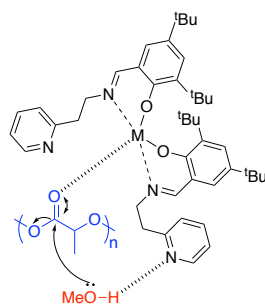


Figure 4.28. A series of Zn(II)- and Mg(II)-complexes reported by Mazzeo and co-workers that facilitate rapid PLA methanolysis at room temperature.^[14,15]

Recently, work within this group has focused on exploring a tBu-substituted variation of the aforementioned tridentate {ONN} ligand to generate a series of homoleptic and heteroleptic Zn(II)- (**30,32**) and Mg(II)-complexes (**31,33**) (Figure 4.28).^[15] For a commercial PLLA sample, complex **32** exhibited comparable activity to **29** under identical conditions. Conversely, **30** and **31** required prolonged reaction times to be appreciably active ($X_{\text{int}} = 83 - 86\%$ and $Y_{\text{Me-LA}} = 21 - 29\%$ within 7 h), although enhanced performance was observed at 65

°C (up to 59% Me-LA yield within 15 min using **30**), contrasting findings in publication 4. Interestingly, **33** was shown to be completely inactive, which was attributed to poor catalyst tolerance. Such reactivity trends contrast those discussed for Zn(**1**)₂ and Mg(**1**)₂. Moreover, a Mg(II)-analogue (**34**) inspired by recent work from McKeown *et al.*^[6] was also shown to be inactive, highlighting the importance of the pendant pyridine donor. Indeed, it is proposed the pendant pyridine arm potentially assists proton-transfer *via* activation of the external nucleophile, as depicted in Scheme 4.1. Pendant amine groups in ancillary ligands have previously been shown to adopt a similar role in polymerisation reactions operating *via* a ligand-assisted activated monomer mechanism.^[6,16] Solvent-free degradations were found to proceed through progressive erosion of the polymer initiated at the chain-end, consistent with **29**. Additionally, both studies fail to investigate process efficiency and selectivity using mixed waste feeds despite a clear industry need.



Scheme 4.1. Ligand-assisted nucleophilic activation mechanism proposed by Mazzeo and co-workers for PLA methanolysis mediated by either **30** or **31**.^[15]

Despite such progress, examples of discrete metal-mediated PLA transesterification remain rare, particularly for metals beyond Zn(II), with work in publication 4 highlighting the potential of Mg(II). However, the field is garnering increasing momentum, evidenced by recent work from Hermann *et al.*^[17] (**35–36**) and D’Alterio *et al.*^[18] (**37**), which highlight recent efforts devoted to diversifying ligand scope (Figure 4.29). Indeed, such catalysts were found to exhibit inferior activity ($k_{app} = 0.037 - 0.059 \text{ min}^{-1}$) relative to Mg(**1**)₂ and Zn(**1**)₂ under comparably mild reaction conditions in THF $\{m_{PLLA} = 0.25 \text{ g}, V_{THF}:V_{MeOH} = 4:1, n_{MeOH}:n_{ester} = 7:1, 1 \text{ mol}\% \text{ catalyst (relative to ester linkages), } 40 - 60 \text{ }^\circ\text{C}\}$.

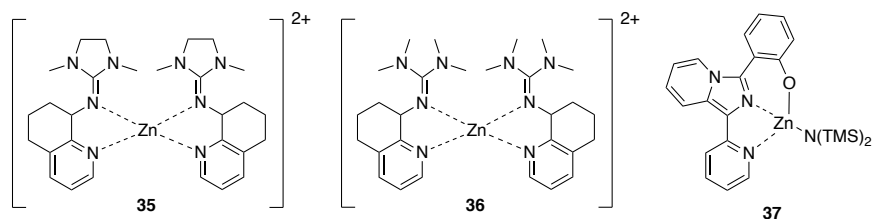


Figure 4.29. Zn(II)-complexes reported by Hermann *et al.*^[17] (**35–36**) and D’Alterio *et al.*^[18] (**37**) active for PLA methanolysis.

Furthermore, chemical recycling need not be limited to small molecule recovery. Indeed, Wang *et al.*^[19] recently reported a ‘DE-RE polymerisation’ strategy for commercial PLA samples of varying molecular weight ($M_n = 29,800 - 63,300 \text{ g mol}^{-1}$) and dispersity ($D = 1.74 - 2.70$). Specifically, PLA could be controllably transesterified in the presence of $\text{Zn}(\text{HMDS})_2$ and MeOH to a pre-determined molecular weight. By virtue of the degraded polymer possessing chain growth activity, monomer could be re-introduced to recover the polymer chain length, which proceeded uniformly due to a difference in chain propagation rates of repolymerisation. This work creates new opportunities for ‘polymer to polymer’ recycling, circumventing often costly and undesirable separation processes, whilst also demonstrating a clear opportunity to develop both highly active and controlled systems.

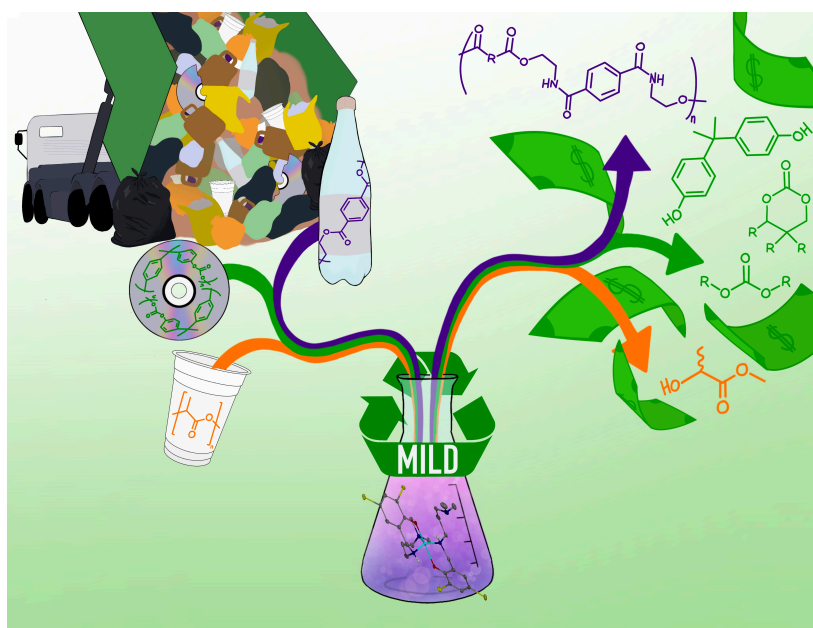
4.4. References

- [1] C. M. Thomas, *Chem. Soc. Rev.* **2010**, *39*, 165–173.
- [2] O. Santoro, X. Zhang, C. Redshaw, *Catalysts* **2020**, *10*, 800.
- [3] K. C. Gupta, A K. Sutar, *Coord. Chem. Rev.* **2008**, *252*, 1420–1450.
- [4] P. G. Cozzi, *Chem. Soc. Rev.* **2004**, *33*, 410–421.
- [5] L. A. Román-Ramírez, P. McKeown, M. D. Jones, J. Wood, *ACS Catal.* **2019**, *9*, 409–416.
- [6] P. McKeown, L. A. Román-Ramírez, S. Bates, J. Wood, M. D. Jones, *ChemSusChem* **2019**, *12*, 5233–5238.
- [7] P. McKeown, S. N. McCormick, M. F. Mahon, M. D. Jones, *Polym. Chem.* **2018**, *9*, 5339–5347.
- [8] C. K. Williams, L. E. Breyfogle, S. K. Choi, W. Nam, V. G. Young, M. A. Hillmyer, W. B. Tolman, *J. Am. Chem. Soc.* **2003**, *125*, 11350–11359.
- [9] A. Rahimi, J. M. García, *Nat. Chem. Rev.* **2017**, *1*, 0046.
- [10] C. Jehanno, J. W. Alty, M. Roosen, S. De Meester, A. P. Dove, E. Y.-X. Chen, F. A. Leibfarth, H. Sardon, *Nature* **2022**, *603*, 803–814.
- [11] L. D. Ellis, N. A. Rorrer, K. P. Sullivan, M. Otto, J. E. McGeehan, Y. Román-Leshkov, N. Wierckx, G. T. Beckham, *Nat. Catal.* **2021**, *4*, 539–556.
- [12] K. Fukushima, J. M. Lecuyer, D. S. Wei, H. W. Horn, G. O. Jones, H. A. Al-Megren, A. M. Alabdulrahman, F. D. Alsewailem, M. A. McNeil, J. E. Rice, J. L. Hedrick, *Polym. Chem.* **2013**, *4*, 1610–1616.
- [13] P. McKeown, M. Kamran, M. G. Davidson, M. D. Jones, L. A. Román-Ramírez, J. Wood, *Green Chem.* **2020**, *22*, 3721–3726.
- [14] F. Santulli, M. Lamberti, M. Mazzeo, *ChemSusChem* **2021**, *14*, 5470–5475.
- [15] F. Santulli, G. Gravina, M. Lamberti, C. Tedesco, M. Mazzeo, *Mol. Catal.* **2022**, *528*, 112480.
- [16] B. Liu, T. Roisnel, L. Maron, J. F. Carpentier, Y. Sarazin, *Chem. Eur. J.* **2013**, *19*, 3986–3994.
- [17] A. Hermann, T. Becker, M. A. Schäfer, A. Hoffmann, S. Herres-Pawlis, *ChemSusChem* **2022**, e202201075.
- [18] M. C. D’Alterio, I. D’Auria, L. Gaeta, C. Tedesco, S. Brenna, C. Pellecchia, *Macromolecules* **2022**, *55*, 5115–5122.
- [19] R. Yang, G. Xu, B. Dong, H. Hou, Q. Wang, *Macromolecules* **2022**, *55*, 1726–1735.

Chapter 5.

Metal-mediated Chemical Upcycling Strategies for Commercial Polyester and Polycarbonate Waste

Publication 5. Versatile Chemical Recycling Strategies: Value-Added Chemicals from Polyester and Polycarbonate Waste



Acknowledgement: The work presented in this chapter has been published in the journal ‘*ChemSusChem*’, volume 15, issue 8, e202200255 and is reproduced with the permission of Wiley-VCH. The electronic supporting information (ESI) has been amended into a supporting experimental section for clarity.

5. Preamble

Zn(II)- and Mg(II)-complexes based on a simple tridentate {ONN} ligand were found to be active for the degradation of various commercial polyesters in Chapter 4, noting high activity for PLA methanolysis under mild conditions and the importance of H-bond donors. Furthermore, ligand flexibility was previously shown in Chapter 1 to dramatically influence the activity of Zn(II)-complexes for polyester degradation.^[1,2] Consequently, our attention shifted to combining such adventitious attributes into a ligand design that is both easy to synthesise and scalable.

Initial work focused on preparation of the propylene analogue of the ligand exploited in Chapter 4 (1H), however, synthesis attempts proved unsuccessful. However, it was swiftly realised the monoanionic half-salan equivalent would not only encompass the aforementioned desirable design features, but also provide greater scope for ligand functionality, and thus catalyst fine tuning. Indeed, half-salan ligands remain vastly underexplored compared to their salan counterparts, which have been widely exploited in lactide polymerisation.^[3-7] Moreover, McKeown *et al.*^[1,2] have previously demonstrated comparable Zn(II)-half-salen complexes to facilitate mild and rapid PLA alcoholysis, highlighting the untapped potential of such systems.

Whilst polyesters have been the primary focus for chemical recycling applications in Chapters 3 and 4, it was postulated whether such processes were amenable to other polymer classes that possess cleavable linkages. Consequently, polycarbonates were identified as a key area of opportunity for sustainable and metal-mediated solutions, with poly(bisphenol A carbonate) (BPA-PC) being the market dominant product.^[8] As such, Chapter 5 aims to provide an overview for the chemical recycling of BPA-PC through a mini-review. This is comparable to that presented for PLA and PET in Chapter 1, with a particular focus on organocatalysed and metal-mediated transesterification (*e.g.* alcoholysis and glycolysis), which is most pertinent herein.

In this chapter, Zn(II)-half-salan complexes are shown to facilitate the mild and selective degradation of various commercial polyesters and polycarbonates into value-added products (*e.g.* green solvents and chemical building blocks). The first example of discrete metal-mediated BPA-PC methanolysis being appreciably active at room temperature is demonstrated, with further kinetic analysis confirming such catalysts to be the fastest reported to date. Process efficiency was found to be dependent on a number of parameters including temperature, $n_{\text{carbonate}}:n_{\text{MeOH}}$, catalyst loading and reaction time. Inspired by recent work from Sardon and co-workers, a completely circular upcycling approach for bottle-grade PET waste is demonstrated through the production of several renewable poly(ester-amide)s (PEAs), which exhibited excellent thermal properties.^[9]

5.1. Introduction

5.1.1. Polycarbonates

Polycarbonates are a class of thermoplastic polymer generally revered for their high thermal resistance, excellent mechanical properties and good optical clarity. Consequently, such materials lend themselves to a wide range of applications, notably in the engineering and construction sectors, for example in optical media storage, electronics and automobiles.^[8,10,11] Presently, PC production equates to *ca.* 5 million tonnes p/a, with poly(bisphenol A carbonate) (BPA-PC) (Figure 5.1) being the most widely used, which will form the primary focus of this introduction.^[8] Indeed, PC production is projected to increase to *ca.* 8 million tonnes p/a by 2024, equating to a global market value of *ca.* \$25 billion.^[12]

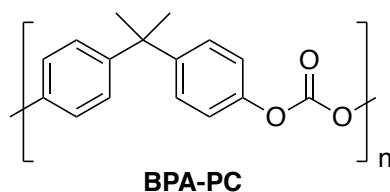
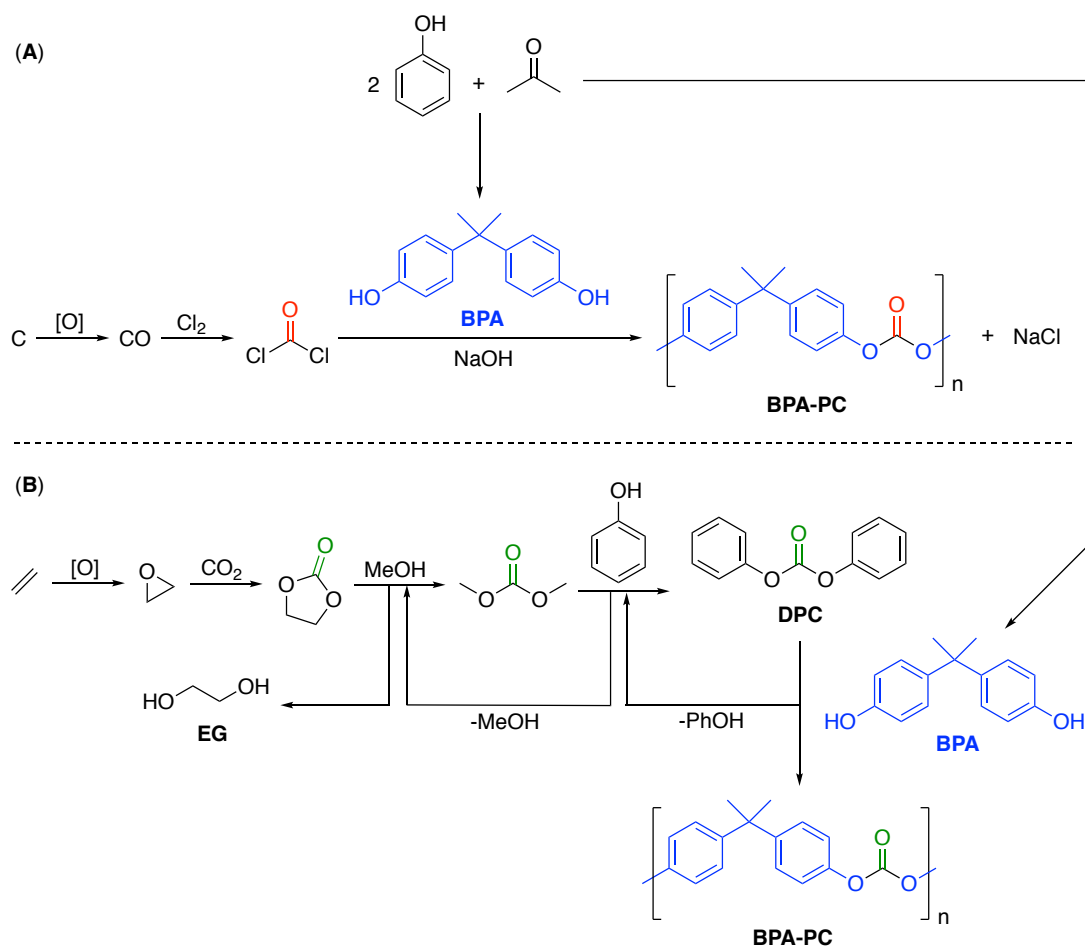


Figure 5.1. Polymeric structure of BPA-PC.

5.1.1.1. Industrial production of BPA-PC

BPA-PC was first commercialised in the 1950s by Bayer and General Electric concurrently and can be produced *via* two distinct processes (Scheme 5.1).^[8,13] Industrially, the interfacial process (Scheme 5.1, **A**) has been the most widely used production method. This process relies on the reaction of phosgene with the sodium salt of bisphenol A (BPA), which reside in the organic (DCM) and aqueous phase, respectively, with polymerisation proceeding at the phase interface. However, this method is limited by safety concerns relating to the use of toxic reagents and solvents. Additionally, energy intensive product purification (*e.g.* solvent residue removal) and the treatment of chemical waste (*e.g.* saline water and organics) post-polymerisation incur significant additional process costs. Indeed, such features are clearly undesirable in accordance to ‘The 12 Principles of Green Chemistry’ as outlined previously by Warner and Anastas.^[14] Such concerns are remedied through the use of a melt process (Scheme 5.1, **B**) developed by Asahi Kasei.^[8,15,16] Specifically, phosgene is substituted for diphenyl carbonate (DPC), which undergoes rapid transesterification in the presence of BPA. Phenol is liberated as a by-product, which can be removed under reduced pressures, shifting the product equilibrium towards BPA-PC. Polymerisation proceeds in the melt, negating the need for a solvent, which are traditionally a significant source of waste in industry.^[17,18] Additionally, all waste by-products are either recycled (PhOH and MeOH) or redirected to

another process (EG). Crucially, this method is also economically competitive with the traditional interfacial process. Consequently, most recent production capacity expansion has relied on the use of the melt process.^[8]



Scheme 5.1. Commercial BPA-PC production methods: interfacial (A) and melt (B) processing.

Critically, both processes rely on chemicals derived from a depleting fossil reserve. However, recent attention in the literature has been devoted to the synthesis of renewable polycarbonate alternatives, exemplified by the ring-opening copolymerisation (ROCOP) of various bio-based epoxide monomers with CO₂.^[19-22] Specifically, bio-based aliphatic polycarbonates (APCs) have seen a re-emergence since they possess, in some instances, intrinsic biocompatibility/biodegradability and superior material properties relative to their conventional petroleum-based counterparts. Consequently, such materials lend themselves to applications beyond traditional BPA-PC materials, notably within the biomedical sector (*e.g.* drug delivery).^[10,23-26]

5.1.1.2. Toxicity of BPA

BPA was first developed as a synthetic estrogen in the 1890s and is now one of the highest volume chemicals produced worldwide.^[27,28] Global production exceeded 6 million tonnes in

2017 and the market is projected to have a compound annual growth rate of *ca.* 6% between 2019 – 2024. Indeed, polycarbonate and epoxies manufacturing accounted for *ca.* 68% and 30% of BPA production capacity demand, respectively, in 2019.^[28] However, BPA has recently been subject to intense scrutiny due to it being a potentially damaging xenostrogenic pollutant.^[8,27-32] Consequently, the use of BPA-PC has been banned in numerous countries, notably in food packaging and baby care applications.^[33,34] A number of BPA analogues have been reported to address such concerns, which are depicted in Figure 5.2 below. However, such analogues are neither considered safer nor renewable, although research into bio-based alternatives remains an ongoing endeavour.^[28,35,36]

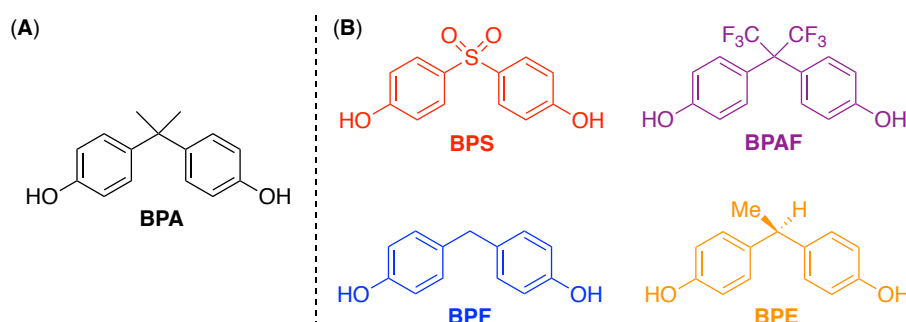


Figure 5.2. Structure of BPA (A) and bisphenol analogues (B).

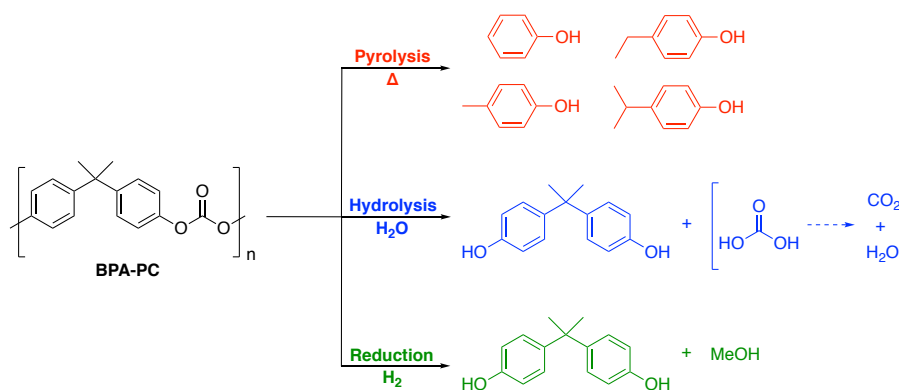
5.1.1.3. End-of-life (EoL) options

Toxicity concerns associated with BPA serve to further exacerbate issues relating to BPA-PC waste management within a linear plastics economy. Indeed, landfill is not a viable option due to the slow release of BPA as BPA-PC degrades, which poses a hazard to both the natural environment and human health. Alarmingly, however, landfill and incineration remain the primary methods of choice for BPA-PC waste management, which fail to address such concerns and align with a wasteful linear model. Whilst mechanical recycling aligns with a circular economy approach, the method is not impervious to BPA leakage and eventual material downcycling inevitably directs such waste towards either landfill or energy recovery.^[8,10] In addition to developing environmentally benign alternatives for BPA, chemical recycling represents a promising solution to such mounting environmental concerns.

5.1.2. Chemical recycling of BPA-PC

Whilst chemical recycling has the potential to address such crucial challenges within the field, notably regarding safe and responsible BPA management, the area has received surprisingly underwhelming attention within the last 10 years.^[8,10-12] This is particularly concerning given the anticipated increase in BPA-PC demand noted in section 5.1.1. However, a diverse range of BPA-PC recycling strategies have been reported, including pyrolysis, hydrolysis and

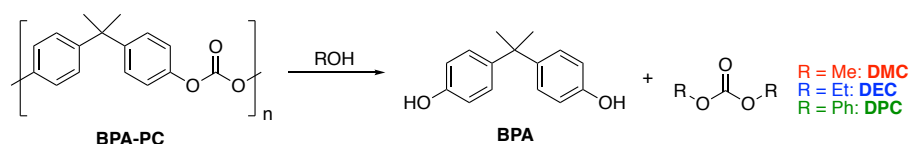
reduction (Scheme 5.2), which have been comprehensively reviewed in the literature.^[8,11,37] Traditionally, such systems exhibit comparable limitations to those discussed for PLA and PET in Chapter 1 (e.g. high temperature and pressure regimes). Furthermore, such transformations fall beyond the scope of this introduction and thus will not be detailed herein. Instead, key developments and recent advancements relating to various upcycling strategies (e.g. alcoholysis and glycolysis) will be discussed, with a particular focus on organocatalysed and metal-mediated transesterification.



Scheme 5.2. Chemical recycling of BPA-PC via pyrolysis, hydrolysis and reduction.

5.1.2.1. Alcoholysis

In addition to judicial BPA management, chemical recycling strategies should endeavour to retain the inherent high value carbonyl functionality embedded within BPA-PC, which is lost during pyrolysis, hydrolysis and reduction (Scheme 5.2).^[8,11] Indeed, conventional methods for installing such functionality relies on the use of toxic sources, namely phosgene, carbon monoxide and their corresponding derivatives.^[38] Consequently, BPA-PC waste could potentially be a green source of carbonyl functionality in chemical synthesis, which inherently lends itself to plastic upcycling.^[39] One such strategy that fulfils this criteria is alcoholysis as shown in Scheme 5.3 below.



Scheme 5.3. BPA-PC alcoholysis into BPA and either DMC (methanolysis), DEC (ethanolysis) or DPC (phenolysis).

5.1.2.1.1. Metal-mediated transesterification

Pioneering work relating to BPA-PC alcoholysis was first conducted by Oku and co-workers over 20 years ago.^[40-42] In the presence of excess MeOH and catalytic amounts of NaOH (17

mol%), BPA-PC was found to undergo minimal degradation, yielding only 7% BPA within 330 min at 60 °C $\{m_{BPA-PC} = 1.27 \text{ g}, n_{\text{carbonate}}:n_{\text{MeOH}} = 1:10\}$. This was mainly attributed to poor polymer solubility under mild conditions. However, the introduction of toluene as a solvent was found to assist with polymer swelling, enabling near quantitative conversion to BPA and dimethyl carbonate (DMC) within 70 min under analogous treatment $\{V_{\text{toluene}}:V_{\text{MeOH}} = 1:1, n_{\text{carbonate}}:n_{\text{MeOH}} = 1:5\}$.^[40] Oku and co-workers subsequently investigated diversification of the nucleophile employed (e.g. dithiols, aminothiols and glycols), which allowed a range of high value carbonates to be accessed, including ethylene carbonate (EC).^[41,42] Indeed, DMC and EC are of significant commercial value, with uses in a wide range of applications, for example as green solvents, battery electrolytes and chemical building blocks.^[43-45] In a follow up study, Piñero *et al.*^[46] implemented the alkali-metal methanolysis process reported by Oku and co-workers in a semi-continuous lab-plant.^[40] Promisingly, optimisation in continuous flow removed the need for an auxiliary solvent, further increasing the processes green credentials. Indeed, BPA was produced in quantitative yield above 100 °C, whilst the yield of DMC was found to be sensitive to the conditions employed due to a competing pathway to Na₂CO₃, consistent with observations by Oku and co-workers.^[40] This could be overcome through the use of elevated temperatures (120 – 140 °C) and methanol pressures (10 MPa), affording DMC in near quantitative yield.

Recently, the application of ultrasound to BPA-PC methanolysis catalysed by NaOH was demonstrated by Pandit and co-workers, although the use of THF as a solvent is required.^[47] Indeed, a significant rate enhancement was observed, achieving complete BPA-PC consumption within 15 min at 30 °C $\{m_{BPA-PC} = 5 \text{ g}, m_{\text{NaOH}} = 0.1 \text{ g} (12.7 \text{ mol}\% \text{ relative to carbonate linkages}), m_{\text{carbonate}}:m_{\text{THF}}:m_{\text{MeOH}} = 1:3:1, n_{\text{carbonate}}:n_{\text{MeOH}} = 1:6\}$. Promisingly, BPA and DMC were recovered in 97% and 91% yield, respectively. Comparatively, Liu *et al.*^[48] have shown rapid BPA-PC methanolysis is possible by conventional heating in the presence of NaOH (12.7 mol%) under relatively mild conditions. Specifically, near quantitative consumption of BPA-PC and over 95% BPA yield was obtainable within 35 min at 40 °C $\{m_{BPA-PC} = 5 \text{ g}, n_{\text{carbonate}}:n_{\text{MeOH}} = 1:8\}$. This result contrasts previous findings by Oku and co-workers and serves to highlight the importance of the solvent employed with regards to process optimisation.^[40] The system was also found to be amenable to BPA-PC hydrolysis, although polymer dissolution within 1,4-dioxane and a reaction temperature of 100 °C was required to achieve appreciable activity.

Metal-mediated BPA-PC methanolysis has also been investigated under microwave irradiation. Notably, Enthaler and co-workers demonstrated a range of simple and commercially available alkali-metal halides (e.g. KF, LiCl, NaBr, NaI and KI) to be highly active for BPA-PC methanolysis.^[49] Indeed, such catalysts yielded quantitative conversion to

BPA within 5 min at 180 °C under solvent-free conditions, although a large excess of MeOH is noted $\{m_{BPA-PC} = 0.34 \text{ g}, n_{\text{carbonate}}:n_{\text{MeOH}} = 1:(23 - 46), 2.5 \text{ mol\% catalyst (relative to carbonate linkages), TOFs up to } 1844 \text{ h}^{-1}\}$. Such activity was attributed to the ability of the alkali-metal halides to act as bifunctional Lewis acid/base catalysts. Specifically, this is characterised by simultaneous activation of the polymer carbonyl and incoming nucleophile, akin to that described for PET and PLA in Chapters 1 (Figure 6 in publication 1) and 4 (Scheme 4.1), respectively. Comparatively, Neverov *et al.*^[50] have shown complete BPA-PC consumption and a high BPA yield (> 90%) is attainable under milder microwave irradiation conditions (100 °C) in the presence of a lanthanum-based catalyst, namely $[\text{La}_2(\text{OCH}_3)_2]^{4+}$. However, a solvent is required to assist with polymer swelling. Whilst literature examples remain scarce, there are lingering concerns pertaining to the translation of microwave-based techniques to industry.

Whilst significant work has focused on BPA-PC methanolysis catalysed by simple metal-based salts, particularly NaOH, such systems remain limited by the use of high catalyst loadings (up to 17%), temperatures (up to 180 °C) and corrosivity. Furthermore, such studies fail to address concerns associated with catalyst recovery and reuse, which is of paramount importance to industry. To this end, a number of heterogeneous metal-based alternatives have been reported, which include mesoporous nanocomposites of SBA-15 in combination with a number of metal oxides (*e.g.* CaO, BaO, SrO and CaO-CeO₂).^[51-54] Such systems offer superior durability and facile catalyst recovery and reuse, as expected.^[55] However, generally higher reaction temperatures (100 – 130 °C) and prolonged reaction times (2 – 7 h) are employed relative to the aforementioned homogeneous-based examples catalysed by NaOH.^[40,47,48] Thus, clear scope remains for the development of heterogeneous catalysts that facilitate BPA-PC methanolysis under mild conditions.

Inspired by work pertaining to polycarbonate hydrolysis, supercritical methanolysis and ethanolysis have also been investigated.^[56-58] Importantly, the critical temperatures used (T_c (MeOH) = 240 °C; T_c (EtOH) = 241 °C) are significantly milder relative to hydrolysis (T_c (H₂O) = 373 °C). This assists with preventing further monomer decomposition, yielding BPA and either DMC or diethyl carbonate (DEC) in good purity. Whilst such temperatures are considerably higher relative to other methods detailed herein, Ikenaga *et al.*^[59] have recently demonstrated enhanced heating efficiency through the application of microwave irradiation, highlighting scope for further system optimisation.

Beyond traditional methanolysis, Iannone *et al.*^[54] and Alberti *et al.*^[60] have reported the phenolysis of BPA-PC into DPC and BPA (Scheme 5.3). Promisingly, DPC can be directly repolymerised in the melt process (Scheme 5.1, **B**) to afford virgin polycarbonate and thus

possibly represents the simplest closed-loop recycling pathway. However, the transformation remains challenging owing to the poor nucleophilicity of phenol, which necessitates the use of forcing reaction conditions and/or prolonged reaction times. Furthermore, the removal of phenol regenerates polycarbonate through the reaction of BPA and DPC, adding additional cost and complexity to post-depolymerisation operations.

5.1.2.1.2. Organocatalysed transesterification

In pursuit of more sustainable and practical systems, organocatalysts have been widely explored for BPA-PC alcoholysis owing to their inherent green attributes.^[8,61,62] Inspired by carbonates and esters possessing comparable chemical reactivity, organic bases that exhibit high transesterification activity, such as DBU and TBD, have been widely investigated for BPA-PC alcoholysis (Figure 5.3).^[63-67]

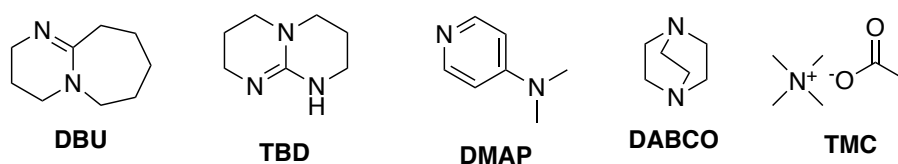


Figure 5.3. Selected examples of organocatalysts reported for BPA-PC alcoholysis.^[64-67]

The first example of BPA-PC alcoholysis in the presence of an organic superbases, namely DBU, was reported by Quaranta and co-workers (Figure 5.3).^[64] Methanolysis proceeded under solvent-free conditions, yielding BPA and DMC exclusively at 100 °C. Indeed, short to moderate reaction times were required to obtain near quantitative monomer recovery, dependent on the catalyst loading of DBU employed (1.8 and 6 h at 10 and 1 mol%, respectively). Besides removing the need for an auxiliary solvent, DBU could be reused *in situ* through the addition of fresh polycarbonate. Furthermore, DBU could be recovered from the reaction mixture as an adduct with BPA, which could then be reused, observing excellent productivity and selectivity retention across 7 successive runs. DABCO and DMAP were also tested, however, prolonged reaction times were observed due to reduced basicity relative to DBU.

TBD has since emerged as a superior catalyst for BPA-PC alcoholysis owing to its dual-activation behaviour, which was previously highlighted in Chapter 1 for PLA and PET transesterification (Figure 5.3).^[63,65,68] Kim and co-workers have demonstrated its efficacy for BPA-PC methanolysis, achieving >98% BPA and DMC yield within 12 h $\{m_{BPA-PC} = 0.13 \text{ g}, n_{\text{carbonate}}:n_{\text{MeOH}} = 1:10, 2 \text{ mol\% TBD (relative to carbonate linkages)}\}$.^[65] Importantly, the process makes use of an environmentally friendly solvent, namely 2-methyltetrahydrofuran (2-MeTHF), and proceeds under ambient conditions. The study also found TBD to offer superior activity relative to NaOH and KOH under such conditions, whilst $\text{Ti}(\text{O}^i\text{Pr}_4)$ and

Zn(TAC), a μ -oxo-tetranuclear zinc cluster, were found to be inactive. Whilst TBD exhibited inferior performance under solvent-free conditions relative to DBU, the auxiliary solvent could be removed by conducting the reaction in excess DMC at 50 °C.^[64] Indeed, DMC offers superior BPA-PC compatibility and processability relative to neat alcohol as a solvent. Catalyst recovery and reuse methods discussed for DBU were also applicable to TBD, which retained excellent performance across 5 catalytic cycles at 75 °C in DMC.^[64,65] Recently, Mckeown *et al.*^[66] reported an organocatalyst, namely TMC (Figure 5.3), that facilitates the mild and selective degradation of various commercial polymers, including BPA-PC, although inferior performance was observed relative to both TBD and DBU.^[64,65]

Traditionally, DMAP exhibits significantly lower reactivity relative to DBU or TBD (Figure 5.3). However, Alberti *et al.*^[67] recently compensated for this through the use of microwave irradiation, which enabled excellent BPA recovery (>99%) within 10 min at 180 °C ($m_{BPA-PC} = 0.34$ g, $n_{carbonate}:n_{MeOH} = 1:46$, 1 mol% DMAP (relative to carbonate linkages)). However, the yield of DMC was consistently low under such conditions (55 – 69%), which was attributed to hydrolysis in the presence of residual water. Such findings are consistent with previous work by Cocero and co-workers.^[46]

Beyond simple organic bases, ionic liquids (ILs) have also been explored for BPA-PC alcoholysis (Figure 5.4), which was first reported by Liu and co-workers.^[69,70] [Bmim][Cl] (**38**) was found to afford >95% conversion to BPA and DMC within 2.5 h at 105 °C ($m_{BPA-PC} = 2$ g, $m_{BPA-PC}:m_{MeOH}:m_{IL} = 2:3:2$, $n_{carbonate}:n_{MeOH} = 1:9$), observing comparable efficiency with [Bmim][Ac] (**39**), although at a slightly lower temperature (90 °C). Indeed, this can likely be attributed to the acetate anions assisting with BPA-PC dissolution owing to structural similarity. In both instances, the catalyst could be easily recovered and reused, retaining excellent performance across 6 to 8 cycles.

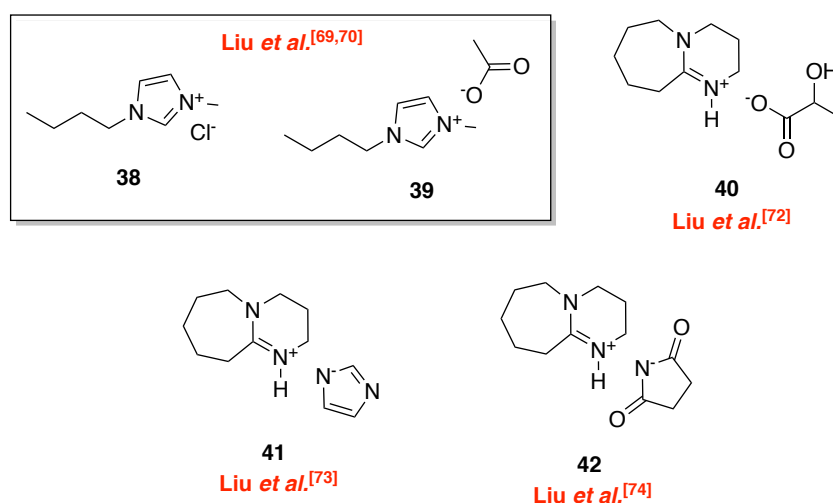


Figure 5.4. Selected examples of ILs reported for BPA-PC alcoholysis.^[69,70,72-74]

In a follow up study, Guo *et al.*^[71] investigated increasing the Lewis acidity of **38** through doping with FeCl₃. Whilst FeCl₃ exhibited negligible activity for BPA-PC methanolysis in isolation, complete BPA-PC consumption and a high BPA yield of *ca.* 97% was achieved within 3 h at 120 °C using **38**·2.0FeCl₃ {*m*_{BPA-PC} = 4 g, *n*_{carbonate:MeOH} = 1:6, 5 mol% catalyst (relative to carbonate linkages)}, which could be reused up to 6 times. Furthermore, the reaction was found to be first-order with an activation energy of 98.9 kJ mol⁻¹, which is considerably lower relative to that reported for **39** (*E*_a = 167 kJ mol⁻¹).^[70]

Subsequent studies have focused primarily on optimisation of the anion and cation employed (Figure 5.4). Initial work by Liu *et al.*^[72] found an IL composed of DBU and lactic acid, namely [HDBU][LAc] (**40**), to be reasonably active for BPA-PC methanolysis. Indeed, complete BPA-PC consumption and quantitative conversion to BPA and DMC was achieved within 1 h at 120 °C {*m*_{BPA-PC} = 4 g, *n*_{carbonate:MeOH} = 1:5, 0.80 mol% catalyst (relative to carbonate linkages)}. Subsequent work within this group demonstrated enhanced activity and lower reaction temperatures (70 °C) were accessible through anion substitution, namely with those derived from imidazole and succinimide.^[73,74] Specifically, [HDBU][Im] (**41**) was found to be highly active, observing complete polymer consumption within 1 h and near quantitative monomer recovery within 2 h at 70 °C under solvent-free conditions {*m*_{BPA-PC} = 4 g, *n*_{carbonate:MeOH} = 1:5, 1.6 mol% catalyst (relative to carbonate linkages)}. Moreover, the catalyst could be easily recovered by extraction and no activity loss was observed across 6 cycles.^[73] [HDBU][Suc] (**42**) exhibited comparable performance under similar reaction conditions, although a significantly higher catalyst loading is noted (30 mol%).^[74] Such studies routinely investigate BPA-PC alcoholysis using higher chain alcohols (*e.g.* ethanol, propanol and butanol), however, longer reaction times are typically observed due to a reduction in nucleophilicity.^[64,65,71,72]

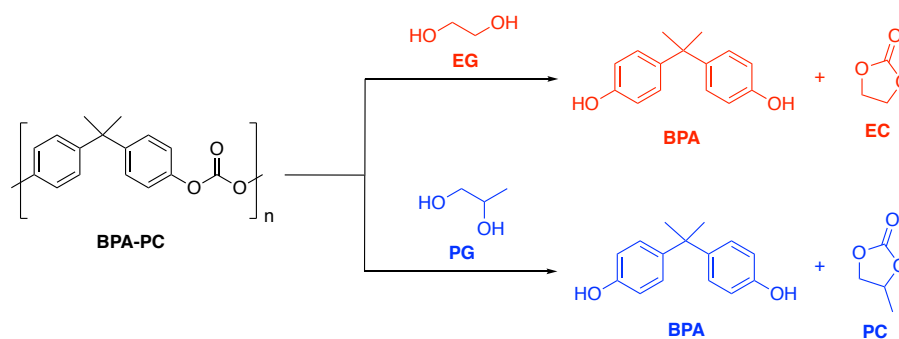
Recently, D'Anna *et al.*^[75] reported the first example of exploiting the synergistic action between ultrasound irradiation and task specific ILs, which enabled BPA-PC methanolysis to proceed under ambient conditions. Such work promises to create new opportunities for utilising ILs to facilitate polycarbonate under mild conditions. Deep eutectic solvents (DESs) have also been reported for BPA-PC methanolysis, although currently remain limited by the use of high reaction temperatures (≥ 120 °C).^[76,77] Indeed, general limitations associated with organic superbases and ILs detailed in Chapter 1 can be extended to those discussed in this section.

5.1.2.2. Glycolysis

BPA-PC glycolysis has also attracted significant attention in the literature since a range of high value linear and cyclic carbonates can be accessed through judicious choice of the reagent

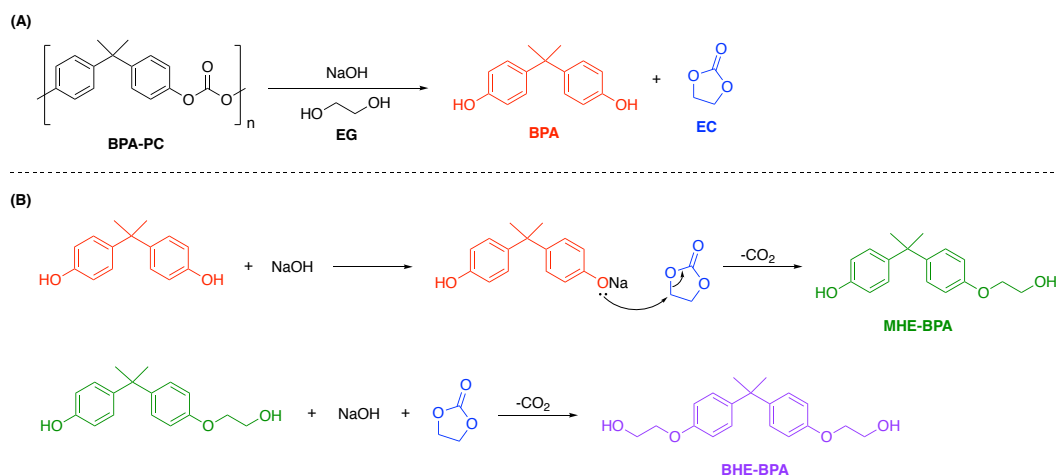
and reaction conditions used. Such precursors are potentially useful chemical building blocks and are traditionally derived from toxic phosgene or CO, creating an appetite for greener alternatives.^[8]

Pioneering work by Kim and co-workers demonstrated the solvent-free depolymerisation of BPA-PC in the presence of ethylene glycol (EG) with no catalyst (Scheme 5.4).^[78] A BPA yield of *ca.* 96% was achieved within 85 min at 220 °C $\{n_{BPA-PC}:n_{EG} = 1:1\}$. Whilst cyclic carbonate formation was observed *via* SEC and FTIR, EC could not be isolated, which was attributed to subsequent decomposition into linear carbonate and CO₂ under the forcing reaction conditions used. In a similar study, Quaranta and co-workers employed propylene glycol (PG), affording BPA and propylene carbonate (PC) in excellent yield (95% and 94%, respectively) within 110 min at 180 °C $\{n_{BPA-PC}:n_{PG} = 1:12\}$ (Scheme 5.4).^[64]



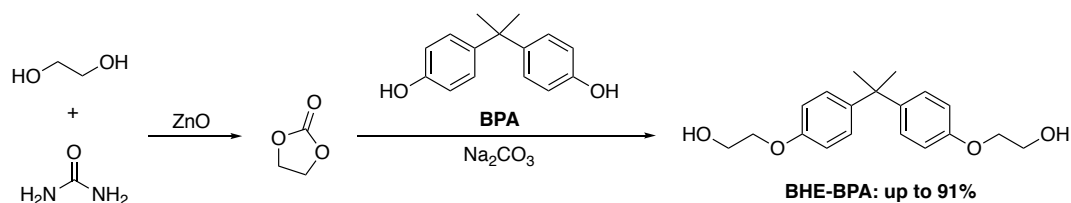
Scheme 5.4. BPA-PC glycolysis in the presence of either EG or PG.

Comparatively, Oku *et al.*^[41] found BPA-PC glycolysis catalysed by NaOH (0.1 mol%) in the presence of EG afforded a mixture of products within 10 min at 180 °C, which included BPA $\{m_{BPA-PC} = 1.27$ g, $n_{BPA-PC}:n_{EG} = 1:10\}$. Specifically, whilst EC is initially produced (Scheme 5.5, **A**), it subsequently reacts to afford mono- and bis-hydroxyethyl ethers (MHE-BPA and BHE-BPA, respectively) of BPA through the liberation of CO₂ (Scheme 5.5, **B**). Indeed, such alkyl-BPA ethers represent potentially promising monomers for polymer synthesis. In a complimentary study, Nikje investigated the impact of NaOH loading on BPC-PC glycolysis with EG under microwave irradiation.^[79] Indeed, an enhanced BPA yield was observed upon increasing catalyst concentration and reaction time. Frediani and co-workers conducted an extensive study into microwave assisted BPA-PC glycolysis, investigating various catalysts (*e.g.* NaOH, KOH, Na₂CO₃ and CaO) and glycols, including EG and PG.^[80] Whilst microwave irradiation reduced the reaction time to 10 min for EG (relative to conventional heating), the production of MHE-BPA and BHE-BPA persisted (Scheme 5.5, **B**).^[8]



Scheme 5.5. BPA-PC glycolysis catalysed by NaOH in the presence of EG (A) and subsequent alkyl-BPA ether formation (B).^[41]

Dai and co-workers have developed a method for maximising hydroxyalkyl ether production from BPA through further treatment of the reaction mixture with urea (Scheme 5.6).^[81] In the presence of a ZnO catalyst, additional EC is generated through the reaction of urea and EG, which subsequently reacts with BPA to generate BHE-BPA in up to 91% yield. Indeed, numerous studies have exploited BHE-BPA as a building block for the production of polyurethane resins and co-polyesters.^[8,81-83]



Scheme 5.6. High BHE-BPA conversion strategy reported by Dai and co-workers *via in situ* EC generation using urea and a ZnO catalyst.^[81]

Nacci and co-workers have previously demonstrated a recyclable and bifunctional Lewis acid/base catalyst consisting of ZnO nanoparticles (ZnO-NPs) and tetrabutylammonium chloride (NBu₄Cl) to be highly efficient for BPA-PC glycolysis.^[54] Glycolysis was conducted in a large excess of various 1,2- and 1,3-diols, employing THF as the reaction solvent. Whilst an increase in reaction temperature coincided with enhanced conversion, poorer product selectivity was observed. Organocatalysts such as DBU and TBD have also been reported for BPA-PC glycolysis.^[65,84] Notably, Kim and co-workers exploited the use of TBD to facilitate the production of numerous high value cyclic carbonates, including EC (92%), PC (97%), styrene carbonate (92%) and cyclopentane carbonate (89%), within 12 h in 2-MeTHF under ambient conditions $\{m_{BPA-PC} = 0.13 \text{ g}, n_{BPA-PC}:n_{glycol} = 1:10, 1 \text{ mol\% TBD (relative to carbonate linkages)}\}$.^[65] Importantly, the undesired hydroxyalkyl ether forming side reaction between

BPA and cyclic carbonate was not observed, despite the use of highly basic TBD, which can likely be attributed to the low reaction temperature employed.

Recent exemplary work by Sardon and co-workers demonstrated the application of TBD:MSA for the production of 5- and 6-membered cyclic carbonates through the chemical upcycling of BPA-PC in the presence of various 1,2- and 1,3-diols (Figure 5.5).^[85]

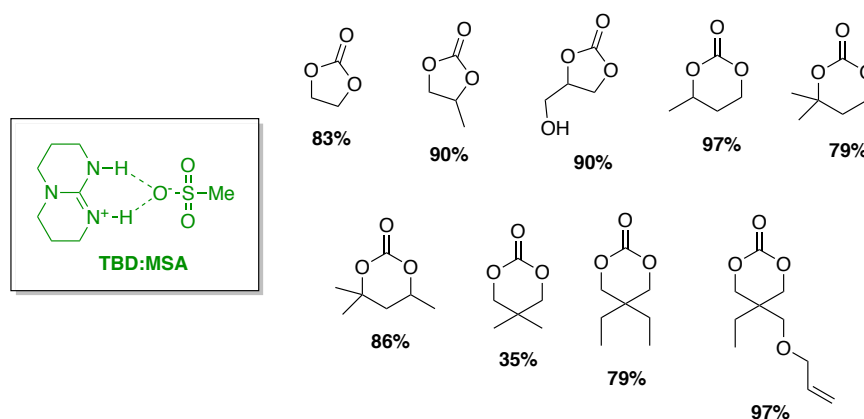
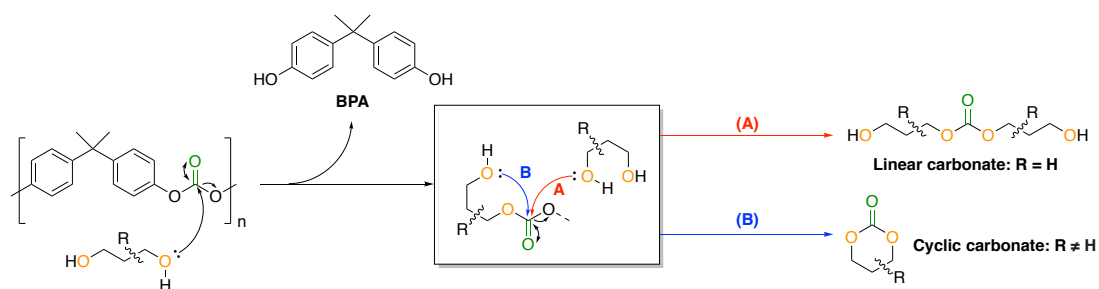


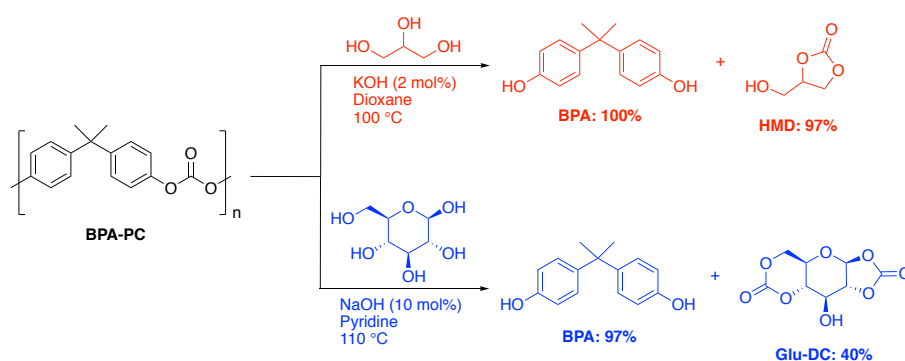
Figure 5.5. Selected examples of 5- and 6-membered cyclic carbonates (with yields) produced *via* the chemical upcycling of BPA-PC in the presence of TBD:MSA as reported by Sardon and co-workers.^[85]

Interestingly, linear carbonate was formed exclusively in the presence of 1,3-propanediol, whilst substituted diols with greater steric bulk favoured formation of the cyclic product. It was proposed in the absence of steric bulk intermolecular attack of a second incoming nucleophilic diol is favoured, resulting in formation of the linear carbonate product (Scheme 5.7, **A**). Conversely, in accordance to the Thorpe-Ingold effect, increasing steric hindrance results in a conformational distortion that promotes intramolecular ring-closure to afford the six-membered cyclic product (Scheme 5.7, **B**). As discussed in section 1.2.2.3. of Chapter 1, TBD:MSA has also been employed for the selective recycling of a mixed BPA-PC/PET waste feed *via* glycolysis.^[86]



Scheme 5.7. Two possible routes for the chemical upcycling of BPA-PC using 1,3-propanediol derivatives: nucleophilic attack of a second diol (**A**) and ring-closure of the carbonate (**B**).^[85]

Subsequent work within this group has extended the reaction scope to higher chain aliphatic 1,n-diols such as 1,4-butanediol and 1,5-pentanediol.^[87] Additionally, this study confirmed double attack on the carbonate group of BPA-PC is responsible for linear carbonate formation (Scheme 5.7, **B**), which have potential uses as battery electrolytes. Partial BPA-PC glycolysis to telechelic polymers has also been actively explored as a possible upcycling route.^[8,88,89] Furthermore, Oku and co-workers have previously demonstrated the use of glycerol and glucose for the production of value-added organic carbonates from waste BPA-PC (Scheme 5.8).^[90] Glucose exists in equilibrium with several structural isomers, which resulted in the formation of multiple products. Glu-DC was identified as the major product, which was characterised and isolated in significantly lower yield relative to HMD.



Scheme 5.8. BPA-PC glycolysis in the presence of glycerol and glucose for the production of high value organic carbonates as reported by Oku and co-workers.^[90]

5.1.2.3. Other methods

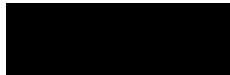
Beyond alcoholysis and glycolysis, a diverse range of chemical upcycling strategies for BPA-PC have been reported (*e.g.* aminolysis, thiolysis and reductions), which have been comprehensively reviewed in a number of recent excellent reviews.^[8,37,91-94] Whilst not pertinent herein, such work serves to highlight the plethora of value-added chemicals accessible from BPA-PC waste, which have applications in both organic and polymer sciences as solvents and chemical building blocks (*e.g.* reagents and monomers). For example, Hedrick and co-workers have previously demonstrated a simple one-pot transformation of BPA-PC into value-added poly(aryl ether sulfone)s in the presence of carbonate salt and bis(aryl fluorides).^[95]

5.1.2.4. Summary

Traditionally, BPA-PC alcoholysis and glycolysis employ the use of a simple metal-based salt or organocatalyst. However, such systems generally remain limited by the use of elevated reaction temperatures, high catalyst loadings and/or prolonged reaction times. High catalyst cost and/or corrosivity serve to confound such issues, notably for NaOH and the organic

superbases/ILs. Discrete homogeneous metal-based catalysts represent a promising solution to such challenges; however, no such examples have been reported to date. Thus, a clear opportunity exists to leverage judicious catalyst design in pursuit of robust and sustainable catalytic chemical recycling strategies for BPA-PC that are cheaper and more environmentally friendly. Ideally, such processes will exhibit high activity and selectivity under mild and solvent-free conditions, thus lending themselves to industry.

5.2. Statement of Authorship

This declaration concerns the article entitled:			
Versatile Chemical Recycling Strategies: Value-Added Chemicals from Polyester and Polycarbonate Waste			
Publication status (tick one)			
Draft manuscript <input type="checkbox"/> Submitted <input type="checkbox"/> In review <input type="checkbox"/> Accepted <input type="checkbox"/> Published <input checked="" type="checkbox"/>			
Publication details (reference)	J. M. Payne, M. Kamran, M. G. Davidson, M. D. Jones, <i>ChemSusChem</i> 2022 , 15, e202200255 (DOI: 10.1002/cssc.202200255)		
Copyright status (tick the appropriate statement)			
I hold the copyright for this material <input checked="" type="checkbox"/> Copyright is retained by the publisher, but I have been given permission to replicate the material here <input type="checkbox"/>			
Candidate's contribution to the paper (provide details, and also indicate as a percentage)	<p>The candidate predominantly executed the work presented in the paper.</p> <p>Formulation of ideas:</p> <p>Ideas were discussed and planned with MK and MDJ. The manuscript draft was prepared by JMP with editing from MK and MDJ during the editing stage. [JMP = 80%, MK = 8%, MGD = 2%, MDJ = 10%]</p> <p>Design of methodology:</p> <p>Experiments were discussed and planned with MK and MDJ. [JMP = 80%, MK = 10%, MGD = 0%, MDJ = 10%]</p> <p>Experimental work:</p> <p>Experimental work and data analysis were conducted by JMP. X-ray crystallographic data was collected and processed by MDJ. PEA synthesis and characterisation (NMR, DSC and TGA) was undertaken by MK. [JMP = 80%, MK = 12%, MGD = 0%, MDJ = 8%]</p> <p>Presentation of data in journal format:</p> <p>NMR, DSC and TGA spectra for the PEAs were prepared by MK. All remaining figures, tables and schemes were prepared by JMP. [JMP = 90%, MK = 10%]</p>		
Statement from Candidate	This paper reports on original research I conducted during the period of my Higher Degree by Research candidature.		
Signed		Date	8/6/2022

Versatile Chemical Recycling Strategies: Value-Added Chemicals from Polyester and Polycarbonate Waste

Jack M. Payne,^[a, b] Muhammad Kamran,^[a, b] Matthew G. Davidson,^[a, b] and Matthew D. Jones^{*[a, b]}

Zn^{II}-complexes bearing half-salan ligands were exploited in the mild and selective chemical upcycling of various commercial polyesters and polycarbonates. Remarkably, we report the first example of discrete metal-mediated poly(bisphenol A carbonate) (BPA-PC) methanolysis being appreciably active at room temperature. Indeed, Zn(2)₂ and Zn(2)Et achieved complete BPA-PC consumption within 12–18 mins in 2-Me-THF, noting high bisphenol A (BPA) yields (S_{BPA} = 85–91 %) within 2–

4 h. Further kinetic analysis found such catalysts to possess k_{app} values of 0.28 ± 0.040 and $0.47 \pm 0.049 \text{ min}^{-1}$ respectively at 4 wt%, the highest reported to date. A completely circular upcycling approach to plastic waste was demonstrated through the production of several renewable poly(ester-amide)s (PEAs), based on a terephthalamide monomer derived from bottle-grade poly(ethylene terephthalate) (PET), which exhibited excellent thermal properties.

Introduction

The “Plastic Age” has delivered unparalleled prosperity in virtually every facet of society from healthcare and transport to agriculture and communications.^[1] However, rapid modernization has highlighted several major drawbacks associated with a linear plastics economy at scale (367 million tonnes in 2020).^[2] Firstly, production is unsustainable based on a depleting fossil reserve, equating to ca. 99% of all processed plastics.^[3] Secondly, short-sighted product design has inadvertently rendered traditional plastics (e.g. robust and durable) a persistent environmental pollutant. This, coupled with irresponsible handling at end-of-life (EoL), underpin plastic pollution, exemplified by ocean plastics.^[4] To this end, renewable and/or biodegradable alternatives, such as poly(lactic acid) (PLA) and poly(ethylene furanoate) (PEF), have been developed.^[3,5] Whilst compostable materials represent a possible solution to system leakage, a linear approach fails to capture embedded material value. This is particularly problematic in sectors dominated by single-use plastics, such as packaging.^[3] Thus, a sustainable and green plastic economy relies on transitioning towards a circular model, with recycling a promising enabler.^[6] Industrially, mechanical recycling is primarily used, accounting almost entirely for Europe’s (EU 28+2) packaging recycling rate in

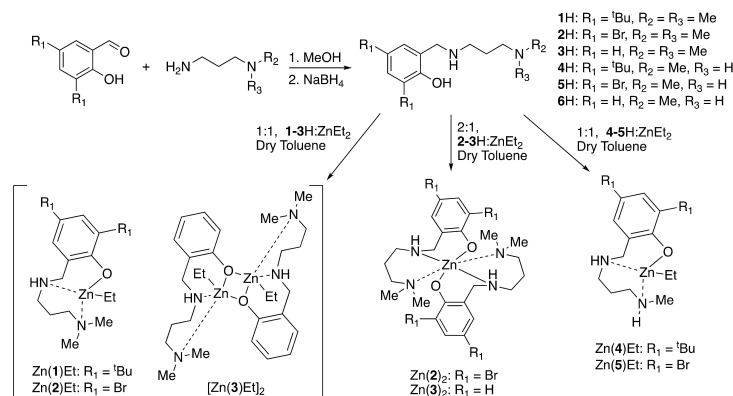
2018.^[7] However, this method is limited by eventual material downcycling, necessitating product repurposing to lower value applications, which creates uncertainty surrounding long-term material value retention.^[6a,8] Conversely, chemical recycling enables product quality to be preserved over an infinite number of cycles. Moreover, scope for both monomer recovery and derivatization of platform/value-added chemicals provides additional economic benefits to industry.^[9] However, barriers to adoption within industry remain, which include high CAPEX/operating costs and energy intensity.^[1c,9g] There is therefore a clear opportunity to develop sustainable chemical recycling strategies to overcome such challenges, with catalysis central to such innovation. Polymer classes relevant to this study include polyesters (e.g. PLA and poly(ethylene terephthalate) (PET) and polycarbonates (e.g. poly(bisphenol A carbonate) (BPA-PC)). PLA recycling methods have recently been reviewed and include strategies such as pyrolysis, hydrogenation and hydrosilylation.^[1c,6a,10] Metal-mediated transesterification is most pertinent herein, although literature examples remain scarce, particularly relative to lactide polymerization.^[11,12] Given the proliferation of plastic pollution, it is imperative future innovation is not limited to emerging plastics and encompasses established commercial products, such as PET and BPA-PC. Additionally, the latter is also a significant source of bisphenol A (BPA), a damaging xenoestrogenic pollutant.^[1a,13a] Both are used in a diverse range of applications, notably packaging and engineering, and are largely amenable to chemical recycling strategies.^[1c,13] PET glycolysis is a commonly used method, often employing a metal acetate transesterification catalyst to furnish bis(2-hydroxyethyl)terephthalate (BHET), which can be repolymerized or redirected for upcycling.^[1c,13d] PET aminolysis has also been reported, yielding value-added terephthalamides for use in the production of additives and high-performance materials.^[13d,14] Catalysts for PET alcoholysis and glycolysis have been widely investigated, although discrete metal-based examples remain rare.^[12f,15] Comparatively, BPA-PC remains vastly underexplored and is limited almost exclusively to the use of

[a] J. M. Payne, Dr. M. Kamran, Prof. M. G. Davidson, Prof. M. D. Jones
Centre for Sustainable and Circular Technologies
University of Bath
Claverton Down, Bath, BA2 7AY (United Kingdom)

[b] J. M. Payne, Dr. M. Kamran, Prof. M. G. Davidson, Prof. M. D. Jones
Department of Chemistry
University of Bath
Claverton Down, Bath, BA2 7AY (United Kingdom)
E-mail: mj205@bath.ac.uk

Supporting information for this article is available on the WWW under <https://doi.org/10.1002/cssc.202200255>

© 2022 The Authors. ChemSusChem published by Wiley-VCH GmbH. This is an open access article under the terms of the Creative Commons Attribution License, which permits use, distribution and reproduction in any medium, provided the original work is properly cited.



Scheme 1. Preparation of half-salan ligands and their corresponding homo- and heteroleptic Zn^{II}-complexes.

organocatalysts.^[13a,16] Notable examples include TBD- and DBU-catalysed methanolysis reported by Do et al.^[16a] and Quaranta et al.^[16b] respectively. Traditionally, such systems rely on elevated temperatures ($\geq 70^\circ\text{C}$), high catalyst loadings (≥ 5 mol%) and/or prolonged reaction times.^[13a] However, simple alkali-metal catalysed methanolysis using NaOH has been shown to be an efficient alternative.^[17] Indeed, Liu et al.^[17a] reported over 95% BPA yield within 35 min at 40°C in THF ($m(\text{BPA-PC}):m(\text{MeOH}) = 1:1$, 2 wt% NaOH). Alongside BPA, organic carbonates (e.g. dimethyl carbonate (DMC)) are also produced. Such chemicals are commercially important with a variety of uses, for example as green solvents, battery electrolytes and chemical building blocks.^[13a,18] Whilst metal-mediated degradation is a possible solution to such crucial challenges in the field, a clear industry appetite remains for cheap and environmentally benign alternatives through judicious catalyst design.

Herein, we report a series of Zn^{II}-complexes bearing half-salan ligands and their application to the mild and selective degradation of several commercial polyesters and polycarbonates. Various strategies (e.g. alcoholysis, glycolysis and aminolysis) were used to obtain a diverse range of value-added chemicals. A completely circular upcycling approach to plastic waste is demonstrated through the production of several renewable poly(ester-amide)s based on a terephthalamide monomer derived from bottle-grade PET.

Results and Discussion

We have previously shown ligand flexibility and hydrogen bond donors to dramatically influence the activity of Zn^{II}-complexes for polyester degradation.^[12g,h,i] Thus, we sought to design new industrially relevant ligands that combine such adventitious attributes. A range of monoanionic half-salan ligands (1-6H) were prepared *via* a facile two-step process (Scheme 1) and

characterized by multinuclear NMR spectroscopy and high resolution ESI-MS (Figures S1–S18). A variety of heteroleptic ZnL^HEt monomers and homoleptic ZnL^HEt₂ complexes were formed upon reaction with ZnEt₂, where L^H denotes the half-salan ligand (Scheme 1). Complexes were isolated and characterized in solution (Figures S19–S44) and in the solid-state (Figure 1 and Figure 2).

To assess polymerization activity all Zn^{II}-complexes were trialed in PLA production, specifically the ring-opening polymerization (ROP) of lactide (Scheme S2). The racemic monomer (*rac*-LA) was used to assess possible catalyst stereoselectivity. Industrially preferred melt conditions (130 and 180°C) were used (Table S1), negating the need for an auxiliary solvent.^[11] In summary, Zn^{II}-complexes were generally highly active in the melt, achieving high conversion (78–94%) within minutes under immortal conditions at 130°C ($\{\textit{rac}\text{-LA}\}:[\text{M}]:[\text{BnOH}] = 10000:1:33\}$) (Table S1). Catalyst colour and low metal loading (0.01 mol%) enabled the production of highly desirable white

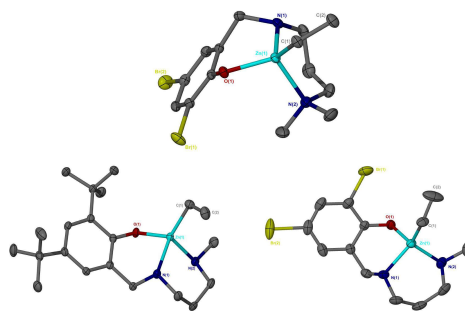


Figure 1. Solid-state structures of Zn(2)Et (top centre), Zn(4)Et (bottom left) and Zn(5)Et (bottom right). Thermal ellipsoids shown at 50% probability. All hydrogen atoms have been omitted for clarity.

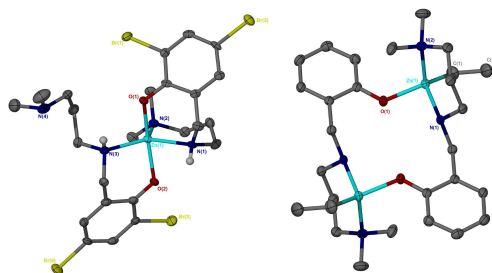


Figure 2. Solid-state structures of Zn(2)₂ (left) and [Zn(3)Et]₂ (right). Thermal ellipsoids shown at 50% probability. All hydrogen atoms, except those bound to N(1) and N(3) for Zn(2)₂, have been omitted for clarity. [Zn(3)Et]₂ has a centre of inversion to complete the macrocycle.

polymer, which was atactic ($P_r = 0.54\text{--}0.59$). Zn(2)₂ was the outstanding candidate, achieving TOFs up to 273000 h⁻¹ (Table S1, Entry 6), competitive with the industry standard; Sn(Oct)₂.^[11,12]

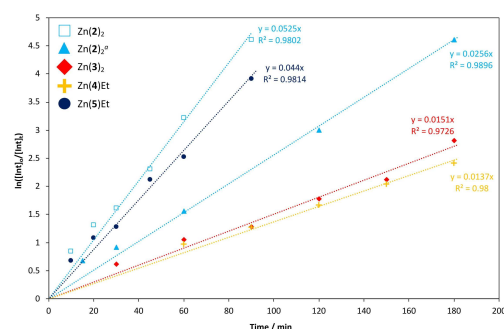


Figure 3. Pseudo-first-order logarithmic plot for the degradation of a PLLA (0.25 g, $M_n = 45510 \text{ g mol}^{-1}$) cup using Zn(2-3)₂ and Zn(4-5)Et at 8 wt% (0.02 g, 0.72–1.4 mol% relative to ester linkages) in THF at 50 °C. Reaction conditions: $V_{\text{THF}}:V_{\text{MeOH}} = 4:1$, $n_{\text{MeOH}}:n_{\text{ester}} = 7:1$. [a] Zn(2)₂ = 4 wt% (0.01 g, 0.36 mol% relative to ester linkages).

Superior M_n control ($M_{n,\text{theo}} = 13200 \text{ g mol}^{-1}$, $M_n = 19350 \text{ g mol}^{-1}$) and narrower dispersities ($D = 1.69$) were realized upon modifying the [M]:[BnOH] ratio to 1:100, suggesting a more efficient initiation process (Table S1, Entry 6). Further polymerization and materials characterization data can be found in the Supporting Information.

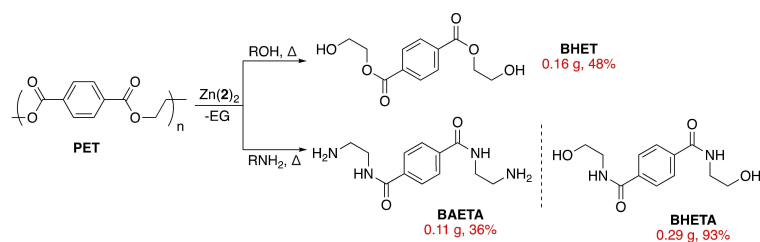
All Zn^{II}-complexes were also investigated in the metal-mediated degradation of commercial PLA into methyl lactate (Me-LA), a high value green solvent (Table S2).^[1c,6a] In short, Zn(2-3)₂ and Zn(4-5)Et were taken forward for further kinetic analysis under mild reaction conditions (Figure 3 and Table S3). Reactivity trends could generally be attributed to ligand effects, with the presence of hydrogen bond donors and Lewis acidity of the Zn^{II} centre being particularly important.^[12e,g,i] Notably, Zn(2)₂ and Zn(5)Et were reasonably active at 8 wt%, exhibiting k_{app} values of 0.053 and 0.044 min⁻¹ respectively in THF at 50 °C (Table S3, Entries 2 and 5). Such values are comparable to previously reported Zn^{II}-complexes.^[12g,i]

Chemical Recycling of PET

Following PLA degradation success, our attention shifted to other commercial polyesters. Consequently, PET was selected, which accounted for ca. 23% of plastic use within the packaging sector in 2015.^[3] Zn(2)₂ was pursued due to its ease of preparation, stability and high activity. Unless otherwise stated, bottle-grade PET ($M_n \sim 40000 \text{ g mol}^{-1}$) was used. All reaction times reflect the time taken to achieve complete PET dissolution, indicative of reaction completion. Degradation products were isolated as white solids *via* washing or recrystallization and characterized by ¹H/¹³C{¹H} NMR spectroscopy (Figures S59–S64).

PET Glycolysis

Initial work focused on PET glycolysis, an established commercial process.^[13c] Degradation products include BHET and EG, constituting to monomer recovery (Scheme 2 and S4). Herein, a reaction temperature of 180 °C and an excess of EG (20.6 equiv.) in the presence of Zn(2)₂ (4–8 wt%) were chosen based on previous work (Table S4).^[12g] Zn(OAc)₂·2H₂O is generally consid-



Scheme 2. Metal-mediated PET glycolysis and aminolysis using Zn(2)₂.

ered the benchmark catalyst, and thus was selected as a commercially available and air-stable reference.^[1c] BHET was recovered *via* recrystallization from deionized H₂O.

Zn(2)₂ was reasonably active at 8 wt%, affording BHET in 48% yield within 1.5 h (Table S4, Entry 6), competitive with previously reported discrete metal-based complexes.^[12f,g,15] Interestingly, a PET thin-film could be completely deconstructed within 1 h at 4 wt% ($Y_{BHET} = 61\%$; Table S4, Entry 4), highlighting activity dependence on sample morphology. For both sources of PET, Zn(2)₂ exhibited higher activity relative to Zn(OAc)₂·2H₂O (Table S4, Entries 1 and 2). In all instances, BHET yields < 65% were observed, presumably due to the production of water-soluble higher chain oligomers despite the use of a large excess of EG.^[1c,13c]

PET Aminolysis

In pursuit of alternative value-added chemicals from PET waste, our attention swiftly shifted to aminolysis for the production of terephthalamides (Scheme 2). Two commercially available aliphatic amines were chosen, namely ethanolamine and ethylenediamine.^[14] Lower reaction temperatures (110–120 °C) were used relative to glycolysis due to the aliphatic amines (6.4–16 equiv.) rendering the reaction more thermodynamically favourable (Table S5).^[1c,14a]

In the presence of Zn(2)₂ at 8 wt%, terephthalamides were furnished in moderate to excellent yield (36–93%) within 1–2 h (Table S5, Entries 2 and 4). Whilst BHETA results were comparable to previously reported systems, this work remains a rare example of discrete metal-based aminolysis.^[1c,12g] BAETA was obtained in significantly lower yield ($Y_{TPA} = 36\%$) relative to BHETA ($Y_{TPA} = 93\%$), which could be attributed to product loss during arduous work-up.

Production of Poly(ester-amide)s (PEAs)

To achieve a completely circular upcycling approach, BHETA was selected for repolymerization owing to its ease of preparation. Recently, poly(ester-amide)s (PEAs) have emerged as a promising hybrid material for both commodity and high-performance applications, notably in the biomedical sector. Indeed, such materials could potentially be engineered to capture desirable qualities of both respective homopolymers (e.g. thermomechanical and possible biodegradability/recyclability).^[19] Thus, PEAs were targeted in proof-of-concept work.

Herein, we report PEA synthesis based on a range of aliphatic and aromatic diesters (Figure 4 and Table 1), employing transesterification by melt polycondensation as a model green polymerization process (see Supporting Information). Diesters were selected based on their ability to be renewably sourced, enabling such PEAs to be of 100% recycled and bio-based content.^[20] Moreover, PEA(1–4) lend themselves to chemical recycling due to the presence of cleavable ester

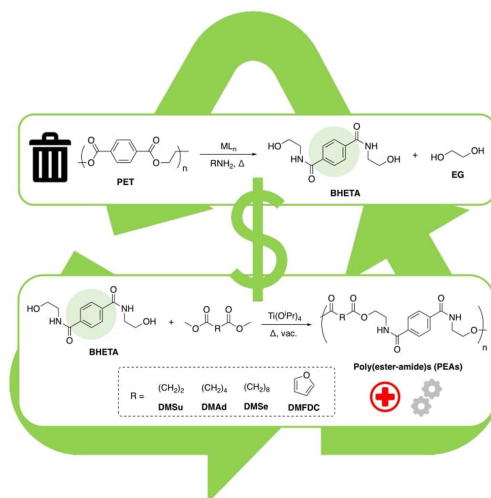


Figure 4. Melt polycondensation of BHETA with various diesters for PEA production.

Diester	PEA	$M_n^{[a]}$ [g mol ⁻¹]	$\mathcal{D}^{[a]}$	$T_g^{[b]}$ [°C]	$T_d-5^{[c]}$ [°C]	$T_d-50^{[c]}$ [°C]
DMSu	PEA(1)	1750	3.36	118	296	392
DMAAd	PEA(2)	2150	3.72	114	293	397
DMSe	PEA(3)	3150	2.91	98	293	388
DMFDC	PEA(4)	2450	3.24	126	275	345

Reaction conditions: BHETA (0.23 mg, 0.92 mmol), diester (0.13–0.21 g, 0.92 mmol) and Ti(OPr)₄ (400 ppm, stock solution, 20 μL mL⁻¹ in toluene). Polycondensation step conducted at 210 °C for 3 h under a dynamic vacuum (< 1 mbar). [a] Determined *via* SEC analysis in *N,N*-DMAc with 0.1% w/v LiBr. [b] Determined by DSC analysis. [c] T_{d-5} and T_{d-50} values refer to 5% and 50% weight loss respectively during TGA analysis under an argon atmosphere.

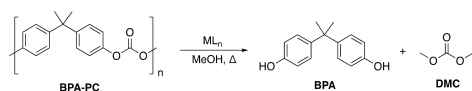
linkages. Titanium alkoxides are well-known ROP and polycondensation catalysts, thus Ti(OPr)₄ was used.^[21]

¹H NMR spectroscopic analysis (Figures S65–S68) confirmed PEA production. Notably, we report the synthesis of PEA(3) and PEA(4) for the first time. Indeed, PEA(4) represents new opportunities for bio-based aromatic polymers, which have previously been hindered by limited monomer scope and challenging synthesis.^[20] SEC analysis revealed PEA(1–4) to be of moderate M_n (1750–3150 g mol⁻¹) and highly disperse ($\mathcal{D} = 2.91$ –3.72) (Table 1). These M_n values imply a loss in stoichiometric balance, evidenced by the presence of residual BHETA in PEA(1–3) (Figures S65–S67). This is possibly due to a number of factors including trace monomer impurities, side reactions and mass transfer limitations.^[22] However, such results are amenable to further optimization. Demartea et al.^[14b] have previously reported PEA(1–2), achieving comparable M_n with narrower dispersities ($\mathcal{D} = 1.34$ –1.46). However, DSC analysis (Figure S70)

revealed PEA(1-2) to possess significantly higher T_g values of 118 and 114 °C (relative to 7 and 18 °C respectively), evidencing greater hydrogen bonding interactions. For PEA(1-3) an increase in diester chain length coincided with a decrease in T_g as expected, although PEA(3) retained an impressive T_g of 98 °C (Table 1, Entry 3). Substitution of the flexible DMSe linker for DMFDC yielded the highest T_g of 126 °C (Table 1, Entry 4), owing to increased polymer rigidity. TGA analysis (Figure S71) was used to determine T_{d-5} and T_{d-50} values, which highlight good polymer thermal stability and robustness (Table 1). Such thermal properties are truly exceptional compared to conventional PEAs and other commercial plastics including PET and PEF.^[3,19] We anticipate this discovery to inspire new and exciting developments in both PET waste management and PEA design, particularly for bio-based aromatic polymers.

Chemical Recycling of BPA-PC

We then sought to explore $Zn(2)_2$ for the recycling of other polymer classes, identifying polycarbonates (PC) as a key area of opportunity for metal-based and sustainable solutions. Presently, PC production equates to ca. 5 million tonnes p/a, with BPA-PC being the market dominant polymer.^[13a]



Scheme 3. Metal-mediated BPA-PC methanolysis into BPA and DMC.

BPA-PC Methanolysis

Preliminary experiments were conducted at 75 °C based on previous state-of-the-art organocatalytic systems.^[16] Commercial BPA-PC pellets ($M_w \sim 45000 \text{ g mol}^{-1}$) and 4 wt% $Zn(2)_2$ (1.3 mol%) were used. 2-Me-THF (solvent) and an initial $n_{\text{carbonate}}:n_{\text{MeOH}}$ ratio of 1:25 were chosen based on previous work in our group.^[16h] Reaction progress was monitored using $^1\text{H NMR}$ (Figures S72–S75), observing BPA and DMC as the main degradation products (Scheme 3). Unless otherwise stated, complete BPA-PC consumption was observed. S_{BPA} and S_{OC} refer to BPA and organic carbonate selectivity respectively.

Promisingly, $Zn(2)_2$ was shown to facilitate rapid BPA-PC methanolysis at 75 °C (Figure 5a). Thus, the effect of various reaction parameters on activity was explored (Figure 5).

Effect of Reaction Parameters

Between 25–75 °C (Figure 5a), an increase in temperature coincided with enhanced BPA yield (up to 95 %) and a reduction in BPA-PC consumption rate (5–20 min). Beyond Arrhenius behaviour, it is proposed higher reaction temperatures favour BPA-PC dissolution and swelling.^[16c,17a] Prior to BPA formation, mono- (MC-BPA) and di-carbonate BPA (DC-BPA) were formed, which were considerably more pronounced at 25 °C despite a prolonged reaction time of 1 h. To assess the need for an auxiliary solvent, reactions between 50–75 °C were repeated in DMC (Table S6, Entries 1 and 2). Unsurprisingly, solvent exchange exasperated the production of MC-BPA and DC-BPA, resulting in a lower yield of BPA ($S_{\text{BPA}} = 68\text{--}80\%$).^[16h] Consequently, 2-Me-THF was retained, citing its green credentials.^[23] A

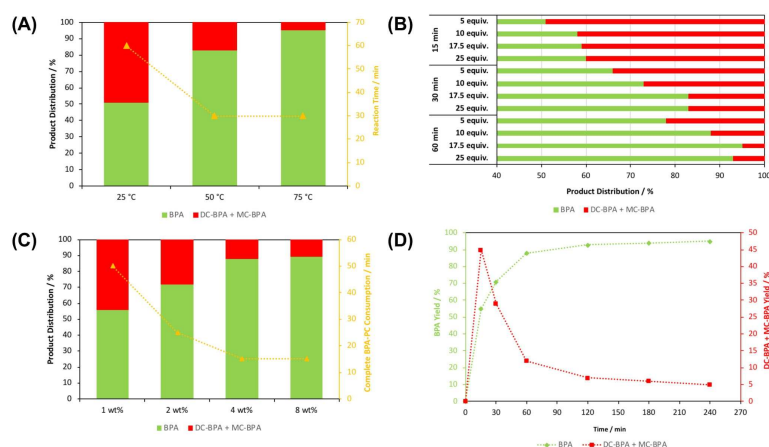


Figure 5. Effect of different reaction parameters on BPA-PC methanolysis: reaction temperature ($n_{\text{carbonate}}:n_{\text{MeOH}} = 1:25$) (A), $n_{\text{carbonate}}:n_{\text{MeOH}}$ (B), catalyst loading ($Zn(2)_2 = 1\text{--}8 \text{ wt}\% = 0.0025\text{--}0.02 \text{ g} = 0.32\text{--}2.5 \text{ mol}\%$ (relative to carbonate linkages), $n_{\text{carbonate}}:n_{\text{MeOH}} = 1:10$, 1 h) (C) and reaction time ($n_{\text{carbonate}}:n_{\text{MeOH}} = 1:10$) (D). Reaction conditions: BPA-PC (0.25 g, $M_w \sim 45000 \text{ g mol}^{-1}$), solvent: 2-methyltetrahydrofuran (2-Me-THF, 4 mL), $Zn(2)_2 = 4 \text{ wt}\%$ (0.01 g, 1.3 mol% relative to carbonate linkages) and 50 °C.

reaction temperature of 50 °C was chosen in the interest of potential cost-energy savings.

To reduce process waste, the influence of $n_{\text{carbonate}}:n_{\text{MeOH}}$ on activity was investigated with time (Figure 5b). Reaction progress was characterized by the consumption of MC-BPA and DC-BPA, resulting in superior BPA yield. Good process efficiency was maintained between 1:25 to 1:10 ($n_{\text{carbonate}}:n_{\text{MeOH}}$), achieving between 88–95% BPA yield within 1 h. Further decreasing the $n_{\text{carbonate}}:n_{\text{MeOH}}$ molar ratio to 1:5 resulted in a significant drop in productivity (78% BPA yield), which could be attributed to dilution effects. The rate of BPA-PC consumption (15 min) appeared independent of $n_{\text{carbonate}}:n_{\text{MeOH}}$ implying product distribution is equilibrium limited. A $n_{\text{carbonate}}:n_{\text{MeOH}}$ ratio of 1:10 was optimal for this reaction.

Catalyst loading was shown to impact both BPA yield and the rate of BPA-PC consumption (Figure 5c). Between 1–4 wt% the yield of BPA gradually improved from 56 to 88%, whilst the rate of BPA-PC consumption decreased from 50 to 15 min. No appreciable impact on process efficiency was observed between 4–8 wt%. Indeed, catalyst saturation has previously been shown to adversely impact productivity by catalysing detrimental side reactions.^[17c] Thus, optimal BPA recovery was possible at 4 wt% (1.3 mol%).

The effect of reaction time on BPA yield was also monitored (Figure 5d). The yield of BPA increased rapidly to 88% within the first hour before plateauing, consistent with the reaction intermediate consumption profile and previous reports.^[16c,17] Whilst a slight increase in BPA yield (up to 95%) was observed with prolonged stirring (4 h), 1 h was deemed sufficient to avoid a protracted reaction time.

Such optimized conditions are promising compared to previously reported systems, in particular the use of low temperatures and loadings.^[13a,16,17]

Reaction Scope

Under the optimized conditions ($n_{\text{carbonate}}:n_{\text{MeOH}} = 1:10$, 4 wt% catalyst, 1 h at 50 °C), reaction scope was further probed (Table S6). Surprisingly, Zn(2)Et maintained excellent performance relative to Zn(2)₂ under analogous conditions (Figure 6). Zn(OAc)₂·2H₂O was virtually inactive at 50 °C, highlighting the need for ligated complexes. Impressive Zn(2)₂ and Zn(2)Et tolerance was demonstrated through the use of mixed feeds and the degradation of a compact disc (CD), which represented a challenging BPA-PC composite (Table S6, Entries 3 and 7–9). Solvent-free methanolysis using 4 wt% Zn(2)Et at 50 °C was unsuccessful, which could be attributed to poor polymer solubility in MeOH (Table S6, Entry 10).^[13a] Organic carbonate substrate scope was extended to diethyl carbonate (DEC) *via* ethanolysis using Zn(2)Et, further promoting a green approach since ethanol can be renewably derived (Table S6, Entry 6 and Figure S77).^[24] However, an extended reaction time of 2 h was conceded to achieve comparable BPA yield ($S_{\text{BPA}} = 88\%$), owing to ethanol being a poorer nucleophile. In all instances, organic carbonate yield was *ca.* 10% lower relative to BPA values (Table S6). Indeed, the presence of residual H₂O has previously

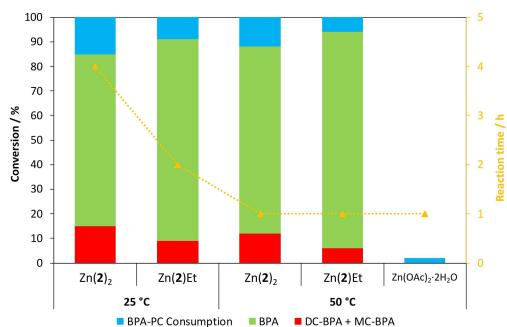


Figure 6. Catalyst performance comparison for BPA-PC methanolysis. Reaction conditions: BPA-PC (0.25 g, $M_w \sim 45000 \text{ g mol}^{-1}$), $n_{\text{carbonate}}:n_{\text{MeOH}} = 1:10$, Zn^{II}-complexes = 4 wt% (0.01 g, 1.3–2.2 mol% relative to carbonate linkages), Zn(OAc)₂·2H₂O = 4 wt% (0.01 g, 4.4 mol% relative to carbonate linkages), solvent: 2-Me-THF (4 mL).

been shown to inhibit DMC formation, consistent with the use of wet solvents.^[17c]

More importantly, we report the first example of discrete metal-mediated BPA-PC methanolysis being appreciably active at RT. Indeed, high BPA yields ($S_{\text{BPA}} = 85\text{--}91\%$) were obtainable within 2–4 h (Figure 6), surpassing previous state-of-the-art organocatalysts, such as TBD and DBU, which required prolonged stirring at RT (12–160 h).^[16a,b] Zn(2)Et furnished BPA in notably higher yields in reduced time relative to Zn(2)₂. This can likely be attributed to Zn(2)₂ being present in a slightly lower molar loading of 1.3 mol% (relative to 2.2 mol%) at 4 wt%, which could be compensated for by an increase in temperature to 50 °C (Figure 6). An acid control using dilute HCl (1 mol%) revealed no BPA-PC consumption after 4 h at RT, further highlighting the promise of these catalysts (Table S6, Entry 14). For Zn(2)₂, increasing the $n_{\text{carbonate}}:n_{\text{MeOH}}$ molar ratio to 1:25 had no effect on activity, as expected (Table S6, Entry 4). An ambient and selective recycling strategy using a mixed BPA-PC:PET feed in the presence of Zn(2)Et at 4 wt% was demonstrated on a multigram scale (Table S6, Entry 12). Crucially, process efficiency was maintained, whilst ¹H NMR and isolated BPA yields (88–89%) were comparable (Figure S76).

Degradation Kinetics

Whilst initial work established a product distribution dependence on temperature (Figure 5a and Figure 6), comparable BPA-PC consumption rates were observed between 25–50 °C (*ca.* 15 min). Thus, kinetic analysis was pursued at RT (Figure 7 and Table S7). A plot of $\ln(1/(1-X))$ against time, where X refers to BPA-PC conversion by weight, exhibited a linear relationship. This suggests the reaction proceeds pseudo-first-order with respect to BPA-PC consumption, consistent with previous work by Song and co-workers.^[16f] Consequently, the gradient of the

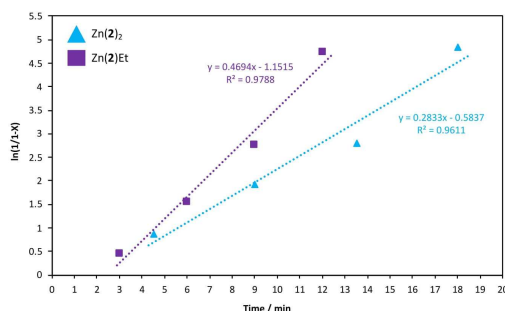


Figure 7. Pseudo-first-order logarithmic plot for BPC-PC (0.25 g, M_n ~45000 g mol^{-1}) methanolysis using Zn(2)_2 and Zn(2)Et at 4 wt% (0.01 g, 1.3–2.2 mol% relative to carbonate linkages) at room temperature. Reaction conditions: $n_{\text{carbonate}}:n_{\text{MeOH}} = 1:10$, solvent: 2-Me-THF (4 mL).

logarithmic plot is equivalent to the apparent rate constant, k_{app} .

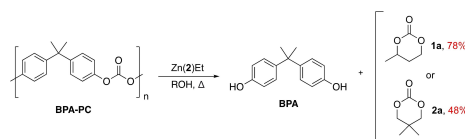
Remarkably, Zn(2)_2 and Zn(2)Et exhibited k_{app} values of 0.28 and 0.47 min^{-1} respectively at 4 wt% (Table S7, Entries 1 and 2), the highest reported to date. This breakthrough provides the foundation for further metal-mediated innovation, opening new possibilities for polycarbonate recycling under mild conditions.

Catalyst Stability

Stability testing in excess MeOH at RT was conducted to further probe the active species. ^1H NMR analysis revealed Zn(2)_2 to be stable (Figure S47). However, a change in coordination number around the metal center during methanolysis cannot be excluded due to lability of the pendant amine.^[12] Conversely, Zn(2)Et reacted to generate the corresponding -OMe analogue (Zn(2)OMe) via elimination of the terminal -Et to afford dissolve ethane (Figure S48). DOSY analysis of Zn(2)OMe revealed one species exists exclusively in solution with a diffusion constant (D) of $0.71 \times 10^{-9} \text{ m}^2 \text{ s}^{-1}$ (Figure S49). Despite having comparable M_r values, this was lower relative to Zn(2)Et ($D = 0.90 \times 10^{-9} \text{ m}^2 \text{ s}^{-1}$; Figure S30), possibly evidencing the formation of a dimer in solution.

BPA-PC Glycolysis

Recent work has highlighted the potential to access valuable cyclic carbonate monomers via BPA-PC glycolysis.^[16f,g] Traditionally, such chemicals are derived from toxic phosgene or CO, creating an appetite for greener alternatives.^[25] Consequently, we sought to diversify product scope. Reaction progress was monitored using ^1H NMR analysis (Figures S78–S80), employing tetramethylsilane (TMS) as an internal standard to determine product yields (Table S8). Zn(2)Et was selected due to catalyst availability.



Scheme 4. Metal-mediated BPA-PC glycolysis using Zn(2)Et where ROH refers to *rac*-butane-1,3-diol (**1a**) and 2,2-dimethyl-1,3-propanediol (**2a**) respectively.

Promisingly, high value cyclic carbonates (Scheme 4) were obtained in moderate to good yield (48–78%; Table S8, Entries 1 and 4), demonstrating catalyst versatility.^[9e] Cyclic carbonate selectivity (S_{CC}) was shown to be dependent on both reaction time and $n_{\text{glycol}}:n_{\text{carbonate}}$ (Table S8). Lower reaction temperatures (75 °C), catalyst loadings (2.2 mol%) and reduced reaction times (1 h) were used relative to an organocatalyst (TBD:MSA) reported by Jehanno et al.,^[16f] highlighting the promise of metal-mediated solutions for such green transformations. Additionally, excellent BPA recovery ($S_{\text{BPA}} = 96$ –99%) was observed under all reaction conditions (Table S8).

Chemical Recycling of Poly(propylene carbonate)

Finally, we endeavoured to extend Zn(2)_2 and Zn(2)Et to other commercial polycarbonates, such as poly(propylene carbonate) (PPC). PPC is a copolymer based on propylene oxide (PO) and CO_2 with uses in packaging and biomedical materials, among others.^[26] Reductive depolymerization strategies for PPC have been widely reported, although typically rely on precious metals and forcing reaction conditions.^[10c]

To the best of our knowledge, we report the first example of PPC methanolysis (Scheme S11), producing propylene carbonate (PC) in moderate to good yield (up to 58% in 1.5 h) at 50 °C (Table S9, Entry 2). PC is both a valuable green solvent and intermediate for the production of DMC via transesterification.^[18c] ^1H NMR analysis revealed the production of unidentified side-products, likely due to competing product equilibria (Figure S81), which appeared dependent on both $n_{\text{carbonate}}:n_{\text{MeOH}}$ and reaction time (Table S9). In the absence of catalyst, no PPC consumption was observed (Table S9, Entry 1). This was monitored via ^1H NMR, necessitating the use of THF to circumvent solvent/polymer peak overlapping (Figure S82).

Conclusion

A range of Zn^{II} -complexes based on half-salan ligands have been prepared and fully characterized in both the solution and solid-state. Catalyst versatility and robustness was demonstrated through the mild and selective degradation of various commercial polyesters and polycarbonates. A range of strategies (e.g. alcoholysis, glycolysis and aminolysis) were employed to obtain a diverse range of value-added chemicals with

uses as green solvents and chemical building blocks. Remarkably, Zn(2)₂ and Zn(2)Et were shown to facilitate rapid BPA-PC methanolysis (12–18 min) at room temperature in 2-Me-THF under low loadings. Further kinetic analysis found such catalysts to possess k_{app} values of 0.28 ± 0.040 and $0.47 \pm 0.049 \text{ min}^{-1}$ respectively at 4 wt%, the highest reported to date. Product distribution was found to be dependent on a number of parameters including temperature, $n_{\text{carbonate}}:n_{\text{MeOH}}$, catalyst loading and reaction time. Proof-of-concept work demonstrated a completely circular upcycling approach to plastic waste through the production of several renewable PEAs based on a terephthalamide monomer derived from bottle-grade poly(ethylene terephthalate) (PET). These materials displayed excellent thermal properties, observing T_g values up to 126 °C, whilst noting scope for further optimization. Such findings promise to stimulate new and exciting developments in both polymer design and recycling, enabling key challenges associated with a dynamic and evolving plastics economy to be addressed. Further work is ongoing to explore the optimization of such catalysts for chemical recycling applications.

Experimental Section

Exemplar procedures are provided below, see Supporting Information for full details.

Materials

The synthesis and characterization of all metal complexes was performed under an inert atmosphere of argon using standard Schlenk or Glovebox techniques. All chemicals used were purchased from Sigma-Aldrich and used as received, with the exception of rac-lactide (rac-LA), which was recrystallized once from anhydrous toluene prior to use. Dimethyl succinate (98%+, Alfa Aesar), dimethyl adipate (99%, Acros Organics), dimethyl sebacate (97%, Alfa Aesar) and dimethyl 2,5-furandicarboxylate (99%, Sarchem laboratories) were sourced from alternative suppliers. Commercial poly(lactic acid) (PLA) samples were purchased (PLLA cup, $M_n=45,510 \text{ g mol}^{-1}$, Vegware™; R600Y-VW) and cut up into $0.1 \times 0.1 \text{ cm}^2$ pieces before degradation. PLLA-based 3D printing material was kindly provided by Filamentive. Bottle-grade poly(ethylene terephthalate) (PET) (Coke Bottle, The Coca-Cola Company™, $M_n \sim 40,000 \text{ g mol}^{-1}$) was sourced from a local grocery store (Fresh, University of Bath), rinsed with acetone, air-dried and cut up into $0.1 \times 0.1 \text{ cm}^2$ pieces before degradation. PET thin-films represent waste from the manufacturing sector and were kindly donated by Avery Dennison. Poly(bisphenol A carbonate) (BPA-PC) ($M_w \sim 45,000 \text{ g mol}^{-1}$) and poly(propylene carbonate) ($M_n \sim 50,000 \text{ g mol}^{-1}$) pellets were sourced from Sigma-Aldrich and used as received. All dry solvents used in handling all metal complexes were obtained via SPS (solvent purification system).

Ligand

2H: To a solution of 3,5-dibromosalicylaldehyde (0.56 g, 2 mmol) in MeOH (5 mL), 3-(dimethylamino)-1-propylamine (0.25 mL, 2 mmol) was added dropwise and the resulting solution was stirred for 3 h at room temperature. NaBH₄ (0.19 g, 5 mmol, 2.5 equiv.) was added portion-wise with stirring, observing rapid precipitation of a white powder in a colourless solution, which was stirred for 1 h at room temperature. The reaction mixture was quenched with deionized

H₂O (5 mL) and the solvent concentrated *in vacuo*. A white powder was isolated by Buchner filtration, washed with deionized H₂O (4 × 5 mL) and dried *in vacuo*.

Zn^{II}-Complex

Zn(2)₂: To a solution of 2H (0.55 g, 1.5 mmol) in dry toluene (7.5 mL), ZnEt₂ (0.75 mL, 0.75 mmol, 1.0 M in hexane) was added dropwise with stirring, observing rapid precipitation of a white powder. The resulting suspension was stirred at 80 °C overnight under a static argon atmosphere. The product was redissolved upon vigorous heating with stirring and the flask transferred to a freezer. After 3 days at –18 °C, a white solid powder was isolated by cannula filtration and dried *in vacuo* at 80 °C for 4 h.

BPA-PC Degradation

General procedure: A J Young's ampoule was charged with BPA-PC pellets (0.25 g, $M_w \sim 45,000 \text{ g mol}^{-1}$) and metal complex (1–8 wt%, 0.0025–0.02 g, 0.32–2.5 mol% relative to carbonate linkages) in a glovebox filled with argon. 2-Me-THF (4 mL) and a desired amount of MeOH (0.21–1 mL, 5–25 equiv.) were added under a dynamic flow of argon and the ampoule was submerged in a pre-heated oil bath (50 °C), observing complete polymer dissolution within 15 to 30 min. Sample aliquots were taken under a flow of argon and analysed by ¹H NMR (CDCl₃) spectroscopy.

Acknowledgements

We wish to thank the EPSRC for funding and the University of Bath and MC² for use of their analysis facilities. We would like to thank the EPSRC for funding (EP/L016354/1) for a PhD studentship to J.P. and EP/R027129/1 for MK and MGD.

Conflict of Interest

The authors declare no conflict of interest.

Data Availability Statement

The data that support the findings of this study are available in the supplementary material of this article.

Keywords: chemical upcycling · green chemistry · homogeneous catalysis · polycarbonates · polyesters

- [1] a) R. C. Thompson, C. J. Moore, F. S. vom Saal, S. H. Swan, *Philos. Trans. R. Soc. B* **2009**, *364*, 2153–2166; b) R. A. Sheldon, M. Norton, *Green Chem.* **2020**, *22*, 6310–6322; c) J. Payne, M. Jones, *ChemSusChem* **2021**, *14*, 4041–4070.
- [2] Statista, Global plastic production 1950–2020, <https://www.statista.com/statistics/282732/global-production-of-plastics-since-1950/>, (Accessed: 5th November 2021).
- [3] M. Rabnawaz, I. Wyman, R. Auras, S. Cheng, *Green Chem.* **2017**, *19*, 4737–4753.
- [4] a) R. Geyer, J. R. Jambeck, K. L. Law, *Sci. Adv.* **2017**, *3*, e1700782; b) Ellen MacArthur Foundation, The New Plastics Economy: Rethinking the

- Future of Plastics, <https://ellenmacarthurfoundation.org/the-new-plastics-economy-rethinking-the-future-of-plastics>, (Accessed: 8th November 2021); c) J. R. Jambeck, R. Geyer, C. Wilcox, T. R. Siegler, M. Perryman, A. Andrady, R. Na, *Science* **2015**, *347*, 768–771; d) L. Lebreton, B. Slat, F. Ferrari, B. Sainte-Rose, J. Aitken, R. Marthouse, S. Hajbane, S. Cunsolo, A. Schwarz, A. Levirier, K. Noble, P. Debeljak, H. Maral, R. Schoeneich-Argent, R. Brambini, J. Reisser, *Sci. Rep.* **2018**, *8*, 4666.
- [5] a) R. Auras, B. Harte, S. Selke, *Macromol. Biosci.* **2004**, *4*, 835–864; b) K. M. Nampoothiri, N. J. Nair, R. P. John, *Bioresour. Technol.* **2010**, *101*, 8493–8501; c) C. Vilela, A. F. Sousa, A. C. Fonseca, A. C. Serra, J. F. J. Coelho, C. S. R. Freire, A. J. D. Silvestre, *Polym. Chem.* **2014**, *5*, 3119–3141; d) A. F. Sousa, C. Vilela, A. C. Fonseca, M. Matos, C. S. R. Freire, G. J. M. Gruter, J. F. J. Coelho, A. J. D. Silvestre, *Polym. Chem.* **2015**, *6*, 5961–5983.
- [6] a) J. Payne, P. McKeown, M. D. Jones, *Polym. Degrad. Stab.* **2019**, *165*, 170–181; b) M. Hong, E. X.-Y. Chen, *Green Chem.* **2017**, *9*, 3692–3706.
- [7] PlasticsEurope, Plastics—the Facts 2019. An Analysis of European Plastics Production, Demand and Waste Data, https://www.plasticseurope.org/application/files/9715/7129/9584/FINAL_web_version_Plastics_the_facts2019_14102019.pdf, (Accessed: 8th November 2021).
- [8] K. Ragaert, L. Delva, K. Van Geem, *Waste Manage.* **2017**, *69*, 24–58.
- [9] a) A. Rahimi, J. M. Garcia, *Nat. Chem. Rev.* **2017**, *1*, 0046; b) G. W. Coates, Y. D. Y. L. Getzler, *Nat. Rev. Mater.* **2020**, *5*, 501–516; c) D. K. Schneiderman, M. A. Hillmyer, *Macromolecules* **2017**, *50*, 3733–3749; d) X. Zhang, M. Fevre, G. O. Jones, R. M. Waymouth, *Chem. Rev.* **2018**, *118*, 839–885; e) P. S. Roy, G. Garnier, F. Allais, K. Saito, *ChemSusChem* **2021**, *14*, 4007–4027; f) Y. Fan, C. Zhou, X. Zhu, *Catal. Rev. Sci. Eng.* **2009**, *51*, 293–324; g) M. G. Davidson, R. A. Furlong, M. C. McManus, *J. Cleaner Prod.* **2021**, *293*, 126163.
- [10] a) P. McKeown, M. D. Jones, *Sustainable Chem.* **2020**, *1*, 1–22; b) S. C. Kosloski-Oh, Z. A. Wood, Y. Manjarrez, J. Pablo de los Rios, M. E. Fieser, *Mater. Horiz.* **2021**, *8*, 1084–1129; c) A. C. Fernandes, *Green Chem.* **2021**, *23*, 7330–7360.
- [11] a) O. Dechy-Cabaret, B. Martin-Vaca, D. Bourissou, *Chem. Rev.* **2004**, *104*, 6147–6176; b) C. M. Thomas, *Chem. Soc. Rev.* **2010**, *39*, 165–173; c) M. J. Stanford, A. P. Dove, *Chem. Soc. Rev.* **2010**, *39*, 486–494; d) R. H. Platel, L. M. Hodgson, C. K. Williams, *Polym. Rev.* **2008**, *48*, 11–63.
- [12] a) H. Liu, X. Song, F. Liu, S. Liu, S. Yu, *J. Polym. Res.* **2015**, *22*, 135–141; b) R. Petrus, D. Bykowski, P. Sobota, *ACS Catal.* **2016**, *6*, 5222–5235; c) E. L. Whitelaw, M. G. Davidson, M. D. Jones, *Chem. Commun.* **2011**, *47*, 10004–10006; d) C. Flideld, D. Vila-Viçosa, M. J. Calhorda, S. Dagorne, T. Avilés, *ChemCatChem* **2014**, *6*, 1357–1367; e) J. Payne, P. McKeown, M. F. Mahon, E. A. C. Emanuelsson, M. D. Jones, *Polym. Chem.* **2020**, *11*, 2381–2389; f) J. Payne, P. McKeown, O. Driscoll, G. Kociok-Köhn, E. A. C. Emanuelsson, M. D. Jones, *Polym. Chem.* **2021**, *12*, 1086–1096; g) J. M. Payne, G. Kociok-Köhn, E. A. C. Emanuelsson, M. D. Jones, *Macromolecules* **2021**, *54*, 8453–8469; h) L. A. Román-Ramírez, P. McKeown, M. D. Jones, *J. Wood, ACS Catal.* **2019**, *9*, 409–416; i) P. McKeown, L. A. Román-Ramírez, S. Bates, J. Wood, M. D. Jones, *ChemSusChem* **2019**, *12*, 5233–5238; j) R. Yang, G. Xu, C. Lv, B. Dong, L. Zhou, Q. Wang, *ACS Sustainable Chem. Eng.* **2020**, *8*, 18347–18353; k) F. Santulli, M. Lamberti, M. Mazzeo, *ChemSusChem* **2021**, *14*, 5470–5475.
- [13] a) J. G. Kim, *Polym. Chem.* **2020**, *11*, 4830–4849; b) E. V. Antonakou, D. S. Achillas, *Waste Biomass Valorization* **2013**, *4*, 9–21; c) V. Sinha, M. R. Patel, J. V. Patel, *J. Polym. Environ.* **2010**, *18*, 8–25; d) N. George, T. Kurian, *Ind. Eng. Chem. Res.* **2014**, *53*, 14185–14198; e) S. M. Al-Salem, P. Lettieri, J. Baeyens, *Waste Manage.* **2009**, *29*, 2625–2643.
- [14] a) K. Fukushima, J. M. Lecuyer, D. S. Wei, H. W. Horn, G. O. Jones, H. A. Al-Megren, A. M. Alabdulrahman, F. D. Alsewaillem, M. A. McNeil, J. E. Rice, J. L. Hedrick, *Polym. Chem.* **2013**, *4*, 1610–1616; b) J. Demarteau, I. Olazabal, C. Jehanno, H. Sardon, *Polym. Chem.* **2020**, *11*, 4875–4882; c) J. Natarajan, G. Madras, K. Chatterjee, *ACS Appl. Mater. Interfaces* **2017**, *9*, 28281–28297.
- [15] a) K. Troev, G. Grancharov, R. Tsevi, I. Gitsov, *J. Appl. Polym. Sci.* **2003**, *90*, 1148–1152; b) S. Wang, C. Wang, H. Wang, X. Chen, S. Wang, *Polym. Degrad. Stab.* **2015**, *114*, 105–114; c) R. Esquer, J. J. Garcia, *J. Organomet. Chem.* **2019**, *902*, 120972; d) L. Deng, R. Li, Y. Chen, J. Wang, H. Song, *J. Mol. Liq.* **2021**, *334*, 116419.
- [16] a) T. Do, E. R. Baral, J. G. Kim, *Polymer* **2018**, *143*, 106–114; b) E. Quaranta, D. Sgherza, G. Tartaro, *Green Chem.* **2017**, *19*, 5422–5434; c) M. Liu, J. Guo, Y. Gu, J. Gao, F. Liu, *ACS Sustainable Chem. Eng.* **2018**, *6*, 15127–15134; d) F. Liu, Z. Li, S. Yu, X. Cui, X. Ge, *J. Hazard. Mater.* **2010**, *174*, 872–875; e) F. Liu, L. Li, S. Yu, Z. Lv, X. Ge, *J. Hazard. Mater.* **2011**, *189*, 249–254; f) C. Jehanno, J. Demarteau, D. Mantione, M. C. Arno, F. Ruipérez, J. L. Hedrick, A. P. Dove, H. Sardon, *ACS Macro Lett.* **2020**, *9*, 443–447; g) E. Quaranta, C. C. Minichetti, G. Tartaro, *ACS Omega* **2018**, *3*, 7261–7268; h) P. McKeown, M. Kamran, M. G. Davidson, M. D. Jones, L. A. Román-Ramírez, J. Wood, *Green Chem.* **2020**, *22*, 3721–3726; i) X. Song, W. Hu, W. Huang, H. Wang, S. Yan, S. Yu, F. Liu, *Chem. Eng. J.* **2020**, *388*, 124324.
- [17] a) F. Liu, Z. Li, S. Yu, X. Cui, C. Xie, X. Ge, *J. Polym. Environ.* **2009**, *17*, 208–211; b) L.-C. Hu, A. Oku, E. Yamada, *Polymer* **1998**, *39*, 3841–3845; c) R. Piñero, J. García, M. J. Cocero, *Green Chem.* **2005**, *7*, 380–387.
- [18] a) R. Tundo, M. Selva, *Acc. Chem. Res.* **2002**, *35*, 706–716; b) M. A. Pacheco, C. L. Marshall, *Energy Fuels* **1997**, *11*, 2–29; c) B. Schäffner, F. Schäffner, S. P. Verevkin, A. Börner, *Chem. Rev.* **2010**, *110*, 4554–4581.
- [19] a) A. C. Fonseca, M. H. Gil, P. N. Simoes, *Prog. Polym. Sci.* **2014**, *39*, 1291–1311; b) A. Rodriguez-Galan, L. Franco, J. Puiggali, *Polymer* **2011**, *3*, 65–99.
- [20] a) R. Mülhaupt, *Macromol. Chem. Phys.* **2013**, *214*, 159–174; b) K. Yao, C. Tang, *Macromolecules* **2013**, *46*, 1689–1712; c) B. M. Stadler, C. Wulf, T. Werner, S. Tin, J. G. de Vries, *ACS Catal.* **2019**, *9*, 8012–8067; d) A. Gandini, T. M. Lacerda, *Prog. Polym. Sci.* **2015**, *48*, 1–39.
- [21] E. Le Roux, *Coord. Chem. Rev.* **2016**, *306*, 65–85.
- [22] Q. Cai, X. Li, W. Zhu, *Macromolecules* **2020**, *53*, 2177–2186.
- [23] D. F. Aycock, *Org. Process Res. Dev.* **2007**, *11*, 156–159.
- [24] R. T. Mathers, *J. Polym. Sci. Part A: Polym. Chem.* **2012**, *50*, 1–15.
- [25] M. North, R. Pasquale, C. Young, *Green Chem.* **2010**, *12*, 1514–1539.
- [26] J. An, Y. Ke, X. Cao, Y. Ma, F. Wang, *Polym. Chem.* **2014**, *5*, 4245–4250.

Manuscript received: February 2, 2022
Accepted manuscript online: February 3, 2022
Version of record online: ■■■, ■■■■

5.3. Experimental

Exemplar procedures, full characterisation data and representative spectra are provided herein, see ESI for full details: https://chemistry-europe.onlinelibrary.wiley.com/action/downloadSupplement?doi=10.1002%2Fessc.202200255&file=cssc202200255-sup-0001-misc_information.pdf

5.3.1. General experimental methods

General methods detailed in sections 2.3.1., 3.2.1. and 4.2.1. of Chapter 2, 3 and 4, respectively, were used. Additional material details are provided in the experimental section of publication 5.

VT NMR experiments were run on a Bruker 500 MHz spectrometer.

5.3.2. General polymerisation procedures

5.3.2.1. Lactide polymerisation

PLA production and subsequent materials characterisation was conducted as detailed in section 2.3.2.1. of Chapter 2.

5.3.2.2. PEA production

Diester (0.13 – 0.21 g, 0.92 mmol) and BHETA (0.23 g, 0.92 mmol) were charged into a glass vial to which $\text{Ti}(\text{O}^i\text{Pr})_4$ (400 ppm, stock solution, 20 $\mu\text{L mL}^{-1}$ in toluene) was added. The vial was then positioned within a heating block, which was connected to a vacuum/argon line. The heating block was evacuated once and purged with argon for at least 45 min before initiating the reaction. The first transesterification step was conducted under a constant flow of argon for 1 h at both 190 and 200 °C, and then at 210 °C for 30 min. The polycondensation step was carried out at 210 °C for 3 h under dynamic vacuum (< 1 mbar). Finally, the heating was stopped, and the vacuum removed with the introduction of argon. The samples were allowed to cool gradually to RT and retained for materials characterisation as detailed below.

PEAs derived from PET were found to be insoluble in THF, thus *N,N*-dimethylacetamide (*N,N*-DMAc) was used as an alternative eluent. Subsequent analysis was performed on an Agilent 1260 infinity instrument using a flow rate of 1 mL min^{-1} at 50 °C with a *N,N*-DMAc and 0.1% w/v LiBr eluent and a Polargel-M 300 \times 7.5 mm column. The system was referenced against 11 narrow molecular weight poly(methylmethacrylate) (PMMA) standards with detection *via* refractive index response.

Differential scanning calorimetry (DSC) analysis was conducted on a TA-instrument Q20 differential scanning calorimeter. All runs were performed under a nitrogen atmosphere with a constant flow rate of 50 mL min⁻¹. The sample (4 – 6 mg) was first equilibrated at –10 °C and then heated to 225 – 250 °C at a heating rate of 20 °C min⁻¹ to construct the first heating curve. The sample was held isothermally for 1 min before starting the cooling scan. In the cooling scan, the sample was cooled at a rate of 10 °C min⁻¹ down to –10 °C, which was maintained for 1 min. Finally, in the second heating scan, the temperature was increased from –10 to 225 – 250 °C using a heating rate of 10 °C min⁻¹. The glass transition temperature (T_g) was measured on the second heating scan.

Thermogravimetric analysis (TGA) was performed on a Setsys Evolution TGA 16/18 from Setaram. The sample (8 – 12 mg) was loaded into a 170 µL alumina crucible and the furnace purged with argon for at least 30 min at RT. The sample was then heated from RT to 120 °C at a heating rate of 10 °C min⁻¹, which was maintained for 20 min to remove any residual water. The sample was then further heated to 700 °C at a heating rate of 10 °C min⁻¹, all under a constant flow of argon.

5.3.3. General PLA degradation procedures

5.3.3.1. PLA methanolysis

PLA methanolysis was conducted as detailed in section 3.2.3.1. of Chapter 3.

5.3.3.2. PLA methanolysis kinetics

PLA methanolysis kinetic data was obtained according to the method detailed in section 3.2.3.2. of Chapter 3.

5.3.4. General PET degradation procedures

5.3.4.1. PET glycolysis

PET glycolysis was conducted as detailed in section 3.2.4.1. of Chapter 3.

5.3.4.2. PET aminolysis

Diamine terephthalamide products derived from PET aminolysis were prepared and characterised in accordance to previous work by Fukushima *et al.*^[96] BHETA was prepared in accordance to the method detailed in section 4.2.4.3.2. of Chapter 4.

5.3.4.2.1. *N,N'*-bis(2-aminoethyl)terephthalamide (BAETA)

A J Young's flask was charged with bottle-grade PET pieces (0.24 g, 0.1 × 0.1 cm², *The Coca-Cola Company*TM, $M_n \sim 40,000$ g mol⁻¹) and Zn(2)₂ (8 wt%, 0.019 g, 1.9 mol% relative to ester

linkages) in a Glovebox filled with argon. Ethylenediamine (1.34 mL, 20 mmol) was added under a dynamic flow of argon. The flask was submerged in a preheated oil bath (110 °C) and stirred for 1 h, observing the formation of an off-white slurry. The homogenous slurry was poured into hot toluene (25 mL) and filtered hot. The residual solid was redissolved in hot MeOH (25 mL) and filtered hot to remove a small amount of insoluble. The filtrate was collected, and the solvent removed *in vacuo* to afford an off-white solid, which was washed with copious amounts of isopropanol (50 mL) and dried *in vacuo* at 100 °C. The product was isolated as a white powder. Yield = 0.11 g, 36%.

5.3.5. General BPA-PC degradation procedures

5.3.5.1. BPA-PC methanolysis

A general BPA-PC methanolysis procedure is provided in the experimental section of publication 5.

General procedure for BPA isolation: Following reaction completion, diethyl ether (10 mL) was added and the volatile components were removed *in vacuo* to afford a crude white solid, which was recrystallised from hot deionised H₂O. The resulting solid was isolated by filtration and dried *in vacuo* at 90 °C for 3 h to afford a white powder.

5.3.5.2. BPA-PC methanolysis kinetics

Reaction kinetic analysis was performed as described previously by Song and co-workers.^[76] A total of 4 data points were obtained in equal intervals prior to the complete consumption of BPA-PC using the methanolysis method detailed in section 5.3.5.1. After the desired amount of time elapsed, residual BPA-PC was recovered by filtration and dried at 140 °C for 1 h or until constant weight was achieved. The pseudo-first-order rate constant (k_{app}) was determined by plotting $\ln(1/1-X)$ against time, where X corresponds to the conversion of BPA-PC, equating to depolymerisation by weight at a reaction time t.

5.3.5.3. BPA-PC glycolysis

Cyclic carbonates derived from BPA-PC glycolysis were prepared and characterised in accordance to methods described previously by Jehanno *et al.*^[85]

A J Young's flask was charged with BPA-PC pellets (0.25 g, $M_w \sim 45,000 \text{ g mol}^{-1}$) and Zn(2)Et (4 wt%, 0.01 g, 2.2 mol% relative to carbonate linkages) in a Glovebox filled with argon. 2-Me-THF (4 mL) and the desired amount of glycol (1.5 – 10 equivalents relative to carbonate linkages) were added under a dynamic flow of argon and the flask was submerged into a pre-heated oil bath (75 °C). Sample aliquots of the crude (50 μL) were taken under a flow of argon

and analysed by ^1H NMR ($\text{D}_6\text{-DMSO}$) spectroscopy. Tetramethylsilane (TMS, 10 μL , 73.5 μmol) was employed as an internal standard for calculating conversion.

5.3.6. General PPC degradation procedures

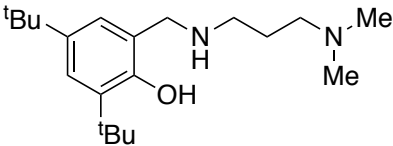
5.3.6.1. PPC methanolysis

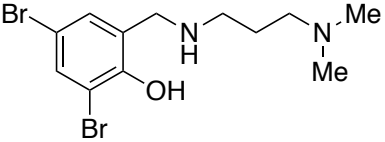
A J Young's flask was charged with PPC pellets (0.25 g, $M_n \sim 50,000 \text{ g mol}^{-1}$) and metal complex (4 wt%, 0.01 g, 0.51 – 0.88 mol% relative to carbonate linkages) in a Glovebox filled with argon. THF (4 mL) was added under a dynamic flow of argon and the flask submerged into a pre-heated oil bath (50 $^\circ\text{C}$), achieving a homogeneous solution within 30 min, with heat and stirring assisting polymer dissolution. A desired amount of MeOH (0.15 – 1 mL, 1.5 – 10 equivalents relative to carbonate linkages) was then added and the solution stirred for a predetermined amount of time (1 – 1.5 h), after which an aliquot of the crude (50 μL) was taken for ^1H NMR (CDCl_3) spectroscopic analysis. Tetramethylsilane (TMS, 10 μL , 73.5 μmol) was employed as an internal standard for calculating conversion.

5.3.7. Synthesis and characterisation

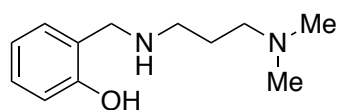
5.3.7.1. Half-salan ligands

A general synthesis procedure for a half-salan ligand (**2H**) is provided in the experimental section of publication 5. HSQC analysis assisted with peak assignment.

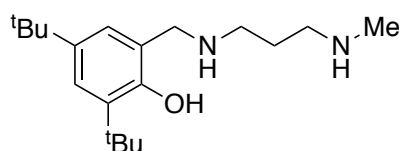
 **1H**: Isolated as a white oil (0.39 g, 1.22 mmol, 61%). ^1H NMR (C_6D_6 , 400 MHz): $\delta = 7.51$ (d, $J = 2$ Hz, 1H; ArH), 6.93 (d, $J = 2$ Hz, 1H; ArH), 3.56 (s, 2H; Ar- CH_2), 2.30 (t, $J = 7$ Hz, 2H; CH_2), 1.98 (t, $J = 7$ Hz, 2H; CH_2), 1.95 (s, 6H; $\text{N}(\text{CH}_3)_2$), 1.74 (s, 9H; $\text{C}(\text{CH}_3)_3$), 1.39 (s, 9H; $\text{C}(\text{CH}_3)_3$), 1.27 (p, $J = 7$ Hz, 2H; CH_2). *N.B.* Unaccounted for -OH and -NH resonances, likely due to rapid proton exchange in solution. $^{13}\text{C}\{^1\text{H}\}$ NMR (C_6D_6 , 125 MHz): $\delta = 155.8$, 140.4, 136.2, 123.5, 122.9, 122.8 (Ar), 58.2 (CH_2), 54.0 (Ar- CH_2), 47.5 (CH_2), 45.5 ($\text{N}(\text{CH}_3)_2$), 35.4, 34.4 ($\text{C}(\text{CH}_3)_3$), 32.1, 30.1 (CH_3), 27.3 (CH_2). ESI-MS (+ve, MeOH): Calculated m/z [$\text{C}_{20}\text{H}_{37}\text{N}_2\text{O}$] $^+$ = 321.2906; found $m/z = 321.2946$.

 **2H**: Isolated as a white solid (0.55 g, 1.50 mmol, 76%). ^1H NMR (C_6D_6 , 400 MHz): $\delta = 7.60$ (d, $J = 2$ Hz, 1H; ArH), 6.71 (d, $J = 2$ Hz, 1H; ArH), 3.06 (s, 2H; Ar- CH_2), 2.05 (t, $J = 6$ Hz, 2H; CH_2), 1.89 (s, 6H; $\text{N}(\text{CH}_3)_2$), 1.87 (t, $J = 6$ Hz, 2H; CH_2), 1.10 (p, $J = 6$ Hz, 2H; CH_2). *N.B.* Unaccounted for -OH and -NH resonances, likely due to rapid proton exchange in solution. $^{13}\text{C}\{^1\text{H}\}$ NMR (C_6D_6 , 125 MHz): $\delta = 155.8$, 134.3, 130.2, 125.5, 112.0, 110.3 (Ar),

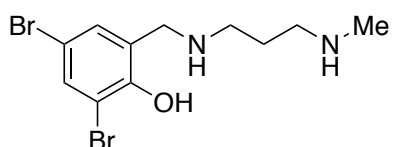
58.3 (CH₂), 52.2 (Ar-CH₂), 47.6 (CH₂), 45.4 (N(CH₃)₂), 26.6 (CH₂). ESI-MS (+ve, MeOH): Calculated m/z [C₁₂H₁₉Br₂N₂O]⁺ = 366.9844; found m/z = 366.9823.



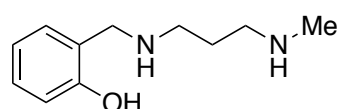
3H: Isolated as a pale yellow oil (0.41 g, 1.97 mmol, 98%). ¹H NMR (CDCl₃, 400 MHz): δ = 7.15 (td, *J* = 8, 2 Hz, 1H; ArH), 6.98 (dd, *J* = 7, 1 Hz, 1H; ArH), 6.82 (dd, *J* = 8, 1 Hz, 1H; ArH), 6.76 (td, *J* = 7, 1 Hz, 1H; ArH), 3.98 (s, 2H; Ar-CH₂), 2.73 (t, *J* = 7 Hz, 2H; CH₂), 2.33 (t, *J* = 7 Hz, 2H; CH₂), 2.20 (s, 6H; N(CH₃)₂), 1.70 (p, *J* = 7 Hz, 2H; CH₂). *N.B.* Unaccounted for -OH and -NH resonances, likely due to rapid proton exchange in solution. ¹³C{¹H} NMR (CDCl₃, 125 MHz): δ = 158.6, 128.7, 128.4, 122.7, 119.0, 116.5 (Ar), 58.2 (CH₂), 53.0 (Ar-CH₂), 47.8 (CH₂), 45.7 (N(CH₃)₂), 27.4 (CH₂). ESI-MS (+ve, MeOH): Calculated m/z [C₁₂H₂₁N₂O]⁺ = 209.1654; found m/z = 209.1640.



4H: Isolated as a white oil (0.48 g, 1.57 mmol, 79%). ¹H NMR (CDCl₃, 400 MHz): δ = 7.22 (d, *J* = 3 Hz, 1H; ArH), 6.86 (d, *J* = 3 Hz, 1H; ArH), 3.95 (s, 2H; Ar-CH₂), 2.76 (t, *J* = 7 Hz, 2H; CH₂), 2.66 (t, *J* = 7 Hz, 2H; CH₂), 2.42 (s, 3H; N(CH₃)), 1.73 (p, *J* = 7 Hz, 2H; CH₂), 1.42 (s, 9H; C(CH₃)₃), 1.28 (s, 9H; C(CH₃)₃). *N.B.* Unaccounted for -OH and -NH resonances, likely due to rapid proton exchange in solution. ¹³C{¹H} NMR (CDCl₃, 125 MHz): δ = 154.9, 140.5, 135.9, 123.2, 123.0, 122.2 (Ar), 53.8 (Ar-CH₂), 50.4, 47.3 (CH₂), 36.8 (N(CH₃)), 35.0, 34.3 (C(CH₃)₃), 31.8 (CH₃), 29.8 (CH₂), 29.8 (CH₃). ESI-MS (+ve, MeOH): Calculated m/z [C₁₉H₃₅N₂O]⁺ = 307.2749; found m/z = 307.2782.



5H: Isolated as pale-yellow solid (0.32 g, 0.91 mmol, 45%). ¹H NMR (CDCl₃, 400 MHz): δ = 7.53 (d, *J* = 2 Hz, 1H; ArH), 7.04 (d, *J* = 2 Hz, 1H; ArH), 3.95 (s, 2H; Ar-CH₂), 2.75 (t, *J* = 7 Hz, 2H; CH₂), 2.68 (t, *J* = 7 Hz, 2H; CH₂), 2.41 (s, 3H; N(CH₃)), 1.71 (p, *J* = 7 Hz, 2H; CH₂). *N.B.* Unaccounted for -OH and -NH resonances, likely due to rapid proton exchange in solution. ¹³C{¹H} NMR (CDCl₃, 125 MHz): δ = 155.2, 134.0, 130.1, 125.1, 111.5, 110.0 (Ar), 52.4 (Ar-CH₂), 50.8, 48.0 (CH₂), 36.6 (N(CH₃)), 28.9 (CH₂). ESI-MS (+ve, MeOH): Calculated m/z [C₁₁H₁₇N₂O₁Br₂]⁺ = 350.9708; found m/z = 350.9744.

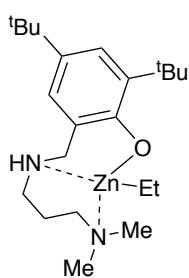


6H: Isolated as clear colourless oil (0.19 g, 0.98 mmol, 49%). ¹H NMR (CDCl₃, 400 MHz): δ = 7.16 (td, *J* = 8, 2 Hz, 1H; ArH), 6.98 (d, *J* = 8 Hz, 1H; ArH), 6.82 (dd, *J* = 8, 1 Hz, 1H; ArH), 6.76 (td, *J* = 7, 1 Hz, 1H; ArH), 3.99 (s, 2H; Ar-CH₂), 2.75 (t, *J* = 7 Hz, 2H; CH₂), 2.66 (t, *J* = 7 Hz, 2H; CH₂), 2.41 (s, 3H; N(CH₃)), 1.72 (p, *J* = 7 Hz, 2H; CH₂). *N.B.* Unaccounted for -OH and -NH resonances, likely due to rapid proton exchange in solution. Relative peak

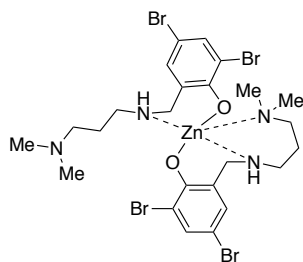
area (RPA) of aromatic resonances higher than expected, indicative of residual product impurities, which remain unidentified. One possible impurity is the presence of a minor cyclic by-product (6^*H_{cyc}) generated *via* cyclisation of the salen (6^*H) prior to reduction. This is consistent with an additional singlet resonance at $\delta = 3.98$ ppm corresponding to a methine proton (-NCH). $^{13}C\{^1H\}$ NMR ($CDCl_3$, 125 MHz): $\delta = 158.5, 128.7, 128.4, 122.7, 119.0, 116.5$ (Ar), 52.93 (Ar-CH₂), 50.48, 47.49 (CH₂), 36.73 (N(CH₃)), 29.67 (CH₂). *N.B.* Additional peaks observed due the presence of residual impurities. Purification by complexation pursued. ESI-MS (+ve, MeOH): Calculated $m/z [C_{11}H_{19}N_2O]^+ = 195.1498$; found $m/z = 195.1488$.

5.3.7.2. Zn(II)-half-salan complexes

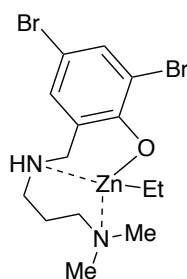
A general synthesis procedure for a Zn(II)-half-salan complex (Zn(2)₂) is provided in the experimental section of publication 5. HSQC analysis assisted with peak assignment.



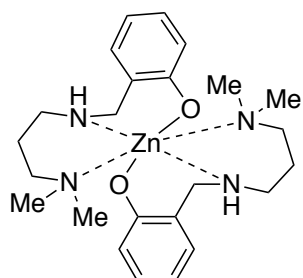
Zn(1)Et: Isolated as a white solid (0.13 g, 0.31 mmol, 55%). 1H NMR (C_6D_6 , 500 MHz): $\delta = 7.64$ (d, $J = 3$ Hz, 1H; ArH), 6.97 (d, $J = 2$ Hz, 1H; ArH), 3.46 (t, $J = 11$ Hz, 1H; Ar-CH), 3.22 (d, $J = 12$ Hz, 1H; Ar-CH), 2.16 – 2.06 (m, 1H; CH), 1.89 (br s, 16H; N(CH₃)₂; CH; C(CH₃)₃), 1.85 – 1.79 (m, 2H; CH), 1.78 – 1.71 (m, 2H; CH), 1.54 (s, 9H; C(CH₃)₃), 1.52 (t, $J = 8$ Hz, 3H; Zn-Et), 1.11 – 0.95 (m, 2H; CH, NH), 0.62 – 0.52 (m, 1H; CH), 0.45 – 0.30 (m, 2H; Zn-Et). *N.B.* Higher RPA than expected observed for $\delta = 1.85 - 1.79$ (m, 2H; CH) and 1.78 – 1.71 (m, 2H; CH), which can likely be attributed to baseline broadening. Consequently, it is proposed both resonances correspond to a single -CH resonance (RPA = 1), consistent with HSQC analysis. Broad singlet observed at $\delta = 1.89$, which could be attributed to overlapping -N(CH₃)₂ and -CH resonances with a -C(CH₃)₃ singlet. This was treated as a single peak for RPA analysis. Peak broadening can likely be attributed to structural fluxionality. $^{13}C\{^1H\}$ NMR (C_6D_6 , 125 MHz): $\delta = 164.9, 138.4, 133.9, 125.1, 124.0, 121.9$ (Ar), 60.9 (CH₂), 54.0 (Ar-CH₂), 48.7 (CH₂), 47.1 (N(CH₃)₂), 36.0, 34.3 (C(CH₃)₃), 32.5, 30.4 (CH₃), 22.8 (CH₂), 14.5 (CH₃; Zn-Et), -3.5 (CH₂; Zn-Et). *N.B.* Low signal intensity observed for -N(CH₃)₂ resonance ($\delta = 47.1$), indicative of fluxionality on the $^{13}C\{^1H\}$ NMR timescale, consistent with 1H NMR analysis. Elemental analysis: Calculated for $C_{22}H_{40}N_2O_1Zn$: C, 63.83%; H, 9.74%; N, 6.77%. Found: C, 61.64%; H, 9.52%; N, 6.61%. Elemental analysis more consistent with a degree of hydroxide during analysis, indicating poor hydrolytic stability. Zn(1)OH, theoretical: C, 59.77%; H, 9.03%; N, 6.97%.



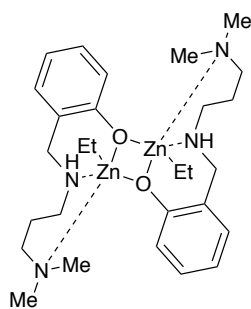
Zn(2)₂: Isolated as a white solid (0.36 g, 0.45 mmol, 60%). ¹H NMR (CDCl₃, 500 MHz): δ = 7.52 (d, *J* = 2 Hz, 1H; ArH), 7.02 (d, *J* = 3 Hz, 1H; ArH), 3.84 (br s, 2H; Ar-CH₂), 3.03 (br s, 2H; CH₂), 2.47 (s, 2H; CH₂), 2.24 (s, 6H; (N(CH₃)₂)), 1.79 (br s, 2H; CH₂). *N.B.* Unaccounted for -NH resonance, likely due to rapid proton exchange in solution. Evidence of peak broadening for -CH resonances, indicating structural fluxionality. ¹³C{¹H} NMR (CDCl₃, 125 MHz): δ = 161.9, 134.4, 132.0, 126.9, 115.7, 103.6 (Ar), 62.0 (CH₂), 52.0 (Ar-CH₂), 49.3 (CH₂), 46.8 (N(CH₃)₂), 24.0 (CH₂). *N.B.* Low -CH₂ signal intensity observed, indicative of fluxionality on the ¹³C{¹H} NMR timescale, consistent with ¹H NMR analysis. Elemental analysis: Calculated for C₂₄H₃₄Br₄N₄O₂Zn: C, 36.23%; H, 4.31%; N, 7.04%. Found: C, 37.02%; H, 4.42%; N, 6.84%.



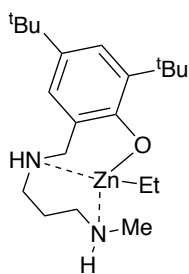
Zn(2)Et: Isolated as a white solid (0.54 g, 1.18 mmol, 78%). ¹H NMR (C₆D₆, 500 MHz): δ = 7.88 (s, 1H; ArH), 6.86 (s, 1H; ArH), 3.48 (d, *J* = 12 Hz, 1H; Ar-CH), 2.62 (d, *J* = 11 Hz, 1H; Ar-CH), 2.21 – 1.63 (br m, 9H; N(CH₃)₂, CH), 1.55 (t, *J* = 8 Hz, 4H; Zn-Et, CH), 1.44 – 1.37 (br m, 1H; CH), 0.85 (br s, 1H; NH), 0.52 (br s, 1H; CH), 0.45 – 0.33 (m, 1H; Zn-Et), 0.33 – 0.20 (m, 1H; Zn-Et). *N.B.* -CH resonances were observed to be inequivalent and broad, indicative of catalyst asymmetry and structural fluxionality. Consequently, overlapping peaks between δ = 2.21 – 1.63 ppm were treated as a single multiplet. ¹³C{¹H} NMR (C₆D₆, 125 MHz): δ = 163.1, 135.4, 132.8, 124.2, 117.0, 102.7 (Ar), 61.0 (CH₂), 52.7 (Ar-CH₂), 47.5, 24.2 (CH₂), 14.2 (CH₃; Zn-Et), -3.5 (CH₂; Zn-Et). *N.B.* Unaccounted for -N(CH₃)₂ resonance, consistent with the absence of a well-defined signal in the ¹H NMR, indicating fluxionality on the ¹³C{¹H} NMR timescale. Elemental analysis: Calculated for C₁₄H₂₂Br₂N₂O₁Zn: C, 36.59%; H, 4.83%; N, 6.10%. Found: C, 36.55%; H, 4.76%; N, 6.10%.



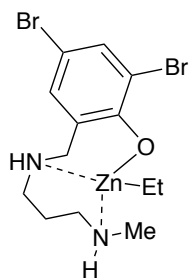
Zn(3)₂: Isolated as a white solid (0.21 g, 0.44 mmol, 44%). ¹H NMR (CDCl₃, 500 MHz): δ = 7.12 (td, *J* = 7, 2 Hz, 1H; ArH), 6.94 (d, *J* = 7 Hz, 1H; ArH), 6.75 (d, *J* = 8 Hz, 1H; ArH), 6.48 (t, *J* = 7 Hz, 1H; ArH), 3.92 (s, 2H; Ar-CH₂), 2.90 (t, *J* = 6 Hz, 2H; CH₂), 2.33 (t, *J* = 6 Hz, 2H; CH₂), 2.14 (s, 6H; N(CH₃)₂), 1.64 (p, *J* = 6 Hz, 2H; CH₂). *N.B.* Unaccounted for -NH resonance, likely due to rapid proton exchange in solution. ¹³C{¹H} NMR (CDCl₃, 125 MHz): δ = 166.9, 130.5, 130.3, 123.1, 120.2, 114.3 (Ar), 60.0 (CH₂), 53.2 (Ar-CH₂), 49.7 (CH₂), 46.3 (N(CH₃)₂), 24.6 (CH₂). Elemental analysis: Calculated for C₂₄H₃₈N₄O₂Zn: C, 60.06%; H, 7.98%; N, 11.67%. Found: C, 59.96%; H, 7.84%; N, 11.60%.



[Zn(3)Et]₂: Isolated as an off-white solid (0.23 g, 0.38 mmol, 27%). ¹H NMR (Toluene-*d*₈, 248 K, 500 MHz): δ = 7.30 (t, *J* = 8 Hz, 1H; ArH), 7.06 (d, *J* = 7 Hz, 1H; ArH), 6.95 (s, 1H; ArH), 6.71 (t, *J* = 7 Hz, 1H; ArH), 4.77 (d, *J* = 13 Hz, 1H; Ar-CH), 4.11 (t, *J* = 12 Hz, 1H; NH), 3.20 (t, *J* = 12 Hz, 1H; Ar-CH), 2.63 (d, *J* = 11 Hz, 1H; CH), 2.04 – 1.94 (m, 1H; CH), 1.86 (s, 3H; N(CH₃)), 1.84 (t, *J* = 8 Hz, 3H; Zn-Et), 1.70 – 1.63 (m, 1H; CH), 1.52 (s, 3H; N(CH₃)), 1.14 (d, *J* = 13 Hz, 1H; CH), 0.65 (q, *J* = 8 Hz, 2H; Zn-Et), 0.58 – 0.38 (m, 2H; CH). ¹³C{¹H} NMR (Toluene-*d*₈, 248 K, 125 MHz): δ = 167.9, 131.2, 130.1, 125.9, 119.3, 113.1 (Ar), 61.3 (CH₂), 53.9 (Ar-CH₂), 49.5 (N(CH₃)), 48.6 (CH₂), 42.8 (N(CH₃)), 24.5 (CH₂), 15.3 (CH₃; Zn-Et), -3.3 (CH₂; Zn-Et). Elemental analysis: Calculated for C₂₈H₄₈N₄O₂Zn₂: C, 55.73%; H, 8.02%; N, 9.28%. Found: C, 54.68%; H, 7.82%; N, 9.08%.



Zn(4)Et: Isolated as a white solid (0.33 g, 0.83 mmol, 53%). ¹H NMR (C₆D₆, 500 MHz): δ = 7.64 (d, *J* = 3 Hz, 1H; ArH), 7.02 (d, *J* = 3 Hz, 1H; ArH), 3.32 (dd, *J* = 11, 8 Hz, 1H; Ar-CH), 3.20 (d, *J* = 10 Hz, 1H; Ar-CH), 2.07 – 1.99 (m, 2H; CH), 1.89 (s, 9H; C(CH₃)₃), 1.86 (d, *J* = 6 Hz, 3H; N(CH₃)H), 1.79 – 1.70 (m, 1H; CH), 1.70 – 1.62 (m, 1H; CH), 1.55 (t, *J* = 8 Hz, 3H; Zn-Et), 1.52 (s, 9H; C(CH₃)₃), 1.30 – 1.25 (m, 1H; NH), 1.03 – 0.93 (m, 2H; CH, NH), 0.58 (d, *J* = 14 Hz, 1H; CH), 0.43 (qd, *J* = 8, 1 Hz, 2H; Zn-Et). *N.B.* Evidence of peak broadening for -CH resonances, indicating structural fluxionality. ¹³C{¹H} NMR (C₆D₆, 125 MHz): δ = 164.9, 138.6, 134.2, 125.0, 124.1 (Ar), 53.8 (Ar-CH₂), 52.2, 50.3 (CH₂), 37.3 (N(CH₃)H), 35.9, 34.3 (C(CH₃)₃), 32.5, 30.4 (CH₃), 25.5 (CH₂), 14.6 (CH₃; Zn-Et), -3.9 (CH₂; Zn-Et). *N.B.* Unaccounted for Ar resonance, likely due to peak overlapping with solvent resonance (δ = 128.06). Additional peaks can be attributed to the presence of residual *n*-hexane. Elemental analysis: Calculated for C₂₁H₃₈N₂O₁Zn: C, 63.07%; H, 9.58%; N, 7.00%. Found: C, 62.52%; H, 9.58%; N, 6.94%.



Zn(5)Et: Isolated as a white solid (0.25 g, 0.56 mmol, 62%). ¹H NMR (C₆D₆, 500 MHz): δ = 7.81 (d, *J* = 3 Hz, 1H; ArH), 6.82 (d, *J* = 2 Hz, 1H; ArH), 3.11 (br s, 1H; Ar-CH), 2.35 (br s, 2H; Ar-CH, CH), 2.17 (d, *J* = 6 Hz, 3H; N(CH₃)H), 1.91 – 1.73 (m, 3H; CH, NH), 1.64 (d, *J* = 12 Hz, 1H; CH), 1.55 (t, *J* = 8 Hz, 3H; Zn-Et), 0.89 – 0.78 (m, 2H; CH, NH), 0.63 (d, *J* = 15 Hz, 1H; CH), 0.43 – 0.31 (m, 2H; Zn-Et). *N.B.* Evidence of peak broadening for -CH resonances, indicating structural fluxionality. ¹³C{¹H} NMR (C₆D₆, 125 MHz): δ = 162.2, 135.5, 135.3, 132.3, 116.7, 104.0 (Ar), 52.8 (CH₂), 50.9 (Ar-CH₂), 49.9 (CH₂), 38.0 (N(CH₃)H), 25.2 (CH₂), 14.1 (CH₃; Zn-Et), -4.1 (CH₂; Zn-Et). Elemental analysis: Calculated for C₁₃H₂₀Br₂N₂O₁Zn: C, 35.05%; H, 4.53%; N, 6.29%. Found: C, 33.36%; H, 4.22%; N, 5.70%. Elemental analysis more consistent with a degree of hydroxide during analysis, indicating poor hydrolytic stability. Zn(5)OH, theoretical: C, 30.48%; H, 3.72%; N, 6.46%.

5.3.7.3. Representative NMR spectra

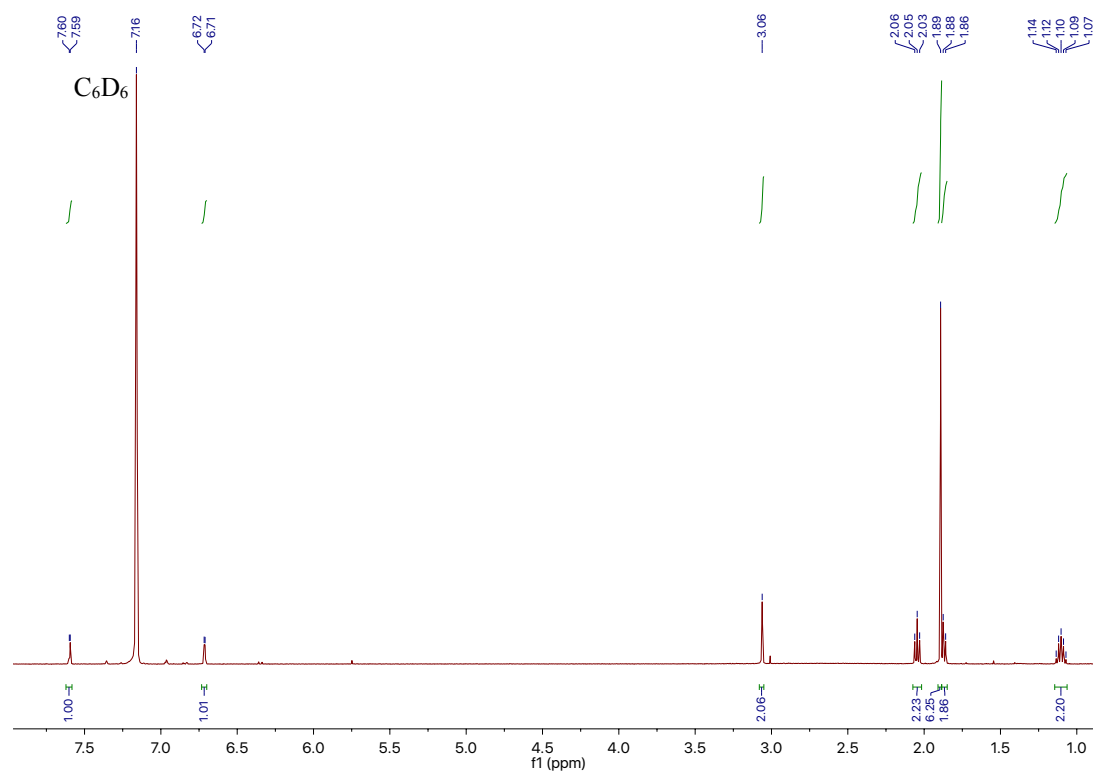


Figure 5.6. ^1H NMR (C_6D_6 , 400 MHz) spectrum of **2H**. *N.B.* Figure S4 in ESI.

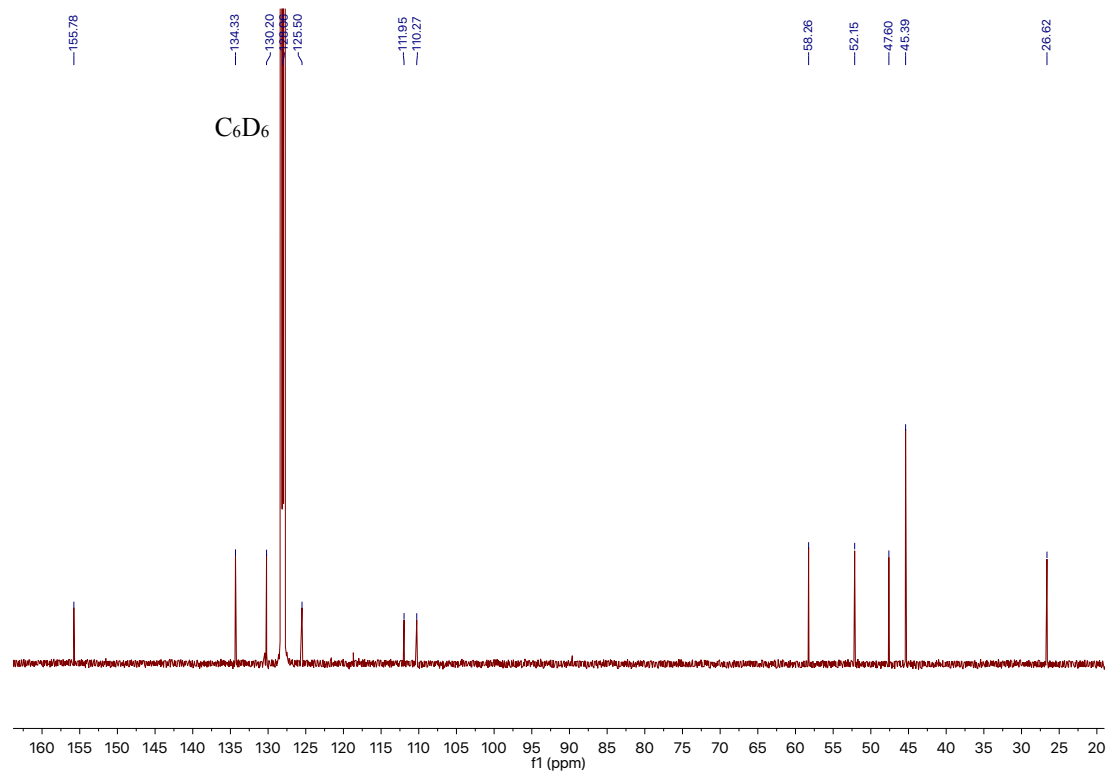


Figure 5.7. ^{13}C (^1H) NMR (C_6D_6 , 125 MHz) spectrum of **2H**. *N.B.* Figure S5 in ESI.

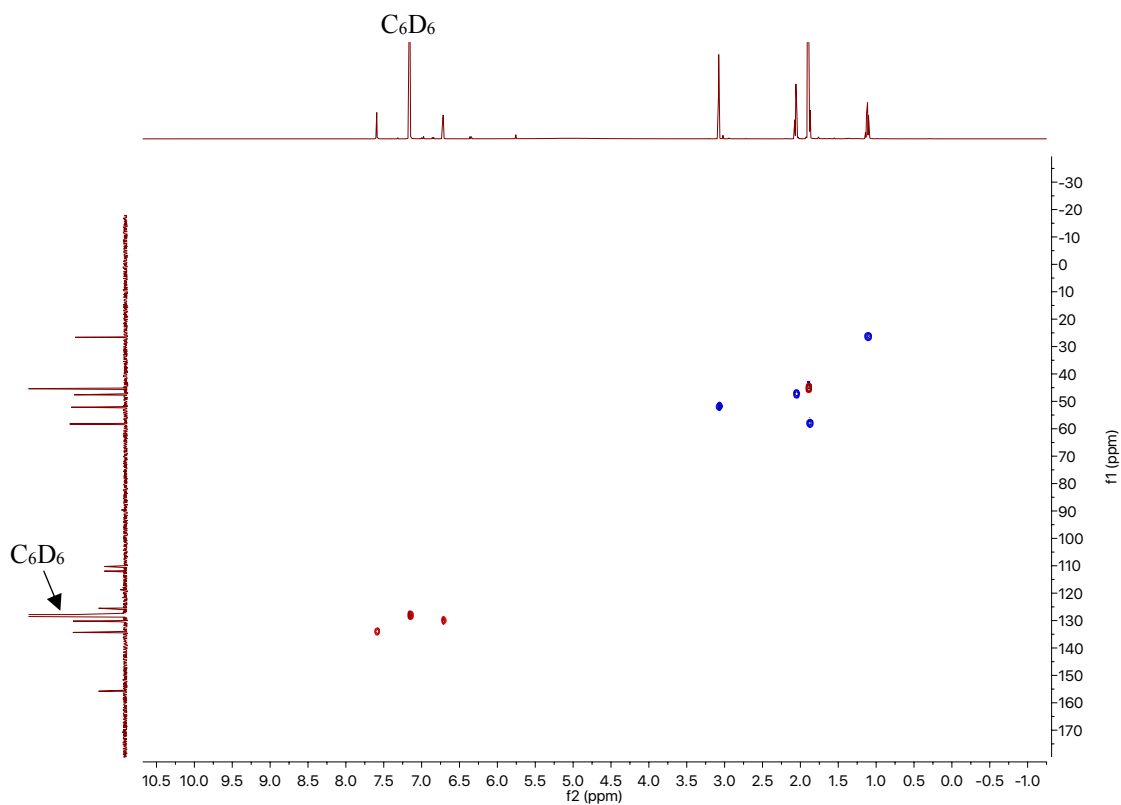


Figure 5.8. HSQC NMR (C_6D_6 , 125 MHz) spectrum of **2H**. *N.B.* Figure S6 in ESI.

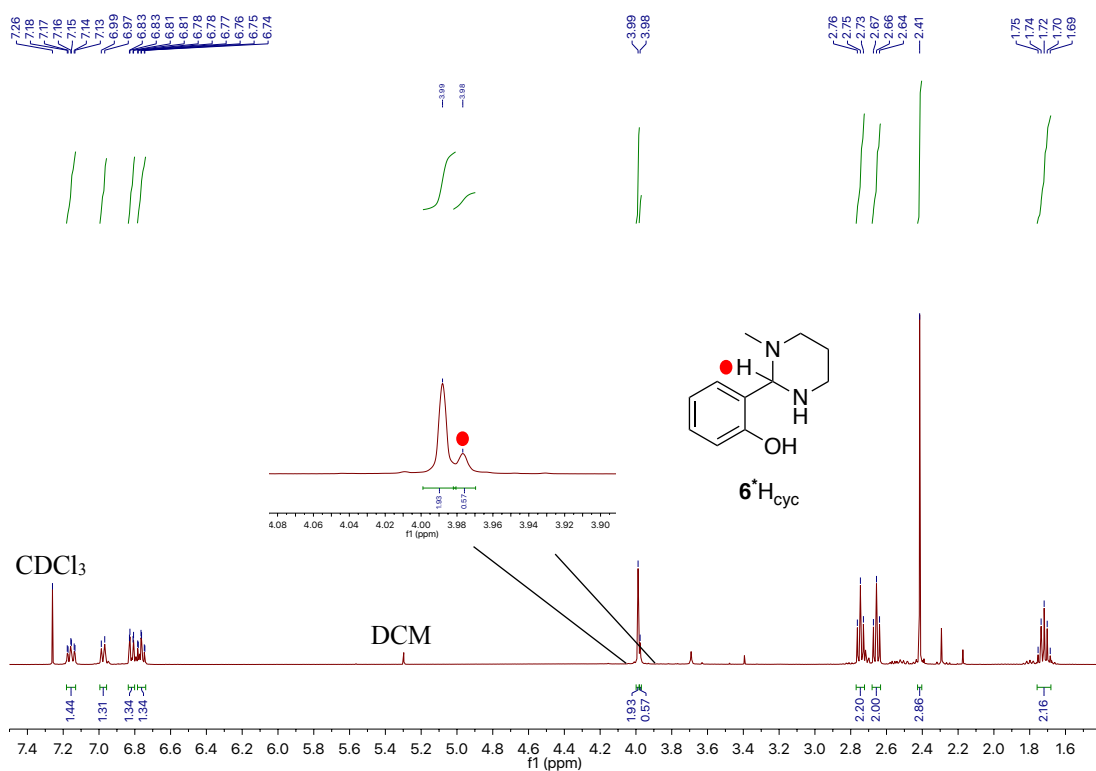


Figure 5.9. 1H NMR ($CDCl_3$, 400 MHz) spectrum of **6H**. *N.B.* Figure S16 in ESI.

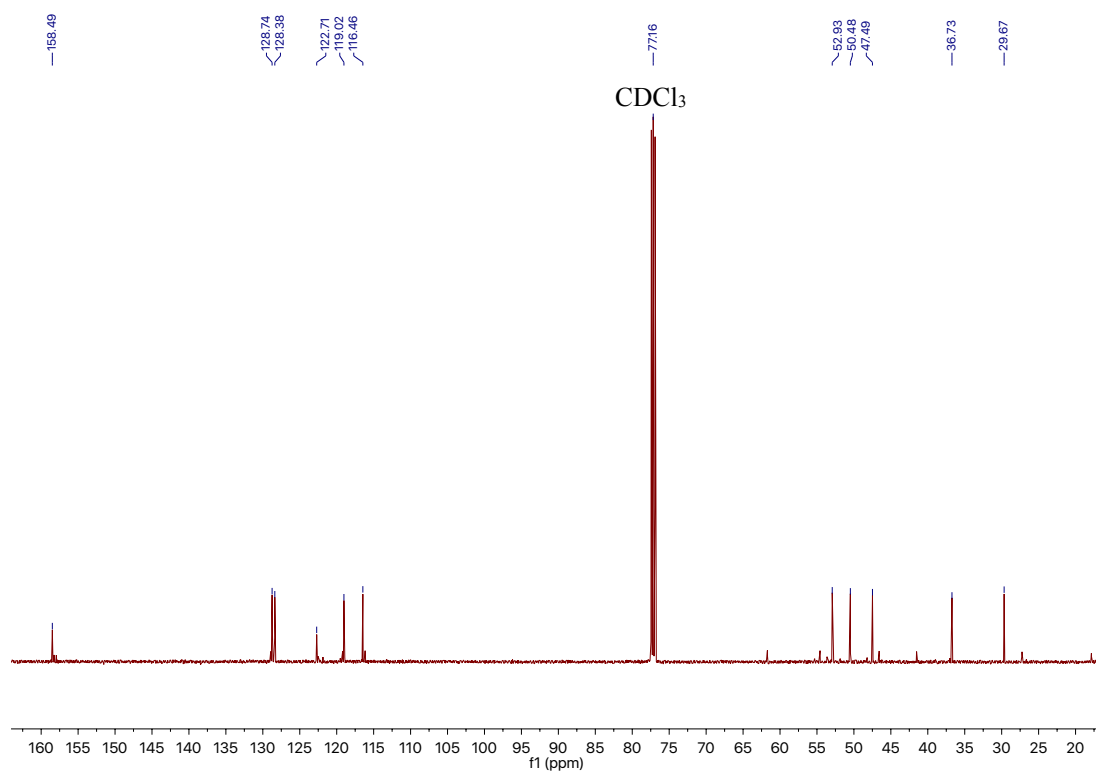


Figure 5.10. $^{13}\text{C}\{^1\text{H}\}$ NMR (CDCl_3 , 125 MHz) spectrum of **6H**. *N.B.* Figure S17 in ESI.

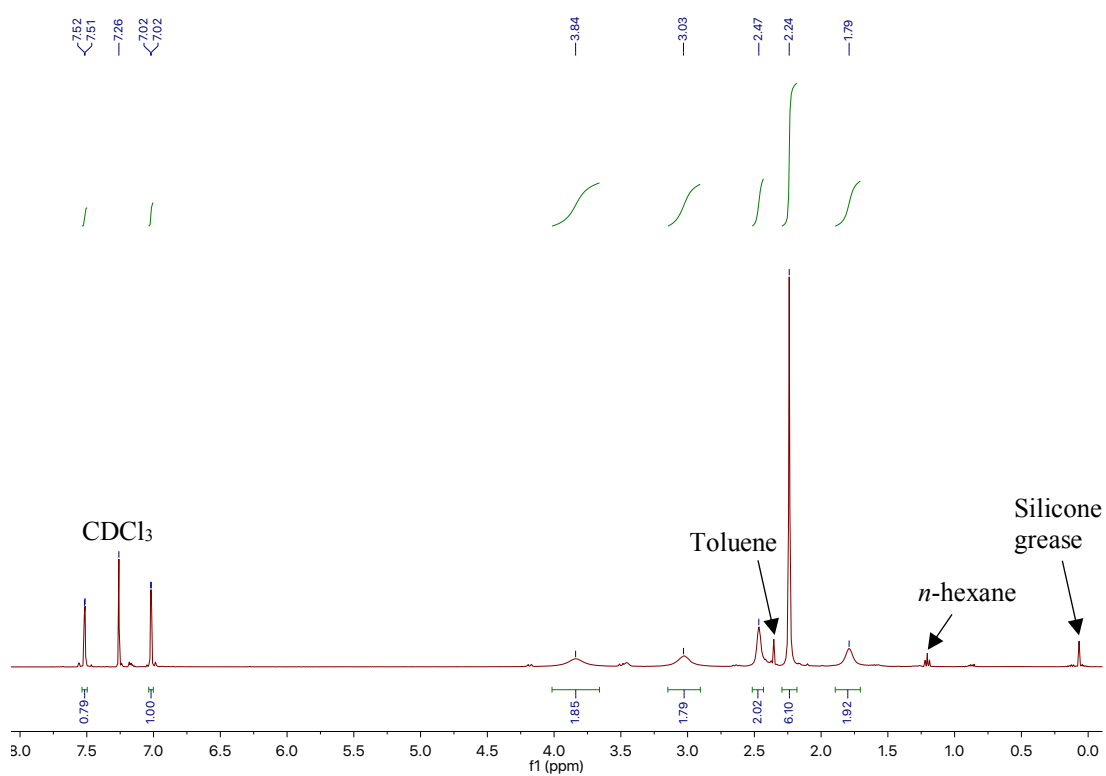


Figure 5.11. ^1H NMR (CDCl_3 , 500 MHz) spectrum of $\text{Zn}(\mathbf{2})_2$. *N.B.* Figure S23 in ESI.

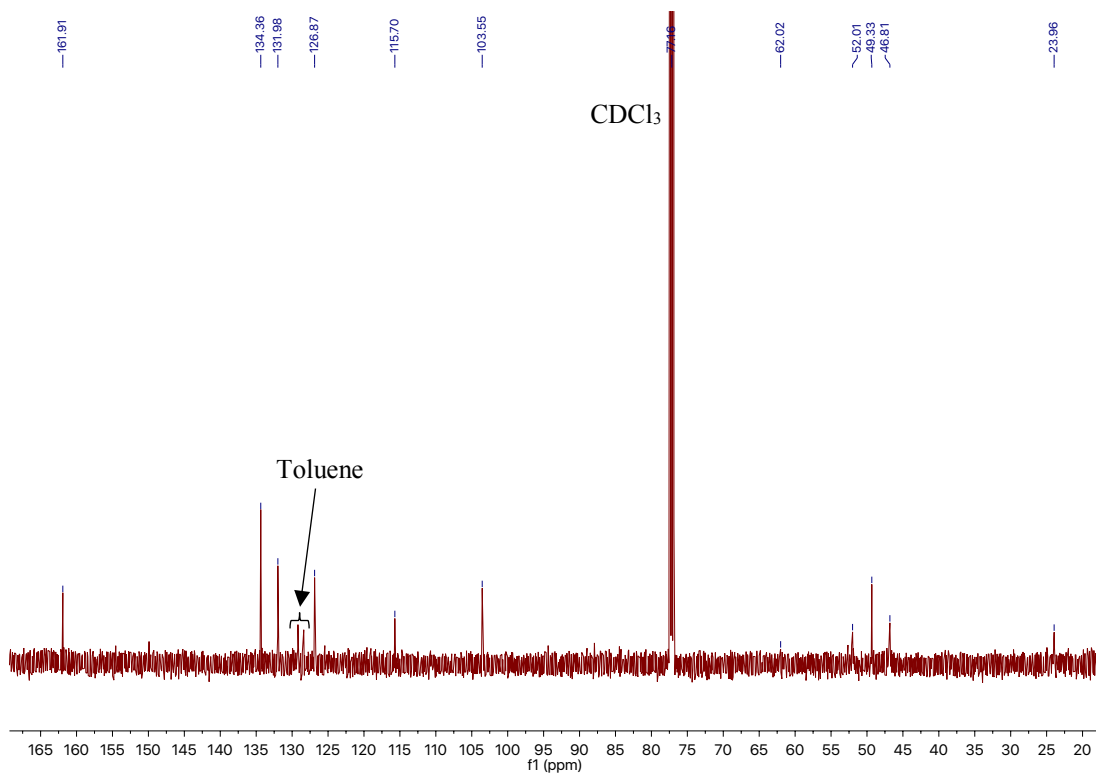


Figure 5.12. $^{13}\text{C}\{^1\text{H}\}$ NMR (CDCl_3 , 125 MHz) spectrum of $\text{Zn}(\mathbf{2})_2$. *N.B.* Figure S24 in ESI.

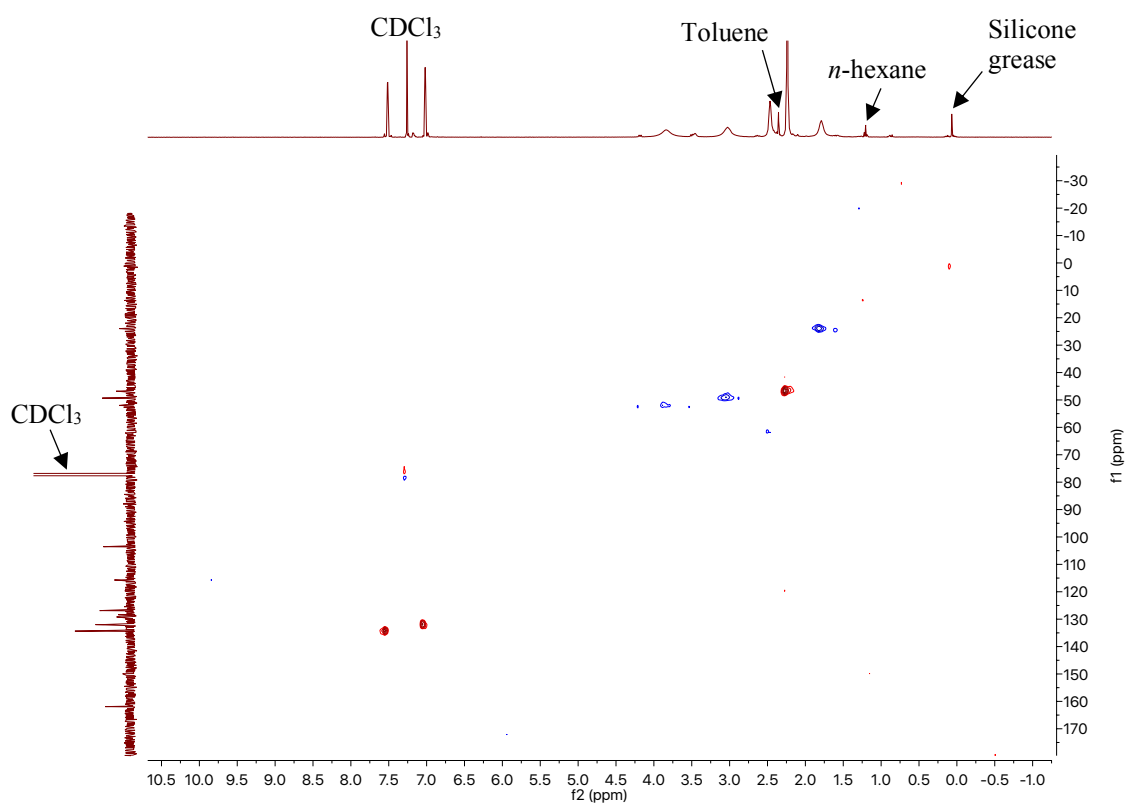


Figure 5.13. HSQC NMR (CDCl_3 , 125 MHz) spectrum of $\text{Zn}(\mathbf{2})_2$. *N.B.* Figure S25 in ESI.

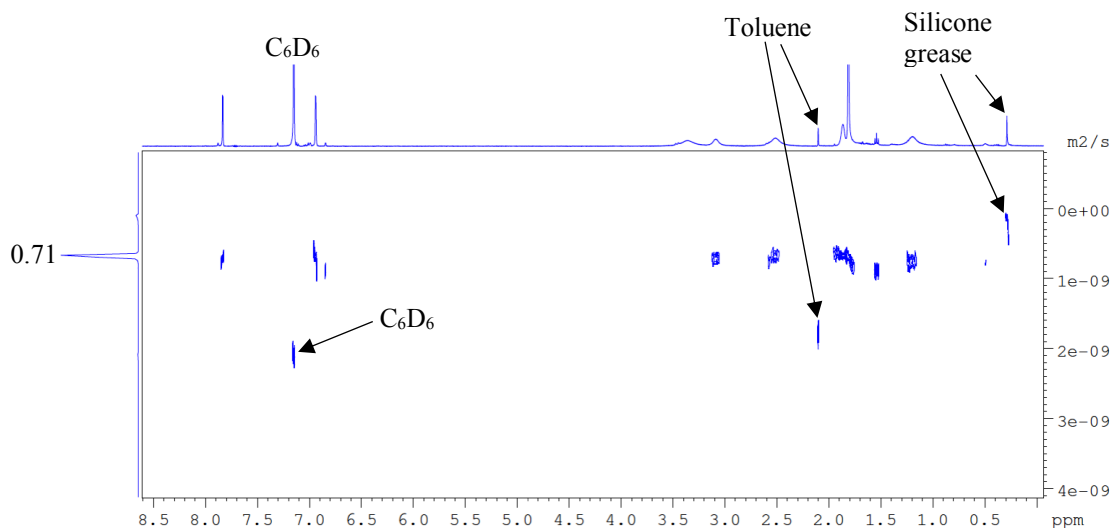


Figure 5.14. DOSY NMR (C_6D_6 , 500 MHz) spectrum of $\text{Zn}(\mathbf{2})_2$, indicating only one species present in solution, with a diffusion constant of $0.71 \times 10^{-9} \text{ m}^2 \text{ s}^{-1}$. *N.B.* Figure S26 in ESI.

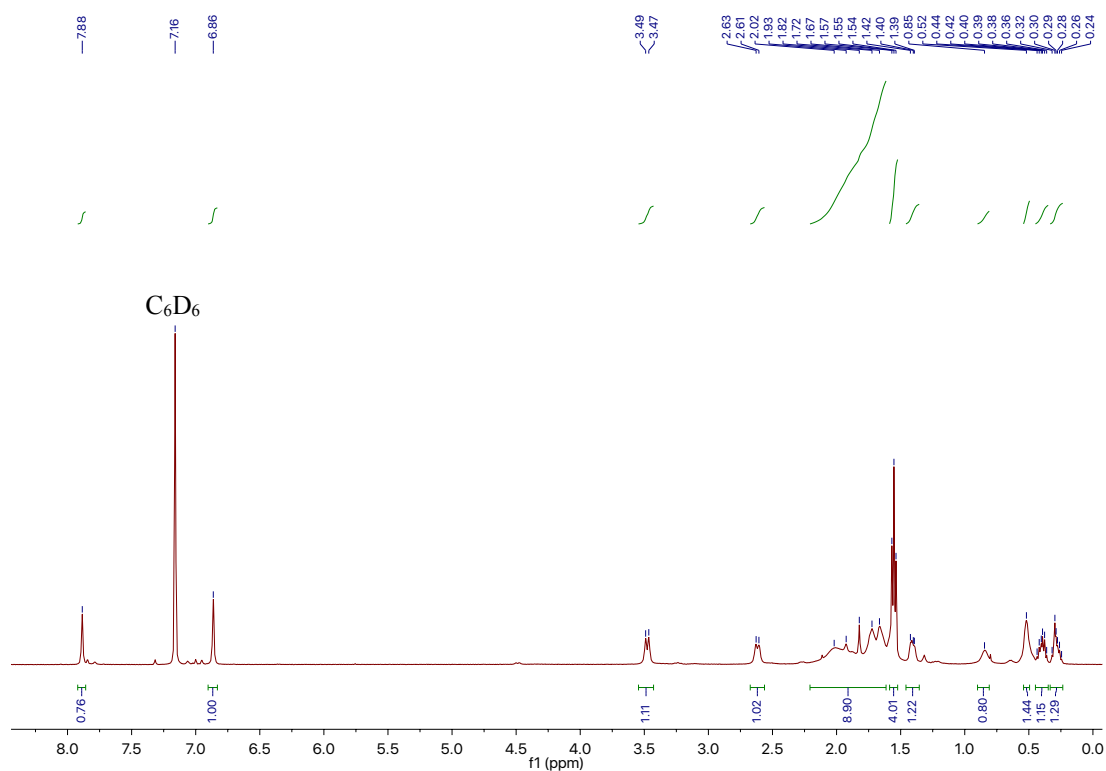


Figure 5.15. ^1H NMR (C_6D_6 , 500 MHz) spectrum of $\text{Zn}(\mathbf{2})\text{Et}$. *N.B.* Figure S27 in ESI.

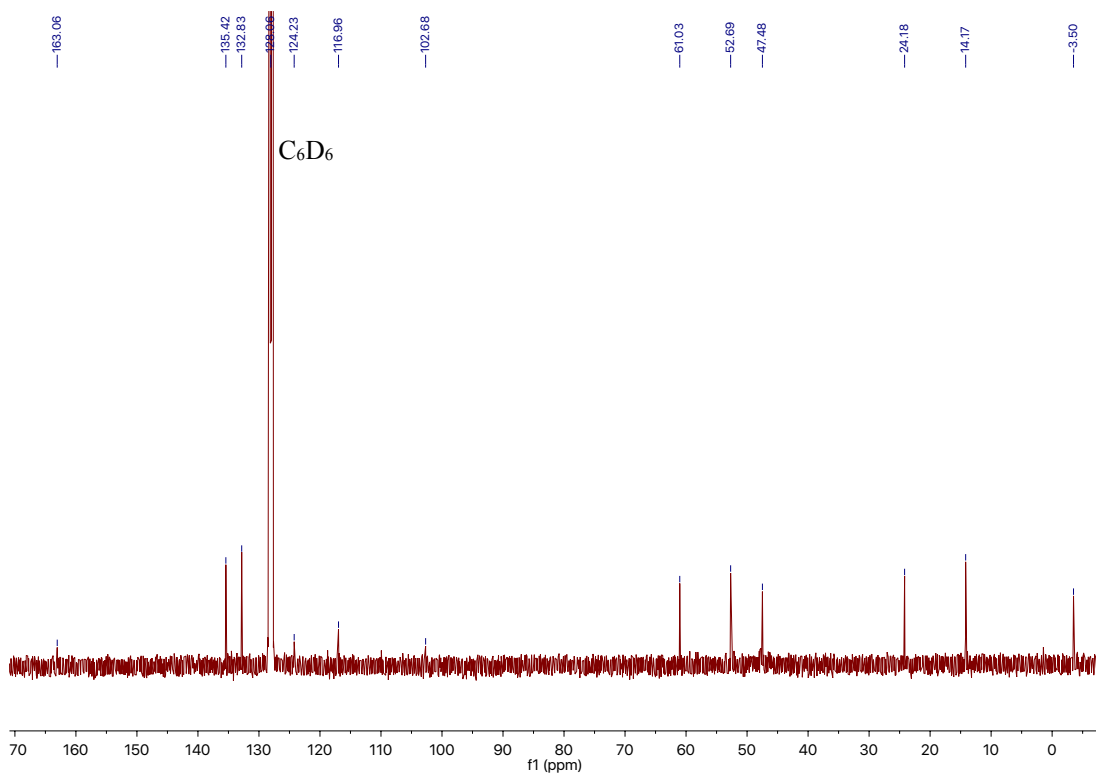


Figure 5.16. $^{13}\text{C}\{^1\text{H}\}$ NMR (C_6D_6 , 125 MHz) spectrum of $\text{Zn}(\mathbf{2})\text{Et}$. *N.B.* Figure S28 in ESI.

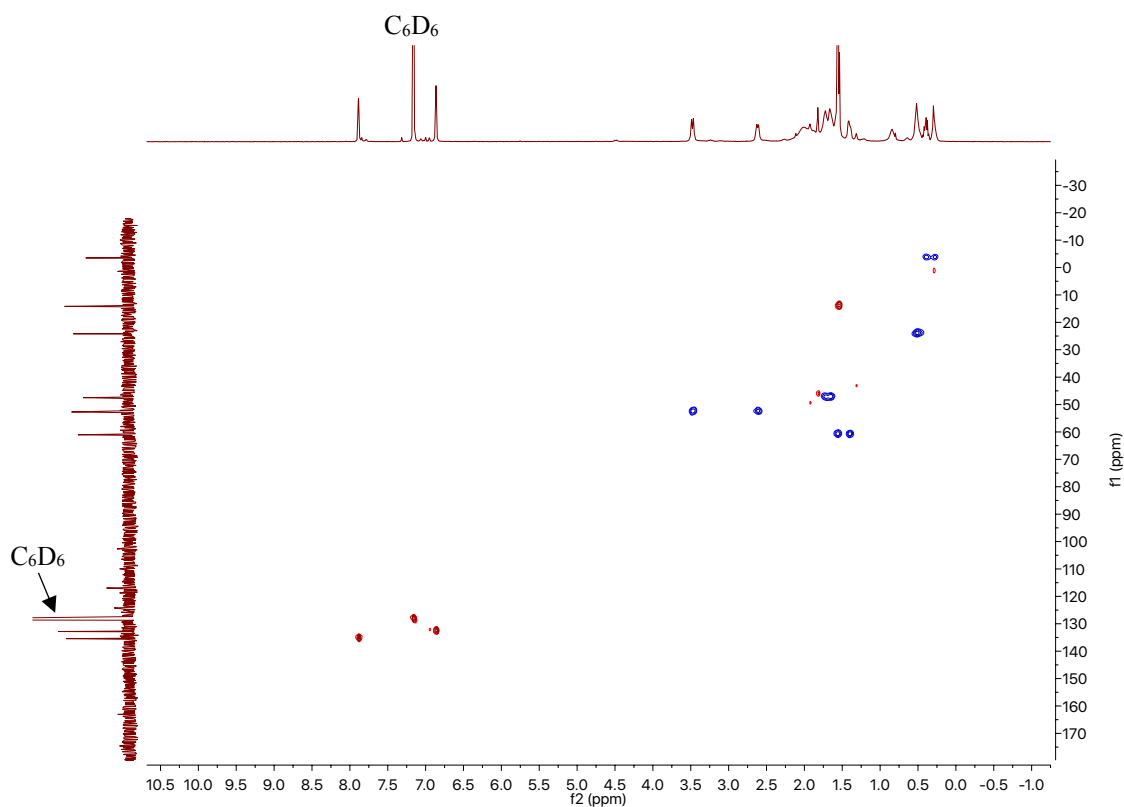


Figure 5.17. HSQC NMR (C_6D_6 , 125 MHz) spectrum of $\text{Zn}(\mathbf{2})\text{Et}$. *N.B.* Figure S29 in ESI.

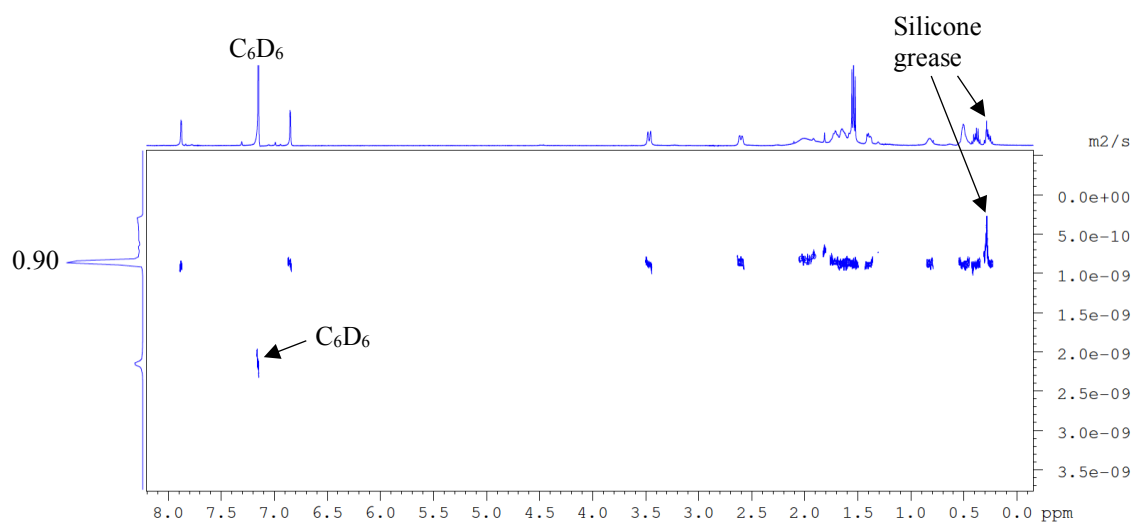


Figure 5.18. DOSY NMR (C₆D₆, 500 MHz) spectrum of Zn(2)Et, indicating only one species present in solution, with a diffusion constant of $0.90 \times 10^{-9} \text{ m}^2 \text{ s}^{-1}$. *N.B.* Figure S30 in ESI.

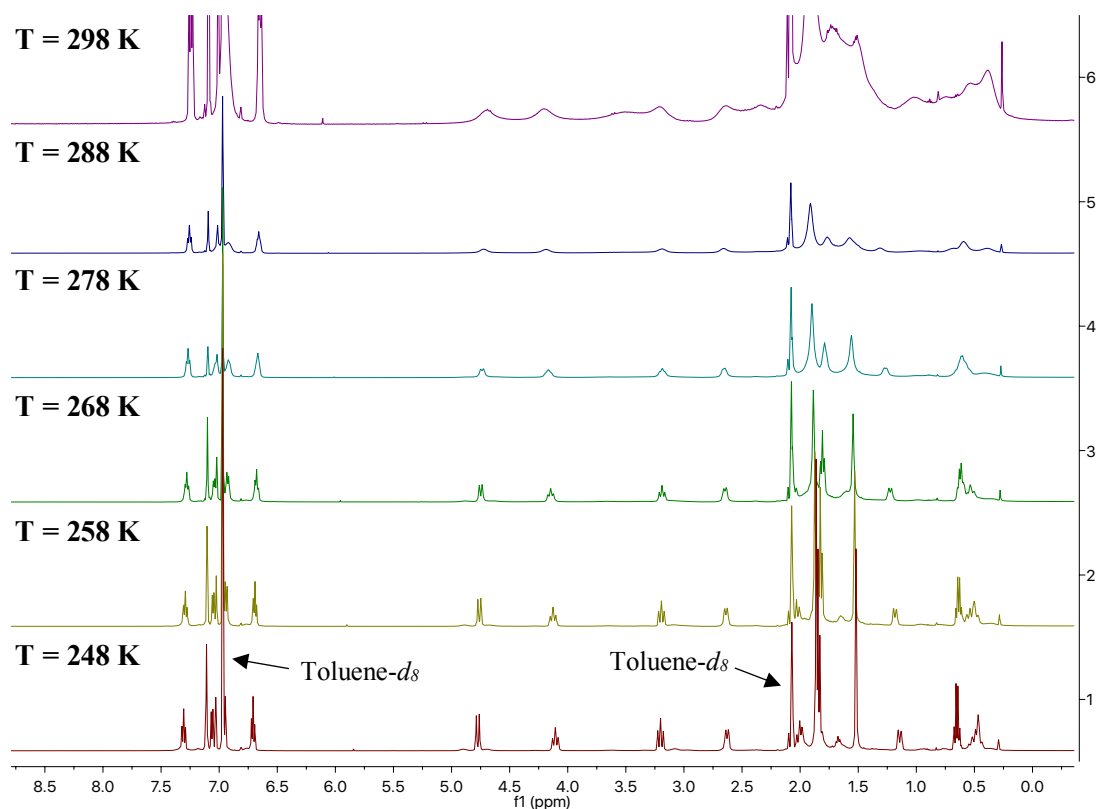


Figure 5.19. VT ¹H NMR (Toluene-*d*₈, 500 MHz) spectrum of [Zn(3)Et]₂ between 248 to 298 K. *N.B.* Figure S36 in ESI.

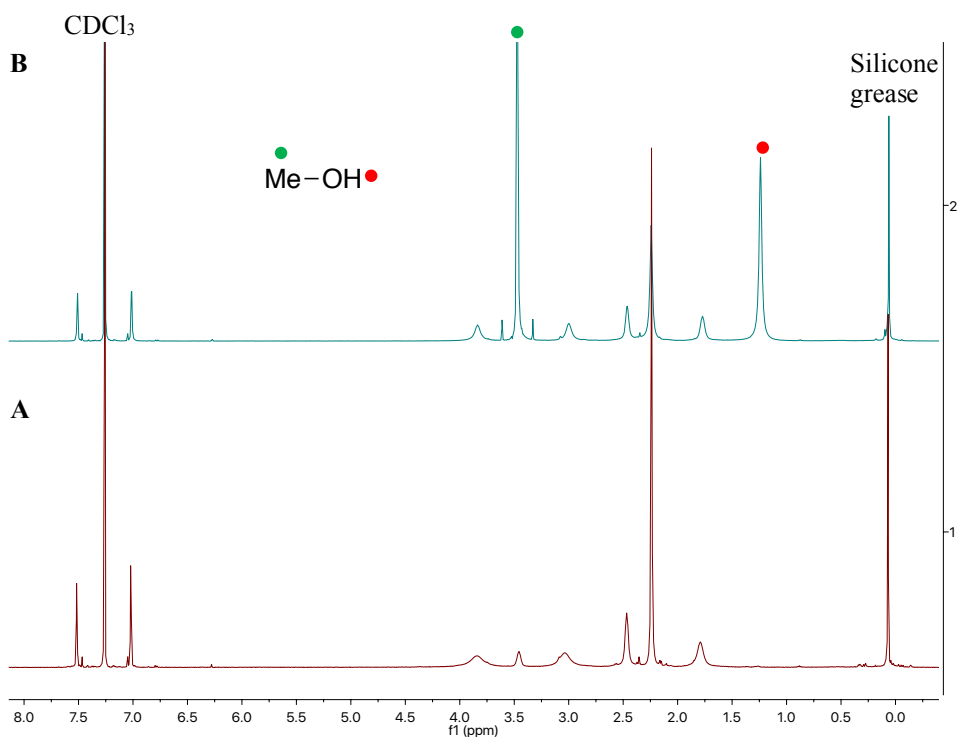


Figure 5.20. Stacked ^1H NMR (CDCl_3 , 500 MHz) spectra assessing the stability of $\text{Zn}(\mathbf{2})_2$ with MeOH at RT: (A) $\text{Zn}(\mathbf{2})_2$, and; (B): $\text{Zn}(\mathbf{2})_2 + \text{MeOH}$. *N.B.* Figure S47 in ESI.

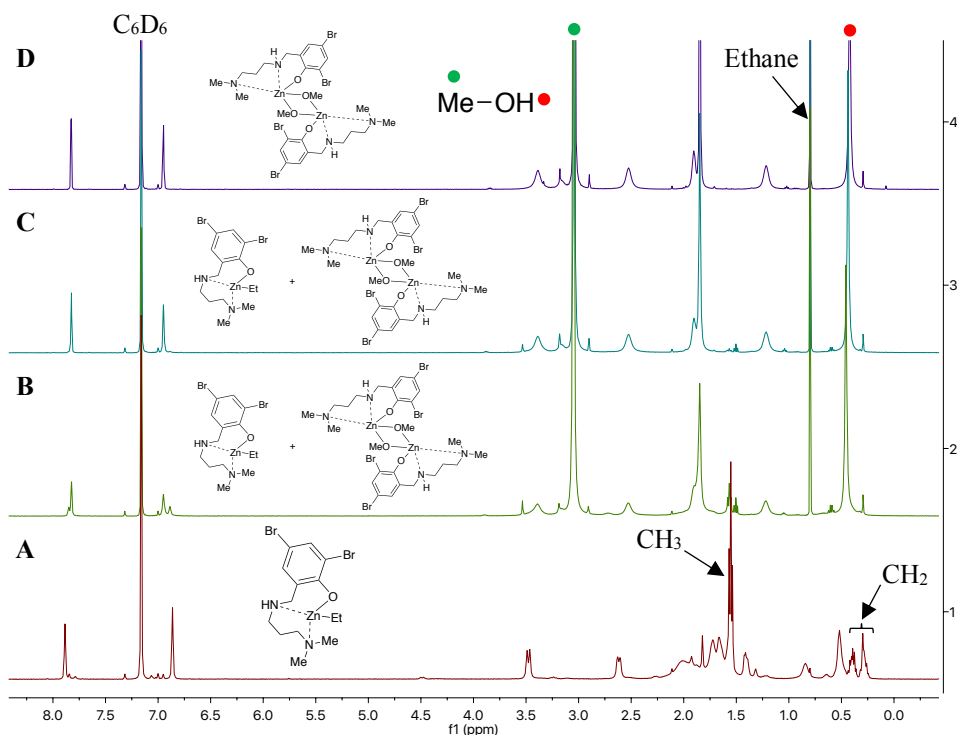


Figure 5.21. Stacked ^1H NMR (C_6D_6 , 500 MHz) spectra assessing the stability of $\text{Zn}(\mathbf{2})\text{Et}$ with excess MeOH at RT: (A) $\text{Zn}(\mathbf{2})\text{Et}$, (B) $\text{Zn}(\mathbf{2})\text{Et} + \text{MeOH}$ after 15 min, (C) $\text{Zn}(\mathbf{2})\text{Et} + \text{MeOH}$ after 30 min, and; (D) $\text{Zn}(\mathbf{2})\text{Et} + \text{MeOH}$ after 1 h. *N.B.* $\text{Zn}(\mathbf{2})\text{OMe}$ is shown to adopt a dimeric structure based on DOSY analysis. Dissolved ethane resonance appears at $\delta = 0.80$ ppm, consistent with the literature.^[97] Figure S48 in ESI.

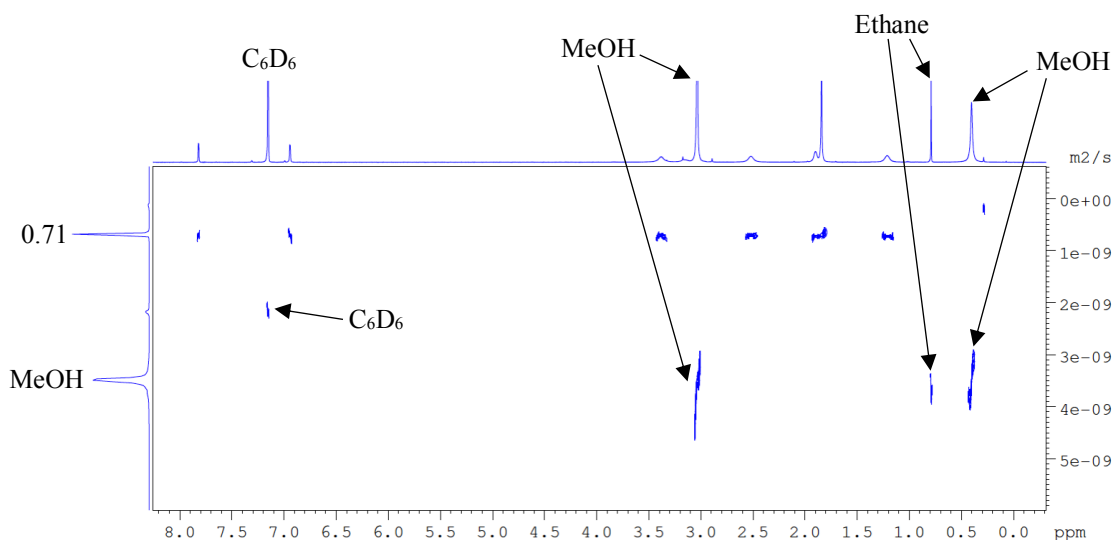


Figure 5.22. DOSY NMR (C_6D_6 , 500 MHz) spectrum of $Zn(2)OMe$, indicating only one species present in solution, with a diffusion constant of $0.71 \times 10^{-9} \text{ m}^2 \text{ s}^{-1}$. *N.B.* Figure S49 in ESI.

5.3.8. Polymer characterisation

5.3.8.1. PLA

5.3.8.1.1. Representative 1H NMR spectrum

A representative 1H NMR spectrum of PLA is provided in section 2.3.4.1. of Chapter 2.

5.3.8.1.2. Representative SEC spectra

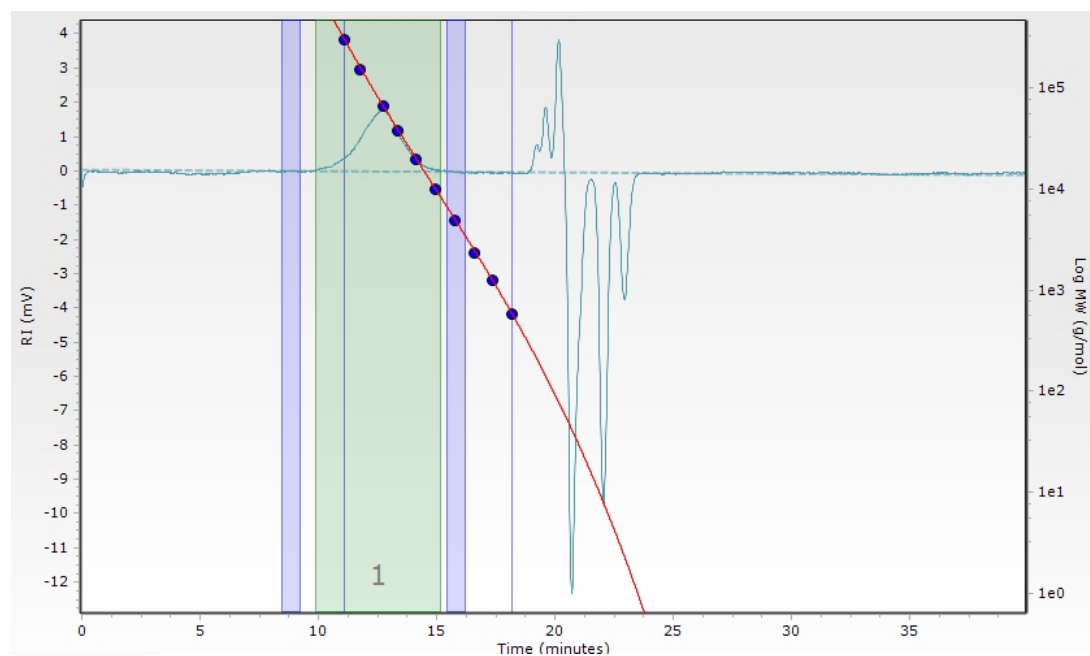


Figure 5.23. Monomodal SEC spectrum of purified PLA obtained from the melt polymerisation of *rac*-LA at 130 °C using $Zn(2)_2$ $\{[rac-LA]:[Zn]:[BnOH] = 10000:1:33\}$ (Table 5.4, Entry 5 in publication 5). *N.B.* Figure S51 in ESI.

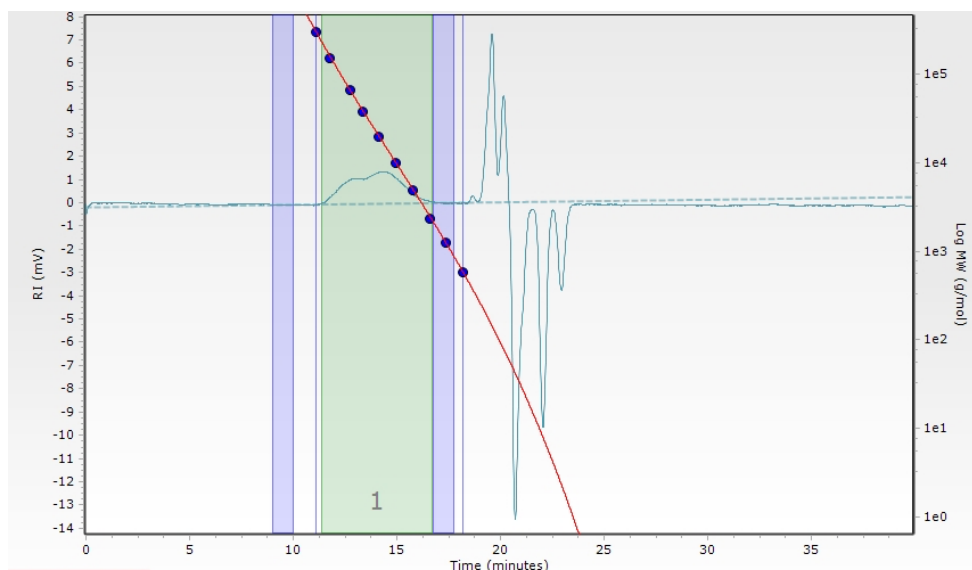


Figure 5.24. Bimodal SEC spectrum of purified PLA obtained from the melt polymerisation of *rac*-LA at 130 °C using Zn(3)₂ {[*rac*-LA]:[Zn]:[BnOH] = 10000:1:33} (Table 5.4, Entry 9). *N.B.* Figure S52 in ESI.

5.3.8.1.3. Representative homonuclear decoupled ¹H NMR spectrum

Representative spectra are provided in section 2.3.4.3. of Chapter 2.

5.3.8.1.4. MALDI-ToF spectra

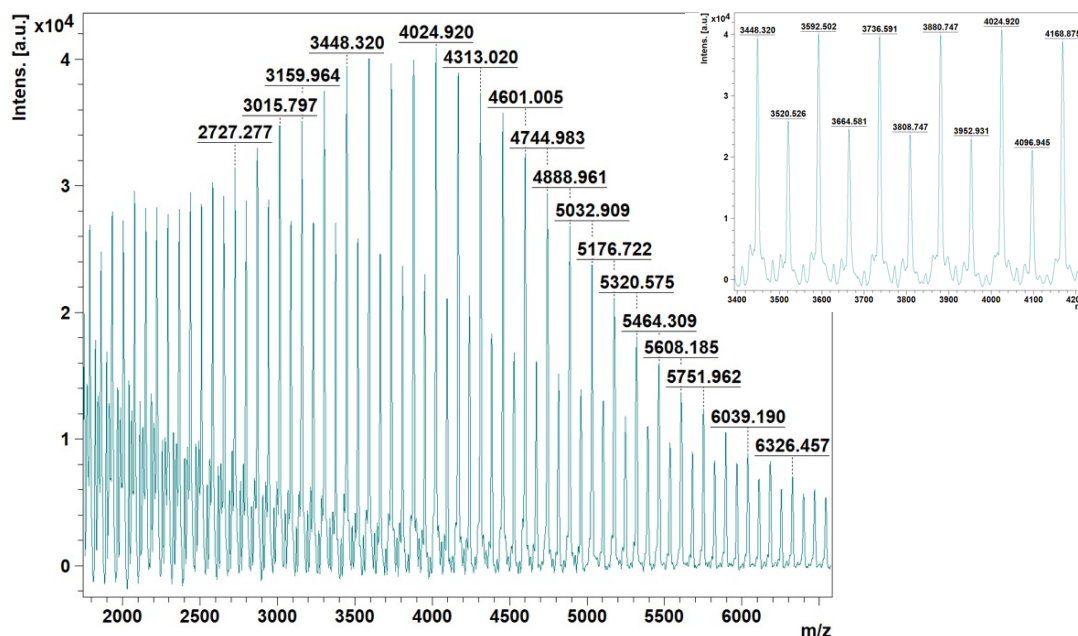


Figure 5.25. MALDI-ToF spectrum of purified PLA obtained from the melt polymerisation of *rac*-LA using Zn(1)Et at 180 °C {[*rac*-LA]:[Zn]:[BnOH] = 10000:1:100} (Table 5.4, Entry 3). Magnified version of secondary series provided to assist in identifying the repeat unit and end group. *N.B.* Figure S54 in ESI.

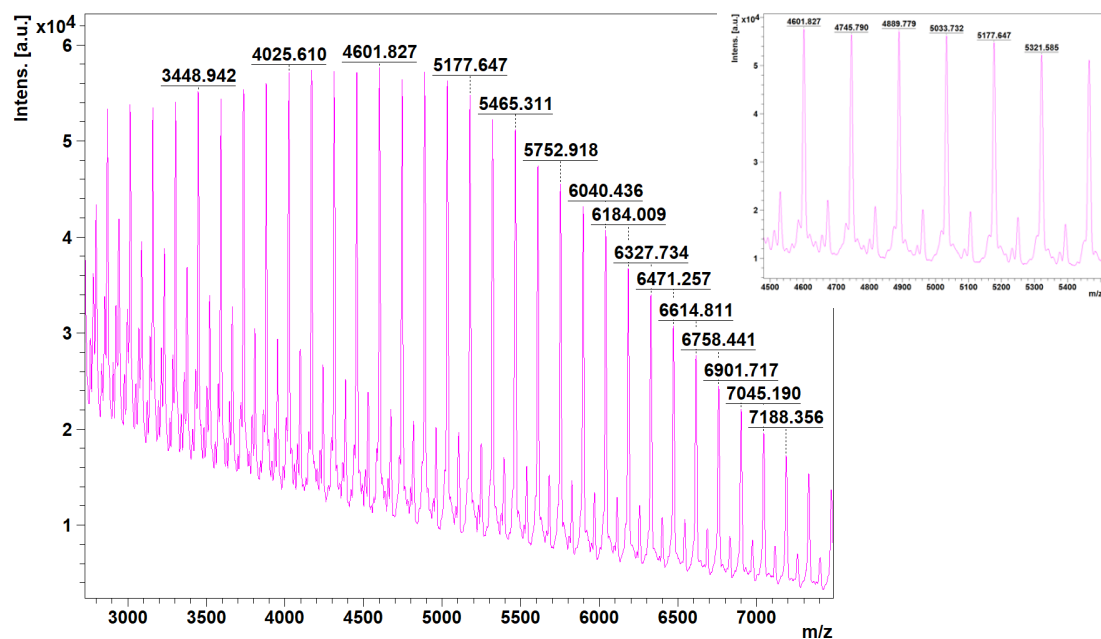


Figure 5.26. MALDI-ToF spectrum of purified PLA obtained from the melt polymerisation of *rac*-LA using Zn(2)₂ at 180 °C {[*rac*-LA]:[Zn]:[BnOH] = 10000:1:100} (Table 5.4, Entry 7). Magnified version of secondary series provided to assist in identifying the repeat unit and end group. *N.B.* Figure S55 in ESI.

5.3.8.2. PEA

5.3.8.2.1. Representative ¹H NMR spectra

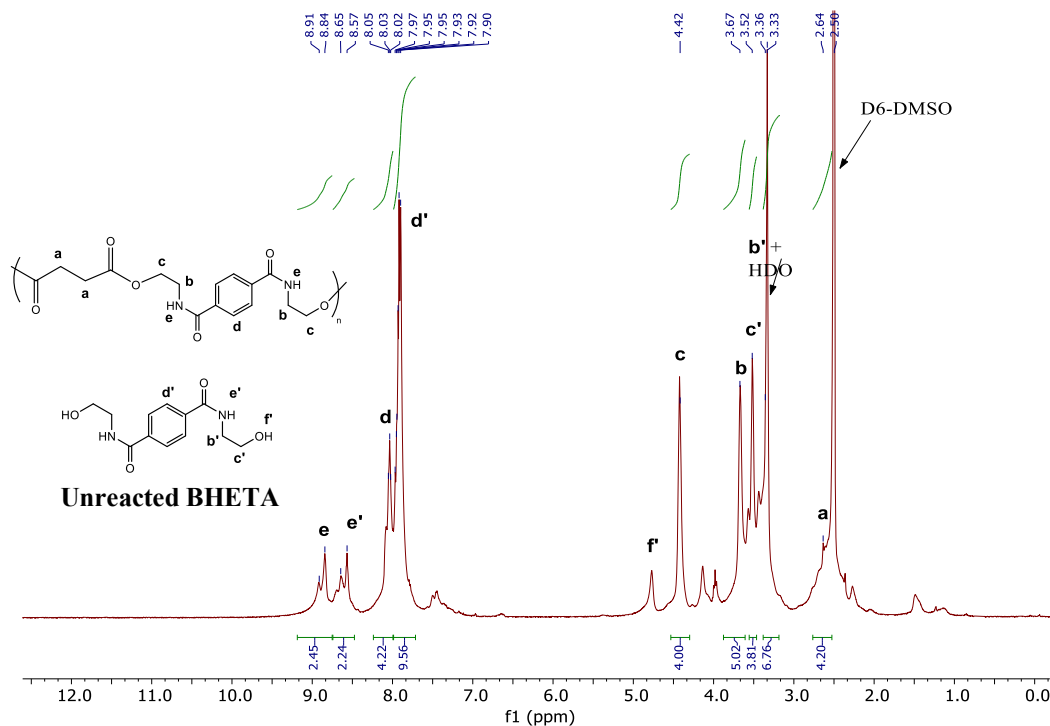


Figure 5.27. ¹H NMR (D₆-DMSO, 500 MHz) spectrum of PEA(1). *N.B.* Figure S65 in ESI.

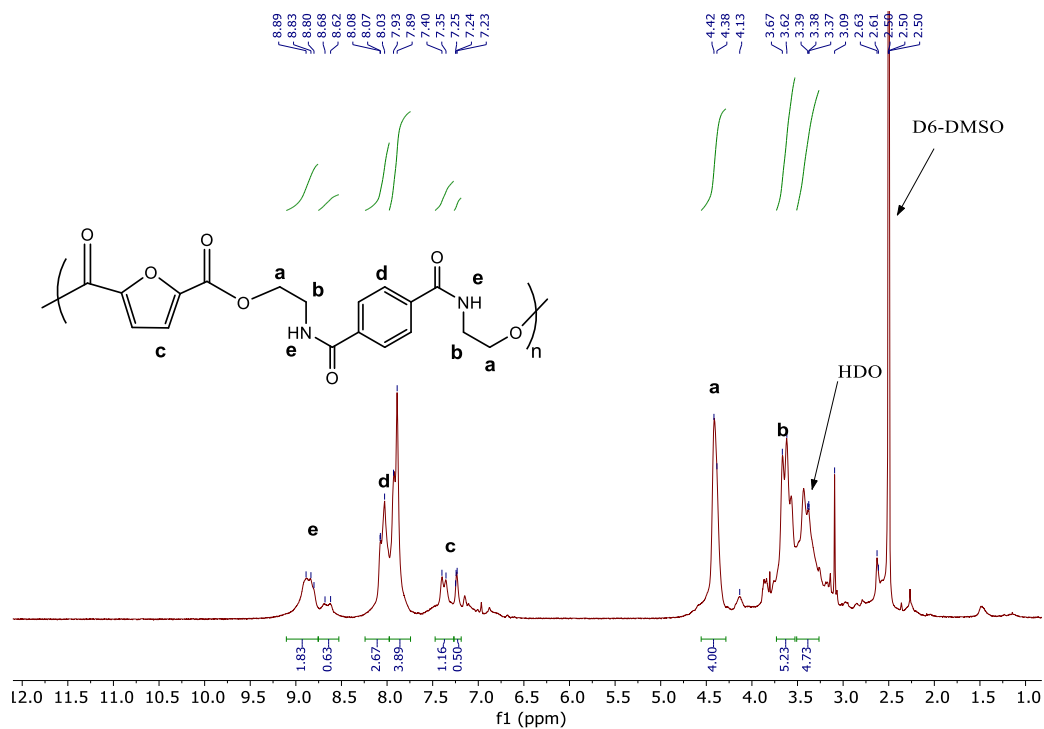


Figure 5.28. ¹H NMR (D₆-DMSO, 500 MHz) spectrum of PEA(4). *N.B.* Figure S68 in ESI.

5.3.8.2.2. Representative SEC spectrum

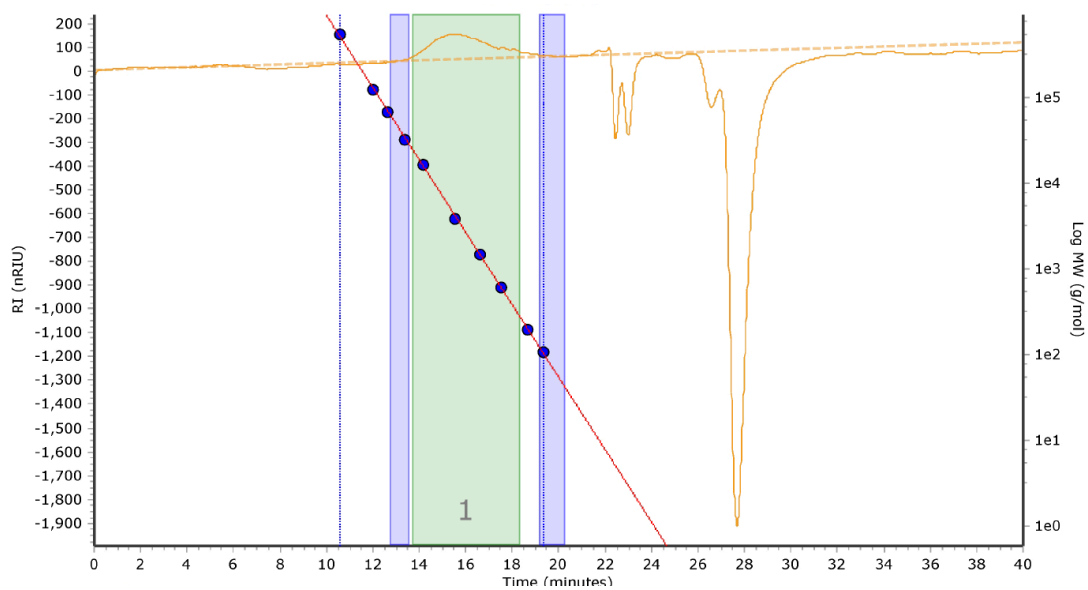


Figure 5.29. Monomodal SEC spectrum of PEA(4) produced from the melt polycondensation of BHETA and DMFDC in the presence of Ti(OⁱPr)₄. *N.B.* Figure S69 in ESI.

5.3.8.2.3. Thermal analysis

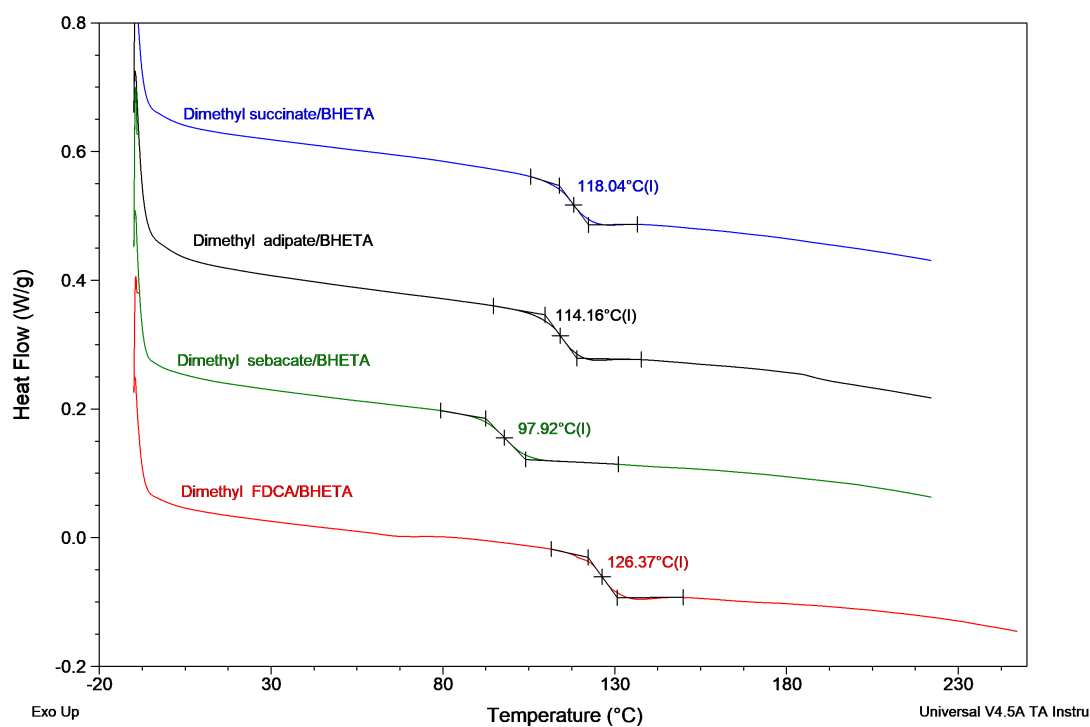


Figure 5.30. Stacked DSC traces of PEA(1-4) produced from the melt polycondensation of BHETA and renewable diesters in the presence of $\text{Ti}(\text{O}^i\text{Pr})_4$. *N.B.* Figure S70 in ESI.

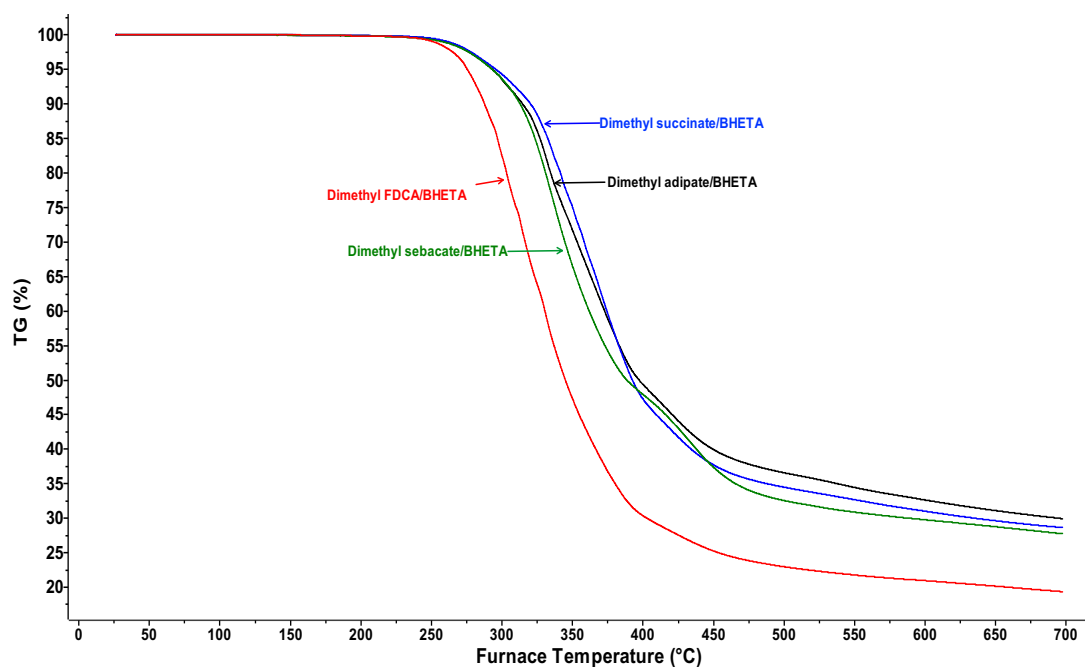


Figure 5.31. TGA plot of PEA(1-4) produced from the melt polycondensation of BHETA and renewable diesters in the presence of $\text{Ti}(\text{O}^i\text{Pr})_4$. *N.B.* Figure S71 in ESI.

5.3.9. Degradation characterisation

5.3.9.1. PLA methanolysis

Representative ^1H NMR spectra of PLA methanolysis are provided in section 3.2.7.1. of Chapter 3.

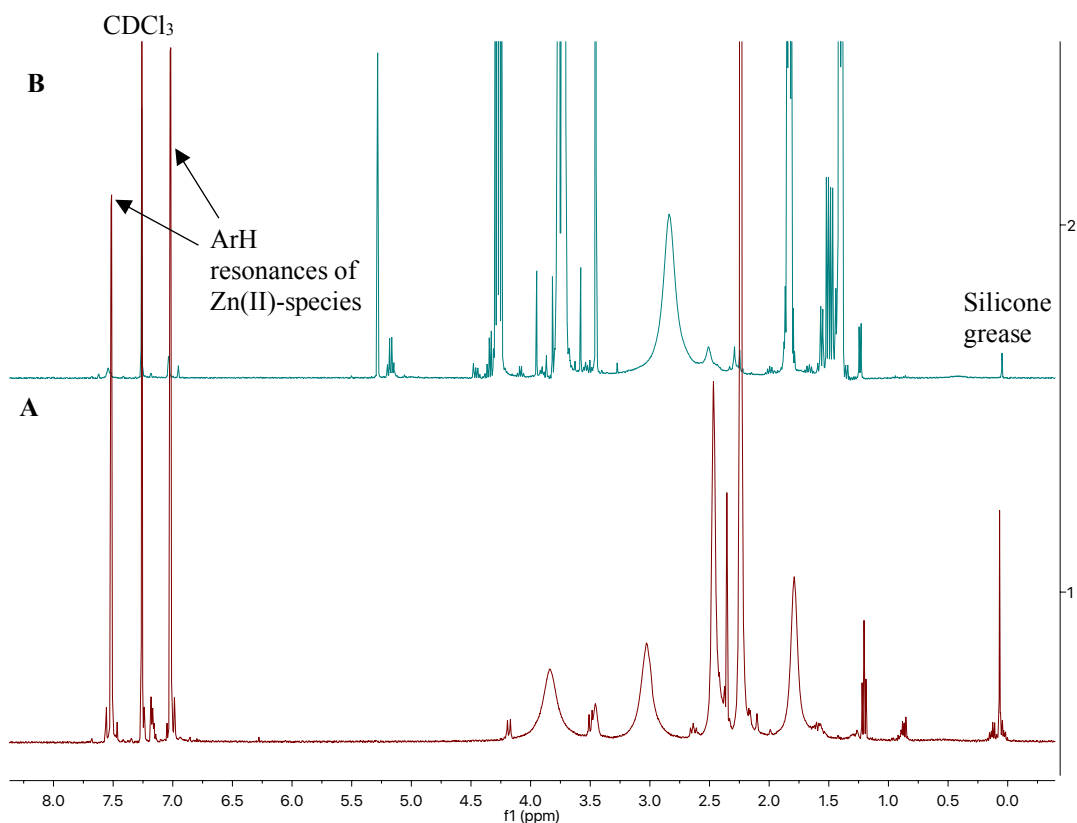


Figure 5.32. Stacked ^1H NMR (CDCl_3 , 500 (A) and 400 (B) MHz) spectra assessing the stability of Zn(2)_2 before and after PLA methanolysis: (A) Zn(2)_2 , and; (B) PLA cup (0.25 g, $M_n = 45,510 \text{ g mol}^{-1}$) degradation into methyl lactate (Me-LA) using Zn(2)_2 (8 wt %, 0.02 g, 0.72 mol% relative to ester linkages) at 50°C for 1.5 h in THF (solvent removed). *N.B.* Figure S58 in ESI.

5.3.9.2. PET glycolysis

A representative ^1H NMR spectrum of BHET is provided in section 3.2.7.2. of Chapter 3.

5.3.9.3. PET aminolysis

Representative NMR spectra of a terephthalamide product (BHETA) is provided in section 4.2.8.4. of Chapter 4.

5.3.9.4. Representative ^1H NMR spectra of BPA-PC methanolysis

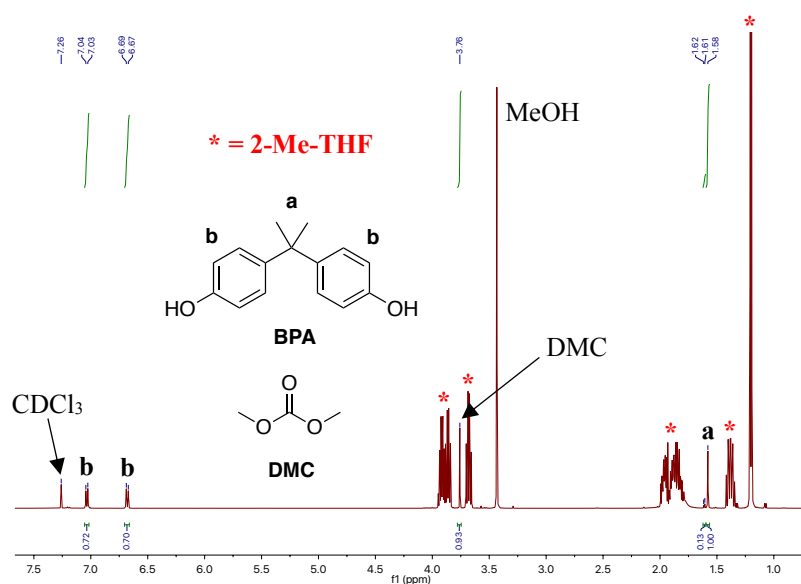


Figure 5.33. ^1H NMR (CDCl_3 , 500 MHz) spectrum of BPA-PC pellet (0.25 g, $M_w \sim 45,000$ g mol^{-1}) methanolysis (10 equiv. MeOH) reaction aliquot after 1 h at 50 °C using $\text{Zn}(\mathbf{2})_2$ (4 wt%, 0.01 g, 1.3 mol% relative to carbonate linkages) in 2-Me-THF. ^1H NMR peak assignments based on a literature example.^[66] Selectivity calculated based on methyl region at $\delta = 1.60$ ppm (a). *N.B.* Figure S72 in ESI.

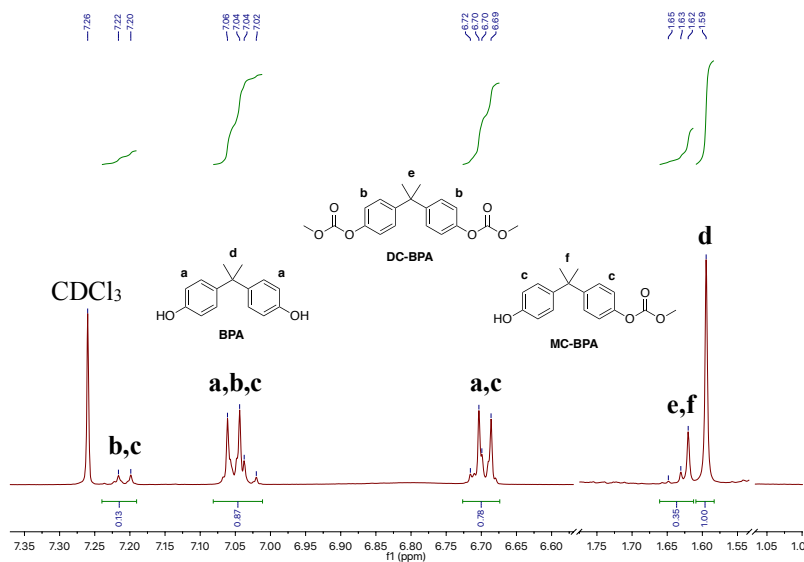


Figure 5.34. ^1H NMR (CDCl_3 , 500 MHz) spectrum of BPA-PC pellet (0.25 g, $M_w \sim 45,000$ g mol^{-1}) methanolysis (10 equiv. MeOH) reaction aliquot after 30 min at 50 °C using $\text{Zn}(\mathbf{2})_2$ (4 wt%, 0.01 g, 1.3 mol% relative to carbonate linkages) in 2-Me-THF. ^1H NMR peak assignments based on a literature example.^[66] Selectivity calculated based on methyl region at $\delta = 1.60$ ppm (d). Signals from carbonates (MC-BPA and DC-BPA) overlap with solvent resonances. *N.B.* Figure S73 in ESI.

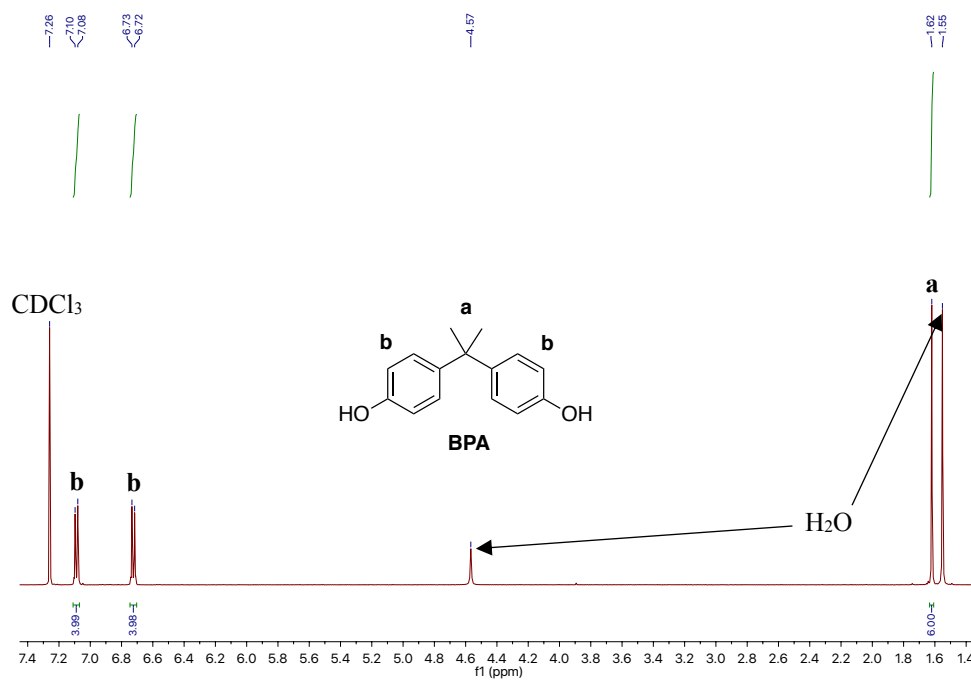


Figure 5.35. ^1H NMR (CDCl_3 , 500 MHz) spectrum of recrystallised BPA from BPA-PC pellet (0.25 g, $M_w \sim 45,000 \text{ g mol}^{-1}$) methanolysis (10 equiv. MeOH) using Zn(2)Et (4 wt%, 0.01 g, 2.2 mol% relative to carbonate linkages) in 2-MeTHF at RT for 2 h. *N.B.* Figure S76 in ESI.

5.3.9.5. Representative ^1H NMR spectrum of BPA-PC ethanolsis

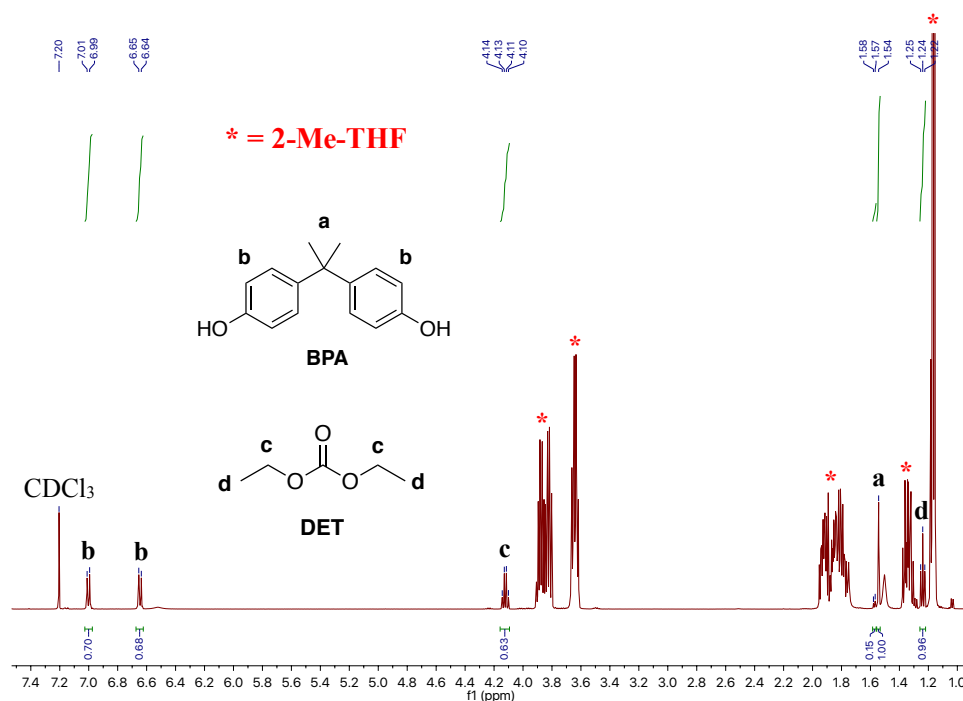


Figure 5.36. ^1H NMR (CDCl_3 , 500 MHz) spectrum of BPA-PC pellet (0.25 g, $M_w \sim 45,000 \text{ g mol}^{-1}$) ethanolsis (10 equiv. EtOH) reaction aliquot after 2 h at 50°C using Zn(2)Et (4 wt%, 0.01 g, 2.2 mol% relative to carbonate linkages) in 2-MeTHF. Selectivity calculated based on methyl region at $\delta = 1.60 \text{ ppm}$ (a). *N.B.* Figure S77 in ESI.

5.3.9.6. Representative ^1H NMR spectrum of BPA-PC glycolysis

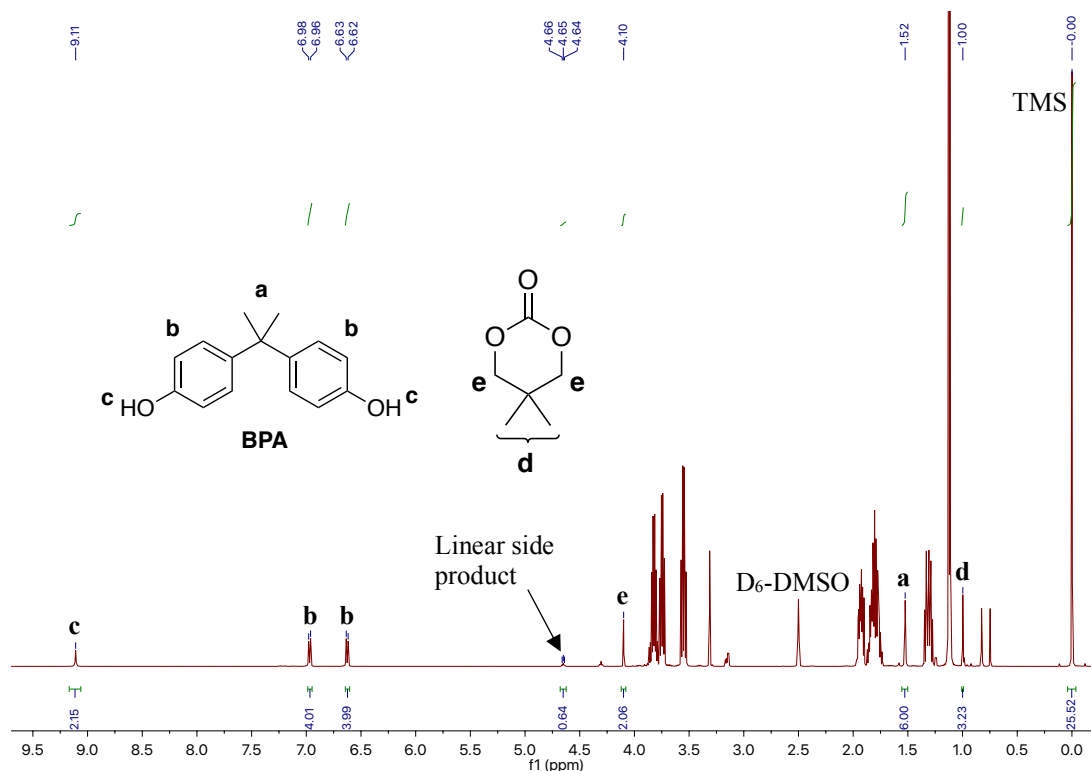


Figure 5.37. ^1H NMR (D_6 -DMSO, 500 MHz) spectrum of BPA-PC pellet (0.25 g, $M_w \sim 45,000 \text{ g mol}^{-1}$) glycolysis reaction aliquot (50 μL) after 1 h at 75 $^\circ\text{C}$ using 2,2-dimethyl-1,3-propanediol (0.15 g, 1.5 equiv.) in the presence of Zn(2)Et (4 wt%, 0.01 g, 2.2 mol% relative to carbonate linkages) in 2-MeTHF. ^1H NMR peak assignments based on a literature example.^[85] Tetramethylsilane (TMS, 10 μL , 73.5 μmol) was employed as an internal standard for calculating conversion. *N.B.* Unassigned peaks can be attributed to residual 2,2-dimethyl-1,3-propanediol. In accordance to previous work by Jehanno *et al.*^[85], the additional triplet at $\delta = 4.65$ ppm can likely be attributed to a linear side product arising from the attack of a second nucleophile on the active carbonate species, which competes with ring-closure (Scheme 5.7). Figure S80 in ESI.

5.3.9.7. Representative ^1H NMR spectra of PPC methanolysis

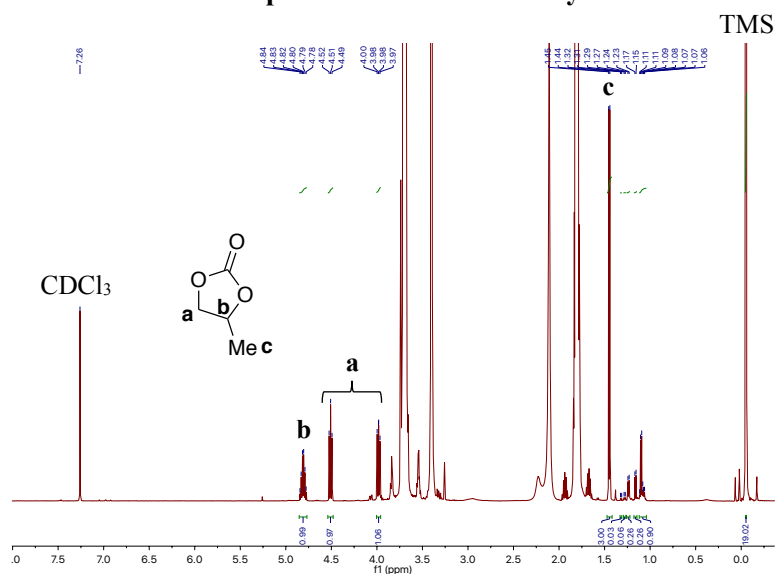


Figure 5.38. ^1H NMR (CDCl_3 , 500 MHz) spectrum of PPC pellet (0.25 g, $M_n \sim 50,000 \text{ g mol}^{-1}$) methanolysis (10 equiv. MeOH) reaction aliquot (50 μL) after 1 h at 50 $^\circ\text{C}$ using Zn(2)Et (4 wt%, 0.01 g, 0.88 mol% relative to carbonate linkages). ^1H NMR peak assignments based on a literature example.^[98] Tetramethylsilane (TMS, 10 μL , 73.5 μmol) was employed as an internal standard for calculating conversion. *N.B.* Unassigned peaks can be attributed to excess MeOH and solvent (THF). Additional peaks between $\delta = 1.06 - 1.23 \text{ ppm}$ can likely be attributed to linear side products, including oligomer and ring-opened carbonates. Figure S81 in ESI.

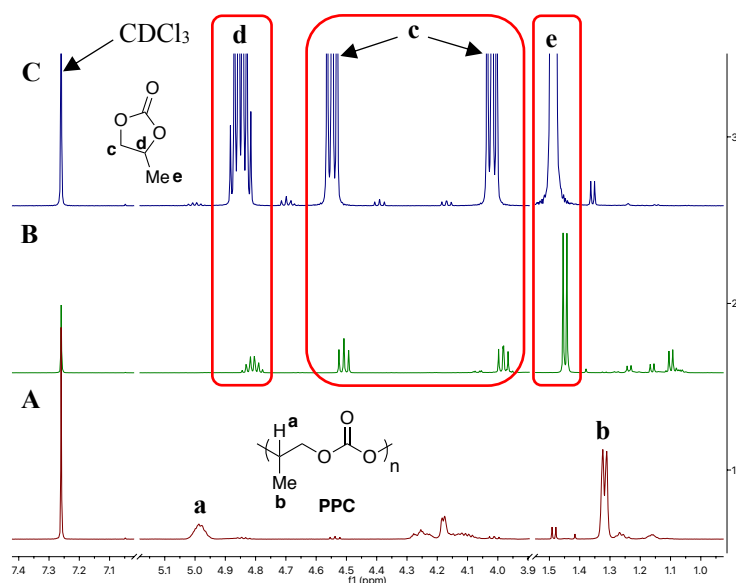


Figure 5.39. Stacked ^1H NMR (CDCl_3 , 500 MHz) spectra assessing PPC consumption and PC formation: (A) Neat PPC in THF, (B) PPC pellet (0.25 g, $M_n \sim 50,000 \text{ g mol}^{-1}$) methanolysis (10 equiv. MeOH) reaction aliquot (50 μL) after 1 h at 50 $^\circ\text{C}$ using Zn(2)Et (4 wt%, 0.01 g, 0.88 mol% relative to carbonate linkages), and; (C) Neat PC. *N.B.* PPC consumption determined by ^1H NMR (CDCl_3) analysis of the methine ($\delta = 4.99 \text{ ppm}$, **a**). Figure S82 in ESI.

5.3.10. Crystallographic data

Table 5.1. Crystallographic data for Zn(2)₂, Zn(2,4-5)Et and [Zn(3)Et]₂. *N.B.* [Zn(3)Et]₂ has a centre of inversion to complete the macrocycle. Table S10 in ESI.

Compound reference	Zn(2) ₂	Zn(2)Et	[Zn(3)Et] ₂	Zn(4)Et	Zn(5)Et
Empirical formula	C ₂₄ H ₃₄ Br ₄ N ₄ O ₂ Zn	C ₁₄ H ₂₂ Br ₂ N ₂ O ₁ Zn	C ₃₅ H ₅₆ N ₄ O ₂ Zn ₂	C ₂₁ H ₃₈ N ₂ OZn	C ₁₃ H ₂₀ Br ₂ N ₂ O ₁ Zn
Formula Mass	795.56	459.52	695.57	399.90	445.50
Crystal system	Triclinic	Orthorhombic	Triclinic	Monoclinic	Orthorhombic
<i>a</i> /Å	11.3914(5)	9.8615(3)	9.7149(9)	12.4990(4)	13.7352(2)
<i>b</i> /Å	12.0168(7)	16.0324(8)	10.0750(12)	10.9531(4)	16.3456(3)
<i>c</i> /Å	12.9805(9)	21.1643(11)	10.6705(10)	15.9078(7)	14.5299(2)
<i>α</i> /°	109.286(5)	90	79.627(9)	90	90
<i>β</i> /°	98.468(5)	90	69.221(9)	96.302(3)	90
<i>γ</i> /°	116.077(5)	90	65.761(11)	90	90
Unit cell volume/Å ³	1413.97(16)	3346.2(3)	889.66(18)	2164.66(14)	3262.11(9)
Temperature/K	150.00(10)	150.01(10)	150.00(10)	150.01(10)	150.00(10)
Space group	P-1	Pbca	P-1	P21/c	Pbcn
No. of formula units per unit cell, <i>Z</i>	2	8	1	4	8
Radiation type	Cu Kα	Cu Kα	Cu Kα	Cu Kα	Cu Kα
No. of reflections measured	8669	40504	12022	28971	65654
No. of independent reflections	5002	3171	3239	3951	3281
<i>R</i> _{int}	0.0343	0.0368	0.0379	0.0275	0.0490
Final <i>R</i> _{<i>i</i>} values (<i>I</i> > 2σ(<i>I</i>))	0.0424	0.0190	0.0246	0.0242	0.0466
Final <i>wR</i> (<i>F</i> ²) values (<i>I</i> > 2σ(<i>I</i>))	0.1103	0.0449	0.0655	0.0671	0.1124
Final <i>R</i> _{<i>i</i>} values (all data)	0.0477	0.0206	0.0253	0.0253	0.0482
Final <i>wR</i> (<i>F</i> ²) values (all data)	0.1156	0.0456	0.0660	0.0681	0.1138

Table 5.2. Selected bond lengths for Zn(2)₂, Zn(2,4-5)Et and [Zn(3)Et]₂. *N.B.* Table S11 in ESI.

Catalyst	Bond	Bond length / Å
Zn(2) ₂	Zn(1)-N(1) {NH}, Zn(1)-N(2) {NMe ₂ }, Zn(1)-N(3) {NH}	2.104(3), 2.109(3), 2.120(3)
Zn(2)Et	Zn(1)-N(1) {NH}, Zn(1)-N(2) {NMe ₂ }	2.1073(16), 2.1721(16)
[Zn(3)Et] ₂	Zn(1)-N(1) {NH}, Zn(1)-N(2) {NMe ₂ }	2.1043(13), 2.1631(13)
Zn(4)Et	Zn(1)-N(1) {NH}, Zn(1)-N(2) {NHMe}	2.1204(11), 2.1352(11)
Zn(5)Et	Zn(1)-N(1) {NH}, Zn(1)-N(2) {NHMe}	2.119(3), 2.086(4)

Table 5.3. Selected bond angles for Zn(2)₂, Zn(2,4-5)Et and [Zn(3)Et]₂ with calculated τ_{4/5} values. Ideal tetrahedral and trigonal bipyramidal geometries correspond to τ₄ and τ₅ = 1, respectively. *N.B.* Table S12 in ESI.

Catalyst	Bond	Bond angle / °	τ _{4/5}
Zn(2) ₂	O(1)-Zn(1)-O(2), N(1)-Zn(1)-N(3)	165.65(11), 133.00(13)	0.54
Zn(2)Et	O(1)-Zn(1)-O(2), N(1)-Zn(1)-N(3)	127.27(7), 117.97(7)	0.81
[Zn(3)Et] ₂	O(1)-Zn(1)-C(1), C(1)-Zn(1)-N(1)	129.66(7), 117.72(7)	0.80
Zn(4)Et	O(1)-Zn(1)-O(2), N(1)-Zn(1)-N(3)	124.83(5), 120.93(5)	0.81
Zn(5)Et	C(1)-Zn(1)-N(1), C(1)-Zn(1)-N(2)	126.33(16), 117.12(16)	0.83

5.3.11. Additional polymerisation and degradation data

Table 5.4. Melt polymerisation of *rac*-LA using Zn(II)-complexes. *N.B.* Table S1 in ESI.

Initiator	Time / min	Conversion ^[a] / %	$M_{n,theo}$ ^[b] / g mol ⁻¹	M_n ^[c] / g mol ⁻¹	\bar{D} ^[c]	P_r ^[d]
Zn(1)Et	2	84	36750	65150	3.23	0.57
	2 ^[e]	88	12800	21450	3.83	0.57
	60 ^[f]	55	8050	9200	1.55	0.55
Zn(2)Et	4	94	41100	75500 ^[g]	3.97 ^[g]	0.54
Zn(2) ₂	2	85	37200	55800	1.91	0.57
	2 ^[e]	91	13200	19350	1.69	0.58
	60 ^[f]	62	9050	11350	1.69	0.59
	60 ^[h]	24	10600	- ^[i]	- ^[i]	- ^[i]
Zn(3) ₂	20	44	19300	15550 ^[g]	2.38 ^[g]	0.56
[Zn(3)Et] ₂	20	21	9250	- ^[i]	- ^[i]	- ^[i]
Zn(4)Et	30	51	21900	25700	4.30	0.56
Zn(5)Et	2	78	34150	51450	3.68	0.55

Reaction conditions: *rac*-LA (3.0 g), solvent-free (130 °C), {[*rac*-LA]:[Zn]:[BnOH]} = 10000:1:33}. [a] Determined *via* ¹H NMR spectroscopy. [b] Theoretical average number molecular weight (M_n) dependent on conversion and co-initiator added $\{(M_{r,LA} \times 3.03 \times \%_{conv.}) + M_{r,BnOH}\}$. [c] Determined *via* SEC analysis (in THF). [d] Determined *via* homonuclear decoupled NMR spectroscopy. [e] {[*rac*-LA]:[Zn]:[BnOH]} = 10000:1:100}. [f] {[*rac*-LA]:[Zn]:[BnOH]} = 10000:1:100} at 180 °C. [g] Bimodal SEC. Calculated M_n and \bar{D} values correspond to peaks treated together. [h] *L*-lactide used (*L*-LA). [i] Insufficient polymeric material isolated for material characterisation due to low monomer conversion. *N.B.* [Zn]:[BnOH] = 1:1 corresponds to 1 equivalent of BnOH per Zn(II) centre.

Table 5.5. PLA methanolysis using Zn(II)-complexes. *N.B.* Table S2 in ESI.

Catalyst	Time / h	T / °C	Catalyst loading / wt%	Y_{Me-LA} / %	S_{Me-LA} / %	X_{int} / %
Zn(1)Et	3	50	4	7	16	44
Zn(2)Et	3	50	4	2	10	22
Zn(2) ₂	3	50	4	70	72	97
				0 ^[a]	0 ^[a]	22 ^[a]
				0 ^[b]	0 ^[b]	17 ^[b]
				22 ^[c]	32 ^[c]	67 ^[c]
				12 ^[d]	24 ^[d]	70 ^[d]
	1.5	50	8	94	94	100
Zn(3) ₂	3	50	4	9	19	49
	3	50	8	42	48	89
[Zn(3)Et] ₂	3	50	4	5	11	45
Zn(4)Et	3	50	4	5	13	35
	3	50	8	29	36	81
Zn(5)Et	3	50	4	62	64	96
	1.5	50	8	85	85	100

Reaction conditions: PLA cup (0.25 g, $M_n = 45,510$ g mol⁻¹), $V_{THF}:V_{MeOH} = 4:1$, $n_{MeOH}:n_{ester} = 7:1$, Zn(II)-complex = 4 – 8 wt% (0.01 – 0.02 g, 0.36 – 1.4 mol% relative to ester linkages). Y_{Me-LA} , S_{Me-LA} and X_{int} determined by ¹H NMR (CDCl₃) upon solvent removal. [a] Solvent: 2-Me-THF. [b] PLA-based 3D printing material. [c] Mixed feed: PLA cup (0.25 g, $M_n = 45,510$ g mol⁻¹) + bottle-grade PET (0.25 g, $M_n \sim 40,000$ g mol⁻¹). [d] Mixed feed: PLA cup (0.25 g, $M_n = 45,510$ g mol⁻¹) + bottle-grade PET (0.25 g, $M_n \sim 40,000$ g mol⁻¹) + PVC (0.025 g, 10 wt%, $M_n = 22,000$ g mol⁻¹).

Table 5.6. PLA cup methanolysis using Zn(2-3)₂ and Zn(4-5)Et in THF. *N.B.* Table S3 in ESI.

Catalyst	Time / h	T / °C	Catalyst loading / wt%	Y_{Me-LA} / %	k_{app} / min ⁻¹
Zn(2) ₂	3	50	4	71	0.026 ± 0.00077
	1.5	50	8	76	0.053 ± 0.0016
Zn(3) ₂	3	50	8	42	0.015 ± 0.0010
Zn(4)Et	3	50	8	27	0.014 ± 0.00027
Zn(5)Et	1.5	50	8	63	0.044 ± 0.0018

Reaction conditions: PLA cup (0.25 g, $M_n = 45,510$ g mol⁻¹), $V_{THF}:V_{MeOH} = 4:1$, $n_{MeOH}:n_{ester} = 7:1$, Zn(II)-complex = 4 – 8 wt% (0.01 – 0.02 g, 0.36 – 1.4 mol% relative to ester linkage). *N.B.* Y_{Me-LA} refers to maximum Me-LA conversion in solution determined *via* ¹H NMR (CDCl₃).

Table 5.7. PET glycolysis using Zn(2)₂ at 180 °C. *N.B.* Table S4 in ESI.

Catalyst	Time / h	T / °C	Catalyst loading / wt%	EG / equiv.	<i>Y</i> _{BHET} / g
Zn(OAc) ₂ ·2H ₂ O	3 ^[a]	180	4	20.6	0.17 (52%)
	4	180	8	20.6	0.14 (42%)
Zn(2) ₂	3	180	4	20.6	0.14 (42%)
	1 ^[a]	180	4	20.6	0.20 (61%)
	3 ^[b]	180	4	20.6	0.06 (18%)
	1.5	180	8	20.6	0.16 (48%)

Reaction conditions: Bottle-grade PET (0.25 g, *M_n* ~ 40,000 g mol⁻¹), 20.6 (1.5 mL) equiv. of EG (relative to ester linkages), Zn(OAc)₂·2H₂O = 4 – 8 wt% (0.01 – 0.02 g, 3.4 – 6.5 mol% relative to ester linkages), Zn(2)₂ = 4 – 8 wt% (0.01 – 0.02 g, 0.96 – 1.9 mol% relative to ester linkages). *Y*_{BHET} refers to the isolated yield of pure BHET recrystallised from deionised H₂O followed by drying at 90 °C for 3 h *in vacuo*. Both mass (g) and % yield (bracketed value) are reported for *Y*_{BHET}. [a] PET thin-film (0.25 g). [b] Mixed feed: bottle-grade PET (0.25 g, *M_n* ~ 40,000 g mol⁻¹) + PVC (0.025 g, 10 wt%, *M_n* = 22,000 g mol⁻¹).

Table 5.8. PET aminolysis into terephthalamides using Zn(2)₂. *N.B.* Table S5 in ESI.

Catalyst	Time / h	T / °C	Cat. loading / wt%	Amine / equiv.	TPA	<i>Y</i> _{BHET} / g
No cat.	2	110	-	16	BAETA	0.034 (11%)
Zn(2) ₂	1	110	8	16		0.11 (36%)
No cat.	3	120	-	6.4	BHETA	0.28 (88%)
Zn(2) ₂	2	120	8	6.4		0.29 (93%)

Reaction conditions: Bottle-grade PET (0.25 g, *M_n* ~ 40,000 g mol⁻¹), Zn(2)₂ = 8 wt% (0.02 g, 1.9 mol% relative to ester linkages). Ethylenediamine (16 equiv.) and ethanolamine (6.4 equiv.) were used for the production of BAETA and BHETA respectively. *Y*_{TPA} refers to the isolated yield of terephthalamide. Both mass (g) and % yield (bracketed value) are reported for *Y*_{TPA}.

Table 5.9. Additional BPA-PC methanolysis data using Zn(2)₂ and Zn(2)Et. *N.B.* Table S6 in ESI.

Catalyst	Time / h	T / °C	Catalyst loading / wt%	Alcohol / equiv.	S _{BPA} / %	S _{OC} / %
Zn(2) ₂	0.5 ^[a]	75	4	25	80	-
	1 ^[a]	50	4	25	68	-
	1 ^[b]	50	4	10	87	76
	4	25	4	25	82	73
	4	25	4	10	85	79
Zn(2)Et	2 ^[c]	50	4	10	88	84
	1 ^[d]	50	4	10	94	85
	1 ^[b]	50	4	10	96	86
	1 ^[e]	50	4	10	93	84
	1 ^[f]	50	4	10	0	0
	2	25	4	10	91 [85]	80
	2 ^[g]	25	4	10	88 [89]	75
Zn(OAc) ₂ ·2H ₂ O	1 ^[h]	50	4	10	0	0
HCl	4 ^[i]	25	1 ^[j]	10	0	0

Reaction conditions: BPA-PC pellets (0.25 g, $M_w \sim 45,000$ g mol⁻¹), 10 – 25 equiv. (0.41 – 1 mL) of MeOH (relative to carbonate linkages), Zn(II)-complexes = 4 wt% (0.01 g, 1.3 – 2.2 mol% relative to carbonate linkages), Zn(OAc)₂·2H₂O = 4 wt% (0.01 g, 4.4 mol% relative to carbonate linkages), solvent: 2-Me-THF (4 mL). *S*_{BPA} and *S*_{OC} refer to BPA and organic carbonate selectivity respectively. Bracketed values correspond to isolated yields. Unless otherwise stated, complete BPA-PC consumption was observed. For reactions where incomplete polymer dissolution was observed, BPA-PC was recovered by filtration and dried at 140 °C to constant weight. [a] Solvent: dimethyl carbonate (DMC). [b] Mixed feed: BPA-PC pellets (0.25 g, $M_w \sim 45,000$ g mol⁻¹) + bottle-grade PET (0.25 g, $M_n \sim 40,000$ g mol⁻¹) + PVC (0.025 g, 10 wt%, $M_n = 22,000$ g mol⁻¹). [c] Ethanolysis, yielding diethyl carbonate (DEC). [d] Mixed feed: BPA-PC pellets (0.25 g, $M_w \sim 45,000$ g mol⁻¹) + bottle-grade PET (0.25 g, $M_n \sim 40,000$ g mol⁻¹). [e] Compact disc (CD) (0.25 g). [f] Solvent-free. Incomplete BPA-PC consumption, m(BPA-PC recovered) = 0.2240 g, corresponding to 10% depolymerisation by weight. [g] Mixed feed scale-up: BPA-PC pellets (2.5 g, $M_w \sim 45,000$ g mol⁻¹) + bottle-grade PET (2.5 g, $M_n \sim 40,000$ g mol⁻¹). [h] Incomplete BPA-PC consumption, m(BPA-PC recovered) = 0.2460 g, corresponding to 2% depolymerisation by weight. [i] Incomplete BPA-PC consumption, m(BPA-PC recovered) = 0.2526 g, corresponding to 0% depolymerisation by weight. [j] Molar ratio of [catalyst]/[BPA-PC].

Table 5.10. BPA-PC methanolysis using Zn(2)₂ and Zn(2)Et in 2-MeTHF at RT. *N.B.* Table S7 in ESI.

Catalyst	Time / h	T / °C	Catalyst loading / wt%	S _{BPA} / %	k _{app} / min ⁻¹
Zn(2) ₂	4	25	4	85	0.28 ± 0.040
Zn(2)Et	2	25	4	91	0.47 ± 0.049

Reaction conditions: BPC-PC pellets (0.25 g, $M_w \sim 45,000 \text{ g mol}^{-1}$), $n_{\text{carbonate}}:n_{\text{MeOH}} = 1:10$, Zn(II)-complex = 4 wt% (0.01 g, 1.3 – 2.2 mol% relative to carbonate linkages), solvent: 2-MeTHF (4 mL).

Table 5.11. BPA-PC glycolysis using Zn(2)Et. *N.B.* Table S8 in ESI.

Catalyst	Time / h	T / °C	Catalyst loading / wt%	Glycol	Glycol / equiv.	S _{BPA} / %	S _{CC} / %
Zn(2)Et	1	75	4	<i>rac</i> -butane-1,3-diol	10	96	78
	1	75	4		5	99	12
	4	75	4	2,2-dimethyl-1,3-propanediol	5	99	7
	1	75	4		1.5	96	48
	4	75	4		1.5	96	26

Reaction conditions: BPC-PC pellets (0.25 g, $M_w \sim 45,000 \text{ g mol}^{-1}$), solvent: 2-Me-THF (4 mL), 1.5 – 10 equiv. (0.15 – 0.89 g) of glycol (relative to carbonate linkages), Zn(2)Et = 4 wt% (0.01 g, 2.2 mol% relative to carbonate linkages). S_{BPA}, S_{CC} and S_{LC} refer to BPA, cyclic carbonate and linear carbonate respectively.

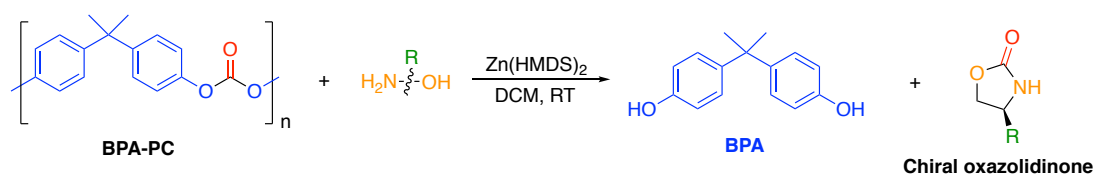
Table 5.12. PPC methanolysis using Zn(2)₂ and Zn(2)Et. *N.B.* Table S9 in ESI.

Catalyst	Time / h	T / °C	Catalyst loading / wt%	MeOH / equiv.	S _{PC} / %	PPC consumption / %
No cat.	1.5	50	4	1.5	0	0
Zn(2) ₂	1.5	50	4	1.5	58	100
	1	50	4	10	38	100
Zn(2)Et	1	50	4	5	39	100
	1.5	50	4	1.5	50	100

Reaction conditions: PPC pellets (0.25 g, $M_n \sim 50,000 \text{ g mol}^{-1}$), solvent: THF (4 mL), 1.5 – 10 equiv. (0.15 – 0.5 mL) of MeOH (relative to carbonate linkages), Zn(II)-complex = 4 wt% (0.01 g, 0.51 – 0.88 mol% relative to carbonate linkages). S_{PC} refers to propylene carbonate selectivity. *N.B.* All reaction times refer to the time taken to achieve complete PPC consumption as determined *via* ¹H NMR analysis.

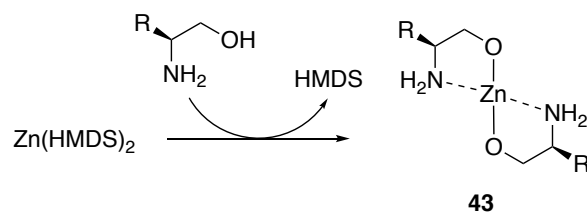
5.4. Post-publication Commentary

Wang and co-workers recently reported the chemical upcycling of BPA-PC into value-added chiral 2-oxazolidinones *via* an amino-alcoholysis strategy catalysed by $\text{Zn}(\text{HMDS})_2$ (Scheme 5.9).^[99] This work represents a rare example of BPA-PC conversion into high value chiral compounds, with chiral 2-oxazolidinones being widely used as pharmaceutical intermediates in medicinal chemistry and as chemical building blocks (*e.g.* Evans chiral auxiliaries) in organic synthesis.^[99-101] Furthermore, such compounds are traditionally derived from toxic phosphene or its analogues, thus there is a clear need to develop safer and greener synthesis routes.



Scheme 5.9. Chemical upcycling of BPA-PC into high value chiral 2-oxazolidinones *via* an amino-alcoholysis strategy catalysed by $\text{Zn}(\text{HMDS})_2$ as reported by Wang and co-workers.^[99]

Promisingly, the reaction proceeds under ambient conditions in DCM, affording BPA and chiral 2-oxazolidinones in good to excellent yield (80 – 99% and 79 – 99%, respectively) $\{m_{\text{BPA-PC}} = 0.25 \text{ g}, n_{\text{BPA-PC}}:n_{\text{amino alcohol}} = 1:2, 2 \text{ mol\% } \text{Zn}(\text{HMDS})_2 \text{ (based on carbonate linkages)}\}$.^[99] Reaction times varied between 1 – 168 h, which was dependent on the nucleophilicity of the amino alcohol employed. For (*S*)-phenylglycinol, a range of simple and cheap Lewis acid catalyst alternatives to $\text{Zn}(\text{HMDS})_2$ were screened (*e.g.* MgCl_2 , AlCl_3 , CaCl_2 , FeCl_2 , ZnCl_2 , ZnO and $\text{Zn}(\text{OAc})_2$), however, significantly reduced activity was observed. Indeed, for $\text{Zn}(\text{HMDS})_2$ high process efficiency was retained upon exchanging the solvent for 2-Me-THF and toluene, although a prolonged reaction time of 6 h was required to achieve comparably high yields in ethyl acetate. Further mechanistic investigation found **43** to likely be the active catalytic species and a coordination-insertion mechanism was proposed (Scheme 5.10). Moreover, a sequential depolymerisation strategy for a mixed BPA-PC/PET feed was demonstrated on a multigram scale.



Scheme 5.10. Reaction of $\text{Zn}(\text{HMDS})_2$ pre-catalyst with chiral 2-oxazolidinones to form the active catalytic species (**43**).

Subsequent work within this group has extended the use of $\text{Zn}(\text{HMDS})_2$ for the chemical recycling of a variety of commercial plastics (e.g. PLA, poly(butylene succinate) (PBS), poly(butylene adipate terephthalate) (PBAT) and PCL) and mixed waste feeds (e.g. PLA/PBDS and PLA/PBAT) *via* sequential, one-pot depolymerisation strategies.^[102] Surprisingly, despite both studies complimenting the work detailed in publication 5, no kinetic data was provided to enable a comparison between the activity of either $\text{Zn}(\mathbf{2})_2$ or $\text{Zn}(\mathbf{2})\text{Et}$ with $\text{Zn}(\text{HMDS})_2$.^[99,102] Indeed, kinetic data for BPA-PC alcoholysis remains scarce in the literature, which should become a routine endeavour as the field progresses. Additionally, no further examples of discrete homogeneous metal-based catalysts for BPA-PC alcoholysis have been reported beyond those detailed in publication 5.

Finally, the incomplete catalyst series presented in publication 5 can be attributed to challenges associated with catalyst preparation. $\text{Zn}(\mathbf{2-3})_2$ formation required prolonged stirring (18 h) at elevated temperatures (80 °C) to drive reaction completion. Despite numerous attempts, $\text{Zn}(\mathbf{1,4})_2$ could not be isolated pure due to high product solubility in a range of polar (DCM, THF) and non-polar solvents (toluene, hexane). To overcome solubility issues, heteroleptic analogues of $\mathbf{1-6H}$ were also targeted. Attempts to isolate homoleptic complexes based on $\mathbf{5-6H}$ were unsuccessful, which could be extended to $\text{Zn}(\mathbf{6})\text{Et}$. Generally, such complexes exhibited a degree of structural fluxionality at RT, which was reflected in peak broadening during ^1H NMR spectroscopic analysis. This was more pronounced in $\text{Zn}(\mathbf{3})\text{Et}$, requiring variable-temperature (VT) NMR for structural elucidation, with a decrease in temperature resulting in superior peak resolution (Figure 5.19). At 248 K in d_8 -toluene, the $-\text{NMe}_2$ resonance was observed to be inequivalent, observing two distinct singlets at $\delta = 1.52$ and 1.86 ppm, indicating restricted movement of the ligand side arm (Figure S35 in publication 5). This demonstrates possible reversible binding of the $-\text{NMe}_2$ moiety to the metal centre in solution, consistent with work by Pongpanit *et al.*^[103], which can likely be extended to $\text{Zn}(\mathbf{2})_2$ (Figure 5.11). In contrast, $\text{Zn}(\mathbf{3})_2$ exhibited a well-defined spectrum, suggesting the ligand is locked to the metal centre (Figure S31 in publication 5). Conversely, ^1H NMR spectroscopic analysis of $\text{Zn}(\mathbf{1-5})\text{Et}$ was generally more complex relative to $\text{Zn}(\mathbf{2-3})_2$, noting diastereotopic Ar-CHN resonances between *ca.* $\delta = 2.30$ and 4.80 ppm upon coordination to Zn(II) (see ESI). This suggests the ligand is locked in position and the metal centre to be asymmetric. Additionally, a characteristic triplet between *ca.* $\delta = 1.50$ and 1.90 ppm integrated to 3 ($\text{Zn-CH}_3\text{-CH}_2$), indicating one $-\text{Et}$ moiety is associated per metal centre.

5.5. References

- [1] L. A. Román-Ramírez, P. McKeown, M. D. Jones, J. Wood, *ACS Catal.* **2019**, *9*, 409–416.
- [2] P. McKeown, L. A. Román-Ramírez, S. Bates, J. Wood, M. D. Jones, *ChemSusChem* **2019**, *12*, 5233–5238.
- [3] O. Dechy-Cabaret, B. Martin-Vaca, D. Bourissou, *Chem. Rev.* **2004**, *104*, 6147–6176.
- [4] C. M. Thomas, *Chem. Soc. Rev.* **2010**, *39*, 165–173.
- [5] R. H. Platel, L. M. Hodgson, C. K. Williams, *Polym. Rev.* **2008**, *48*, 11–63.
- [6] M. J. Stanford, A. P. Dove, *Chem. Soc. Rev.* **2010**, *39*, 486–494.
- [7] M. J.-L. Tschan, R. M. Gauvin, C. M. Thomas, *Chem. Soc. Rev.* **2021**, *50*, 13587–13608.
- [8] J. G. Kim, *Polym. Chem.* **2020**, *11*, 4830–4849.
- [9] J. Demarteau, I. Olazabal, C. Jehanno, H. Sardon, *Polym. Chem.* **2020**, *11*, 4875–4882.
- [10] Y. Liu, X.-B. Lu, *J. Polym. Sci.* **2022**, 1–13.
- [11] E. V. Antonakou, D. S. Achilias, *Waste Biomass Valor.* **2013**, *4*, 9–21.
- [12] R. Singh, S. Shahi, Geetanjali, *ChemistrySelect* **2018**, *3*, 11957–11962.
- [13] D. J. Brunelle, P. M. Smigelski Jr., E. P. Boden, *ACS Symp. Ser.* **2004**, *898*, 8–21.
- [14] P. T. Anastas, J. C. Warner in *Green chemistry: theory and practice*, (Eds.: P. T. Anastas, J. C. Warner), Oxford University Press, **1998**, pp. 29–56.
- [15] S. Fukuoka, M. Kawamura, K. Komiya, M. Tojo, H. Hachiya, K. Hasegawa, M. Aminaka, H. Okamoto, I. Fukawa, S. Konno, *Green Chem.* **2003**, *5*, 497–507.
- [16] S. Fukuoka, M. Tojo, H. Hachiya, M. Aminaka, K. Hasegawa, *Polym. J.* **2007**, *39*, 91–114.
- [17] J. Payne, P. McKeown, M. D. Jones, *Polym. Degrad. Stab.* **2019**, *165*, 170–181.
- [18] M. J. Raymond, C. S. Slater, M. J. Savelski, *Green Chem.* **2010**, *12*, 1826–1834.
- [19] Y. Zhu, C. Romain, C. K. Williams, *Nature* **2016**, *540*, 354–362.
- [20] S. Paul, Y. Zhu, C. Romain, R. Brooks, P. K. Saini, C. K. Williams, *Chem. Commun.* **2015**, *51*, 6459–6479.
- [21] M. J.-L. Tschan, E. Brulé, P. Haquette, C. M. Thomas, *Polym. Chem.* **2012**, *3*, 836–851.
- [22] C. K. Williams, M. A. Hillmyer, *Polym. Rev.* **2008**, *48*, 1–10.
- [23] J. Xu, E. Feng, J. Song, *J. Appl. Polym. Sci.* **2014**, *131*, 39822.
- [24] J. Feng, R. X. Zhuo, X. Z. Zhang, *Prog. Polym. Sci.* **2012**, *37*, 211–236.
- [25] W. Chen, F. H. Meng, R. Cheng, C. Deng, J. Feijen, Z. Y. Zhong, *J. Controlled Release* **2014**, *190*, 398–414.

- [26] R. P. Brannigan, A. P. Dove, *Biomater. Sci.* **2017**, *5*, 9–21.
- [27] J. R. Rochester, *Reprod. Toxicol.* **2013**, *42*, 132–155.
- [28] F. Liguori, C. Moreno-Marrodan, P. Barbaro, *Chem. Soc. Rev.* **2020**, *49*, 6329–6363.
- [29] A. M. Calafat, J. Weuve, X. Ye, L. T. Jia, H. Hu, S. Ringer, K. Huttner, R. Hauser, *Environ. Health Perspect.* **2009**, *117*, 639–644.
- [30] S. Biedermann, P. Tschudin, K. Grob, *Anal. Bioanal. Chem.* **2010**, *398*, 571–576.
- [31] L. N. Vandenberg, R. Hauser, M. Marcus, N. Olea, W. V. Welshons, *Reprod. Toxicol.* **2007**, *24*, 139–177.
- [32] C. A. Staples, P. B. Dome, G. M. Klecka, S. T. Oblock, L. R. Harris, *Chemosphere* **1998**, *36*, 2149–2173.
- [33] C. M. Metz, *Workspace Health Saf.* **2016**, *64*, 28–36.
- [34] S. A. Vogel, *Am. J. Public Health* **2009**, *99*, S559–S566.
- [35] N. Andújar, Y. Gálvez-Ontiveros, A. Zafra-Gómez, L. Rodrigo, M. J. Álvarez-Cubero, M. Aguilera, C. Monteagudo, A. Rivas, *Nutrients* **2019**, *11*, 2136–2154.
- [36] K. Pelch, J. A. Wignall, A. E. Goldstone, P. K. Ross, R. B. Blain, A. J. Shapiro, S. D. Holmgren, J. H. Hsieh, D. Svoboda, S. S. Auerbach, F. M. Parham, S. A. Masten, V. Walkera, A. Rooney, K. A. Thayer, *Toxicology* **2019**, *424*, 152235.
- [37] A. C. Fernandes, *Green Chem.* **2021**, *23*, 7330–7360.
- [38] P. T. Anastas, M. M. Kirchhoff, *Acc. Chem. Res.* **2002**, *35*, 686–694.
- [39] M. Hong, E. Y.-X. Chen, *Green Chem.* **2017**, *19*, 3692–3706.
- [40] L.-C. Hu, A. Oku, E. Yamada, *Polymer* **1998**, *39*, 3841–3845.
- [41] A. Oku, S. Tanaka, S. Hata, *Polymer* **2000** *41*, 6749–6753.
- [42] S. Hata, H. Goto, S. Tanaka, A. Oku, *J. Appl. Polym. Sci.* **2003**, *90*, 2959–2968.
- [43] R. Tundo, M. Selva, *Acc. Chem. Res.* **2002**, *35*, 706–716.
- [44] M. A. Pacheco, C. L. Marshall, *Energy Fuels* **1997**, *11*, 2–29.
- [45] B. Schöffner, F. Schöffner, S. P. Verevkin, A. Börner, *Chem. Rev.* **2010**, *110*, 4554–4581.
- [46] R. Piñero, J. García, M. J. Cocero, *Green Chem.* **2005**, *7*, 380–387.
- [47] C. S. Bhogle, A. B. Pandit, *Ultrason. Sonochem.* **2019**, *58*, 104667.
- [48] F. Liu, Z. Li, S. Yu, X. Cui, C. Xie, X. Ge, *J. Polym. Environ.* **2009**, *17*, 208–211.
- [49] C. Alberti, S. Enthaler, *Asian J. Org. Chem.* **2020**, *9*, 359–363.
- [50] A. A. Neverov, L. D. Chen, S. George, D. Simon, C. I. Maxwell, R. S. Brown, *Can. J. Chem.* **2013**, *91*, 1139–1146.
- [51] Y. Zhao, X. Zhang, X. Song, F. Liu, *Catal. Lett.* **2017**, *147*, 2940–2949.
- [52] Y. Yang, C. Wang, F. Liu, X. Sun, G. Qin, Y. Liu, J. Gao, *J. Mater. Sci.* **2019**, *54*, 9442–9455.
- [53] F. Liu, Y. Xiao, X. Sun, G. Qin, X. Song, Y. Liu, *Chem. Eng. J.* **2019**, *369*, 205–214.

- [54] F. Iannone, M. Casiello, A. Monopoli, P. Cotugno, M. C. Sportelli, R. A. Picca, N. Cioffi, M. M. Dell'Anna, A. Nacci, *J. Mol. Catal. A: Chem.* **2017**, *426*, 107–116.
- [55] N. Mizuno, M. Misono, *Chem. Rev.* **1998**, *98*, 199–217.
- [56] L. Chen, Y. Wu, Y. Ni, K. Huang, Z. Zhu, *Acta Sci. Circumstantiae* **2004**, *24*, 60–64.
- [57] H. Jie, H. Ke, Z. Qing, C. Lei, W. Yongqiang, Z. Zibin, *Polym. Degrad. Stab.* **2006**, *91*, 2307–2314.
- [58] D. Kim, B.-K. Kim, Y. Cho, M. Han, B.-S. Kim, *Ind. Eng. Chem. Res.* **2009**, *48*, 6591–6599.
- [59] K. Ikenaga, K. Higuchi, S. Kohri, K. Kusakabe, *IOP Conf. Ser.: Mater. Sci. Eng.* **2018**, *458*, 012037.
- [60] C. Alberti, F. Scheliga, S. Enthaler, *ChemistryOpen* **2019**, *8*, 822–827.
- [61] V. G. Oliveira, M. F. Cardoso, L. M. Forezi, *Catalysts* **2018**, *8*, 605.
- [62] B. List, *Chem. Rev.* **2007**, *107*, 5413–5415.
- [63] B. G. G. Lohmeijer, R. C. Pratt, F. Leibfarth, J. W. Logan, D. A. Long, A. P. Dove, F. Nederberg, J. Choi, C. Wade, R. M. Waymouth, J. L. Hedrick, *Macromolecules* **2006**, *39*, 8574–8583.
- [64] E. Quaranta, D. Sgherza, G. Tartaro, *Green Chem.* **2017**, *19*, 5422–5434.
- [65] T. Do, E. R. Baral, J. G. Kim, *Polymer* **2018**, *143*, 106–114.
- [66] P. McKeown, M. Kamran, M. G. Davidson, M. D. Jones, L. A. Román-Ramírez, J. Wood, *Green Chem.* **2020**, *22*, 3721–3726.
- [67] C. Alberti, S. Enthaler, *Waste Biomass Valorization* **2020**, *11*, 4621–4629.
- [68] J. Payne, M. D. Jones, *ChemSusChem* **2021**, *14*, 4041–4070.
- [69] F. Liu, Z. Li, S. Yu, X. Cui, X. Ge, *J. Hazard. Mater.* **2010**, *174*, 872–875.
- [70] F. Liu, L. Li, S. Yu, Z. Lv, X. Ge, *J. Hazard. Mater.* **2011**, *189*, 249–254.
- [71] J. Guo, M. Liu, Y. Gu, Y. Wang, J. Gao, F. Liu, *Ind. Eng. Chem. Res.* **2018**, *57*, 10915–10921.
- [72] M. Liu, J. Gao, Y. Gu, J. Gao, F. Liu, S. Yu, *ACS Sustainable Chem. Eng.* **2018**, *6*, 13114–13121.
- [73] M. Liu, J. Guo, Y. Gu, J. Gao, F. Liu, *ACS Sustainable Chem. Eng.* **2018**, *6*, 15127–15134.
- [74] F. Liu, J. Gao, P. Zhao, M. Jia, M. Liu, J. Gao, *Polym. Degrad. Stab.* **2019**, *169*, 10899.
- [75] F. D'Anna, M. Sbacchi, G. Infurna, N. Tz. Dintcheva, S. Marullo, *Green Chem.* **2021**, *23*, 9957–9967.
- [76] X. Song, W. Hu, W. Huang, H. Wang, S. Yan, S. Yu, F. Liu, *Chem. Eng. J.* **2020**, *388*, 124324.

- [77] W. Huang, H. Wang, W. Hu, D. Yang, S. Yu, F. Liu, X. Song, *RSC Adv.* **2021**, *11*, 1595–1604.
- [78] D. Kim, B. K. Kim, Y. Cho, M. Han, B. S. Kim, *Ind. Eng. Chem. Res.* **2009**, *48*, 685–691.
- [79] M. M. A. Nikje, *Polimery* **2011**, *56*, 381–384.
- [80] L. Rosi, M. Bartoli, A. Undri, M. Frediani, P. Frediani, *J. Mol. Catal. A: Chem.* **2015**, *408*, 278–286.
- [81] C.-H. Lin, H.-Y. Lin, W.-Z. Liao, S. A. Dai, *Green Chem.* **2007**, *9*, 38–43.
- [82] M. Vannini, L. Finelli, N. Lotti, M. Colonna, C. Lorenzetti, N. Munari, *J. Polym. Sci., Part B: Polym. Phys.* **2005**, *43*, 1441–1454.
- [83] C. Berti, M. Colonna, L. Finelli, C. Lorenzetti, N. Lotti, M. Vannini, *Macromol. Chem. Phys.* **2004**, *205*, 2473–2485.
- [84] E. Quaranta, C. C. Minischette, G. Tartaro, *ACS Omega* **2018**, *3*, 7261–7268.
- [85] C. Jehanno, J. Demarteau, D. Mantione, M. C. Arno, F. Ruipérez, J. L. Hedrick, A. P. Dove, H. Sardon, *ACS Macro Lett.* **2020**, *9*, 443–447.
- [86] C. Jehanno, J. Demarteau, D. Mantione, M. C. Arno, F. Ruipérez, J. L. Hedrick, A. P. Dove, H. Sardon, *Angew. Chem. Int. Ed.* **2021**, *60*, 6710–6717.
- [87] K. Saito, C. Jehanno, L. Meabe, J. L. Olmedo-Martínez, D. Mecerreyes, K. Fukushima, H. Sardon, *J. Mater. Chem. A* **2020**, *8*, 13921–13926.
- [88] T. Rufino, M. C. Breitzkreitz, M. I. Felisberti, *Ind. Eng. Chem. Res.* **2017**, *56*, 3983–3992.
- [89] B. Li, F. Xue, J. Wang, E. Ding, Z. Li, *Prog. Rubber, Plast. Recycl. Technol.* **2017**, *33*, 39–50.
- [90] K. Hidaka, Y. Iwakawa, T. Maoka, F. Tanimoto, A. Oku, *J. Mater. Cycles Waste Manage.* **2009**, *11*, 6–10.
- [91] E. A. Gilbert, M. L. Polo, J. M. Maffi, J. F. Guastavino, S. E. Vaillard, D. A. Estenoz, *J. Polym. Sci.* **2022**, 1–34.
- [92] P. S. Roy, G. Garnier, F. Allais, K. Saito, *ChemSusChem* **2021**, *14*, 4007–4027.
- [93] H. Chen, K. Wan, Y. Zhang, Y. Wang, *ChemSusChem* **2021**, *14*, 4123–4136.
- [94] C. Jehanno, J. W. Alty, M. Roosen, S. De Meester, A. P. Dove, E. Y.-X. Chen, F. A. Leibfarth, H. Sardon, *Nature* **2022**, *603*, 803–814.
- [95] G. O. Jones, A. Yuen, R. J. Wojtecki, J. L. Hedrick, J. M. García, *Proc. Natl Acad. Sci. USA* **2016**, *113*, 7722–7726.
- [96] K. Fukushima, J. M. Lecuyer, D. S. Wei, H. W. Horn, G. O. Jones, H. A. Al-Megren, A. M. Alabdulrahman, F. D. Alsewailem, M. A. McNeil, J. E. Rice, J. L. Hedrick, *Polym. Chem.* **2013**, *4*, 1610–1616.

- [97] G. R. Fulmer, A. J. M. Miller, N. H. Sherden, H. E. Gottlieb, A. Nudelman, B. M. Stoltz, J. E. Bercaw, K. I. Goldberg, *Organometallics* **2010**, *29*, 2176–2179.
- [98] T. Zhou, Z. Zou, J. Gan, L. Chen, M. Zhang, *J. Polym. Res.* **2011**, *18*, 2071–2076.
- [99] Z. Wang, R. Yang, G. Xu, T. Liu, Q. Wang, *ACS Sustainable Chem. Eng.* **2022**, *10*, 4529–4537.
- [100] D. A. Evans, J. Bartroli, T. L. Shih, *J. Am. Chem. Soc.* **1981**, *103*, 2127–2129.
- [101] Y. Liu, Z. Yi, X. Yang, H. Wang, C. Yin, M. Wang, X.-Q. Dong, X. Zhang, *ACS Catal.* **2020**, *10*, 11153–11161.
- [102] R. Yang, G. Xu, B. Dong, X. Guo, Q. Wang, *ACS Sustainable Chem. Eng.* **2022**, *10*, 9860–9871.
- [103] T. Pongpanit, T. Saeteaw, P. Chumsaeng, P. Chasing, K. Phomphrai, *Inorg. Chem.* **2021**, *60*, 17114–17122.

Chapter 6.

6. Concluding Remarks

The work presented within this thesis aimed to address the following aims and objectives of the PhD:

1. Develop simple, cheap and environmentally benign discrete metal-based catalysts for PLA production *via* the ROP of *rac*-LA, prioritising high activity and stereocontrol, particularly under industrially melt conditions (**Chapter 2**).
2. Assess the ability of such catalysts to facilitate the mild and selective degradation of various commercial polyesters, such as PLA and PET, with a particular focus on chemical upcycling into value-added products (*e.g.* green solvents and chemical building blocks) (**Chapters 3, 4 and 5**).
3. Explore judicious metal and ligand diversification for the optimisation of such systems for the chemical recycling of polyesters, whilst ensuring catalyst design remains industrially relevant in accordance to Aim 1 above (**Chapters 3, 4 and 5**).
4. Investigate the potential to extend catalyst scope to other types of plastics that possess cleavable linkages (*e.g.* polycarbonates) (**Chapters 5**).

In Chapter 1, an overview of the plastics industry was provided, and key challenges and opportunities were identified in the context of transitioning to a sustainable and circular plastics economy. Chemical recycling was introduced as a possible enabler and compared with the industry standard, namely mechanical recycling. Social, economic and environmental challenges associated with the uptake of such technology, in addition to governing thermodynamic and kinetics principles, were discussed before introducing polyesters as a possible class of plastics amenable to chemical recycling. A comprehensive overview of key contributions and recent developments for the catalytic chemical recycling of PLA and PET were highlighted, focusing on upcycling strategies (*e.g.* solvolysis, alcoholysis and reductive depolymerisation) and the use of metal-based catalysts. Importantly, Chapter 1 highlights discrete metal-mediated systems remain rare despite being a promising solution for a number of key challenges in the field, including process efficiency and selectivity.

In Chapter 2, the adventitious design features of two established ligand classes, namely the salen and catam, were incorporated into the design of a new ligand framework: the catalen (**1-3H₂**). In combination with Al(III), such initiators were found to facilitate rapid PLA production in the melt (TOFs up to 45,300 h⁻¹), affording polymer of high M_n (> 10,000 g mol⁻¹) under industrially relevant loadings (0.033 mol%) for the first time. Promisingly, high activity was

retained in DCM at room temperature, noting an unusual stereoselectivity switch dependent on the ligand substituents employed {Al(**1**)Me, $P_r = 0.30$; Al(**3**)Me, $P_r = 0.72$ }. Al(**3**)Me was found to be inactive for PLA methanolysis, presumably due to poor hydrolytic stability and adverse electronic/steric effects.

In pursuit of catalysts active for PLA methanolysis, metal diversification was explored in Chapter 3 as a possible solution to the limitations noted in Chapter 2. Metal exchange was found to adversely impact polymerisation activity under both melt and solution conditions, which can likely be attributed to a shift in the polymerisation mechanism in operation. This was reflected in Zn(**1-3**)₂ and Mg(**1,3**)₂ exhibiting markedly poorer performance relative to their Al(III)-counterparts. However, the first example of PLA methanolysis mediated by a discrete Mg(II)-complex was demonstrated under relatively mild conditions (80 °C). Significantly reduced activity was observed in the analogous Zn(II)-complexes, possibly due to catalyst aggregation, which appeared less prevalent in the Mg(II)-complexes. Such findings are generally consistent with the Al(III)-catalen dimers detailed in Chapter 2, where kinetically limited dissociation was highlighted as a possible cause for poor polymerisation control in solution. Preliminary work successfully demonstrated the application of such catalysts to the chemical recycling of PET from various commercial sources, demonstrating catalyst versatility.

In Chapter 4, a simple monoanionic tridentate {ONN} building block (**1H**), initially used for the production of the catalen ligands employed in Chapters 2 and 3, was investigated as a possible ligand for the production of homoleptic and monomeric Zn(II)- and Mg(II)-complexes. Crucially, Zn(**1**)₂ and Mg(**1**)₂ were found to facilitate rapid PLA methanolysis under mild conditions (50 °C) and are among the fastest reported to date. Catalyst versatility was demonstrated through the degradation of various commercial polyesters (*e.g.* PET and PCL), employing a range of upcycling strategies (*e.g.* methanolysis, glycolysis and aminolysis) to achieve a broad value-added substrate scope. Indeed, the application of discrete homogeneous metal-based catalysts to PET aminolysis and PCL methanolysis was reported for the first time. A selective recycling strategy for a mixed PLA/PET feed was also demonstrated on a multigram scale using Zn(**1**)₂. Importantly, metal exchange was found to dramatically influence catalyst activity, which appeared system dependent, whilst elevated temperatures were found to adversely impact PLA methanolysis.

In Chapter 5, learnings pertaining to catalyst design for chemical recycling applications from Chapters 2, 3 and 4 were applied to the synthesis of a series of well-defined Zn(II)-half-salan complexes. Indeed, such complexes were shown to mediate the mild and selective degradation of various commercial polyesters (*e.g.* PLA and PET) and polycarbonates (*e.g.* BPA-PC and PPC). A range of value-added products were produced including green solvents and chemical

building blocks. The first example of discrete metal-mediated BPA-PC methanolysis being appreciably active at room temperature was demonstrated, with further kinetic analysis confirming Zn(2)_2 to be the fastest catalyst reported to date. Process efficiency was found to be dependent on a number of parameters including temperature, $n_{\text{carbonate}} \cdot n_{\text{MeOH}}$, catalyst loading and reaction time. Furthermore, in proof-of-concept work, a completely circular upcycling approach for bottle-grade PET waste was demonstrated through the production of several renewable PEAs, which exhibited excellent thermal properties.

6.1. Future Work

6.1.1. Chapter 2

In Chapter 2, a pronounced stereoselectivity switch dependent on the nature of the ligand backbone employed was observed for the solution phase production of PLA in DCM at RT, as summarised in Figure 6.1 below, which remains poorly understood. Consequently, future work should endeavour to understand the origin of this stereocontrol, possibly through further computational study, which is of paramount importance to future catalyst design and optimisation. Indeed, Marshall *et al.*^[1] and D'Alterio *et al.*^[2] have previously exploited DFT to provide mechanistic insight into the stereoselective ROP of lactide using metal-based catalysts. It is envisaged such studies will provide useful models to address this challenge.

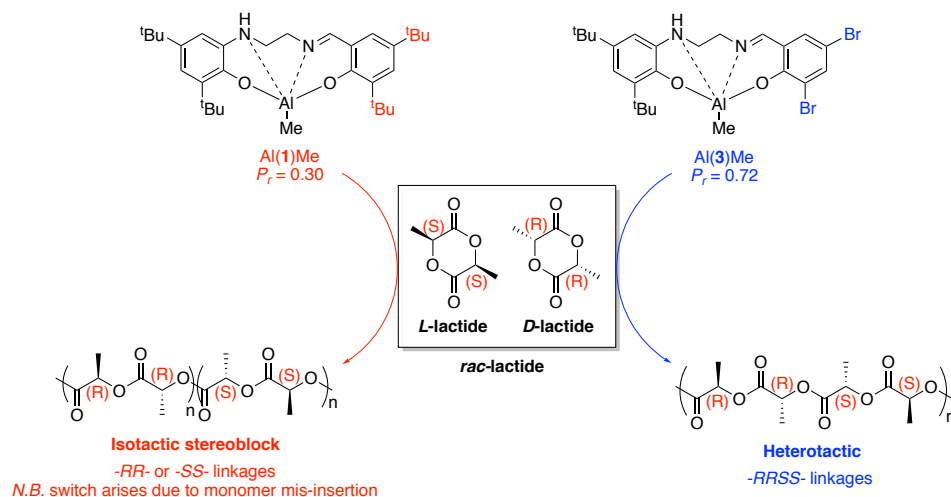


Figure 6.1. Summary of stereoselectivity switch observed between Al(1)Me and Al(3)Me for the solution phase production of PLA at room temperature in DCM $\{[rac\text{-LA}]:[\text{Al}]:[\text{BnOH}] = 100:1:1\}$.

Significant scope also remains for diversification of the catalen ligand. Indeed, Mckeown *et al.*^[3,4] have previously shown ligand flexibility to dramatically influence the activity of Zn(II) -complexes for polyester degradation. It is likely this would also result in enhanced polymerisation activity, with possible further ramifications on observed stereocontrol,

consistent with previous work by Romain and co-workers.^[5,6] Thus, future work should endeavour to prepare the propyl analogues of **1-3H₂** for an initiator performance comparison study with Chapter 2 (Figure 6.2, **A**). Further derivatisation could also include reduction of the imine to afford the corresponding ‘catalan’ (Figure 6.2, **B**), analogous to the established salan ligand, which has been widely exploited in the ROP of cyclic esters. Indeed, salan-based complexes are often white powders, and thus produce polymer of superior optical clarity, which is of considerable interest to industry.^[7-10] Moreover, the introduction of a second -NH donor, in combination with a more flexible ligand backbone, will likely result in superior polymerisation activity. Importantly, judicious diversification of the catalen ligand may also create new opportunities to exploit discrete Al(III)-based complexes in chemical recycling applications.

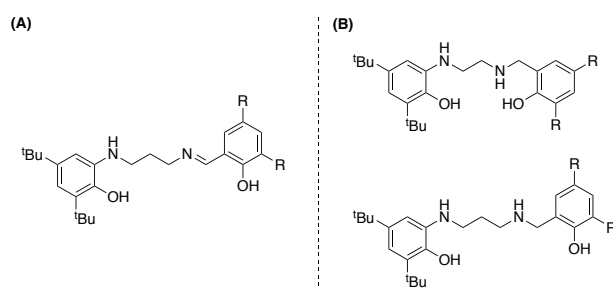


Figure 6.2. Possible diversification routes of the catalen to afford the corresponding propyl (**A**) and catalan (**B**) analogues. *N.B.* R denotes either ^tBu, Cl or Br.

Future work should also endeavour to better understand the kinetically limited dissociation exhibited by $[Al(\mathbf{1-3})\{OBn\}]_2$, which could be addressed through adopting a complimentary computational (*e.g.* DFT) and experimental (*e.g.* reaction kinetic analysis to determine catalyst order) approach. Indeed, a fundamental understanding of the factors that govern catalyst association will help inform both future catalyst design, in pursuit of systems that afford superior polymerisation control, and the mechanism in operation. Indeed, Mehrkhodavandi and co-workers have previously highlighted a number of factors that influence catalyst association in dinuclear catalysts for the ROP of lactide, which included metal size, ligand flexibility and bulk, and the nature of the initiating group employed.^[11] Furthermore, Romain *et al.*^[12] have previously employed reaction kinetic analysis to investigate the impact of chirality-induced catalyst aggregation on the speciation and activity of enantiopure chiral Al(III)-complexes in the ROP of cyclic esters, which could possibly be adapted to this work.

6.1.2. Chapter 3

Diversification strategies discussed for the catalen ligands in section 6.1.1. could also be applied to the Zn(II)- and Mg(II)-complexes detailed in Chapter 3. Moreover, modification of the Schiff-base moiety also represents a promising route to accessing new monoanionic and

dianionic catalen frameworks, enabling factors such as electronic and steric effects, structural rigidity and pendant arm lability to be further investigated (Figure 6.3). Indeed, Mazzeo and co-workers have previously shown the importance of a pendant pyridine donor in facilitating superior PLA methanolysis efficiency *via* a ligand-assisted nucleophilic activation mechanism (Scheme 4.1).^[13,14] Specifically, the pendant pyridine arm likely assists with proton-transfer *via* activation of the external nucleophile, comparable to a ligand-assisted activated monomer mechanism observed in some polymerisation reactions.^[4,15]

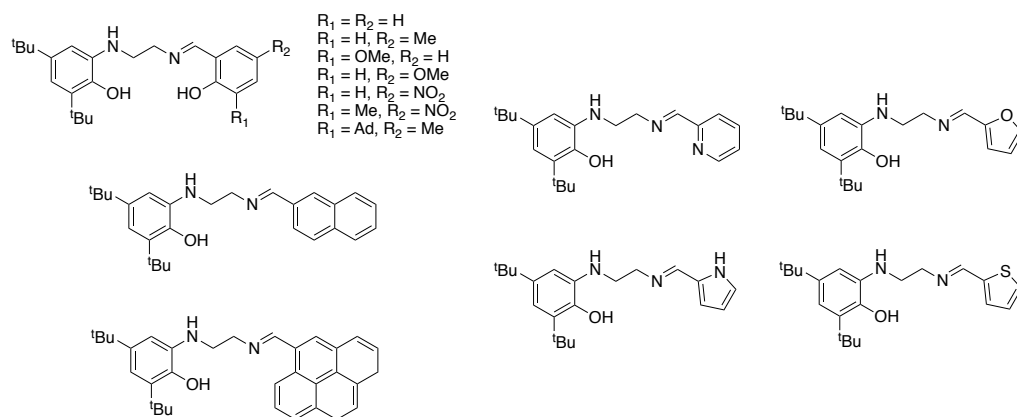


Figure 6.3. Example modifications of the Schiff-base moiety to access a diverse range of new monoanionic and dianionic catalen frameworks.

Recent work within this group has also investigated the impact of structure-activity relationships on PLA alcoholysis mediated by Zn(II)-complexes (**44-49**) bearing tridentate {ONN} Schiff-base-type ligands (Figure 6.4).^[16] Whilst electron donating groups were found to increase the rate of methanolysis, contrasting previous findings of the preceding MRes project to this PhD, the steric hinderance of the substituents employed had a greater impact on activity reduction.^[17] A greater understanding of structure-activity relationships within such systems will enable a targeted approach to catalyst design and optimisation to be adopted, thus accelerating progress within the field and possible translation to industry.

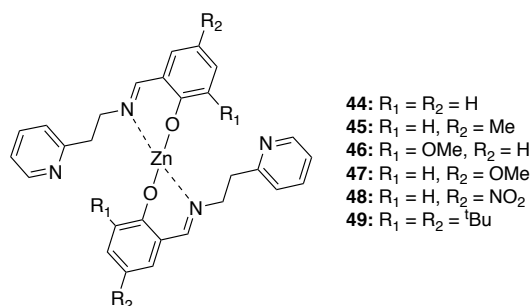


Figure 6.4. Homoleptic Zn(II)-complexes based on tridentate {ONN} Schiff-base-type ligands reported by Mazzeo and co-workers for PLA production and alcoholysis.^[16]

Possible catalen modifications depicted in Figure 6.3. could also be extended to the propyl and catalan analogues shown in Figure 6.2, which serves to generate significant scope for catalyst fine-tuning. Furthermore, diversification of the catalen backbone may also help remedy concerns associated with catalyst aggregation, which appeared prevalent in the Zn(II)-complexes, resulting in poorer PLA methanolysis performance than expected. Indeed, for divalent metals, such as Zn(II) and Mg(II), it is anticipated the use of a monoanionic ligand will enable access to well-defined homoleptic and monomeric complexes, which will likely help address this issue.

Recently, Driscoll *et al.*^[18] demonstrated the first example of simple ligand types and classes, namely salen, salalen, salophen and salan, facilitating epoxide/anhydride ROCOP, specifically between phthalic anhydride (PA) and cyclohexene oxide (CHO). Intuitively, **1-3H₂**, and any subsequent catalen variations or derivatives, could potentially offer a simplistic, metal- and halide-free organocatalytic approach for the production of highly alternating polyesters, which should be explored.

6.1.3. Chapter 4

Initial future work should focus on expansion of the catalyst suite with potential tridentate {ONN} ligand backbone candidates provided in Figure 6.5. below. Indeed, these half-catalen-type structures would represent a new and emerging class of ligand in the field, creating new opportunities for catalyst development. Whilst synthesis attempts to prepare the propyl analogue of **1H** were unsuccessful in this thesis, alternative strategies (*e.g.* Dean-Stark apparatus and protecting groups) should be explored. This is due to the potential to realise significantly enhanced catalyst activity relative to Zn(**1**)₂ and Mg(**1**)₂ through additional ligand flexibility, consistent with previous work by Mckeown *et al.*^[3,4]

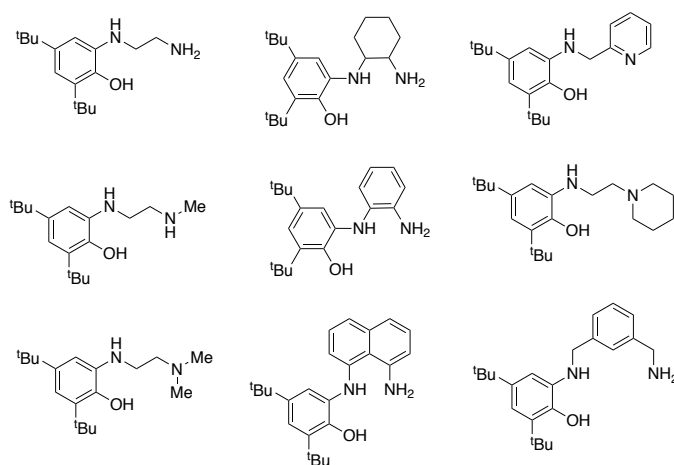
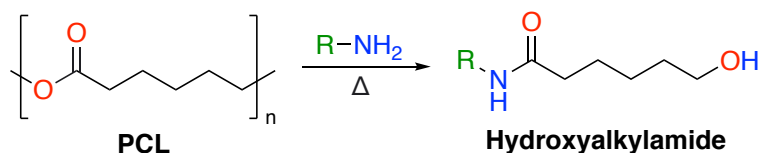


Figure 6.5. Possible tridentate {ONN} ligand candidates based on commercially available reagents.

Following the successful development of more highly active catalysts, PLA alcoholysis using higher chain alcohols, such as EtOH, ⁱPrOH and ⁿBuOH, should also be explored. Presently, the Et-LA market is projected to reach \$92 million by 2024 and currently trades at £2.54 – 3.49 per kg relative to £1.69 per kg for virgin PLA.^[20,21] Indeed, providing intrinsic economic benefits to industry through plastic upcycling is of paramount importance to overcoming inevitable barriers to adoption within industry.

Surprisingly, both Zn(1)₂ and Mg(1)₂ exhibited inferior PLA methanolysis performance at elevated temperatures, potentially due to thermal degradation. Whilst non-Arrhenius behaviour has previously been reported by Wood and co-workers for a Zn(II)-complex bearing a propylenediamine ligand, this phenomenon remains poorly understood in relation to the work presented in Chapter 4.^[20,22] To this end, Flow NMR spectroscopy represents a potentially powerful tool for identifying and monitoring catalytic species in real-time. Indeed, this technique has previously been used to monitor photochemical and radical polymerisation reactions, to name but a few, and can likely be readily extended to degradation.^[23,24] Crucially, this could provide further insight into the active catalytic species, in addition to any competing deactivation pathways, which will assist with future process optimisation. This technique could also compliment work detailed in Chapters 2, 3 and 5.

Recently, the chemical upcycling of PCL *via* alcoholysis has received increasing interest in the literature.^[25-29] Beyond traditional methods, PCL aminolysis represents a promising route to accessing high value hydroxyalkylamides (Scheme 6.1), which are widely used in surfactants, carrier-prodrugs and pharmaceutical intermediates, to name but a few.^[30] However, to the best of our knowledge, current examples of hydroxyalkylamide production remain primarily limited to the ROP of the corresponding lactone, for example ε-caprolactone or lactide, *via* aminolysis.^[30-33] There is therefore a clear opportunity to explore PCL waste as a possible feedstock for the production of such chemicals.



Scheme 6.1. PCL aminolysis for the production of high value hydroxyalkylamides.

6.1.4. Chapter 5

The application of discrete metal-based catalysts to the chemical recycling of BPA-PC *via* alcoholysis remains vastly underexplored. Thus, immediate future work should focus on further catalyst development. Firstly, the Mg(II)-analogues of Zn(2)₂ and Zn(2)Et, as shown in Figure 6.6 below, should be prepared to assess the impact of the metal centre on activity,

which was previously shown in Chapter 4 to dramatically influence both polymerisation and degradation activity. Indeed, all remaining Zn(II)-half-salan complexes, and their corresponding Mg(II)-analogues, detailed in Chapter 5 should also be screened for their BPA-PC methanolysis and glycolysis efficacy.

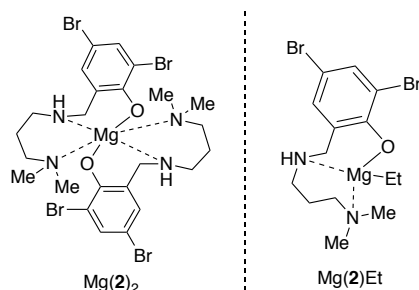


Figure 6.6. Mg(II)-analogues of Zn(2)₂ and Zn(2)Et.

Secondly, diversification of the half-salan ligand backbone should then be pursued, for example variation of the propylamine fragment (Figure 6.7, **A**), prioritising the use of cheap and commercially available reagents in the interest of industrial relevance. Additionally, this may also help address catalyst synthesis challenges detailed in Chapter 5. Finally, analogous metal-half-salen complexes should also be assessed for a performance comparison, which will assist with ascertaining a better understanding of structure-activity relationships (Figure 6.7, **B**). Indeed, such ligands are accessible *via* inexpensive, simple one-pot processes, which is desirable from an industry perspective. Furthermore, if such complexes retain high process efficiency, the academic community need look no further than the literature for a bountiful source of inspiration for future catalyst development.^[7-10,34,35] Additionally, homoleptic metal-complexes will offer superior catalyst stability relative to their heteroleptic counterparts (*i.e.* Zn-Et), and thus should be prioritised for ease of handling and use.

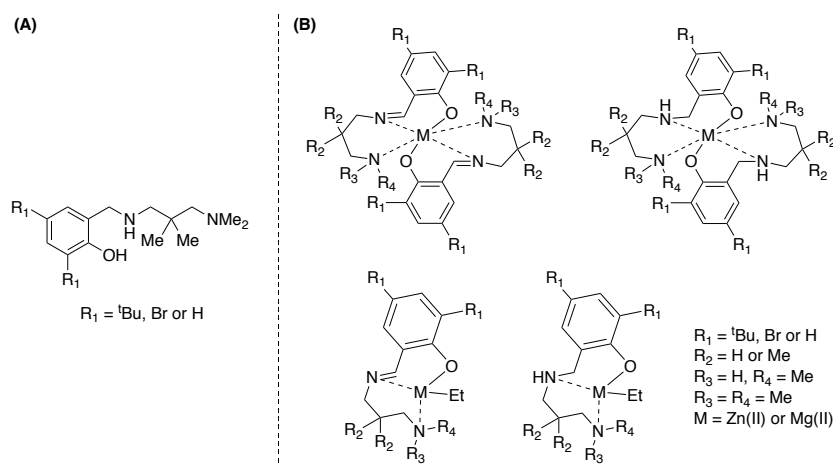


Figure 6.7. Possible diversification of the half-salan backbone (**A**) and the corresponding homoleptic and heteroleptic half-salan and half-salen metal-complexes (**B**).

Whilst Zn(2)_2 and Zn(2)Et offer exceptional activity for BPA-PC methanolysis, concerns remain regarding catalyst recovery and reuse, a common limiting feature of homogeneous catalysis.^[36] A potential solution to this challenge is the development of heterogeneous-based alternatives *via* immobilisation of such catalysts on a support, for example inert polystyrene (PS) or silica.^[36-39] Furthermore, adapting such systems to operate in flow could offer a number of benefits relative to batch, particularly with regards to the handling of mixed plastic waste feeds and from a product separation perspective.^[40] Indeed, continuous flow reactors have recently been coupled with online monitoring tools and reaction telescoping for the precise engineering of polymeric materials. Promisingly, this enabled rapid process optimisation, streamlining and machine-learning based reactor automatisation.^[41] It is envisioned such principles could be extended to the reverse process, namely degradation. However, to the best of our knowledge, no such examples have yet been reported for either PLA, PET or BPA-PC. Catalyst immobilisation could also be pursued following optimisation of the systems reported in Chapter 4.

Upon successful catalyst immobilisation, there is also the possibility to explore process scalability (> 200 mL) on a novel spinning disc reactor (SDR) (Figure 6.8). This could be achieved through a collaboration with Dr Emma Emanuelsson in the Chemical Engineering Department at the University of Bath. A form of process intensification, the SDR relies on centrifugal (shear) forces to generate a thin-film, which promotes superior mass and heat transfer.^[42,43] Whilst SDRs have previously been exploited for polycondensation reactions, to the best of our knowledge, no such examples have yet been reported for the chemical recycling of plastics.^[44] Complimentary computational work could include process modelling using design-of-experiments (DoE) and MATLAB to assist with system optimisation.



Figure 6.8. SDR located in 9W 0.04 at the University of Bath (Emanuelsson group), which could possibly be amended for chemical recycling applications.

In Chapter 5, PEA(1-4) were found to exhibit promising thermal properties, observing T_g values up to 126 °C, however, remain limited by low M_n values (1750 – 3150 g mol⁻¹) and broad dispersities ($D = 2.91 - 3.72$). Thus, future work should endeavour to optimise the synthesis procedure to achieve PEAs of high and well-defined M_n . Further materials characterisation (*e.g.* tensile testing, dynamic mechanical analysis (DMA) and thermomechanical analysis (TMA)) should also be conducted. This will assist with identifying future applications of such materials, for example in the biomedical sector.^[45,46] Furthermore, PEA(4) represents new opportunities for bio-based aromatic polymers, which have previously been hindered by limited monomer scope and challenging synthesis.^[47-50] Consequently, particular attention should be given to dimethyl 2,5-furandicarboxylate (DMFDC) in combination with various terephthalamide monomers for the production of renewable polyamides (Figure 6.9). Indeed, Kamran *et al.*^[51] recently reported semi-aromatic polyamides based on a renewable monomer, namely furandicarboxylic acid (FDCA). Importantly, such polymers exhibited comparable T_g values (up to 140 °C) and thermal properties (T_{d-max} up to 446 °C) relative to their petroleum-based counterparts, highlighting the promise of such polymeric materials. Furthermore, previous work by Fukushima *et al.*^[52] provides a plethora of terephthalamide monomers easily accessible *via* PET aminolysis, examples of which are given below in Figure 6.9. Intuitively, such work could be extended to the remaining renewable diester monomers employed in Chapter 5.

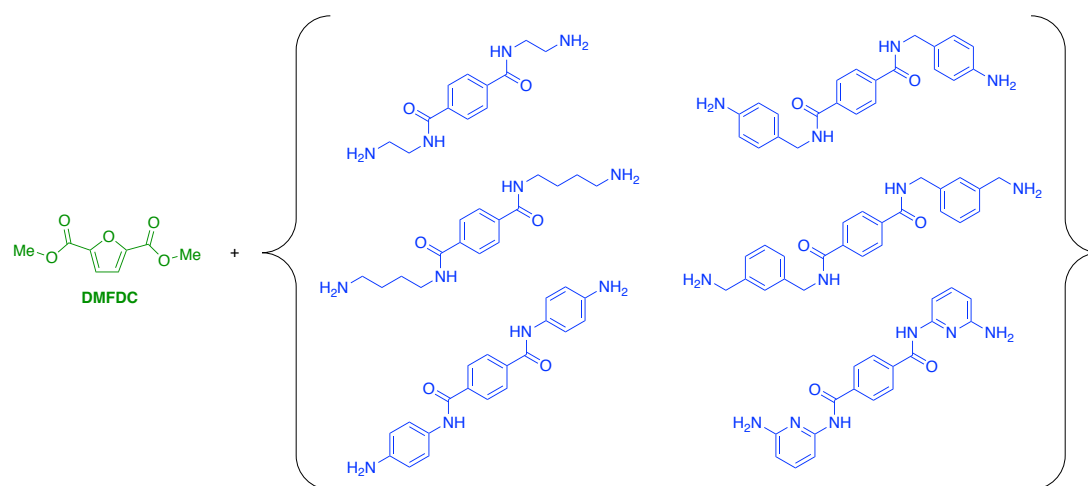


Figure 6.9. Polymerisation of DMFDC with various terephthalamide monomers derived from PET waste *via* aminolysis for the production of renewable polyamides.

6.2. References

- [1] E. L. Marshall, V. C. Gibson, H. S. Rzepa, *J. Am. Chem. Soc.* **2005**, *127*, 6048–6051.
- [2] M. C. D'Alterio, C. De Rosa, G. Talarico, *Chem. Commun.* **2021**, *57*, 1611–1614.
- [3] L. A. Román-Ramírez, P. McKeown, M. D. Jones, J. Wood, *ACS Catal.* **2019**, *9*, 409–416.
- [4] P. McKeown, L. A. Román-Ramírez, S. Bates, J. Wood, M. D. Jones, *ChemSusChem* **2019**, *12*, 5233–5238.
- [5] S. Gesslbauer, H. Cheek, A. J. P. White, C. Romain, *Dalton Trans.* **2018**, *47*, 10410–10414.
- [6] S. Gesslbauer, R. Savela, Y. Chen, A. J. P. White, C. Romain, *ACS Catal.* **2019**, *9*, 7912–7920.
- [7] O. Dechy-Cabaret, B. Martin-Vaca, D. Bourissou, *Chem. Rev.* **2004**, *104*, 6147–6176.
- [8] C. M. Thomas, *Chem. Soc. Rev.* **2010**, *39*, 165–173.
- [9] M. J. Stanford, A. P. Dove, *Chem. Soc. Rev.* **2010**, *39*, 486–494.
- [10] M. J.-L. Tschan, R. M. Gauvin, C. M. Thomas, *Chem. Soc. Rev.* **2021**, *50*, 13587–13608.
- [11] A. B. Kremer, P. Mehrkhodavandi, *Coord. Chem. Rev.* **2019**, *380*, 35–57.
- [12] S. Gesslbauer, G. Hutchinson, A. J. P. White, J. Burés, C. Romain, *ACS Catal.* **2021**, *11*, 4084–4093.
- [13] F. Santulli, M. Lamberti, M. Mazzeo, *ChemSusChem* **2021**, *14*, 5470–5475.
- [14] F. Santulli, G. Gravina, M. Lamberti, C. Tedesco, M. Mazzeo, *Mol. Catal.* **2022**, *528*, 112480.
- [15] B. Liu, T. Roisnel, L. Maron, J. F. Carpentier, Y. Sarazin, *Chem. Eur. J.* **2013**, *19*, 3986–3994.
- [16] S. D'Aniello, S. Laviéville, F. Santulli, M. Simon, M. Sellitto, C. Tedesco, C. M. Thomas, M. Mazzeo, *Catal. Sci. Technol.* **2022**, Advance Article.
- [17] J. Payne, P. McKeown, M. F. Mahon, E. A. C. Emanuelsson, M. D. Jones, *Polym. Chem.* **2020**, *11*, 2381–2389.
- [18] O. J. Driscoll, J. A. Stewart, P. McKeown, M. D. Jones, *Macromolecules* **2021**, *54*, 8443–8452.
- [19] J. M. García, *Chem* **2016**, *1*, 813–815.
- [20] F. M. Lamberti, L. A. Román-Ramírez, P. McKeown, M. D. Jones, J. Wood, *Processes* **2020**, *8*, 738.
- [21] L. A. Román-Ramírez, M. Powders, P. McKeown, M. D. Jones, J. Wood, *J. Polym. Environ.* **2020**, *28*, 2956–2964.

- [22] L. A. Román-Ramírez, P. McKeown, M. D. Jones, J. Wood, *ACS Omega* **2020**, *5*, 5556–5564.
- [23] A. M. R. Hall, R. Broomfield-Tagg, M. Camilleri, D. R. Carbery, A. Codina, D. T. E. Whittaker, S. Coombes, J. P. Lowe, U. Hintermair, *Chem. Commun.* **2018**, *54*, 30–33.
- [24] J. H. Vrijsen, I. A. Thomlinson, M. E. Levere, C. L. Lyall, M. G. Davidson, U. Hintermair, T. Junkers, *Polym. Chem.* **2020**, *11*, 3546–3550.
- [25] R. Yang, G. Xu, C. Lv, B. Dong, L. Zhou, Q. Wang, *ACS Sustainable Chem. Eng.* **2020**, *8*, 18347–18353.
- [26] R. Yang, G. Xu, B. Dong, X. Guo, Q. Wang, *ACS Sustainable Chem. Eng.* **2022**, *10*, 9860–9871.
- [27] B. Dong, G. Xu, R. Yang, Q. Wang, *Chem. Asian J.* **2022**, e202200.
- [28] P. McKeown, M. Kamran, M. G. Davidson, M. D. Jones, L. A. Román-Ramírez, J. Wood, *Green Chem.* **2020**, *22*, 3721–3726.
- [29] E. Cheung, C. Alberti, S. Bycinskij, S. Enthaler, *ChemistrySelect* **2021**, *6*, 8063–8067.
- [30] X. Liang, P. Yu, C. Fu, Y. Shen, *Tetrahedron Lett.* **2021**, *66*, 152821.
- [31] M. Hölderle, G. Bar, R. Mülhaupt, *J. Polym. Sci. A: Polym. Chem.* **1997**, *35*, 2539–2548.
- [32] P. Garg, H. Keul, D. Klee, M. Möller, *Des. Monomers Polym.* **2009**, *12*, 405–424.
- [33] V. R. Chintareddy, H.-A. Ho, A. D. Sadow, J. G. Verkade, *Tetrahedron Lett.* **2011**, *52*, 6523–6529.
- [34] R. H. Platel, L. M. Hodgson, C. K. Williams, *Polym. Rev.* **2008**, *48*, 11–63.
- [35] O. Santoro, X. Zhang, C. Redshaw, *Catalysts* **2020**, *10*, 800.
- [36] N. Mizuno, M. Misono, *Chem. Rev.* **1998**, *98*, 199–217.
- [37] I. C. Howard, C. Hammond, A. Buchard, *Polym. Chem.* **2019**, *10*, 5894–5904.
- [38] C. Di Iulio, M. D. Jones, M. F. Mahon, D. C. Apperley, *Inorg. Chem.* **2010**, *49*, 10232–10234.
- [39] M. D. Jones, M. G. Davidson, C. G. Keir, L. M. Hughes, M. F. Mahon, D. C. Apperley, *Eur. J. Inorg. Chem.* **2009**, 635–642.
- [40] M. B. Plutschack, B. Pieber, K. Gilmore, P. H. Seeberger, *Chem. Rev.* **2017**, *117*, 11796–11893.
- [41] N. Zaquen, M. Rubens, N. Corrigan, J. Xu, P. B. Zetterlund, C. Boyer, T. Junkers, *Prog. Polym. Sci.* **2020**, *107*, 101256.
- [42] K. V. K. Boodhoo, M. C. Flickinger, J. M. Woodley, E. A. C. Emanuelsson, *Chem. Eng. Process.* **2022**, *172*, 108793.
- [43] F. Visscher, J. van der Schaaf, T. A. Nijhuis, J. C. Schouten, *Chem. Eng. Res. Des.* **2013**, *91*, 1923–1940.
- [44] K. V. K. Boodhoo, R. J. Jachuck, *Green Chem.* **2000**, *2*, 235–244.

- [45] A. C. Fonseca, M. H. Gil, P. N. Simoes, *Prog. Polym. Sci.* **2014**, *39*, 1291–1311.
- [46] A. Rodriguez-Galan, L. Franco, J. Puiggali, *Polymer* **2011**, *3*, 65–99.
- [47] R. Mülhaupt, *Macromol. Chem. Phys.* **2013**, *214*, 159–174.
- [48] K. Yao, C. Tang, *Macromolecules* **2013**, *46*, 1689–1712.
- [49] B. M. Stadler, C. Wulf, T. Werner, S. Tin, J. G. de Vries, *ACS Catal.* **2019**, *9*, 8012–8067.
- [50] A. Gandini, T. M. Lacerda, *Prog. Polym. Sci.* **2015**, *48*, 1–39.
- [51] M. Kamran, M. G. Davidson, V. Tsanaktsis, S. van Berkel, S. de Vos, *Eur. Polym. J.* **2022**, *178*, 111496.
- [52] K. Fukushima, J. M. Lecuyer, D. S. Wei, H. W. Horn, G. O. Jones, H. A. Al-Megren, A. M. Alabdulrahman, F. D. Alsewailem, M. A. McNeil, J. E. Rice, J. L. Hedrick, *Polym. Chem.* **2013**, *4*, 1610–1616.